EPA-600/3-83-015
April 1983

EPA COMPLEX TERRAIN MODEL DEVELOPMENT
Second Milestone Report - 1982

by

David G. Strimaitis
Akula Venkatram
Benjamin R. Greene
Steven Hanna
Steven Heisler
Thomas F. Lavery
Arthur Bass
Bruce A. Egan

ENVIRONMENTAL RESEARCH & TECHNOLOGY, INC.
696 Virginia Road, Concord, Massachusetts 01742

Contract No. 68-02-3421

Project Officer

Francis A. Schiermeier
Meteorology and Assessment Division
Environmental Sciences Research Laboratory
Research Triangle Park, North Carolina 22771

ENVIRONMENTAL SCIENCES RESEARCH LABORATORY
OFFICE OF RESEARCH AND DEVELOPMENT
U.S. ENVIRONMENTAL PROTECTION AGENCY
RESEARCH TRIANGLE PARK, NORTH CAROLINA 22771

NOTICE

This document has been reviewed in accordance with U.S. Environmental Protection Agency policy and approved for publication. Mention of trade names or commercial products does not constitute endorsement or recommendation for use.

FOREWORD

The Environmental Sciences Research Laboratory (ESRL) conducts an intramural and extramural research program in the physical sciences to detect, define, and quantify air pollution and its effects on urban, regional, and global atmospheres and the subsequent impact on water quality and land use. The Laboratory is responsible for planning, implementing, and managing research and development programs designed to quantify the relationships between emissions of pollutants from all types of sources with air quality and atmospheric effects, and to uncover and characterize hitherto unidentified air pollution problems. Information from ESRL programs and from the programs of other government agencies, private industry, and the academic community are integrated by the Laboratory to develop the technical basis for air pollution control strategies for various pollutants.

The Complex Terrain Model Development (CTMD) project is designed to develop reliable atmospheric dispersion models that are applicable to large pollutant sources located in complex terrain. The first major field study of this five-year program was conducted during 1980 at Cinder Cone Butte near Boise, Idaho. Data from this field study along with measurements of scaled physical simulations performed in the EPA Fluid Modeling Facility are being used to quantify the effects of terrain obstacles on stable plume dispersion. The first milestone report presented the performance evaluations of four existing complex terrain models and described the initial developmental stages of two proposed new models. This second milestone report documents subsequent improvements to the two new models and presents detailed case studies to illustrate and contrast various flow situations and ranges of model performance.

A. H. Ellison

A.H. Ellison
Director
Environmental Sciences Research Laboratory

ABSTRACT

The U.S. Environmental Protection Agency (EPA) is sponsoring the Complex Terrain Model Development (CTMD) program, a multi-year integrated program to develop and validate practical plume models of known reliability and accuracy for simulating 1-hour average ground-level concentrations downwind of elevated sources during stable atmospheric conditions in complex terrain. The first major component of the CTMD was a field program conducted during the fall of 1980 at Cinder Cone Butte (CCB), a roughly axisymmetric, isolated 100-meter tall hill located in the broad Snake River Basin near Boise, Idaho. The field program consisted of ten flow visualization experiments and 18 multi-hour tracer gas experiments conducted during stable flow conditions.

The CCB data were used to develop and evaluate two new, preliminary modeling algorithms (called the Impingement and Neutral models) and to evaluate the performance of current EPA complex terrain plume dispersion models (Valley, COMPLEX I, COMPLEX II, and PFM). For the model evaluations, 45 hours were selected from the 18 field experiment days. The meteorological and tracer data were used in a "hands-off" mode: no modifications were made to the models to improve their predictions. This study was described in the CTMD first milestone report (Lavery et. al., 1981).

This second milestone report documents work accomplished from fall 1981 through April 1982 to improve the Impingement and Neutral modeling approaches, to refine the meteorological and tracer gas data bases, and further analyze the data to relate plume behavior and observed meteorological conditions.

The Wrap and Lift models (modified versions of the Impingement and Neutral models) are described in detail, and aspects of the more general theory of stable flow and dispersion near hills is summarized to motivate the concepts behind these model formulations, and to identify important phenomena not yet incorporated into the models. Both the new and former versions of the models are evaluated on a subset of the CCB data base.

Unlike the hands-off evaluations described in the first milestone report, the approach taken in this report is a case study analysis. From the 45 hours used in the first report, 14 hours were selected for detailed individual case study to illustrate and contrast various flow situations and ranges of model performance.

Corrections to the UVW propellor wind set data are formulated to account for non-cosine response characteristics of the propellors used, wake effects of one propellor on another, and wake effects of a propellor shaft

or junction box on an adjacent propellor. Furthermore, adjustments to cup and vane wind set data as well as UVW propellor wind set data are devised to account for wake effects (shadowing) caused by the supporting tower structure.

New mathematical functions are developed to fit gas chromatograph calibrations. These functions provide a better fit to the calibration curves. Both SF_6 and Freon 13B1 concentrations are recalculated and analyzed to estimate the precision and the lower quantifiable limit of the analysis method.

Lidar measurements of plume size and near-field vertical plume spread angles estimated from photographs are analyzed, intercompared, and compared with turbulence data to evaluate the consistency between methods of measuring plume size, and to evaluate the performance of methods of estimating plume size from meteorological data. The analysis includes averaging times shorter than 1 minute as well as averaging times equal to or in excess of one hour. The comparison with turbulence data underscores the importance of accounting for spatial/temporal wind variability, and the characteristics of this variability are explored by means of time-series analysis.

Streamline heights well upwind of the hill and over the crest of the hill are inferred from temperature profiles at the 150 m tower 2 km to the north of CCB, and at the 30 m tower on the south peak of CCB. Details of the method employed and the implications for modeling the flow above the dividing streamline height are discussed.

This second milestone report also contains, as an appendix, a report prepared by the EPA Fluid Modeling Facility. The report describes a series of wind tunnel and tow tank experiments designed to study various aspects of stratified, sheared flow over a variety of simple obstacles, as well as flow over a model of CCB. In particular, the dividing-streamline concept is evaluated for obstacles of differing aspect ratio embedded in stably stratified flows both with, and without wind shear; and the effects of hill slope and wind shear on the flow patterns is discussed.

This report was submitted in partial fulfillment of Contract 68-02-3421 by Environmental Research & Technology, Inc. under the sponsorship of the U.S. Environmental Protection Agency. This report covers the period June 2, 1981 to June 1, 1982.

ACKNOWLEDGEMENT

The authors gratefully acknowledge the cooperation of the NOAA Wave Propagation Lab, and Wynn Eberhard in particular, in providing us with the reduced lidar data for so many of the CCB experiment hours studied in this report. The quality and unique attributes of the lidar data have been and will continue to be instrumental in formulating and evaluating plume dispersion models for CCB.

We also thank William Snyder, Roger Thompson, Robert Eskridge, Robert Lawson, Ian Castro, J.T. Lee, Julian Hunt, and Yasushi Ogawa for allowing us to include their draft paper as an appendix in advance of its possible journal publication. Its content certainly illuminates many flow phenomena which are central to modeling pollutant plumes in complex terrain.

Julian Hunt provided many useful suggestions for modeling the flow phenomena at CCB. Don DiCristofaro, Tony Curreri, and Jack Beebe performed much of the data analysis and modeling work that forms the basis of this report. And Frank Schiermeier and George Holzworth deserve much credit for keeping the CTMD program in motion.

CONTENTS

Foreward iii
Abstract iv
Figures ix
Tables xix
Symbols and Abbreviations xxi
Acknowledgement xxv

1. Introduction 1
2. Modeling Concepts 5
   2.1 The Froude Number and Dividing Streamline Height 5
   2.2 Flow in Region 1 7
   2.3 Dispersion in Region 1 10
   2.4 Flow in Region 2 11
   2.5 Summary 16
3. Modeling of CCB 17
   3.1 Model Description 17
   3.2 Comparison of Photographs and Lidar Plume Observations with Meteorological Observations 29
   3.3 Isentropic Analysis 50
4. Case Study Analyses 59
   4.1 Experiment 202, Hour 4 59
   4.2 Experiment 202, Hour 5 74
   4.3 Experiment 204, Hour 1 88
   4.4 Experiment 205, Hour 4 104
   4.5 Experiment 205, Hour 5 122
   4.6 Experiment 206, Hour 4 136
   4.7 Experiment 206, Hour 6 151
   4.8 Experiment 206, Hour 8 164
   4.9 Experiment 209, Hour 1 178
   4.10 Experiment 209, Hour 7 192
   4.11 Experiment 210, Hour 3 207
   4.12 Experiment 210, Hour 7 224
   4.13 Experiment 211, Hour 1 234
   4.14 Experiment 211, Hour 5 251
   4.15 Summary 266
5. Quality Assurance and Refinement of CCB Data 274
   5.1 Refinement of Tracer Gas Data 274
   5.2 Refinement of Meteorological Data 286
6. Summary, Conclusions, and Recommendations for Further Study 306
   6.1 Principal Accomplishments and Key Findings 306

6.2 Conclusions 311
6.3 Recommendations for Further Study 313

References 316
Appendices

A. The Structure of Strongly Stratified Flow Over Hills--
Dividing-Streamline Concept 319

FIGURES

Number		Page
1	Schematic diagram of plume behavior in stable flows around obstacles	6
2	Schematic of flow around a three-dimensional obstacle at very low Froude number	8
3	Definition of notation for describing flow in region 2 . .	12
4	Plume dispersion in the region of horizontal flow	18
5	Geometry used in formulating the Neutral model for high Froude number flows	20
6	Schematic used to derive the probability density function for specified θ_m	23
7	Geometry used to derive the effective radius of curvature R_e for the portion of the hill above H_c, and to incorporate the wind direction probability distribution function $P(\theta)$ in the Lift model	26
8	Observed 5-minute average i_z versus i_z (tower)	31
9	Time series of 5-minute average i_z (photo) and i_z (tower) from Experiment 201	33
10	Average tower i_z versus photo i_z. Circled points are those for which H_s = 60 m and H_t = 40 m	35
11	Observed hourly σ_y plotted as a function of $i_y x$ for selected experiment hours, based on Equation 51 . .	37
12	Observed hourly lidar σ_y as a function of the stability parameter U_o/N	38
13	Averages of observed individual scan lidar σ_y plotted as a function of x for selected experiment hours	40

FIGURES

Number		Page
14	Observed hourly lidar σ_z as a function of $i_z x$ for for selected experiment hours	42
15	Averages of observed individual scan lidar σ_z plotted as a function of x for selected experiment hours	43
16	Observed hourly i_z at 40 m level as a function of hourly scalar wind speed	44
17	Comparison of lidar-derived hourly σ_z values and calculated σ_z	46
18	Five minute wind speed record at 10 m elevation, its autocorrelogram, and its energy spectrum for Experiment 211	48
19	Estimated upwind height of streamlines that pass through the 10 m level and 30 m level of Tower B on the crest of Cinder Cone Butte during Experiments 201-203	51
20	Estimated upwind height of streamlines that pass through the 10 m level and 30 m level of Tower B on the crest of Conder Cone Butte during Experiments 204-208	53
21	Estimated upwind height of streamlines that pass through the 10 m level and 30 m level of Tower B on the crest of Cinder Cone Butte during Experiments 209-213	54
22	Estimated upwind height of streamlines that pass through the 10 m level and 30 m level of Tower B on the crest of Cinder Cone Butte during Experiments 214-218	55
23	Relationship between inferred streamline heights, the dividing streamline height H_c, and the quantities n_m, ZA	56
24	Height of the source streamline above the crest of CCB for various effective source heights inferred from temperature measurements at Tower A and Tower B. Values are scaled by the effective hill height	57
25	Plume centroid positions calculated from lidar data. Experiment 202, Hour 4	62
26	Calculated dividing streamline heights and bulk hill Froude numbers above H_c for Experiment 202	64

FIGURES

Number		Page
27	Tower A wind speeds during Experiment 202, Hour 4.	65
28	Calculated wind direction distribution functions for Experiment 202, Hour 4.	66
29	Observed SF_6 concentrations for Experiment 202, Hour 4. Source: r = 1014.6 m, r = 319.0°, net height = 13 m, Q = .082 g/s	68
30	Observed 10-minute averages SF_6 concentrations for Experiment 202, Hour 4	69
31	SF_6 concentrations estimated for Experiment 202, Hour 4 by the Neutral and Lift models.	75
32	Plume centroid positions calculated from lidar data. Experiment 202, Hour 5	77
33	Tower A wind speeds during Experiment 202, Hour 5.	79
34	Calculated wind direction distribution functions for Experiment 202, Hour 5.	80
35	Observed SF_6 concentrations for Experiment 202, Hour 5. Source: r = 1014.6 m, θ = 319.0°, net height = 23 m, Q = .086 g/s	81
36	Observed 10-minute average SF_6 concentrations for Experiment 202, Hour 5	82
37	SF_6 concentrations estimated for Experiment 202, Hour 5 by the Neutral and Lift models	87
38	Plume centroid positions calculated from lidar data. Experiment 204, Hour 1	92
39	Calculated dividing streamline heights and bulk hill Froude numbers above H_c for Experiment 204	94
40	Tower A wind speeds during Experiment 204, Hour 1	95
41	Calculated wind direction distribution functions for Experiment 204, Hour 1	96
42	Observed SF_6 concentrations for Experiment 204, Hour 1. Source: r = 1035.7 m, θ = 4.5°, net height = 23.2 m, Q = .094 g/s	97

FIGURES

Number		Page
43	Observed 10-minute average SF_6 concentrations for Experiment 204, Hour 1	99
44	SF_6 concentrations estimated for Experiment 204, Hour 1 by the Impingement and Wrap models	103
45	View of the 5-minute average plume trajectory between 0325 and 0330 MST taken from behind the release during Experiment 205, Hour 4	107
46	Preselected camera locations	108
47	Plume centroid positions calculated from lidar data. Experiment 205, Hour 4	110
48	Calculated dividing streamline heights and bulk hill Froude numbers above H_c for Experiment 205	111
49	Tower A wind speeds during Experiment 205, Hour 4	112
50	Calculated wind direction distribution functions for Experiment 205, Hour 4	114
51	Observed SF_6 concentrations for Experiment 205, Hour 4. Source: $r = 1155.1$ m, $\theta = 120.1°$, net height = 31.1 m, $Q = .083$ g/s	115
52	Observed 10-minute average SF_6 concentrations for Experiment 205, Hour 4	116
53	SF_6 concentrations estimated for Experiment 205, Hour 4 by the Neutral and Lift models	121
54	View of the 5-minute average plume trajectory between 0415 and 0420 MST taken from behind the release during Experiment 205, Hour 5	124
55	Plume centroid positions calculated from lidar data. Experiment 205, Hour 5	125
56	Tower A wind speeds during Experiment 205, Hour 5	127
57	Calculated wind direction distribution functions for Experiment 205, Hour 5	128

FIGURES

Number		Page
58	Observed SF_6 concentrations for Experiment 205 Hour 5. Source: r = 1155.1 m, θ = 120.1°, net height = 41.1 m, Q = .087 g/s	129
59	Observed 10-minute average SF_6 concentrations for Experiment 205, Hour 5	131
60	SF_6 concentrations estimated for Experiment 205, Hour 5 by the Neutral and Lift models	135
61	View of the 5-minute average plume trajectories between 0335 and 0340, and between 0340 and 0345 MST taken from behind the release during Experiment 206, Hour 4	138
62	Plume centroid positions calculated from lidar data. Experiment 206, Hour 4	139
63	Calculated dividing streamline heights and bulk hill Froude numbers above H_c for Experiment 206	141
64	Tower A wind speeds during Experiment 206, Hour 4	142
65	Calculated wind direction distribution functions for Experiment 206, Hour 4	143
66	Observed SF_6 concentrations for Experiment 206, Hour 4. Source: r = 595.9 m, θ 123.6°, net height = 29.5 m, Q = .039 g/s	144
67	Observed 10-minute average SF_6 concentrations for Experiment 206, Hour 4	145
68	SF_6 concentrations estimated for Experiment 206, Hour 4 by the Neutral and Lift models	150
69	Half-hour sequence of 5-minute average plume trajectories between 0500 and 0530 MST taken from behind the release during Experiment 206, Hour 6	153
70	Plume centroid positions calculated from lidar data. Experiment 206, Hour 6	155
71	Tower A wind speeds during Experiment 206, Hour 6	156
72	Calculated wind direction distribution functions for Experiment 206, Hour 6	157

FIGURES

Number		Page
73	Observed SF_6 concentrations for Experiment 206, Hour 6. Source: r = 595.9 m, θ = 123.6°, net height = 29.5 m, Q = .062 g/s	159
74	Observed 10-minute average SF_6 concentrations for Experiment 206, Hour 6	160
75	SF_6 concentrations estimated for Experiment 206, Hour 6 by the Impingement and Wrap models	165
76	View of the plume trajectory at 0721 MST taken from behind the release during Experiment 206, Hour 8	168
77	Tower A wind speeds during Experiment 206, Hour 8	169
78	Calculated wind direction distribution functions for Experiment 206, Hour 8	170
79	Observed SF_6 concentrations for Experiment 206, Hour 8. Source: r = 595.9 m, θ = 123.6°, net height = 29.5 m, Q = .062 g/s	172
80	Observed 10-minute average SF_6 concentrations for Experiment 206, Hour 8	173
81	SF_6 concentrations estimated for Experiment 206, Hour 8 by the Impingement and Wrap models	177
82	Two views of the plume trajectory at 1715 and 1746 MST taken from behind the release and taken off to the side of the release during Experiment 209, Hour 1	180
83	Plume centroid positions calculated from lidar data. Experiment 209, Hour 1	182
84	Calculated dividing streamline heights and bulk hill Froude numbers above Hc for Experiment 209	183
85	Tower A wind speeds during Experiment 209, Hour 1	184
86	Calculated wind direction distribution functions for Experiment 209, Hour 1	186
87	Observed SF_6 concentrations for Experiment 209, Hour 1. Source: r = 986.1 m, θ = 315.9°, net height = 33 m, Q = .156 g/s	187

FIGURES

Number		Page
88	Observed 10-minute average SF_6 concentrations for Experiment 209, Hour 1	188
89	SF_6 concentrations estimated for Experiment 209, Hour 1 by the Neutral and Lift models.	193
90	Two views of the plume trajectory between 2320 and 2325 MST taken from the top of the north peak and taken from behind the release during Experiment 209, Hour 7	196
91	Tower A wind speeds during Experiment 209, Hour 7.	198
92	Calculated wind direction distribution functions for Experiment 209, Hour 7	199
93	Observed SF_6 concentrations for Experiment 209, Hour 7. Source: $r = 999.2$ m, $\theta = 100.9°$, net height = 35.3 m, Q = .160 g/s.	200
94	Observed 10-minute average SF_6 concentrations for Experiment 209, Hour 7	202
95	SF_6 concentrations estimated for Experiment 209, Hour 7 by the Impingement and Wrap models.	206
96	Two views of the plume trajectory between 0215 and 0220 MST taken from the top of the north peak and taken off to the side of the release during Experiment 210, Hour 3	211
97	Plume centroid positions calculated from lidar data. Experiment 210, Hour 3	212
98	Calculated dividing streamline heights and bulk hill Froude numbers above H_c for Experiment 210	214
99	Tower A wind speeds during Experiment 210, Hour 3.	215
100	Calculated wind direction distribution functions for Experiment 210, Hour 3	216
101	Observed SF_6 concentrations for Experiment 210, Hour 3. Source: $r = 1084.3$ m, $\theta = 113.7°$, net height = 49.8 m, Q = .169 g/s	218

FIGURES

Number		Page
102	Observed 10-minute average SF_6 concentrations for Experiment 210, Hour 3	219
103	SF_6 concentrations estimated for Experiment 210, Hour 3 by the Neutral and Lift models	223
104	Two views of the plume trajectory between 0615 and 0620, and between 0610 and 0620 MST taken from the top of the south peak and taken from behind the release during Experiment 210, Hour 7	226
105	Tower A wind speeds during Experiment 210, Hour 7.	228
106	Calculated wind direction distribution functions for Experiment 210, Hour 7	229
107	Observed SF_6 concentrations for Experiment 210, Hour 7. Source: $r = 1086.2$ m, $\theta = 122.2°$, net height = 49.8 m, $Q = .178$ g/s	230
108	Observed 10-minute average SF_6 concentrations for Experiment 210, Hour 7	231
109	SF_6 concentrations estimated for Experiment 210, Hour 7 by the Neutral and Lift models	236
110	Plume centroid positions calculated from lidar data. Experiment 211, Hour 1	239
111	Calculated dividing streamline heights and bulk hill Froude numbers above H_c for Experiment 211	241
112	Tower A wind speeds during Experiment 211, Hour 1.	242
113	Calculated wind direction distribution functions for Experiment 211, Hour 1	243
114	Observed SF_6 concentrations for Experiment 211, Hour 1 Source: $r = 1001.2$ m, $\theta = 101.4°$, net height = 25.3 m, $Q = .179$ g/s	245
115	Observed 10-minute average SF_6 concentrations for Experiment 211, Hour 1	246
116	SF_6 concentrations estimated for Experiment 211, Hour 1 by the Impingement and Wrap models	250

FIGURES

Number		Page
117	Three views of the plume trajectory between 0410 and 0415, and between 0450 and 0455 MST taken from behind the release, taken from the top of the south peak, and taken off to the side of the release during Experiment 211 Hour 5	255
118	Tower A wind speeds during Experiment 211, Hour 5.	257
119	Calculated wind direction distribution functions for Experiment 211, Hour 5	258
120	Observed SF_6 concentrations for Experiment 211, Hour 5. Source: $r = 1155.1$ m, $\theta = 120.1°$, net height = 11.1 m, $Q = .175$ g/s	259
121	Observed 10-minute average SF_6 concentrations for Experiment 211, Hour 5	260
122	SF_6 concentrations estimated for Experiment 211, Hour 5 by the Impingement and Wrap models	265
123	Least-squares fit of old calibration function to calibration of gas chromatograph No. 7, S^3, with SF_6 at 0615 MST on November 11, 1980. Note the consistent over-prediction of concentrations by the least-squares fit below 1,000 ppt	276
124	Least-squares fit of new calibration function to calibration of gas chromatograph No. 7, S^3, with SF_6 at 0615 MST on November 11, 1980. The new function fits concentrations below 1,000 ppt better than the old function shown in Figure 123	278
125	Least-squares fit of power-law function to calibration of the AID gas chromatograph with SF_6 at 0600 MST on November 11, 1980	279
126	Least-squares fit of power-law function to calibration of the AID gas chromatograph with Freon 13B1 at 0615 MST on November 11, 1982	280
127	F_u, fraction of cosine response of U-propellor, from wind tunnel experiments as a function of wind direction as mounted in the field	290

FIGURES

Number		Page
128	F_V, fraction of cosine response of V-propellor, from wind-tunnel experiments as a function of wind direction as mounted in the field	291
129	F_u and F_V from wind tunnel experiments plotted symmetrically. Responses at 5 and 10 m/s for UVW set A only	292
130	Difference at 150 m level of Tower A between cup-derived wind speed SP and propellor-derived wind speed WS plotted as ratio (SP-WS)/SP as a function of vane direction DR before correction of data.	299
131	Sketch of geometry of tower, booms, and wind instruments at 150 m level, Tower A	300
132	Difference at 150 m level of Tower A between cup-derived wind speed SP and propellor-derived wind speed WS plotted as ratio (SP-WS)/SP as a function of vane direction DR, after correction of data	302
133	Difference at 150 m level of Tower A between wind direction DR derived from cup-and-vane set and direction WD derived from propellors as a function of DR before correction	304
134	Difference at 150 m level of Tower A between wind direction DR derived from cup-and-vane set and wind direction WD derived from propellors after correction. .	305

TABLES

Number		Page
1	Comments on Tower and Photo i_z Observations	34
2	Time Periods at Which Maximum Turbulent Energy Occurs for Six CCB Experiments.	49
3	Summary of Data Used to Select Case Study Hours	60
4	Neutral and Lift Model Calculations - Experiment 202, Case Hour 4	73
5	Neutral and Lift Model Calculations - Experiment 202, Case Hour 5	85
6	Impingement and Wrap Model Calculations - Experiment 204, Case Hour 1	102
7	Neutral and Lift Model Calculations - Experiment 205, Case Hour 4	120
8	Neutral and Lift Model Calculations - Experiment 205, Case Hour 5	134
9	Neutral and Lift Model Calculations - Experiment 206, Case Hour 4	149
10	Impingement and Wrap Model Calculations - Experiment 206, Case Hour 6	163
11	Impingement and Wrap Model Calculations - Experiment 206, Case Hour 8	176
12	Neutral and Lift Model Calculations - Experiment 209, Case Hour 1	191
13	Impingement and Wrap Model Calculations - Experiment 209, Case Hour 7	205
14	Neutral and Lift Model Calculations - Experiment 210, Case Hour 3	222
15	Neutral and Lift Model Calculations - Experiment 210, Case Hour 7	235

TABLES

Number		Page
16	Impingement and Wrap Model Calculations - Experiment 211, Case Hour 1	249
17	Impingement and Wrap Model Calculations - Experiment 211, Case Hour 5	264
18	Summary of Meteorological Data and the Associated Tracer Plume Behaviors	267
19	Summary Performance Statistics for the Lift and Neutral Models	271
20	Summary of Peak Modeled and Observed 1-Hour Average SF_6 Concentrations	273
21	Average Absolute Precent Differences of Recount Data by Concentration Ranges	282
22	Cumulative Frequency Distribution of SF_6 Concentrations	284
23	Precision of SF_6 Analysis	285
24	Average Fractions of Cosine Response Shown by U and V Propellor Anemometers: CCB Field Data, CSU Wind Tunnel Data, and Value Applied as Correction Factor to Field Data	295

LIST OF SYMBOLS AND ABREVIATIONS

SYMBOL	
$a(z)$	Radius of an ideal hill in horizontal cross-section
α_m	Angular horizontal plume spread, including meander
α_s	Angular horizontal plume spread, without meander
A	Least-squares fit calibration factor
B	Least-squares fit calibration factor
ß	Stable boundary layer profile constant
ß	Plume horizontal distortion factor
C	Assumed wind speed deficit in the center of a tower wake
C	Concentration
C_i	Instantaneous concentration
C_{max}	Maximum hourly averaged concentration
C_o	Observed concentration
C_p	Modeled concentration
C_T	Wind speed tower wake deficit correction
$C(\sigma_\phi)$	Refined correction factor for σ_ϕ
d	Distance of the source from the stagnation point
d	Absolute percent deviation
δ	Thickness of the inner surface layer
D	Effective radius of curvature minus the dividing streamline height
$\Delta u, \Delta v, \Delta w$	Velocity perturbations
E	Plume spread angle in the vertical
$F(\phi)$	Correction factor for σ_ϕ
F_u, F_v	Fraction of cosine response in propellor data
Fr_H	Froude number based upon hill height
Fr_L	Froude number based upon hill length
g	Acceleration due to gravity

h	Terrain height function
H	Hill height (crest)
H_c	Critical dividing streamline height
H_s	Plume height at the source
H_T	Instrument height on meteorological tower
H_*	$H-H_c$
η	Streamline deflection in the vertical
η^a,η^u	Streamline deflections due to hill slope and wind shear
θ	Wind direction
θ_o	Mean wind direction of approach flow
θ_o	Wind direction along center of tower wake
Θ	Potential temperature
i_x,i_y,i_z	Turbulence intensities alongwind, crosswind, and verticle
k	von Karman constant
ℓ_w	Vertical length scale of turbulence
L	Half-length (horizontal alongwind scale) of the hill
L_m	Monin-Obuhkov length scale
n	Number (in a summation)
n_m	Height of plume streamline over the hill crest
N	Number (in a summation)
N	Brunt-Vaisala frequency
p	Pressure
p'	Pressure perturbation
$P(\theta)$	Wind direction probability distribution function
Q	Tracer emission rate
r,θ,z	Polar coordinate system
ρ	Density
R	Response of GC
R_e	Effective radius of curvature
s	Distance from source to receptor
s_a	Distance along terrain from impingement point to receptor
σ	Standard deviation
σ_θ	Standard deviation of horizontal wind direction
σ_w	Standard deviation of vertical velocity fluctuations

σ_ϕ	Standard deviation of wind flow elevation angle
σ_y, σ_z	Crosswind and vertical standard deviation of tracer concentrations
σ_{yf}, σ_{zf}	Crosswind and vertical standard deviation of tracer concentrations in flat terrain setting
S	Scorer parameter
t_ℓ	Integral time scale
T	Time period for $P(\theta)$
T_c	Terrain factor
T_m	Terrain factor computed by model
T_{max}	Time period at which maximum turbulent energy occurs
T_o	Terrain factor computed from observed concentrations.
u,v,w	Wind tunnel wind speed measurements - UVW props
u_o	Wind tunnel flow speed
u_*	Surface friction velocity
U_o	Approach flow wind speed profile
ϕ	Wind flow elevation angle
ϕ	Plume spread distortion angle
ϕ_m	Indicator function for $P(\theta)$
W	Width of tower wake
x	Distance downwind from source
x_r, y_r, z_r	Tracer release coordinates
x_R, y_R, z_R	Receptor coordinates
z_o	Roughness length
z_r	Plume release height
ZA	Streamline height at tower A inferred from isentrope analysis

ABBREVIATIONS

AGE	Absolute Gross Error
CCB	Cinder Cone Butte
CTMD	Complex Terrain Model Development
DBMS	Data Base Management System
EPA	U.S. Environmental Protection Agency

ERT	Environmental Research & Technology
ESRL	Environmental Sciences Research Laboratory
FMF	Fluid Modeling Facility
GC	Gas chromatograph
Hz	Hertz
MRI	Meteorology Research, Inc.
MST	Mountain Standard Time
NAWC	North American Weather Consultants
NOAA	National Oceanographic and Atmospheric Administration
ppb	Parts per billion by volume
ppt	Parts per trillion by volume
PDF	Probability distribution function
RMSE	Root mean square error
RTD	Resistance Thermometric Device
TRC	TRC Environmental Consultants, Inc.
WPL	Wave Propagation Laboratory

SECTION 1

INTRODUCTION

The U.S. Environmental Protection Agency (EPA) Complex Terrain Model Development (CTMD) program is a multi-year study to develop improved models for calculating ground-level air pollutant concentrations that result from large emission sources located in mountainous terrain. These models are to be used in a wide variety of applications, such as the siting of new energy-development facilities and other air pollution sources, regulatory decision making, and environmental planning. Therefore, the models should be easy to understand, easy to use with conveniently obtained meteorological data as inputs, and of known accuracy and limitations.

In July 1979 the EPA convened an expert technical workshop to consider the issues and problems of simulating air pollutant dispersion in complex terrain (Hovind et al. 1979). The objective of the workshop was to recommend the design of a research program to support the development of improved complex terrain models. The consensus of the workshop was that the EPA should conduct field tracer experiments to provide data for model development and testing. The participants recommended starting with controlled field experiments on relatively isolated terrain features with simple geometric shapes and then proceeding to a large-scale experiment in the vicinity of an operating power plant.

Following the workshop recommendations, the EPA developed a conceptual design for a multi-year integrated program with emphasis on the "production of a useful model (or models) with demonstrated reliability and prescribed applicability" (Holzworth 1980). During the field measurements and laboratory experiments, the observational needs of the modelers were to be foremost in importance. The program was perceived as "an integrated and highly coordinated effort that involves:

1) model development/evaluation/improvement,
2) scaled physical modeling in a fluid modeling laboratory,
3) field measurements/experiments centered on isolated simple terrain features, and
4) field measurements/experiments centered on a full-scale plant....in terrain with opportunities for plume impaction and other types of plume-terrain interactions" (Holzworth 1980).

The CTMD program was subsequently begun in June 1980. Its primary goal is to develop reliable, practical models to calculate 1-hour average ground-level concentrations during stable atmospheric conditions in complex terrain settings. The models will be developed, refined, and evaluated

using field measurement data, physical modeling results, and recent theoretical work.

The first major field program was conducted during the fall of 1980 at Cinder Cone Butte (CCB)*, a roughly axisymmetric, isolated 100-m tall hill in the broad Snake River Basin near Boise, Idaho. The field program consisted of a preliminary learning phase followed by an intensive measurement phase. The data base compiled at CCB includes the following components:

- Source information: emission rates, locations and heights of SF_6, CF_3Br, and oil-fog releases.
- Meteorological data: measurements of the mesoscale valley flow in the vicinity of CCB as well as information on flow and dispersion on and over CCB itself.
- Tracer gas concentrations on the hill surface: data from more than 14,000 individual bag samples collected over the 18 days of experiments from as many as 80 sampler locations in a given experiment.
- Lidar data: sections across the plume characterizing the plume trajectory and plume spread upwind of CCB.
- Photographic data: still photographs taken from fixed locations on and around CCB, aerial photographs taken from an aircraft flying overhead, and (occasional) 16 mm movies and videotapes.

The CCB data were used to develop and evaluate two new, preliminary modeling algorithms (called the Impingement and Neutral models) and to evaluate the performance of current EPA complex terrain plume dispersion models (Valley, COMPLEX I, COMPLEX II, and PFM). The Impingement model simulates dispersion during strongly stable flows in which plumes remain approximately horizontal and impinge on and travel around the sides of CCB. The Neutral model simulates dispersion during slightly stable and neutral flows in which plumes rise over CCB. For the model evaluations, 45 hours were selected from the 18 field experiment days. The meteorological and tracer data were used in a "hands-off" mode: no modifications were made to the models to improve their predictions.

---

*The prime contractor for the CTMD is Environmental Research and Technology, Inc. (ERT). Its principal subcontractors for the CCB experiments were Western Scientific Services, Inc. (WSSI), responsible for fixed meteorological data (towers, instrumentation and data communication) and North American Weather Consultants (NAWC), responsible for the experimental field program (tracer and smoke releases, tracer data collection, photography, mobile meteorology, and field logistics). In allied activities, the EPA Fluid Modeling Facility (FMF) has provided laboratory fluid modeling support; the NOAA Wave Propagation Laboratory (WPL) has supported the field program with a manned lidar system; and TRC Environmental Consultants, Inc. has provided independent data audits.

The CTMD first milestone report (Lavery et al. 1981) describes the air quality models that were evaluated, the evaluation methods, and overall model performance. The report also provides comparative statistics of the model evaluations. The CCB field experiments and associated quality assurance activities are also described.

This second milestone report documents work accomplished from fall 1981 through April 1982 to improve the Impingement and Neutral modeling approaches, to refine the meteorological and tracer gas data bases, and further analyze the data to relate plume behavior and observed meteorological conditions. Unlike the hands-off evaluations described in the first milestone report, the approach taken in this report is a case study analysis. From the 45 hours used in the first report, 14 hours were selected for detailed individual case study to illustrate and contrast various flow situations and ranges of model performance.

The meteorological data, lidar data, and plume photographs were analyzed in detail to describe the evolution of the observed hourly average SF_6 concentrations. Each hour was modeled with both the earlier and the current versions of either the Impingement or the Neutral model. The results are encouraging: the modified models tend to give more realistic simulations and less scatter between model estimates and observations. It must be emphasized, however, that although the models show progress, much more can be done with the CCB data to further improve the models.

The model nomenclature used in this report will retain the "Neutral" and "Impingement" labels for the two algorithms discussed in the first CTMD milestone report. However, names more reflective of the central plume path assumptions of each of these models will be used to refer to the latest versions of these algorithms. The modified Neutral model will be called the Lift model because its formulation is applicable to plumes that pass freely over the top of a hill. The modified Impingement model will be called the Wrap model because its formulation is applicable to plumes which impinge on and wrap around a hill. This terminology will hopefully avoid potential misunderstandings about when these models should be applied. For example, in one particular stable flow, a plume released at one height may lift freely over the top of a hill, but one released closer to the surface might run into the hill and wrap around the sides. Consequently, some plumes in decidedly non-neutral flows may still lift over terrain, as in the Neutral (or Lift) model, and the application of neutral flow modeling techniques is appropriate.

In January 1982, EPA exercised Option 1 of the CTMD program. The work under this option includes continuing model development and evaluations with the CCB data and performing a second small hill impaction study at the Hogback* (a long, roughly 100 m tall ridge near Farmington, New Mexico). The information collected at the Hogback will enlarge the modeling data base to include measurements of flows and tracer gas concentrations in the vicinity of a long ridge. It is expected that these new data will provide a good basis for testing and extending the dividing streamline concept for two-dimensional ridges.

This report consists of five major sections. Section 2 discusses the modeling concepts and physical principles that form the basis for the CTMD program. Section 3 provides details on the Impingement, Wrap, Neutral and Lift models and how they are applied to the CCB data base. The case study analyses are given in Section 4. The refined meteorological and tracer gas data bases are discussed in Section 5. Section 6 presents the summary and conclusions, and gives recommendations for further work, including the second small hill study.

*ERT is continuing to provide overall project management and is conducting the modeling and analysis tasks. Through an Interagency Agreement with EPA, NOAA Air Resources Laboratory Field Research Office (ARLFRO) will conduct the flow visualization and tracer experiments during the next field program. NOAA WPL will provide lidar and other remote meteorological measurements.

SECTION 2

MODELING CONCEPTS

This section reviews the physical processes that govern the dispersion of pollutants around obstacles placed in stable flows. The primary emphasis is on the results obtained from simple models of dispersion and flow around hills. This section provides the basis for the models applied to the CCB data base and described in Section 3.

2.1 The Froude Number and Dividing Streamline Height

Although the complete physics of dispersion around obstacles in stably stratified flows is complicated and only partially understood, for an ideal flow with a constant velocity U_o and Brunt-Vaisala frequency N approaching a hill of height H, the essential flow properties are described by the hill Froude number, Fr_H

$$Fr_H \equiv U_o/NH \tag{1}$$

The hill Froude number is the square root of the ratio of the kinetic energy of the approaching fluid to the potential energy it acquires in surmounting the hill.

Experiments and theory (Sheppard 1956, Drazin 1961, Hunt and Snyder 1980, Snyder, Britter and Hunt 1980, Rowe et al. 1981) indicate that the Froude number describes two distinct regimes of flow around the hill (Figure 1). In region 1, which extends from the base of the hill to a height $H(1 - Fr_H)$, the flow does not have enough kinetic energy to go over the hill and remains roughly horizontal as it goes around the hill. (On the downwind side, this flow separates into a recirculating wake.) In region 2, which lies above the dividing streamline that separates the two regions, the flow has enough energy to pass up and over the hill. The concept of the critical dividing streamline height $H_c \equiv H(1 - Fr_H)$ is related to the notion that a fluid parcel can rise only through a height U_o/N.

If the wind speed and stratification are functions of height (as is generally the case), H_c is defined as follows

$$\frac{1}{2} U_o^2(H_c) = \int_{H_c}^{H} N^2(z)(H - z)dz \tag{2}$$

8205078

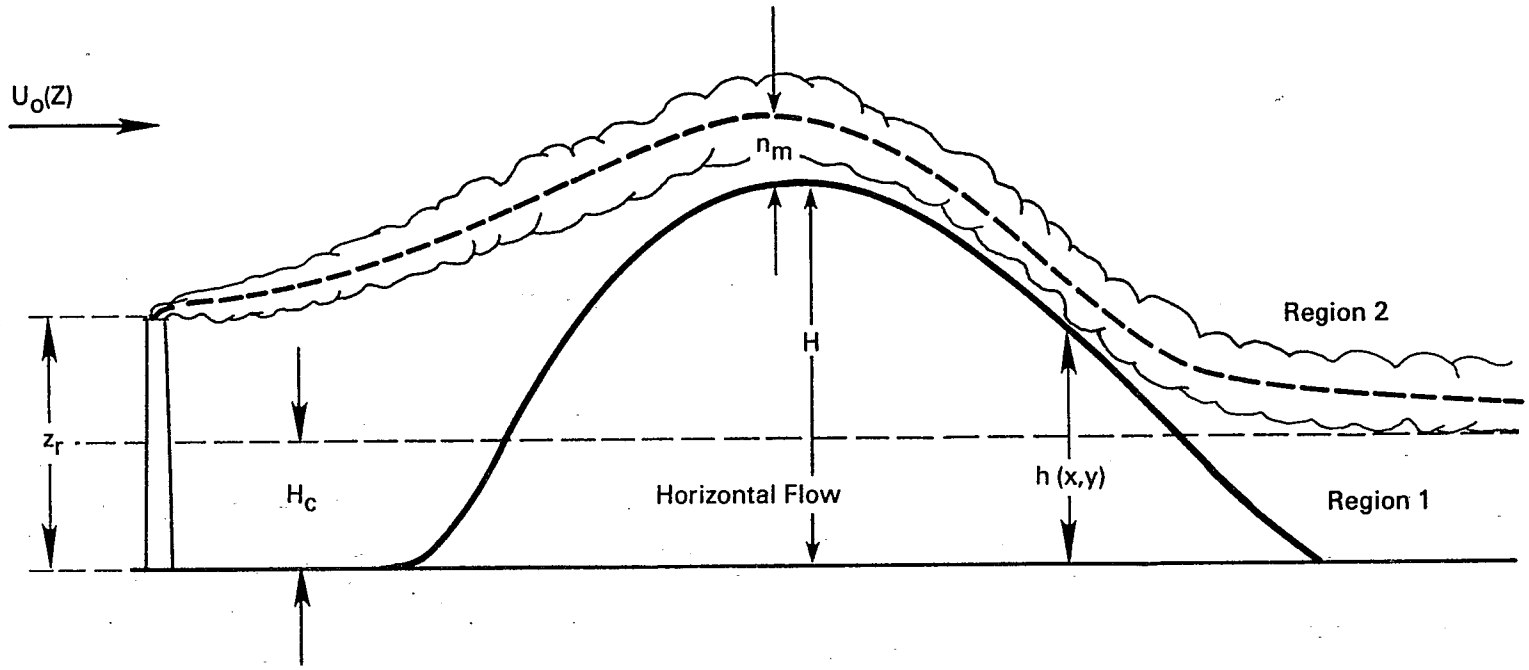

Figure 1. Schematic diagram of plume behavior in stable flows around obstacles.

where $U_o(H_c)$ is the wind speed at $z = H_c$ and $N(z)$ is the local Brunt-Vaisala frequency defined by

$$N(z) = [g/\Theta(z)\ (\partial\Theta/\partial z)]^{1/2} \tag{3}$$

where g is the acceleration due to gravity, and Θ is the potential temperature (°K). The left-hand side of the Equation 2 is the kinetic energy of the fluid at $z = H_c$, and the right-hand side is the potential energy gained by the fluid in rising through the height $H - H_c$.

Note that H_c, as defined, depends only on the height of the hill; it does not account for the shape of the hill as "seen" by the flow. We do not expect a sharp boundary between regions 1 and 2; nevertheless, the concept of a well-defined H_c is useful in studying stable flows over hills.

2.2 Flow in Region 1 (Strongly Stratified Flow)

Although the flow in region 1 is largely horizontal (i.e., two-dimensional in the horizontal plane), the variation of the radius of an idealized hill a(z) (see Figure 2) with height and the vertical velocity gradient give rise to pressure fluctuations that cause small deflections of the streamlines. Drazin (1961) showed that the relationship between the pressure fluctuation $p'(x,y,z)$ and the deflection $\eta(x,y,z)$ of the streamline at z is

$$\frac{\partial p'}{\partial z} = - g\frac{d\rho}{dz}\,\eta \tag{4}$$

and p' (calculated from two-dimensional potential theory) can be expressed in the form

$$p'(r,\theta,z) = \frac{1}{2}\,\rho\ U_o^2\ f(r/a(z),\theta) \tag{5a}$$

where

$$f(r/a,\theta) = [1 - U^2(r/a,\theta)/U_o^{\ 2}] \tag{5b}$$

and (r,θ,z) are the cylindrical coordinates. When the approach flow U_o is uniform with height, Equations 4 and 5 indicate that the streamline deflection η is positive upwind of stagnation points of the hill and zero at the stagnation points. The streamlines are deflected downwards as the flow passes around the sides of the hill and then recover to their initial heights in the downwind region (Hunt and Snyder 1980). However, when U_o varies with height, the pattern of streamline deflections may change. Expressions for the deflections caused by da/dz and dU_o/dz can be obtained by combining Equations 4 and 5

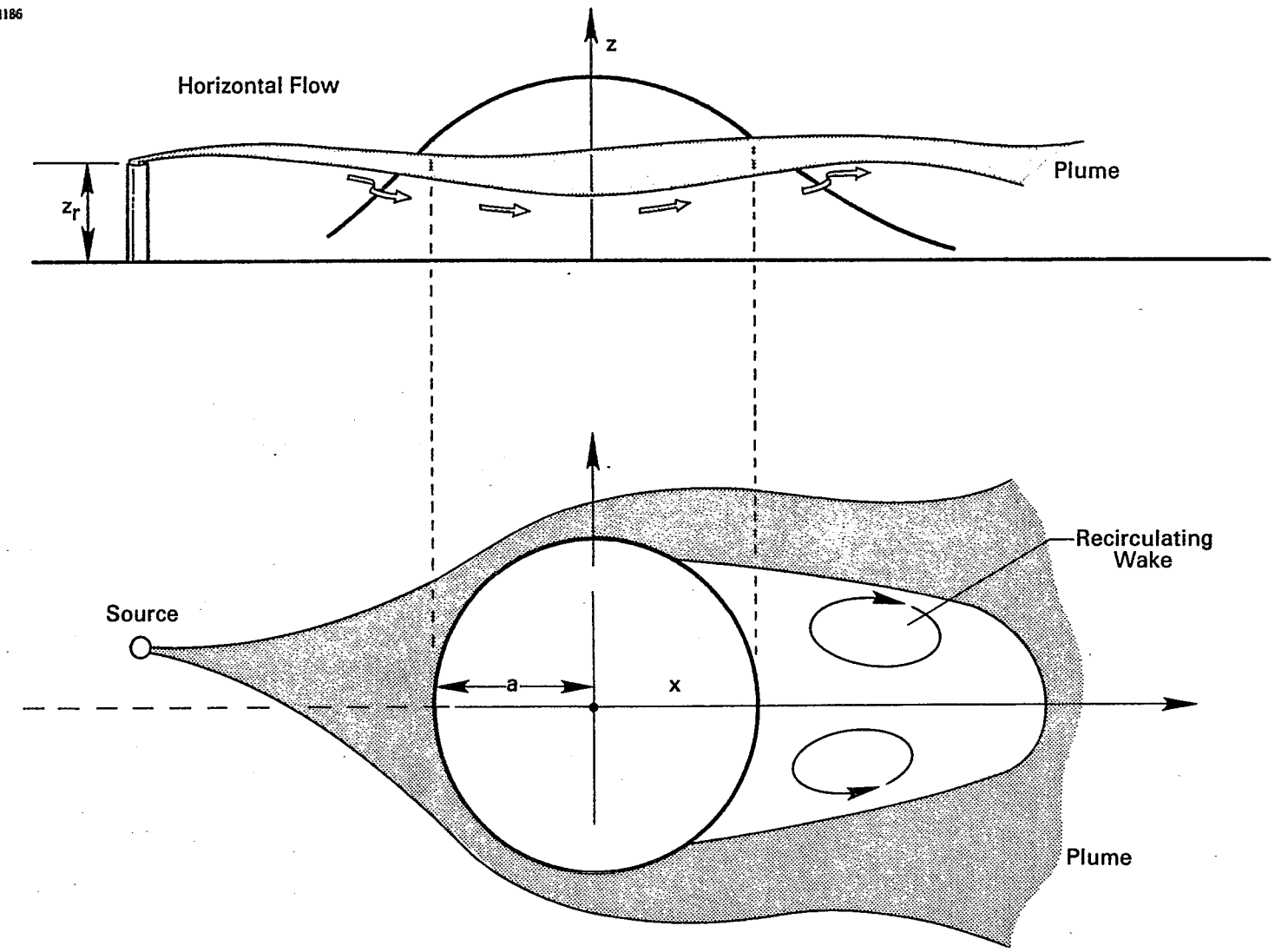

Figure 2. Schematic of flow around a three-dimensional obstacle at very low Froude number.. Adapted from Hunt et al. (1979)

$$\eta^a = \frac{-\rho U_o^2 f'(r/a,\theta)(-r/a^2)(da/dz)}{2g\frac{d\rho}{dz}} * \tag{6a}$$

$$\eta^u = \frac{-\rho U_o (dU_o/dz) f(r/a,\theta)}{g\frac{d\rho}{dz}} * \tag{6b}$$

Because $d\rho/dz < 0$, then $\eta^a > 0$ when $f' > 0$ in front of the hill. Therefore, the streamlines are deflected upward. On the sides of the hill, $f' < 0$ because the velocity decreases along r for a fixed θ. Then Equation 6a shows that the streamlines are deflected downward as they pass around the sides of the hill.

We see from Equation 6b that if the approach flow has a positive velocity gradient ($dU_o/dz > 0$), the deflection η^u associated with it depends on the sign of f. In front of the hill, along the stagnation streamline, $f > 0$ and η^u is negative--the streamlines are depressed downward. On the sides of the hill, $\eta^u > 0$. Even moderate values of (dU_o/dz) can make η^u large. Before Equation 6b can be used to show this, we must point out that the theory used to formulate Equation 6b is valid only if vertical streamline deflections are much smaller than the vertical scale over which a(z) changes

$$\eta << a/\frac{da}{dz} \tag{7}$$

If we put $H = a/(da/dz)$, Equation 7 implies that η should be much smaller than the height of the hill. Keeping this in mind, we will calculate η^u for typical values of the variables in Equation 6b. Near the stagnation point where $U(r/a,\theta) \sim 0$ Equation 6b becomes

$$\eta^u \sim -U_o \frac{dU_o}{dz}/N^2 \tag{8}$$

Because $f \sim 1$ near the stagnation point, η^u has its maximum value here. Let $U_o = 2\ ms^{-1}$ at $z = 10$ m. Then, taking $N \simeq 0.10\ s^{-1}$ (close to the ground) we find that

$$\eta^u \sim 40\ m \tag{9}$$

This calculation is valid only if $H >> 40$ m. However, it does suggest that vertical shear might lead to significant downward deflection of the streamlines even when $\eta \sim H$.

---

*The superscripts indicate the streamline deflection caused by the change in hill radius (a) or wind speed (U_o) with height.

To estimate the maximum size of η^a, Equation 6a is approximated near the stagnation point where $f' \sim 1$ and $r/a \sim 1$. Then, for $H \sim a/(da/dz)$,

$$\left|\eta^a\right| \sim \frac{U_o^2}{N^2 H^2} H = Fr_H^2 H \tag{10}$$

If Fr_H is much less than 1, η^a will be much smaller than H.

Fluid modeling studies performed by Snyder et al. and reported in Appendix A provide experimental data on the relative effect of shear, stratification, and hill slope on vertical streamline deflections upwind of stagnation points. For hills with a large slope, da/dz is small, and the η^u deflection might be expected to overcome the η^a deflection. This tendency appears to be substantiated in the laboratory studies. In fact, streamline height changes are great enough to produce overturning in the fluid, as evidenced by observed vortex formation. For hills of lower slope (CCB for example), da/dz is greater, and no shear-induced vortex formation was observed in the laboratory studies.

2.3 Dispersion in Region 1 (Strongly Stratified Flow)

We have seen that shear and the vertical variation of the radius of the hill can induce vertical deflections of the streamlines. Plumes embedded in such a flow will follow these deflected streamlines, and dispersion calculations will have to account for this phenomenon. Presently available dispersion models do not do so.

When both η^a and η^u can be neglected so that the flow can be considered essentially horizontal, the problem of plume dispersion can be reduced to that of two-dimensional diffusion of a line source around a cylinder (Hunt et al. 1979). Figure 2 shows plume behavior under such conditions. The axis of the relevant cylinder is parallel to the z-axis, and the cylinder has the cross section of the hill at release height z_r.

When the plume is directed along the stagnation streamline corresponding to the cylinder, it will "impinge" on the hill and cause large concentrations. To calculate the concentration at the stagnation (impingement) point, it is necessary to account for the divergence of the flow as it approaches the hill.

Hunt et al. (1979) show that the increase in σ_y caused by the diverging streamlines is almost compensated for by the decrease in U as the stagnation point is approached, and that at the stagnation point (where U goes to zero), $\sigma_y U$ is approximately the same as it would have been in the absence of the hill. Because $\sigma_z \sim \sigma_w \int ds/U(s)$, where s is the distance along the stagnation streamline, σ_z becomes infinite (in

theory) at the stagnation point. However, Hunt et al. (1979) show that the explosive growth of σ_z actually begins very close to the stagnation point. If the source is far enough from the hill,

$$\sigma_z (d - \varepsilon) \simeq \sigma_{zf} [1 + \frac{a}{d}] \tag{11}$$

where d is the distance from the source to the stagnation point, ε is a small distance away from the stagnation point, and σ_{zf} is the vertical spread without the hill. If $d > 3a$, σ_z is not very different from σ_{zf}.

These arguments suggest that the concentration at the stagnation point is approximately equal to that without the hill. Hunt et al. (1979) describe experiments supporting this important result. Therefore in steady flows, we can estimate the impingement concentration without explicitly accounting for the presence of the hill. However, in unsteady flows the hill may increase the large scale meander of the winds at the source. Because most flows are likely to be unsteady, this effect must be incorporated in the dispersion model.

The calculation of impingement concentrations is also complicated by our relative lack of understanding of vertical dispersion of elevated releases in the stable boundary layer. Progress in this area (see Hunt 1981) will be necessary for the development of realistic dispersion models.

2.4 Flow in Region 2 (Weakly Stratified Flow)

In region 2, the flow may go over the hill. The hill Froude number defined with respect to the height of the hill above H_c is unity or greater. Experiments and theory (Britter et al. 1981) show that with the exception of a thin layer close to the surface of the hill, the velocity perturbations induced by the hill can be calculated as if the flow were inviscid.

2.4.1 Flow in the Inner Region

Close to the hill surface (see Figure 3), the gradient of the perturbation shear stress is balanced by the perturbation inertia force. Therefore

$$\frac{U_o(\delta)}{2} \frac{\Delta u}{L} \sim \frac{k u_* \Delta u}{\delta} \tag{12}$$

8205079

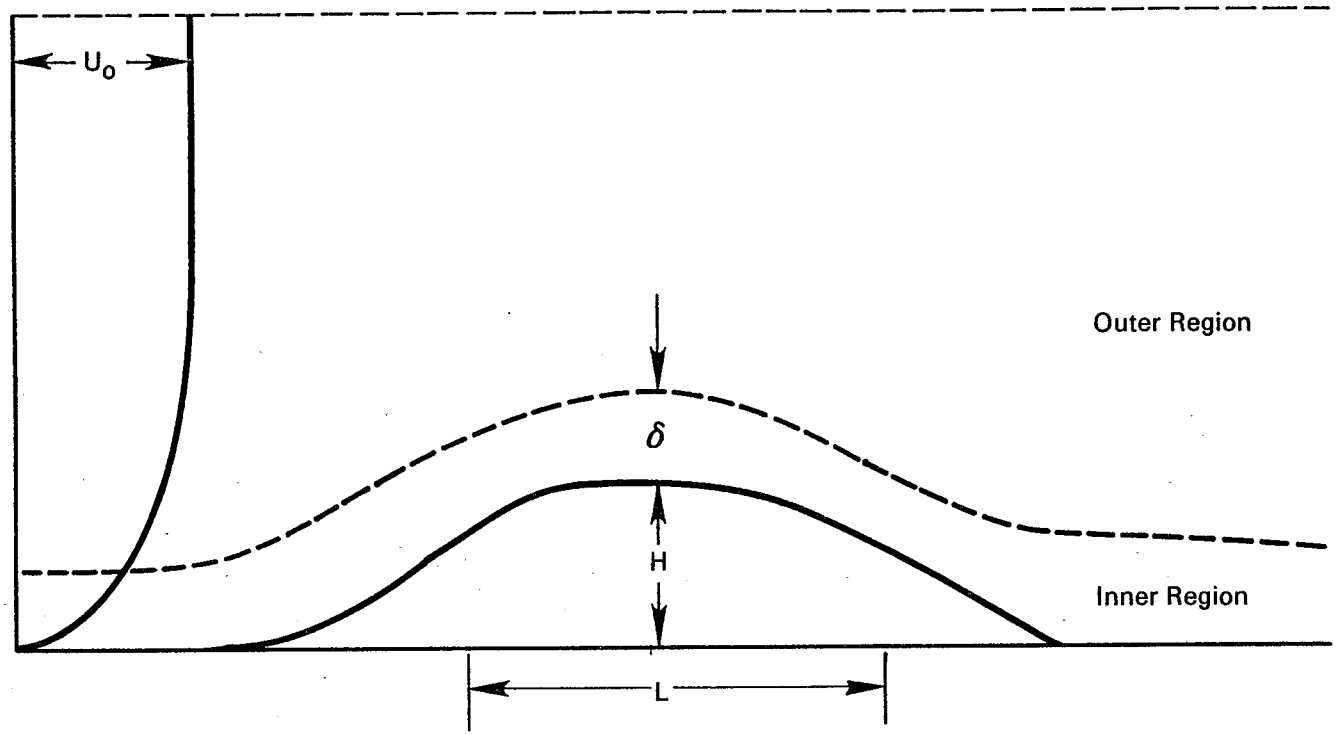

Figure 3. Definition of notation for describing flow in region 2.

where δ is the thickness of the layer, k is the von Karman constant, Δu is the velocity perturbation, L is the half-length of the hill, and u_* is the surface friction velocity. The velocity $U_o(z)$ in the inner region is assumed to be given by the stable similarity profile (Businger 1973)

$$U_o(z) = \frac{u_*}{k}\left[\ln\left(\frac{z}{zo}\right) + \frac{\beta z}{L_m}\right] \tag{13}$$

In Equation 13, L_m is the local Monin-Obuhkov length, z_o is the roughness height and the constant $\beta = 4.7$. Substituting Equation 13 into Equation 12, leads to

$$\delta \simeq 2k^2 L\left[\ln(\delta/z_o) + \frac{\beta\delta}{L_m}\right]^{-1} \tag{14}$$

The velocity perturbation Δu reaches a maximum at $z = \delta$. For low hills, Jackson and Hunt (1975) show that

$$\Delta u(z=\delta) = \frac{U_o(L)H}{L} \tag{15}$$

where for stable flows, $U_o(L)$ is given by Equation 13.

The increase in velocity over the hill is accompanied by a depression of streamlines over the surface. If δ is the initial streamline height upwind of the hill, its height n_m over the crest of a two-dimensional hill is found by conserving mass in the surface layer

$$\frac{n_m}{\delta} = \frac{U_o(\delta)}{U_o(\delta) + \Delta u} \simeq 1 - \frac{\Delta u}{U_o(\delta)} \tag{16}$$

Using Equation 13 and taking $L_m \simeq \beta u_*/N$ (Hunt et al. 1982), Equation 16 becomes (approximately)

$$\frac{n_m}{\delta} = 1 - \frac{2H}{L}\left[1 + \frac{LN}{u_* \ln(L/z_o)}\right] \tag{17}$$

where it is assumed that $\ln(L/z_o)/\ln(\delta/z_o) \simeq 2$. It is seen from Equation 17 that an increase in stability (larger N) leads to a decrease in n_m. This decrease would bring plume material closer to the surface. But the same convergence of streamlines which brings the plume closer will distort the vertical plume spread as well; therefore, it would seem that the ground-level concentration on the hill would remain the same as that without the hill if diffusion were ignored. However, turbulence levels σ_w and σ_v are increased in this inner layer. This effect, together with the larger vertical concentration gradients caused by streamline convergence,

might counteract the effect of streamline convergence, and the net result might be an increase in concentration over the hill. These processes will have to be considered in future model development.

2.4.2 Flow in the Outer Region

When $(H-H_c)/L$ is small, the velocity perturbations in the outer region can be obtained from the linearized inviscid momentum equations. The vertical velocity perturbation Δw satisfies the equation (Scorer 1949)

$$\left(\frac{\partial^2}{\partial x^2} + \frac{\partial^2}{\partial y^2} + \frac{\partial^2}{\partial z^2} + S\right) \Delta w = 0 \tag{18}$$

where S is the "Scorer parameter" defined by

$$S \equiv N^2/U_o^2 - (d^2U_o/dz^2)/U_o \tag{19}$$

When N and U_o are arbitrary functions of z, numerical methods can be used to solve Equation 18. A simple analytic solution is possible when $N^2/U_o^2 << (d^2U_o/dz^2)/U_o$ (Hunt and Richards 1982).

To illustrate the main effects of stratification on the flow, we will consider the case when $S = N^2/U_o^2$ = constant. Then Equation 18 can be rewritten as (Smith 1980)

$$\frac{\partial^2}{\partial x^2} (\nabla^2\eta) + \frac{N^2}{U_o^2} \nabla_H\eta = 0 \tag{20}$$

where η, the vertical displacement of the streamlines, is related to Δw through the equation

$$\Delta w = U_o\eta_x \tag{21}$$

With the linearized boundary condition $\eta(x,y,z = 0) = h(x,y)-H_c$, Equation 20 can be solved for the velocity perturbations using Fourier transform techniques. Details of the solution can be found in Smith (1980). For our purposes, it is sufficient to focus on the expression for η close to the hill's surface and we will assume $H_c = 0$. Close to the surface, the deflection is approximated by a truncated Taylor series expansion

$$\eta(x,y,z) \simeq h(x,y) + \eta_z.z \tag{22}$$

Smith (1980) shows that for a bell-shaped hill described by $h(x,y) = H/(r^2/L^2 + 1)^{3/2}$, η_z becomes

$$\eta_z(x,y,0) = \frac{HN}{U_o}\left(\frac{-L^2}{y^2+L^2}\right)\left[1 + \frac{x(L^2-y^2}{(y^2+L^2)(r^2+L^2)^{1/2}} - \frac{2y^2}{(y^2+L^2)} + \frac{xL^2}{(r^2+L^2)^{3/2}}\right] \tag{23}$$

This solution is valid only if the hill Froude number ($Fr_H = U_o/NH$) is greater than one and if the Froude number based on the length of the hill ($Fr_L = U_o/NL$) is less than one. The height of a streamline above the hill's surface is

$$n_m/z_r = 1 + \eta_z \tag{24}$$

where z_r is the upwind source height. Because $\eta_z < 0$, n_m is always less than z_r. At the crest of the hill x=y=0, and

$$\frac{n_m}{z_r} = 1 - \frac{HN}{U_o} \tag{25}$$

However, the minimum n_m occurs in the lee of the hill at x = 1.4. At this distance,

$$\frac{n_m}{z_r} \simeq 1 - \frac{2HN}{U_o} \tag{26}$$

In contrast to potential flow, the streamline pattern for stable flow in region 2 is not symmetric. The streamline (and hence a plume) can come very close to the surface on the leeward side of the hill. Although this streamline depression is accompanied by streamtube contraction (σ_z decreases), ground-level concentrations may be greater than in the absence of the hill. However, the magnitude of this concentration increase is uncertain. Further work is required before we can develop a formulation for reliably estimating the effects of stratification.

Hunt and Richards (1982) show that the velocity and streamline perturbations can be calculated for arbitrarily shaped hills $h \equiv Hf(x,y)$ in the limits of weak stratification ($Fr_L >> 1$) and strong stratification ($Fr_L << 1$). As an example of the type of expressions they derive, we write n_m for $F_L << 1$

$$\frac{n_m}{z_r} = 1 - \frac{NH}{U_o}\frac{1}{2\pi}\iint_{hill}\frac{f(x',y')\quad(x-x')dx'dy'}{[(x-x')^2 + (y-y')^2]^{3/2}} \tag{27}$$

Note that n_m "follows" the contour of the hill, hence the dipping of the streamline in the lee of the hill. The calculation of Δu, Δv, and Δw involves a straightforward numerical integration over the hill's contour.

2.5 Summary

This section summarizes the concepts that will form the basis of the modeling approach described in Section 3.

(1) Stable flow around an obstacle can be divided into two regions. In region 1, below H_c, the flow can be considered to be essentially horizontal. In region 2, above H_c, the flow goes over the hill. Streamline behavior in region 2 may be modeled by assuming that the surface at H_c constitutes the lower horizontal boundary.

(2) In region 1 (horizontal flow), the plume will impinge directly on the hill when the mean wind is along the stagnation streamline. Theory and laboratory experiments indicate that the concentration at the impingement point is approximately equal to that in the absence of the hill providing that dispersion rates are equivalent.

(3) In region 2, the streamlines approach the hill's surface at heights that are less than their initial heights upwind. This streamline depression is accompanied by streamtube contraction. A plume embedded in this flow would be lowered towards the hill's surface. At the same time, σ_z decreases because of streamtube contraction (streamline convergence). Hence, the ratio of the change of the plume centerline height to the change in σ_z may vary much less than σ_z or n_m individually.

Some of the physical processes not considered in the present models and which will be explored in future modeling efforts are:

(1) Vertical streamline deflection in region 1 caused by wind shear and hill slope.

(2) The interaction between streamline depression, streamline convergence, and turbulence for plume dispersion in region 2.

SECTION 3
MODELING OF CCB

3.1 Model Description

A complicated plume dispersion problem such as that presented by CCB involves many physical processes. To understand the system, it is necessary to identify the essential variables that may control its behavior. One way of doing this is to construct a simple model with empirical parameterization of important effects. Testing this type of model against observations can lead to an understanding of the controlling physical variables. This approach to modeling, adopted to guide new model development, relies heavily on the analysis of concentration observations.

Two preliminary models were described in the first milestone report (Lavery et al. 1981). The Impingement model corresponds to low Froude-number flows (region 1) in which the plume remains horizontal as it impinges on and flows around the hill. The Neutral model corresponds to moderate or large Froude-number flows (region 2) in which the plume goes over the top of the hill. A number of refinements have been made to these two models. For background, the older versions (described in the first milestone report) are reviewed first, and then the newer versions, Wrap and Lift, are described.

3.1.1 The Impingement Model

The Impingement model is applicable to the region below H_c in which the flow is mostly horizontal. Observations indicate considerable meander of the horizontal wind during a typical hour. To model plume behavior in such unsteady conditions, we assume that the hour can be divided into several quasi-steady periods. We also assume that the average angular spread of the plume, α_s, corresponding to these periods is small compared to the total meander during the hour, α_m.

Concentrations are assumed to occur on the hill's surface only when a portion of the plume is directed along the stagnation streamline. Therefore, the maximum concentration occurs at the stagnation point.

During any single quasi-steady period, the concentration at the stagnation point A (see Figure 4) will be non-zero only if the mean wind direction during the period lies within $\alpha_{si}/2$ of the stagnation streamline ($\theta = \theta_d \pm \alpha_{si}/2$). If this concentration is denoted by $C_i(\theta,\theta_d)$, then the average concentration at A, C_{max}, over an hour is given by

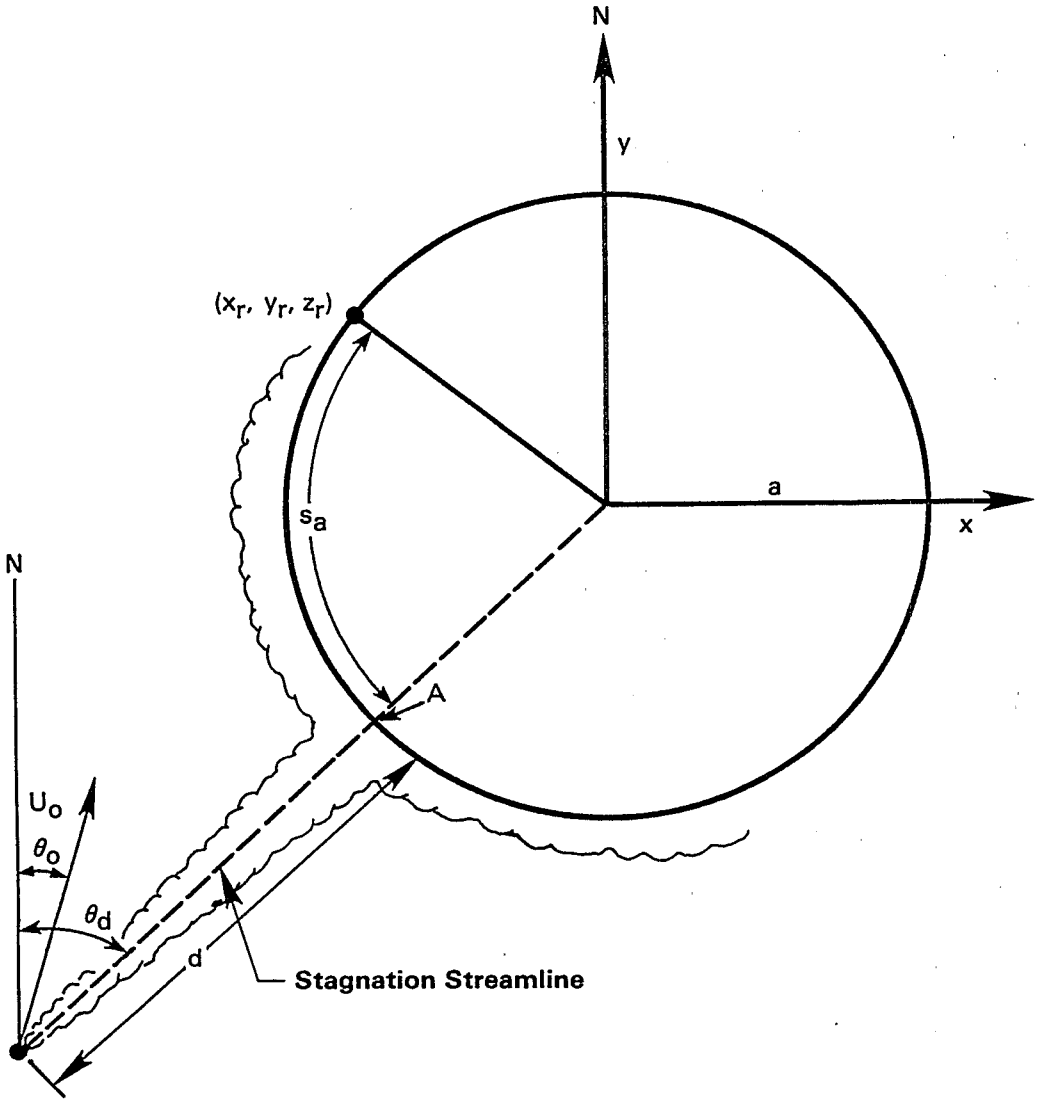

Figure 4. Plume dispersion in the region of horizontal flow.

8205077

$$C_{max} = \int_{\theta} C_i(\theta, \theta_d)\ P(\theta)\ d\theta \tag{28}$$

were $P(\theta)$ is the hourly probability density function of wind directions. If the wind speed, vertical plume spread, and horizontal plume spread angle are nearly constant among quasi-steady periods during the hour, then the only non-zero contributions to the integral in Equation 28 arise for wind directions within $\pm\ \alpha_s/2$ of the stagnation wind direction. Furthermore, if the concentration distribution within the plume during each quasi-steady period is assumed to be uniform, and if the spread due to plume meander during the hour is much greater than α_s, so that $P(\theta_d)$ is nearly constant within the interval α_s, then

$$C_{max} \simeq \overline{C}_i \int_{\theta_d-\alpha_s/2}^{\theta_d+\alpha_s/2} P(\theta)d\theta \simeq \overline{C}\ P(\theta_d)\ \alpha_s \tag{29a}$$

where

$$\overline{C}_i = \frac{Q}{\sqrt{2\pi}\sigma_z U_o \alpha_s d} \tag{29b}$$

In Equation 29b, σ_z, U_o, and α_s represent averages for the relevant hour. If we assume that $P(\theta)$ is Gaussian, Equation 29a becomes

$$C_{max} = \frac{Q}{2\pi\sigma_z U_o \sigma_\theta d} \exp\left[-\frac{(\theta_o - \theta_d)^2}{2\sigma_\theta^2}\right] \tag{30}$$

where σ_θ is the standard deviation of wind direction about the mean direction θ_o during the hour. The first milestone report presents concentration estimates obtained from Equation 30.

3.1.2 The Neutral Model

Figure 5 is a schematic of a plume embedded in region 2. For convenience, an axisymmetric flow is considered. The lower figure shows, in cross section, the plume heading toward the hill. As the plume goes over the hill, it is distorted vertically and horizontally, and the height of the plume centerline above the hill surface varies with the distance along the plume. These effects must be parameterized in a dispersion model.

The following formulation for the concentration on the hill surface is based on the model of Egan (1975)

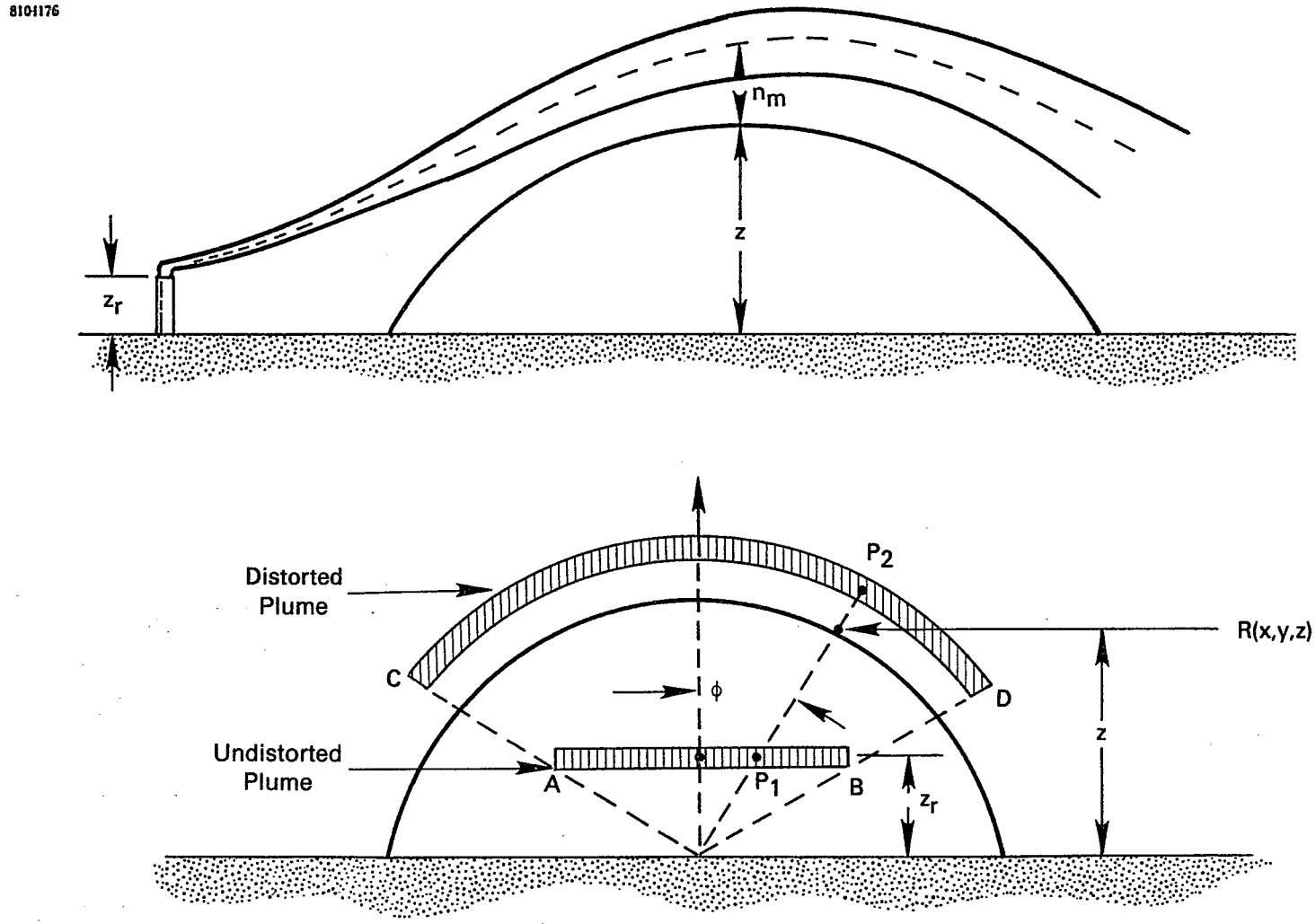

Figure 5. Geometry used in formulating the Neutral model for high Froude number flows.

$$C(x,y) = \frac{2Q}{(2\pi U_o \sigma_y \sigma_z)_f} \exp\left[- \frac{T_c^2 z_r^2}{2 \sigma_{zf}^2}\right] \exp\left[\frac{-(\beta y)^2}{2 \sigma_{yf}^2}\right] \tag{31}$$

where the subscript f denotes values in the absence of the hill. The terrain correction factor T_c accounts for the effects of streamline convergence, streamtube contraction and increased turbulence over the hill. For plumes released well below the height of an obstacle, empirical evidence indicates that T_c is $\simeq 1$ over the crest of nearly two-dimensional obstacles and T_c is no less than 1/2 over the crest of sharply three-dimensional obstacles. This result could be related to the relative height of the plume centerline above the hill. The plume height is smaller for flow over three-dimensional bodies than for that over two-dimensional shapes (Egan 1975). Until we understand more about dispersion over hills we suggest the following formulation for T_c in modeling Cinder Cone Butte

$$\begin{aligned} T_c &= 1 - z/2z_r; \; z \leq z_r \\ &= 1/2; \; z > z_r \end{aligned} \tag{32}$$

When the receptor is not located on elevated terrain, $z = 0$ and $T_c = 1.0$. T_c attains a minimum value of one half for all receptors above the release height.

To estimate the horizontal distortion factor β we use the observation that in axisymmetric flow, the angle ϕ (see Figure 5) remains a constant along a streamline. We next assume that horizontal plume distortion is uncoupled from turbulent plume spread and occurs after the plume has spread because of turbulence. In other words, the segment AB (in Figure 5), which would describe the plume spread at a downwind distance x from the source in the absence of the hill, becomes the plume segment CD at the same downwind distance in the presence of the hill. In effect, the point P_2 maps onto the point P_1 on the "flat terrain" plume. For a plume directed toward the center of the hill, simple geometry shows that $\beta = z_r/z$.*

3.1.3 Dispersion Parameters

Dispersion in stable flows is not fully understood, although some progress has been made in modeling the behavior of surface releases (Van Ulden 1978). The analysis of lidar data collected during the CCB experiment has not been completed by WPL. Because of this lack of complete theory and data, the suggested expressions for sigmas are tentative.

The horizontal meandering of the wind suggests that σ_y can be expressed as

*When the plume direction is not along the radius of the hill, the expression for β is slightly less straightforward, although the concept behind its derivation is still very simple.

$$\sigma_y = \sigma_\theta x \tag{33}$$

where σ_θ is measured at source height and x is the distance downwind. This equation has not yet been fully tested.

For elevated releases in the stable boundary layer, the vertical length scale of turbulence, ℓ_w, can be expressed as

$$\ell_w \sim \sigma_w/N \tag{34}$$

where σ_w is the standard deviation of vertical velocity fluctuations and N is the Brunt-Vaisala frequency. The Lagrangian integral time scale, t_ℓ, should be on the order of 1/N. A typical value of N measured at source height during the CCB experiment is 0.05 s^{-1}, which translates to a t_ℓ of about 20 s. With a typical wind speed $\sim$ 5 ms^{-1}, it is expected that σ_z will approach the large travel- time behavior beyond 200 m from the source. Because the source-to-receptor distance was usually more than 400 m, the following equation for σ_z is proposed

$$\sigma_z^2 = 2\,\frac{\sigma_w^2 x}{U_o N} \tag{35}$$

where all of the variables in Equation 35 refer to source height.

3.1.4 Impingement Model Refinements: The Wrap Model

This section describes the modifications made to the Impingement model to represent the physics of the flow better. This modified version will be referred to as the Wrap Model.

<u>Wind Direction Distribution Function $P(\theta)$</u>

Equation 29a indicates that C_{max} predicted by the Impingement model is sensitive to $P(\theta)$ and to the location of the stagnation point. Therefore, use of the "measured" $P(\theta)$ is an obvious improvement. The method used to calculate $P(\theta)$ can be understood by referring to Figure 6. Let T represent the time period over which we want to calculate $P(\theta)$. Because $P(\theta_m)\,\Delta\theta$ represents the fraction of time spent by the wind in $\Delta\theta$ centered upon θ_m, it follows that

$$P(\theta_m)\,\Delta\theta = (\Delta t_1 + \Delta t_2)/T \tag{36a}$$

or

$$P(\theta_m) = (\Delta t_1 + \Delta t_2)/T\Delta\theta \tag{36b}$$

Then the general expression for $P(\theta_m)$ can be written as

$$P(\theta_m)\Delta\theta = \frac{1}{T}\int_o^T \phi_m(t)\,dt \tag{37}$$

8205070

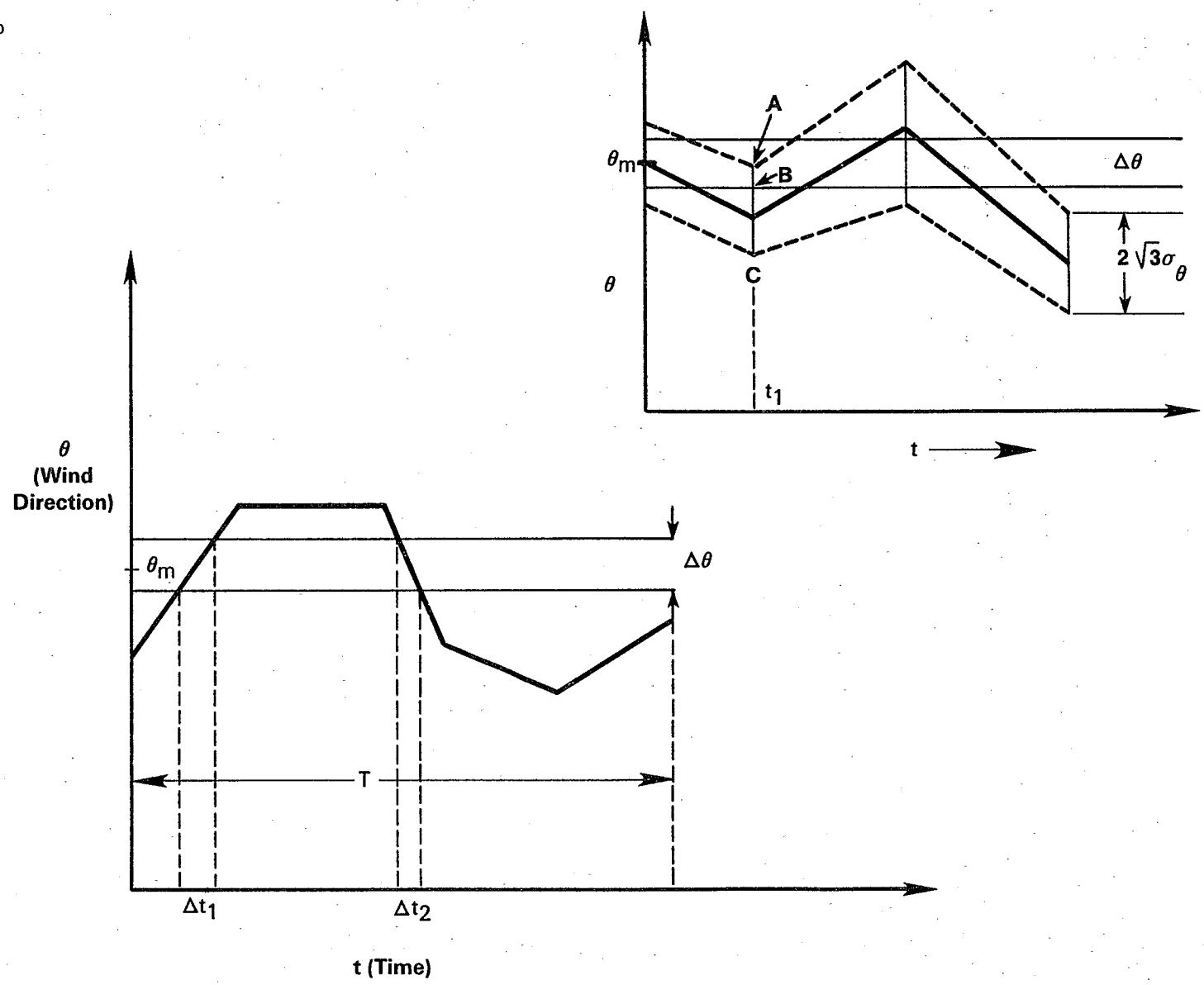

Figure 6. Schematic used to derive the probability density function for specified θ_m.

where the indicator function ϕ_m is defined by the equations

$$\phi_m(t) = 1;\ \theta_m - \frac{\Delta\theta}{2} < \theta < \theta_m + \frac{\Delta\theta}{2} \tag{38a}$$

$$= 0;\ \text{otherwise} \tag{38b}$$

For the CCB experiment we do not have a continuous record of $\theta(t)$ as a function of t; only 5-minute averages of θ and σ_θ are available. To use this information, we assume that θ is uniformly distributed in the interval $2\sqrt{3}\sigma_\theta$ about the 5-minute averaged value θ. We then use linear interpolation to estimate values of θ and σ_θ between measured values.

We see from Figure 6 that at a given time, t_1, the probability that the wind direction is within the interval $\Delta\theta$ about θ_m is AB/AC. Then the expression for $\phi_m(t)$ becomes

$$\phi_m(t) = \frac{\Delta I}{2\sqrt{3}\,\sigma_\theta(t)} \tag{39a}$$

where

$$\Delta I = (\theta_m - \frac{\Delta\theta}{2},\ \theta_m + \frac{\Delta\theta}{2})\ \Lambda\ (\bar{\theta} - \sqrt{3}\,\sigma_\theta,\ \bar{\theta} + \sqrt{3}\,\sigma_\theta) \tag{39b}$$

and Λ denotes intersection. Note that $\Delta I = 0$ when there is no intersection between the two intervals. Also, $\phi_m = 1$ if the interval $(\theta - \sqrt{3}\,\sigma_\theta,\ \theta + \sqrt{3}\,\sigma_\theta)$ is contained within $(\theta_m - \Delta\theta/2,\ \theta_m + \Delta\theta/2)$.

As noted before, C_{max} can be very sensitive to the location of the stagnation point, which we now assume corresponds to that of a circular cylinder "fitted" to the cross section of CCB at the height of release. This approximation can cause an uncertainty in the estimation of C_{max}. In applying the model to the CCB data, greater potential uncertainty in maximum estimated concentrations is expected when the mean wind is near the stagnation streamline, and $P(\theta)$ is sharply peaked. By aligning the peak in $P(\theta)$ with the stagnation streamline in two such cases (206, hours 6 and 8- see Section 4), C_{max} increases by 30 to 35%. In the future, we hope to make improvements by calculating the two-dimensional flow around a more appropriately shaped cylinder at the relevant height.

Modification to Compute Concentrations Over the Hill

The Impingement model provided estimates only of the maximum concentration at the stagnation point. This estimate was compared with the maximum observations anywhere on the hill. To make the model more general, we have made the following modification. From Figure 4, we see that the impinging plume is assumed to wrap around the hill. Therefore, the concentration at the receptor x_R, y_R at the height of release is

$$C(x_R, y_R, z_r) = \frac{Q\ P(\theta_d)}{\sqrt{2\pi} U_o \sigma_z} \cdot \frac{1}{d+s_a} \tag{40}$$

Note that s_a is the extra distance beyond the impingement point traveled by the plume to the receptor and that σ_z is evaluated at the downwind distance $d + s_a$. To estimate the concentration at a height z_R above or below the height of release z_r, we simply assume that

$$C(x_R, y_R, z_R) = C(x_R, y_R, z_r) \frac{1}{\sqrt{2\pi}\sigma_z} \exp\left[\frac{-\Delta Z^2}{2\sigma_z^2}\right] \tag{41}$$

where $\Delta Z = (z_R - z_r)$. Equation 41 cannot be valid for large ΔZ. However, there is little reason to improve Equation 40 because we are primarily interested in the maximum concentrations at release height. Furthermore, since σ_z is usually small under stable conditions, the concentration falls off rapidly in the z-direction.

3.1.5 Neutral Model Refinements: The Lift Model

This section describes the modifications made to the Neutral model to better represent the physics of the flow. This modified version will be referred to as the Lift model.

<u>H_c and the Effective Radius of Curvature</u>

On the basis of the discussion of Section 2, we now assume that only the flow above H_c goes over the hill. The surface at H_c constitutes the "base" of the "cut-off" hill. This suggests that all vertical distances be measured with respect to H_c.

Because the hill may have an aspect ratio greater than 1, it is necessary to define an effective radius of curvature R_e for the hill. This radius determines the horizontal plume distortion factor ß. We see from Figure 7 that R_e can be written as follows

$$R_e^2 = D^2 + a^2 = (H_* + D)^2 \tag{42a}$$

Then

$$D = (a^2 - H_*^2)/2H_* \tag{42b}$$

In Equation 42, a is the "radius" of the hill at $z = H_c$ and $H_* = H - H_c$. It is readily seen that for a plume heading toward the center of the hill

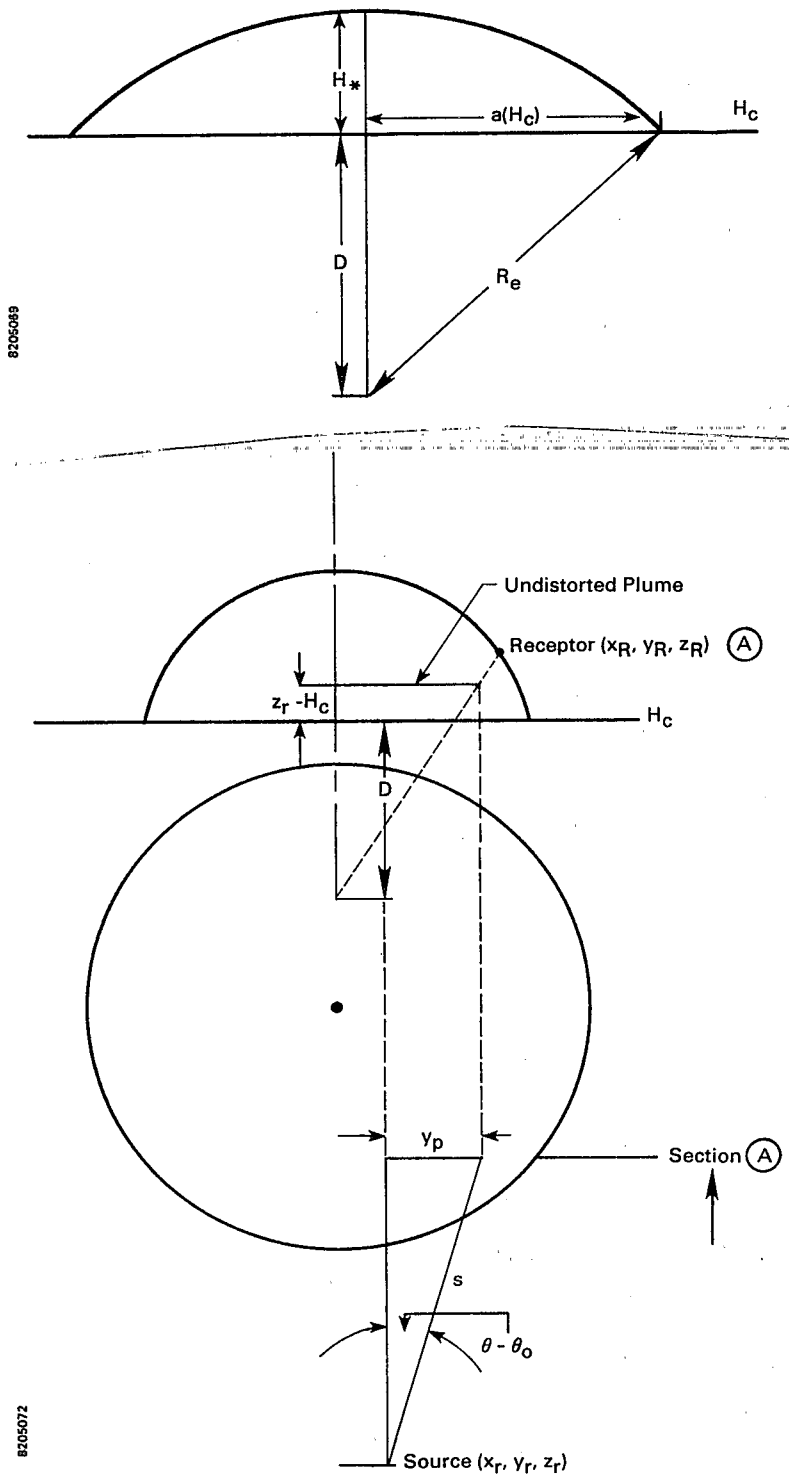

Figure 7. Geometry used to derive the effective radius of curvature R_e for the portion of the hill above H_c, and to incorporate the wind direction probability distribution function $P(\theta)$ in the Lift model.

$$\beta = (z_r - H_c + D)/(z - H_c + D). \tag{43}$$

Note that when $a = H_*$ (the cross-section is approximately a semi- circle), $D = 0$ and we recover the equation used previously for β. When $H_* << a$, the flow becomes essentially two-dimensional; the streamlines are approximately parallel as they pass over the hill. We expect little plume distortion for this type of flow. This behavior is embodied in β: when $H_* << a$, D is very large and β is close to unity, thus suggesting no horizontal plume distortion.

Terrain Correction Factor T_c

The terrain correction factor T_c is approximately one for flows over two-dimensional bodies; for flows over approximately symmetric three-dimensional obstacles, T_c is probably closer to 1/2. An examination of Figure 7 shows that $D/R_e \rightarrow 1.0$ when the hill becomes two-dimensional; $D/R_e = 0$ when the hill cross section becomes a semi-circle. These observations suggest a plausible formulation for T_c

$$T_c = \frac{D}{R_e} + \frac{1}{2}\left(1 - \frac{D}{R_e}\right) \tag{44}$$

While Equation 44 accounts for the type of flow over the hill, it does not include the relationship between the source and receptor heights. However, this is not likely to matter as long as the hill is higher than the source and as long as we are primarily interested in the maximum concentrations close to the top of the hill.

Wind Direction Distribution Function

The probability density function, $P(\theta)$, is incorporated into the neutral flow model by replacing the exponential term for the y-direction in Equation 31 as follows

$$\frac{1}{\sqrt{2\pi}\sigma_y} \exp\left[\frac{-\beta y^2}{2\sigma_y^2}\right] \overset{R}{=} \frac{P(\theta)}{s} \tag{45}$$

where $\overset{R}{=}$ denotes "replaced by." The angle θ is given by

$$\theta = \sin^{-1}(y_p/s) + \theta_o \tag{46}$$

where s is the approximate downwind distance along θ to the receptor. In Equation 46, y_p is the distance of the projection of the receptor $R(x_R, y_R, z_R)$ from the plume centerline. Figure 7 shows the relevant geometry used to derive Equation 46.

3.1.6 Dispersion Parameter Refinement

Equation 35 for σ_z overestimates σ_z when N becomes small. To avoid this problem, we have modified the formulation as follows:

$$\sigma_z = \sigma_w t/(1+ Nt/p)^{1/2} \tag{47a}$$

where $t = x/U_o$ and $p = 1.5$. (47b)

Equation 47 is consistent with the previous formulation for σ_z for $N \simeq 0.05\ s^{-1}$ and reflects the small time behavior $\sigma_z \sim \sigma_w t$ when the Lagrangian time scale $p/N >> t$. The parameter "p" was determined by calibrating Equation 47 against lidar measurements. This is discussed in Section 3.2.2. This formulation for σ_z is incorporated in both the Wrap and Lift models.

3.1.7 Summary

Differences between the Impingement model and the Wrap model are as follows:

- The Gaussian probability density function for the wind direction was replaced by the density function $P(\theta)$ constructed from the 5-minute averaged wind directions.
- The Wrap model allows estimates of concentrations around the hill at the height of release.
- The Wrap model uses a modified formula for σ_z that reduces to the small travel time form when N goes to zero.

Differences between the Neutral model and the Lift model are as follows:

- H_c was subtracted from the vertical coordinate to reflect the two-layer flow over the hill.
- A radius of curvature based on the shape of the hill was incorporated into the expression for the horizontal distortion factor ß and into the expression for T_c.
- The "measured" $P(\theta)$ was used instead of a Gaussian probability density function.
- The Lift model uses a modified formula for σ_z that reduces to the small travel time form when N goes to zero.

The utility of these modifications was tested by comparing model predictions against observations for the 14 hours considered in this report. This evaluation is discussed in Section 4.

3.2 Comparison of Photographs and Lidar Plume Observations with Meteorological Observations

Plume photographs and lidar cross sections are available for most experiment hours. In this section, these data are compared with tower observations of turbulence intensities, and the importance of variability in the wind field during stable conditions is discussed.

3.2.1 Analysis of Vertical Spread From Plume Photographs

The plume photography at CCB was described in detail in the first milestone report. Photographs were taken by cameras at several fixed locations, and additional photographs were taken by observers on the ground and from a small airplane. The oil-fog plume was generally visible to downwind distances of greater than 1 km for most viewing angles. The photos provided information on vertical and lateral plume spreading and on plume trajectory, including plume impaction on CCB and plume streamlines over or around CCB.

Most of these photos were 5-minute time exposures. During each exposure, the plume would be illuminated about ten times by the sweeping beam from an arc lamp rotating at two sweeps per minute. When this lamp provided the only illumination, the photos recorded a superposition of these ten plume images. However, when the moon was shining, the plume was illuminated continuously and the photos provided a true 5-minute average. It is difficult to scale distances and angles from most of the photos because the plume trajectory was seldom at right angles to the line of sight. When it was perpendicular to the line of sight, the plume was often difficult to see at distances of more than a few hundred meters from the source due to the light-scattering angle. The initial analysis of the photos therefore emphasized the vertical spread in the near field.

Specifically, we estimated the vertical angle, E, of the plume on the photos and compared it with the vertical turbulence intensity, i_z, observed on tower A. Usually it was easy to estimate E because the sides of the plume were straight and sharp out to downwind distances of 100-200 m. During some of the 8-hour experiments, only one or two photos were useful; in others, as many as 20 or 30 photos were useful. The effective turbulence intensity on the photo (i_z (photo)) is assumed to be related to the measured angle E through the relation

$$i_z \text{ (photo)} = E/2\sqrt{3} \tag{48}$$

where E is in radians. The constant $2\sqrt{3}$ results from the top-hat distribution assumed for the plume.

In the analyses reported in this section, 5-minute average i_z (photo) observations are compared with concurrent 5-minute average i_z (tower) observations, where the i_z (tower) values are interpolated to source height from tower instrument levels (10 m, 40 m, and 80 m). In Figure 8, i_z (photo) is plotted versus i_z (tower), with data from different experiments indicated by different symbols. About 54% of the points agree within a factor of 2. The median i_z (photo) is 60% larger than i_z (tower).

A small part of this difference can be explained by the initial plume dilution generated by mechanical turbulence in the oil-fog plume. (The photos suggest that source-induced σ_{zo} is about 1 m and that the influence of the source extends downwind about 10 or 20 m.)

A larger part of the disagreement between i_z (photo) and i_z (tower) can be accounted for when the i_z (tower) data is adjusted for propellor response deficiencies. (Propellor response characteristics are discussed at length in Section 5.) Adjustments may be made to measured i_z values by using a correction proposed by Horst (1973). The relationship between the measured value and the "correct" value can be written as

$$i_z \simeq \sigma_\phi = 1.25\ \sigma_{\phi m}\ C(\sigma_\phi) \tag{49a}$$

for small elevation angles ϕ. In the equation, σ_ϕ is the standard deviation of the "correct" elevation angle of the wind, $\sigma_{\phi m}$ is the standard deviation of the measured elevation angle, the factor 1.25 is a bulk correction for the lack of propellor response at small elevation angles, and $C(\sigma_\phi)$ is a refined correction factor which is a function of the distribution of ϕ over the averaging period

$$C^2(\sigma_\phi) = \overline{\sin^2\phi} / \overline{F^2(\phi)\sin^2\phi} \tag{49b}$$

$F(\phi)$ is a correction factor derived for the vertical propellor of the Gill anemometer.

In calculating $C(\sigma_\phi)$, Horst assumes that the azimuth and elevation angles θ and ϕ are independent random variables with normal distributions. This allows him to calculate C as a function of σ_ϕ. These computations are presented in his paper. The resulting function $C(\sigma_\phi)$ increased σ_ϕ most at small values of σ_ϕ. In general, the net adjustment in Equation 49a increased hourly i_z values by 25% to 50%. Because the adjustment requires that ϕ be distributed normally in time, its application to 5-minute values of i_z may not be appropriate.

Another (perhaps major) part of the disagreement between i_z (photo) and i_z (tower) arises because of the physical separation of the tower and the source. When the source is located to the southeast of CCB, the source is about 3 km from the tower. With wind speeds of 2 m/s, it would take the

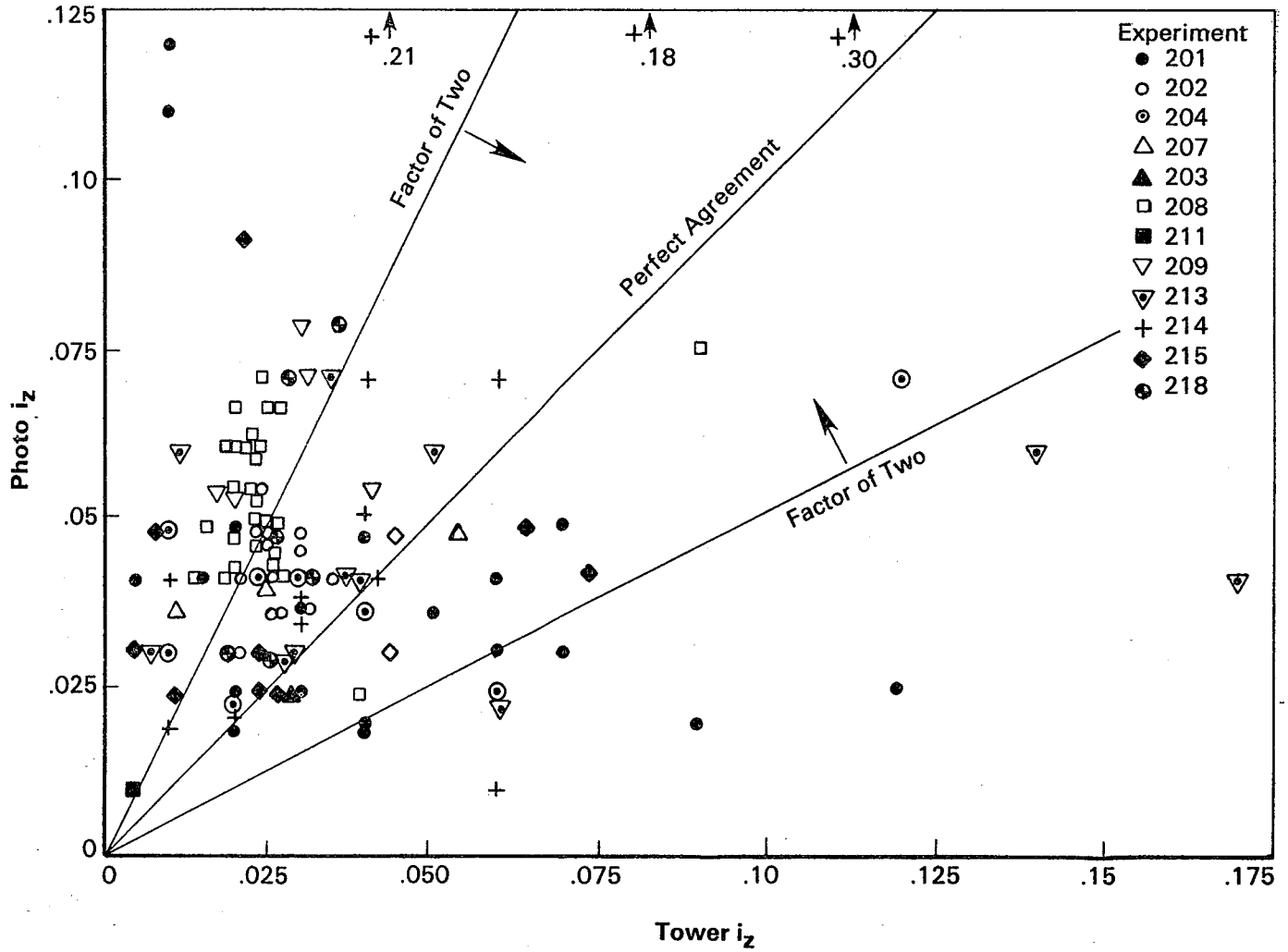

Figure 8. Observed 5-minute i_z (photo) versus i_z (tower).

air about half an hour to traverse this distance. If i_z fluctuations are caused by traveling gravity waves or mesoscale meanders (see Section 3.2.3), a region of high vertical turbulence intensity may arrive at the tower and source at times differing by as much as an hour. This possible effect is suggested in Figure 9 (from Experiment 201), where time series of i_z (photo) and unadjusted i_z (tower) are plotted. Note that the shapes of the curves and their peak magnitudes are similar, but the curves are displaced in time by 30 minutes. This travel-time effect makes it difficult (at least for very light wind situations) to predict 5-minute average plume dispersion from tower A data but probably does not unduly influence hourly averages.

Brief comments on tower and photo i_z's for each experiment are given in Table 1. The agreement is variable. If the data at 40 m on Tower A are available, tower and photo i_z's agree within a factor of two, on the average. If the 40 m level tower data are incomplete (e.g., Experiments 206 and 211), it is difficult to interpolate i_z accurately from the 10 and 80 m levels. In both of these experiments, the tower and tethersonde data suggest that there was a light-wind, high i_z layer extending to heights of 20 m and a high-wind, low i_z layer aloft. A strong inversion containing large wind speed and direction shears separated the layers.

These 5-minute data show not only that it is important to observe i_y and i_z in order to make diffusion calculations but also that these measurements should be taken as close to the source as possible. If the data are taken from a tower located several kilometers from the source or from a height more than 20 m above or below the source, differences of a factor of 2 or 3 or more in i_z can be expected during stable conditions.

The 5-minute data reported above were also combined into longer term averages, and the resulting tower and photo average i_z's are compared in Figure 10. Averaging periods for these data range from 20 minutes to 2 hours, and the average i_z (tower) values have been adjusted for propellor response characteristics as discussed earlier. The average values agree better than the 5-minute values in Figure 8 because the individual differences tend to cancel out over longer averaging times. For example, the averaged i_z in Figure 9 is nearly equal for the two data sets even though the peaks are displaced in time by 30 minutes. The circled points on Figure 10 are those for which the source height (H_S = 60 m) was above the tower level (H_T = 40 m) used to determine tower i_z. In general, excluding these points, the data agree within a factor of two and there is very little bias.

3.2.2 Analysis of Lidar Estimates of σ_y and σ_z

To have confidence in the lidar data taken near CCB (where the flow is definitely perturbed), it is important to determine whether the lidar plume observations are well-behaved in the unperturbed region within a few hundred meters of the source. In this section, lidar-derived σ_y and σ_z

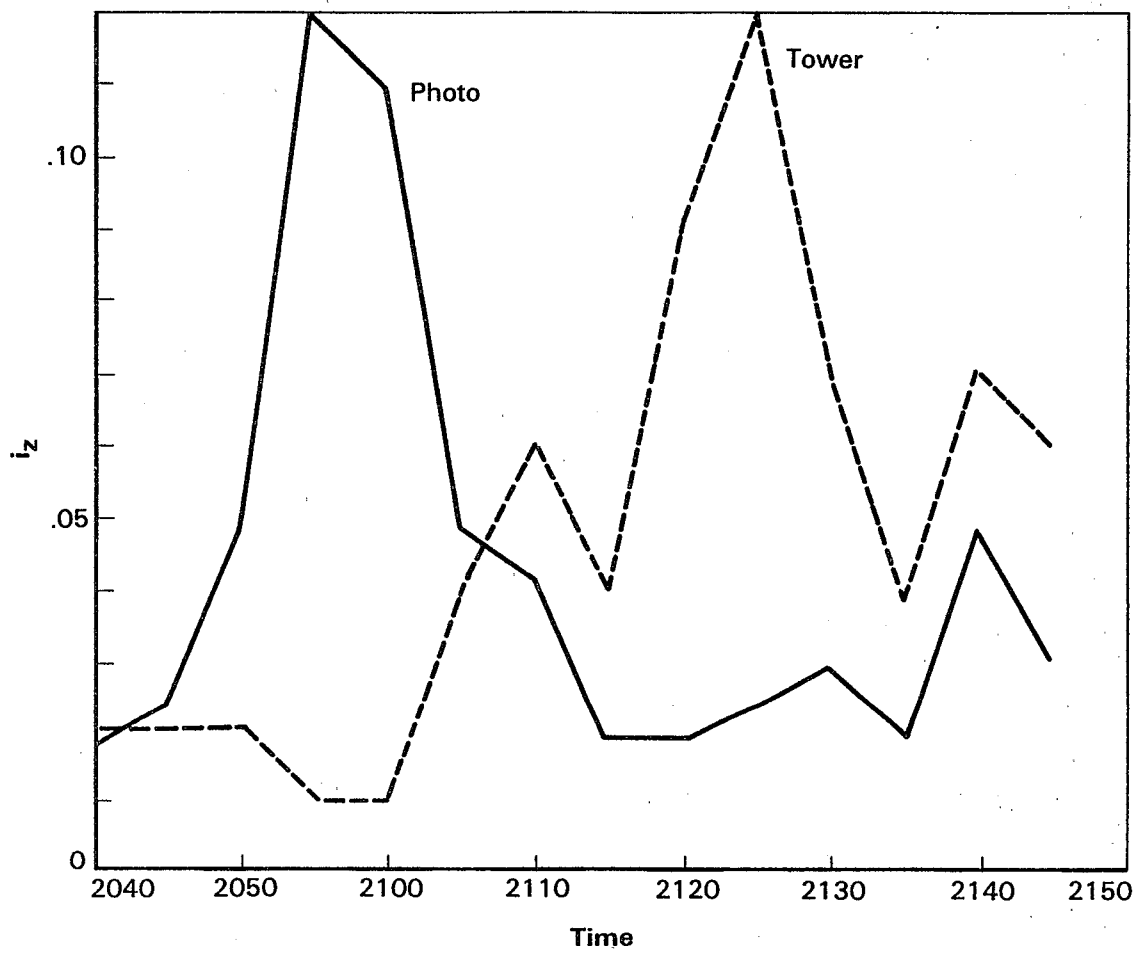

Figure 9. Time series of 5-minute average i_z (photo) and i_z (tower) from Experiment 201.

8205040

TABLE 1

COMMENTS ON TOWER AND PHOTO i_z OBSERVATIONS

Experiment	Number of Photos Analyzed	Source Heights (m)	Coments
201	31	20,30, 40	Tower and photo i_z's agree on average; peaks are displaced in time by 30 minutes.
202	13	20,30	Tower and photo i_z's agree on average.
204	8	30	Tower and photo i_z's agree on average, but individual 5-minute values differ by as much as a factor of ± 5.
206	14	35,46	Tower A 40 m data missing; 10 m tower i_z's are 3-4 times greater than photo i_z's; 80 m tower i_z's are either in agreement or are zero.
207	3	30	Tower and photo i_z's agree on average.
208	35	30	Tower i_z is factor of 2 below photo i_z's.
209	5	40	Tower i_z is factor of 2 below photo i_z's.
211	30	58,40 20	Tower A 40 m data missing; 10 m tower i_z's are 3 times greater than photo i_z's; 80 m tower i_z's are factor of 2 lower.
213	12	30,40 50,60	Tower and photo i_z's agree on average; peaks are factor of 5 higher or lower.
214	16	47	Tower and photo i_z's differ by factor of ± 5.
215	16	30,57	Tower and photo i_z's differ by factor of ± 3.
218	6	30	Tower i_z is consistently a factor of 2 below photo i_z.

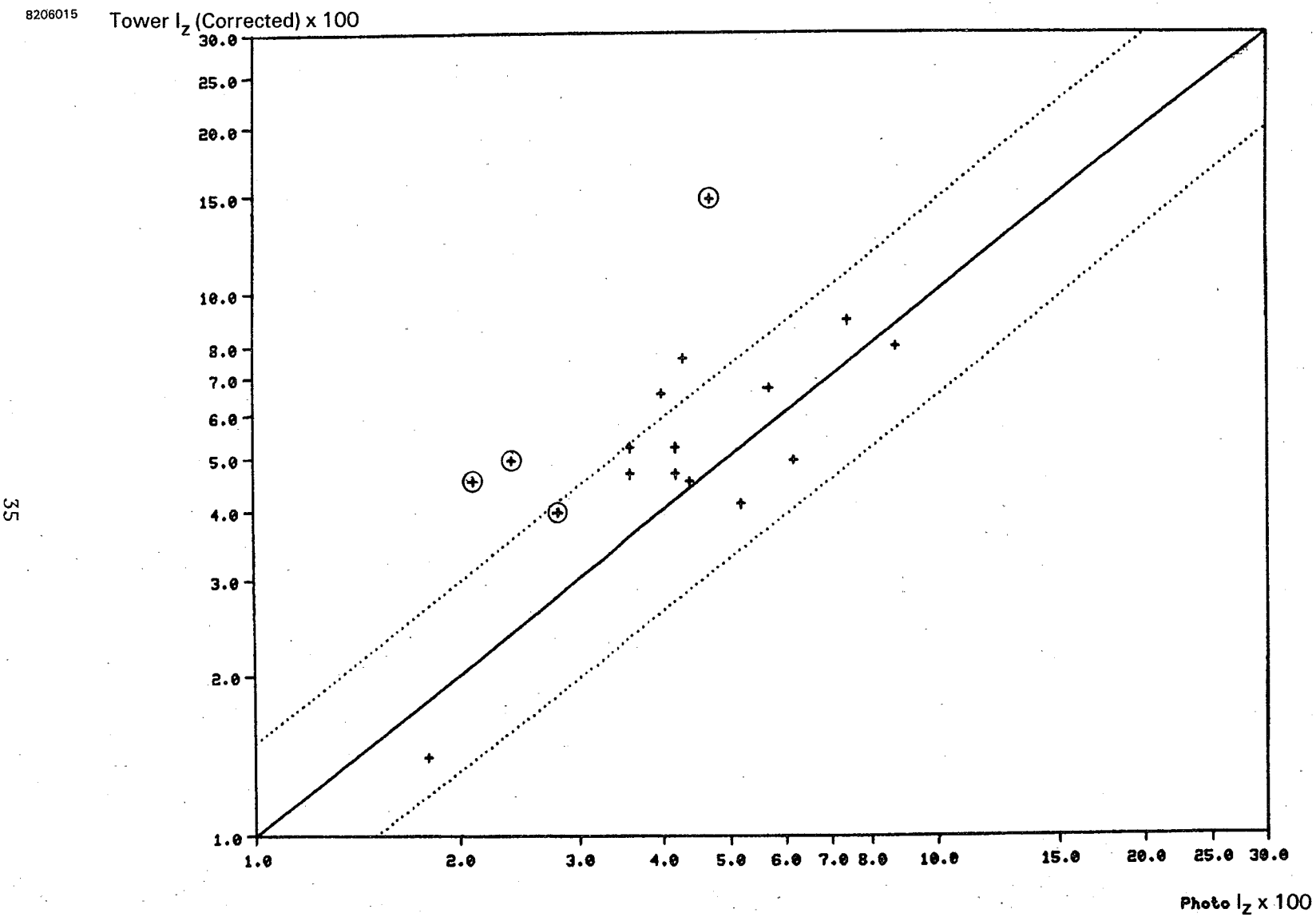

Figure 10. Average tower i_z versus photo i_z. Circled points are those for which H_s = 60 m and H_t = 40 m.

estimates are plotted as a function of downwind distance and compared to observed meteorological parameters such as i_y, i_z, U_o, and N. Hourly averaged lidar data are included in the analysis. Data for all the experiments are not available because data processing work has not yet been completed by the Wave Propagation Laboratory.

Lidar σ_y

The lateral diffusion parameter σ_y can be estimated by the formula (Pasquill 1976)

$$\sigma_y = i_y x \, F_y(x) \tag{50}$$

where i_y is the crosswind turbulence intensity and $F_y(x)$ is a dimensionless function that is close to unity at distances less than 1 km from the source (Briggs 1973). The observed lidar σ_y's upwind of the hill should approximate $i_y x$, where i_y is obtained for the source height by linear interpolation from adjacent tower levels. In Figure 11, the hourly averaged σ_y's are plotted versus $i_y x$ for 13 separate experiment hours. Each hourly σ_y is made up of contributions from individual lidar scans and from the lateral displacement of observed plume centroids

$$\sigma_y^2 = \sum_{i=1}^{n} \sigma_{yi}^2/n + \sum_{i=1}^{n} (y_{ci} - \bar{y}_c)^2/n \tag{51}$$

The parameter y_c is the centroid position, and n is the number of lidar cross-sections at that particular downwind distance during that hour.

Figure 11 shows that the line $\sigma_y = i_y x$ passes through the middle of the data set, but that the data from individual hours can be as much as a factor of 3 different from this line. The curves for individual hours generally have slopes close to unity. Many factors could contribute to the scatter on the figure, including small sample size, unrepresentative tower i_y, and lidar resolution and accuracy.

The contribution to σ_y from lateral displacement of centroids or meandering is greater than the individual scan contribution in about 50% of the cases analyzed. In 20% of the cases, the meander component exceeds the individual scan component by a factor of 5 to 10. The total hourly σ_y observed by the lidar is plotted versus the stability parameter U_o/N in Figure 12, showing that σ_y is relatively small for U_o/N larger than about 200 m but varies widely for U_o/N less than 200 m. Small U_o/N (i.e., low winds and/or strong inversion) is a necessary but not a sufficient condition for large σ_y. This wide range of σ_y may result from gravity waves during light-wind, stable conditions.

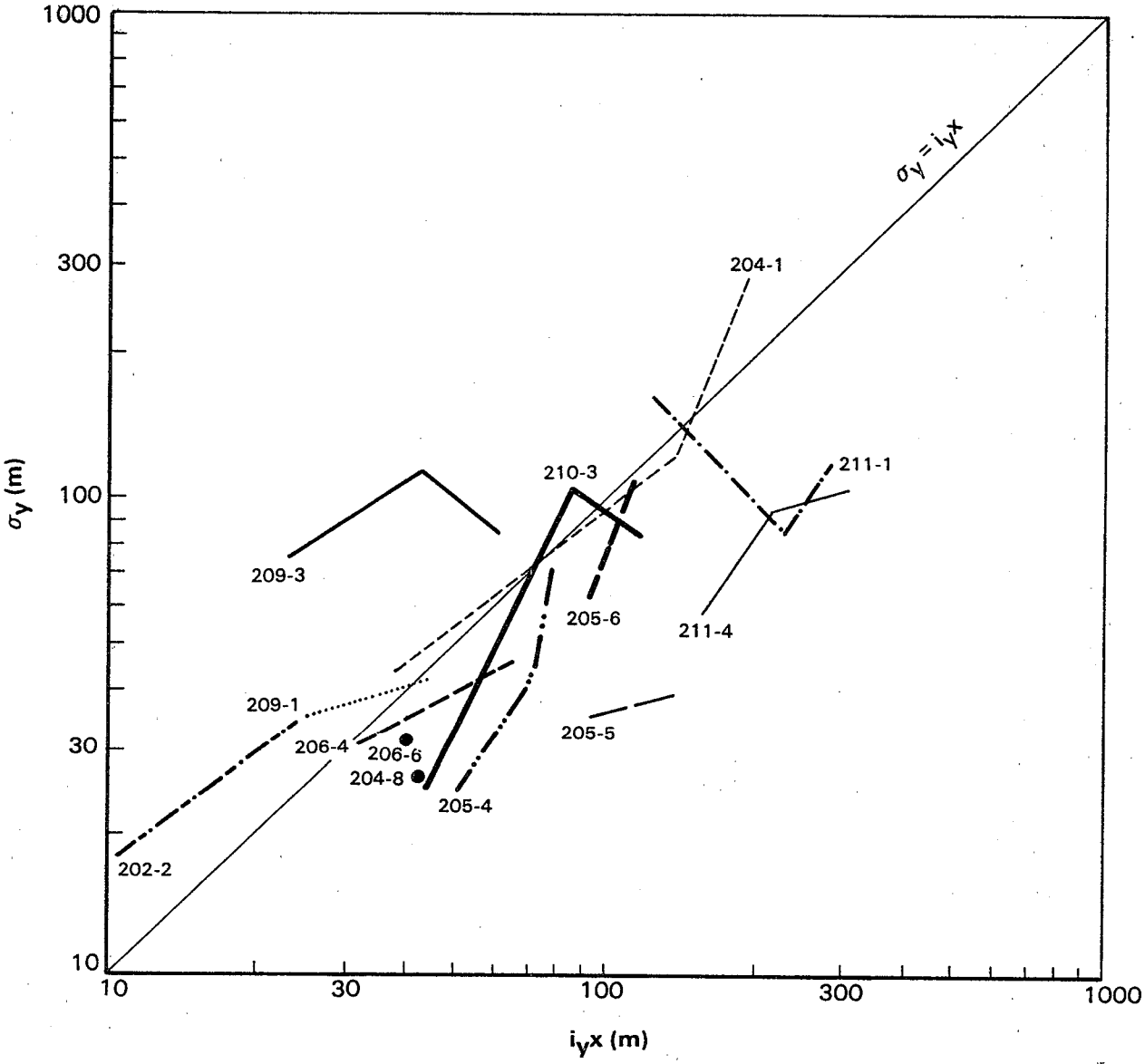

Figure 11. Observed hourly σ_y plotted as a function of $i_y x$ for selected experiment hours, based on Equation 51.

8205049

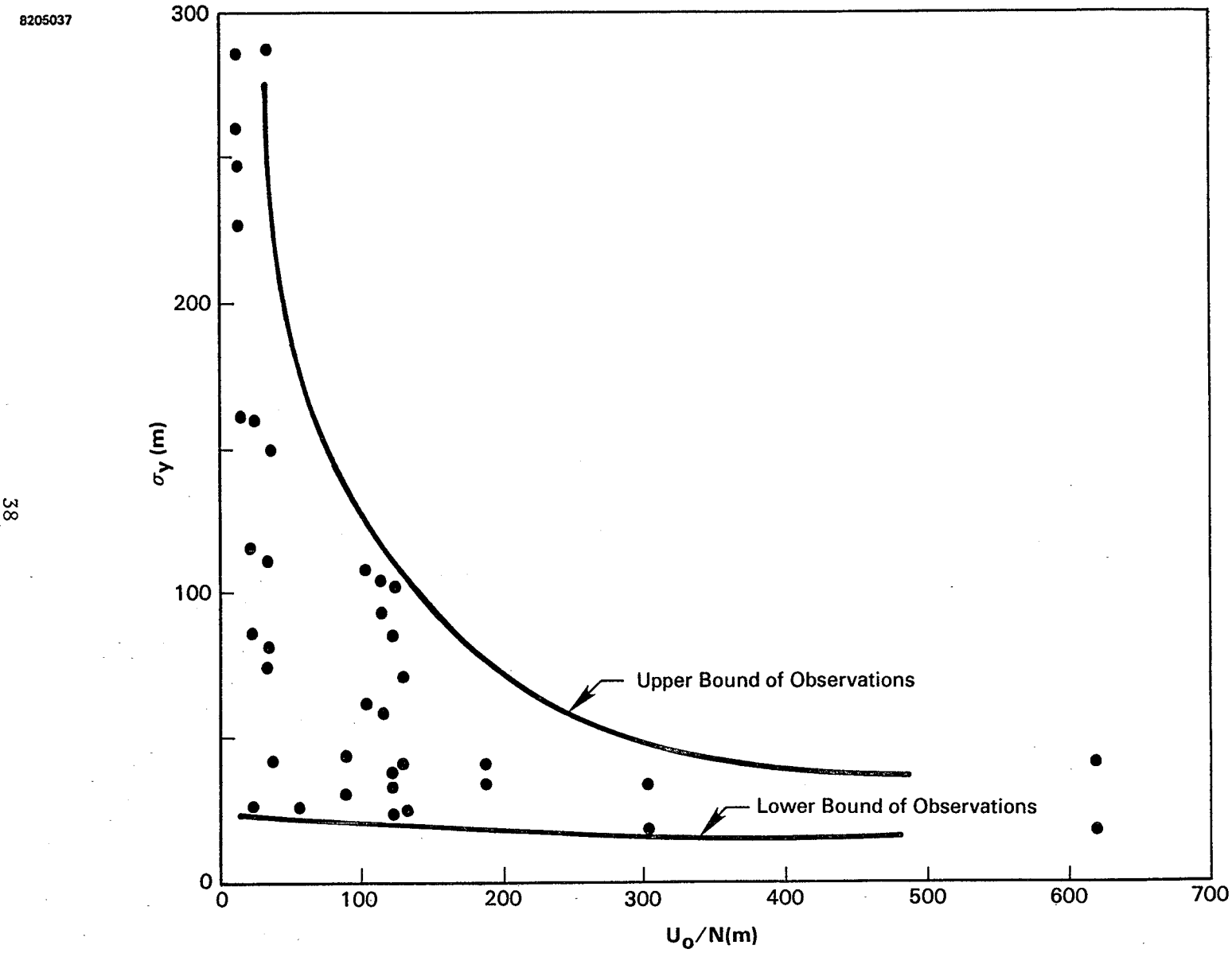

Figure 12. Observed hourly lidar σ_y as a function of the stability parameter U_o/N.

To eliminate the effect of lateral displacement of observed centroids, the individual scan contribution (term 1 in Equation 51) is plotted in Figure 13 as a function of downwind distance. The lateral turbulence intensity i_y is not included because it is not known for the specific times of the lidar cross sections. The interesting aspect of this figure is that all of the individual scan σ_y curves are fairly flat, in disagreement with relative diffusion theory and observations of other instantaneous plumes (Gifford 1977). These theories suggest that slopes of $\sigma_y(x)$ curves for relative diffusion should be greater than slopes for hourly averaged diffusion, even during stable conditions. Furthermore, if the lines on Figure 13 are extrapolated to $x = 0$, they do not come close to $\sigma_y = 0$. (The intercept for most curves is 10-20 m.) The largest initial σ_{yo} that we can justify on the basis of photographic observations of the oil-fog plume is only 1-2 m. Because it is unlikely that the curves in Figure 13 change slope abruptly to the left of their first point, the lidar observation system may have either over-estimated plume size near the source or underestimated plume size further from the source. It is not possible to check these results with the plume photographs, because the plumes were extremely diffuse at the distances of the lidar observations.

Another reason for this behavior could be an alteration of the plume spread caused in some way by the presence of the hill. Many observes noted a significant increase in the apparent width of the visual plume when the trajectory was directed toward the center of the hill rather than to one side of the hill. And this effect appeared to affect the plume size over a significant portion of the trajectory between the source and the hill. Because the sampling frequency of the lidar was not great enough to resolve this variability evenly in all lidar sampling planes, and because Figure 13 ignores this kind of variability within hourly averaging periods, some relative overestimation of σ_y close to the source may have resulted. This possibility is being investigated.

It can be concluded that hourly σ_y observations agree on the average with the formula $\sigma_y = i_y x$. Most of the contribution to σ_y and i_y over a 1-hour period comes from gradual plume meandering. The standard Pasquill-Gifford-Turner stability class scheme cannot account for the meander contribution to σ_y. Averages of individual lidar scan estimates of σ_y appear to overestimate σ_y at small downwind distances.

Lidar σ_z

The vertical diffusion parameter, σ_z, can be estimated by the following formula (Irwin 1979)

$$\sigma_z = i_z x \, F_z(x) \tag{52}$$

where i_z is the vertical turbulence intensity, and $F_z(x)$ is a dimensionless function that equals unity near the source but decreases with distance (more rapidly than $F_y(x)$) during stable conditions. In Figure 14

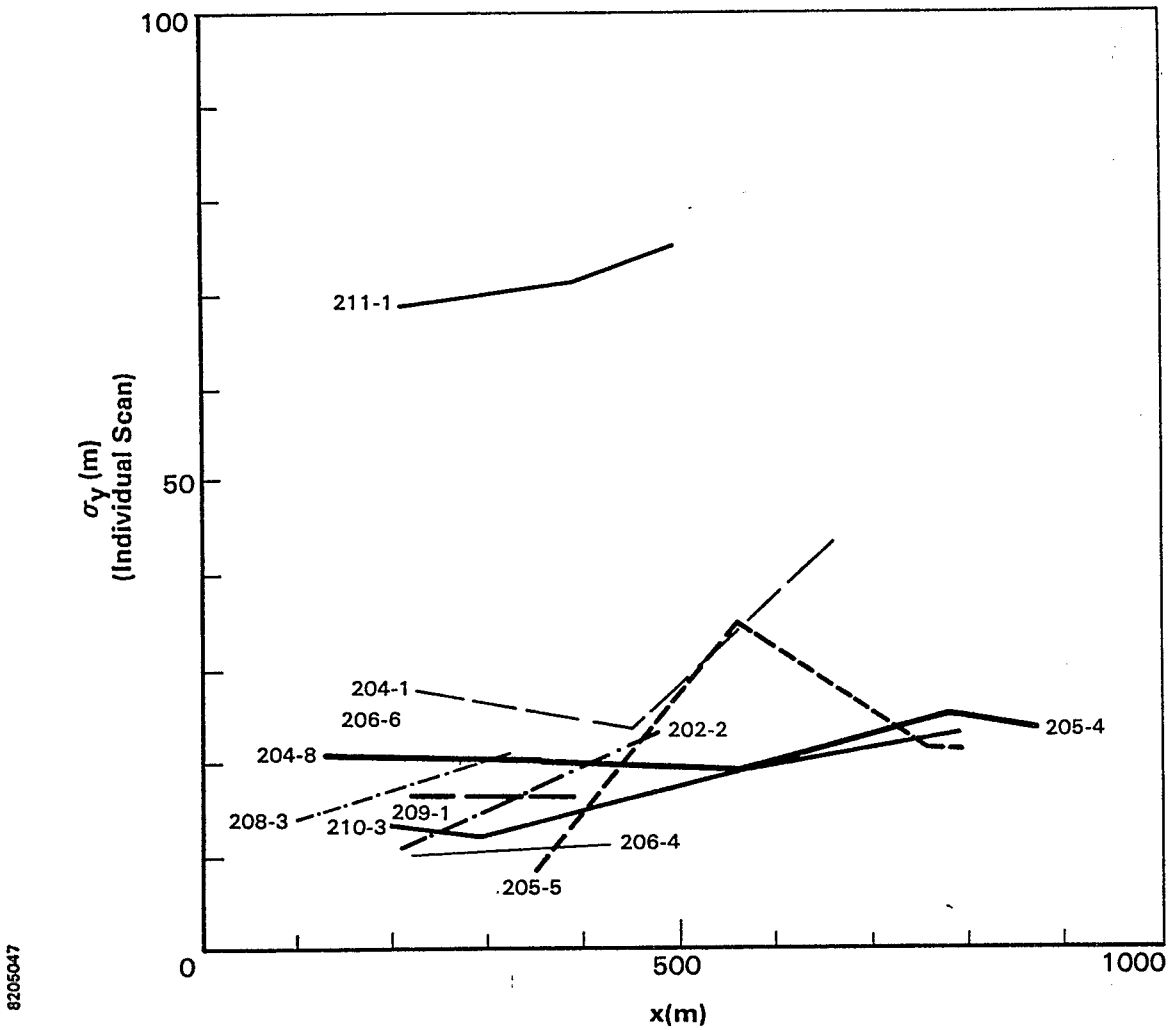

Figure 13. Averages of observed individual scan lidar σ_y plotted as a function of x for selected experiment hours.

the hourly-averaged σ_z's are plotted versus $i_z x$ for 13 separate experiment hours. Total hourly σ_z is made up of individual scan and meandering components (similar to Equation 51 for σ_y); but the meandering component is usually small. The lidar-observed hourly σ_z is proportional to $i_z x$ for $i_z x < 10$, but σ_z grows more slowly with distance at large $i_z x$. It is hard to know if this behavior is real, however, because it is difficult to estimate the appropriate i_z at plume height for cases when i_z data vary rapidly with height (e.g., Experiment 211) or when i_z data are missing at the 40 m level. In Experiment 211, i_z was fairly high (.07) at the 10 m level, missing at the 40 m level, and low (.005) at the 80 m level. The value used for i_z in Figure 14 appears to be too high, as the curves for the two Experiment 211 hours are displaced from the others.

Averages of individual scan σ_z's for selected runs are plotted as a function of downwind distance in Figure 15. These σ_z curves are not quite as flat as the individual scan σ_y curves in Figure 13, but they also give unreasonable intercepts (σ_{zo}) in most cases if the curves are extrapolated to x = 0. Some of the apparent overestimation in σ_z may be attributable to the spatial resolution of the lidar system. The minimum vertical grid resolution for calculating σ_z was 1.5 m. In Figure 15, the minimum grid resolution was 2.25 m for hour 208-3, 1.5 m for hour 206-4, 4.5 m for hour 209-8, and 3.0 m for hour 211-1. Therefore, the relative spacing of the intercepts σ_{zo} for 206-4, 208-3, and 209-8 are at least qualitatively indicative of a grid resolution limit to σ_z at small downwind distances. However, σ_{zo} for 211-1 indicates that other factors must be considered. These are under study.

Because nearly all of the CCB experiments were conducted at night, it can be hypothesized that hours with high wind speeds are the more neutral, and hours with low wind speeds are the more stable. Current point-source dispersion models assume that vertical dispersion decreases monotonically as stability increases. For example, the Pasquill-Gifford-Turner σ_z values for F stability are smaller than those for E stability. According to the conventional stability classification, therefore, the hours of lowest wind speed on clear nights should have the smallest i_z's.

Figure 16 illustrates that the CCB i_z data do not corroborate the wind speed-stability class convention used in current models; i_z can be as much as 0.10 for wind speeds less than about 3 m/s but is never greater than 0.04 for wind speeds greater than about 5 m/s. Panofsky (1982) has been studying turbulence data from the 300 m tower at the Boulder Atmospheric Observatory and concludes that gravity waves which occur during light wind stable conditions have significant vertical components. Perhaps gravity waves are also causing the increased i_z during low winds at CCB. The large observed range in i_z at low winds is consistent with the i_y data in Figure 12; this suggests the intermittent occurrence of gravity waves during low winds. As we have not yet determined whether it is possible to predict gravity waves, it is clear that it is important to measure i_y and i_z directly to estimate diffusion using an equation like Equation 52 under stable flow conditions.

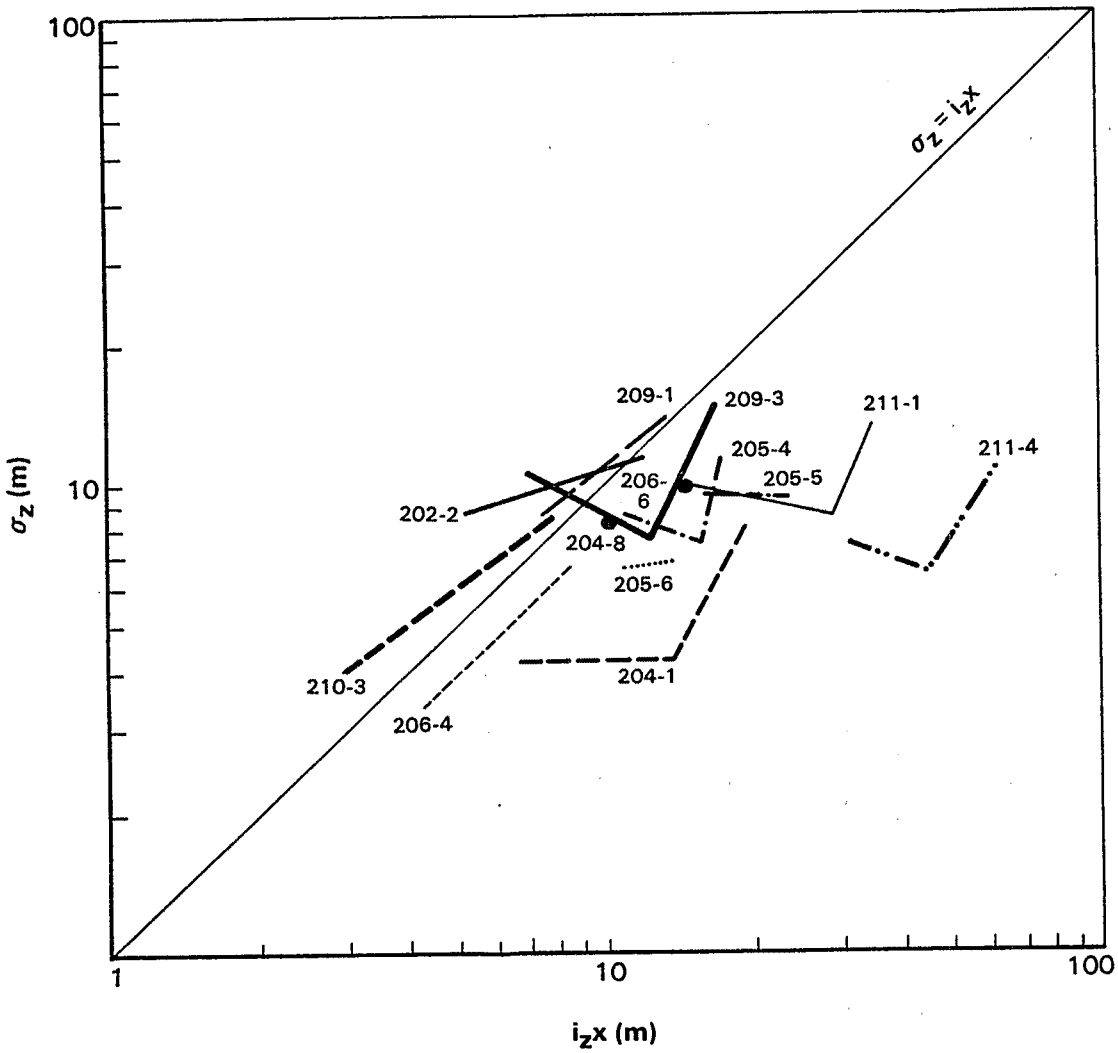

Figure 14. Observed hourly lidar σ_z as a function of $i_z x$ for selected experiment hours.

8205048

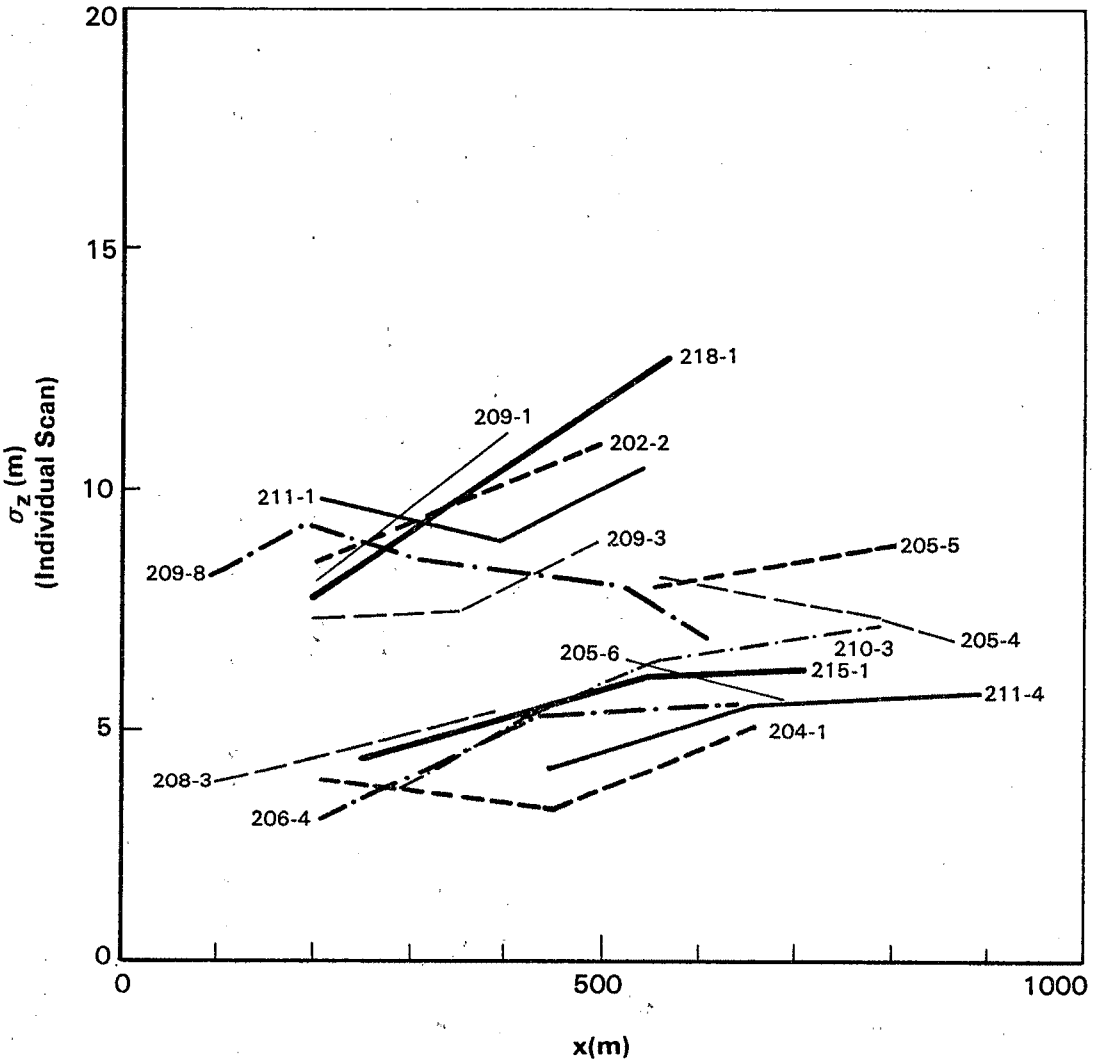

Figure 15. Averages of observed individual scan lidar σ_z plotted as a function of x for selected experiment hours.

8205046

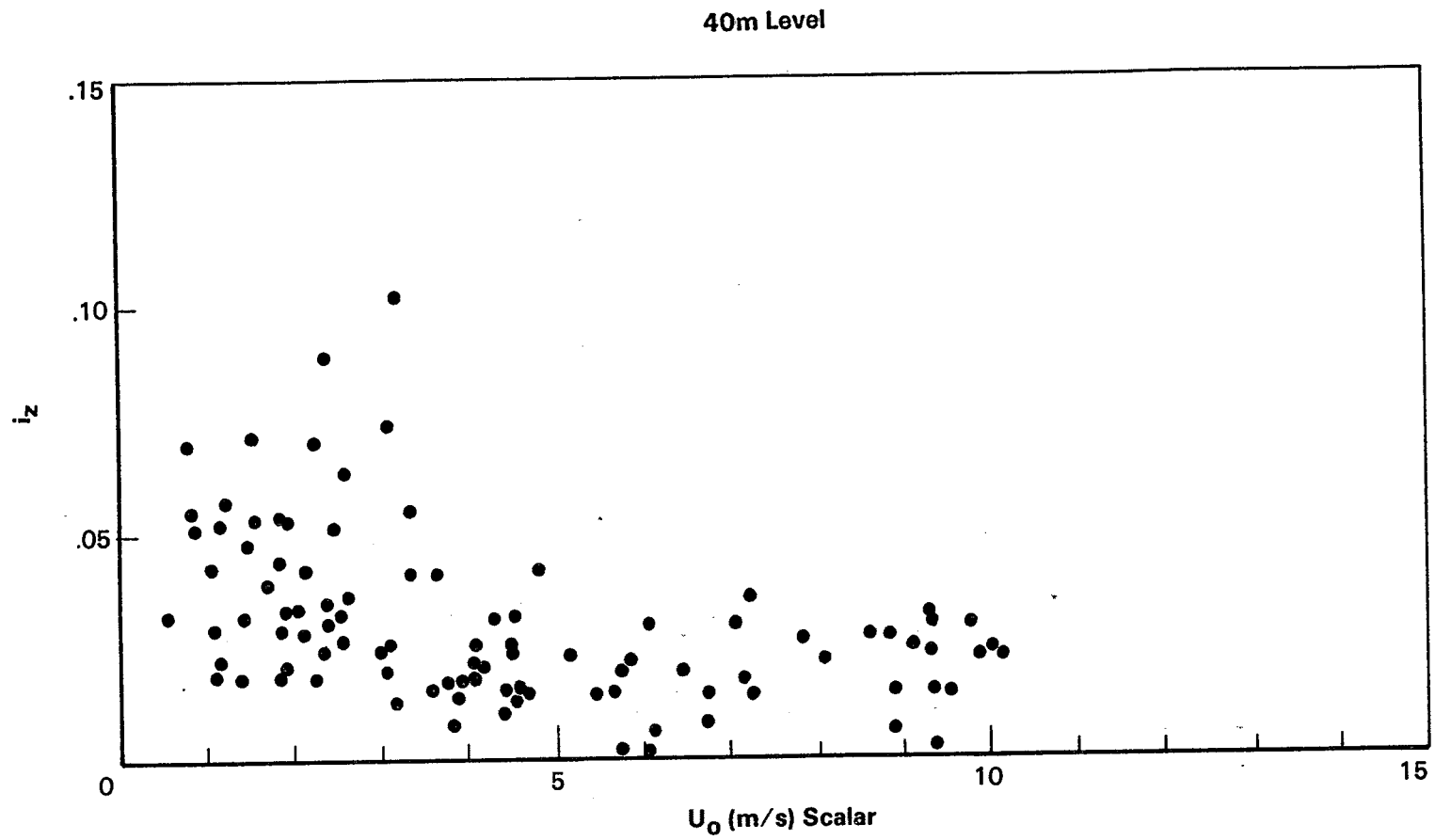

Figure 16. Observed hourly i_z at 40 m level as a function of hourly scalar wind speed.

It is possible to compare the lidar σ_z's with those calculated by our theoretical formula. As indicated earlier, (Equation 47) we have assumed that σ_z in stable flows is described by the equation

$$\sigma_z = \sigma_w t/(1 + tN/p)^{1/2} \tag{53}$$

where p is a parameter. Its value was determined by calibrating Equation 53 against σ_z derived from lidar cross sections. The hourly averaged "measurements" of σ_z were constructed by combining statistics from individual lidar scans available during the hour using an equation like 51 with n-1 weighting. Many of these average sigmas correspond to only two to three instantaneous lidar cross sections. Therefore, their values are uncertain. This should be kept in mind in interpreting the comparison between the results obtained from Equation 53 and the measurements.

Experimentation with several values of p showed that p = 1.5 resulted in reasonable agreement between lidar measurements and calculated σ_z values based on adjusted i_z values. The i_z values used in calculating σ_z were interpolated to source height and then adjusted for propellor response characteristics. The interpolation process involved multiplying i_z values measured above and below the release height by the corresponding mean wind speeds to produce σ_w values, linearly interpolating σ_w to release height, using a power law interpolation to estimate the wind speed at release height, and multiplying this speed by the interpolated σ_w to obtain i_z at the release height (more details are presentd in Section 4.1.2). Figure 17 compares the lidar and calculated σ_z values. These results indicate that Equation 53 serves the intended purpose of providing estimates of σ_z that correspond to "measured" values. This formulation is used in all model calculations presented in Section 4.

3.2.3 Time Series Analysis of Wind Speed Data

Nighttime stable periods are characterized by slow fluctuations in wind speed and direction caused by the passage of gravity waves or terrain-induced eddies. These fluctuations can also be caused by time variations in vertical boundary layer structure (e.g., the collapse of a strong inversion when the Richardson number falls below its critical value) or by the influence of thunderstorms several kilometers away. Time periods of these meanders or mesoscale fluctuations are on the order of 10 minutes to 2 hours. As shown in Section 3.2.2, these large-scale fluctuations often dominate hourly averaged i_y or σ_y observed at CCB.

Some of the CCB experiments exhibit exceptional variability in wind speed and direction. For example, a time series of the 5-minute average scalar wind speed from the 10 m level of tower A for Experiment 211 is plotted in Figure 17. Wind direction was equally variable during this period, going completely around the compass (counterclockwise) during a 20-minute period at the end of hour 3. During Experiment 204, the wind direction went around the compass (clockwise) in hour 5. The range in

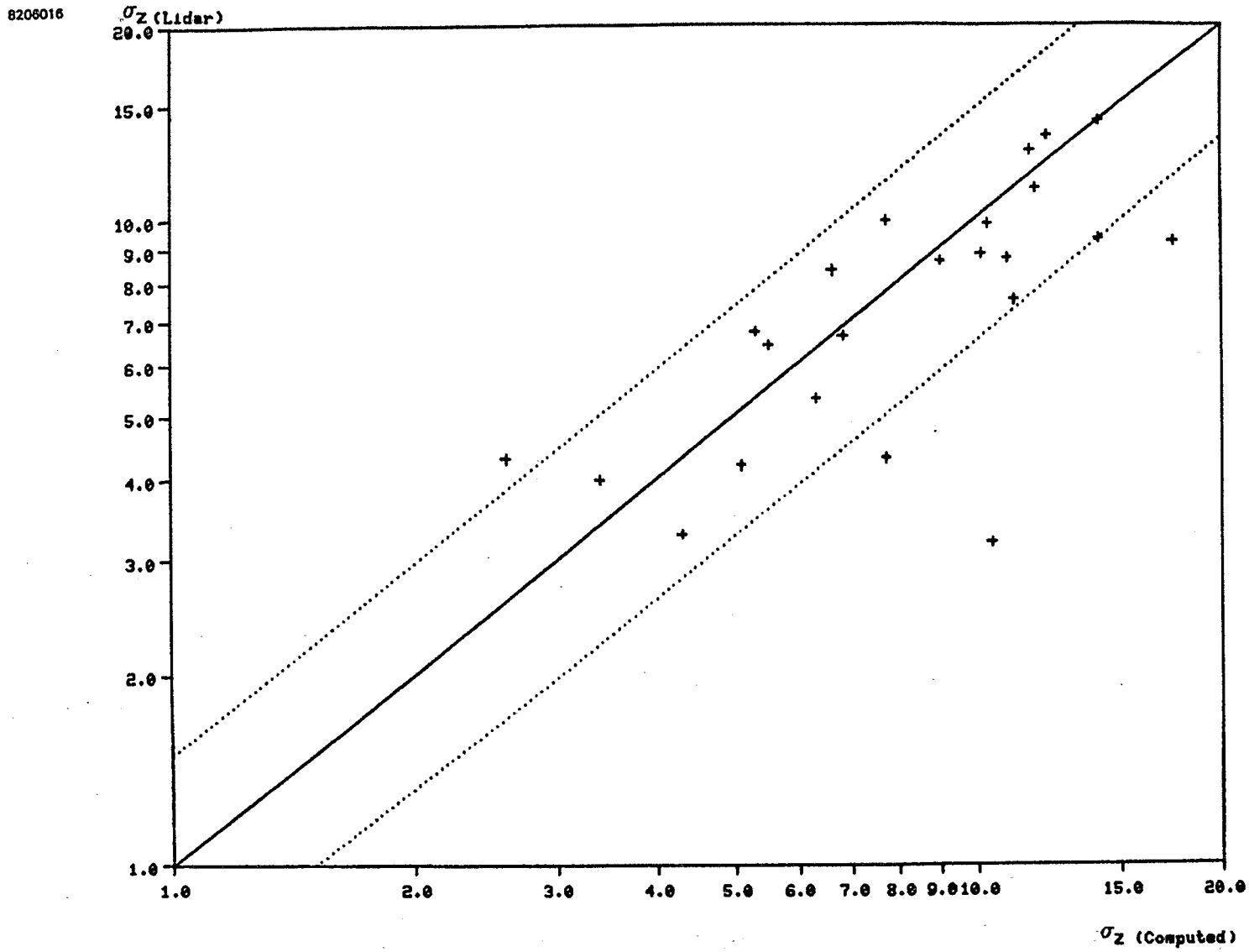

Figure 17. Comparison of lidar-derived hourly σ_z values and calculated σ_z (Equation 53).

5-minute wind speeds (0.4 m/s to 4 m/s) in Experiment 211 is a factor of two greater than the average wind speed during the 8-hour experiment. Visual examination of the figure suggests fluctuations present with periods of about 1 to 1.5 hours (low winds occur at times 0010, 0140, 0250, 0420, 0550, 0730). Other fluctuations with smaller periods are also obvious, however.

Spectral analyses of the data were performed to estimate the amounts of turbulent energy associated with eddies with periods ranging from 10 minutes to 2 hours. A standard Fast Fourier Transform (FFT) computer code was applied to each experiment for wind data from the level closest to the level of the source. The total speed and u and v components of the wind speed were analyzed separately. Autocorrelograms and spectra were plotted for each experiment. The autocorrelograms and energy spectra for the data are also given in Figure 18. Standard procedures were used to remove a linear trend from each time series, since a trend will show up in the spectrum as a great deal of energy at the lowest frequency point. Also the beginning and end of the time series were smoothed to prevent unrealistic behavior of the spectrum at high frequencies (Rayment 1970, Cooley and Tukey 1965).

Peak spectral energy occurs at frequencies of 1-2 cycles per hour, or periods of 30-60 minutes. The presence of these eddies must be recognized in model development for light-wind stable conditions. In particular, it is important to use frequency distributions of actual wind direction to make diffusion calculations during an hour when these eddies are present.

A summary of the time series analysis of six of the CCB cases is given in Table 2. Wind observations at the 40 m level of tower A are used if available; otherwise, the winds at the 80 m level are used. The u and v components of the wind velocity are analyzed separately. The time period T_{max} at which maximum turbulent energy occurs is estimated by two procedures:

- Autocorrelogram Method: $T_{max} = 5T(1/e)$, where $T(1/e)$ is the time lag when the autocorrelogram first drops to 1/e or 0.37. The time period T_{max} of the turbulent fluctuation associated with $T(1/e)$ is obtained by multiplying by 5. The factor 5 comes from calculating the spectrum for an exponential correlogram (Hanna 1981).

- Spectral Method: T_{max} is the period associated with maximum $nS(n)$, where n is frequency and S is energy density in units of m^2/s^2 per unit frequency.

As expected, the T_{max} values determined by the autocorrelogram and spectral methods agree within about ±50%. On the average, T_{max} equals about 1-2 hours for the CCB cases. When averaging times for the meteorological and concentration data are one hour, about one-half to one full cycle can be expected to be captured. It is possible that the winds will continually decrease or increase during the 1-hour period, or decrease for the first 30 minutes and increase for the last 30 minutes of the period,

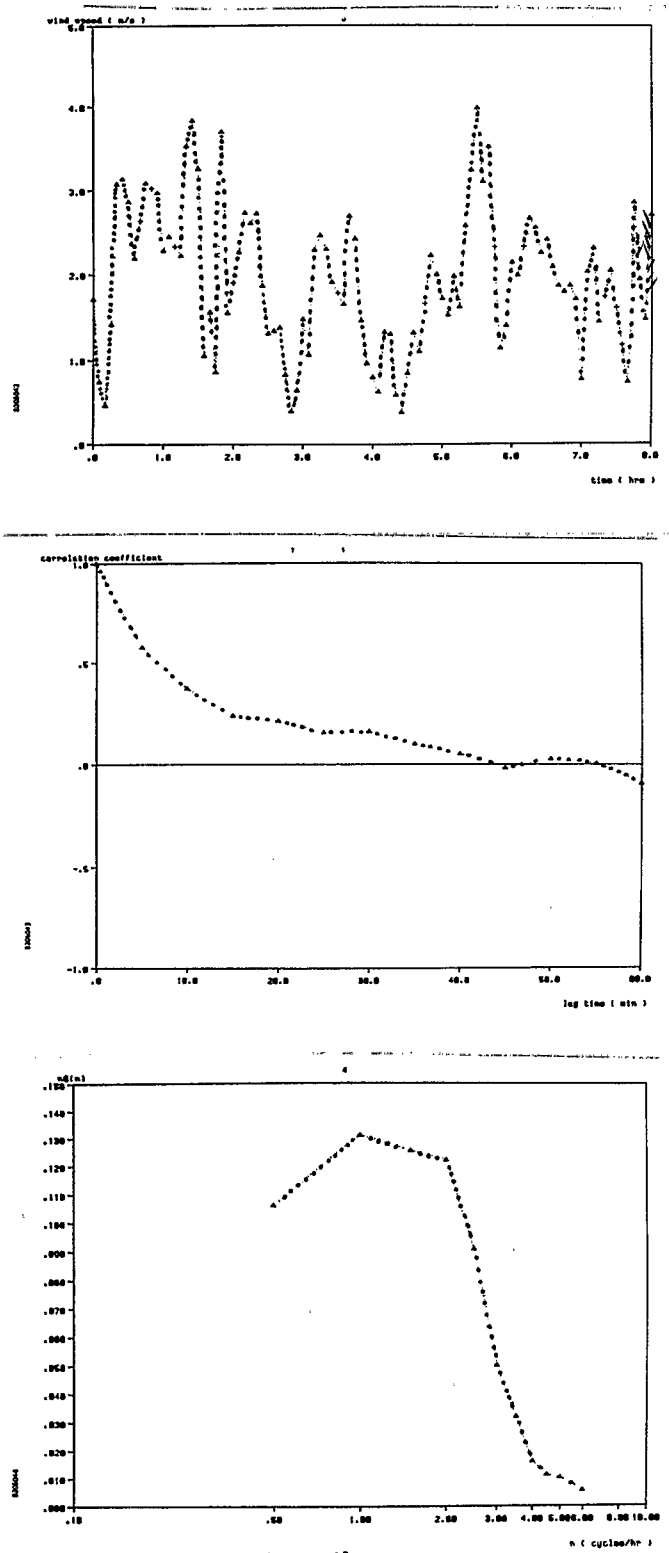

Figure 18. Five minute wind speed record at 10 m elevation, its autocorrelogram, and its energy spectrum for Experiment 211.

TABLE 2

TIME PERIODS AT WHICH MAXIMUM TURBULENT ENERGY OCCURS FOR SIX CCB EXPERIMENTS

Experiment	Elevation	Component	(Autocorrelogram)	(Spectrum)
202	40 m	u	2 hr	2.5 hr
		v	2.5 hr	2 hr
204	40 m	u	1.5 hr	1.5 hr
		v	2 hr	50 min
206	80 m	u	1.5 hr	2 hr
		v	3 hr	2 hr
209	40 m	u	1.5 hr	2 hr
		v	50 min	50 min
210	80 m	u	3 hr	30 min, 4 hr
		v	50 min	30 min, 1.5 hr
211	80 m	u	2 hr	1-2 hr
		v	2.5 hr	2 hr

depending on the portion of the sinusoidal wind cycle that is captured. This mesoscale energy thus appears as slow meander during a 1-hour period rather than as a turbulent fluctuation. Because these time scales are comparable to the averaging periods of interest, the effects of mesoscale meander must be accounted for explicitly. Therefore, as previously described, the actual observed hourly probability distributions of wind direction (rather than some conjectured distribution) should be used in modeling hourly average plume transport and impacts.

3.3 Isentropic Analysis

Five-minute average temperature data from tower A and tower B have been analyzed to estimate the original, or upwind, heights of streamlines that pass through measurement heights on tower B. The relationships between streamline heights upwind of the hill and those at tower B over the crest of the hill may be compared with calculations from potential flow theory and with data obtained in tow tank and wind tunnel experiments. Of particular interest is the relationship between the observed streamline lift in the flow above H_c and that found in weakly stratified flow experiments.

If streamline lifting is adiabatic, streamlines follow surfaces of constant potential temperature (isentropic surfaces). In considering the flow over a hill, the vertical motion can be assumed adiabiatic if heat transfer or mixing is negligible. Therefore, only data from 10 m and 30 m on tower B are considered. Other sources of uncertainty in calculating upwind streamline heights include temporal and spatial inhomogeneity in the temperature field between tower A and tower B, errors in measuring weak temperature gradients on tower A, and the lack of vertical resolution in the temperature profile between 100 m and 150 m on tower A.

Initially, potential temperatures were matched for every available 5-minute period in which no temperatures on either tower were missing. This first attempt did not provide enough data to complete the analysis, so missing data in the tower A profile were interpolated in height from adjacent levels or in time from adjacent time periods. Time interpolation was the preferred interpolation method, and height interpolation was used only as a last resort.

The resulting upwind streamline heights on tower A during Experiment 201 are presented in the upper portion of Figure 19. The solid line marks a streamline that originates at the altitude given in the ordinate and "passes" 10 m above the crest of the south peak; the dotted line marks a streamline that "passes" 30 m above the peak. For example, Figure 19 shows that at 2000 MST a streamline that passed 10 m above the south peak of the hill (102 m) originated at an altitude of about 55 m, thereby indicating a lift of about 57 m.

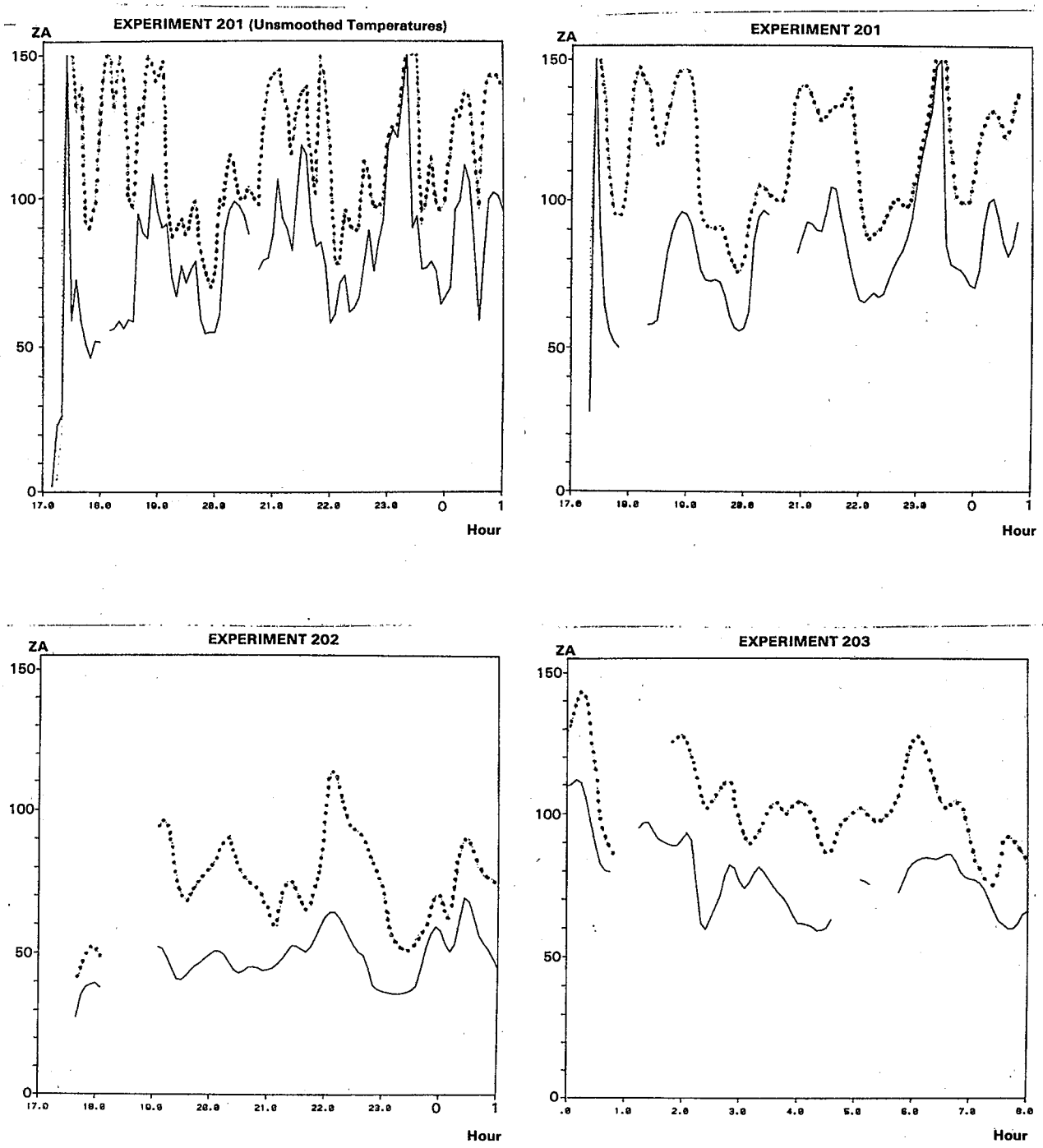

Figure 19. Estimated upwind height (ZA) of streamlines that pass through the 10 m (——) level and 30 m (...) level of Tower B on the crest of Cinder Cone Butte during Experiments 201 - 203.

Considerable variability is seen in this figure. Some of this is probably attributable to the spatial variability in the temperature field. In order to reduce the scatter, a running 3-point (15-minute) average was applied twice to the 5-minute temperature data. This resulted in streamline heights that are better behaved, with far fewer "spikes". The final isentrope plots are presented in Figures 19-22. In these plots, missing temperature data from tower A were interpolated only in time because data interpolated in height may be inappropriately influenced by strong temperature stratification. However, little difference was found between the two interpolation procedures.

Data from these figures have been used to evaluate the relationship between the streamline heights upwind and over the hill crest, and the relative importance of the density stratification. Scaled streamline heights are referred to as $n_m/H*$ and $z_r/H*$. As shown in Figure 23, $n_m/H*$ is the ratio of the streamline height over the hill crest (n_m) to the height of the hill above the dividing streamline height ($H-H_c$), and $(ZA-H_c)/H*$ is the ratio of the upwind streamline height above the dividing streamline height ($ZA-H_c$) to the height of the hill above the dividing streamline height ($H-H_c$). This inclusion of H_c is motivated by the expectation that the layer of air below H_c is "dead" to the flow above H_c (see below). The plot of $(ZA-H_c)/H*$ versus $z_r/H*$ derived from 1-hour averages of the inferred 5-minute streamline height data are presented in Figure 24.

Five symbols are used in the plot to classify the data by the bulk hill Froude number for the flow above H_c. The bulk hill Froude number is defined as

$$Fr_H = \frac{\overline{U}_o}{N(H-H_c)} \tag{54}$$

where U_o is the average wind speed from H_c to 150 m, and N is the Brunt-Vaisala frequency calculated with the temperature gradient between H_c and 150 m. The H_c and Fr_H values used in this analysis were calculated for each 5-minute period and then averaged over one hour. The streamline heights from Figures 19 through 22 were further smoothed by hand to obtain 1-hour average streamline heights.

Included on the figure are computed curves of $n_m/H*$ versus $(ZA-H_c)/H*$ derived for potential flow over a circular cylinder and potential flow over a sphere. Although neither hill shape is appropriate for CCB, each represents a convenient limiting hill shape to represent flows over a well-defined, three-dimensional hill (sphere) and a well-defined, two-dimensional ridge (cylinder). (Potential flow calculations are appropriate for estimating streamline paths in nonstratified flows as long as the streamline height is above the strongly sheared layer close to the surface.)

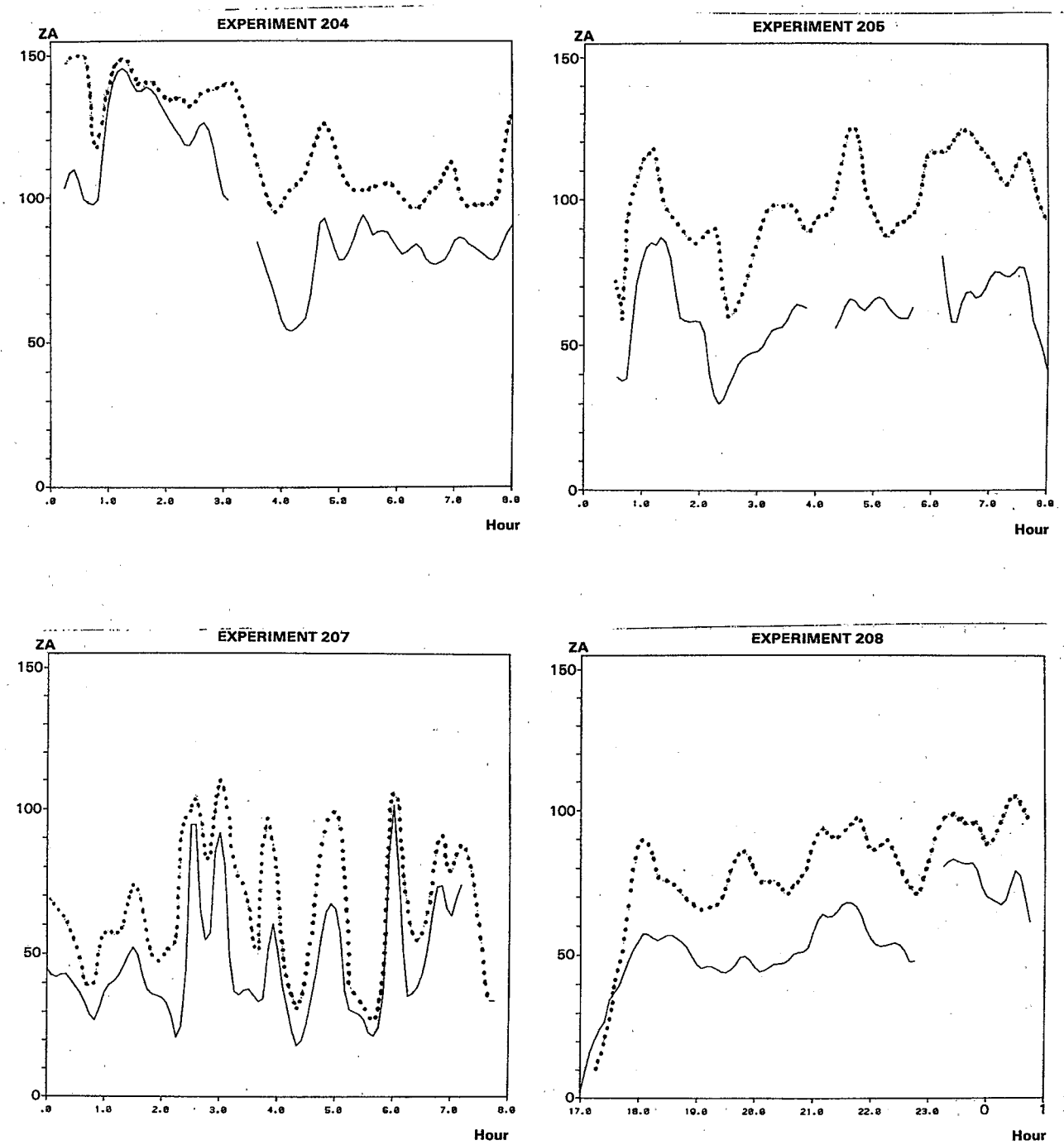

Figure 20. Estimated upwind height (ZA) of streamlines that pass through the 10 m (——) level and 30 m (...) level of Tower B on the crest of Cinder Cone Butte during Experiments 204 - 208.

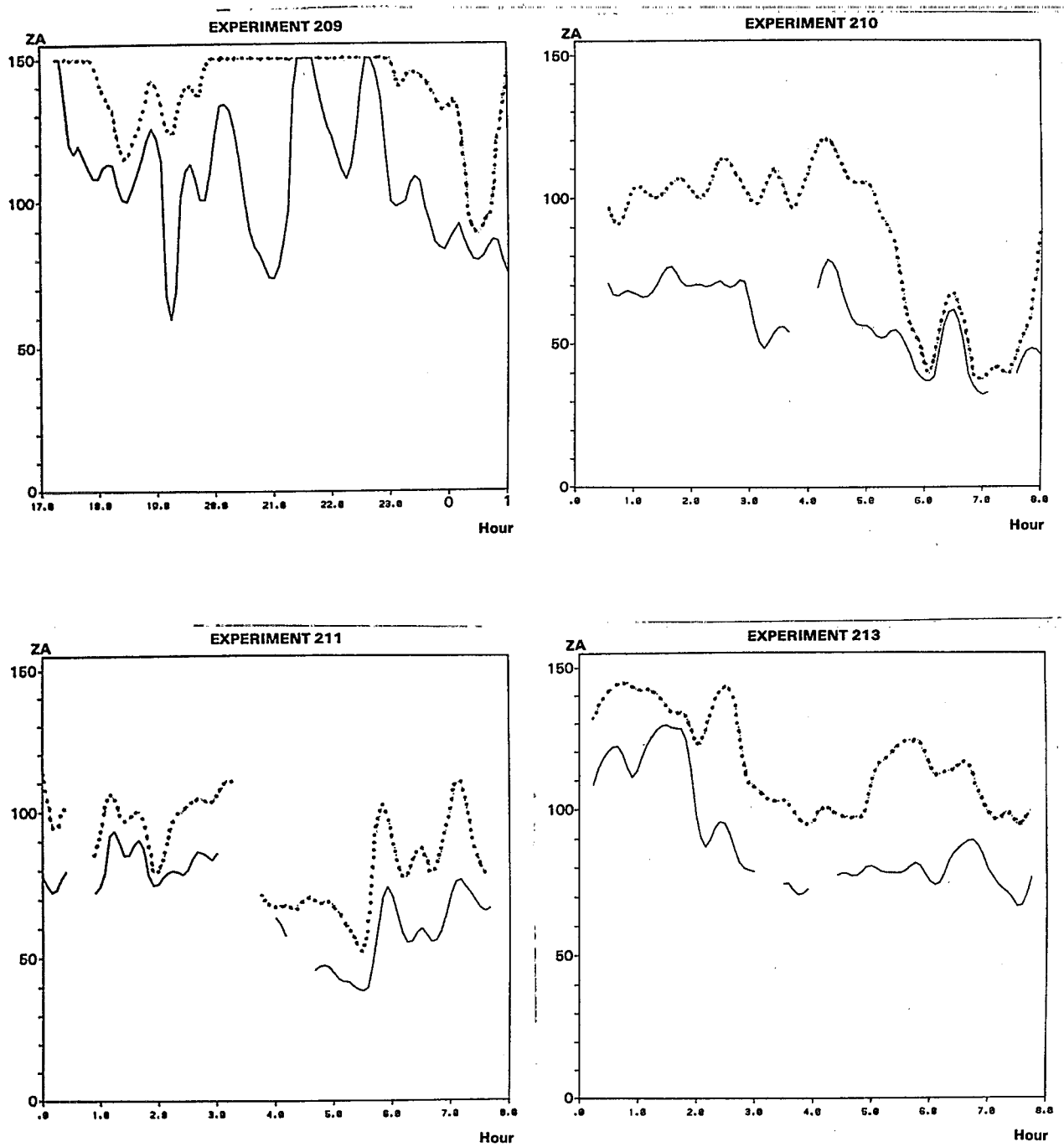

Figure 21. Estimated upwind height (ZA) of streamlines that pass through the 10 m (——) level and 30 m (...) level of Tower B on the crest of Cinder Cone Butte during Experiments 209 - 213.

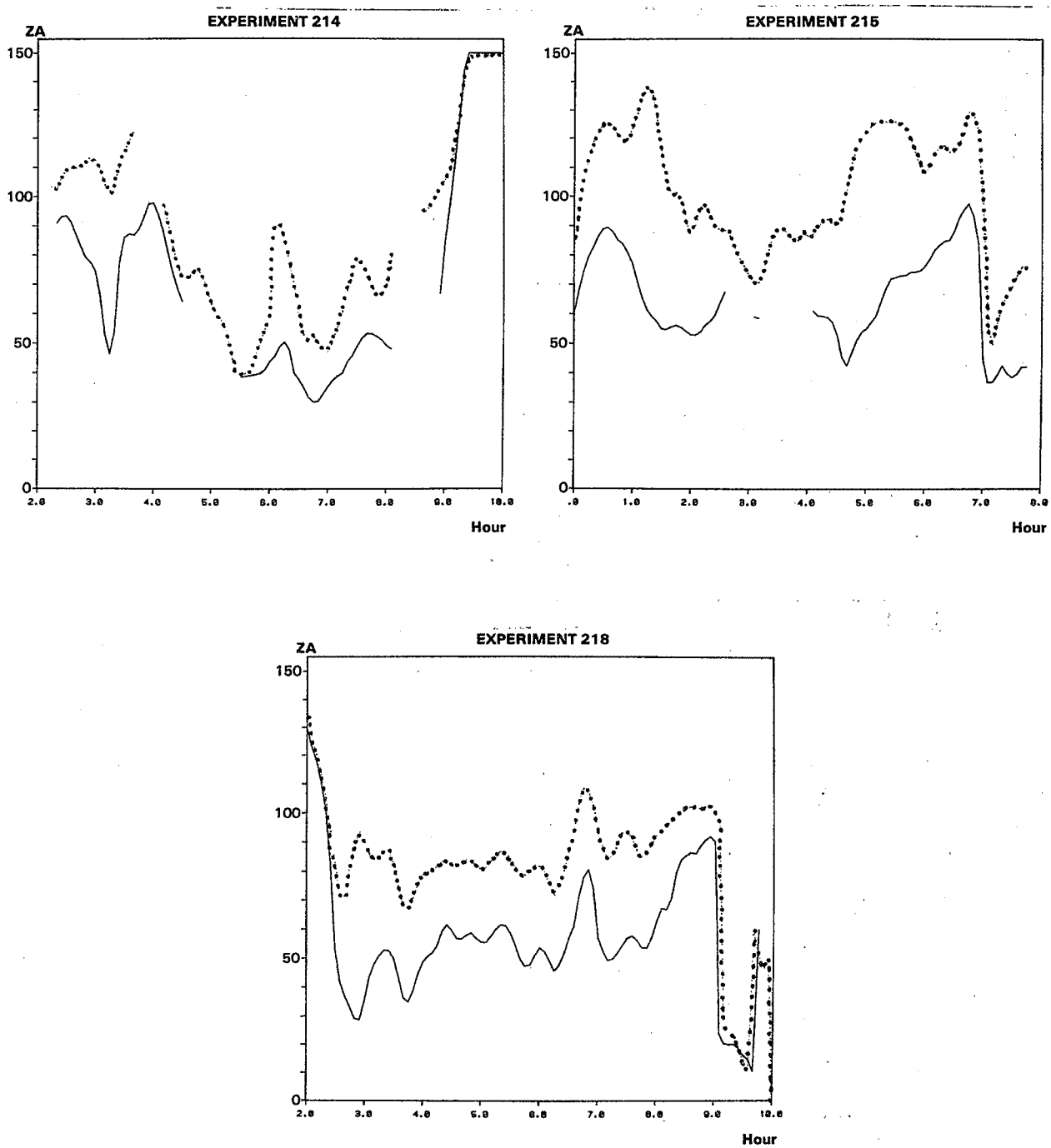

Figure 22. Estimated upwind height (ZA) of streamlines that pass through the 10 m (——) level and 30 m (...) level of Tower B on the crest of Cinder Cone Butte during Experiments 214 - 218.

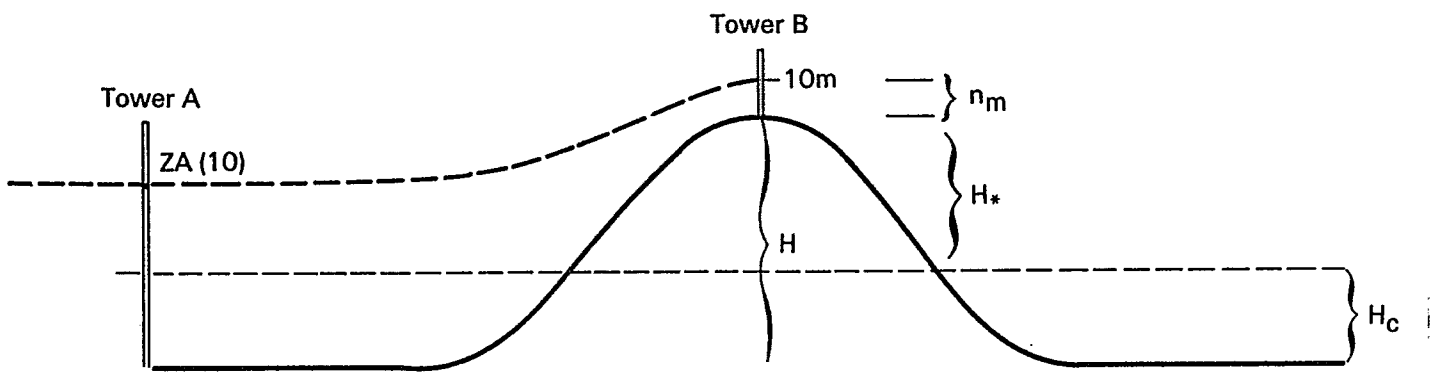

Figure 23. Relationship between inferred streamline heights, the dividing streamline height H_c, and the quantities n_m, ZA.

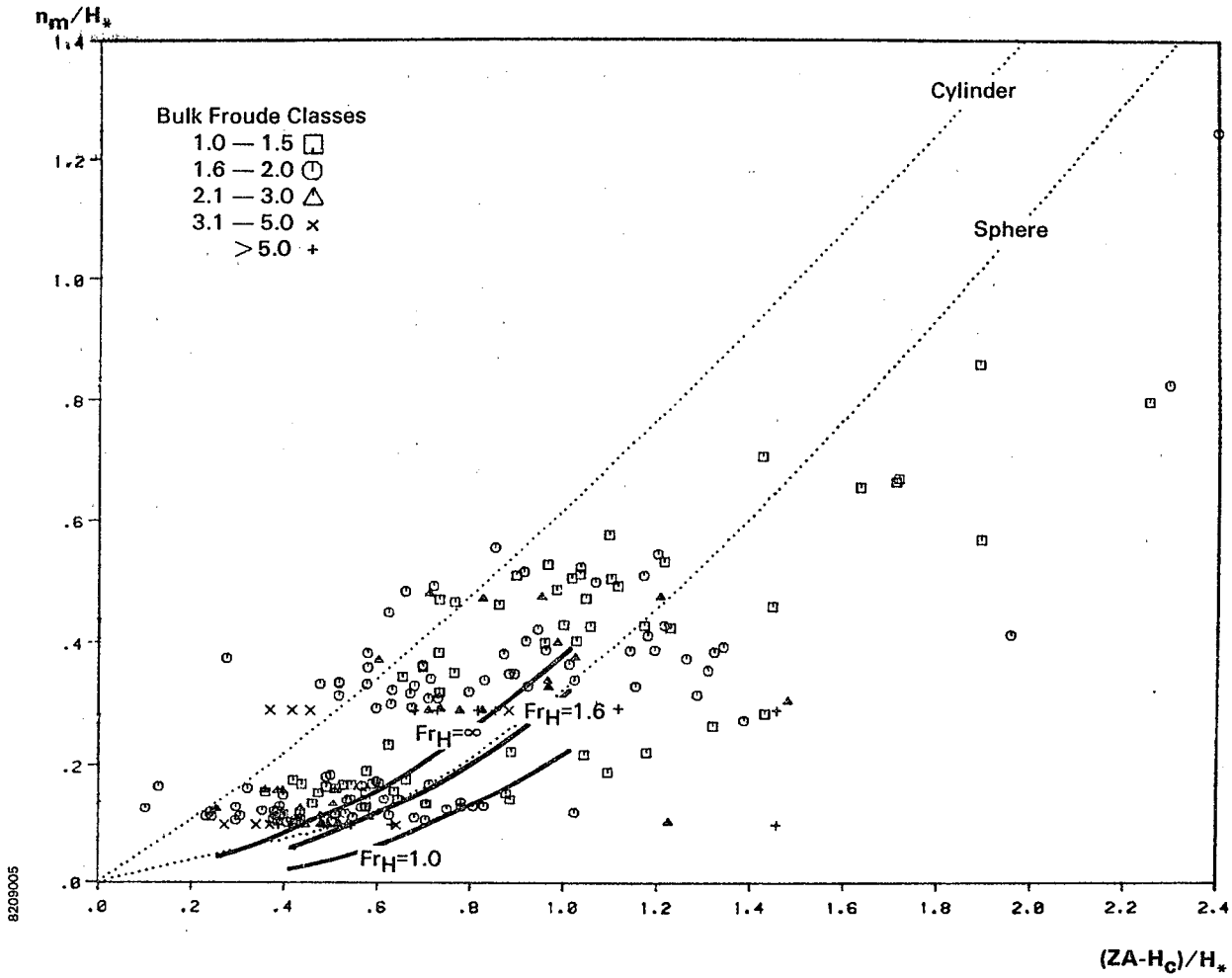

Figure 24. Height of the source streamline (n_m) above the crest of CCB for various effective source heights ($ZA-H_c$) inferred from temperature measurements at Tower A and Tower B. Values are scaled by the effective hill height (H_*).

Note: Dotted lines represent potential flow computations, and solid lines are taken from EPA FMF experiments (Hunt et al. 1978).

Results obtained in the EPA Fluid Modeling Facility tow tank and wind tunnel studies of flow over a bell-shaped hill are also presented in the figure. The dashed lines represent tow tank results for Froude numbers of 1.0 and 1.6 and wind tunnel results for a Froude number of infinity (i.e., unstratified flow).

A comparison of streamlines derived from temperature data measured at CCB, streamlines calculated with potential flow theory, and streamlines created in physical modeling experiments suggests that the flow above the critical dividing streamline height may be modeled as weakly stratified or near-neutral flow. The use of a neutral flow model that treats the layer of air below H_c as "dead" in terms of its effect on the dynamics of the flow above has some merit. Many of the points lying to the right of the potential flow curves fall into the lower Froude number classes, thus following the trend exhibited in the physical modeling of weakly stratified flows. The bulk of the data points falls between the two curves calculated from potential flow theory. Because CCB has a shape between these two extremes, this result indicates that the flow above H_c may behave like unstratified flow much of the time. But note that this analysis addresses streamline behavior only over the crest of the hill; many of the flows characterized as "nearly neutral" on the figure could also have pronounced lee wave effects.

SECTION 4

CASE STUDY ANALYSES

Detailed analyses of several of the hours modeled in the first milestone report are presented in this section. In looking at these hours, we assess the ability of the modeling algorithms discussed in Section 3 to reproduce tracer concentrations measured over the hill surface. This assessment uses all available information, including photographic and lidar data.

A primary determinant in choosing a subset of the 45 hours modeled in the previous report is how well particular hours were modeled by the Neutral and Impingement models. Those hours for which these models did either well or poorly were identified, and a subset of 14 were selected according to whether the SF_6 release was above or below the critical dividing streamline, and also according to the quality and availability of photographic and lidar data. A summary of the criteria for these 14 hours is presented in Table 3.

4.1 Experiment 202, Hour 4 (2000-2100 MST)

4.1.1 Summary Description

Thermofogger oil-fog and SF_6 tracer gas were released from the northwest side of the hill for the entire hour. The release crane was positioned at 1014.6 m, 319.0° at the start of the experiment, and the release height of 20 m was established at the start of the previous hour. Therefore, the tracer plume was well established by the beginning of hour 4.

Local terrain elevations near the release point are estimated to be -7.0 m relative to the zero of the hill coordinate system, so the net release height corresponds to the 13 m height level on the hill. The SF_6 release rate is computed to be 0.082 g/s with an estimated uncertainty of $\pm$0.5%. No Freon was released.

Plume Observations

During the course of this experiment, several people recorded their observations about the appearance of the oil-fog plume and its trajectory. Very few of these observations apply to this hour, however; those that do are presented below.

Time: 1950 It is really cold outside the sampler trailer. Plume appears to be going to the SW, although it might be striking the W knoll. From my viewpoint here the plume is only visible halfway to the

TABLE 3

SUMMARY OF DATA USED TO SELECT CASE STUDY HOURS

Experiment	Hour	$U_o(z_r)$ (m/s)	z_r-H_c (m)	Photo Quality	Lidar	Neutral Model* Max C_p/C_o	Neutral Model* $\overline{C_p/C_o}$	Impingement Model* Max C_p/C_o	Observed** Max C_o/Q
202	4	6.0	16	Fair	Yes	0.71	1.47	0.15	81.6
202	5	6.5	21	Fair	Yes	0.90	0.94	0.03	49.2
204	1	2.0	-33	Good	Yes	1.78	12.11	3.49	14.5
205	4	5.5	22	Excellent	Yes	1.17	1.67	1.73	15.4
205	5	6.0	25	Excellent	Yes	0.30	0.56	0.43	25.5
206	4	4.0	11	Excellent	Yes	0.23	0.47	2.98	56.7
206	6	2.0	-5	Excellent	Yes	0.69	1.20	1.02	124.5
206	8	2.5	-1	Fair	No	0.15	0.30	0.15	154.6
209	1	3.5	33	Excellent	Yes	8.83	34.00	5.94	3.8
209	7	2.0	-20	Poor	No	0.27	0.31	29.17	7.6
210	3	5.5	27	Excellent	Yes	0.31	0.42	3.87	11.5
210	7	6.5	42	Excellent	No	0.92	4.75	1.08	8.1
211	1	1.5	-18	Good	Yes	1.53	2.58	1.23	11.5
211	5	2.0	-8	Excellent	No	0.33	0.77	0.23	97.4

Note: These data are taken from the first milestone report and do not reflect changes in the meteorological and air quality data base.

*Ratio of modeled (C_p) to observed (C_o) SF_6 concentrations. "Max" is the ratio of the maximum calculated and maximum observed concentrations irrespective of location on the hill.

**C_o/Q has units of $(\mu g/m^3)/(g/s)$

butte. It's hard to say what it's doing when it reaches the hill. There is quite a bit of mixing. Conditions continue to be quite unstable.

Time: 1958 I'm watching the mobile crane doing its first transect.

Time: 2053 I've asked the release crew to bring the generator down at 2100, refuel it, and put it back up at 30 meters.

Photographs of the plume provide additional information. The photographs indicate that the wind direction was fairly steady over this hour. In each exposure, the plume appears to be heading toward the south peak of the hill, although the fog becomes too diffuse to tell if it actually heads into the northwest draw or passes around to the south of the hill. Plume trajectories over or around the hill cannot be discerned. Only the first 100 m to 200 m of the trajectory are visible, and this portion appears to be very level. The dispersion of the plume also appears to be unchanging over the hour. Little if any differences are noted in the photos taken from the side.

Lidar data are quite extensive during this hour, showing that the plume trajectory was very steady over the hour. Three planes were sampled by the lidar: two upwind of the hill, and the third just downwind. Plume centroid positions derived from the lidar along these planes are plotted in Figure 25, which indicates how the centroid moved in time. The numbers next to the positions label 5-minute periods associated with each dot (e.g., the centroid position measured at some point during the 5-minute period from 2025 to 2030 is labeled by a "6".) Plume centroid positions in Figure 25 indicate that the plume spent much if not all of its time along the southwest slope of the hill. Plume paths closest to the hill center occur in the latter half of the hour.

Estimates of the wind angle at the release point are made using the plume centroid positions in lidar sampling planes upwind of the hill. These calculations are made with the following assumptions: the calculated centroid of the instantaneous smoke distribution is representative of a 5-minute mean plume centerline position, plume centerline curvature caused by the presence of the hill is negligible at the upwind sampling planes, and potential inaccuracies in the source position and the lidar position are small. Calculated trajectories from the source to the first sampling plane indicate that the wind direction at the start of the hour was nearly 332°, changing to 337° for most of the first half hour. Wind directions in the last half hour varied between 329° and 331°. Because the source was located at a bearing of 319° from the hill center, the plume traveled to the southwest side of the hill.

Trajectory angles are also computed using the second lidar sampling plane (closer to the hill) and the source position. Although the influence of the hill may be greater, errors in the source location relative to the centroid positions have a smaller effect on the trajectory calculation. These calculations produce wind directions of 332° to 335° in the first half hour, and 327° to 329° in the second half hour.

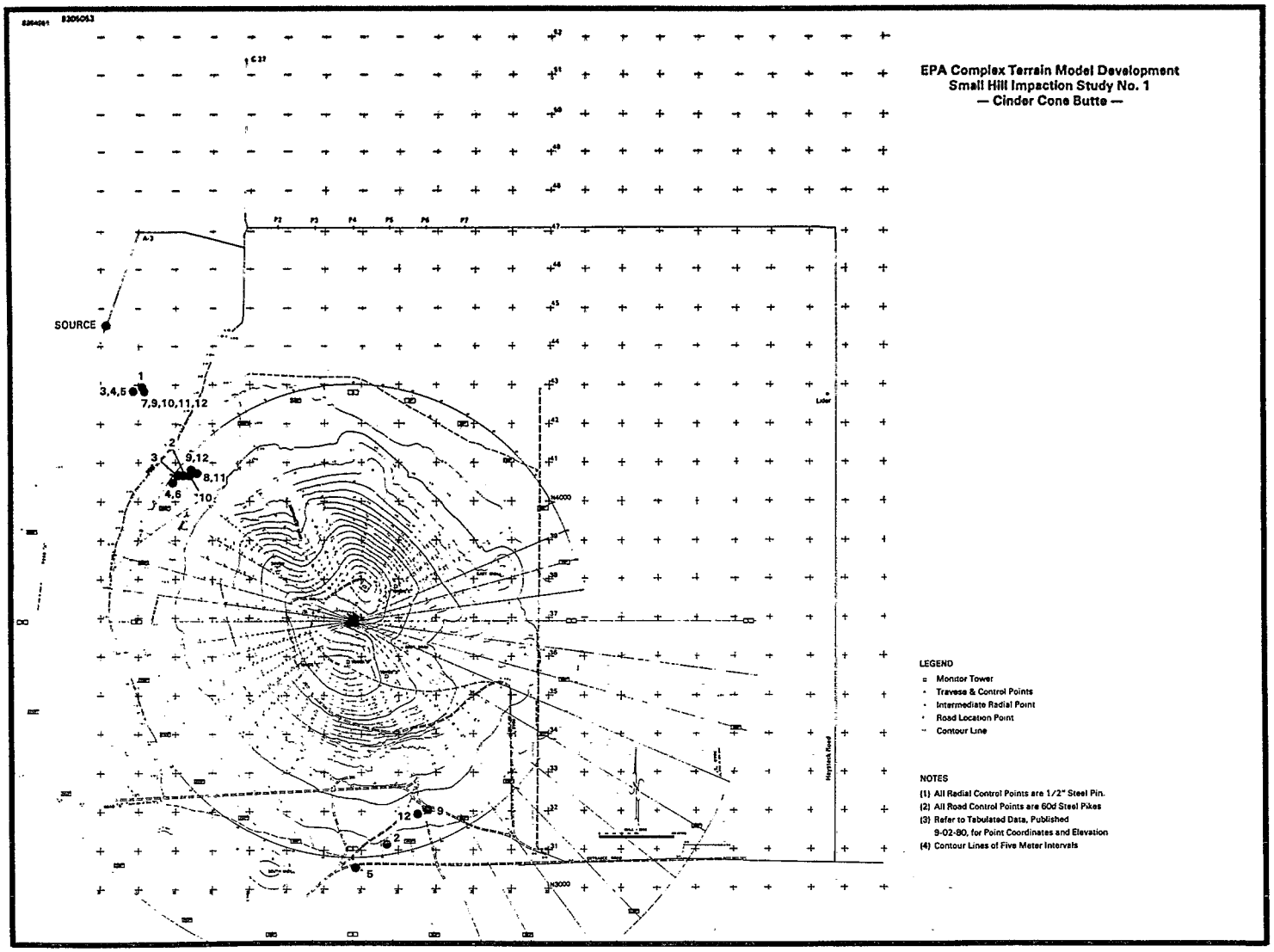

Figure 25. Plume centroid positions calculated from lidar data. Experiment 202, Hour 4 (2000-2100 MST).

Meteorological Information

Wind and temperature data measured at tower A during this hour are used to characterize the flow in terms of the critical dividing streamline height, H_c (see Section 2.1, Equation 2). All wind data used in this section are taken from the UVW propellor wind sets rather than a combination of prop data and cup (and vane) data. The cup data were not explicitly included because these data were measured only at the 2-m, 10-m, and 150-m levels where the data capture by the UVW systems was good, and because the wind data corrections discussed in Section 5 provided an adequate degree of agreement between these cup and prop data. The hourly average of the calculated 5-minute H_c values produced an hourly average H_c that is interpreted to be zero, indicating that none of the flow was forced around (rather than over) the hill. This is also reflected in the value of the hill bulk Froude number for the layer between H_c and 150 m: $Fr_H = 2.5$. The corresponding bulk Froude number based upon the horizontal length scale of the hill is a quarter of this value (H = 100 m, L = 400 m): $Fr_L = 0.625$. These Froude numbers indicate that although all streamlines may have passed freely over the top of the hill, there may have been enough stratification to produce some streamline depression in the lee of the hill.

Figure 26 contains a time series plot of the calculated 5-minute values of H_c and Fr_H for all of Experiment 202. The minimum value of H_c in this figure is 1 m, but because we have no data below 2 m, any value less than 2 m is interpreted as an indication that all streamlines are able to pass over the hill. The data show that a stable layer was just starting to form near the ground during the fourth hour of the experiment but did not become strong enough to block any flow over the hill. The Fr_H plot also shows a weak trend toward a more stable atmosphere during the hour. Because these variations within the hour are small, the 1-hour average values adequately characterize the hour.

Hourly average wind speeds measured by the UVW props at 10 m and 40 m are 5.6 and 9.5 m/s, respectively. The 10 m winds are from 324°, as are the 40 m winds, so the winds were strong and unidirectional across the layer containing the plume. Figure 27 shows the trend in the wind speeds over the hour. The '+' symbols in the figure denote 5-minute values that were interpolated in time. Because the variation is small, the 1-hour average winds characterize the hour very well.

The variation of wind directions measured at tower A at 10 m and 40 m are shown in Figure 28 as frequency distributions. Both distributions are very narrow; this bears out the observations and photographs discussed above. These distributions were computed from the 5-minute average wind directions. However, whenever the recorded data were judged to be bad, missing, or otherwise unavailable, time-interpolated values were used. The method for constructing the distribution is similar to that described in Section 3.1.4, except no use is made of the 5-minute σ_y values.

In summary, this hour is characterized as a high wind speed near neutral hour, with winds very steady both in time and in height.

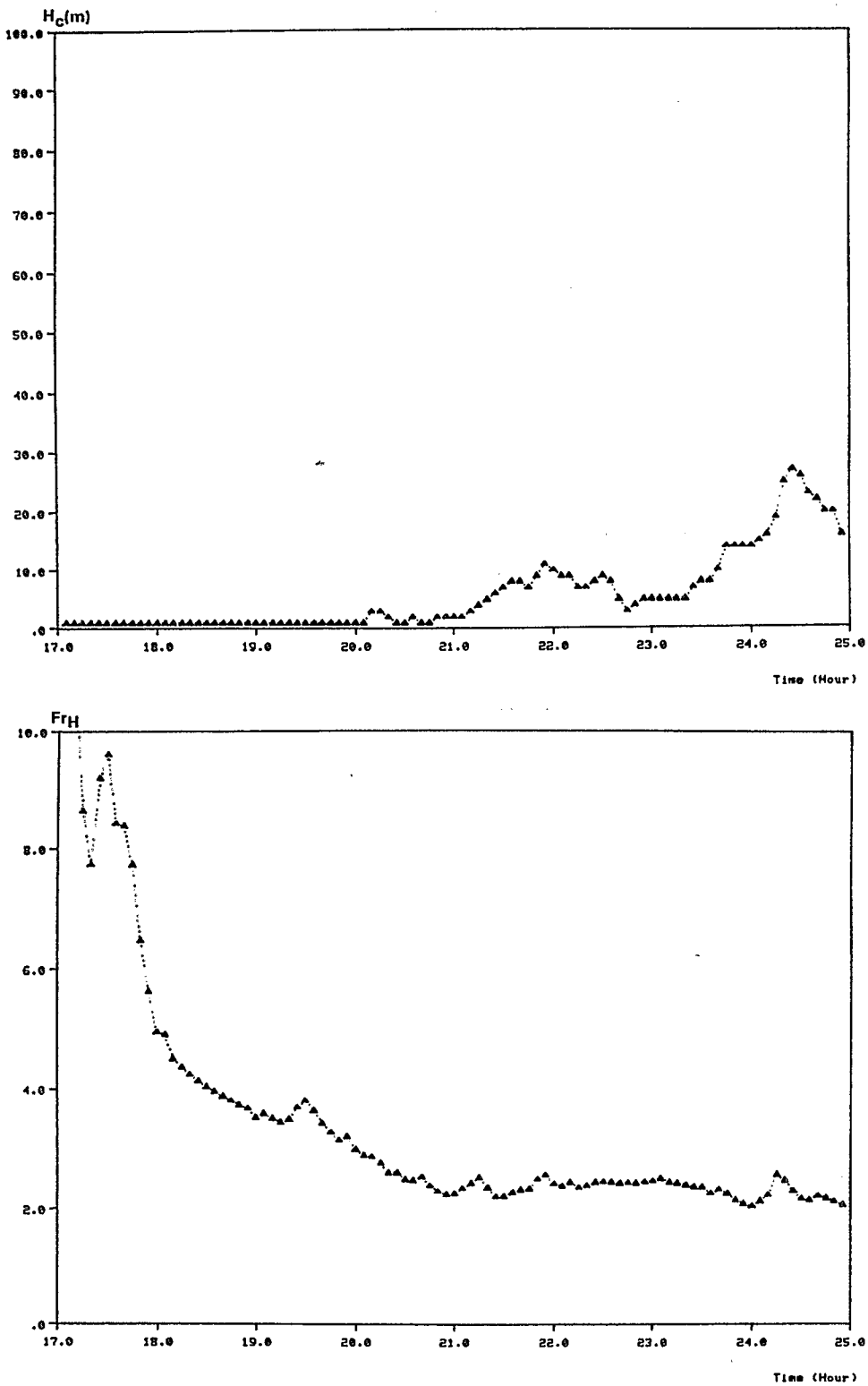

Figure 26. Calculated dividing streamline heights (H_c) and bulk hill Froude numbers above H_c (Fr_H) for Experiment 202.

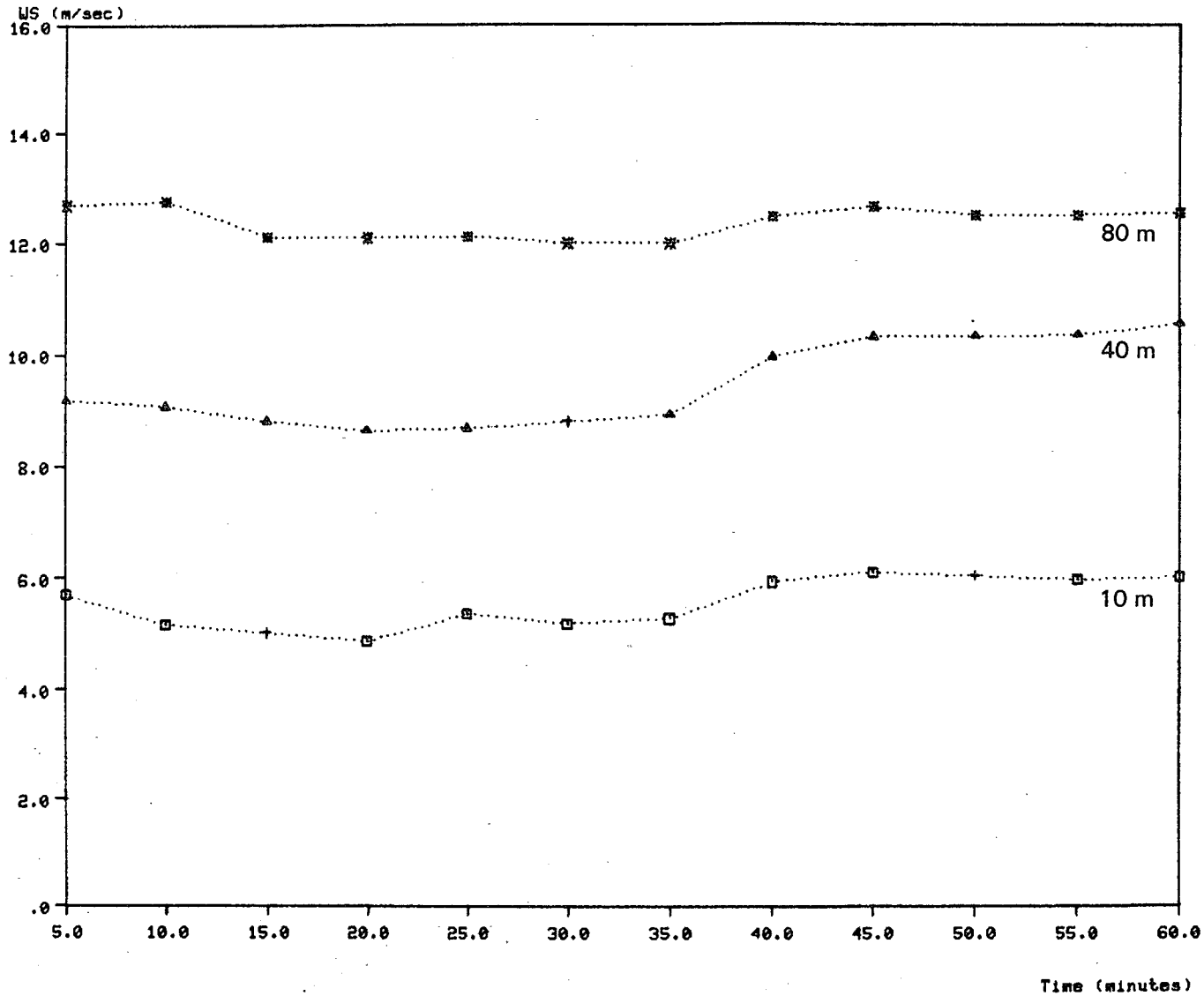

Figure 27. Tower A wind speeds during Experiment 202, Hour 4 (2000-2100 MST).

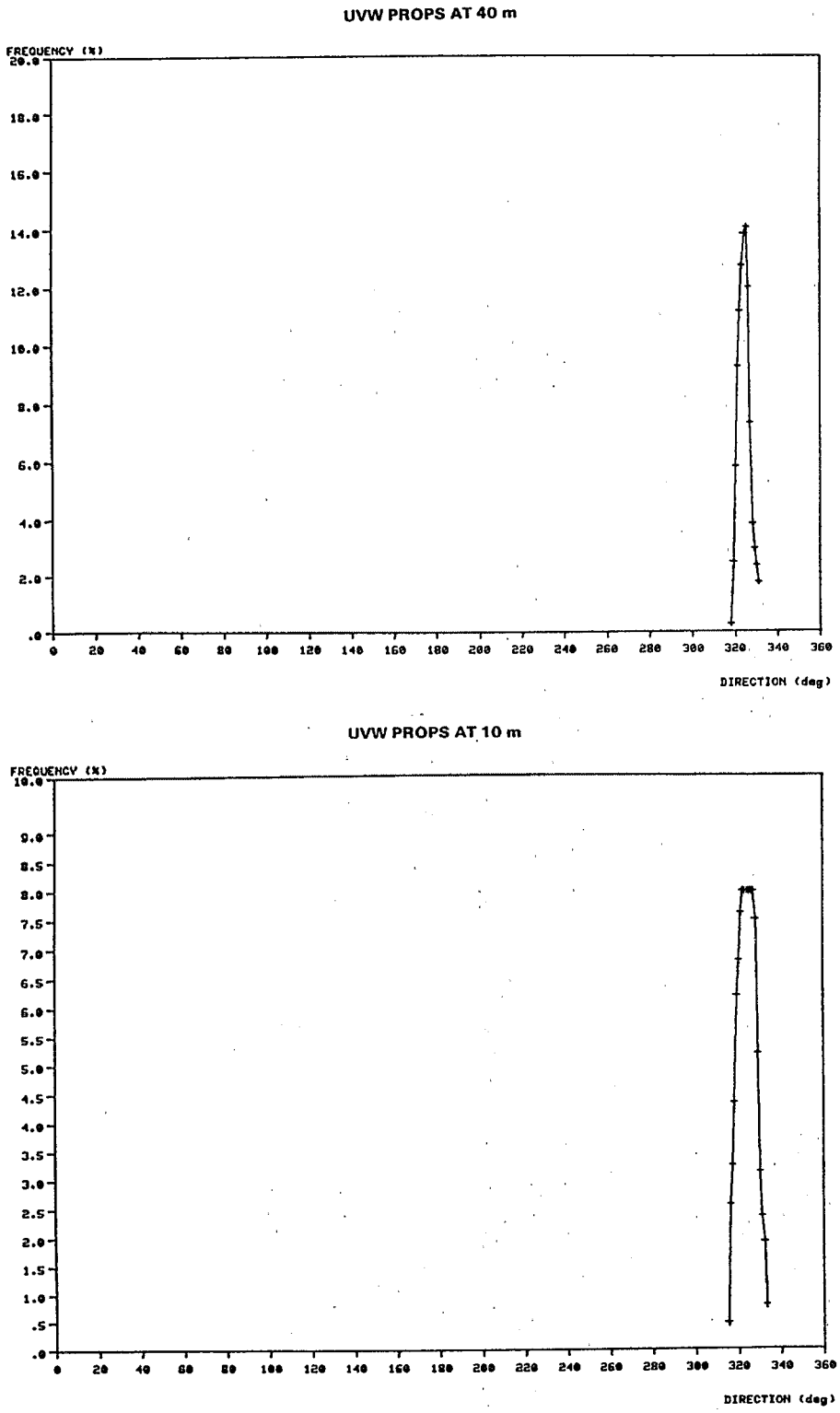

Figure 28. Calculated wind direction distribution functions for Experiment 202, Hour 4 (2000-2100 MST).

SF_6 Concentrations

The distribution of hourly averaged SF_6 concentrations over the hill surface is shown in Figure 29. All concentration labels are placed so that the lower left-hand corner of the right-most digit lies at the sampler location. Height contours are presented at 10 m intervals, beginning with the 5 m height contour. The zero height coincides with 945 m (3,100 ft) above sea level. The grid marks radial distance increments of 100 m and angular increments of 22.5°.

A trail of the highest concentrations extends from the western edge of the hill across the southwestern face. Little plume material was measured on the other sides of the hill. The largest concentration was recorded between the 10 m and 15 m height contours on the ridge that forms the southern side of the northwest draw. Because this height is very close to the relative height of the SF_6 release (13 m); the plume may have risen very little in flowing past the edge of the hill. Other concentrations, higher on the hill, indicate that plume material rose occasionally up the ridge toward the south peak.

All available 10-minute average SF_6 concentrations are presented in Figure 30, and although the coverage across the hill is considerably less than that for the 1-hour average samplers, the data do show that the plume shifted more toward the south peak of the hill at times. This is most evident from 2030 to 2100, as indicated in the lidar data.

4.1.2 Model Performance

This hour has been modeled with the Lift model because all the evidence indicates that streamlines at plume height traveled freely over the hill rather than being forced onto and around the sides of the hill. Meteorological data for the modeling has been constructed from temperature and UVW prop measurements at tower A. Measured values at 10 m and 40 m were used to estimate those for the 20 m release height.

The Lift model requires the following input information:

- average emission rate (g/s),
- release height (m),
- average dividing streamline height (m),
- source location coordinates r (m) θ (degrees),
- average wind speed (m/s),
- average wind direction (degrees),
- average Brunt-Vaisala frequency (1/s),
- average bulk hill Froude number,
- horizontal and vertical turbulence intensities, and
- wind direction probability distribution function (PDF).

Of these, the wind speeds and distributions were interpolated to release height, the Brunt-Vaisala frequency was calculated from the local temperature gradient at release height, and the PDF was selected from what

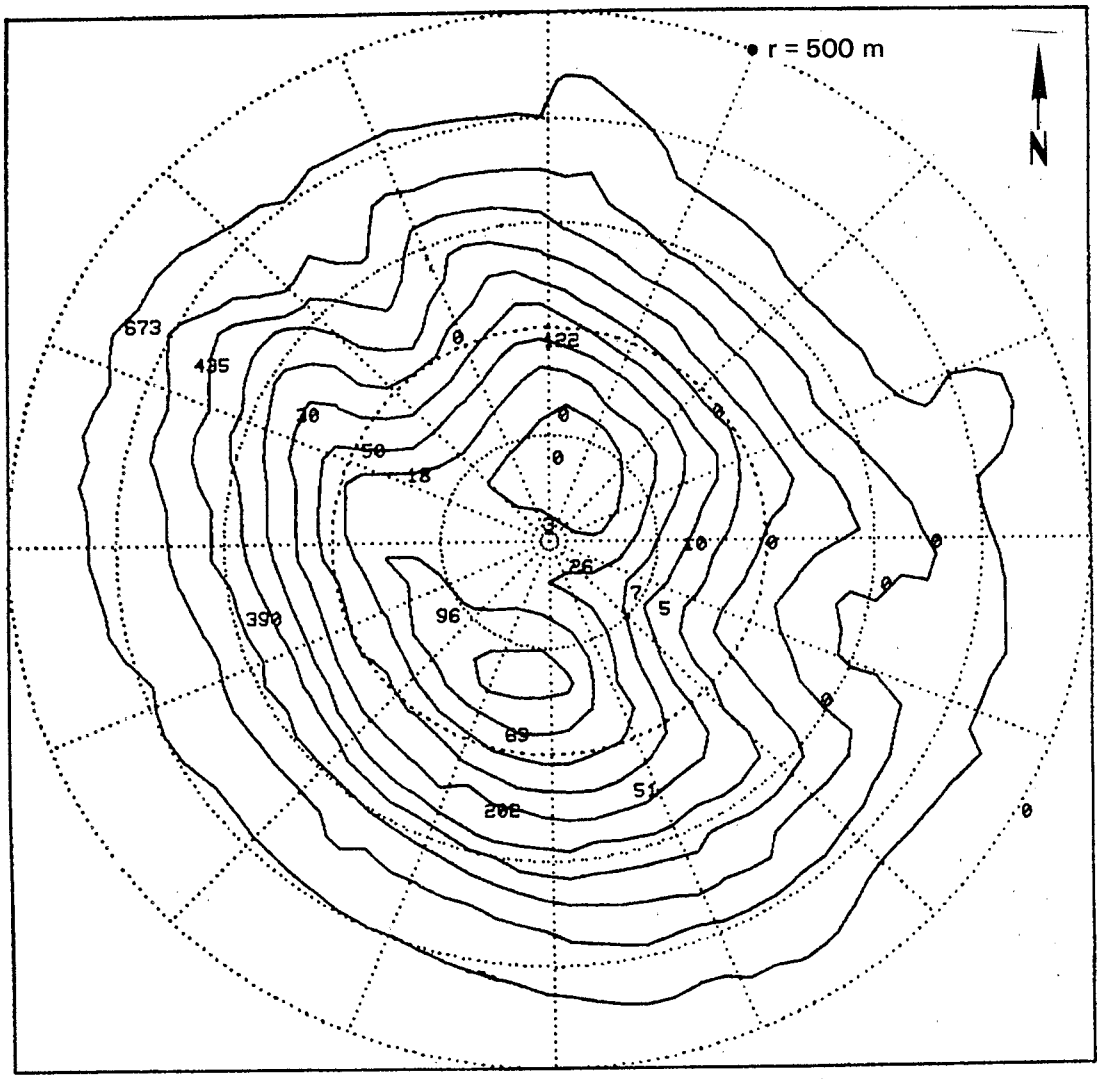

Figure 29. Observed SF_6 concentrations (ppt) for Experiment 202, Hour 4 (2000-2100 MST). Source: r = 1014.6 m, θ = 319.0°, net height = 13 m, Q = .082 g/s.

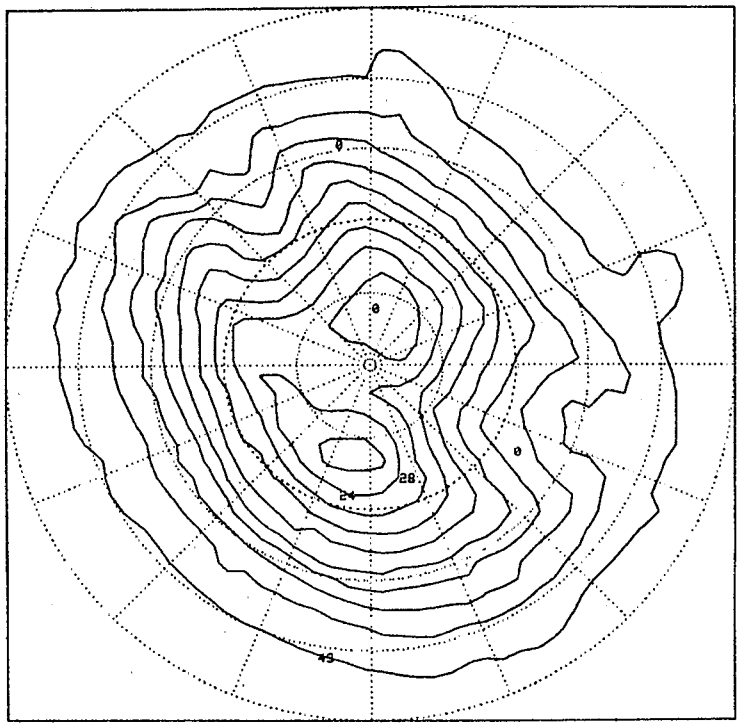

TIME PERIOD 2000-2010

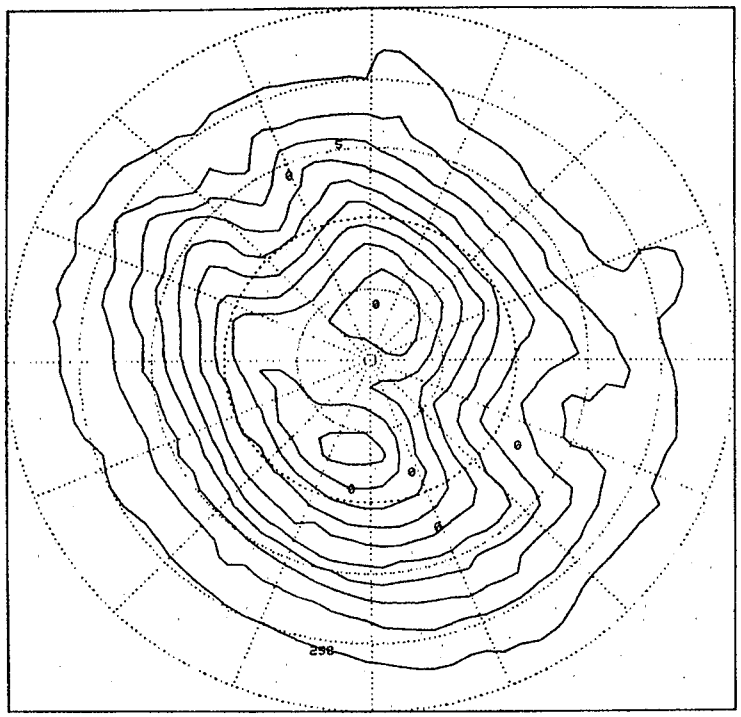

TIME PERIOD 2010-2020

Figure 30. Observed 10-minute averages SF_6 concentrations (ppt) for Experiment 202, Hour 4 (2000-2100 MST).

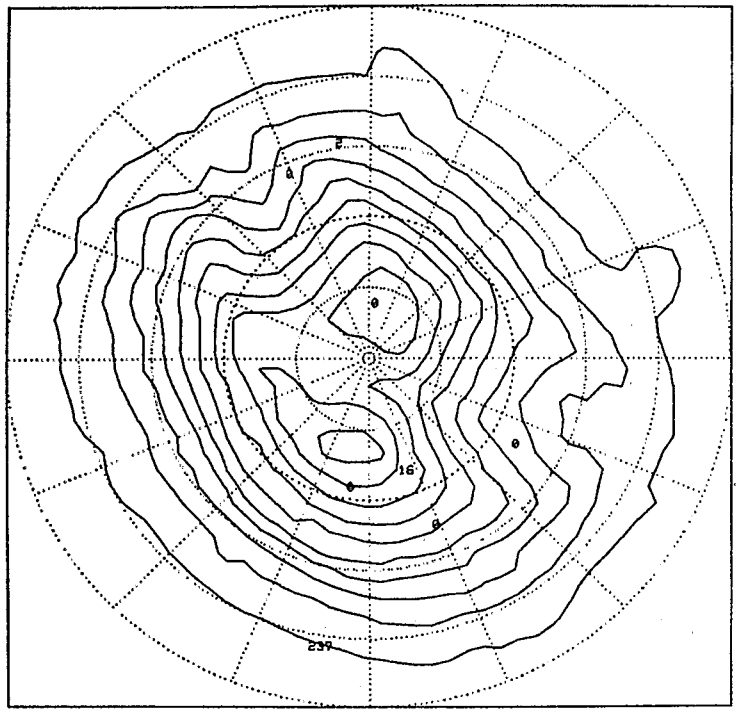

TIME PERIOD 2020-2030

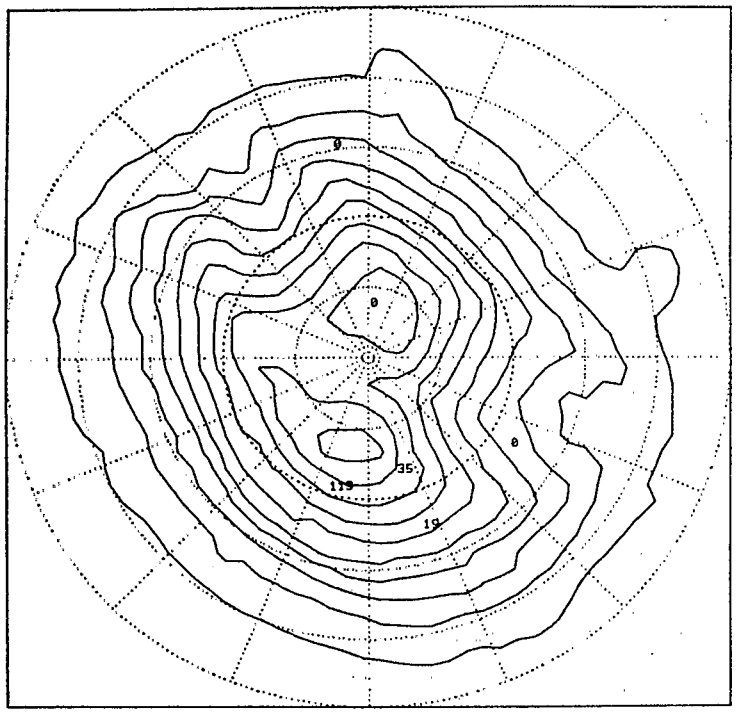

TIME PERIOD 2030-2040

Figure 30. Continued.

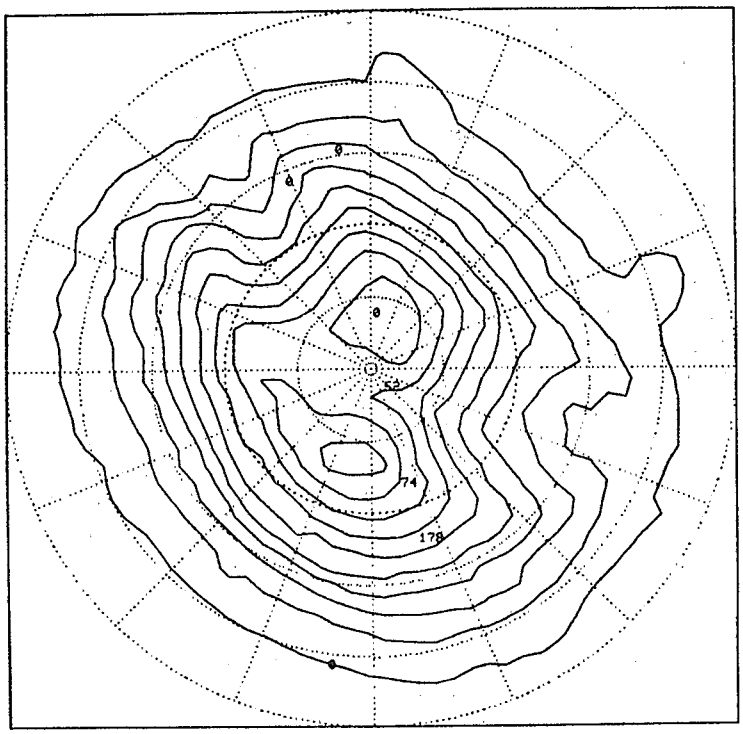

TIME PERIOD 2040-2050

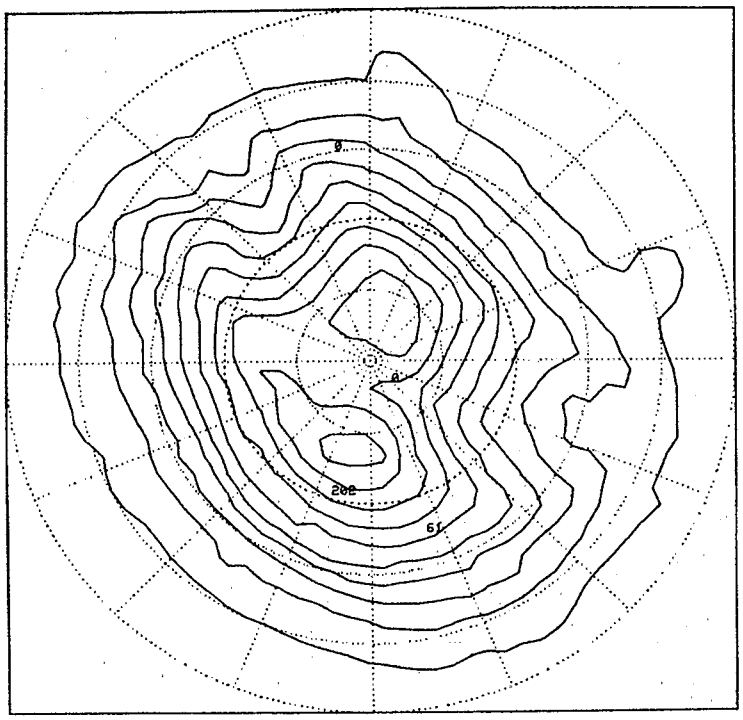

TIME PERIOD 2050-2100

Figure 30. Continued.

is thought to be the most representative instrument level. All other information pertains to either the flow as a whole or to the specifics of the tracer release.

Wind speed interpolation was performed with a power law. Speeds at 10 m and 40 m were used to determine the exponent, and the speed at 20 m was interpolated from the speed at 10 m with this exponent.

Turbulence data were interpolated linearly. The turbulence intensities at 10 m and 40 m were multiplied by the wind speeds at those levels to produce σ_v and σ_w at 10 m and 40 m. The values of σ_v and σ_w were then interpolated to 20 m and divided by the calculated wind speed at 20 m to produce the turbulence intensities at source height. This method was chosen because σ_v and σ_w are nearly constant with height in many cases. Furthermore, when σ_v or σ_w vary significantly with height, there is no apparent pattern (i.e., always increasing, or always decreasing with height) so that linear interpolation is used in these cases as the simplest interpolation method.

Wind directions were not interpolated to release height. Instead, the 1-hour averaged wind directions measured at the tower A measurement levels nearest the local release height were compared with wind directions measured at 10 m and 30 m on top of the south peak, and with plume trajectory information obtained from plume photographs, lidar data, and observer comments. The wind direction thought to be most consistent with these sources of information was chosen for the modeling.

During the fourth hour of Experiment 202, mean tower A wind directions at the nearest levels above and below the release height were both 324°. However, the directions at 10 m and 30 m on tower B were 328° and 329°, respectively; and plume trajectories inferred from lidar data varied from 327° to 335°. Because the plume trajectories sampled by the lidar are judged to be shifted a little to the south and because the directions at tower B are influenced by the topography of CCB, a wind direction of 327° was selected for modeling. The PDF considered most appropriate is that derived from the 40 m level of tower A because the 20° spread in the 10 m PDF at tower A is not consistent with the lidar data. Model input data are summarized in Table 4.

Because the meteorological data and tracer concentrations used in running the model have been changed since the first milestone report (see Section 5), the Neutral model has been rerun for this hour with the revised data. The Neutral model had produced a peak concentration that was 71% of the peak observed concentration. With the refined meteorological and SF_6 data, it also calculates a peak concentration that is 71% of the peak observed value.* The location of the peak modeled concentration in both cases is the same, and the spot lies just uphill from the peak observed concentration. Modeled concentrations across other parts of the hill are

*The new runs of the Neutral model also used the local source height rather than the source height relative to the hill coordinate system. This raises the plume 7 m in this application.

TABLE 4. NEUTRAL AND LIFT MODEL CALCULATIONS - EXPERIMENT 202, CASE HOUR 4

Meteorological Data

wind direction(deg)	=	327.
wind speed(m/s)	=	7.3
critical dividing streamline height(m)	=	.0
Iz	=	.041
Iy	=	.054
N(1/s)	=	.037

Source Data

direction(deg)	=	319.
distance(m)	=	1014.6
release height(m)	=	20.0
SF6 emission rate(g/s)	=	.082

Receptor Coordinates X(m)	Y(m)	Z(m)	Observed SF6 (ppt)	Neutral Predicted SF6 (ppt)	Lift Predicted SF6 (ppt)
360.22	.00	13.26	.00	.00	.00
208.35	.00	31.25	.00	.05	.00
142.00	.00	50.00	9.70	1.92	.00
159.04	122.04	46.91	.00	.05	.00
15.97	121.29	90.94	.00	2.52	.00
10.61	80.56	91.97	.00	4.83	.00
25.15	190.88	65.00	122.10	.27	.00
2.15	18.88	80.00	2.90	10.62	.00
-32.79	-249.09	48.82	202.20	158.93	317.95
-23.49	-178.46	80.00	68.92	63.31	265.66
-84.85	-65.12	90.00	95.80	38.93	302.24
-248.96	-66.71	32.90	390.00	439.51	70.43
95.80	-231.27	52.96	51.44	53.63	124.78
59.13	-154.04	80.00	30.58	34.79	57.89
441.46	-254.87	-2.45	.00	.00	.00
256.81	-148.27	25.29	.00	.41	.00
108.15	-61.12	50.00	4.70	8.28	.00
82.15	-46.12	60.00	7.00	10.50	.00
312.38	-41.13	14.00	.00	.00	.00
-359.96	207.82	8.94	672.80	243.82	154.79
-297.11	171.54	28.07	434.80	478.47	530.18
-153.85	89.88	70.00	50.40	17.59	188.33
-111.85	65.88	80.00	18.00	14.40	9.16
-80.75	194.94	50.00	.00	.74	.00
-40.46	307.35	30.00	.63	.00	.00

smaller and are more in line with observed concentrations. Figure 31 shows the distribution of SF_6 concentrations calculated by Neutral with the new meteorological data. These data are also tabulated in Table 4.

Results of the Lift model calculations are presented in Figure 31 and tabulated in Table 4. The overall magnitude of the estimated concentrations is similar to that of the Neutral results, but the distribution appears to be too narrow and too far up on the south peak when compared with the observed concentrations. The peak modeled concentration is larger, being 79% of the observed peak concentration. These results indicate that when the wind speeds are strong and fairly steady, the use of a PDF that is not measured at the source position could lead to larger errors than does the use of a Gaussian distribution derived from an interpolated value of i_y. Differences in the ways in which the two models treat the terrain factor and H_c are small for the hour compared to the difference in the horizontal plume spread results.

4.2 Experiment 202, Hour 5 (2100-2200 MST)

4.2.1 Summary Description

Thermofogger oil-fog and SF_6 tracer gas were released from the northwest side of the hill at hour 2111 and continued until 2200. The release crane was positioned at 1014.6 m, 319.0° at the start of the experiment and remained there throughout this hour. Both release heights were set at 30 m, 10 m higher than the previous hour. Consequently, SF_6 measurements during this hour may have captured some of the material released at 20 m just before 2100.

Local terrain elevations near the release point are estimated to be -7.0 m relative to the zero of the hill coordinate system, so the net release height corresponds to the 23 m height level on the hill. The SF_6 rate is computed to be 0.086 g/s with an estimated uncertainty of $\pm 5.7\%$. No Freon was released.

Plume Observations

During the course of this experiment, several people recorded their observations about the appearance of the oil-fog plume and its trajectory. Observations that apply to this particular hour are presented below.

Time: 2115 The plume seems to be headed right toward the shoulder by that tower at this time. It looks to be quite well spread in the horizontal and vertical. It's not looking like the coherent stable plume we had last night, in fact, it has quite a surprisingly vertical extent although it is more visible than it was at 1700, so it is obviously more stable.

Time: 2122 Smoke seems to be possibly going to the south of tower F now.

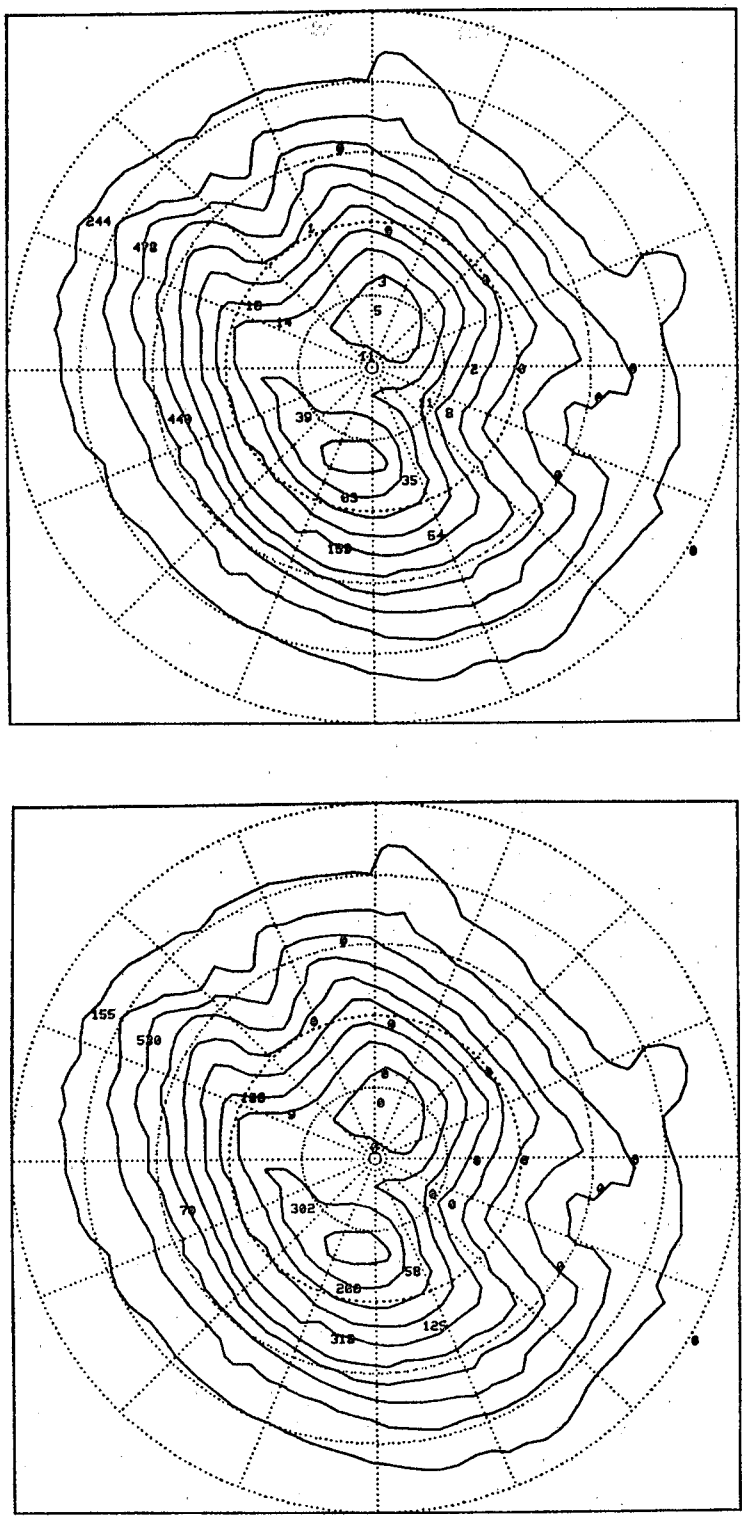

Figure 31. SF_6 concentrations (ppt) estimated for Experiment 202, Hour 4 by the Neutral (top) and Lift (bottom) models.

Time: 2136 From the location of the release crane, it definitely looks like the plume is heading right toward tower F.

These observations indicate that the plume traveled to the southeast, spending much of the time near the ridge along the southwest side of the northwest draw. Consequently, plume material probably passed through the draw and over the saddle at the top of the hill at times.

Photographs of the plume during this hour provide little additional information. The plume photos show the plume traveling toward the hill, but the smoke is too faint to mark the plume path around the hill. Each photo indicates that the plume trajectory was quite steady over the hour. The plume dispersion also appears to be quite steady, although the photos over the last ten minutes show a measurable reduction in the vertical spread of the plume.

Lidar data are quite extensive from 2115 through the end of the hour (the oil-fog was not turned on until 2111). Data were obtained in four sampling planes. Two were upwind of the hill, one was over the center of the hill, and one was just downwind of the hill. Plume centroid positions in each of these planes are plotted in Figure 32 and labeled by 5-minute period.

The centroid positions verify that the wind direction at the release was very steady and transported the plume toward the ridge line on the southwest side of the northwest draw (near tower F). Initial wind trajectories computed with the centroid locations in the lidar sampling plane closest to the source indicate wind directions varying between 329° and 335°. Wind directions derived with the next closest lidar sampling plane vary between 324° and 331°.

Meteorological Information

Wind and temperature data measured at tower A during this hour were used to characterize the flow in terms of H_c. The average of the 5-minute H_c values over the hour is 7 m, which indicates that nearly all streamlines were able to go over the hill. However, because the local release height was 30 m, nearly one-quarter of the flow below the plume height lay below the dividing streamline; the flow above H_c was still quite neutral. The average bulk Froude number from H_c to 150 m is 2.4; thus, Fr_L is 0.6. These Froude numbers indicate that the plume, embedded in the flow above H_c, could pass freely over the top of the hill with a potential for some depression in the lee.

Figure 26 contains plots of the 5-minute H_c and Fr_H values for the experiment. H_c rose steadily through the hour while Fr_H remained constant. This shows that the lower layer was growing but that the balance between buoyancy and inertial forces remained steady in the upper layer.

Hourly averaged wind speeds measured at 10 and 40 m on tower A are 4.7 and 8.9 m/s, respectively. The 10 m winds were from 331°, and the 40 m winds were from 326° and, similar to the winds measured in the previous

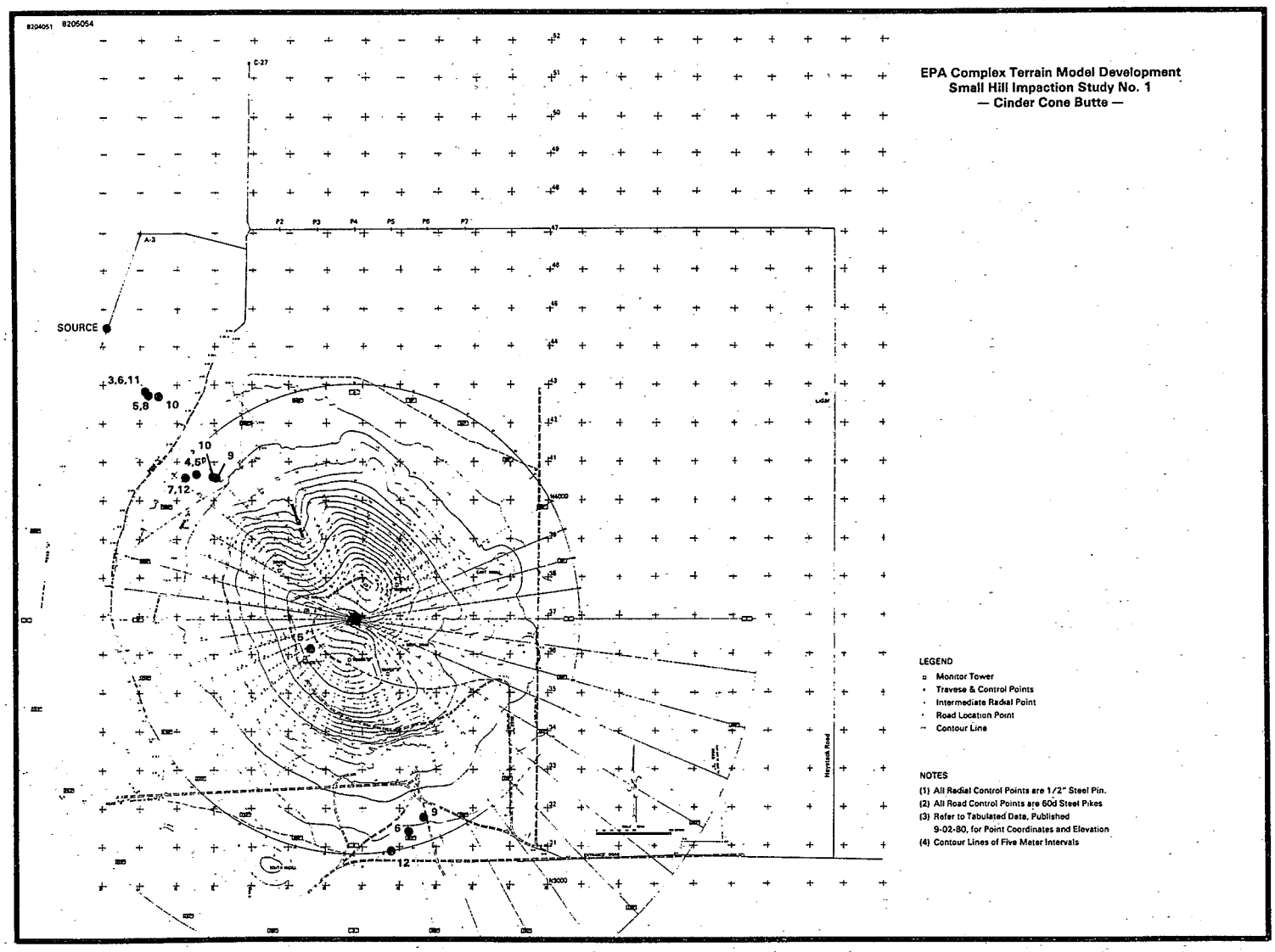

Figure 32. Plume centroid positions calculated from lidar data. Experiment 202, Hour 5 (2100-2200 MST).

hour, are again quite large, with little directional shear across the layer containing the plume. Figure 33 shows the trend in the 5-minute wind speeds over the hour. Because variations in wind speed were small, the 1-hour average winds characterize this hour very well.

Variations in the wind directions measured at tower A at 10 m and 40 m are shown in Figure 34 as frequency of occurrence distributions. Although both distributions are fairly narrow, the 40 m wind distribution is much narrower than the 10 m distributions. Because the tracer plume was released from 30 m, the distribution at 40 m is probably more representative of the meteorology at plume height; this distribution bears out the observations and photographs discussed above.

In summary, this hour was much like the previous hour. The layer containing the plume was near neutral with relatively high wind speeds and little directional wind shear.

SF_6 Concentrations

The distribution of hourly averaged SF_6 concentrations over the hill surface is presented in Figure 35. Although fewer samples were obtained around the south peak than in the previous hour, the overall pattern is similar. High concentrations are again seen along the western side of the hill, and the highest is seen near the 10 m height contour. This is somewhat unusual because the release height in this hour corresponded to a contour height of 23 m. Some plume material collected at the start of the hour could have been released from the lower elevation at the end of the previous hour, but it is not likely that such a dose could dominate the concentration field.

The distribution of 10-minute average SF_6 concentrations is presented in Figure 36. Although no 10-minute data are available in the areas of the largest 1-hour concentrations, there are two samplers on the south face of the hill that do record a relatively small dose of SF_6 during the first 10 minutes of the hour. Because the SF_6 was not turned on until 2111, these concentrations are attributable to SF_6 released at the end of the previous hour, and they indicate that the influence of the release from the previous hour is small.

4.2.2 Model Performance

This hour was modeled with the Lift model because all evidence indicates that streamlines at plume height traveled freely over the hill, as in the previous hour (see Section 4.1.2). The meteorological parameters used in the modeling were prepared in the same way, and are summarized in Table 5.

The tower A 1-hour wind direction measured 20 m below the release height is 331° and that measured 10 m above the release height is 326°. Wind directions at 10 m and 30 m on tower B are 326° and 327°, respectively. Plume trajectories obtained from lidar data range from 324°

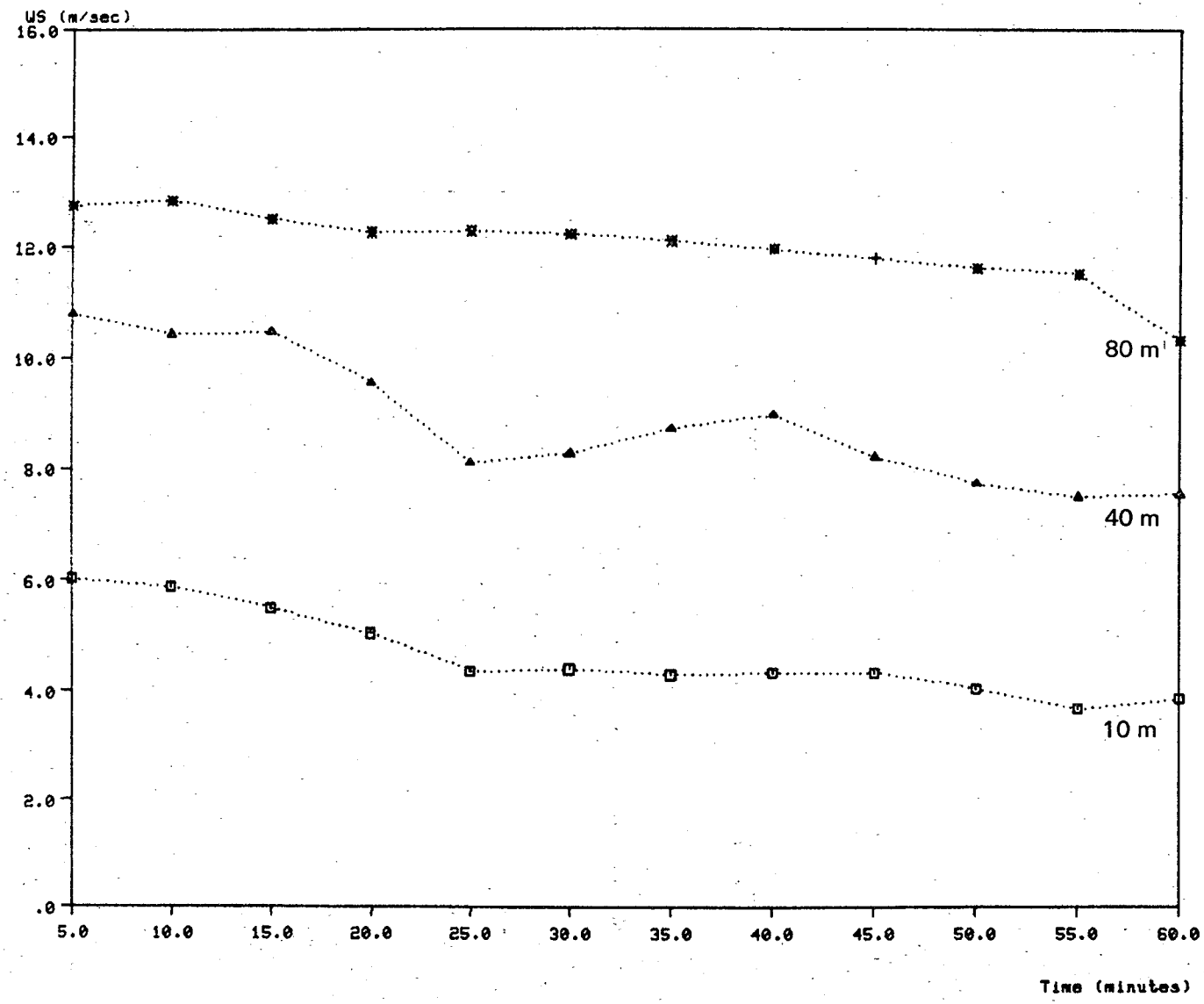

Figure 33. Tower A wind speeds during Experiment 202, Hour 5 (2100-2200 MST).

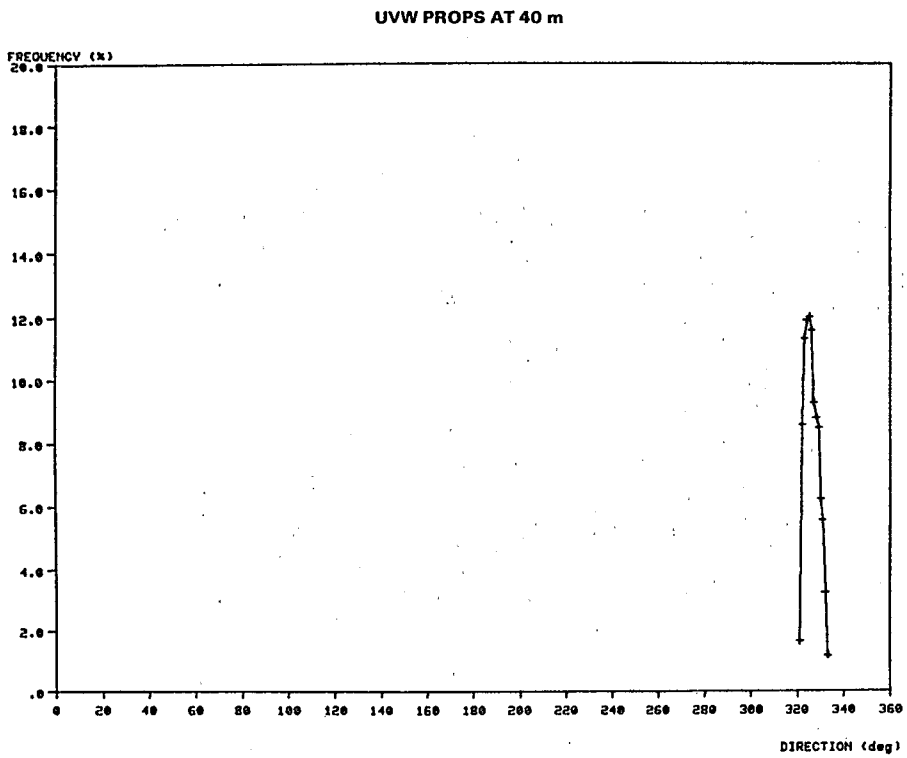

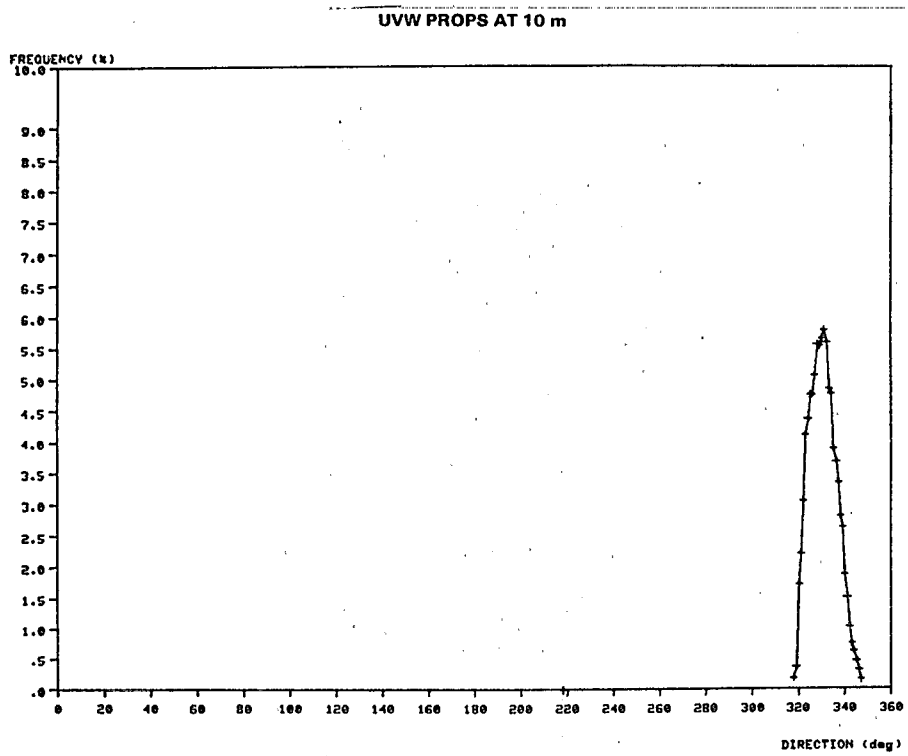

Figure 34. Calculated wind direction distribution functions for Experiment 202, Hour 5 (2100-2200 MST).

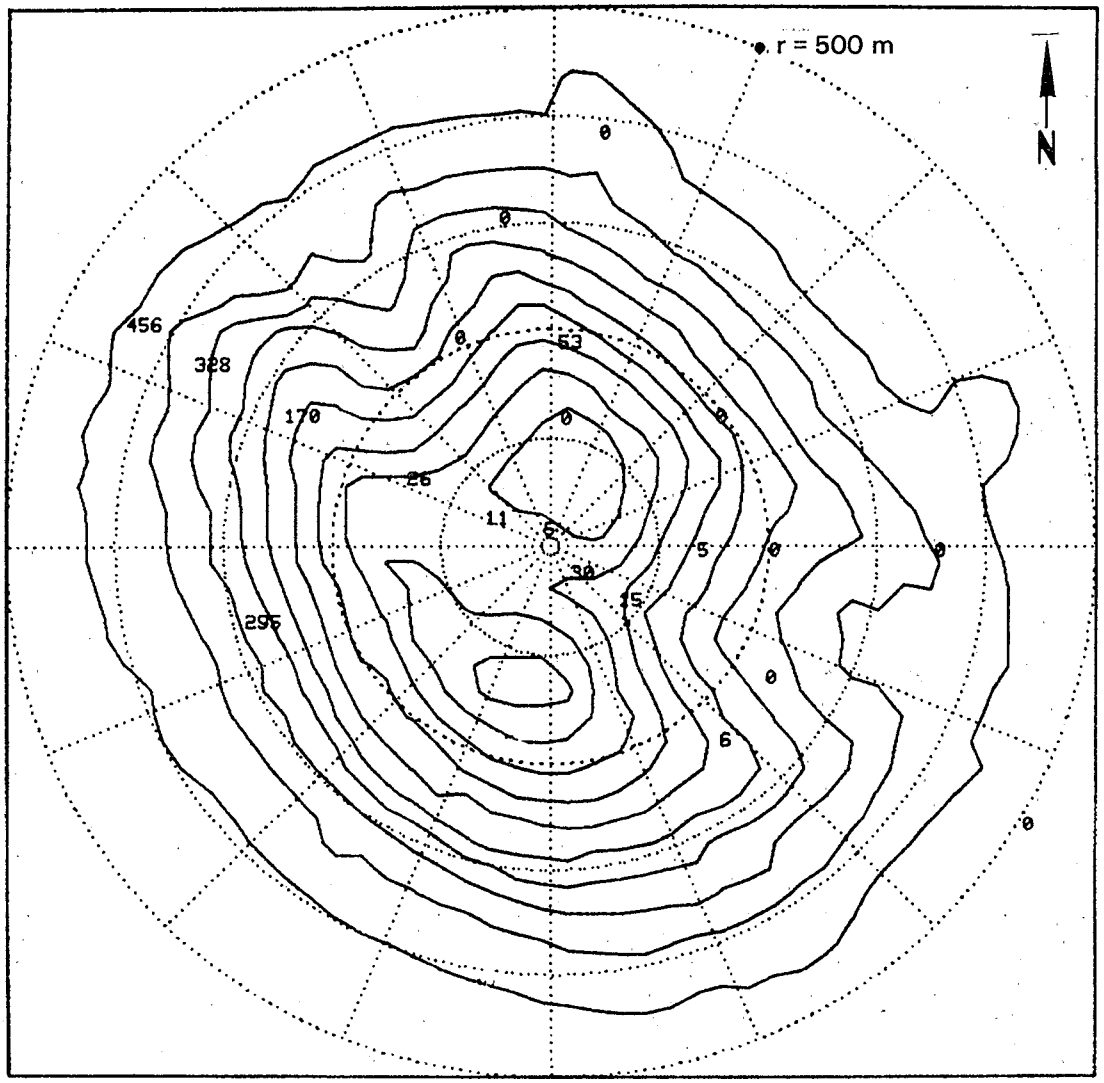

Figure 35. Observed SF_6 concentrations (ppt) for Experiment 202, Hour 5, (2100-2200 MST). Source: r = 1014.6 m, θ = 319.0°, net height = 23 m, Q = .086 g/s.

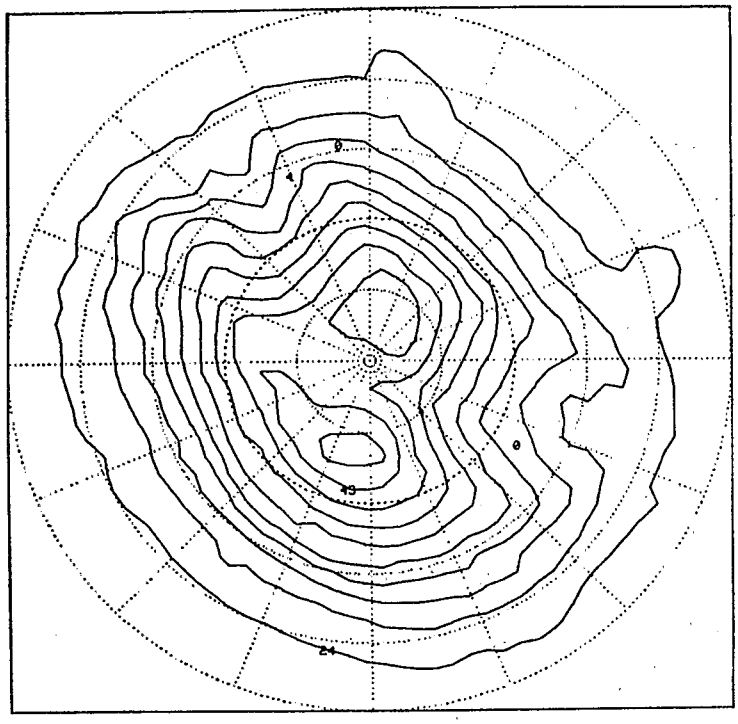

TIME PERIOD 2100-2110

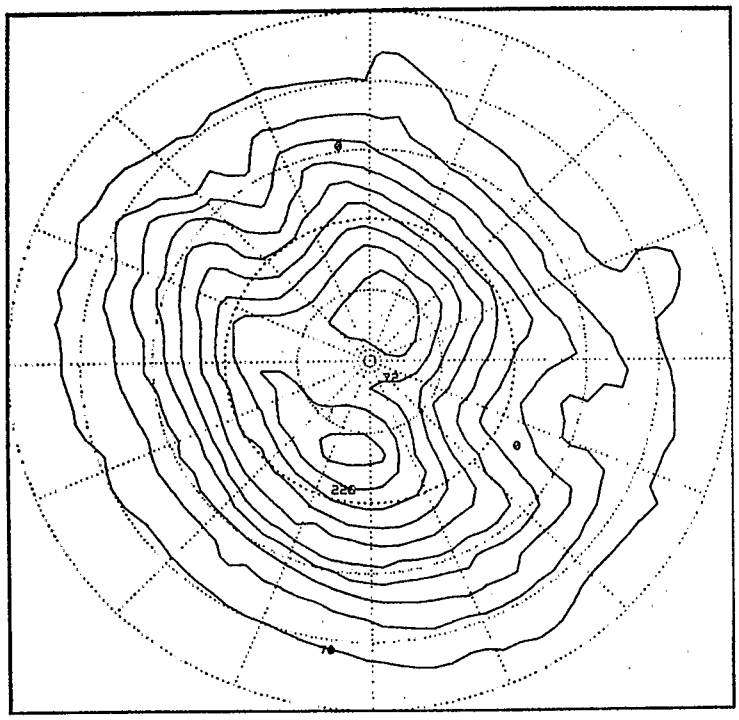

TIME PERIOD 2110-2120

Figure 36. Observed 10-minute average SF_6 concentrations (ppt) for Experiment 202, Hour 5 (2100-2200 MST).

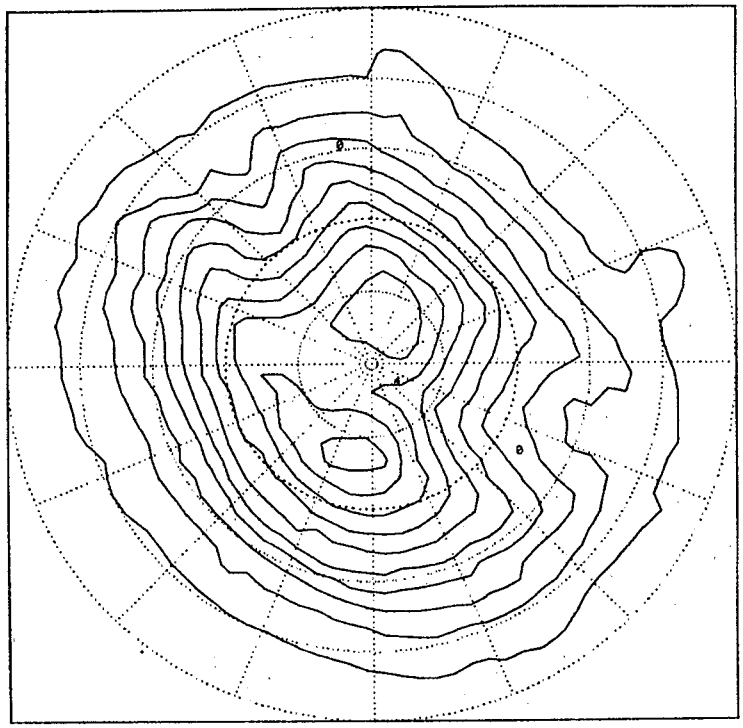

TIME PERIOD 2120-2130

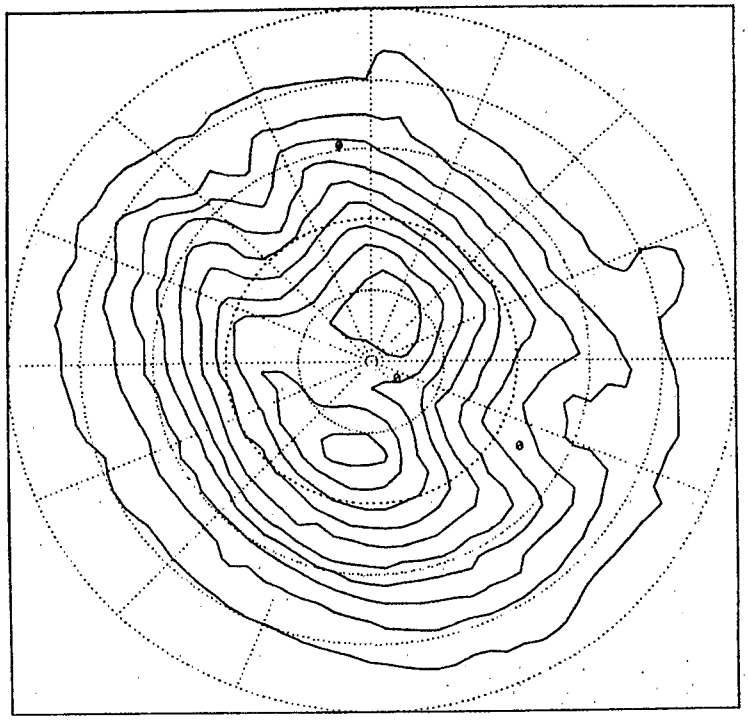

TIME PERIOD 2130-2140

Figure 36. Continued.

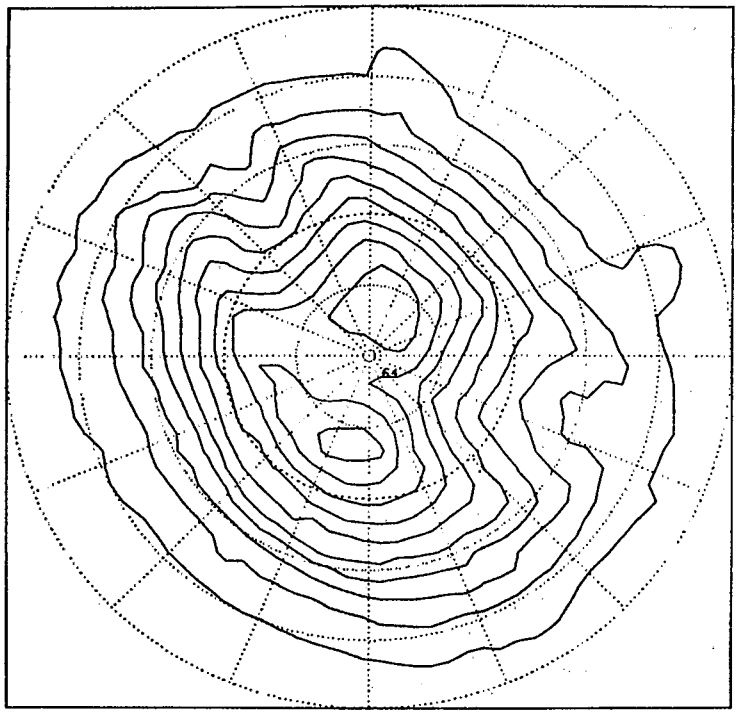

TIME PERIOD 2140-2150

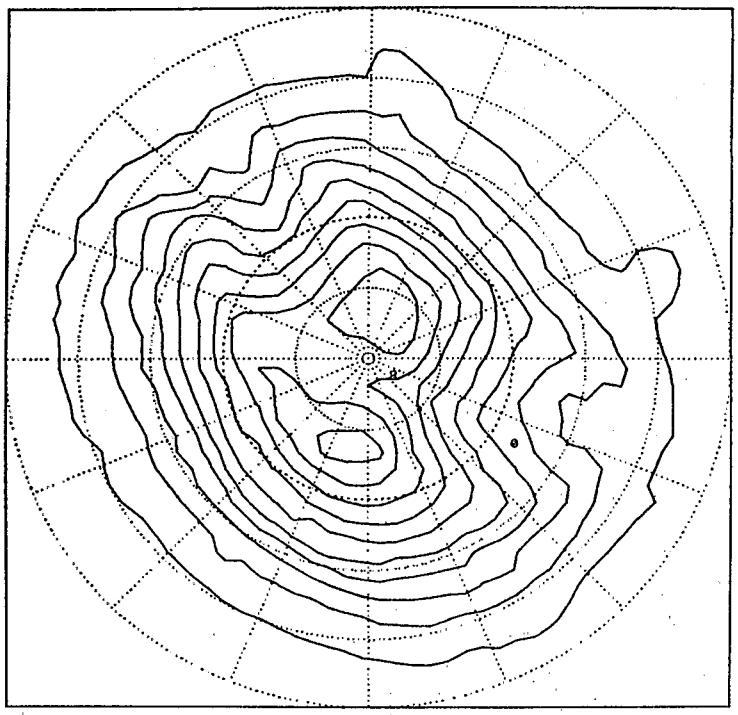

TIME PERIOD 2150-2200

Figure 36. Continued.

TABLE 5. NEUTRAL AND LIFT MODEL CALCULATIONS - EXPERIMENT 202, CASE HOUR 5

Meteorological Data

wind direction(deg)	=	326.
wind speed(m/s)	=	7.8
critical dividing streamline height(m)	=	7.0
Iz	=	.037
Iy	=	.060
N(1/s)	=	.047

Source Data

direction(deg)	=	319.
distance(m)	=	1014.6
release height(m)	=	30.0
SF6 emission rate(g/s)	=	.086

Receptor Coordinates X(m)	Y(m)	Z(m)	Observed SF6 (ppt)	Neutral Predicted SF6 (ppt)	Lift Predicted SF6 (ppt)
360.22	.00	13.26	.00	.00	.00
208.35	.00	31.25	.00	.03	.00
142.00	.00	50.00	4.50	3.80	.00
159.04	122.04	46.91	.00	.05	.00
51.04	387.66	11.78	.00	.00	.00
15.97	121.29	90.94	.00	9.41	.00
25.15	190.88	65.00	53.00	.86	.00
2.15	18.88	80.00	5.10	35.52	.00
-66.52	-505.24	-3.54	.00	5.05	.00
-248.96	-66.71	32.90	294.60	81.17	25.95
163.68	-175.52	50.00	6.00	39.83	.00
441.46	-254.87	-2.45	.00	.05	.00
204.15	-117.12	30.00	.00	2.20	.00
82.15	-46.12	60.00	15.00	27.79	.00
37.15	-21.12	70.00	29.62	37.24	.00
-359.96	207.82	8.94	455.70	88.61	125.61
-297.11	171.54	28.07	328.10	428.14	202.49
-111.85	65.88	80.00	26.10	65.04	36.94
-40.85	28.88	80.00	10.60	47.89	.00
-80.75	194.94	50.00	.00	3.84	.00
-40.46	307.35	30.00	.00	.00	.00

to 331° over the hour. Because the measured wind directions at 40 m on tower A are consistent with both the tower B directions and the lidar trajectories, 326° is selected as the model wind direction. Similarly, the 40 m PDF is also used in the modeling.

Neutral was rerun with the new meteorology; instead of estimating a peak value 90% of the observed peak value, it produced a value 94% of the observed peak. As in the previous hour, the peak observed concentration occurred more toward the base of the hill. Modeled concentrations at other points on the hill are in fair agreement with the observed concentrations. Figure 37 shows the distribution of calculated concentrations; the data are also summarized in Table 5.

Results from Lift computations are displayed in Figure 37 and are also listed in Table 5. Concentration estimates are generally much too low. The peak modeled concentration is only 44% of the peak observed concentration. Furthermore, the third largest observed concentration (along the southwest side of the hill) is underestimated by over a factor of 10 by Lift. Neutral underestimates this concentration by a factor of about 3.5. Therefore, the Lift model performs worse for this hour than Neutral.

Because Lift uses a constant terrain factor at all receptors, it may be instructive to calculate the factor required to reproduce the most important observed concentrations. Modeled and observed concentrations are related by the "modeled" and "observed" terrain factors:

$$\ln \frac{C_m}{C_o} = -\frac{1}{2}\left(\frac{H}{\sigma_{zf}}\right)^2 (T_m^2 - T_o^2) \tag{55}$$

Therefore, the factor needed to produce an observed concentration within the framework of the Lift model can be computed using model variables and the observed concentrations:

$$T_o^2 = T_m^2 + 2\left(\frac{\sigma_{zf}}{H}\right)^2 \ln\frac{C_m}{C_o} \tag{56}$$

The model terrain factor computed for this hour is 0.95. The factor required to reproduce the observed concentration at the point of the largest modeled concentration is $T_o = 0.77$. A T_o of 0.40 would have been needed to reproduce the largest observed concentration. Therefore, Lift would have performed better with a terrain factor between 0.5 and 1.0 but still would not have been able to reproduce the largest observed concentration with any reasonable value of T_o. Note that Neutral overestimates the observed concentration at the location of the greatest modeled concentration because it uses a factor of approximately 0.5 at this receptor, rather than 0.77.

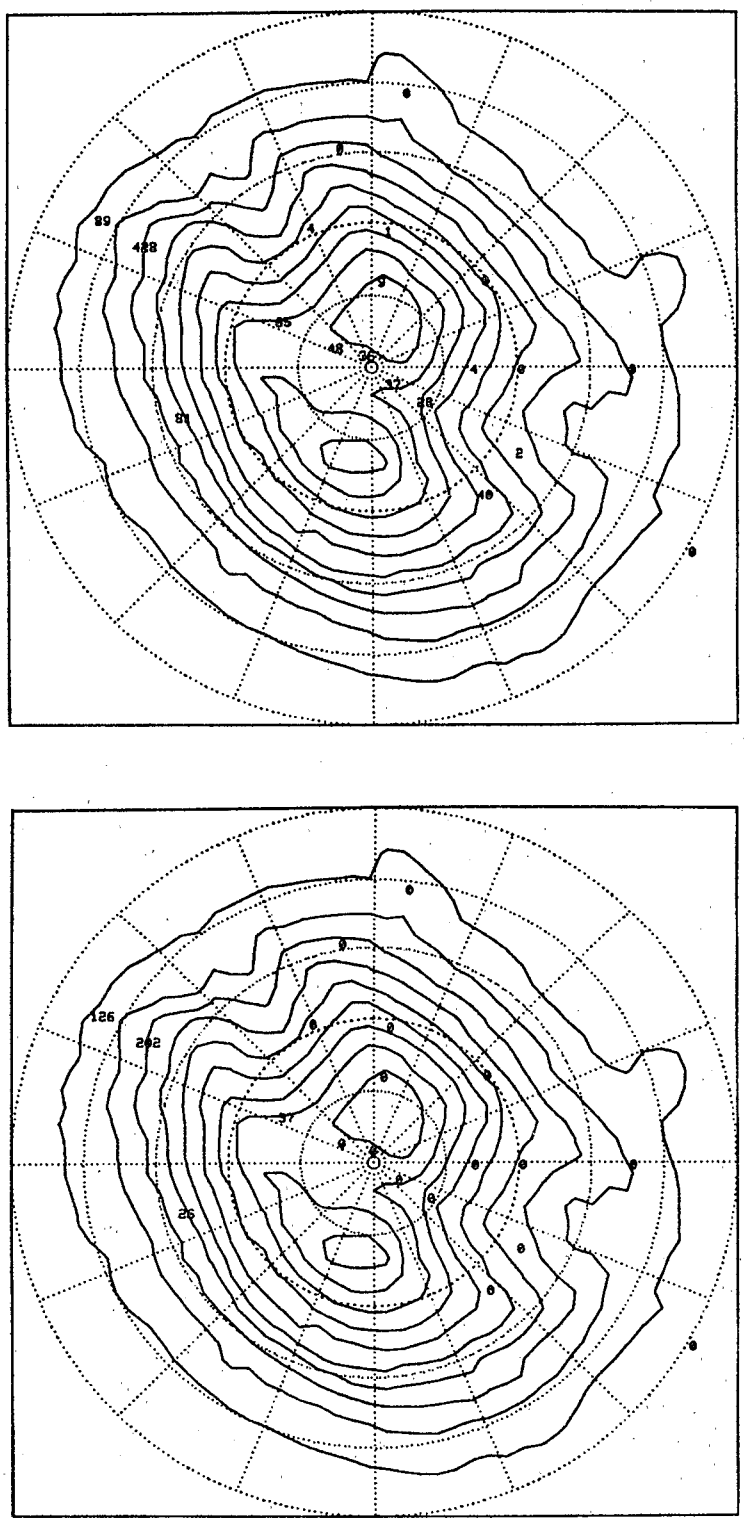

Figure 37. SF_6 concentrations (ppt) estimated for Experiment 202, Hour 5 by the Neutral (top) and Lift (bottom) models.

4.3 Experiment 204, Hour 1 (0000-0100 MST)

4.3.1 Summary Description

Thermofogger oil-fog and SF_6 tracer gas were released from the northern side of the hill for virtually the entire hour. The oil-fog release was begun three minutes before the hour, and the SF_6 release was begun one minute after the start of the hour. The release crane was positioned at 1035.7 m, 4.5°, and the height of both releases was 30 m. Because the SF_6 release did not begin well before the start of the hour, the measured concentrations on the hill may not be true 1-hour averages. Six to seven minutes of travel time could have been lost.

Local terrain elevations near the release point are estimated to be -6.8 m relative to the zero of the hill coordinate system, so the net release height corresponded to the 23.2 m height level on the hill. The SF_6 release rate is computed to be 0.094 g/s with an estimated uncertainty of $\pm$9%. No Freon was released.

Plume Observations

Many observations of the appearance and trajectory of the oil fog plume are available for this hour.

Time: 2357 The plume is just reaching the hill and is beginning to go around the west side. It looks quite stable, although the wind is brisk enough that it's not the really smeared plume we've seen in the past. It's not really smearing at all until it gets close to the hill.

Time: 0002 Plume looks very stable, heading right toward the hill to the west side of center.

Time: 0004 There is a horizontal undulation in the plume caused by a slight wind shift.

Time: 0005 I'm at site D8. The plume is going just east of D8 and is spreading out in a very nice "V" as it comes along. I estimate that as it passes over here, it is about four road widths ($\sim$7 m x 4). As I look downwind it is appearing to kind of go around the hill and then loop back a little bit further east so there is some curvature to the trajectory. Quite a bit of horizontal spread, very pretty. Part of the plume now looks like it is half way between the road and the hill.

Time: 0010 The part of the plume that is half way to the hill now appears to be going more directly toward the north butte and will have to bend very hard to avoid the hill.

Time: 0014 (?) From block house on south butte: I see plume bending, or curving around the west side of the butte and then straightening out downwind of the hill.

Time: 0015 The plume seems to have to take a very definite bend now around the area of tower F and then it hooks and ends up going south of the hill. I can see some of the plume material now in a line between me at D8 and the base of the FAA tower (on the north peak). It actually is going below the base of the FAA tower. The plume is very dense and very compact. There apppears to be very little turbulence at the present time.

Time: 0018 Plume is going directly towards tower F. It appears to be going around the hill to the northwest side. There is a definite bifurcation of the plume at tower F. One plume segment is quite close to the hill, with quite a bit of vertical motion--a lot of eddys. The other to the west of the hill is very flat and much more stable.

Time: 0019 Plume now looks like it will be going through the FAA tower. There is a shift to the north occurring.

Time: 0021 Plume is now coming much closer to the hill and may be fumigating near tower F. The wind seems to be backing at the present time and the plume orientation is now to the northeast part of the hill. Plume centerline is to the east towards the FAA tower.

Time: 0022 Smoke odor is noted at block house. Most of the plume material is going toward tower F. Most of the draw is filled with smoke.

Time: 0023 NAWC 2 can smell smoke at the block house.

Time: 0024 Plume is on the east side of the hill.

Time: 0025 The plume has just wiped them out at the block house.

Time: 0026 The plume is hitting very hard at a point at 60C.

Time: 0028 Now the plume is considerably east of the butte.

Time: 0030 The plume centerline now is traveling at a point to the northeast of the east knoll and it takes a bend at a point right at the east knoll and goes toward the south on the east side of the hill. The plume looks very stratified on the east side of hill.

Time: 0034 Plume is starting to head back toward the hill.

Time: 0036 About two minutes ago, the plume was going directly over the east knoll and now is on its way up the hill. It is now in the small valley between the east knoll and the large hill.

Time: 0040 The plume is approaching the northeast side of the hill. It starts out on a trajectory right towards tower C, then takes an extremely wide berth, completely around the hill heading to the south, but it ends up heading due south in the area of point B3, or B2.

Time: 0047 Trajectory from the release is headed right back toward the hill again. The plume is very wide and, of course, the parent plume is still going to the east about half-a-hill width away from the hill. But the new plume apppears to be heading right toward the north butte right now and we'll see where it goes.

The plume orientation has continued to veer to a point where it is heading directly towards the FAA tower and it looks like it is continuing to veer somewhat. The centerline is now to the west side of the tower.

Time: 0049 The plume is really wide and its initial trajectory is to the west side of the FAA tower.

Time: 0050 The plume is pretty much plastering the hill right now. Up close to the hill you can see that the plume is stratified from the east to the west. There appears to be considerable dispersion in the plume close to the release with a few undulations between the release point and the hill.

Time: 0053 From just below block house, the plume width appears to be about 1-hill width. The plume is smearing across the north ridge that the power line comes up, and is just reaching the northwest draw, as it begins to smear around the west side.

Time: 0055 It has just reached the ridge below tower F. It looks like the creeping plague as it smears around the northwest side of the hill now, streaming over the ridge by tower F, but below tower F.

Time: 0056 Plume appears quite stable as it approaches the north end of the hill; some undulation and considerable vertical spreading as it impacts the hill. Plume is also visible on the south side of the hill. I'm framing the butte in the center of the picture, trying to catch plume on both sides of butte.

Time: 0057 Airplane reports that the plume is on the west side of the hill.

Time: 0059 The plume centerline has continued to veer until about this time. It was at one time pointing towards the northwest side of the hill and now the orientation is starting to back. The plume centerline now is directly toward the FAA tower. The plume has continued to veer in back from the east side of the hill to the west side of the hill, with almost continual fumigation on the north end of the hill.

Time: 0100 Plume is hitting the west side of the hill and northwest draw. Centerline is shifting to the east again, and appears to be heading toward FAA tower. One third of the way to the hill the plume rises abruptly, flowing upward, then leveling out again before smearing against the hill.

The observations clearly indicate that the wind was very unsteady over the hour, carrying the plume from one side of the hill to the other, and back again.

At the start of the hour, the plume was fairly compact, traveling slightly to the west of the center of the hill. By the second 5-minute period, an eastward shift was noted, and the plume trajectory came closer to the hill center. Throughout the second and third periods, the plume came very close to the ridge line below tower F. The plume continued to move eastward in the fourth period, and was clearly hitting the hill in the area of the northwest draw to the east of tower F. This was confirmed by the smoke odors noted at the block house (located on the helicopter landing pad) near the top of the northwest draw. The plume shifted to the northeast face of the hill by the end of the fifth period, and was considerably east of the hill by the end of the sixth period (half past the hour).

The plume remained east of the hill for the next ten minutes (periods 7 and 8), but then started to swing back toward the hill during period 9. This shift continued in period 10, and the plume then appeared very wide as it aimed toward the center of the hill. The plume continued to shift in period 11, and was once again streaming across the ridge line below tower F. The trajectory remained to the northwest side of the hill, until it started to shift toward the center of the north face by the end of the hour.

Photographs of the plume also document the shifts in the plume trajectory. The plume spread from the north face of the hill to the western edge during periods 3 and 4, and it was well to the east during periods 5-8. The shift back toward the hill center is seen during periods 9 and 10, and the plume was spread from the north face around the west side once again during periods 11 and 12.

Data from the lidar also document the plume trajectory descriptions during periods 4-12. Many sampling planes were used because the plume shifted around so much, resulting in fewer than the normal number of samples in each plane. Plume centroid positions in each plane are plotted in Figure 38 and labeled by the corresponding 5-minute period. These centroid positions show the plume trajectory to be toward the western side of the hill during periods 4, 10, 11, and 12, and toward the eastern side of the hill during periods 5, 6, 7, and 8. The easternmost trajectory occurred during period 8, corresponding to an estimated wind direction of about 334°. The westernmost trajectory is unknown because no lidar data were taken during the first 15 minutes, but the westernmost trajectory of those sampled by the lidar corresponds to a wind direction of 030°.

Meteorological Information

Wind and temperature data from tower A were used to characterize the flow during this hour in terms of H_c. The average of the 5-minute H_c values over the hour is 58 m, which is indicative of very stable flow at plume height. Because the plume was released at a local elevation of 30 m, it was well within the layer that is unable to surmount the hill (according

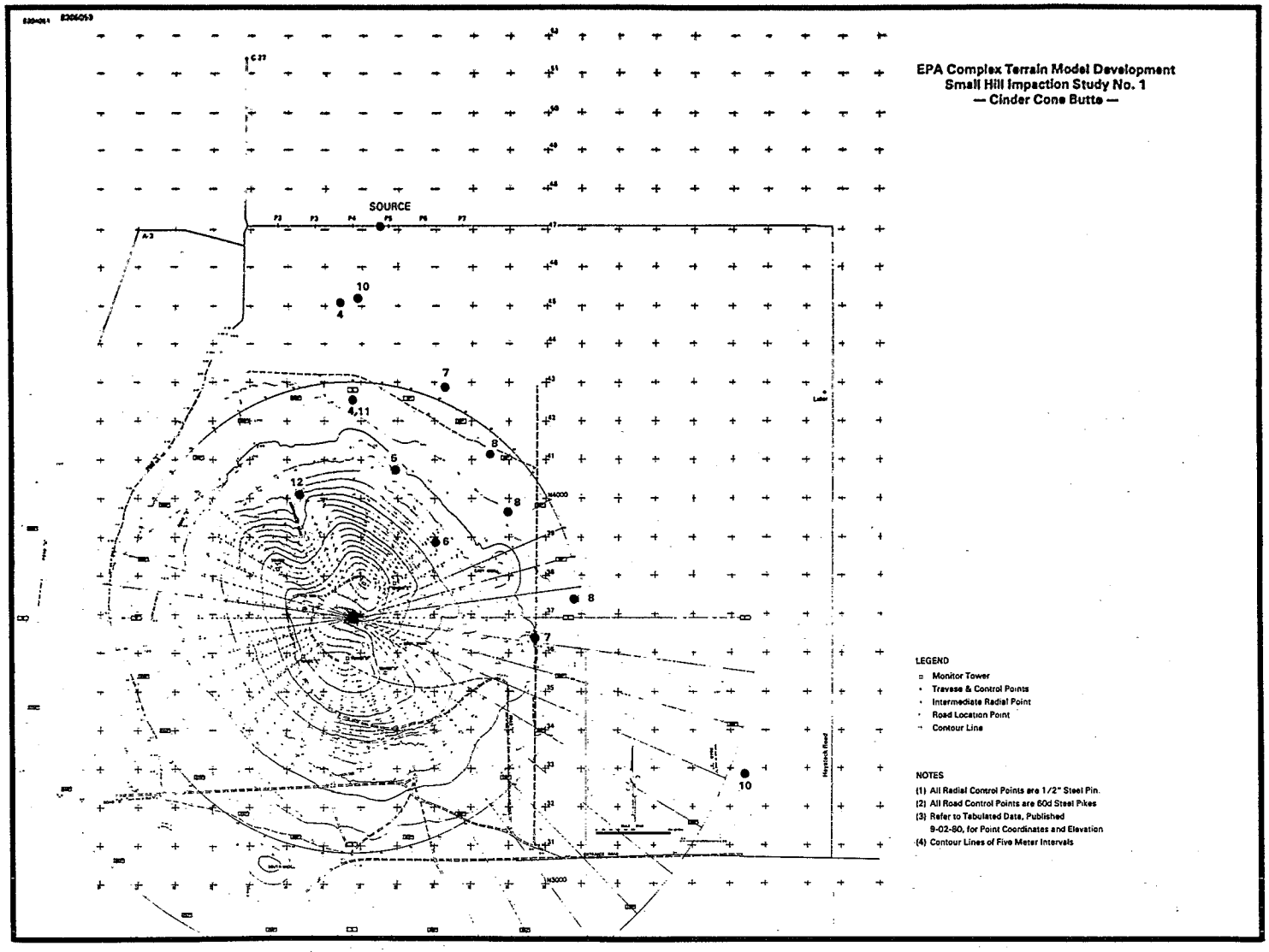

Figure 38. Plume centroid positions calculated from lidar data. Experiment 204, Hour 1 (0000-0100 MST).

to the simplified energy argument used to derive H_c). Above H_c, the bulk hill Froude number is 1.9, so the flow at this level was only weakly stable. Fr_L above H_c is 0.37; hence, a definite depression of streamlines in the lee is expected.

Figure 39 contains plots of the 5-minute H_c and Fr_H values for this experiment. H_c values ranged from 45 m to 74 m over the hour, but these fluctuations are likely to be unimportant in modeling this hour because the plume height remained well below H_c. Fr_H above H_c changed from 1.5 to 3.0 during the hour. The effect of this change on the plume trajectory is unclear.

Hourly averaged wind speeds measured at 10 m and 40 m on tower A are 2.4 and 2.0 m/s, respectively. The 10 m winds were from 010°, and the 40 m winds were from 359°. Therefore, the change in mean wind direction with height over the layer containing the plume was quite small. Figure 40 shows the variation in wind speed during the hour and it too is fairly small. Consequently, the 1-hour average wind speeds are an adequate representation of the hour.

Variations in the wind direction measured at 10 m and 40 m at tower A are shown in Figure 41 as frequency distributions. Both distributions are quite broad, stretching from 340° (320°) to about 65° (40°). The distribution at 40 m has two major peaks, and the trough between the peaks lies close to the wind direction that would have advected the plume toward the hill. This is consistent with the observational data discussed above.

In summary, the plume lay well below H_c and therefore probably traveled around rather than over the hill. The winds were 2-3 m/s from 10 m through 80 m. Wind directions pointed the plume preferentially to the east and west of the hill, so the only impact near the center of the hill occurred during periods of shifting winds. The photographs indicate that such a shift occurred twice during the hour.

SF_6 Concentrations

The distribution of hourly averaged SF_6 concentrations over the surface of the hill is shown in Figure 42. The pattern indicates that plume material smeared widely over the hill, but the higher concentrations are found either on the east or west slopes of the hill.

Because the plume spent a good deal of time to the east of the hill, the highest concentration southeast of the hill at about the 10 m contour is probably due to the length of the time that the plume was nearby, and not to a very strong but momentary dose from the plume. The second highest concentration occurred at a height of about 65 m on the ridge line along the southwest side of the northwest draw, near tower F. The plume was seen to stream by this area early in the hour and again late in the hour. In fact, observers noted that the plume was "fumigating" near tower F at 0021 as the plume swung across the hill.

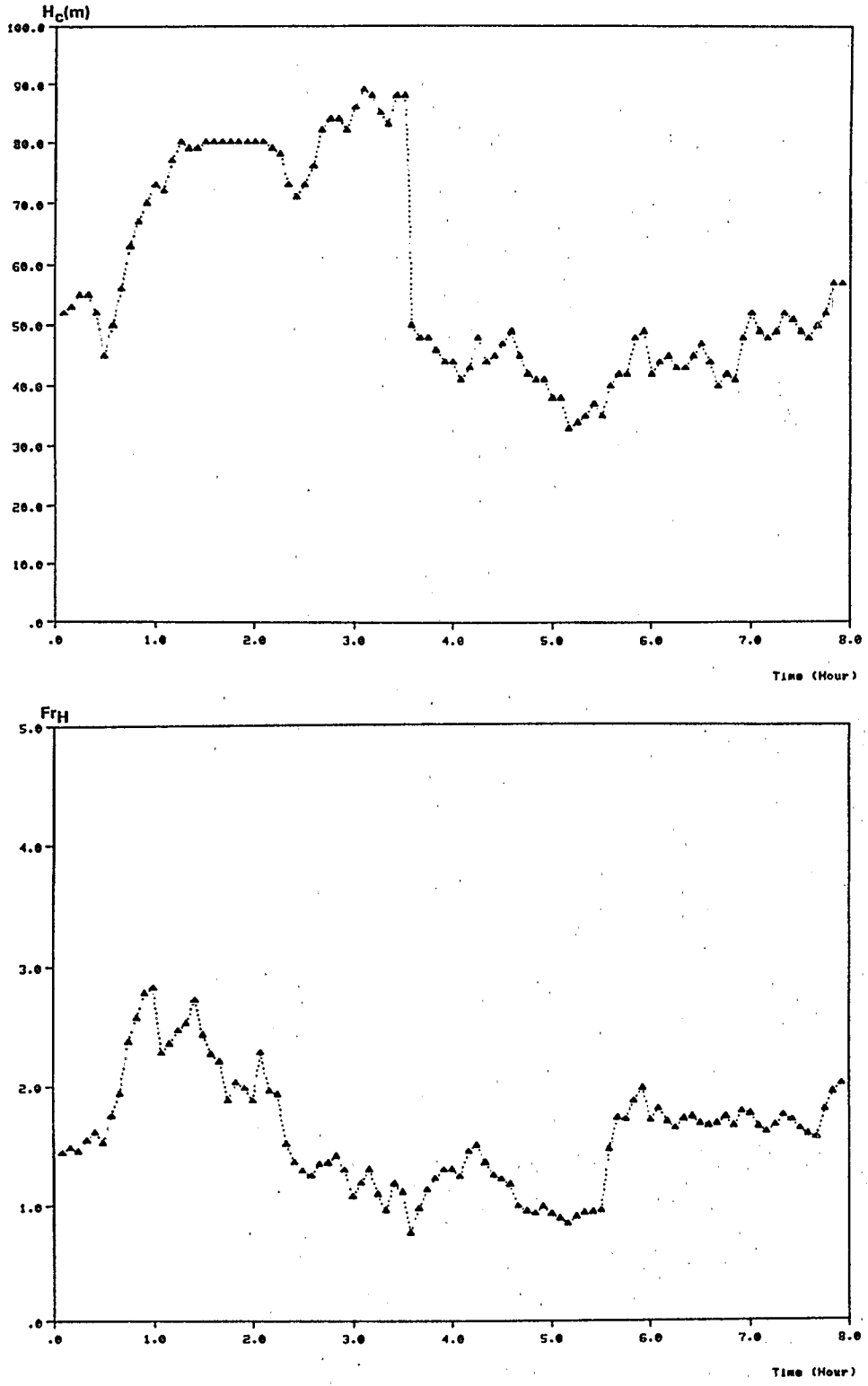

Figure 39. Calculated dividing streamline heights (H_c) and bulk hill Froude numbers above H_c (Fr_H) for Experiment 204.

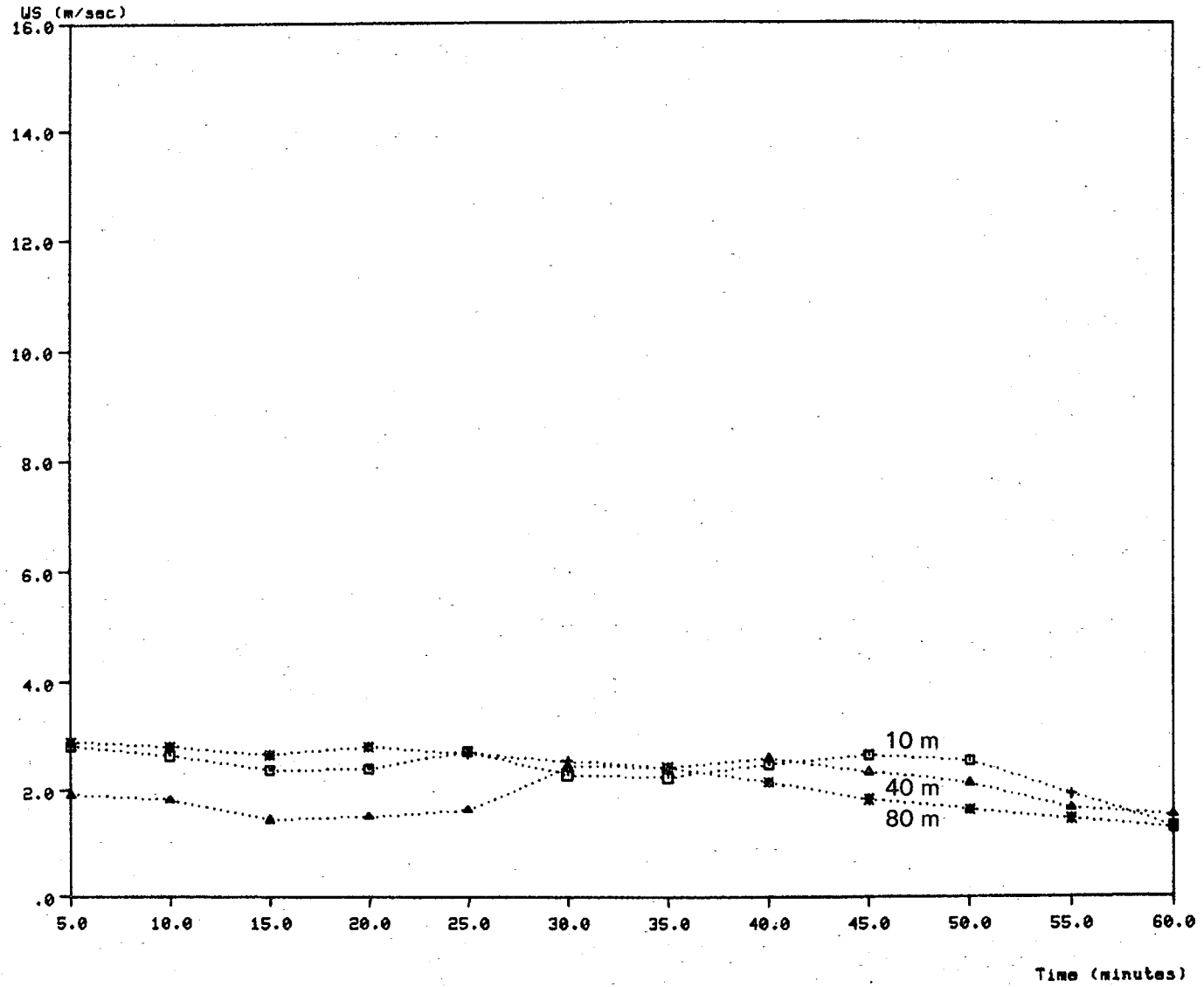

Figure 40. Tower A wind speeds during Experiment 204, Hour 1 (0000-0100 MST).

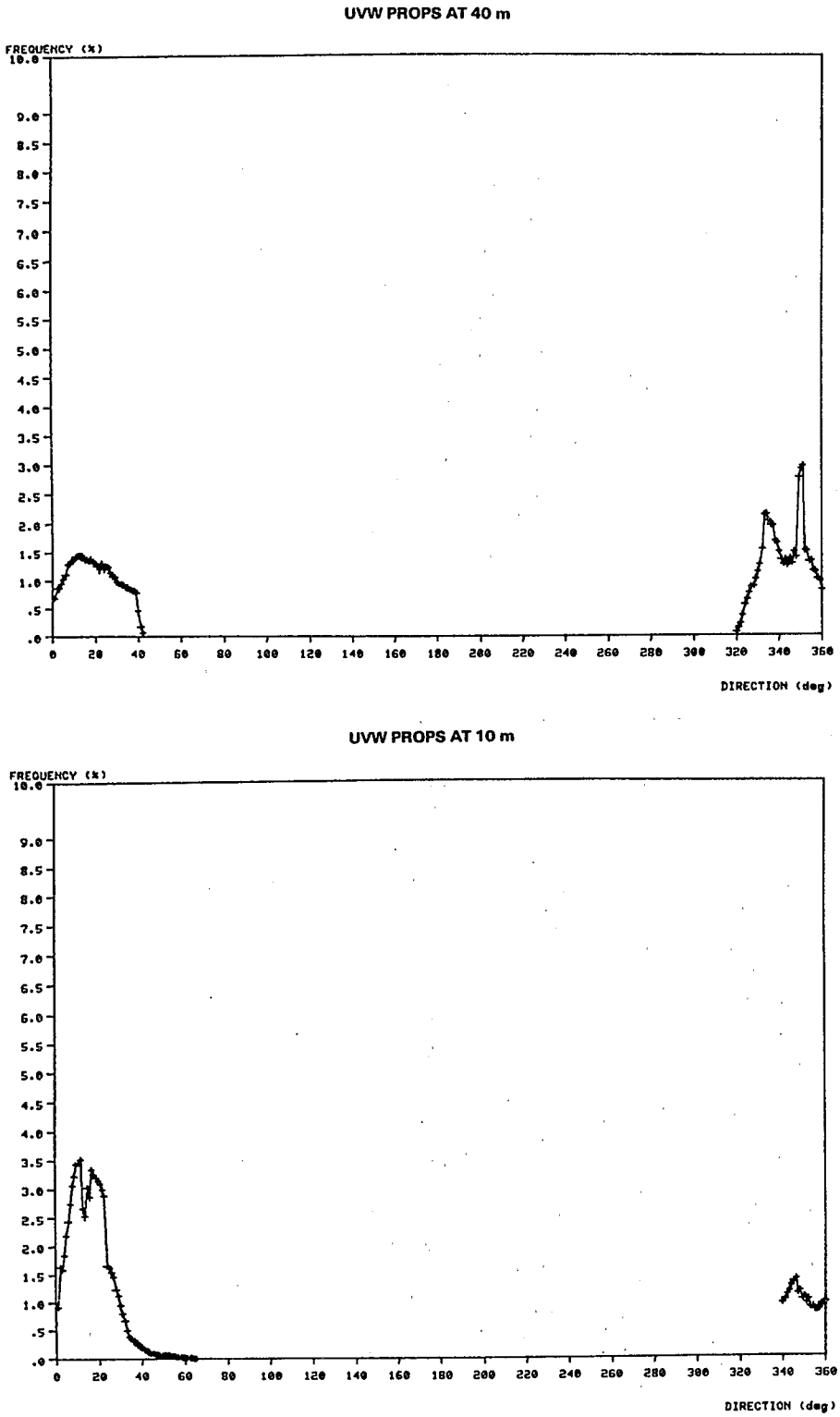

Figure 41. Calculated wind direction distribution functions for Experiment 204, Hour 1 (0000-0100 MST).

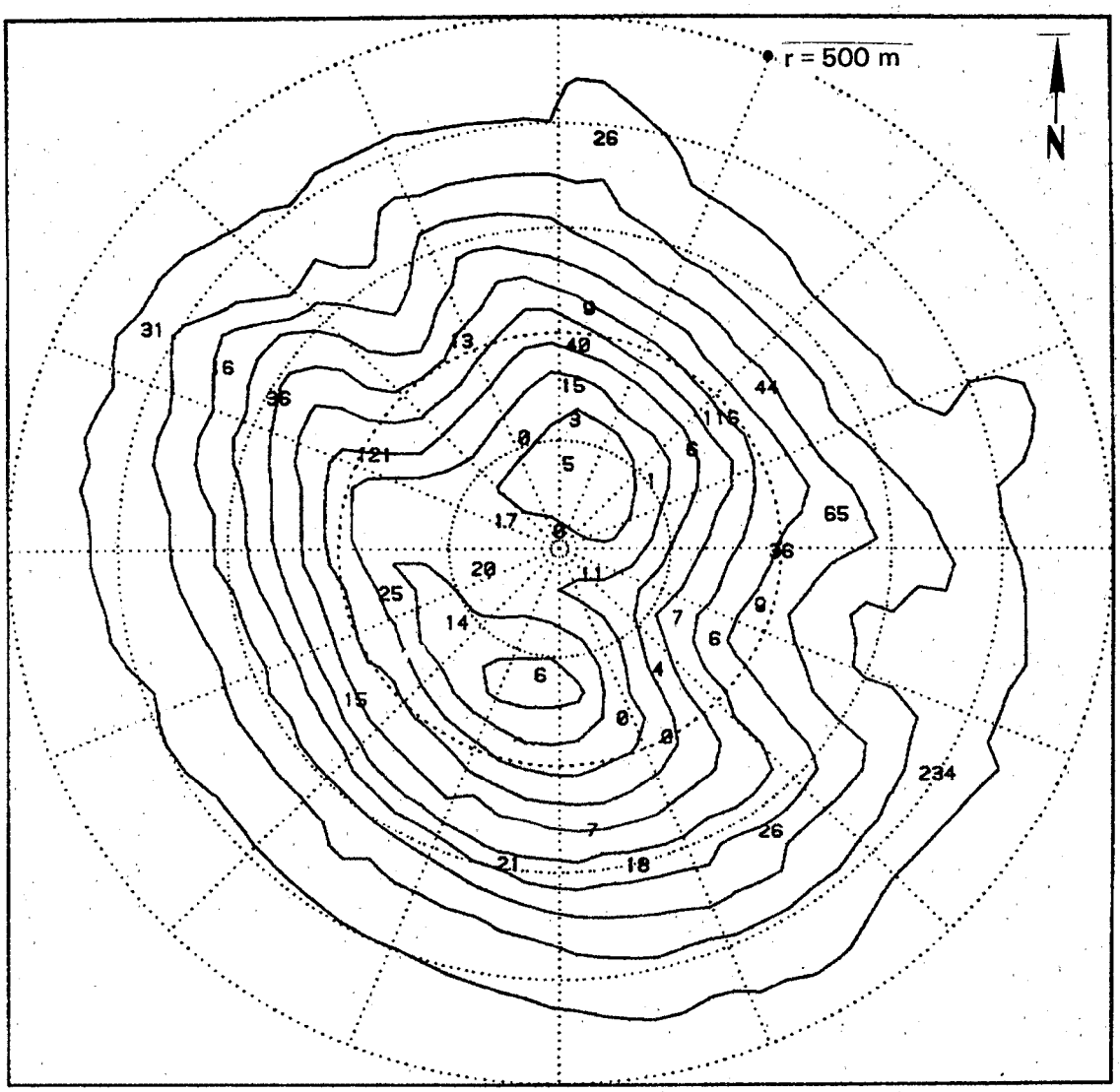

Figure 42. Observed SF_6 concentrations (ppt) for Experiment 204, Hour 1 (0000-0100 MST). Source: r = 1035.7 m, θ = 4.5°, net height = 23.2 m, Q = .094 g/s.

Most of the other "high" concentrations are spread along a band between 45 and 65 m across the north side of the hill. Because the release height corresponded to the 23 m height contour, the plume material must have lifted about 30 m as it flowed up around the hill.

The 10-minute average SF_6 concentration data are presented in Figure 43. Fortunately, two of the higher 1-hour concentrations over the hill were recorded at 10-minute samplers. Nearly all of the SF_6 measured at these two samplers was recorded between 0020 and 0030. During this period, the plume swung from the west wide of the hill to the east side, and reports of strong smoke odors were reported on top of the hill. Probably, most of the concentrations measured on the hill were recorded during this phase of the wind shift.

4.3.2 Model Performance

This hour was modeled with the Wrap model because the plume was released well below H_c, and it was therefore expected that the plume would have run into and curved around the hill rather than over the hill. However, because the winds tended to take the plume well to one side of the hill or the other, the frequency of occurrence of "impingement" wind directions is relatively small.

All meteorological data were prepared for the release height as described in Section 4.1.2. The resulting values are summarized in Table 6. The tower A 1-hour wind direction measured 20 m below the release height is 010°, and the wind direction 10 m above the release height is 359°. Wind directions at 10 m and 30 m on tower B are 351° and 354°, respectively. The lidar and photographic data show a highly variable wind direction during the hour. Because the release height was closest to the 40 m level (359°) and because the winds were so highly variable, 359° is used as the model wind direction. The PDF computed with 40 m wind data is also used in the model.

The Impingement model was modified to calculate concentrations along the sides of the hill, not just at the point of maximum expected concentration. The modified version of Impingement was rerun with the revised meteorology for comparisons with the Wrap model.

The results from both calculations are listed in Table 6 and plotted on a map of CCB in Figure 44. Both modeled sets of concentrations lie within a factor of 2 of the observed concentrations on the hill but are placed incorrectly. This is partly attributable to the basic model formulation. The models assume that the plume remains horizontal as it impinges on the hill at the stagnation point and wraps around the sides of the hill thereafter. In this idealized picture of plume behavior, the high concentrations estimated from the models should be confined to a band around the hill at the height of release. Furthermore, the models compute only concentrations associated with the wind direction that lies along the

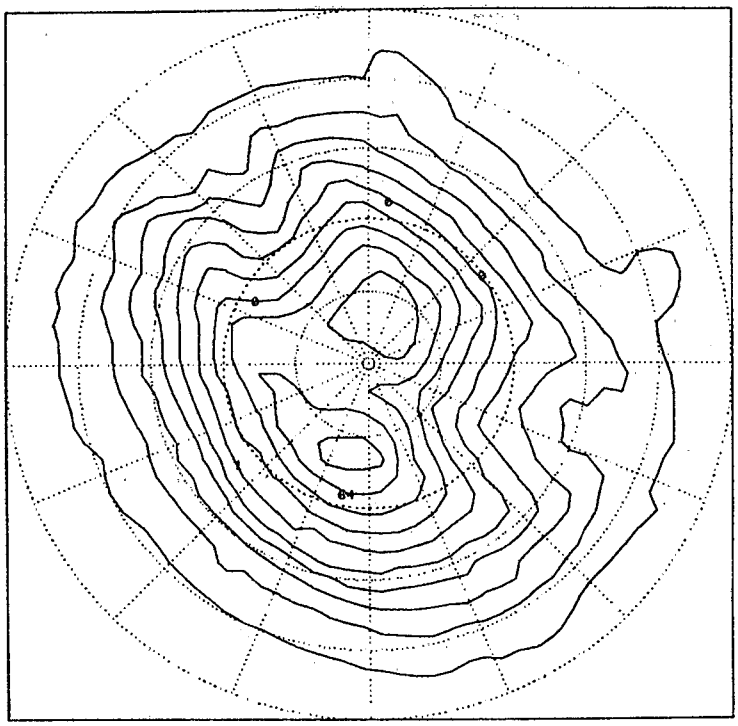

TIME PERIOD 0000-0010

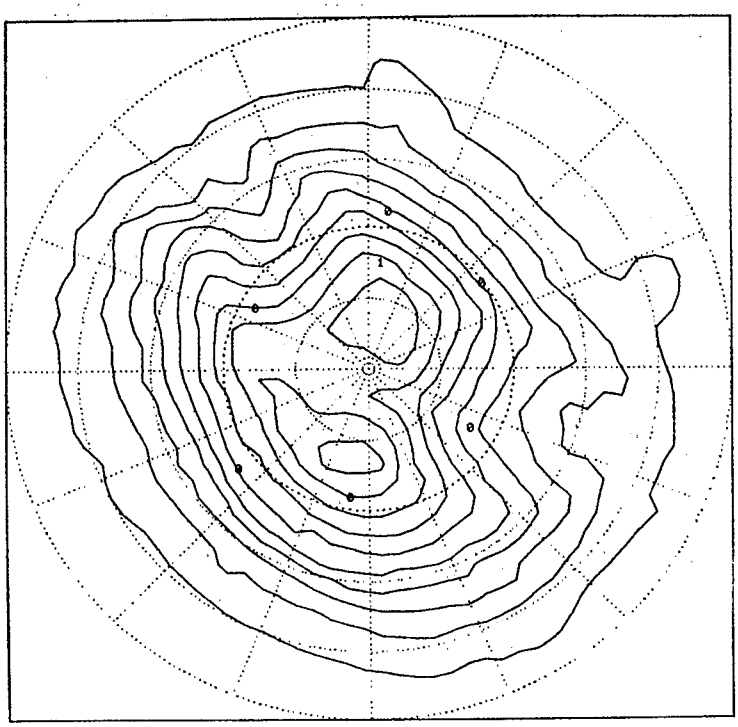

TIME PERIOD 0010-0020

Figure 43. Observed 10-minute average SF_6 concentrations (ppt) for Experiment 204, Hour 1 (0000-0100 MST).

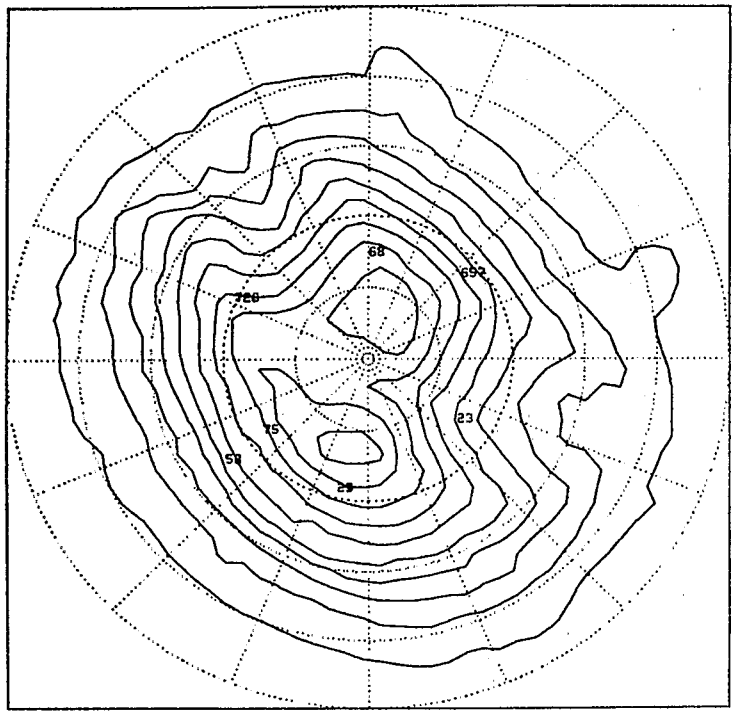

TIME PERIOD 0020-0030

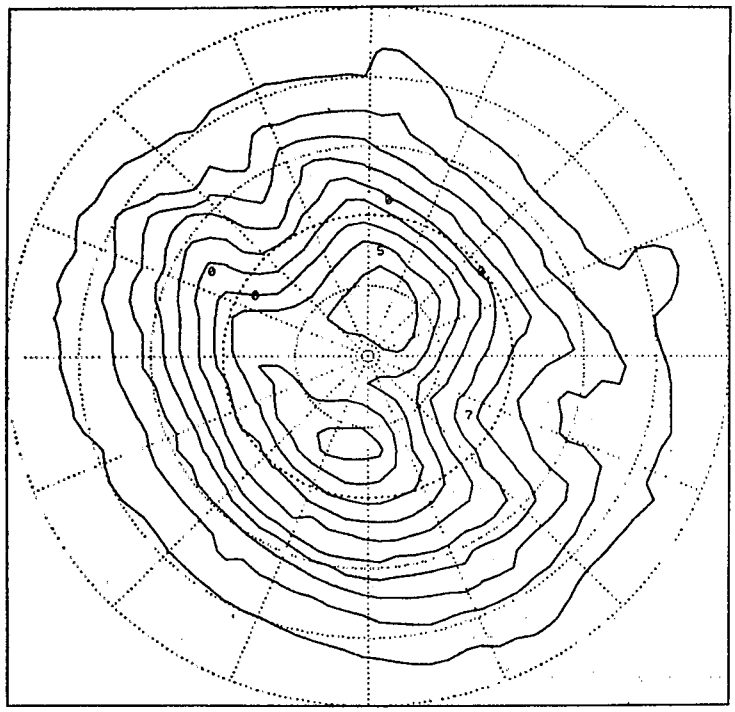

TIME PERIOD 0030-0040

Figure 43. Continued.

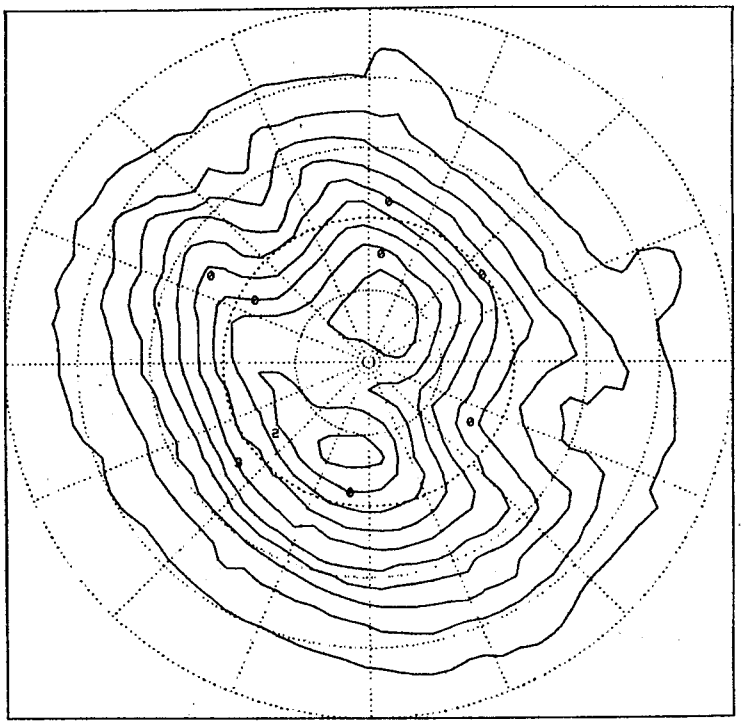

TIME PERIOD 0040-0050

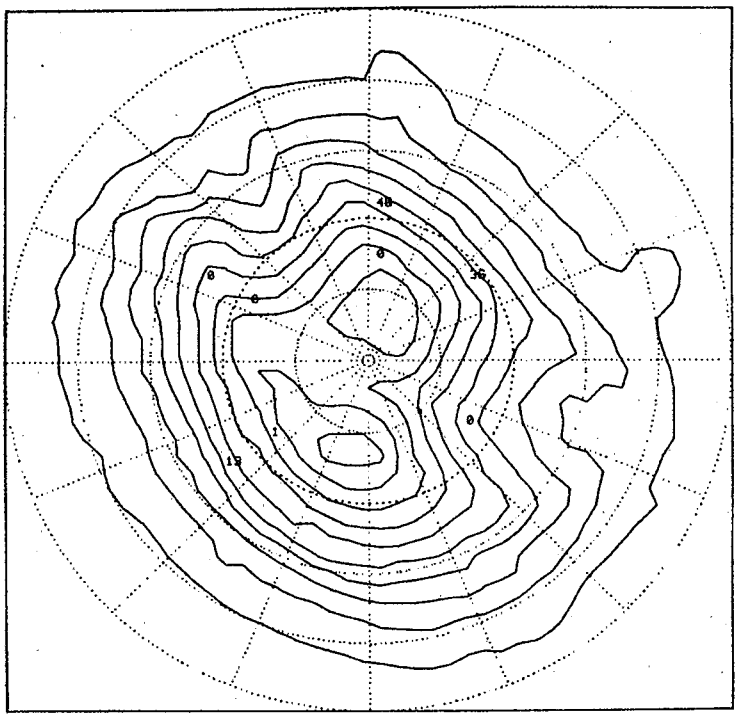

TIME PERIOD 0050-0100

Figure 43. Continued.

TABLE 6. IMPINGEMENT AND WRAP MODEL CALCULATIONS - EXPERIMENT 204, CASE HOUR 1

Meteorological Data

wind direction(deg)	=	359.
wind speed(m/s)	=	2.1
critical dividing streamline height(m)	=	58.0
Iz	=	.049
Iy	=	.341
N(1/s)	=	.051

Source Data

direction(deg)	=	5.
distance(m)	=	1035.7
release height(m)	=	30.0
SF6 emission rate(g/s)	=	.094

Receptor Coordinates X(m)	Y(m)	Z(m)	Observed SF6 (ppt)	Impingement Predicted SF6 (ppt)	Wrap Predicted SF6 (ppt)
208.35	.00	31.25	35.90	195.85	146.14
257.78	33.94	30.00	64.80	205.66	153.79
195.15	149.74	27.41	44.10	246.25	183.50
159.04	122.04	46.91	115.55	120.71	66.86
85.15	64.88	80.00	1.20	.43	.02
51.04	387.66	11.78	26.20	122.14	57.71
29.59	224.79	51.51	9.28	80.02	31.42
20.07	152.45	81.06	14.62	.08	.00
15.97	121.29	90.94	2.80	.00	.00
10.61	80.56	91.97	5.30	.00	.00
25.15	190.88	65.00	39.90	6.80	.90
2.15	18.88	80.00	.00	.11	.00
-38.04	-288.98	32.94	20.80	121.60	89.78
-15.01	-113.99	98.96	5.50	.06	.00
-177.41	-136.13	49.21	14.84	77.46	44.21
-84.85	-65.12	90.00	13.70	.21	.01
-144.85	-38.12	80.00	25.20	1.20	.13
-60.85	-16.12	80.00	20.40	1.20	.13
31.69	-258.06	50.00	7.30	66.65	38.46
77.87	-290.63	35.10	17.50	127.10	92.84
59.13	-154.04	80.00	.00	1.93	.27
199.06	-259.43	30.00	25.90	147.79	109.95
91.36	-109.36	65.00	3.60	16.29	5.08
355.15	-205.04	5.69	234.20	52.71	24.94
142.15	-81.12	40.00	6.14	136.83	94.42
108.15	-61.12	50.00	7.30	76.47	41.88
37.15	-21.12	70.00	11.20	7.43	1.62
183.53	-49.18	30.00	8.70	180.13	134.40
-359.96	207.82	8.94	30.90	78.28	38.08
-297.11	171.54	28.07	16.10	222.07	165.71
-246.20	142.14	47.96	35.80	104.36	57.13
-153.85	89.88	70.00	121.07	5.04	.80
-40.85	28.88	80.00	16.80	.54	.03
-80.75	194.94	50.00	12.60	94.28	43.85
-29.85	104.88	85.00	.00	.04	.00

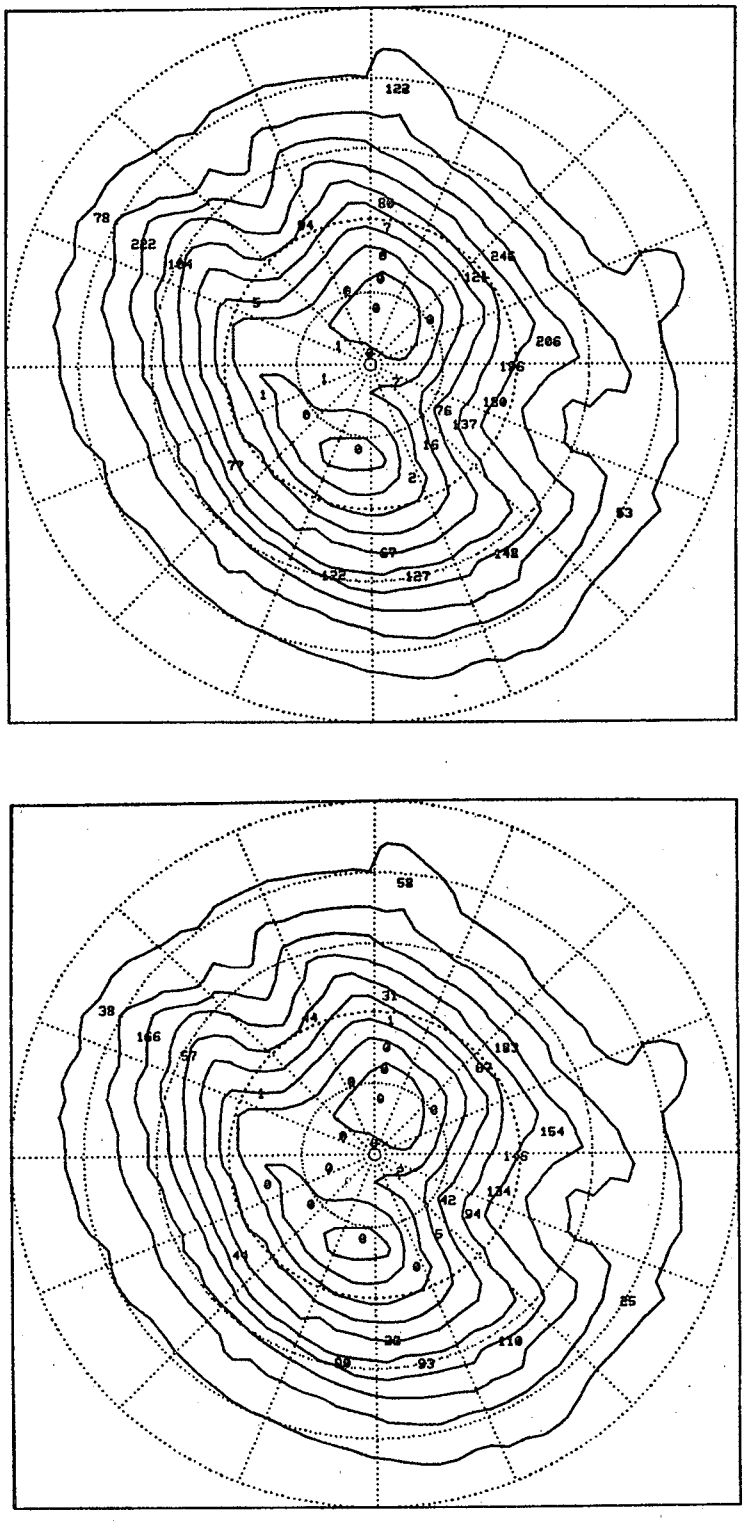

Figure 44. SF_6 concentrations (ppt) estimated for Experiment 204, Hour 1 by the Impingement (top) and Wrap (bottom) models.

stagnation streamline, so concentrations to the side of the hill are not simulated.

We do not expect the model to match observed features away from this impingement region. However, the model can be considered to be useful if it reproduces the most important aspects of the observed concentration pattern. The model is useful if the highest observed concentrations are located within a band near the height of release and if the magnitudes of the model estimates are "reasonably" close to observed concentrations on the hill.

The highest observed concentration of 234 ppt occurred at 5.7 m, close to the base of the hill. This could be associated with the plume when it was located to the east of the hill. (Recall that the model assumes that all concentrations on the hill are caused only by a plume along the stagnation streamline, not elsewhere.) The second highest observed concentration of 121 ppt (see Table 6) occurs near the top of the hill at 70 m. The level-flow assumption in the model cannot account for this implied large upward deflection of the plume.

The highest modeled concentrations from Wrap range from 134 ppt to 183 ppt and occur in the band around the release height of 30 m. These should be compared to the concentration of 116 ppt measured at 47 m.

The estimates from Impingement are 50% to 100% larger than those of Wrap. This result is probably related to the Gaussian probability density distribution used in the Impingement model. This distribution overestimates the probability that the wind blew along the stagnation streamline during this hour.

In summary, the wind direction distribution assumed by the model for this hour is critically important. Because the plume spent very little time near the stagnation streamline during the hour, a distribution that is peaked preferentially along that streamline (such as a Gaussian distribution) will cause any model to perform poorly for this hour. High concentrations away from the hill cannot be estimated well because the model is not designed for these receptors. The high concentrations toward the top of the hill are "fair game" for the model, but their locations cannot be expected to coincide with the peak concentrations predicted from the level-flow models.

4.4 Experiment 205, Hour 4 (0300-0400 MST)

4.4.1 Summary Description

Thermofogger oil-fog and SF_6 tracer gas were released from the southeast side of the hill from 0300 to 0349. The release crane was positioned at 1155.1 m, 120.1°, and the release height was set at 40 m. Because the release was continuous from the previous hour, the sampler measurements correspond to the indicated release data. However, the release terminated 10 minutes early; therefore, the SF_6 may not represent a true

1-hour average. With a wind speed of about 4 m/s at 40 m, the last tracer material released would take 4 to 5 minutes to reach the hill.

Local terrain elevations near the release point are estimated to be -8.9 m relative to the zero of the hill coordinate system, so the net release height corresponded to the 31.1 m height level on the hill. The SF_6 release rate is computed to be 0.083 g/s with an estimated uncertainty of $\pm 2.7\%$. No Freon was released.

Plume Observations

Many observations of the appearance and trajectory of the oil-fog plume are available for this hour.

Time: 0258 Aircraft reports the plume going between the two peaks and I can confirm that from my vantage point, about E4.

Time: 0259 Smoke odor is reported on north butte.

Time: 0300 I am standing on the north butte and it appears that the plume is heading toward the south peak, toward tower D. Neph data is being acquired--should get good data.

Time: 0301 The plume is really bombing the draw area right now.

Time: 0311 Plume is still going directly up the east draw. There is some horizontal spreading as it approaches the butte. Plume strikes the hill and bends sharply upward, flowing through draw at height over north knoll (and probably also over south knoll). Thick smoke in draw now.

Time: 0315 Lidar reports plume still going up draw.

Time: 0316 I am on the north peak and the plume looks like it is going up the draw. Winds are pretty brisk up here. Dan just said about 12 m/s versus about 8 m/s at the equivalent level of the 150 m tower so it appears there is an acceleration of the wind as it goes up the butte.

Time: 0318 The plume is headed toward the north butte now, when just a couple of minutes ago it was on the south butte.

Time: 0321 Strong oil fog odor is noticed on the north butte.

Time: 0322 Plume is going up draw, and can be seen well into the lee side of the hill.

Time: 0323 Lidar reported the plume on the lee side of the hill is elevated. It is really whipping through the draw, accelerating as it goes over the backside of the hill.

Time: 0326 I'm standing on the backside of the draw. The plume is accelerating rapidly up the draw--very strong winds up here.

Time: 0328 The smoke is roaring up the draw and I'm up by the draw now and it is coming through very heavily, I can smell it very strongly. The winds are quite brisk. This is very unusual. We've got a 6 m/s wind roaring up the draw from the southeast. We've never had anything like this.

Time: 0334 The plume is still accelerating up through the draw--you can see pieces coming over the lee side of the hill.

Time: 0338 I am going down the road that services the butte. The plume appears to be going right up the draw from my vantage point. The plume has some vertical growth. It looks like there is some mechanical turbulence that is pulling the plume apart - much more than it was during experiment 204.

Time: 0340 Parked under the plume, I can see it going right up the draw. It is accelerating rapidly as it goes up over the top of the hill.

Time: 0345 Parked near the release crane, it looks like the plume is going towards the north knoll and up the draw.

Time: 0350 We're taking the fogger down to refuel it.

The observations indicate that plume behavior was remarkably steady throughout the hour. Most of the time, the plume was transported into the southeast draw and up over the saddle between the two peaks, and when it wandered from this trajectory, it veered no further than the north or south peaks. Other observations indicate that the trajectory of the plume over the hill rose sharply over the saddle with little discernable depression in the lee. As the plume 'jumped' over the saddle, acceleration in the flow was readily apparent, and the plume appeared to be diffusing steadily in the turbulent flow.

Photographs of the plume illustrate many of these observations, and one characteristic photo is displayed in Figure 45. This photo is part of a series taken from camera position 0-19 (behind the release crane, see Figure 46), toward magnetic bearing 240°. Each photo in the series is a 5-minute time exposure.

Seen from behind the release crane, the plume is fairly compact and very steady. The plume appears to approach the hill along a level trajectory, and then lifts just enough to follow the terrain up and over the hill. Areas between the two peaks above the 50 m height contour appear to receive the most plume material, but the plume becomes very diffuse near the hill top. It therefore cannot be seen clearly just where over the top the bulk of the plume goes when it does not go over the saddle.

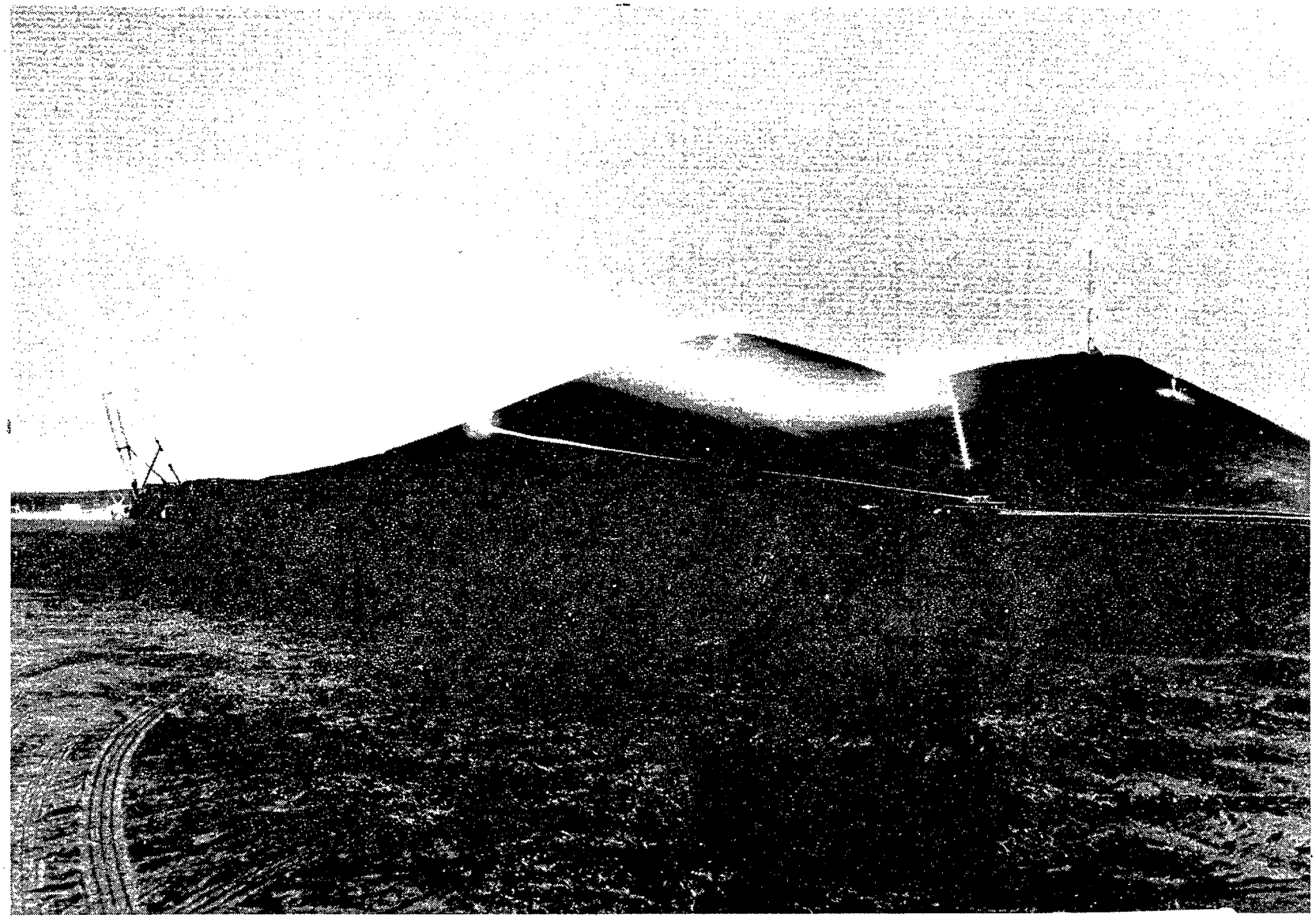

Figure 45. View of the 5-minute average plume trajectory between 0325 and 0330 MST taken from behind the release (position 19) during Experiment 205, Hour 4.

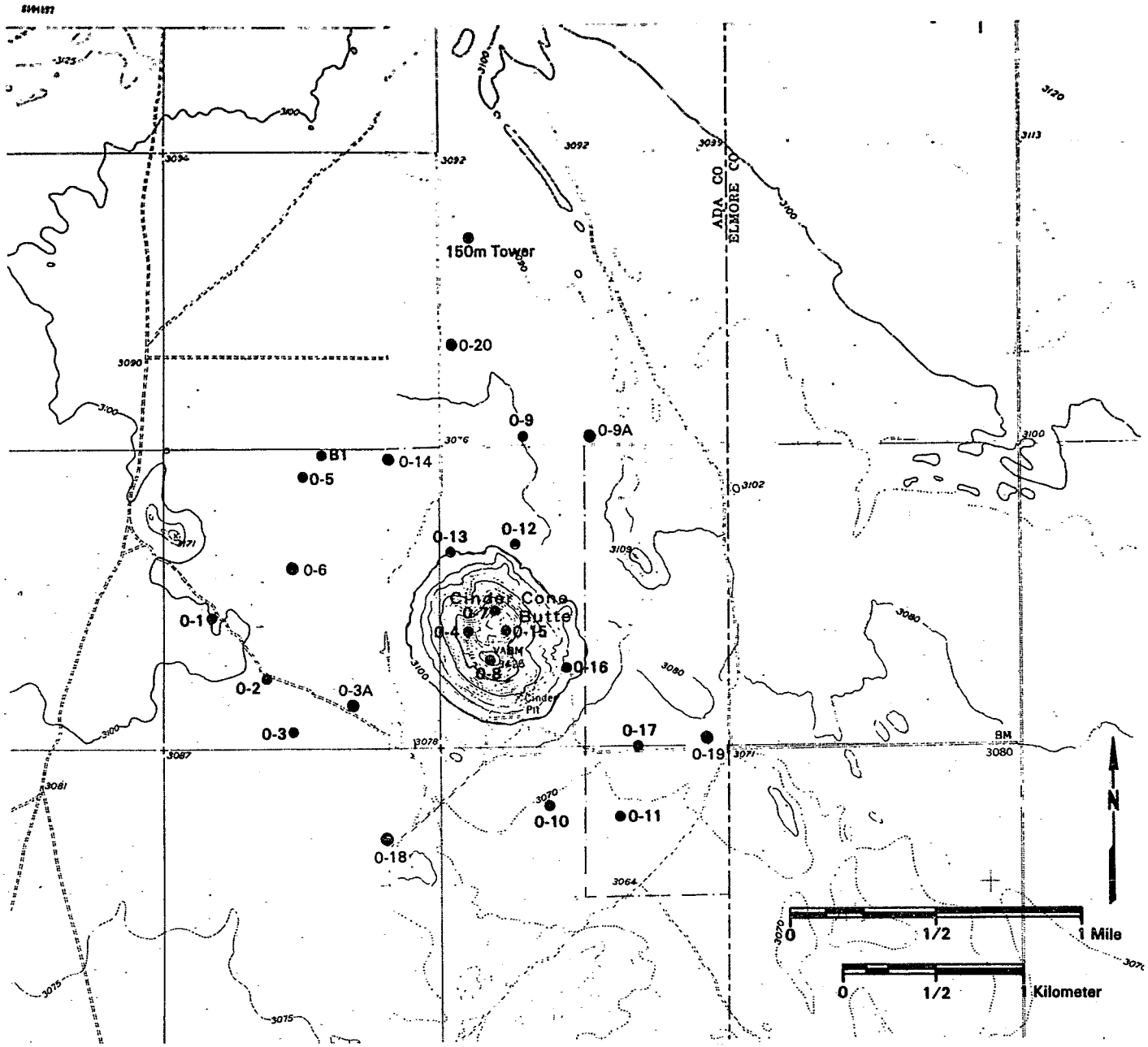

Figure 46. Preselected camera locations.

Lidar data during this hour are fairly sparse, but the plume was so steady that even two or three profiles of the plume in three planes provide useful information. All three lidar sampling planes were on the upwind side of the hill. One of these was near the base of the hillsource, one was near the 20 m height contour, and the third cut across the 50 m height contour of the southeast shoulder of the hill. Plume centroid positions from these planes are plotted in Figure 47 and they agree with plume trajectories seen in the photographs.

Meteorological Information

Wind and temperature data measured at tower A during this hour were used to characterize the flow in terms of H_c. However, because the V-component of the wind set at 40 m was missing during this experiment, wind speeds were inferred for this height before H_c was computed.

Wind speeds at 40 m were inferred from the data from the 80 m wind set and the U-component measured at 40 m. We assumed that the 80 m wind direction was not much different from that at 40 m and therefore, this direction was used to calculate the total wind speed at 40 m. Furthermore, to include the speed adjustment applied to the wind data (see Section 5.1), the computed 40 m wind speed was modified by the same factor used in adjusting the 80 m wind speed. This is an approximate method intended to produce wind speed estimates that are at least partially consistent with the good data obtained at 40 m. Because the winds were from the south-southeast, small errors in wind direction should not have produced large errors in the inferred wind speed.

The hourly averaged value of H_c is 15 m, which indicates that the plume at 40 m should have surmounted the top of the hill. The flow above H_c has a bulk hill Froude number of 3.0; hence, stratification had only a weak effect on the flow over the top. Fr_L for the flow above H_c is 0.74, which indicates a potential for some depression of the plume on the lee side.

Figure 48 contains plots of the 5-minute H_c and Fr_H values for this experiment. H_c was approximately 10 m for the first 35 minutes of the hour and then rose steadily to a peak of more than 30 m by the end of the hour. Fr_H held steady near 3.0 for the hour. However, nothing in the observation logs or in the available photographs indicates that the plume behaved differently during the latter part of the hour as H_c grew from 10 m to 30 m. If the concentration field was similarly insensitive to this change in H_c, then models that treat the flow below H_c as a "dead" layer may be too sensitive to this parameter. (But the 10-minute concentrations do reflect the H_c trend-see below).

The hourly averaged wind speed at 40 m on tower A is estimated to be 5.9 m/s, and the direction from the 80 m level is 123°. Figure 49 shows the trend in wind speeds between 10 m and 80 m during the hour. The wind speed shear is seen to be substantial, and the inferred winds at 40 m appear reasonable. During the first half hour, the winds were fairly constant, but wind speeds at each level fell off during the last half hour. This decrease

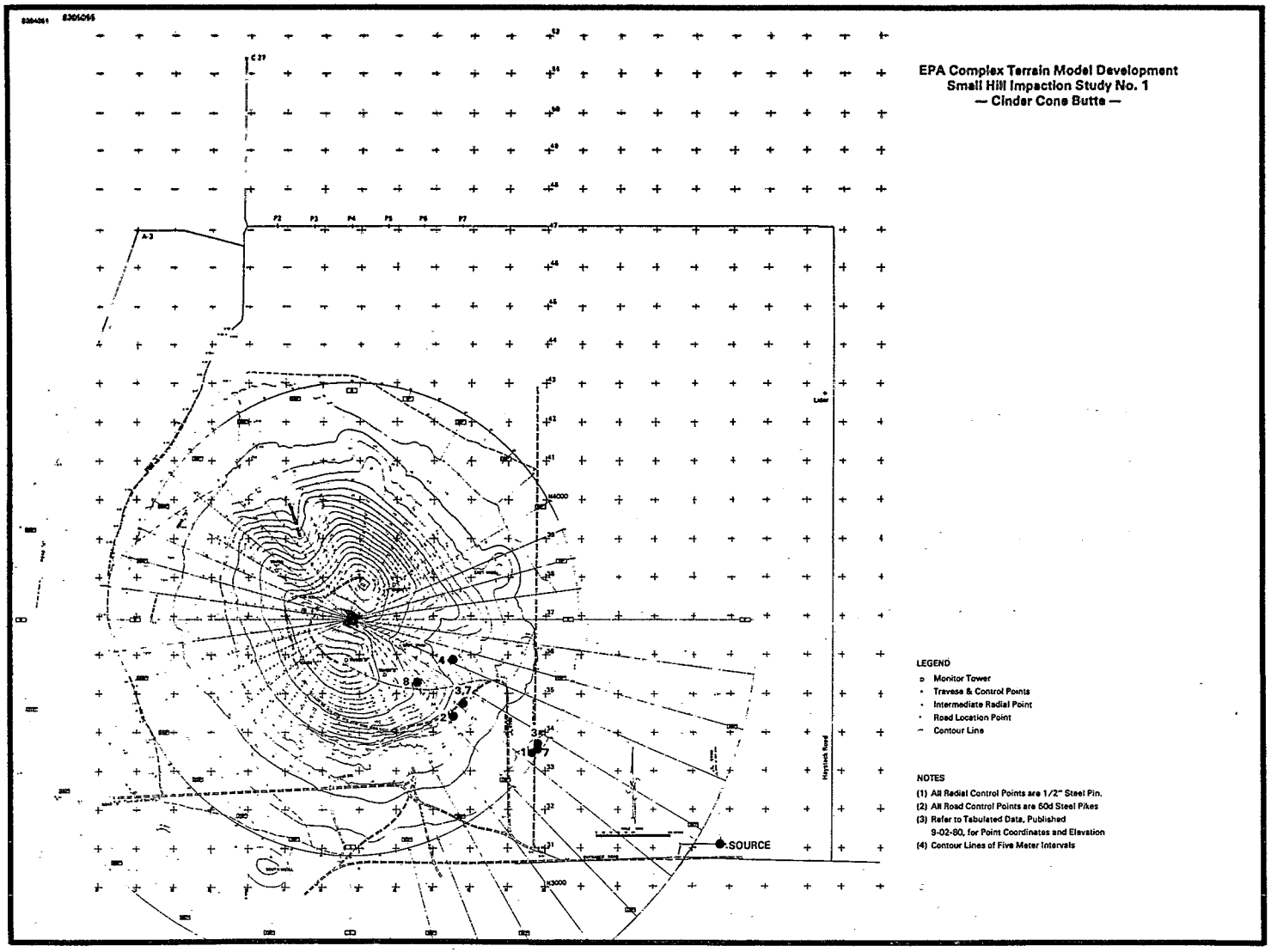

Figure 47. Plume centroid positions calculated from lidar data. Experiment 205, Hour 4 (0300-0400 MST).

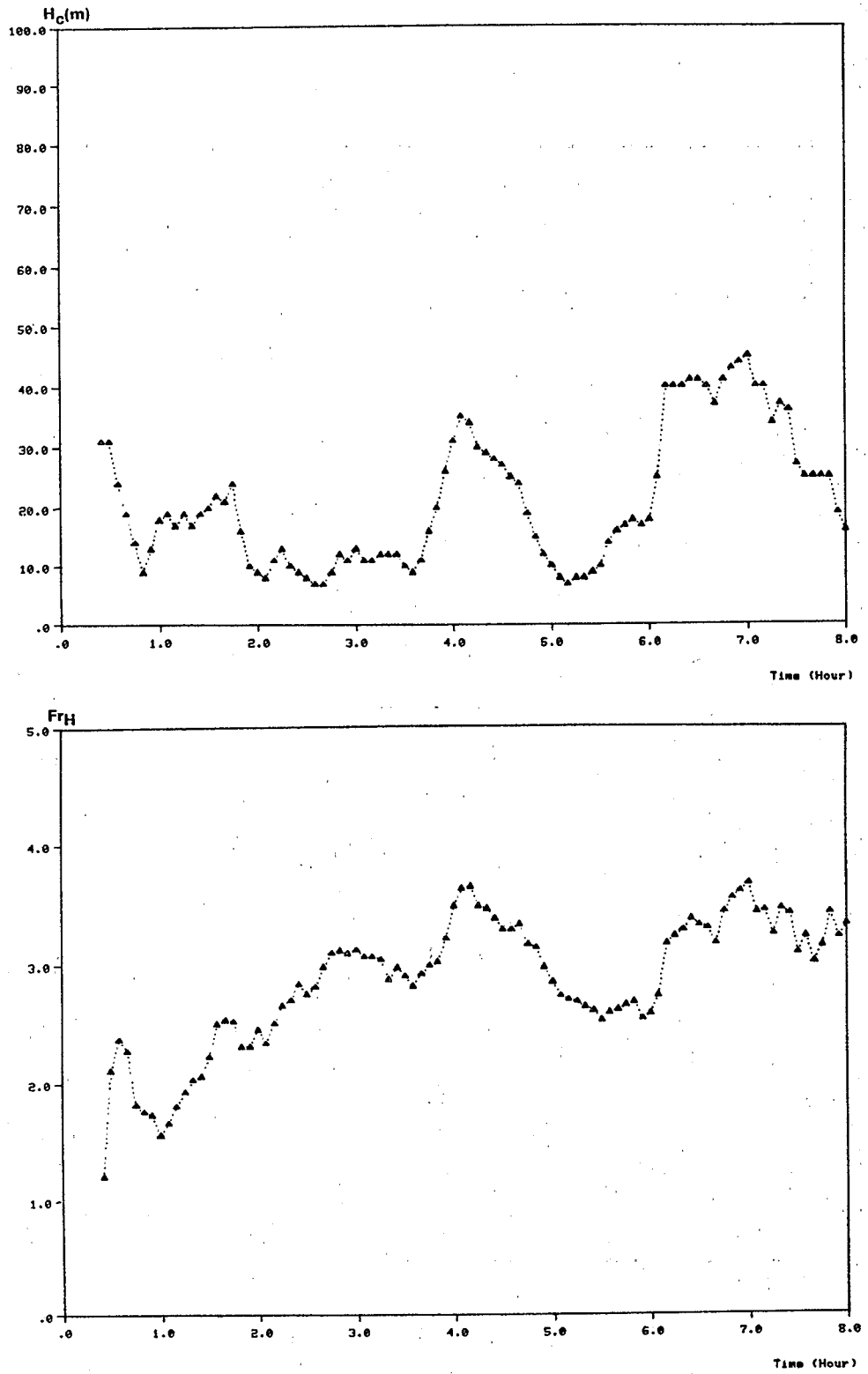

Figure 48. Calculated dividing streamline heights (H_c) and bulk hill Froude numbers above H_c (Fr_H) for Experiment 205.

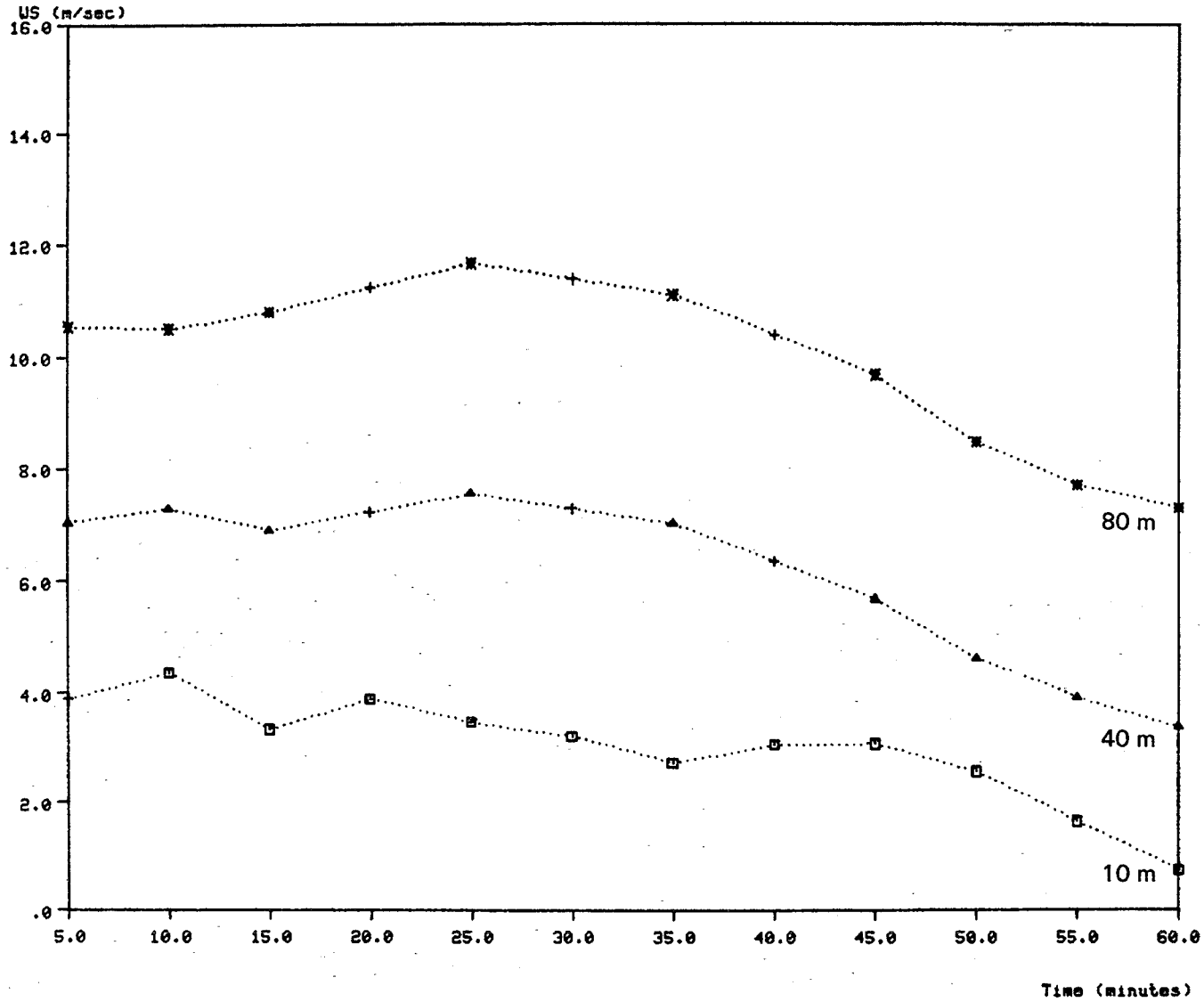

Figure 49. Tower A wind speeds during Experiment 205, Hour 4 (0300-0400 MST).

in speed corresponds to the increase in H_c. Because of the wind speed dilution factor in expressions for computed concentrations and because in the Lift model the increase in H_c brings the plume closer to the hill surface as it travels over the top, concentrations in the latter part of the hour might be expected to be greater than those early in the hour, given similar wind directions.

Variations in the wind directions measured at tower A at 10 and 80 m are presented in Figure 50 as frequency distributions. The distribution of 10 m winds covers a range of 30° and that at 80 m covers about 10°. The 80 m wind distribution is probably more representative of the winds at release height because the photos and the observation log both suggest that the wind direction was very steady.

In summary, the plume was released above H_c in a region characterized by 4 to 7 m/s winds, virtually no wind direction shear, very little wind meander, and large Froude numbers (both Fr_H and Fr_L suggest only weak stratification effects). Therefore, it is likely that the plume traveled horizontally until it got close to the hill and then flowed over the top with some depression in the lee. This is quite consistent with the observations and photos reviewed above.

SF_6 Concentrations

The distribution of hourly averaged SF_6 concentrations over the surface of the hill is shown in Figure 51. The pattern indicates that most of the plume material went over the saddle between the two peaks, producing the highest concentrations in the saddle areas. Other significant concentrations are found between the 30 m contour in the southeast draw on the windward side of the hill and the 35 m contour near the northwest draw. The 30 m height contour corresponds directly to the relative release height. This pattern is consistent with the smoke plume observations and the flow parameters derived from the meteorological data.

The distribution of 10-minute SF_6 concentrations is presented in Figure 52. Very little SF_6 is measured during the first 10-minute period even though the photographs show the oil-fog plume traveling toward the center of the hill. This may be attributable to not having 10-minute average SF_6 data anywhere on the windward side of the hill during this period. Most of the other plots contain data from both the windward and leeward sides of the hill, and concentrations just beyond the saddle (on the lee side) tend to be greater than those upwind. The only time when the concentrations on the windward face exceeded concentrations just beyond the saddle was during the last 10 minutes of the hour. Concentrations were expected to be quite small during this period, because the tracers were shut off at 0350, but those concentrations measured in the southeast draw are nearly as great as any other during the hour. This implies that the increase in H_c late in the hour could have brought the plume closer to the surface, and the material released between 0345 and 0350 (the travel time to the hill center with the 4 m/s winds is about 5 minutes) produced concentrations as large as those produced earlier in the hour over 10-minute time periods.

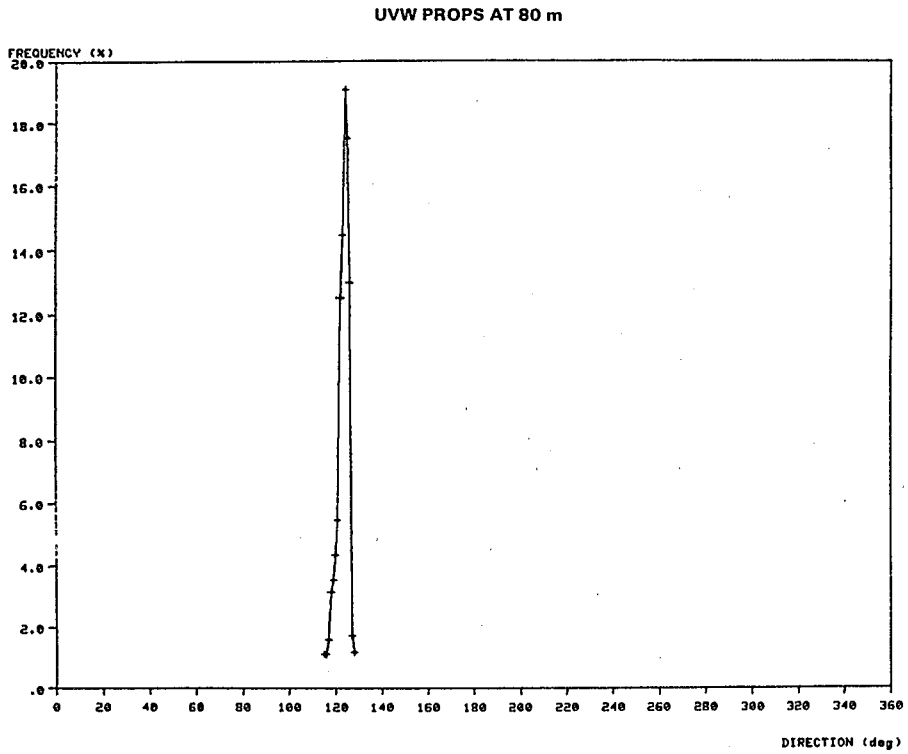

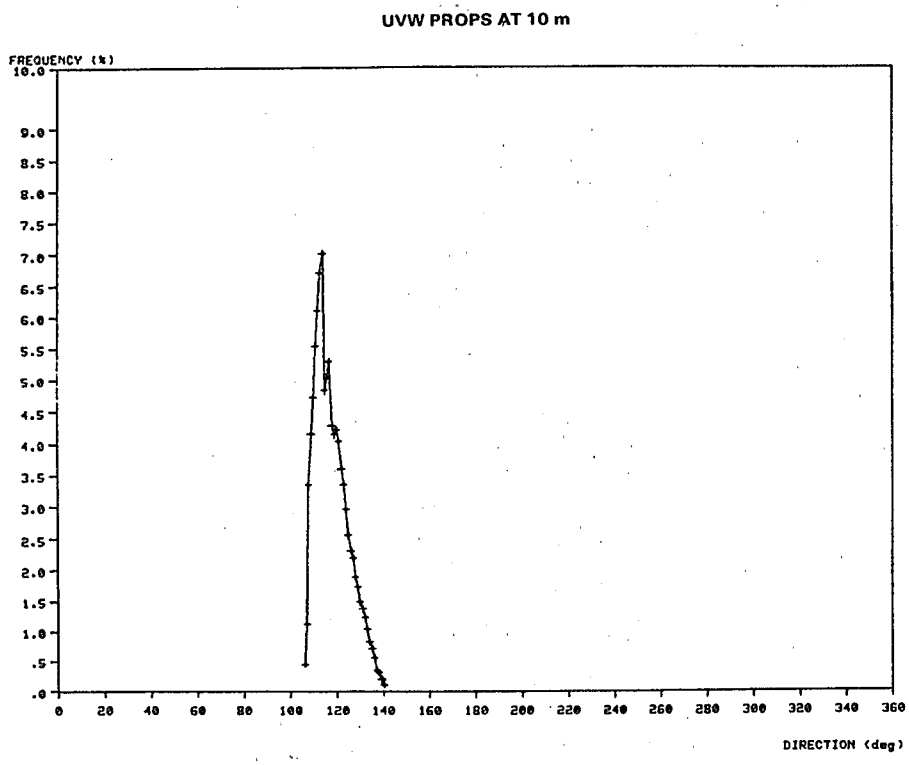

Figure 50. Calculated wind direction distribution functions for Experiment 205, Hour 4 (0300-0400 MST).

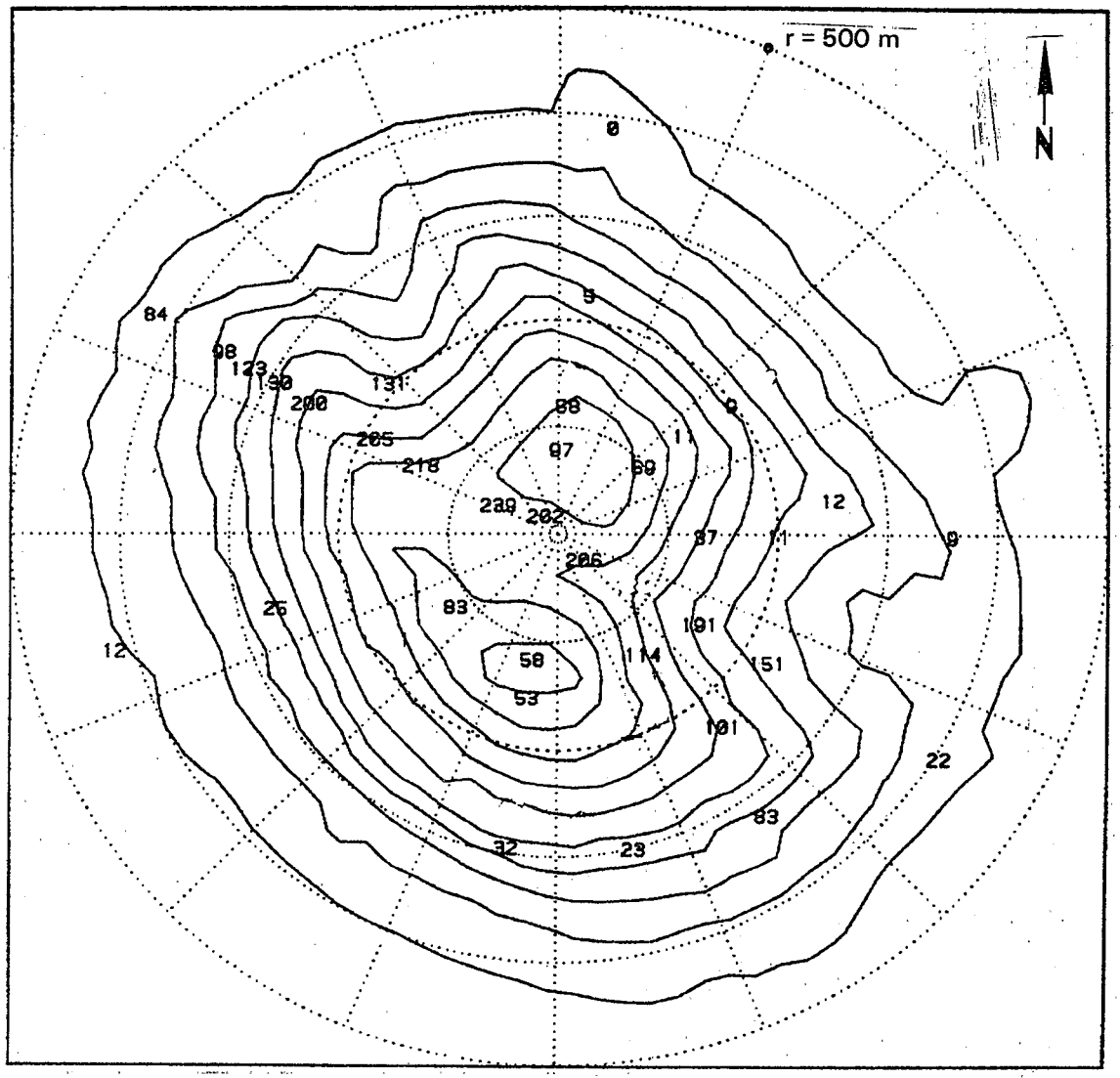

Figure 51. Observed SF_6 concentrations (ppt) for Experiment 205, Hour 4, (0300-0400 MST). Source: r = 1155.1 m, θ = 120.1°, net height = 31.1 m, Q = .083 g/s.

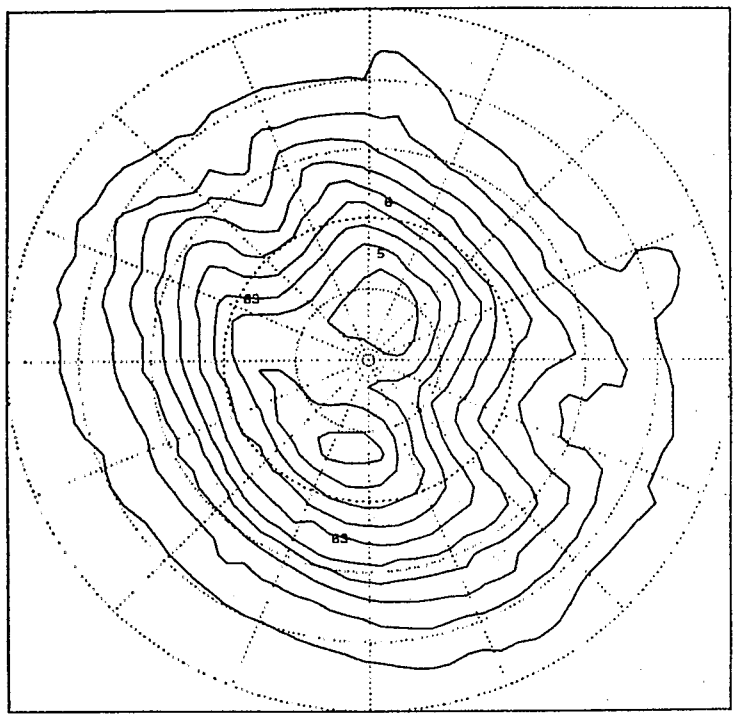

TIME PERIOD 0300-0310

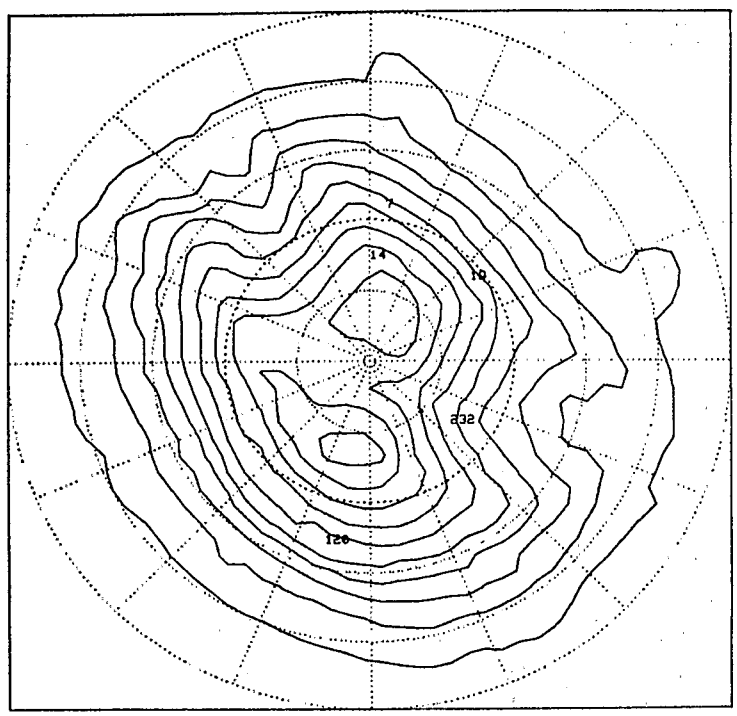

TIME PERIOD 0310-0320

Figure 52. Observed 10-minute average SF_6 concentrations (ppt) for Experiment 205, Hour 4 (0300-0400 MST).

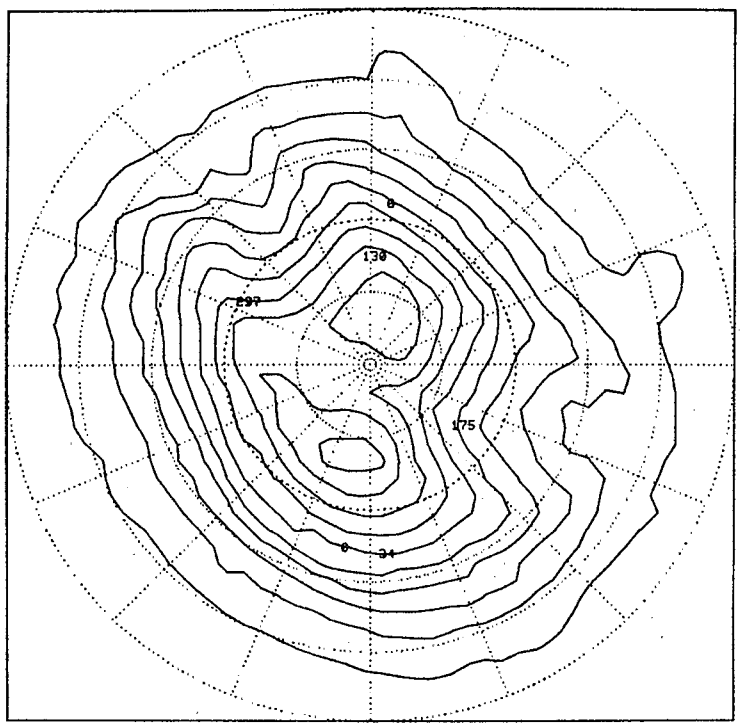

TIME PERIOD 0320-0330

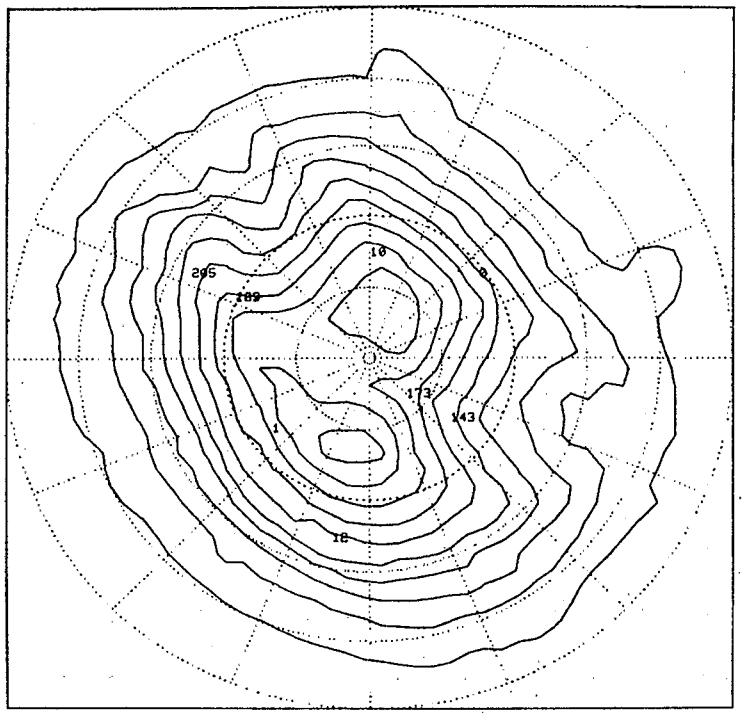

TIME PERIOD 0330-0340

Figure 52. Continued.

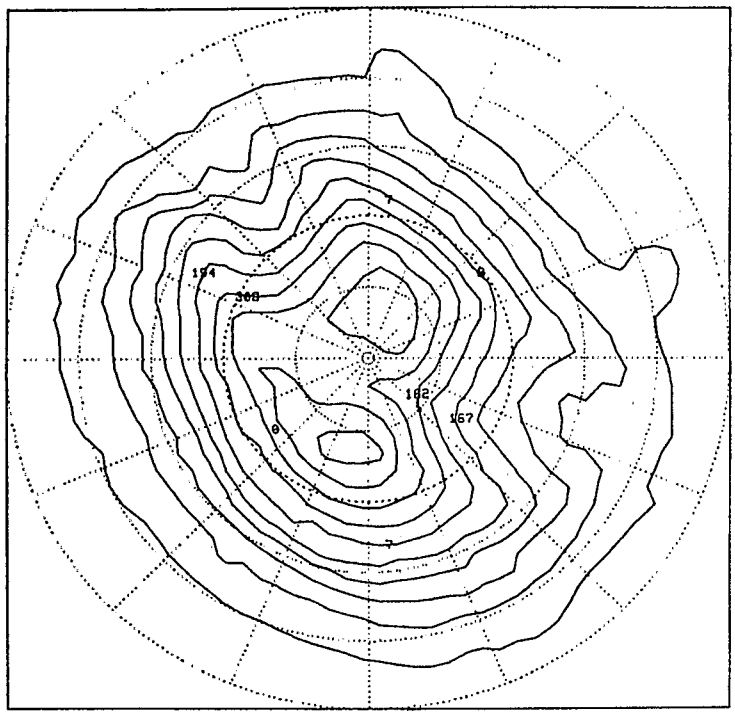

TIME PERIOD 0340-0350

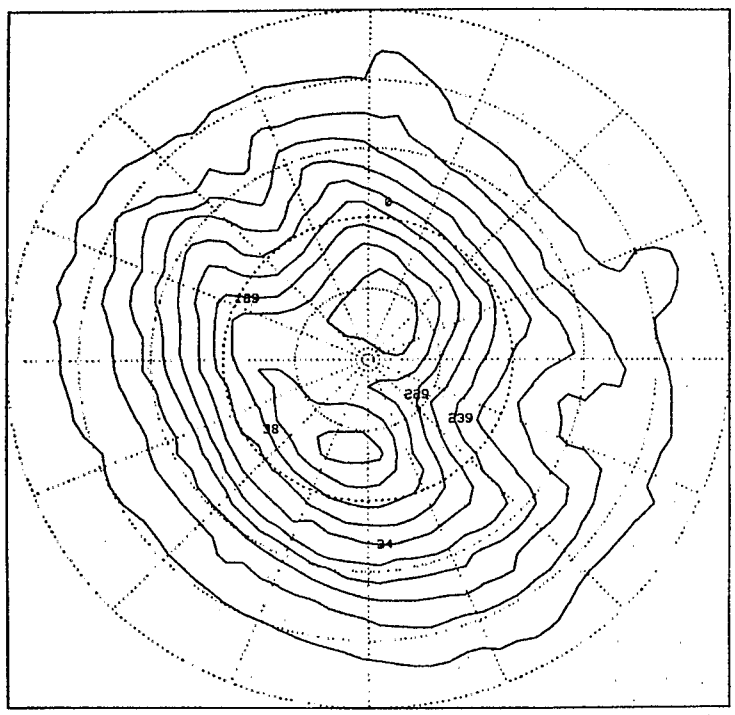

TIME PERIOD 0350-0400

Figure 52. Continued.

4.4.2 Model Performance

This hour was modeled with the Lift model because all evidence indicates that streamlines at plume height traveled freely over the hill. Meteorology used in the modeling was prepared as in Section 4.1.2, except that no interpolation to release height was necessary because the plume was released at 40 m, an instrumented level on tower A. The data are summarized in Table 7.

The 1-hour average wind directions at 10 m and 80 m on tower A (the 40 m wind data were incomplete) are 119° and 123°, and the directions at 10 m and 30 m on tower B are 117° and 119°. Lidar data support a transport wind direction between 117° and 122°, and the photographs support a direction of almost 121°. Therefore, the modeling wind direction for this hour is set to 121°. Because the PDF computed from the 80 m directions is narrower than that at 10 m, the 80 m PDF is judged to be more representative of the wind distribution at source height.

Neutral was rerun with the new meteorological data. Instead of estimating a peak value 117% of the observed peak value, it produced a value 129% of the peak observed. The peak observed value occurs on the saddle above the northwest draw, and the modeled maximum occurs near the height of release in the windward draw. Concentrations in the windward draw area and around the two peaks are generally high, but concentrations elswewhere compare well. Figure 53 shows the distribution of calculated concentrations plotted on a map of CCB, and the results are also summarized in Table 7.

Results from Lift computations are displayed in Figure 53, and are also listed in Table 7. Concentration estimates are generally too low. The maximum occurs halfway down the lee side and is 72% of the largest observed concentration. Some of the discrepancy between modeled and observed concentrations appears to be caused by a slight misalignment in the mean wind direction. The model tends to shift the concentration field too far toward the north peak (more weight should have been given to the wind directions from tower B). Had the patterns been aligned better, the model estimate of 172 ppt on the lee side of the hill would have been comparable to the observed concentrations of 200 ppt to 205 ppt in that same area. But such a shift would not have improved the correspondence on the windward side and over the saddle.

Terrain factors (T_o) computed from model estimates and observed concentrations in the upper portion of the southeast draw and over the saddle vary between 0.73 and 0.83. A couple of concentration estimates on the southern side of the draw produce T_o values near 0.6, but these are probably unrealistically low because of the wind alignment problem. T_o values on the lee side range from 0.76 near the saddle to 1.0 at the base of the hill, and these too are likely to increase (at least near the hilltop) with a shift in the wind direction. Therefore, within the framework of Lift, terrain factors of 0.7 to 0.8 over the top of the hill appear reasonable. Moreover, a factor near unity fits the observations toward the base of the hill, even on the lee side, which indicates that any lee wave

TABLE 7. NEUTRAL AND LIFT MODEL CALCULATIONS - EXPERIMENT 205, CASE HOUR 4

Meteorological Data

wind direction(deg)	=	121.
wind speed(m/s)	=	5.9
critical dividing streamline height(m)	=	10.0
Iz	=	.031
Iy	=	.069
N(1/s)	=	.042

Source Data

direction(deg)	=	120.
distance(m)	=	1155.1
release height(m)	=	40.0
SF6 emission rate(g/s)	=	.083

Receptor Coordinates X(m)	Y(m)	Z(m)	Observed SF6 (ppt)	Neutral Predicted SF6 (ppt)	Lift Predicted SF6 (ppt)
360.22	.00	13.26	9.20	1.20	.00
208.35	.00	31.25	11.00	91.67	8.09
142.00	.00	50.00	37.40	260.29	94.76
257.78	33.94	30.00	12.10	19.05	.00
195.15	149.74	27.41	2.90	2.93	.00
85.15	64.88	80.00	69.00	264.08	13.83
51.04	387.66	11.78	.00	.07	.00
29.59	224.79	51.51	5.16	64.97	.00
15.97	121.29	90.94	58.40	250.81	14.73
10.61	80.56	91.97	96.70	268.29	108.46
2.15	18.88	80.00	201.70	275.42	118.51
-38.04	-288.98	32.94	31.90	.08	.00
-15.01	-113.99	98.96	57.70	210.60	12.64
-19.85	-149.12	90.00	52.50	167.71	8.90
-84.85	-65.12	90.00	82.80	203.51	26.76
-396.68	-106.29	3.44	11.80	.39	.00
-248.96	-66.71	32.90	24.80	17.12	.00
77.87	-290.63	35.10	23.00	.57	.00
199.06	-259.43	30.00	82.80	13.49	.00
91.36	-109.36	65.00	114.00	247.20	25.73
163.68	-175.52	50.00	101.10	178.26	19.93
355.15	-205.04	5.69	21.70	31.67	49.07
204.15	-117.12	30.00	150.90	206.23	77.13
142.15	-81.12	40.00	191.00	308.37	86.34
37.15	-21.12	70.00	205.80	280.53	98.60
-359.96	207.82	8.94	83.60	72.91	116.90
-297.11	171.54	28.07	98.10	151.48	116.11
-269.62	155.66	38.07	123.20	207.05	115.58
-246.20	142.14	47.96	129.50	222.18	115.03
-153.85	89.88	70.00	205.08	239.85	111.86
-111.85	65.88	80.00	217.90	248.22	109.81
-40.85	28.88	80.00	239.20	263.81	105.43
-141.42	141.42	50.00	131.00	236.67	171.54

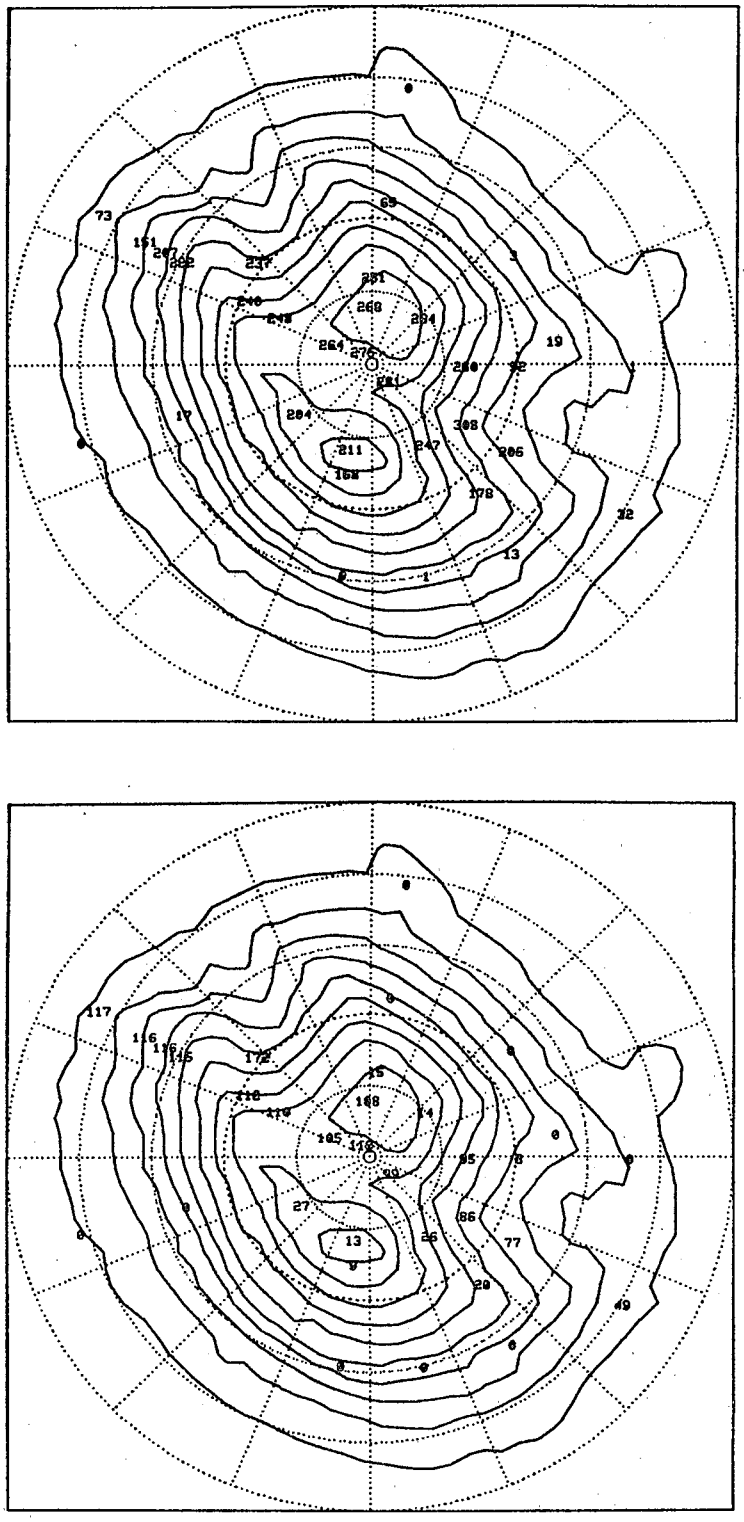

Figure 53. SF_6 concentrations (ppt) estimated for Experiment 205, Hour 4 by the Neutral (top) and Lift (bottom) models.

influence near the hill produced no net change in the symmetry of the terrain factor from the windward side of the hill to the leeward side.

In summary, the use of a terrain factor between 0.7 and 0.8 over the top of the hill would improve the estimates from both the Neutral and Lift models. Furthermore, the narrower horizontal distribution produced by the PDF appears to provide a better representation of observed concentrations than does the Gaussian distribution based on the measured i_z.

4.5 Experiment 205, Hour 5 (0400-0500 MST)

4.5.1 Summary Description

Thermofogger oil-fog and SF_6 tracer gas were released from the southeast side of the hill at 1155.1 m, 120.1° for nearly the entire hour. The SF_6 release began at 0403 and terminated at 0455. The oil-fog ran from 0400 through 0500. The release height was 50 m, 10 m higher than the release height during the previous hour. However, because the release terminated 10 minutes early during the previous hour, the height change is not a factor in interpreting the SF_6 measurements made during hour 5.

Local terrain elevations near the release point are estimated to be -8.9 m relative to the zero of the hill coordinate system, so the net release height corresponds to the 41.1 m height level on the hill. The SF_6 release rate is computed to be 0.087 g/s with an estimated uncertainty of $\pm$7.7%. No Freon was released.

Plume Observations

Many observations of the appearance and trajectory of the oil-fog plume are available for this hour.

Time: 0402 They are back up with the thermofogger at 50 meters.

Time: 0406 (?) Plume is still going up the draw after switching release height to 50 m. Heading right over the mobile crane towards the draw. Plume is a little more wispy looking at this altitude.

Time: (?) Smoke odor is evident outside sampler trailer, but is much stronger over by draw. Odor may be stronger standing up (or on boxes, etc.) than right close to the ground.

Time: 0430 Tethersonde winds at 40 m: 120-130°, 10.5 m/s.

Time: 0437 The lidar was reporting that this new plume at 50 meters was going up and over the hill. From my vantage point, behind the release crane, it looks like that might be possible. The plume travels level toward the hill until it gets in the vicinity of the mobile crane and then does a steep climb. It looks almost like it goes through the draw area, but even with the two peaks, which would put it some 10 meters above the ground or so. Because the wind speed now is so brisk in the 8-9 m/s range, the plume is becoming harder to see.

Time: 0440 I'm down around B3 and it definitely looks like the plume is going over the hill in the vicinity of the draw. This is really beautiful to see, we've talked about this, seeing the plume approach and then just go up and over the hill without appearing to touch it too much, although I'm sure that there is some impact. The tethersonde winds are 120 at 10 m/s.

Time: 0450 Plume is elevated as it goes through the draw (view from north butte); then drops in lee. The plume goes fairly level until it goes in the vicinity of the mobile crane (about 50 m from the crane towards the hill) and then it climbs slowly over the draw. It does quite a hook up and over the hill, returning to some former altitude although it's in back of the hill and I can't see. The plume seems to go across the top of the hill about even with the first light on the FAA tower, which would probably be about 50 to 80 ft above the top of the north butte. Actually I think it is a little bit below the first light on the FAA tower, which is the light 1/2 way up, so maybe it is 30-40 ft above the north butte.

Time: 0459 The plume is dropping to 30 meters.

The observations point out that the plume trajectory was very steady throughout the hour, and very similar to the previous hour (see Section 4.4).

Photographs of the plume illustrate the observations very well. A representative photograph reproduced in Figure 54 was taken from camera position 0-19 (see Figure 46) behind the release crane. The photo is a 5-minute time exposure.

The high wind speed caused so much dilution of the smoke plume that it is difficult to see the plume in the photos taken from the top of the hill. However, enough contrast is generated in the views from position 0-19 to show the plume bending over the saddle. The plume appears to stay quite high as it passes over the hill, so the area of greatest impact was likely to be just over the top of the hill, or possibly a short way down the back side.

The lidar sampled the plume along three planes upwind of the hill, one plane over the center of the hill, and two planes in the lee. Although there were few samples in any one plane, they were spread out over the hour, therefore illustrating how uniform the wind direction was (see Figure 55). The sections in the lee of the hill indicate that the plume returned to its initial height by the time it reached the downwind base of the hill, but the one section 1,200 m downwind of the hill center produced a centroid height of about one-half the release height, indicating that the plume may have continued to drop with increasing downwind distance.

Meteorological Information

Wind and temperature data measured at tower A during this hour have been used to characterize the flow in terms of H_c. However, because the

Figure 54. View of the 5-minute average plume trajectory between 0415 and 0420 MST taken from behind the release (position 19) during Experiment 205, Hour 5.

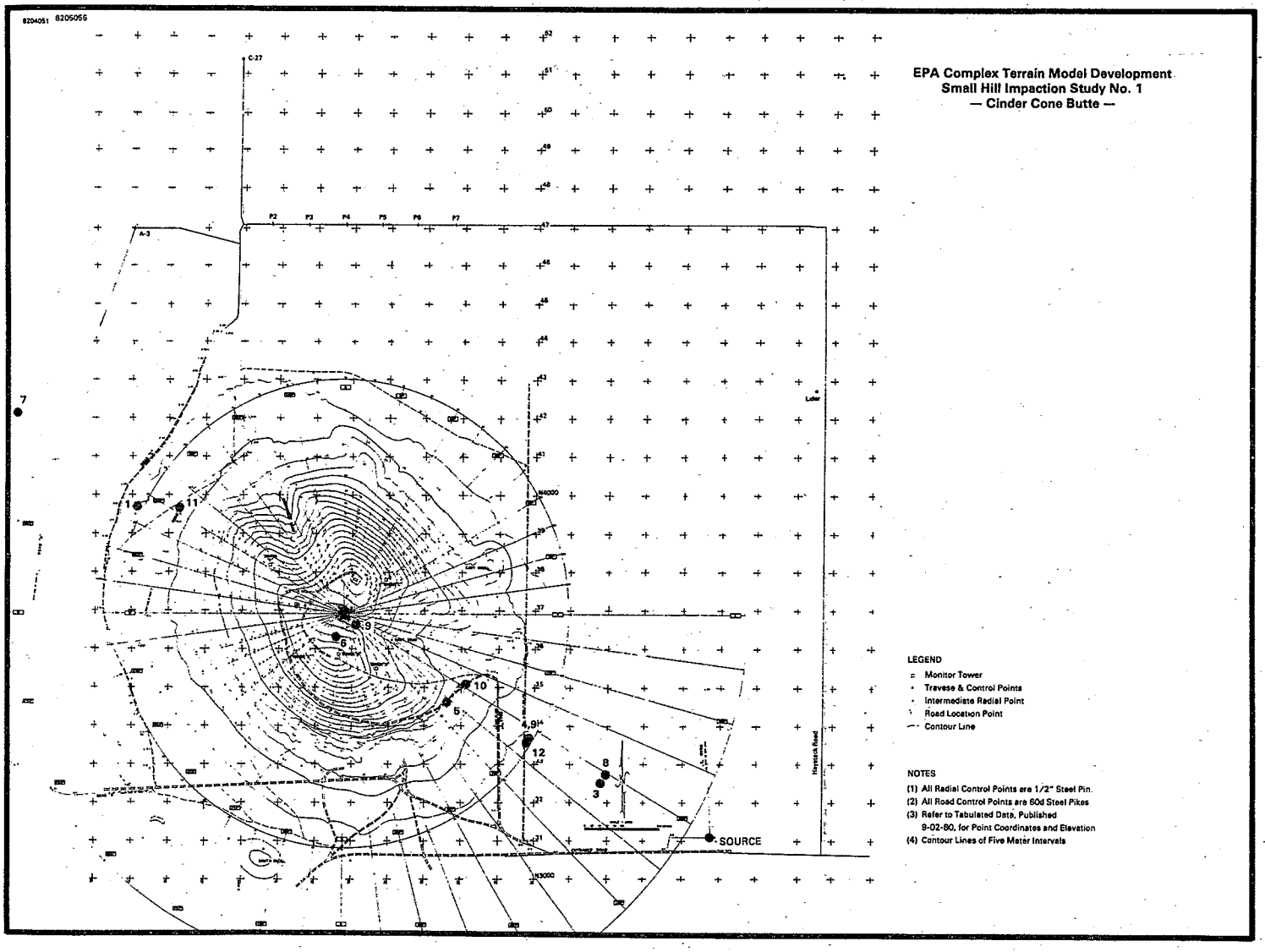

Figure 55. Plume centroid positions calculated from lidar data. Experiment 205, Hour 5 (0400-0500 MST).

U-component of the wind set at 40 m was missing during this experiment, wind speeds were inferred at this height before H_c was computed. The method followed in calculating speeds at 40 m is outlined in Section 4.4.1.

The average H_c over this hour is 24 m, and the bulk hill Froude number above this level is 3.3. Because the local release height was 50 m, the plume was well above H_c and should have behaved like the plume of the previous hour. Fr_L is 0.86, indicating only a weak tendency to produce a streamline depression in the lee. None of the observer comments indicate a depression in the lee and none of the photographs capture one, but the lidar data downwind of the hill show lower plume centroid heights in this area. If a depression is indeed absent, then the lidar might be seeing the results of significant mixing in the wake.

Figure 48 contains plots of the 5-minute H_c and Fr_H values for this experiment. H_c is seen to drop from a high of about 30 m to a low of less than 10 m during the hour (reversing the trend seen during the previous hour); but, on the average, H_c is larger. However, the Fr_H values neither follow the trend of the previous hour nor reverse it. Fr_H increases sharply from 2.9 to 3.5 at the start of the hour and then slowly declines to its initial level. These changes in the H_c and Fr_H did not produce any discernable changes in the observed plume trajectory.

The hourly averaged wind speed at 40 m on tower A is estimated to be 5.2 m/s, and the direction from the 80 m level is 121°. Figure 56 shows the trend in wind speeds between 10 m and 80 m during the hour. Wind speeds increased steadily throughout the hour at all levels from the low of the previous hour. This wind speed increase drove the decrease in calculated H_c values during the hour. Because H_c is largest and wind speed is smallest early in the hour, calculated concentrations would be higher.

Variations in the wind directions measured at tower A at the 10 m and 80 m levels are presented in Figure 57 as frequency distributions. The 80 m distribution covers a range of about 15°, whereas the 10 m distribution spans 160°. Clearly, the 80 m distribution is more consistent with the observational data for this hour.

In summary, this hour was very similar to the previous hour. The plume was again released above H_c in a region with wind speeds in excess of 4 m/s, little wind meander, and high Froude numbers. Photographs indicate that the plume behaved accordingly.

SF_6 Concentrations

The distribution of hourly averaged SF_6 concentrations over the surface of the hill is shown in Figure 58. The highest concentration is found at the base of the southeast draw, and the area of highest concentrations spreads from this point up to the saddle between the peaks. Other moderately high concentrations tend to spread around both sides of the south peak.

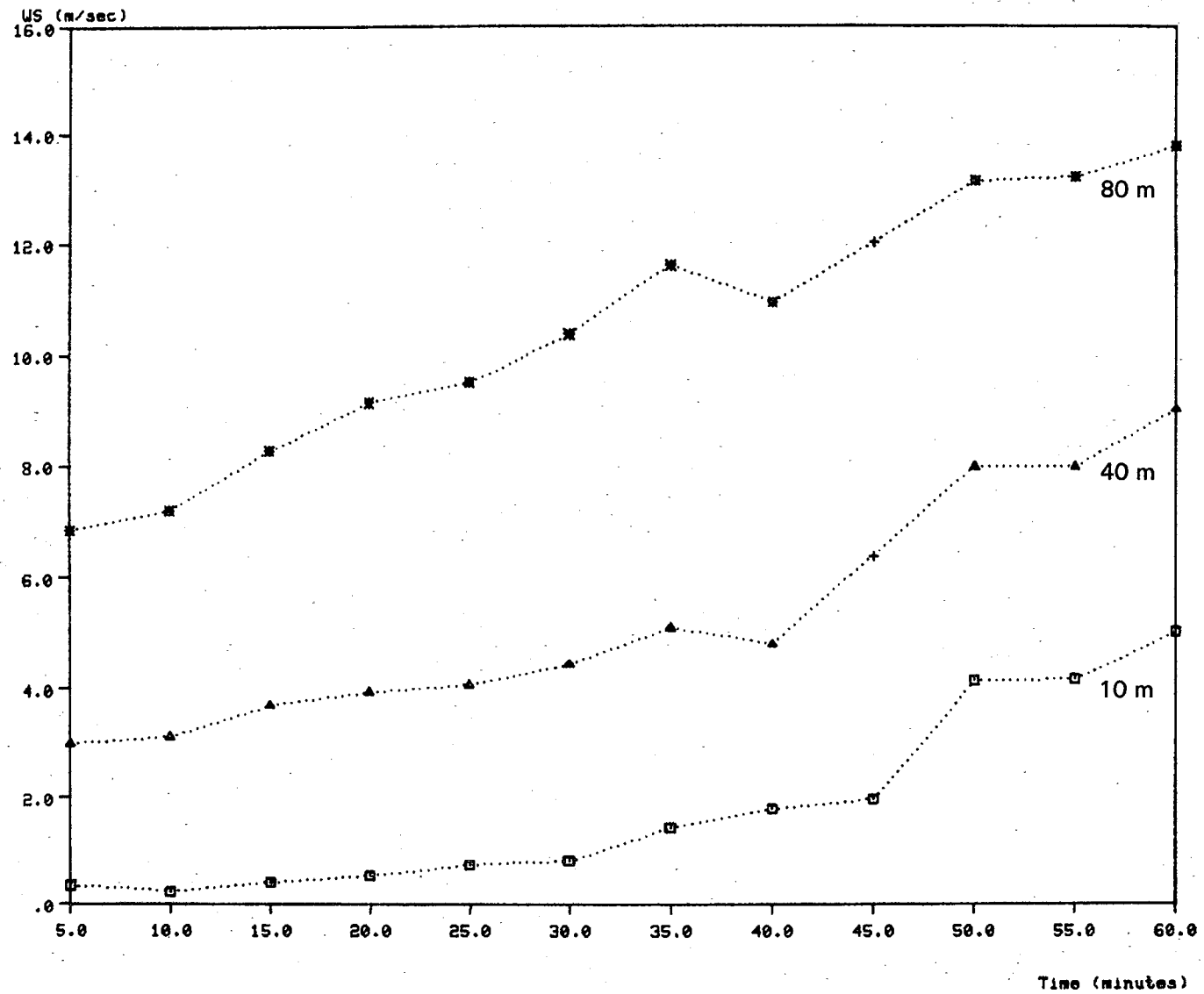

Figure 56. Tower A wind speeds during Experiment 205, Hour 5 (0400-0500 MST).

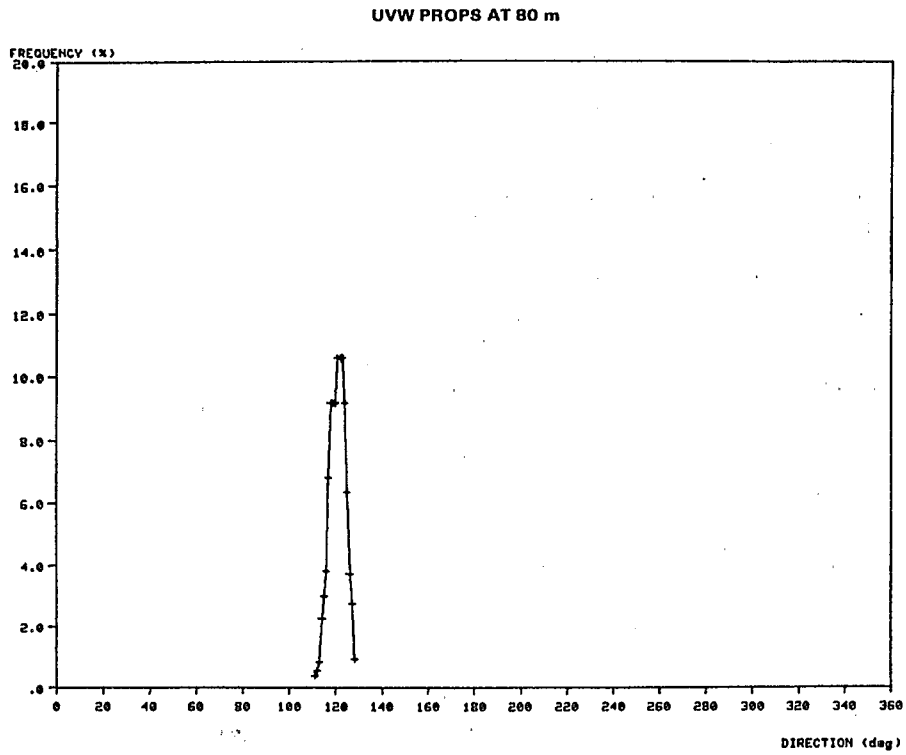

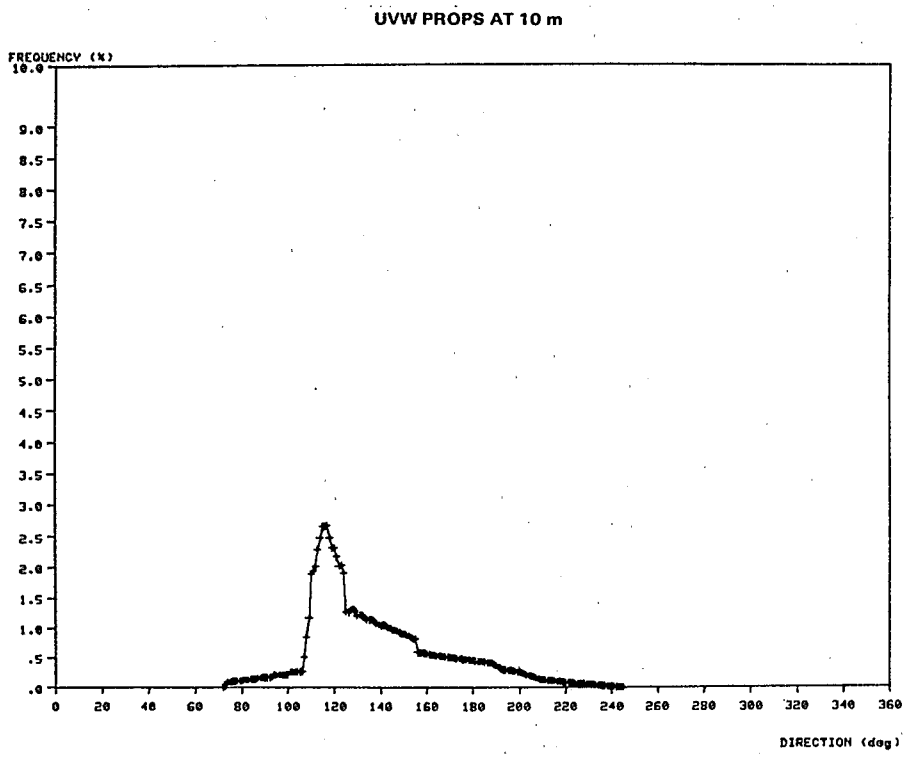

Figure 57. Calculated wind direction distribution functions for Experiment 205, Hour 5 (0400-0500 MST).

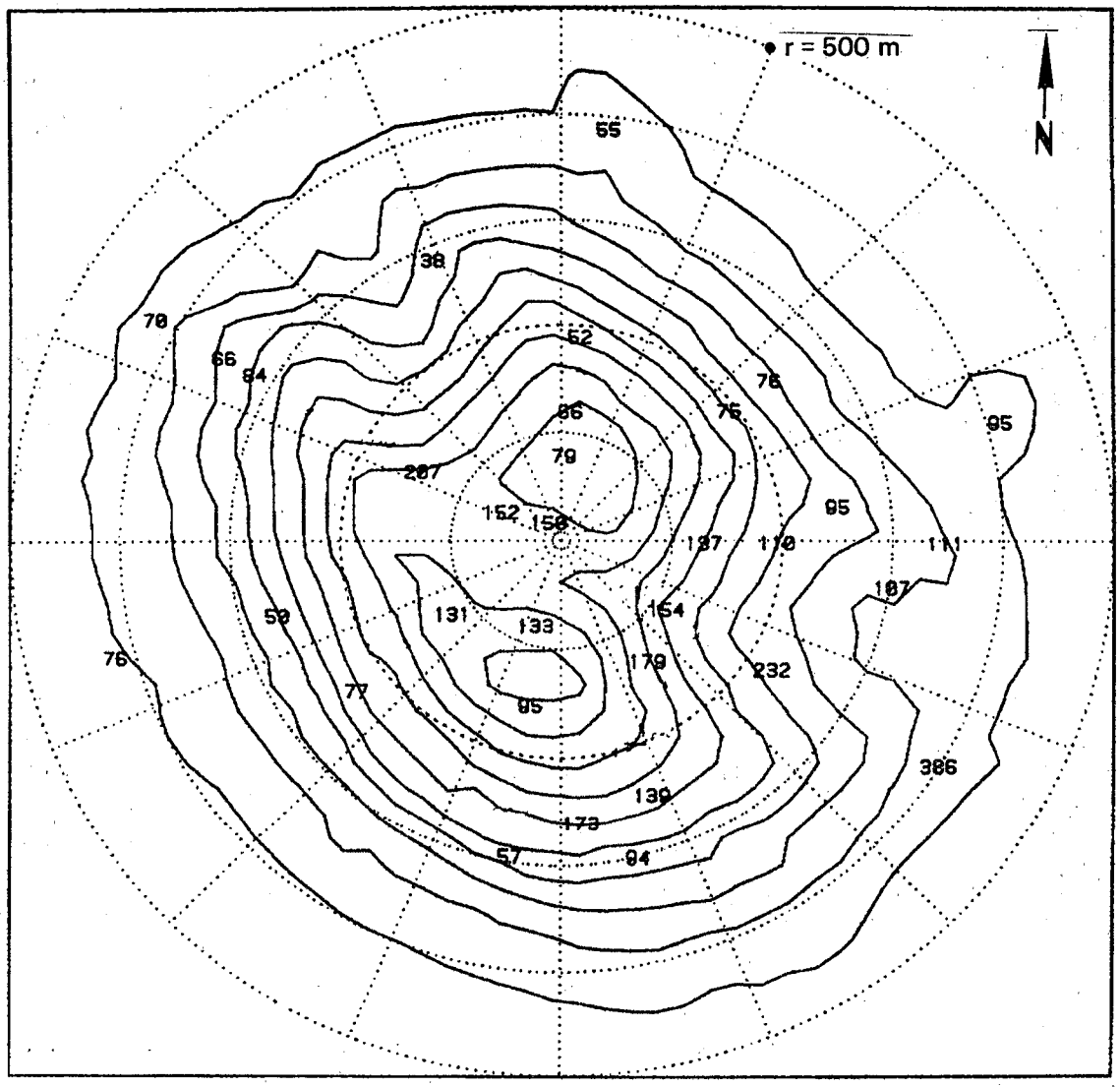

Figure 58. Observed SF_6 concentrations (ppt) for Experiment 205, Hour 5 (0400-0500 MST). Source: r = 1155.1 m, θ = 120.1°, net height = 41.1 m, Q = .087 g/s.

This pattern would seem to indicate a low-level release and substantial dispersion. However, the observational data discussed above describe a very steady, high plume that tended to rise over the hill with little impact. In fact, the major difference between this hour and the last one is that the plume was raised 10 m; consequently, a concentration distribution similar to that shown in Figure 51 would be expected. The patch of high concentrations on the lower part of the windward side of the hill is therefore inconsistent with the SF_6 release height and may be the result of an uncontrolled near-surface release.

The distribution of 10-minute SF_6 concentrations is presented in Figure 59. Concentrations during the first 10-minutes are quite small, indicating that the height change from the previous hour has had no effect on measured concentrations during this hour. The pattern of concentrations during the rest of the hour is consistent with the 1-hour average concentration field. Unfortunately, the 10-minute data provide no further information on the anomalously large SF_6 impact on the windward side of the hill.

4.5.2 Model Performance

This hour was modeled with the Lift model because all evidence indicates that streamlines at plume height traveled freely over the hill. Meteorology used in the modeling was prepared as in Section 4.1.2, and is summarized in Table 8.

Tower A wind directions measured 40 m below and 30 m above the release height are 138° and 121°. Directions measured at 10 m and 30 m on tower B are 116° and 117°. The wind direction inferred from photographic and lidar data varies from 119° to 120°. Therefore, 120° is selected as the model wind direction. The 80 m PDF is considered more representative of the release height than that at 10 m.

Neutral was rerun with the new meteorological data. Instead of estimating a peak value 30% of the peak observed concentration, it produced a value 41% of the peak observed. However, the peak modeled concentration occurs high in the southeast draw, and the observed maximum is found at the base of this draw. With the exception of the larger observed concentrations near the base of the draw, Neutral does an excellent job of reproducing the observed concentration field. Figure 60 shows the distribution of calculated concentrations plotted on a map of CCB, and the results are also summarized in Table 8.

Results of the Lift computations are also presented in Figure 60 and Table 8. The concentrations match observed concentrations better in the lower portion of the southeast draw but are consistently too high elsewhere along the wind trajectory over the hill. Concentrations away from the center of the hill in the crosswind direction also fall off too rapidly to match the observed pattern. These observations indicate that the PDF used in Lift is too narrow and that the distribution based on the interpolated

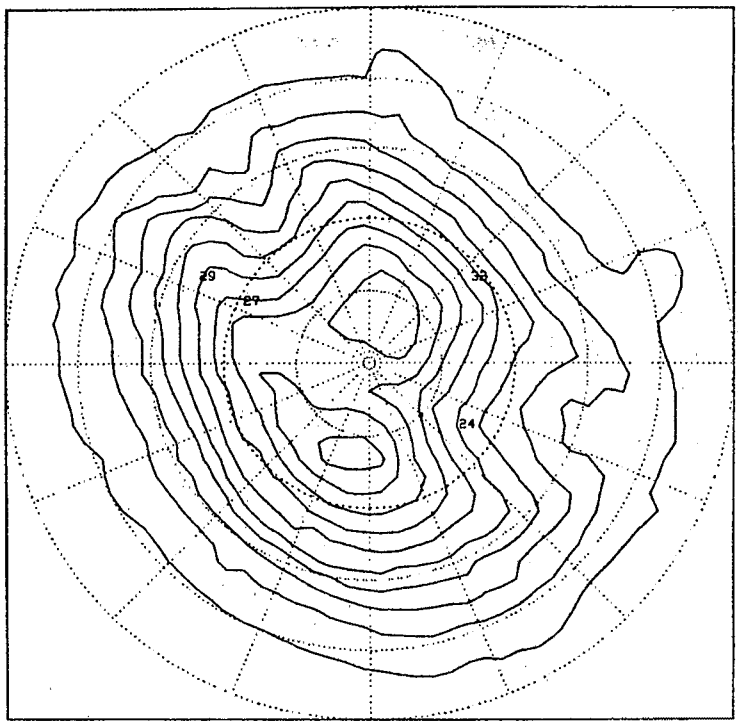

TIME PERIOD 0400-0410

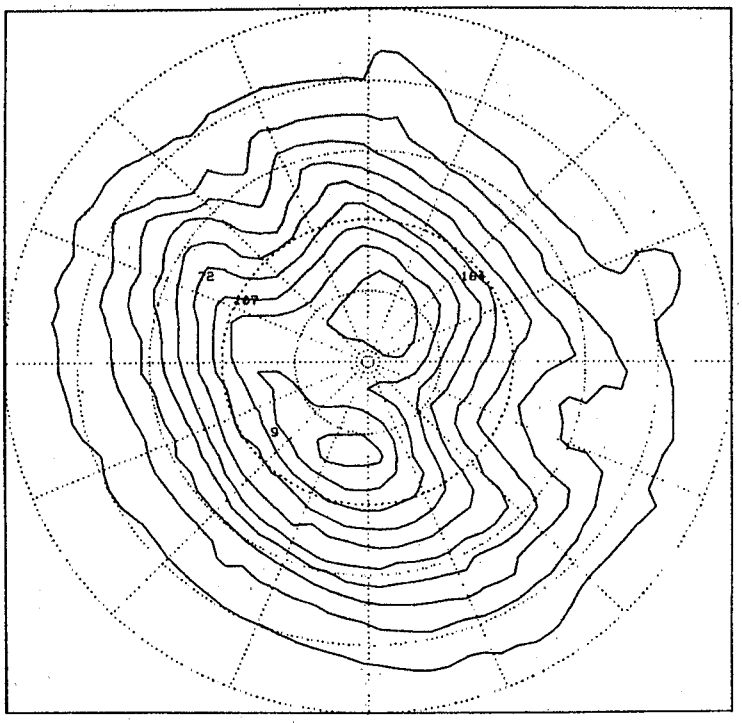

TIME PERIOD 0410-0420

Figure 59. Observed 10-minute average SF_6 concentrations (ppt) for Experiment 205, Hour 5 (0400-0500 MST).

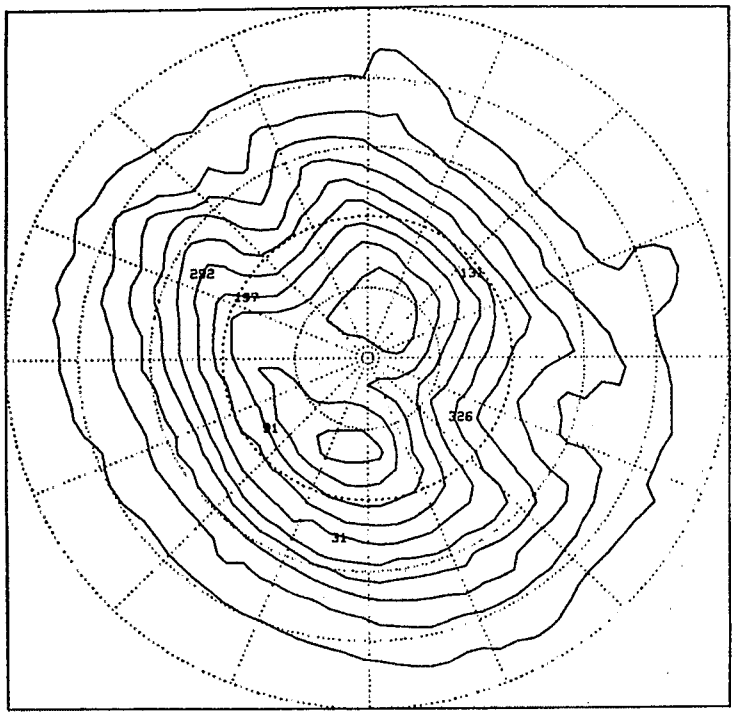

TIME PERIOD 0420-0430

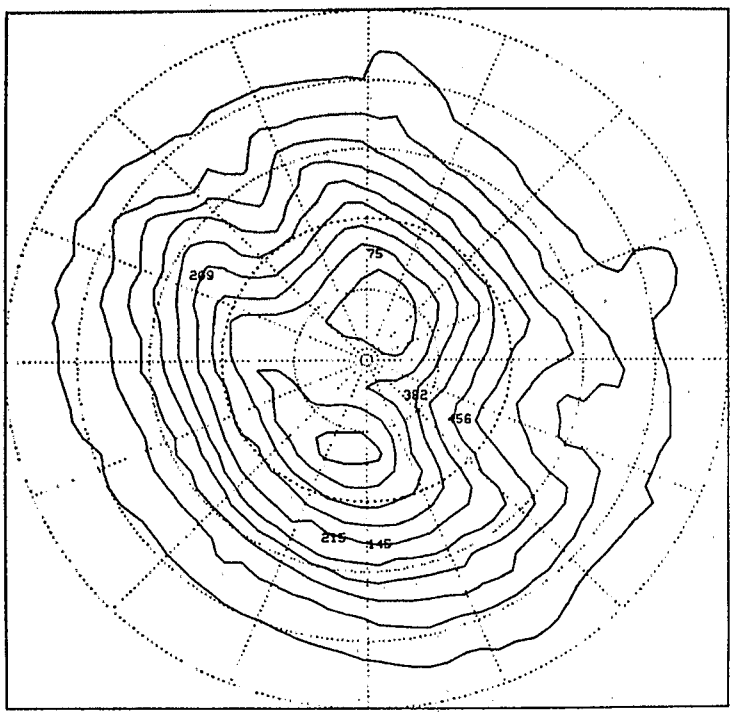

TIME PERIOD 0430-0440

Figure 59. Continued.

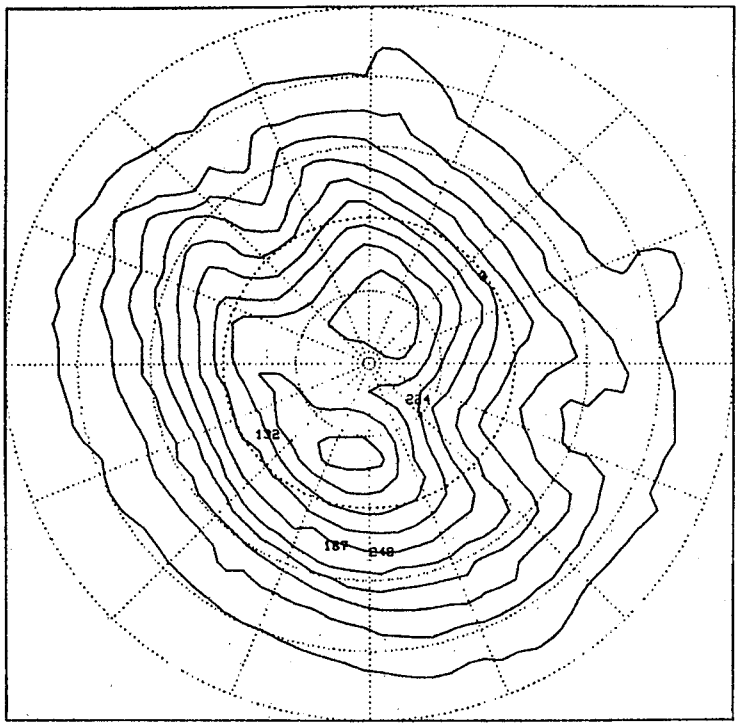

TIME PERIOD 0440-0450

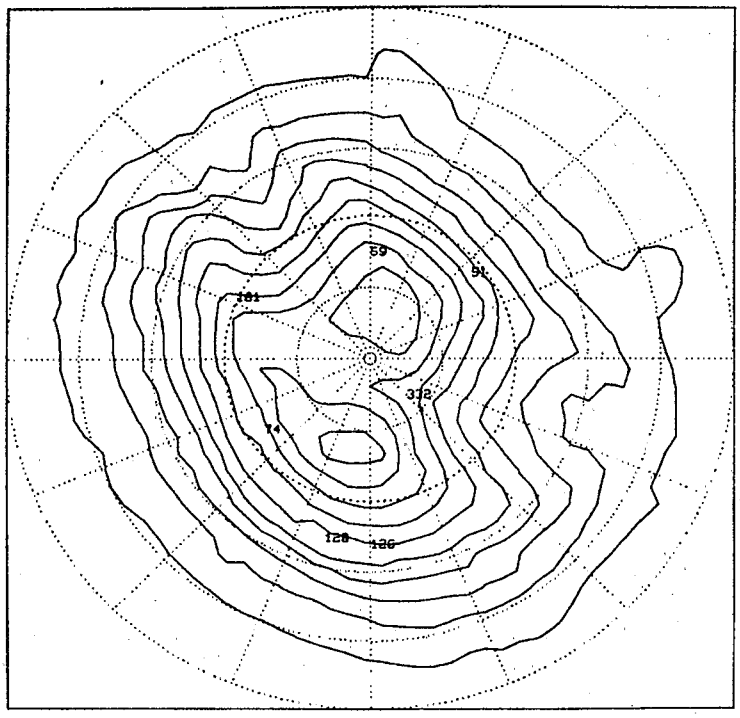

TIME PERIOD 0450-0500

Figure 59. Continued.

TABLE 8. NEUTRAL AND LIFT MODEL CALCULATIONS - EXPERIMENT 205, CASE HOUR 5

Meteorological Data

wind direction(deg)	=	120.
wind speed(m/s)	=	6.5
critical dividing streamline height(m)	=	24.0
Iz	=	.049
Iy	=	.104
N(1/s)	=	.048

Source Data

direction(deg)	=	120.
distance(m)	=	1155.1
release height(m)	=	50.0
SF6 emission rate(g/s)	=	.087

Receptor Coordinates X(m)	Y(m)	Z(m)	Observed SF6 (ppt)	Neutral Predicted SF6 (ppt)	Lift Predicted SF6 (ppt)
360.22	.00	13.26	110.80	7.18	.00
208.35	.00	31.25	110.40	63.22	68.03
142.00	.00	50.00	137.00	127.20	149.81
257.78	33.94	30.00	94.80	28.67	.00
404.91	111.59	10.00	95.00	.19	.00
195.15	149.74	27.41	75.50	10.88	.00
159.04	122.04	46.91	75.48	35.91	.00
51.04	387.66	11.78	55.10	1.58	.00
15.97	121.29	90.94	65.50	119.44	77.69
10.61	80.56	91.97	79.40	130.15	193.84
25.15	190.88	65.00	52.00	73.69	.00
2.15	18.88	80.00	149.70	140.49	227.40
-38.04	-288.98	32.94	57.00	5.28	.00
-19.85	-149.12	90.00	94.60	120.94	51.03
-9.85	-76.12	90.00	133.40	139.06	202.75
-84.85	-65.12	90.00	130.70	125.16	142.43
-396.68	-106.29	3.44	76.10	7.07	.00
-248.96	-66.71	32.90	49.70	39.13	15.95
77.87	-290.63	35.10	93.90	12.27	.00
95.80	-231.27	52.96	138.60	62.65	14.17
91.36	-109.36	65.00	178.50	153.16	218.95
355.15	-205.04	5.69	386.20	41.78	299.86
204.15	-117.12	30.00	232.20	108.85	270.91
108.15	-61.12	50.00	153.80	160.43	250.51
312.38	-41.13	14.00	107.10	25.30	.00
-359.96	207.82	8.94	70.30	49.24	170.02
-297.11	171.54	28.07	66.30	75.15	178.67
-269.62	155.66	38.07	84.00	91.20	182.65
-111.85	65.88	80.00	206.60	126.48	207.91
-40.85	28.88	80.00	152.20	135.78	220.45
-109.07	263.31	30.00	38.10	39.52	17.23

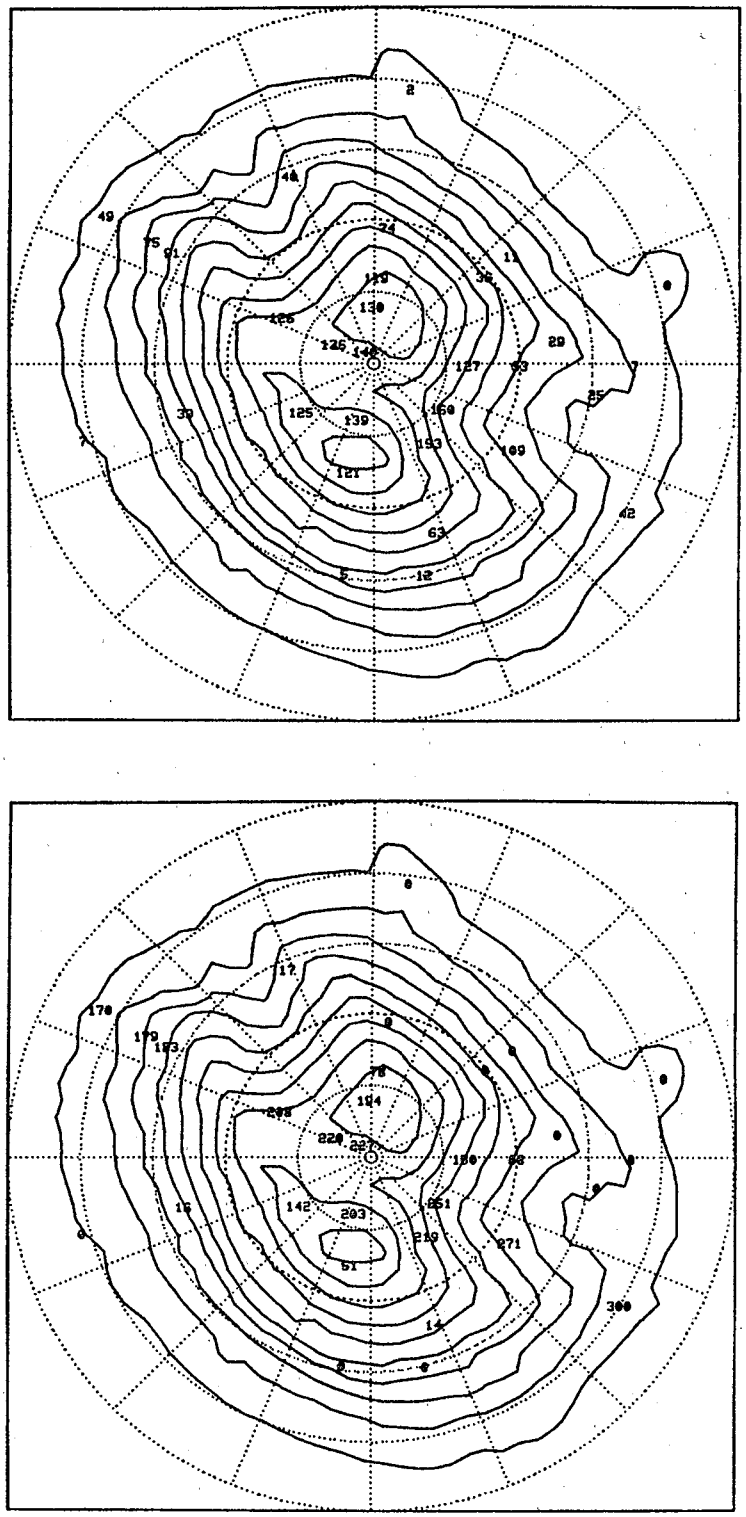

Figure 60. SF_6 concentrations (ppt) estimated for Experiment 205, Hour 5 by the Neutral (top) and Lift (bottom) models.

value of i_y provides a better description. Computed terrain factors (T_o) from the observed concentrations over the hill also indicate a problem with the Lift concentrations because nearly all of the factors are greater than one. However, many of the observed concentrations themselves appear too large when compared against those of the previous hour. Therefore, Neutral computations over the top of the hill may also be too large. Without greater confidence in the SF_6 tracer data for this hour, however, a firm conclusion is impossible.

4.6 Experiment 206, Hour 4 (0300 - 0400 MST)

4.6.1 Summary Description

Thermofogger oil-fog and SF_6 tracer gas were released from the southeast side of the hill at 595.9 m, 123.6° for the entire hour. The release height was 35 m, a change of 11 m from the release height during the previous hour. Because the SF_6 was off for only about 2 minutes during the height change, the SF_6 recorded at the samplers could have come from a 46 m rather than a 35 m height at the start of the hour if the winds at that time were directed toward the hill. The photographs show the plume traveling to the north, so tracer material from the previous hour should have no effect on these concentrations.

Local terrain elevations near the release point are estimated to be -5.5 m relative to the zero of the hill coordinate system, so the net release height corresponds to the 29.5 m height level on the hill. The SF_6 release rate is computed to be 0.039 g/s with an estimated uncertainty of $\pm$3.4%. No Freon was released.

Plume Observations

Several observations of the appearance and the trajectory of the oil-fog plume are available for this hour.

Time: 0259 The thermofogger is dropping now to 35 meters, from 46, at its location about 60K.

Time: 0300 Plume now appears to be going northwest, traveling in a level plane, a horizontal plane. Quite stable conditions right now, really calm at this point.

Time: 0303 The plume is coming very close to the ridge coming down past tower C. It probably stays 3-5 meters above the ground as it goes over.

Time: 0308 The plume is moving around the north side of the hill.

Time: 0322 The plume has shifted. Now it is going up and over the north peak and nearly up the middle draw. As seen from the north peak, the plume has shifted to the right towards the north peak, basically splitting to go around on both sides, meandering a little bit.

Time: 0327 The plume is still hitting in the area of the north butte.

Time: 0335 I've just driven around the west side of the butte, over to the east-west road north of the butte (along the power lines), site 0-9. From my vantage point coming around the west side of the hill I could see the plume rushing through the saddle and coming out over the northwest draw.

Time: 0347 Now driving back around the northwest end of the butte, the arc lamp is illuminating plume material in the draw and above the draw.

Time: 0350 The plume is impacting heavily on the north butte.

Time: 0400 We're putting the plume down to the ground for 10 minutes to refuel.

These observations indicate that the plume spent much of the time wandering from the north side of the hill across the north peak to the southeast draw. This is illustrated better in the photographs. Two representative photographs are reproduced in Figure 61. They are from a series taken from a point behind the release crane to the south at location 0-11 (see Figure 46). Each photo is a 5-minute time exposure.

The photos show that the plume skimmed around the north side of the hill during the first 5-minute period, started to swing back across the face of the north peak during the second period, and sat over the southeast draw and the saddle between the peaks during the third period. No photos are available for periods 4 and 5. When the photos pick up again in the sixth period, the plume appears to be riding up the northern ridge of the southeast draw, and this continues into period 7. The plume once again rested between the peaks during period 8, but slowly shifted across the face of the north peak during periods 9-11 until it again skirted the hill along the north side during period 12. The plume size appears to remain unchanged throughout the hour.

Lidar data were obtained along four sampling planes. Two of the planes crossed the top of the hill, and the other two cut across the southeast face of the hill. Figure 62 displays the plume centroid locations computed from the lidar cross-sections. These data corroborate the photographic record, and indicate that the plume remained near the southern face of the north peak during periods 4 and possibly 5 (for which photographs are unavailable).

Meteorological Information

Wind and temperature data measured at tower A during this hour were used to characterize the flow in terms of H_c. However, because the V-component of the 40 m wind set was missing, wind speeds at this height were inferred before H_c was calculated. The method followed in calculating speeds at 40 m is outlined in Section 4.4.1.

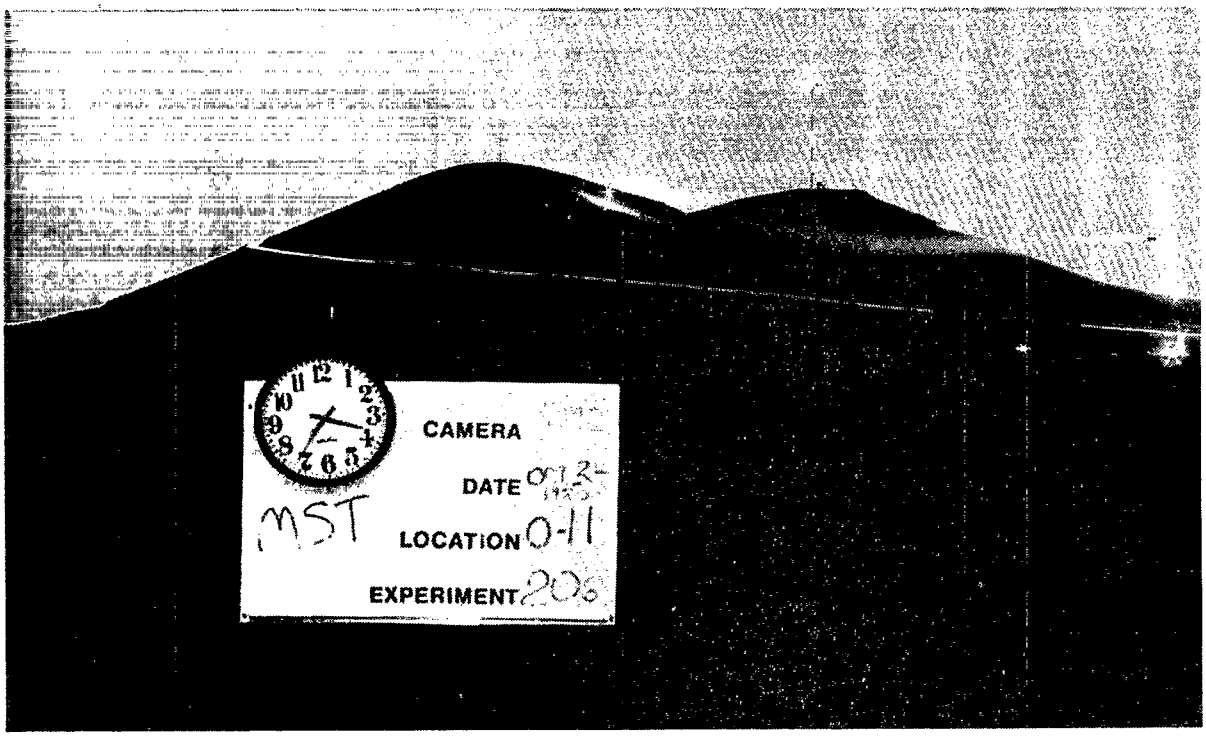

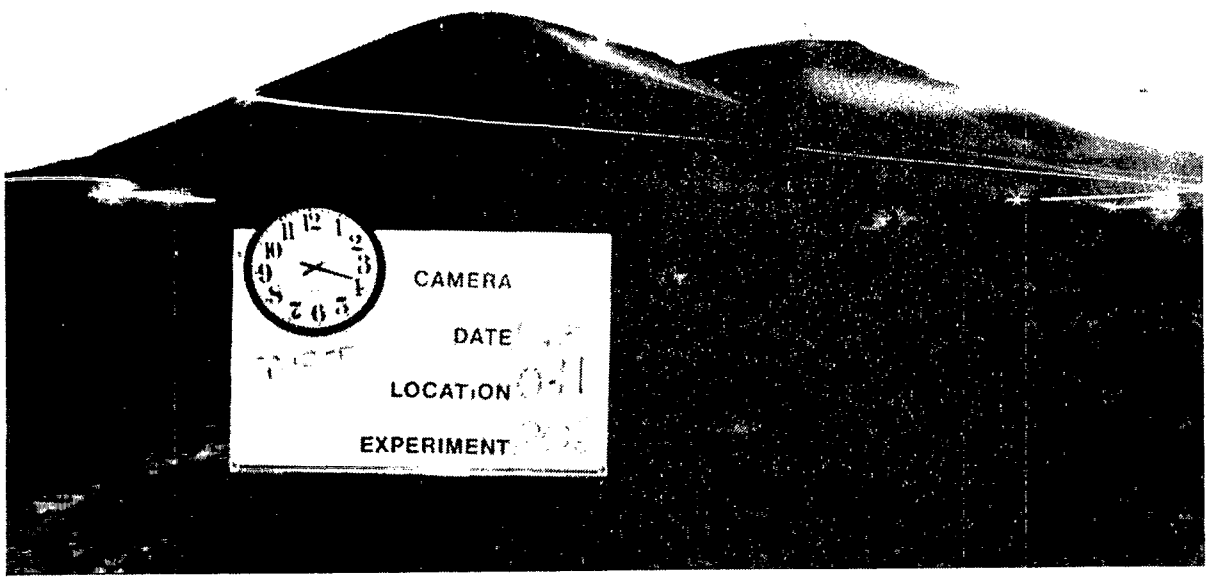

Figure 61. View of the 5-minute average plume trajectories between 0335 and 0340, and between 0340 and 0345 MST taken from behind the release (position 11) during Experiment 206, Hour 4.

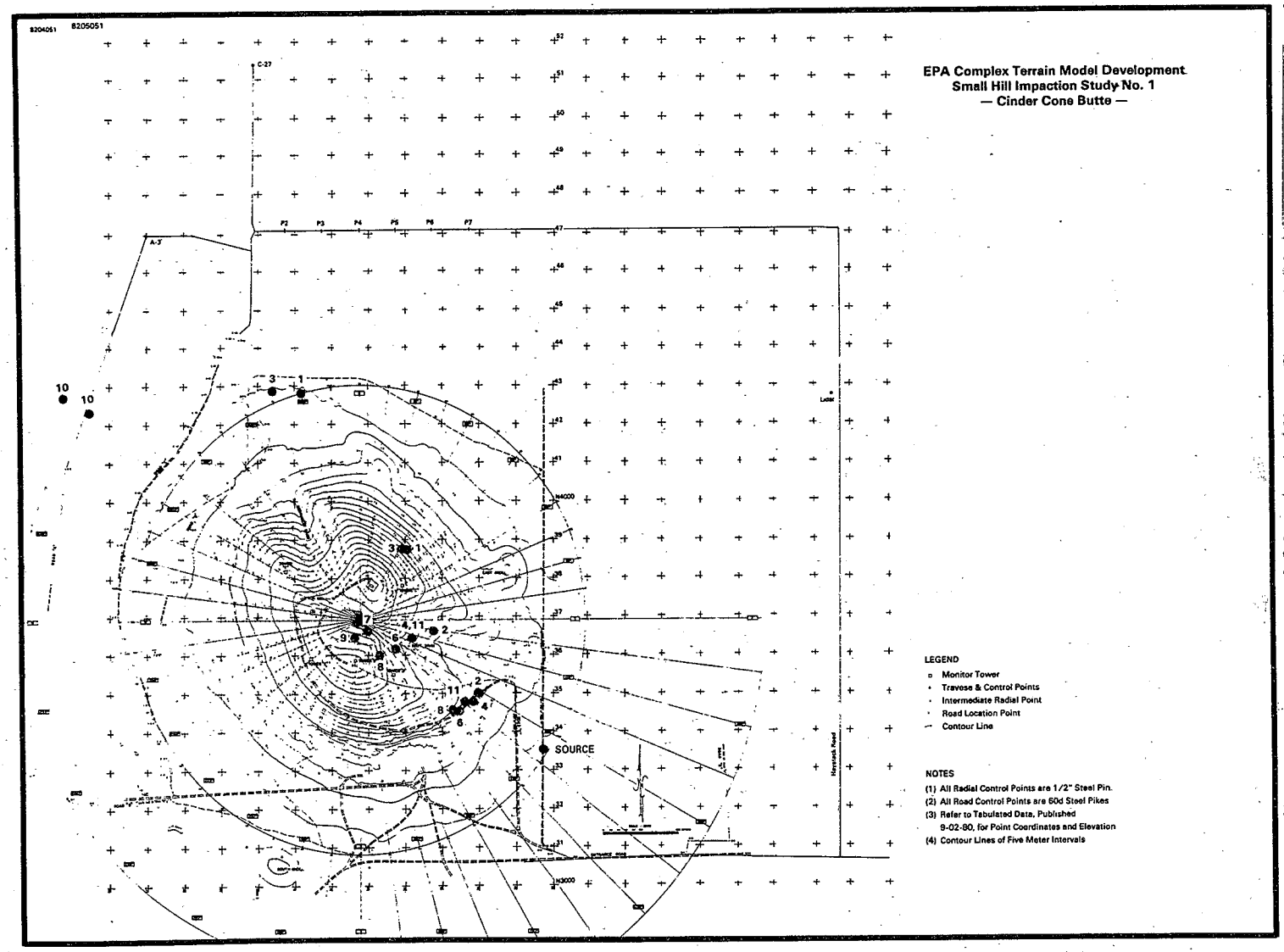

Figure 62. Plume centroid positions calculated from lidar data. Experiment 206, Hour 4 (0300-0400 MST).

The average H_c over this hour is 20 m, and the bulk hill Froude number above this level is 2.1. Because the local release height was 35 m, the size of H_c could have had a substantial effect on computed surface concentrations. Also, Fr_L is 0.53, so a significant degree of streamline depression in the lee of the hill is expected, although no evidence of this feature is contained in the observations reviewed above.

Figure 63 contains plots of the 5-minute H_c and Fr_H values for this experiment. H_c stayed near 21 m for much of the hour, dropping sharply to 16 m by the end of the hour. Fr_H remained nearly constant. The change in H_c was not likely to have produced substantial changes in surface concentrations.

Hourly averaged wind speeds measured at 10 m and estimated at 40 m on tower A are 1.8 and 4.5 m/s, respectively. The direction at 10 m was 141° and that at 80 m, 136°. This shows there was little directional wind shear, but substantial speed shear across the region near plume elevation. Figure 64 shows the trend in wind speeds between 10 m and 80 m during the hour. Although the speeds are nearly constant over the hour, there is a slight tendency toward increasing speed in the latter half hour. This increase corresponds to the drop in H_c noted above.

Variations in the wind directions measured at 10 m and 80 m on tower A are shown in Figure 65 as frequency distributions. The distribution at 80 m is about 10°, substantially narrower than that at 10 m, about 40°. The 10° span is clearly more consistent with the documented plume trajectories.

In summary, the plume was released above H_c into a flow characterized by little wind meander, 5 to 6 m/s wind speeds, and a hill Froude number of about 2. As a result, the plume should have ridden fairly close to the surface over the hill and dropped a little on the lee side.

SF_6 Concentrations

The distribution of hourly averaged SF_6 concentrations over the surface of the hill is shown in Figure 66. The highest concentrations are found on the upper portion of the north side of the north peak. Other high concentrations are found in a band between 50 m and 60 m along the north side of the north peak and also between 30 m and 60 m in the lee of the hill.

This pattern is consistent with the observations discussed above, except that because the concentrations below the 55 m contour are very small, it is now quite clear that the plume rose above the hill surface on the windward side. Also, it appears that the plume may have been depressed in the lee of the hill, because the concentrations along the ridge that form the south side of the northwest draw are much higher at 35 m than at the 75 m contour across the saddle. This would be consistent with the Fr_L value calculated for this hour.

The 10-minute SF_6 concentration distribution is presented in Figure 67. The sequence of concentration patterns throughout the hour follows the plume trajectories documented in the photographs. Very little

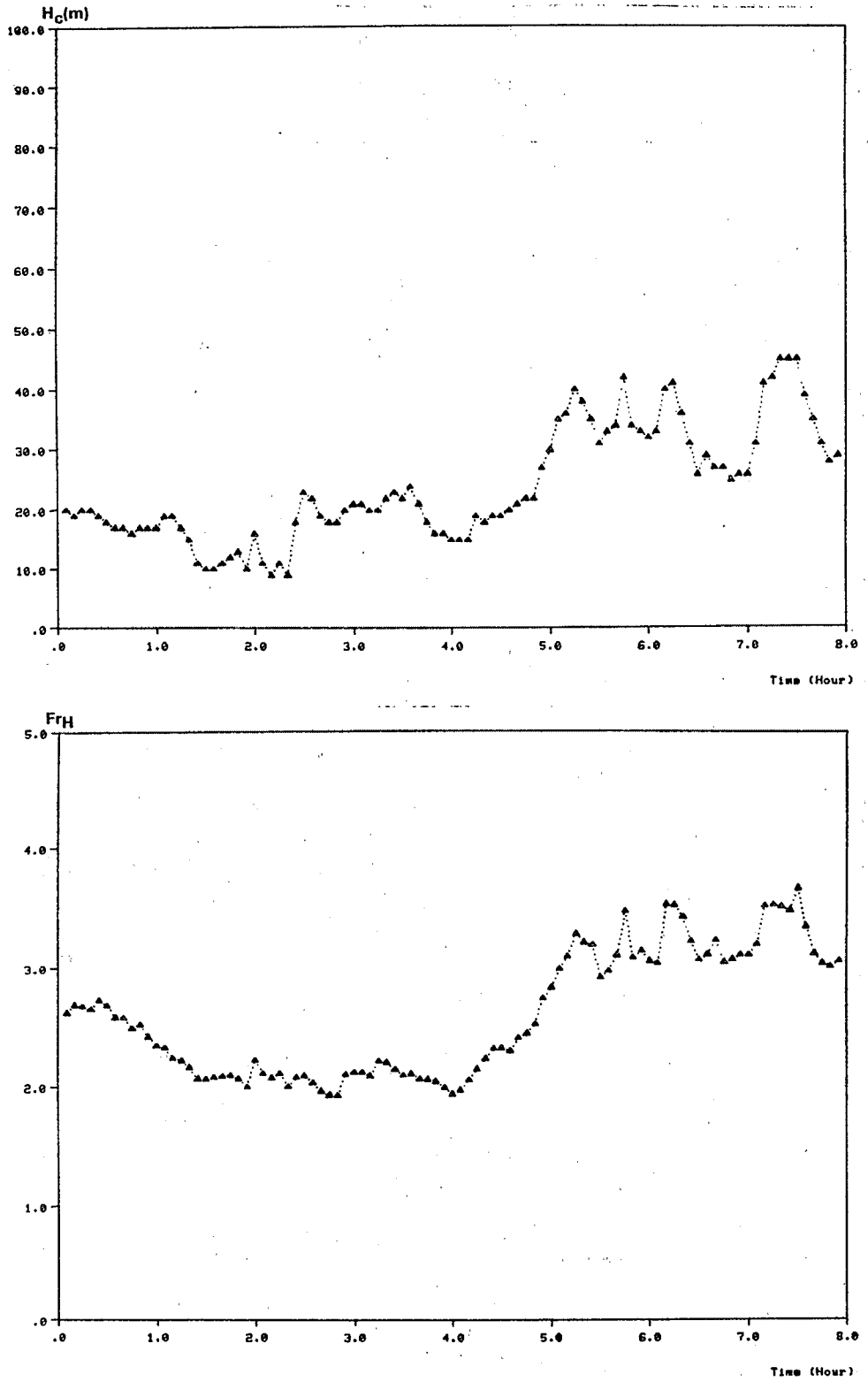

Figure 63. Calculated dividing streamline heights (H_c) and bulk hill Froude numbers above H_c (Fr_H) for Experiment 206.

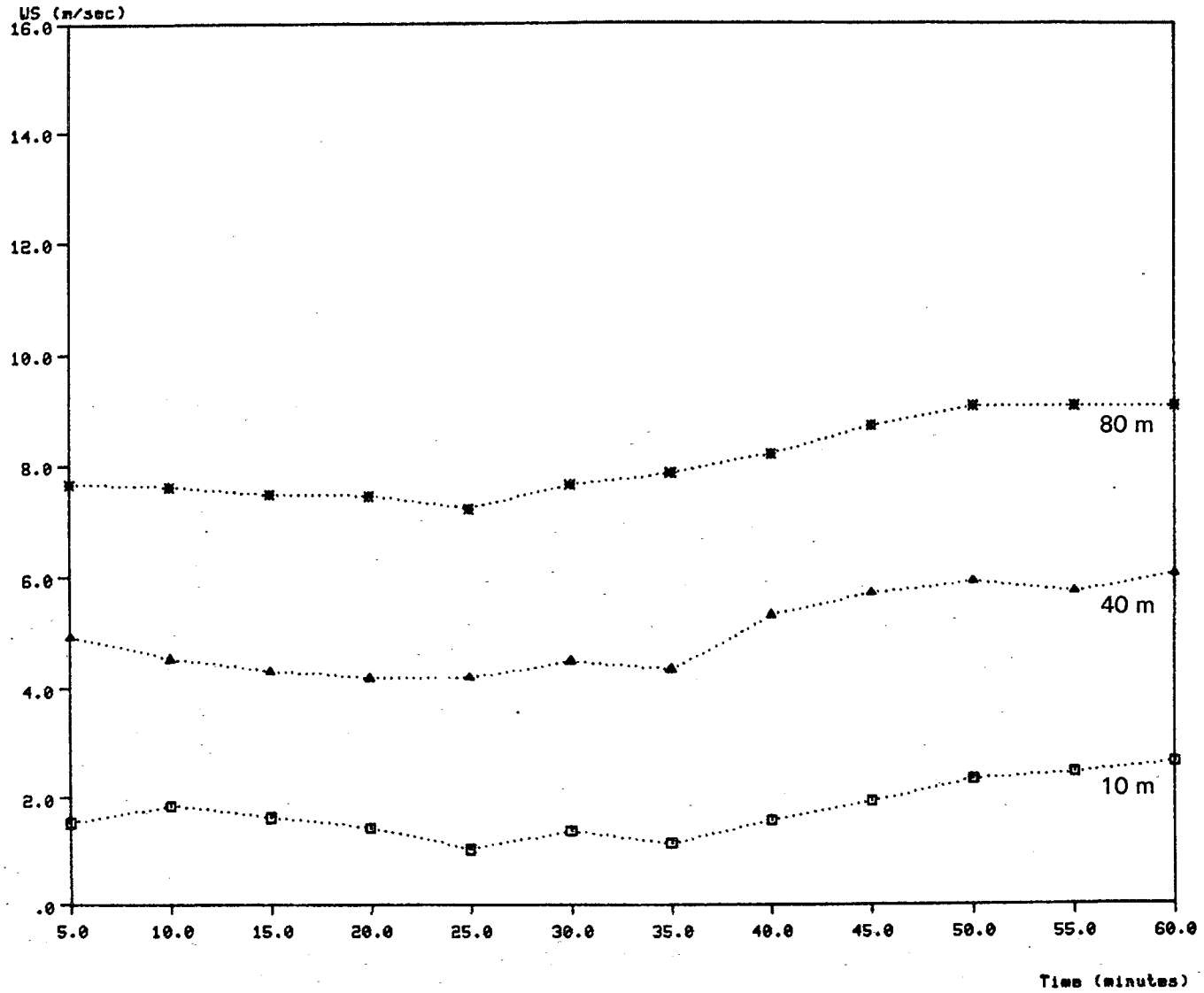

Figure 64. Tower A wind speeds during Experiment 206, Hour 4 (0300-0400 MST).

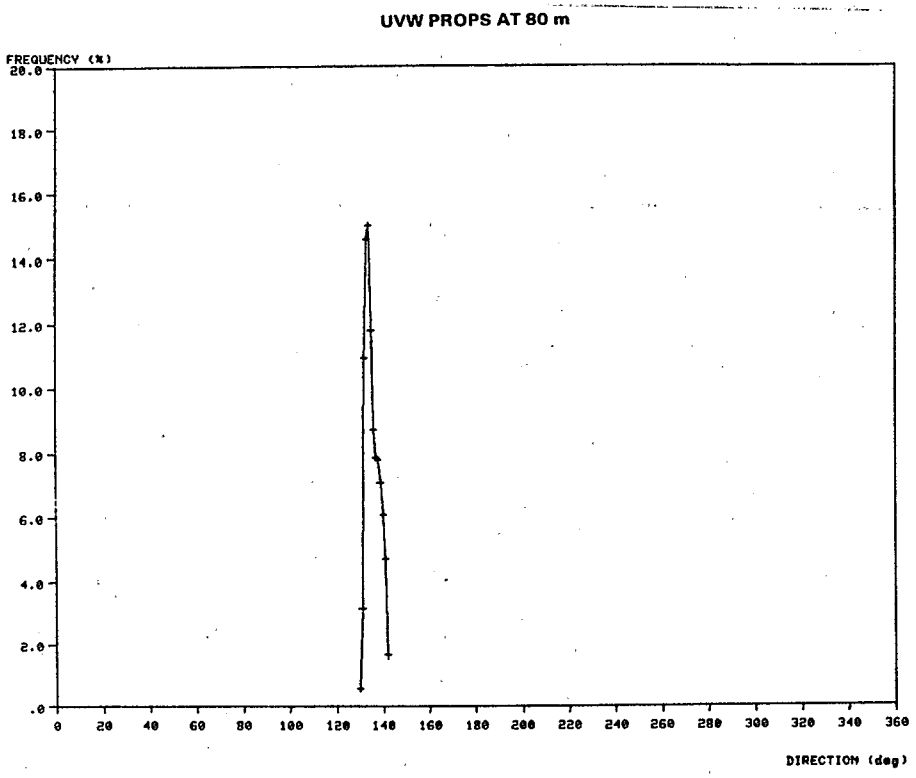

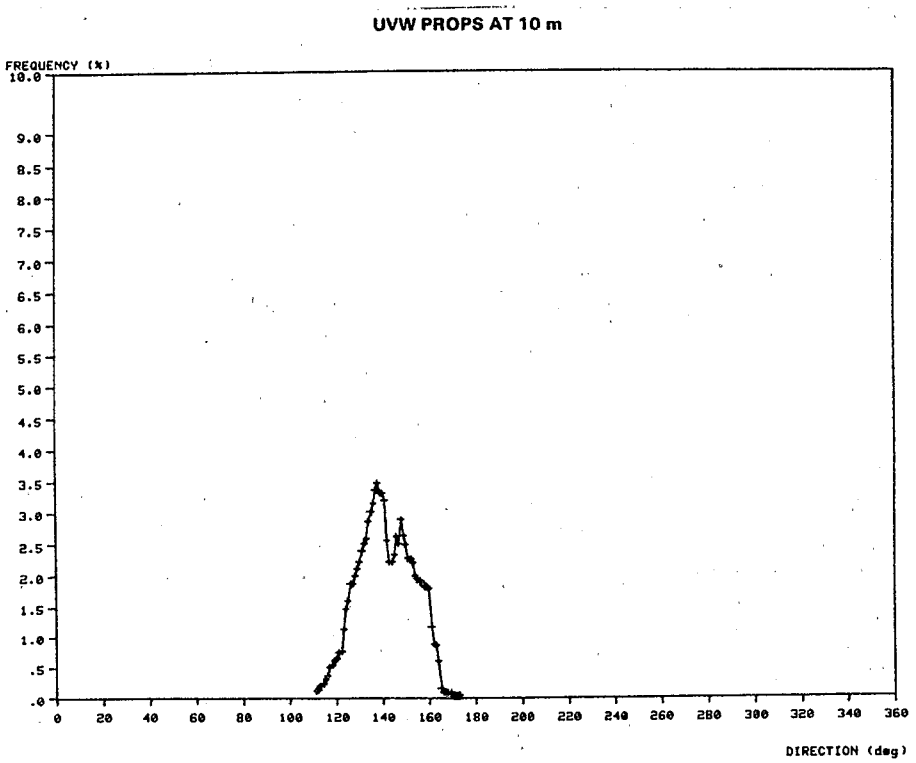

Figure 65. Calculated wind direction distribution functions for Experiment 206, Hour 4 (0300-0400 MST).

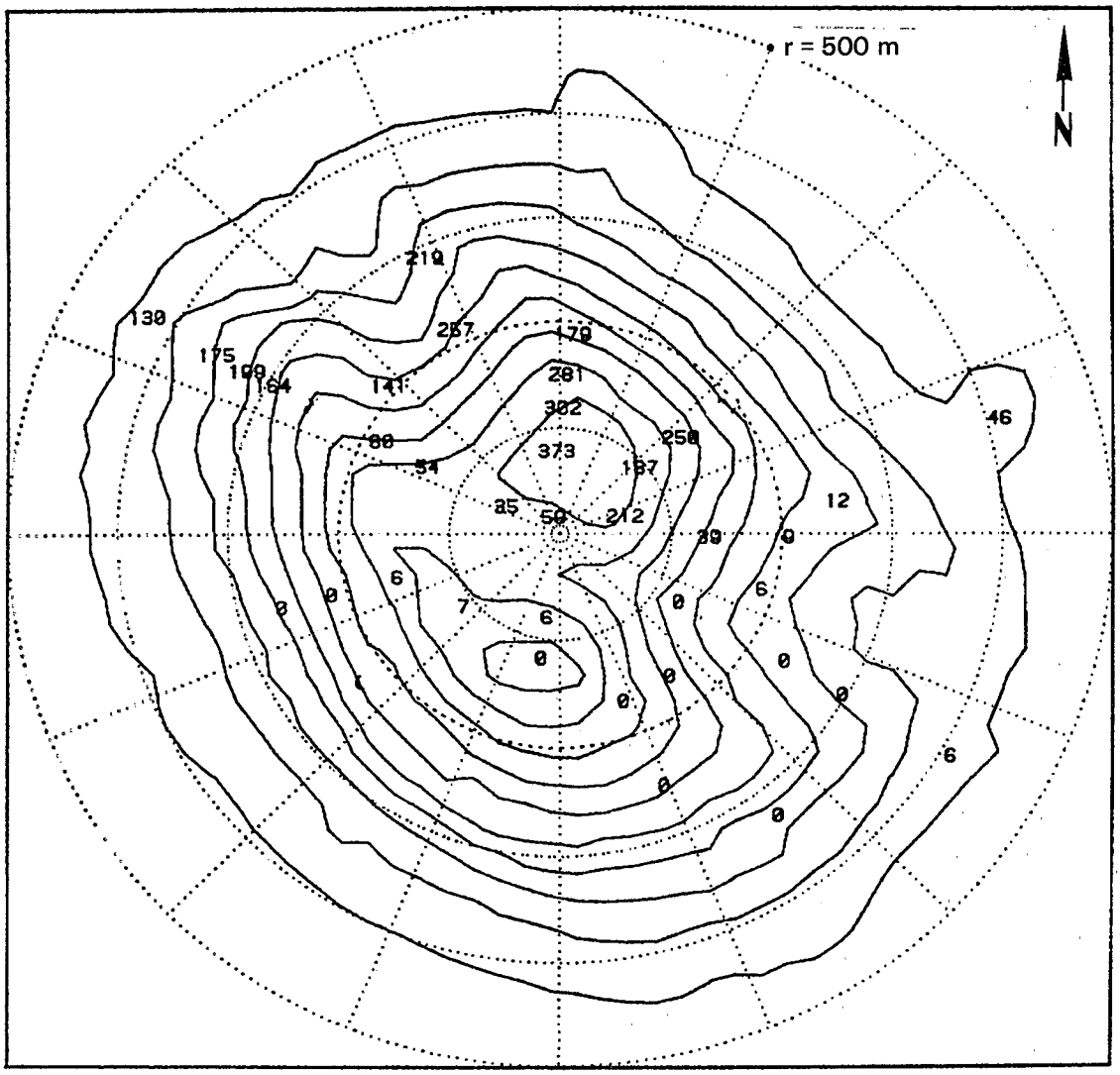

Figure 66. Observed SF_6 concentrations (ppt) for Experiment 206, Hour 4 (0300-0400 MST). Source: r = 595.9 m, θ = 123.6°, net height = 29.5 m, Q = .039 g/s.

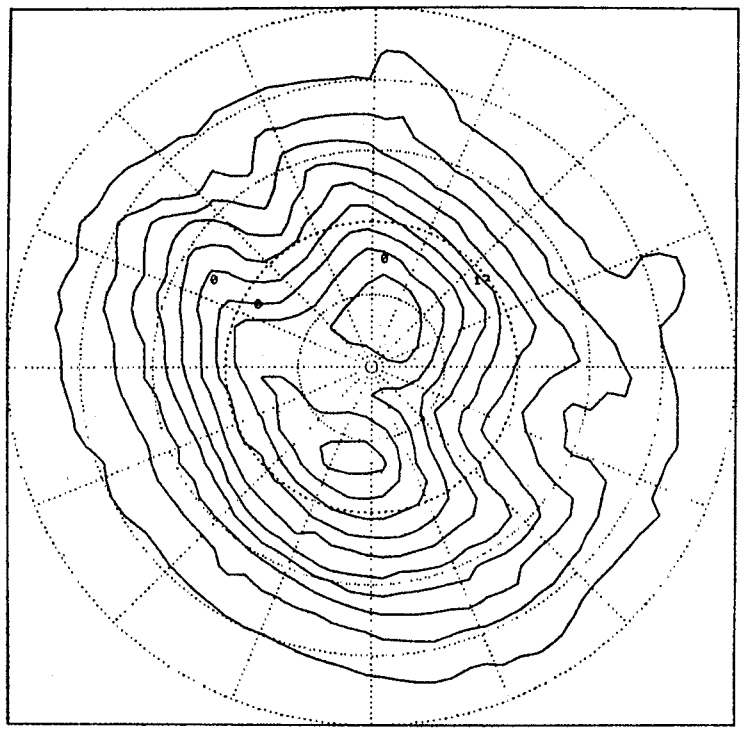

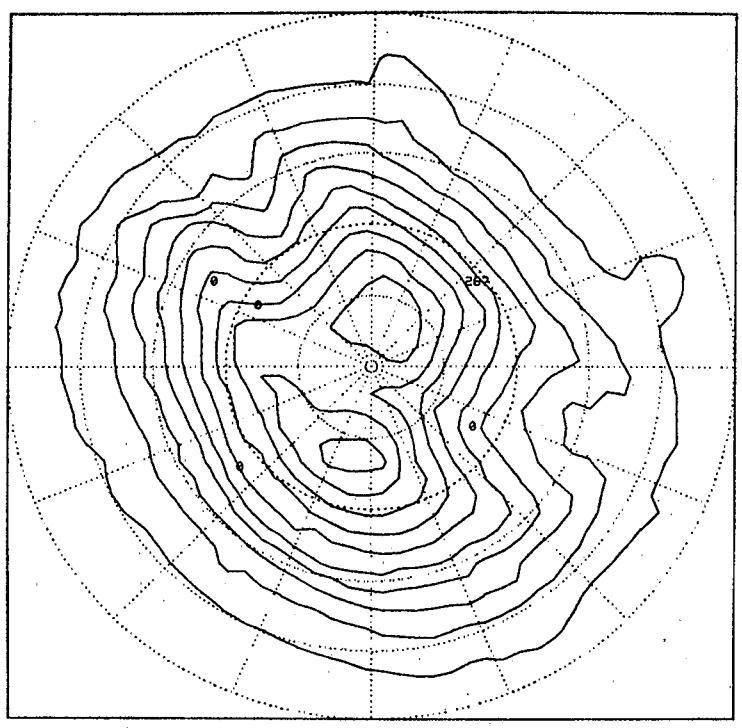

Figure 67. Observed 10-minute average SF_6 concentrations (ppt) for Experiment 206, Hour 4 (0300-0400 MST).

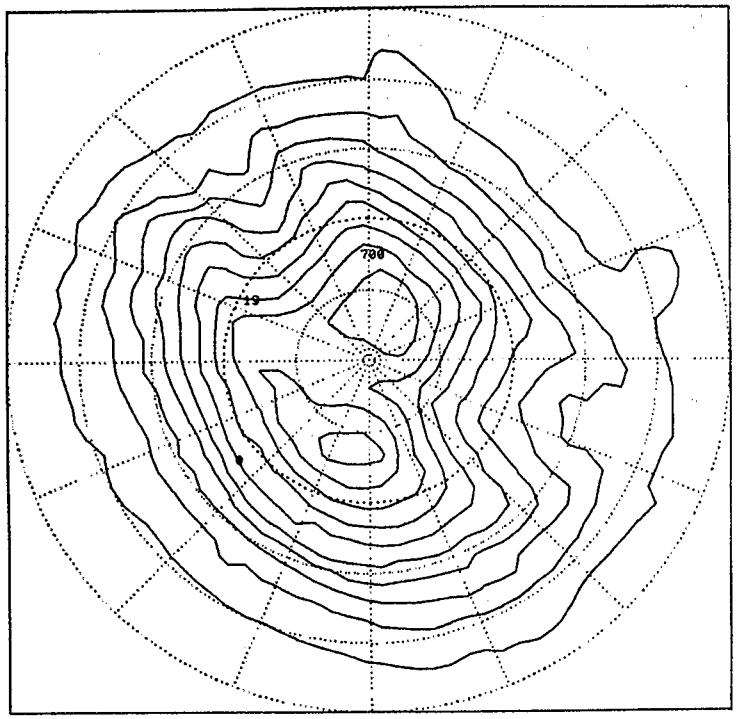

TIME PERIOD 0320-0330

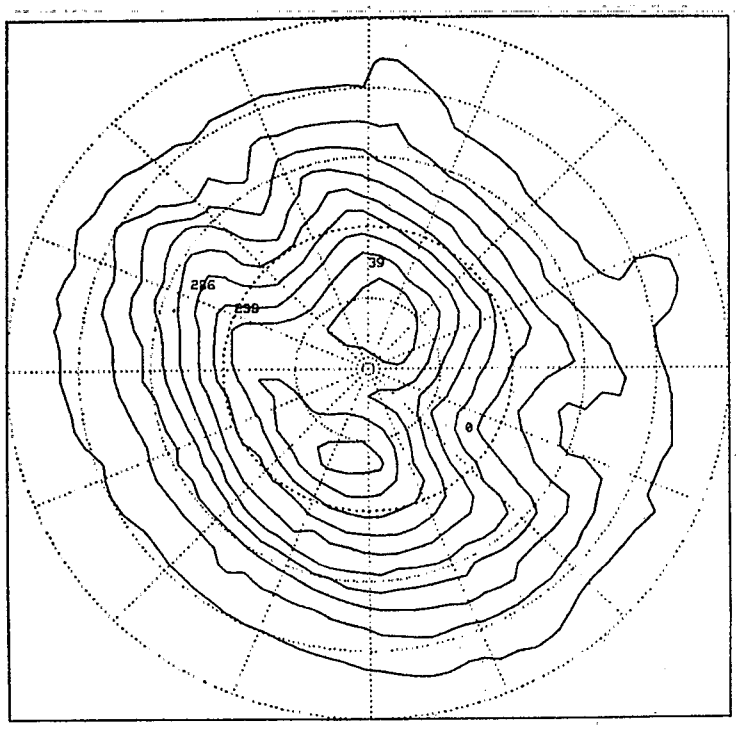

TIME PERIOD 0330-0340

Figure 67. Continued.

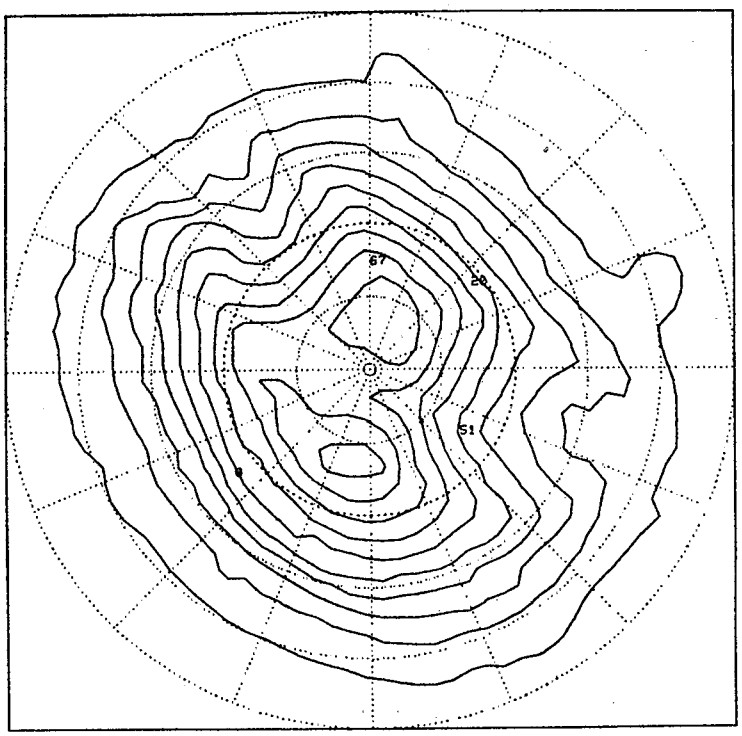

TIME PERIOD 0340-0350

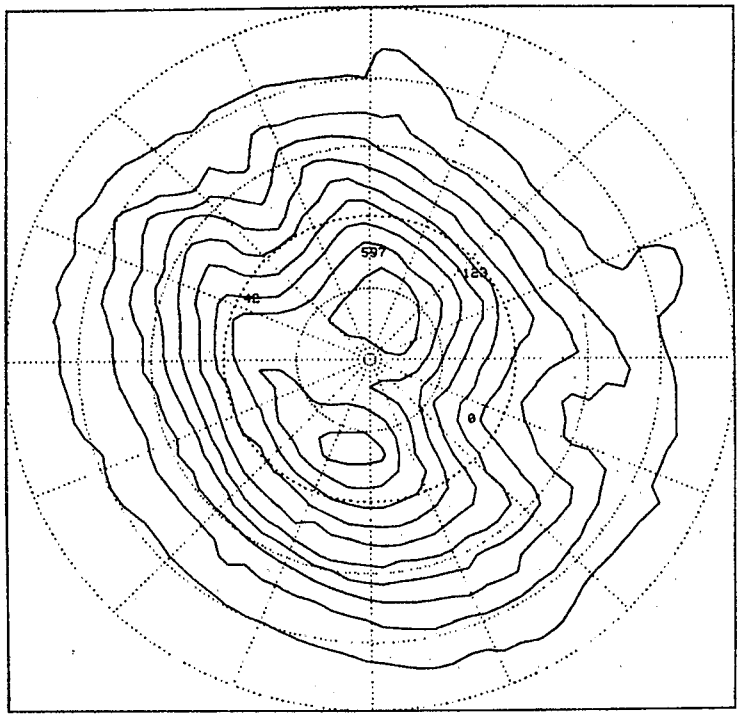

TIME PERIOD 0350-0400

Figure 67. Continued.

SF_6 reached any of the 10-minute samplers during the first 10 minutes, but significant concentrations were recorded around the north peak and downwind of the saddle at times during the rest of the hour.

4.6.2 Model Performance

This hour was modeled with the Lift model because all evidence indicates that streamlines at plume height passed over the hill. However, the dividing streamline height is a significant fraction of the local release height, and therefore may have exerted a significant influence on tracer concentrations. Meteorology used in the modeling was prepared as in Section 4.1.2 and is summarized in Table 9.

The 1-hour averaged wind directions at 10 m and 80 m on tower A are 141° and 136°, respectively. However, plume trajectories inferred from the lidar data and the photographs indicate a wind direction in the 128° to 130° range. No wind direction data are available from tower B. Because the wind directions at 10 m and 80 m are inconsistent with the observed plume trajectory at 35 m, the model wind direction is taken to be 128°. However, the only choices for the PDF are 10 m or 80 m. Because the 10 m distribution appears too broad in view of the lidar and photographic documentation, the 80 m PDF is used in the modeling.

Neutral was rerun with the revised meteorology. Instead of estimating a peak value 23% of the observed peak value, it produced a value 66% of the observed peak. Both the highest observed and modeled concentrations are found near the north peak, but the observed high falls on top of the peak, and the modeled high lies near the windward edge of the top of the north peak. Elsewhere, Neutral 1 tends to overestimate concentrations on the windward side of the hill and underestimate concentrations on the lower portion of the leeward side of the hill. Figure 68 shows the distribution of calculated concentration plotted on a map of CCB, and the results are also summarized in Table 9.

Results from Lift computations are displayed in Figure 68 and are also listed in Table 9. The maximum modeled concentration is 120% of the peak observed concentration but does not occur on the same portion of the hill. It lies halfway down the northwest side of the hill. Concentration estimates in the vicinity of the north peak are overestimated on the south side and underestimated across the top and on the north side. Concentration estimates on the windward side of the hill are substantially overestimated.

These observations indicate that Lift produces a concentration pattern that is too narrow and does not produce enough plume lift on the windward side of the hill. Terrain factors computed from the observed concentrations vary from 0.68 to 1.4 on the lee side of the hill, from 0.79 to 1.4 over the top of the north peak, and from 1.0 to 1.5 on the windward face. Most of the range in T_o at receptors over and beyond the top of the hill may be attributable to the narrow concentration distribution and is therefore difficult to interpret. The factors for the windward face, however, indicate the need for a weaker plume interaction. Because nearly 60% of the

TABLE 9. NEUTRAL AND LIFT MODEL CALCULATIONS - EXPERIMENT 206, CASE HOUR 4

Meteorological Data

wind direction(deg)	=	128.
wind speed(m/s)	=	4.5
critical dividing streamline height(m)	=	20.0
Iz	=	.031
Iy	=	.078
N(1/s)	=	.044

Source Data

direction(deg)	=	124.
distance(m)	=	595.9
release height(m)	=	35.0
SF6 emission rate(g/s)	=	.039

Receptor Coordinates X(m)	Y(m)	Z(m)	Observed SF6 (ppt)	Neutral Predicted SF6 (ppt)	Lift Predicted SF6 (ppt)
208.35	.00	31.25	9.00	7.73	.00
142.00	.00	50.00	38.90	227.60	176.99
257.78	33.94	30.00	12.30	.01	.00
72.15	19.88	80.00	211.60	224.25	251.27
404.91	111.59	10.00	46.10	.00	.00
85.15	64.88	80.00	187.00	247.77	190.68
20.07	152.45	81.06	280.56	232.69	52.49
15.97	121.29	90.94	302.30	238.97	223.66
10.61	80.56	91.97	373.30	225.10	248.39
25.15	190.88	65.00	179.10	170.21	.00
2.15	18.88	80.00	58.90	175.28	352.86
-15.01	-113.99	98.96	.10	38.47	.00
-9.85	-76.12	90.00	6.00	63.73	.00
-84.85	-65.12	90.00	7.10	50.41	.00
-248.96	-66.71	32.90	.00	.02	.00
-204.16	-54.70	52.26	.00	4.33	.00
-144.85	-38.12	80.00	6.00	44.20	.00
95.80	-231.27	52.96	.00	.02	.00
59.13	-154.04	80.00	.00	15.57	.00
199.06	-259.43	30.00	.20	.00	.00
355.15	-205.04	5.69	6.00	.00	9.69
256.81	-148.27	25.29	.10	35.54	199.37
204.15	-117.12	30.00	.30	103.58	299.78
108.15	-61.12	50.00	.20	165.73	318.33
183.53	-49.18	30.00	5.70	92.28	179.98
-359.96	207.82	8.94	129.50	16.30	.00
-297.11	171.54	28.07	175.10	61.50	.00
-269.62	155.66	38.07	199.40	98.60	.00
-246.20	142.14	47.96	164.10	115.80	.00
-153.85	89.88	70.00	59.88	142.26	.00
-111.85	65.88	80.00	54.40	148.79	.00
-40.85	28.88	80.00	34.70	156.60	107.23
-141.42	141.42	50.00	141.20	199.61	447.49
-109.07	263.31	30.00	218.60	57.31	138.74
-80.75	194.94	50.00	257.20	203.19	215.48

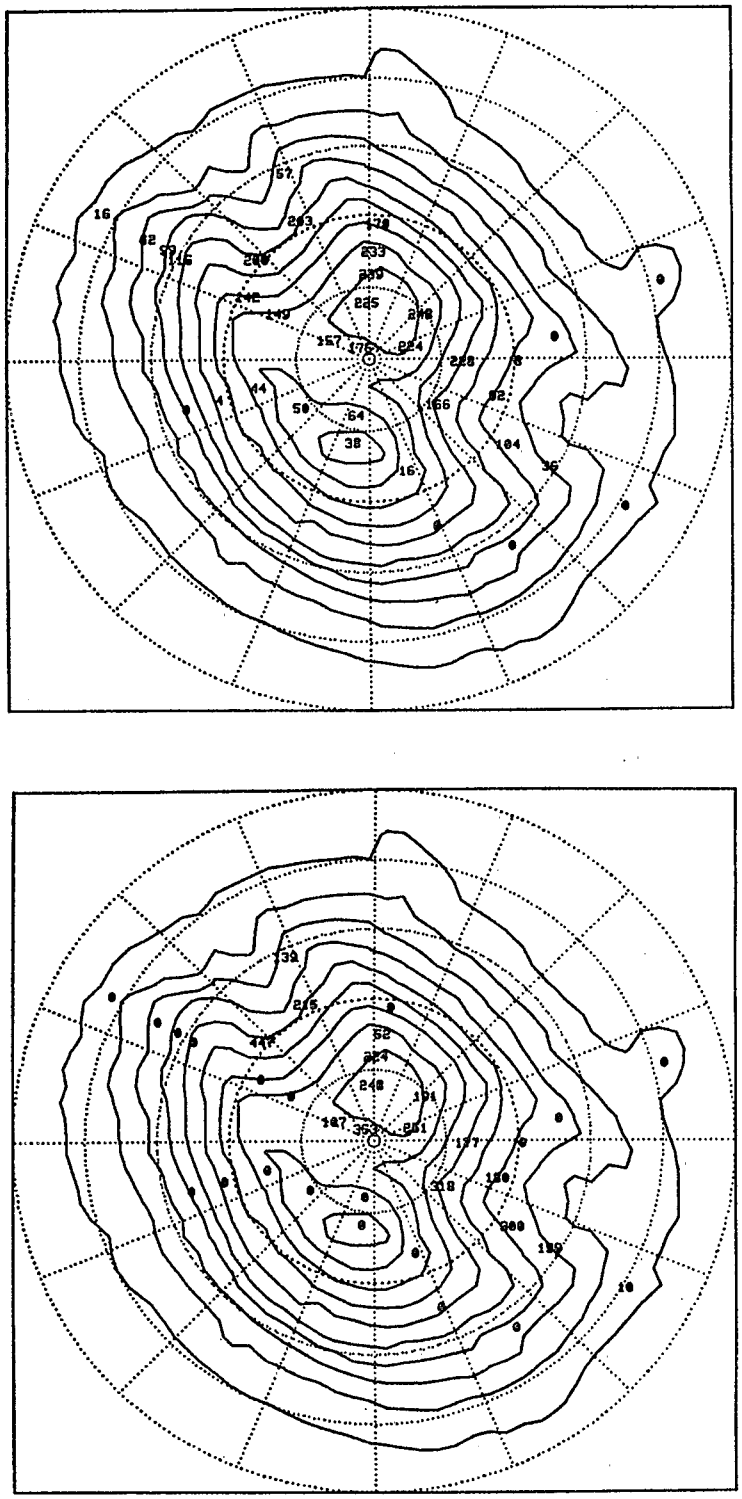

Figure 68. SF_6 concentrations (ppt) estimated for Experiment 206, Hour 4 by the Neutral (top) and Lift (bottom) models.

initial plume height was removed in subtracting H_c from the release height, much of the overestimation on the windward face would be reduced if some allowance were made for an H_c surface able to travel part of the way up the windward slope. For example, a 5 m or 25% decrease in the value of H_c is equivalent to multiplying the net release height above H_c by 1.3 in this experiment hour. This alone could account for a T_o of 1.3.

4.7 Experiment 206, Hour 6 (0500-0600 MST)

4.7.1 Summary Description

Thermofogger oil-fog and SF_6 tracer gas were released from the southeast side of the hill at 595.9 m, 123.6° for the entire hour. All release parameters were the same as those during the previous hour, so there were no discontinuities in the experiment at the start of the hour. The release height was 35 m.

Local terrain elevations near the release point are estimated to be -5.5 m relative to the zero of the hill coordinate system, so the net release height corresponds to the 29.5 m height level on the hill. The SF_6 release rate is computed to be 0.062 g/s with an estimated uncertainty of $\pm$1.0%. No Freon was released.

Plume Observations

Many observations of the appearance and the trajectory of the oil fog plume are available for this hour.

Time: 0455 The plume has stopped going up the draw and is now going back around the north side and its character changes somewhat, the plume width becomes less.

Time: 0500 The plume is going up the draw again and as usual it is much wider than it has been in the past.

Time: 0512 We must have been bombing the butte in the last 10 minutes. The plume is directed right at the north butte, part of it going up the draw or the north side of the draw, and occasionally some of it going around the north side around tower C. We've really been hitting it hard. It seems to be spread quite a bit. It seems to be quite a bit wider all the way back to the source than it was 30 minutes ago when it was going around the N side below tower C.

Time: 0517 The lidar reports that the plume is hitting the hill at the base of the draw.

Time: 0523 From my vantage point, 1/2 mile behind the release crane, it looks like the plume is beginning to run more into the south butte, even to the left of tower D, although my perspective could be wrong.

Time: 0525 Plume is rising coming out of the generator, and I lose sight of it about halfway from the crane to the hill.

Time: 0528 For about the last 5 minutes, the plume has been butting directly into the southeast shoulder of the butte, and is dramatically wide. It is very wide horizontally and very wide vertically, even coming all the way down to the ground at maybe the 3,100 ft level of the butte.

Time: 0529 I'm driving up by the camera location on road F. The plume has come all the way to the ground below the road that goes up and curls around the south side of the butte (smack on the ground from 35 meters). That downward motion doesn't really start dramatically until it has crossed road F.

Time: 0533 We're continuing to bomb the southeast shoulder of the butte.

Time: 0537 The plume character seems to have changed a little bit. It is a slightly better defined plume, with a great deal of vertical and horizontal dispersion. It is bombing the southeast shoulder with tower D on it, going up the draw. Part of it is going around the north shoulder of the butte and part of it is going up the draw, possibly going over the top by the FAA tower.

Time: 0540 I've paced off the width, where I can smell it, and it was 70 meters on that road as it circles up the butte. The approximate location where I did the pacing off is 57D. It might be a horseshoe vortex that is bringing the plume to the ground. Again it is coming to the ground, it is below me, below 57D.

Time: 0547 I'm down here on road F; NAWC 1 is on the road up the hill and between us the plume has very clearly come down to the surface. I can smell it at road F. He was seeing it up at his location before and we're hypothesizing that there is some sort of downflow--maybe a horseshoe vortex; something drawing the plume down to the surface in this area.

Time: 0552 Part of the plume is going up the draw, it appears, and part is climbing quite a bit and is going around the N side.

These observations show that the plume ran into the eastern face of the hill for much of the hour, at times striking the northern section, at times striking the southern section, but mainly striking in between. The most remarkable aspect of the observations, however, is the description of the plume becoming very wide, and striking the surface of the hill at the base of the draw. This plume was not just being deflected over or around the hill. Its trajectory was altered to the extent that the plume material spread dramatically in front of the hill (some of the effect was noticable even at the release point).

Photographs during the hour capture this unusual plume character very well. A half-hour series of photos taken from behind the release at camera location 0-11 (see Figure 46) is reproduced in Figure 69. Each photograph

Figure 69. Half-hour sequence of 5-minute average plume trajectories between 0500 and 0530 MST taken from behind the release (position 11) during Experiment 206, Hour 6.

is a 5-minute time exposure. The change in plume character from periods 1 and 2 to periods 4 and 5 is especially clear. Note that much of the vertical growth in plume size occurred at the bottom of the plume at the start of the spreading sequence (period 3). But as the plume continued to change, the spread became more symmetric about the release height (periods 5 and 6).

Only three plume cross sections were obtained with the lidar during the hour because of equipment failure, but fortunately these three bracket the dramatic change in the plume in periods 1, 3, and 6. The sampling plane cut across the base of the hill just downwind of the source. Plume centroid positions are plotted in Figure 70. The standard deviations of the oil fog distribution as sampled by the lidar show that the instantaneous plume cross-section did not change much in going from period 1 to period 3, but both σ_y and σ_z virtually doubled in period 6.

Meteorological Information

Wind and temperature data measured at tower A during this hour were used to characterize the flow in terms of H_c. As in the previous hour, wind speeds at 40 m were estimated because of the partial failure of the 40 m wind set. The average H_c over this hour is 35 m, and Fr_H above this level is 3.1. Because the local release height was 35 m, H_c had a substantial influence on the plume trajectory.

According to the simplified energy arguments used to derive H_c, the plume had just enough energy to rise over the crest of the hill. However, the precision of the method as well as the vertical resolution of the temperature and wind speed profiles suggest that the uncertainty in H_c is considerably greater than 1 m. Therefore, the plume's trajectory might have been consistent with flow either above or below the dividing streamline. In terms of modeling, however, we have models only for plumes well above or well below H_c.

Figure 63 contains plots of the 5-minute H_c and Fr_H values for this experiment. H_c oscillated between 30 m and 40 m twice during the hour, thus forming a complete but distorted sine wave. Fr_H also followed a similar shape about 3.0. Because H_c oscillated about the local release height, data from this hour may provide an intriguing example of flow along the dividing streamline.

Hourly averaged wind speeds measured at 10 m and estimated at 40 m on tower A are 0.9 and 2.1 m/s, respectively. The direction at 10 m was 26° and that at 80 m, 132°; thus, there was a tremendous directional shear between 10 m and 80 m. Because the plume approached the hill steadily at 35 m in the photographs, the shear region must have occurred between 10 m and 30 m. Perhaps some of the vertical mixing seen in the photographs was driven by this shear just below the release height. The trend in wind speeds between 10 and 80 m is shown in Figure 71.

Variations in wind directions measured at 10 m and 80 m on tower A are shown in Figure 72 as frequency distributions. The winds at 80 m were once

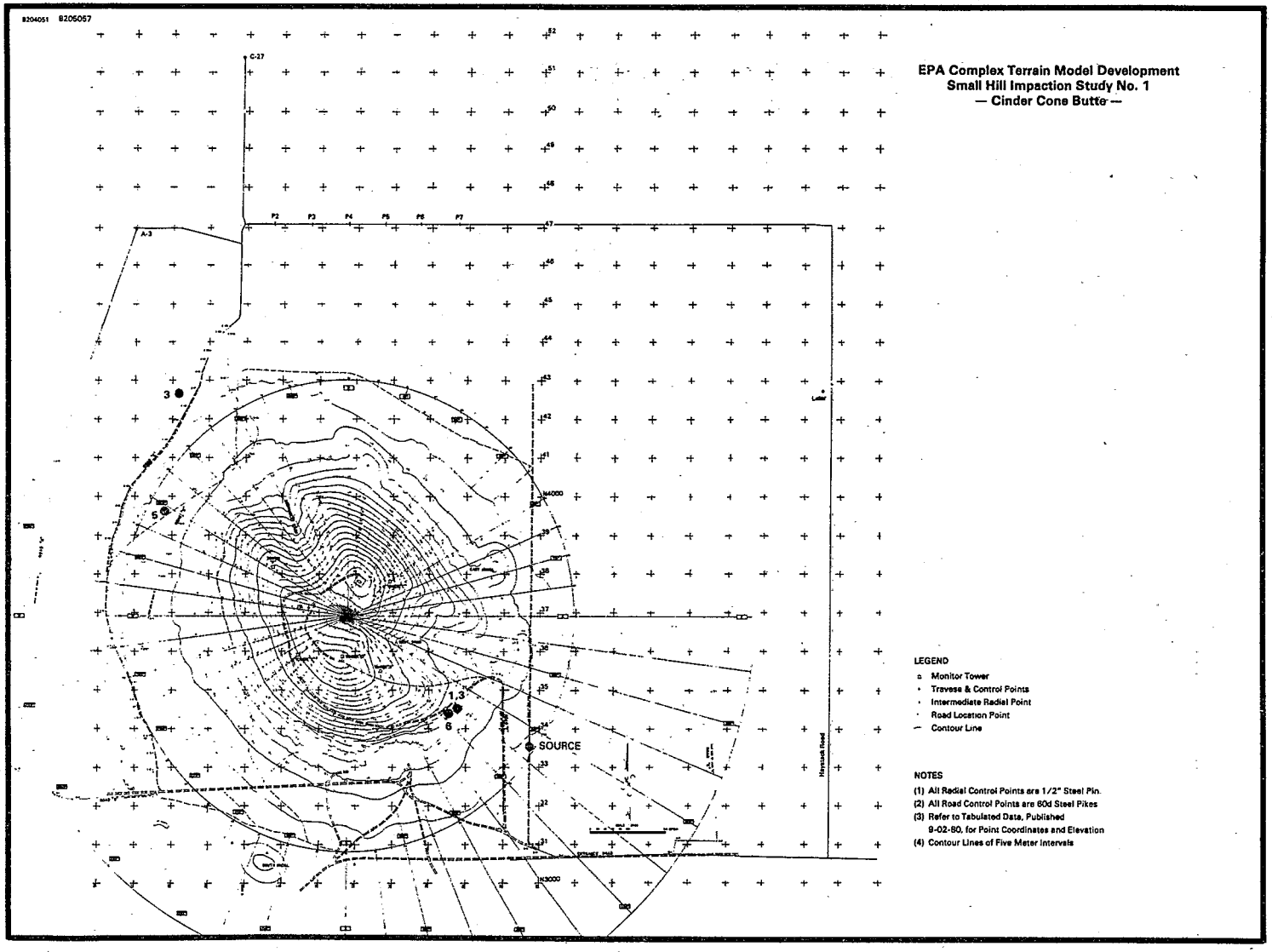

Figure 70. Plume centroid positions calculated from lidar data. Experiment 206, Hour 6 (0500-0600 MST).

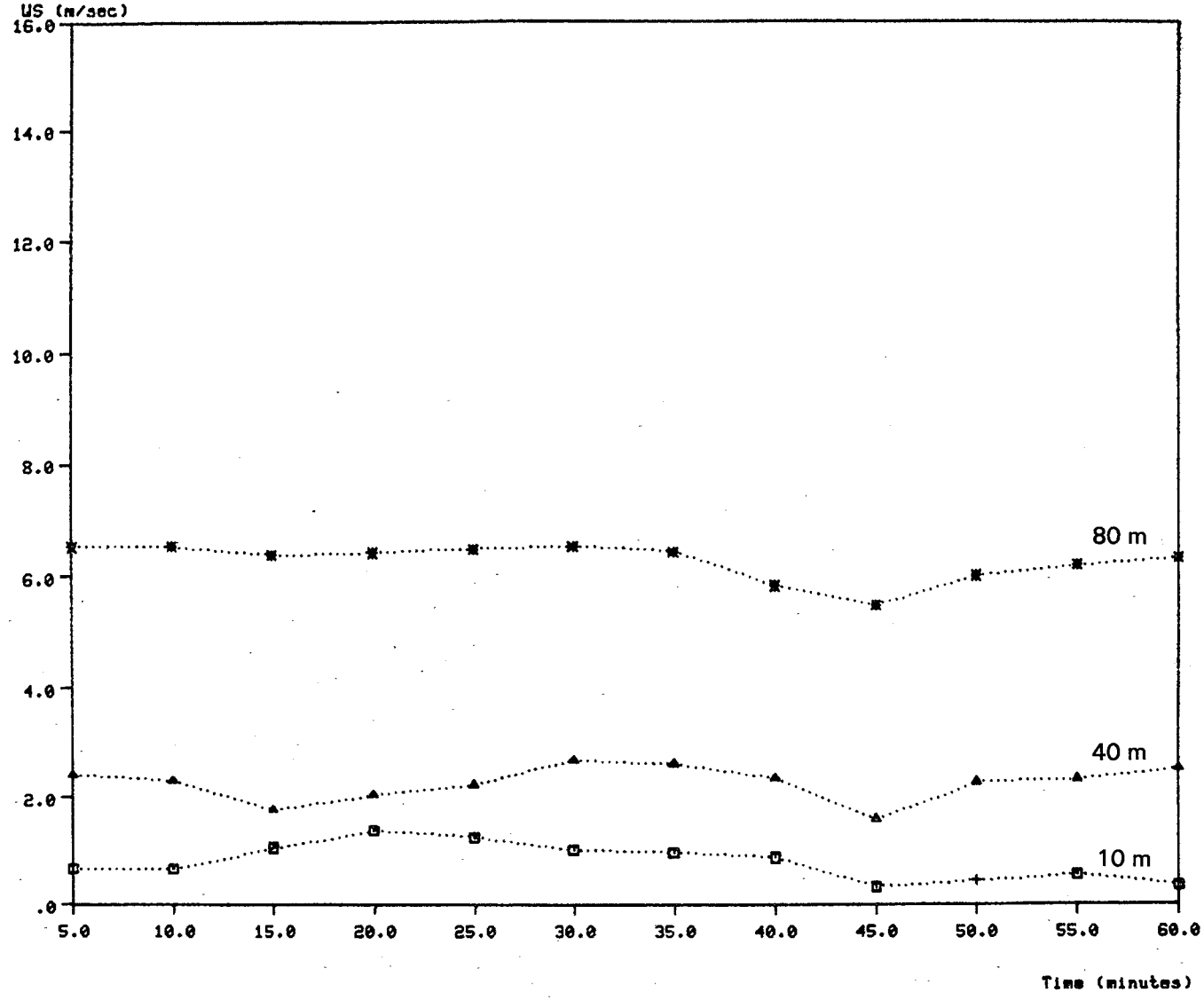

Figure 71. Tower A wind speeds during Experiment 206, Hour 6 (0500-0600 MST).

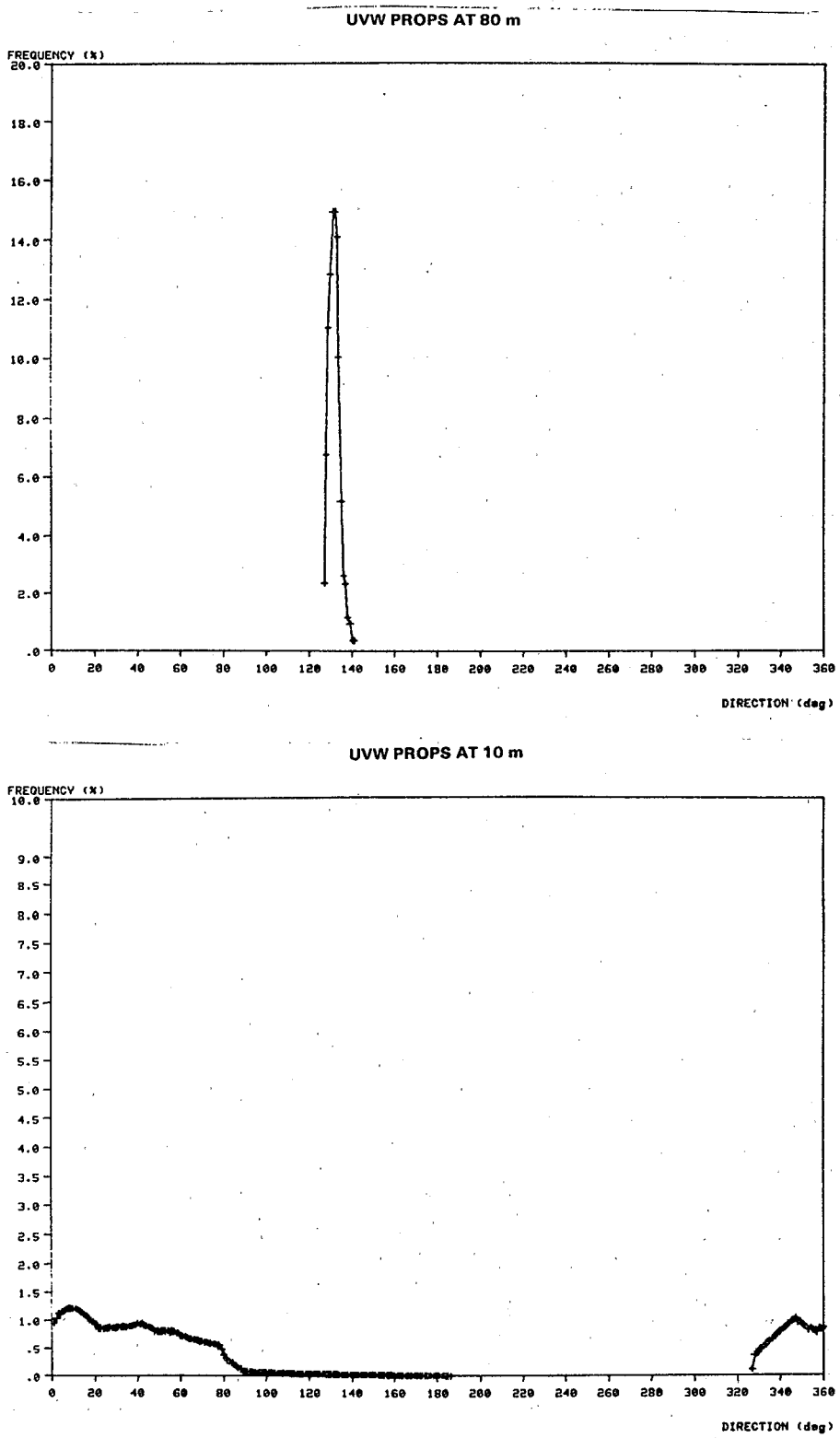

Figure 72. Calculated wind direction distribution functions for Experiment 206, Hour 6 (0500-0600 MST).

again very steady, spanning only about 10°. Because the photographs indicate a steady wind direction toward the hill, this distribution is probably representative of the distribution at source height. It is, at least, more representative than that at 10 m.

In summary, the plume was released virtually at the level of H_c. Wind speeds were fairly low at 2 m/s, but the transport direction was steady towards the hill. This hour is an excellent case in which to study transport properties along streamlines very near the critical dividing streamline in a complicated flow with wind shear.

SF_6 Concentrations

The distribution of hourly averaged SF_6 concentrations over the surface of the hill is shown in Figure 73. Highest concentrations are found above 25 m in the southeast draw right up and over the saddle, with equally high concentrations on the east face of the north peak.

This pattern is quite consistent with the reported observations and the photographs discussed above. Although the qualitative appearance of the flow was similar to that of previous hours, additional vertical mixing was reported; this may account for the high concentrations near the 25 m contour. The relative release height corresponded to the 30 m contour, so the mixing could have produced maximum concentrations below the release height.

The distributions of 10-minute SF_6 concentrations are presented in Figure 74. During the first 10 minutes, the plume apparently traveled preferentially along the north side of the hill, often impinging on the east face of the north peak. Later in the hour, however, the greater concentrations are found in the windward draw area.

4.7.2 Model Performance

This hour was modeled with the Wrap model because the plume was released very close to the calculated critical dividing streamline height. The hour provides an excellent opportunity to look at how the Wrap model performs when the winds were directed quite steadily from the source toward the hill.

The meteorological data were prepared for the release height as in Section 4.1.2. The resulting values are summarized in Table 10.

The 1-hour average wind direction measured 25 m below and 45 m above the release height are 26° and 132°, respectively. Because neither lidar nor tower B data are available for estimating wind directions at plume elevation, the photographs provide the only other check. These photographs suggest mean wind directions between 127° and 130°. Model winds are assumed to be 127°, and the PDF computed with the 80 m wind direction data are assumed valid for the 35 m release.

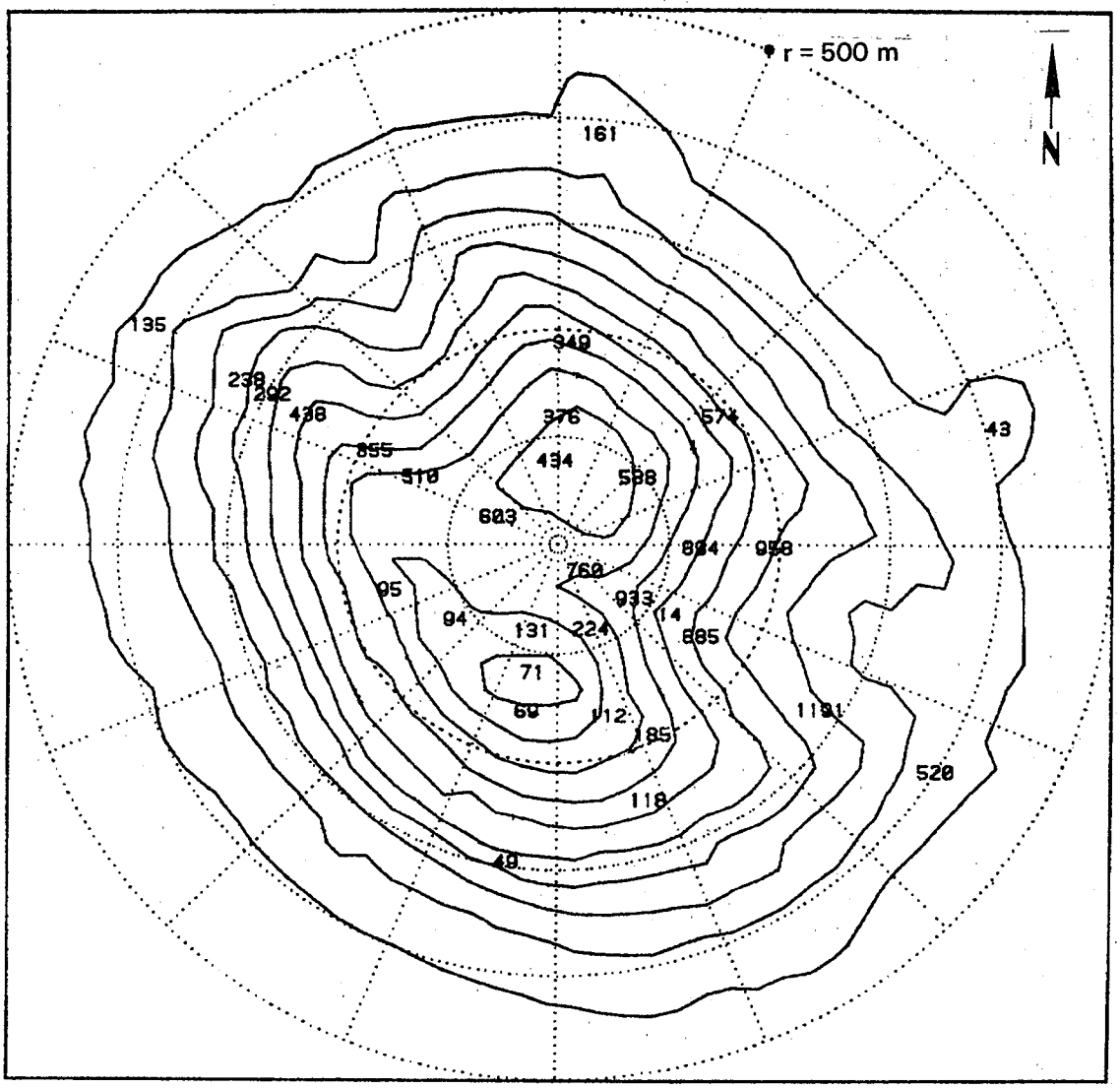

Figure 73. Observed SF_6 concentrations (ppt) for Experiment 206, Hour 6, (0500-0600 MST). Source: r = 595.9 m, θ = 123.6°, net height = 29.5 m, Q = .062 g/s.

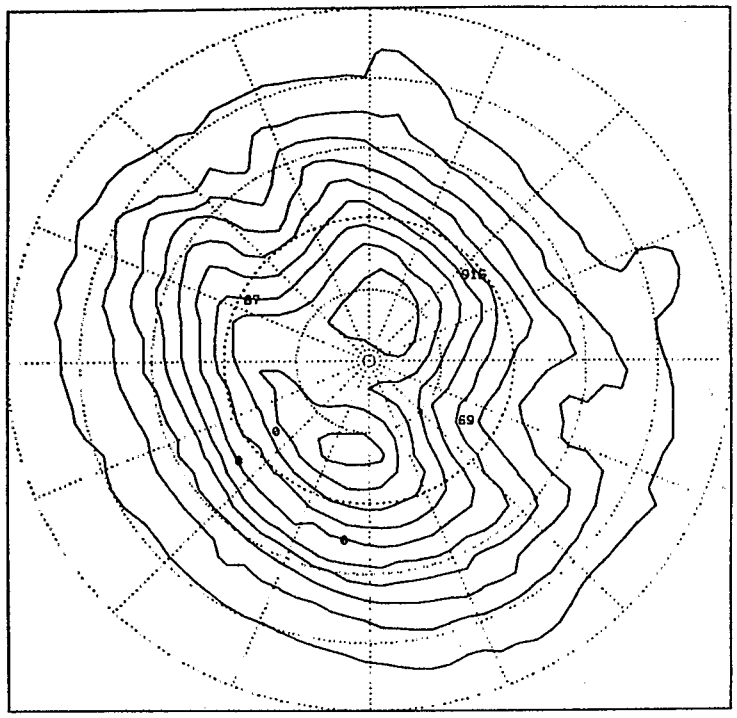

TIME PERIOD 0500-0510

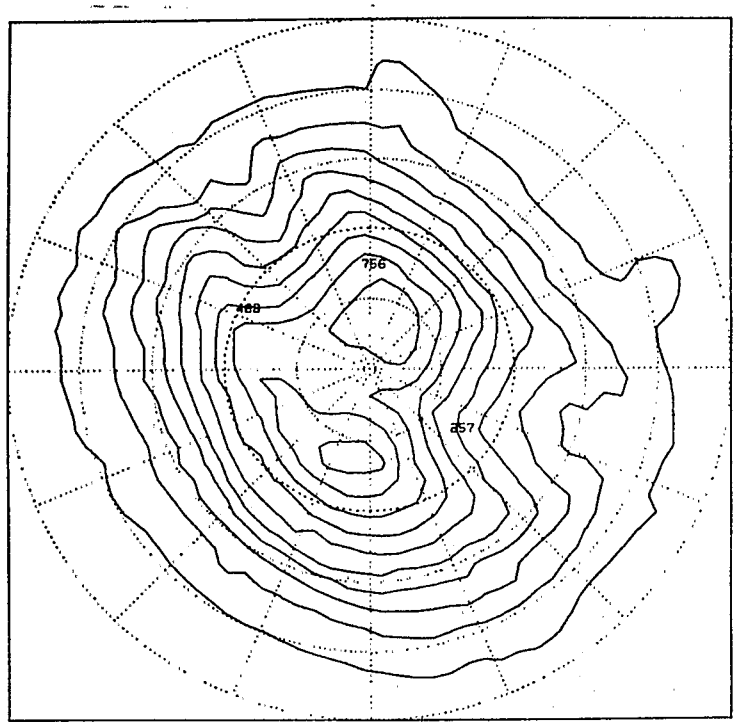

TIME PERIOD 0510-0520

Figure 74. Observed 10-minute average SF_6 concentrations (ppt) for Experiment 206, Hour 6 (0500-0600 MST).

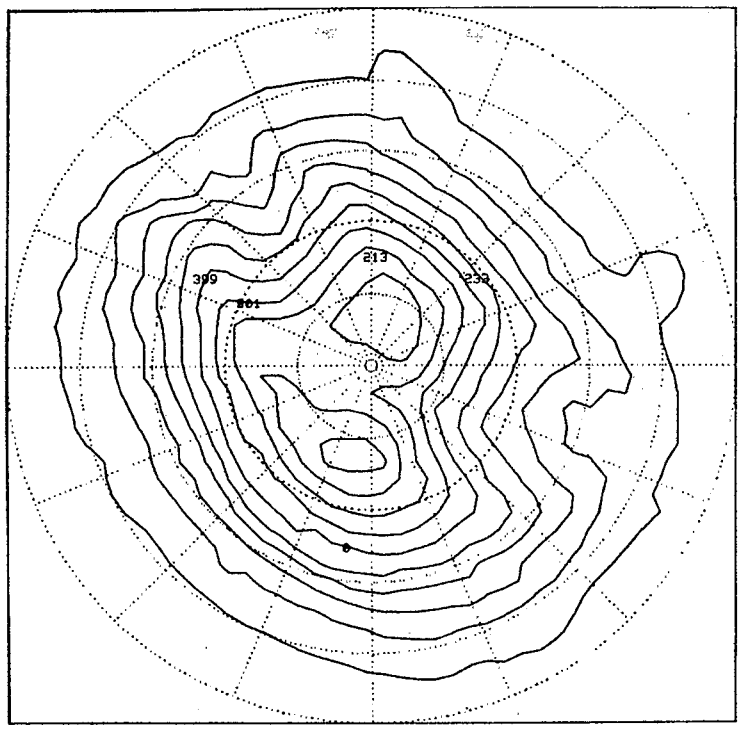

TIME PERIOD 0520-0530

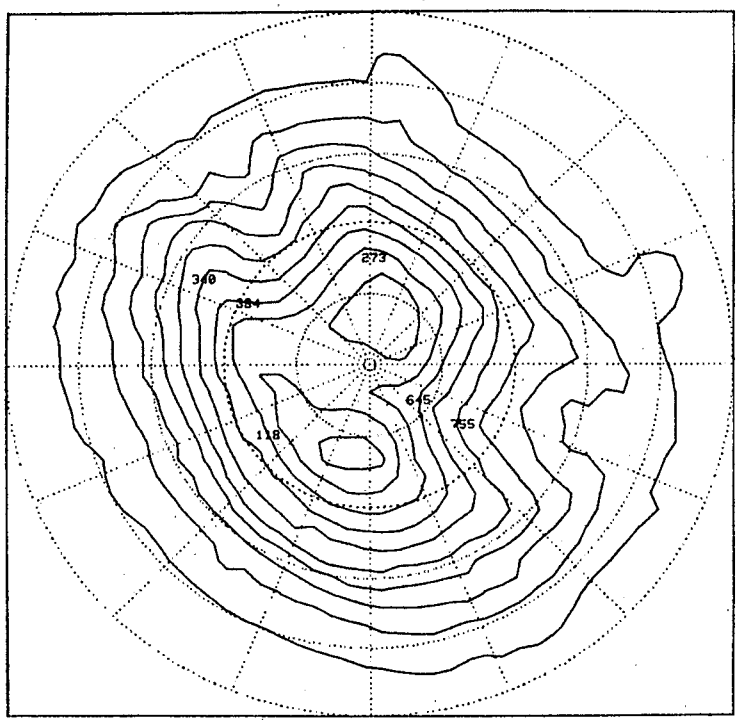

TIME PERIOD 0530-0540

Figure 74. Continued.

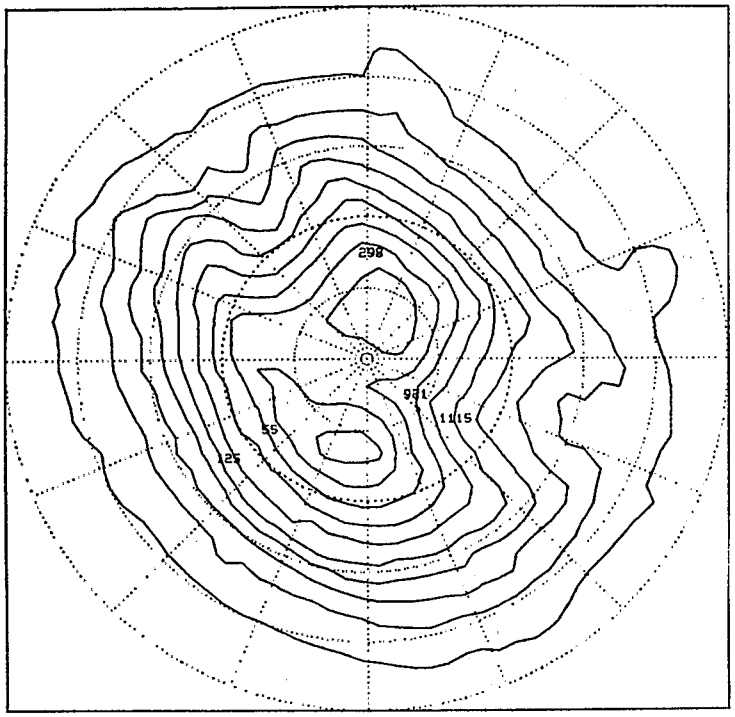

TIME PERIOD 0540-0550

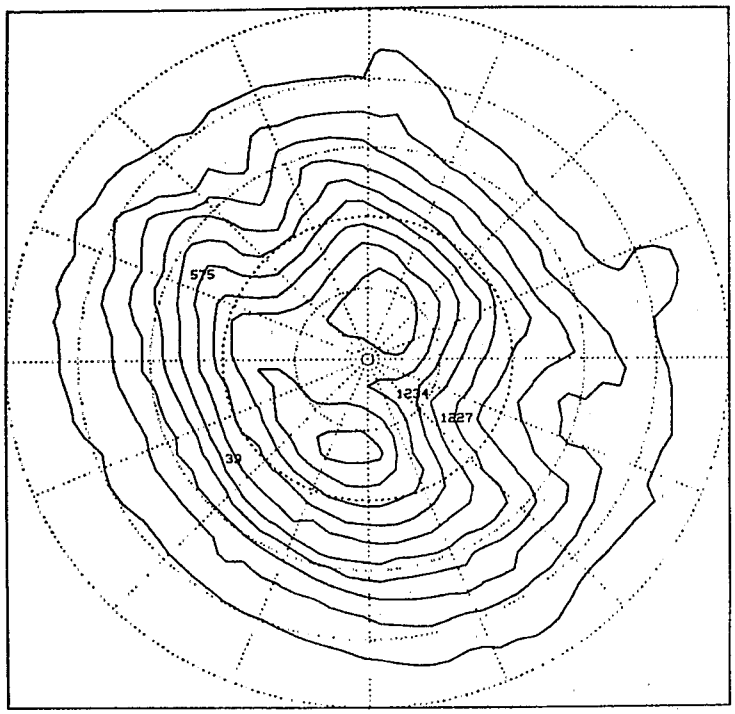

TIME PERIOD 0550-0600

Figure 74. Continued.

TABLE 10. IMPINGEMENT AND WRAP MODEL CALCULATIONS - EXPERIMENT 206, CASE HOUR 6

Meteorological Data

wind direction(deg)	=	127.
wind speed(m/s)	=	2.1
critical dividing streamline height(m)	=	35.0
Iz	=	.086
Iy	=	.212
N(1/s)	=	.035

Source Data

direction(deg)	=	124.
distance(m)	=	595.9
release height(m)	=	35.0
SF6 emission rate(g/s)	=	.062

Receptor Coordinates X(m)	Y(m)	Z(m)	Observed SF6 (ppt)	Impingement Predicted SF6 (ppt)	Wrap Predicted SF6 (ppt)
208.35	.00	31.25	957.70	348.23	1493.01
142.00	.00	50.00	894.00	272.76	1016.32
404.91	111.59	10.00	42.90	154.43	467.95
85.15	64.88	80.00	587.70	39.59	67.96
51.04	387.66	11.78	161.20	108.07	381.60
15.97	121.29	90.94	376.40	19.18	29.92
10.61	80.56	91.97	433.80	17.75	26.71
25.15	190.88	65.00	348.70	84.93	267.64
-38.04	-288.98	32.94	48.70	246.35	1046.51
-15.01	-113.99	98.96	71.20	5.93	3.58
-19.85	-149.12	90.00	68.90	15.69	15.79
-9.85	-76.12	90.00	130.50	15.66	15.72
-84.85	-65.12	90.00	94.30	20.14	31.01
-144.85	-38.12	80.00	94.80	39.48	92.33
95.80	-231.27	52.96	117.50	242.87	848.54
59.13	-154.04	80.00	112.20	34.37	39.80
43.00	-74.48	80.00	224.30	31.90	31.56
355.15	-205.04	5.69	520.20	145.12	262.44
256.81	-148.27	25.29	1190.80	486.23	1958.89
142.15	-81.12	40.00	684.54	539.76	2337.82
108.15	-61.12	50.00	13.90	392.59	1381.63
37.15	-21.12	70.00	759.50	81.57	101.43
-359.96	207.82	8.94	135.40	73.09	259.74
-269.62	155.66	38.07	238.20	102.83	424.59
-246.20	142.14	47.96	292.30	94.85	378.02
-111.85	65.88	80.00	509.50	36.78	96.80
-40.85	28.88	80.00	602.90	36.68	96.83

Both the Impingement and Wrap models were run with the revised meteorological data, and the results are listed in Table 10, and plotted on a map of CCB in Figure 75.

The concentration pattern estimated by the Wrap model compares favorably with that observed, but peak concentrations are overestimated. The highest observed concentration of 1,191 ppt was measured at 25 m on the windward side of the hill. The highest concentration calculated by Wrap (2338 ppt) occurs at 40 m. At this location Impingement predicts 540 ppt. At 25 m, Impingement estimates 486 ppt, which is about one-half of the observed concentration. The corresponding estimate from Wrap is 1,959 ppt, or nearly twice the observed.

In general, both of the models perform reasonably well in reproducing the observed concentration pattern on the windward side of the hill. This is not surprising because both models place the stagnation streamline near the peak of similarly shaped horizontal distribution functions. If the vertical mixing shown near the foot of the hill in the photographs were incorporated into Wrap the model estimates of the peak concentrations would probably improve.

4.8 Experiment 206, Hour 8 (0700-0800 MST)

4.8.1 Summary Description

Thermofogger oil-fog and SF_6 tracer gas were released from the southeast side of the hill at 595.9 m, 123.6° for nearly the entire hour. The release height was 35 m, and all release parameters were the same as those from the previous hour, causing no discontinuities in the experiment at the start of the hour. Although the SF_6 release terminated early at 0753, there may have been nearly a full hour of tracer impact on the hill because the travel time from the source to the hill center at 2 m/s is about 5 minutes.

Local terrain elevations near the release point are estimated to be -5.5 m relative to the zero of the hill coordinate system; the net release height corresponds to the 29.5 m height level on the hill. The SF_6 release rate is computed to be 0.062 g/s, with an estimated uncertainty of $\pm$1.0%. No Freon was released.

Plume Observations

Several observations of the appearance and the trajectory of the oil-fog plume are available for this hour.

Time: 0658 We are going to raise the small secondary fogger up another 5 or 6 meters to a final height of 15 meters.

Time: 0708 I've been standing on road F watching the flow visualization that has been going on. We are seeing very interesting things with the flares going mostly to the southeast at the surface.

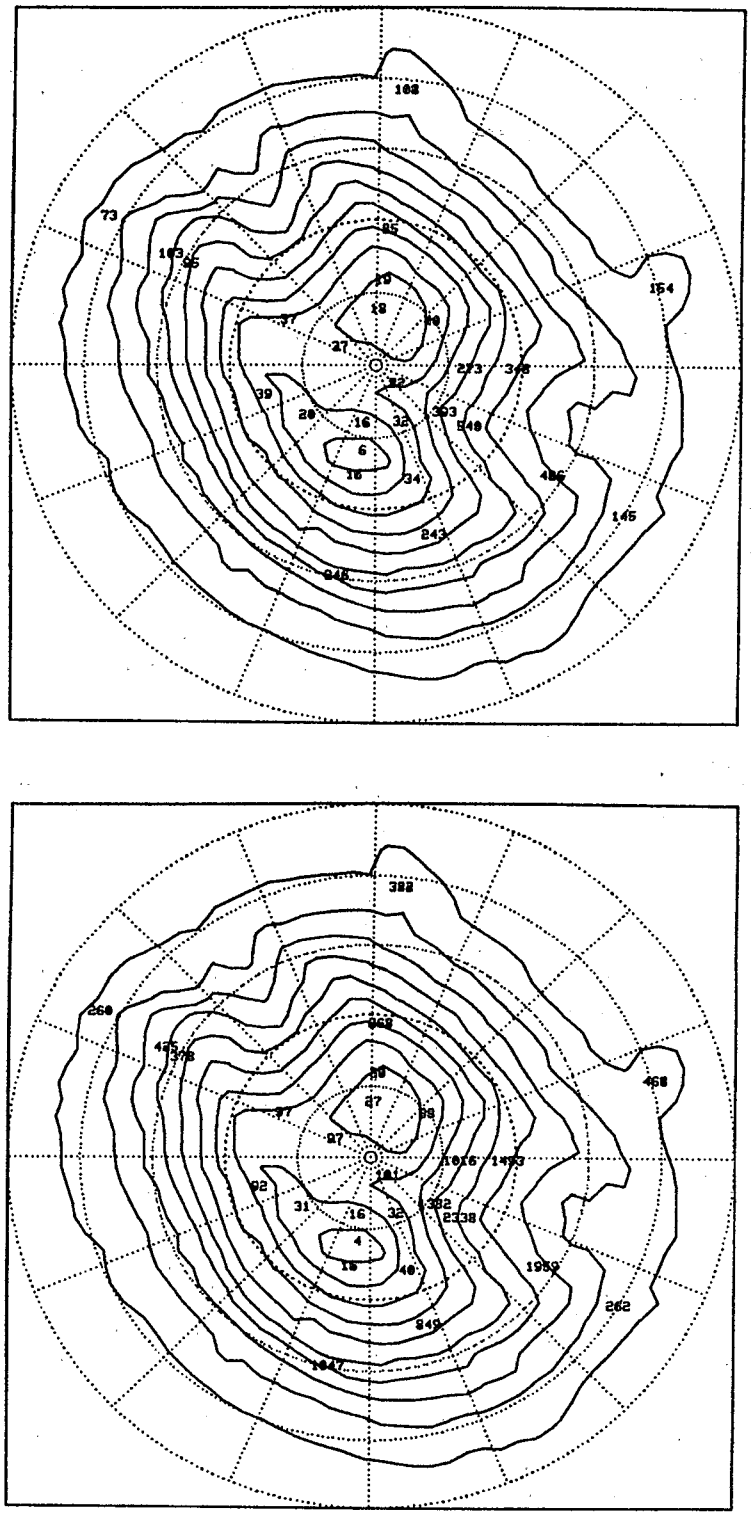

Figure 75. SF_6 concentrations (ppt) estimated for Experiment 206, Hour 6 by the Impingement (top) and Wrap (bottom) models.

The oil-fog from the United Survey generator (up at 15 meters) is going to the west-northwest, but is getting caught in some kind of down draft and being brought down to the ground after it has gone 20-30 meters or less. The main plume is still hitting the north butte and the draw area. It is really smearing around after it gets close, and it is hard for me to see from this location exactly where it is. I would say that it is hitting in the lower third of the draw and then going up the draw, and part of it is going around the north butte, below tower C.

Time: 0713 I'm up the road toward tower D and the plume is coming right at me or just switched off from me. I can smell it quite strongly. I'm about 20 meters below tower D.

We have two releases going now. The primary release is an irregular plume heading for the north knoll, slipping around the north end. The second release is impacting the south end and sinking. Smoke is visible on the ground.

Time: 0715 The elevated smoke plume continues to go toward the north butte with some of the plume material going up the draw and the bulk of it going around the east side of the north butte. Low level flow at the surface is evident by the smoke candles, downslope or towards the east. From the location of the United Survey generator at 15 meters, it is still pretty confused with a lot of vertical motion and a lot of downward mixing.

Time: 0717 We are driving up to the north butte and just past the draw. Smoke material was very visible coming up the draw.

Time: 0719 It looks like the United Survey generator now is up to about 30 meters on the short crane.

Time: 0729 About 3-4 minutes ago I noticed that the main plume has switched from coming right up the butte to being caught in some very strong eddies. As I am looking back at the release from the north butte, it is a vortex that rotates clockwise and it is bringing the plume all the way to the ground by the time it hits the road up the butte. The plume now is headed more up the southeast ridge, and the United Survey plume is down.

Time: 0735 It looks to me like all the other extraneous sources of smoke are gone and the nephelometer measurements should be good again.

Time: 0742 The plume is mixing down from the 35-meter release all the way to the ground by the time it gets to road F. The crane is on the mobile crane road, and the plume is hitting the western edge of road F.

Time: 0743 Now the plume is back up again. You get momentary parts of the plume coming down.

Time: 0750 Plume is irregular (vertically) and only visible to the north knoll.

The observations indicate that there was large directional wind shear between the surface and some level below 15 m. The main plume containing the tracer gas traveled between the southeast shoulder of the hill and the north side throughout the hour. At times, strong eddies appear to have brought the plume to the ground on the lower part of the hill. Reportedly, the eddies gave the plume a rotating appearance as the observer looked back at the source along the plume axis.

Although the still photographs cannot document this rotation, they do show marked plume dilution near the hill. A representative photo from the series taken from behind the release at camera position 0-11 (see Figure 46) is reproduced in Figure 76. Each photo in the series is an automatic exposure, so it represents nearly a instantaneous picture of the plume rather than a 5- or 10-minute average.

The plume appears to sweep back and forth over the draw between the two peaks for much of the hour. The rapid dilution of the plume noted in the observations does not become readily apparent until 0730.

Meteorological Information

Wind and temperature data measured at tower A during this hour were used to characterize the flow in terms of H_c. As in the previous hours of Experiment 206, wind speeds at 40 m were estimated because of the partial failure of the 40 m wind set. The average H_c over this hour is 37 m, and Fr_H above this level is 3.3. Because the local release height is 35 m, H_c had a substantial influence on the plume trajectory (as discussed in Section 4.7.1).

Figure 63 contains plots of the 5-minute H_c and Fr_H values for this experiment. H_c began the hour at about 26 m but quickly rose above 40 m. Over the latter half hour, however, H_c fell steadily to below 30 m. Fr_H during the same period exhibited a similar pattern, rising as high as 3.5. Because H_c varied about the release height by ±5 m, this hour is very similar to hour 6 of the same experiment (see Section 4.7.1).

Hourly averaged wind speeds measured at 10 m and estimated for 40 m on tower A are 0.7 and 2.0 m/s, respectively. The direction at 10 m was 356° and that at 80 m, 131°; thus, the strong directional shear noted during hour 6 persisted. Again, the plume at 35 m is directed toward the hill so that the shear must take place below this height. The trend in wind speeds between 10 and 80 m is shown in Figure 77. Both the 10 m and 80 m levels hold fairly constant, although even slight variations at 10 m represent large percentage changes because of the extremely low wind speeds recorded. The estimated winds at 40 m go through a significant decrease during the first half hour, however. This dip produces the rapid rise of H_c at this time.

Variations in wind directions measured at 10 m and 80 m on tower A are shown in Figure 78 as frequency distributions. The 10 m distribution is once again characterized by a wide range of wind directions, whereas

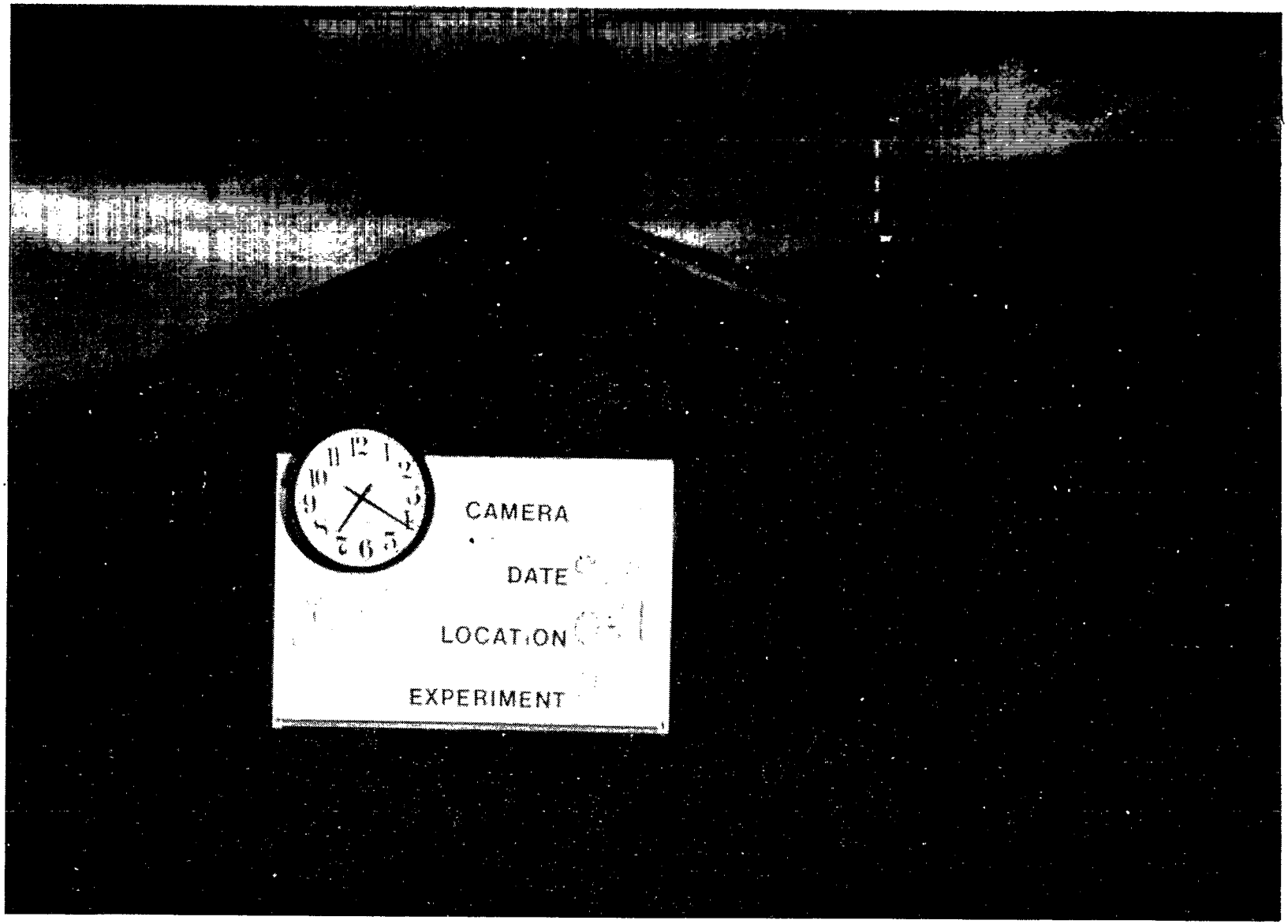

Figure 76. View of the plume trajectory at 0721 MST taken from behind the release (position 11) during Experiment 206, Hour 8.

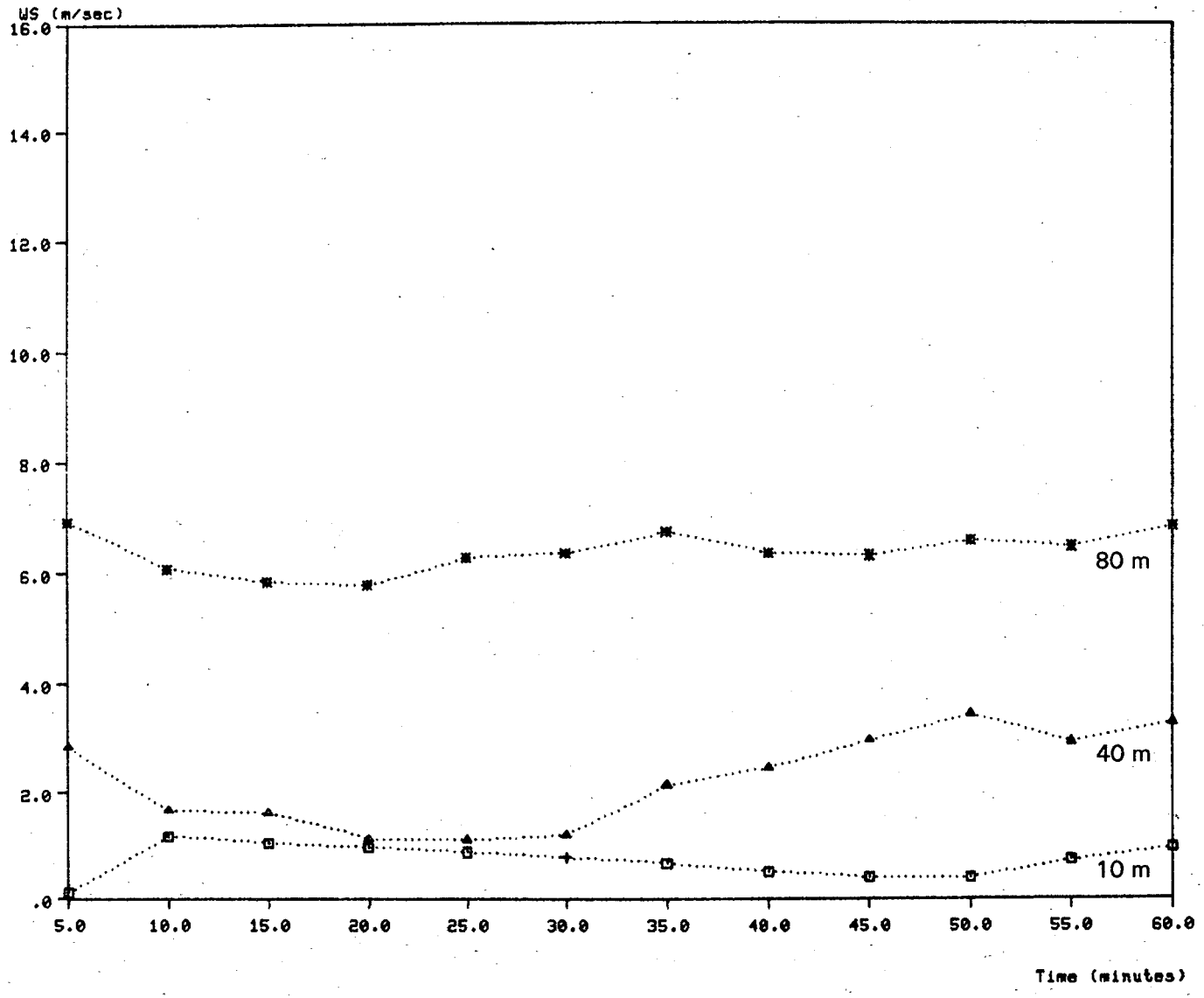

Figure 77. Tower A wind speeds during Experiment 206, Hour 8 (0700-0800 MST).

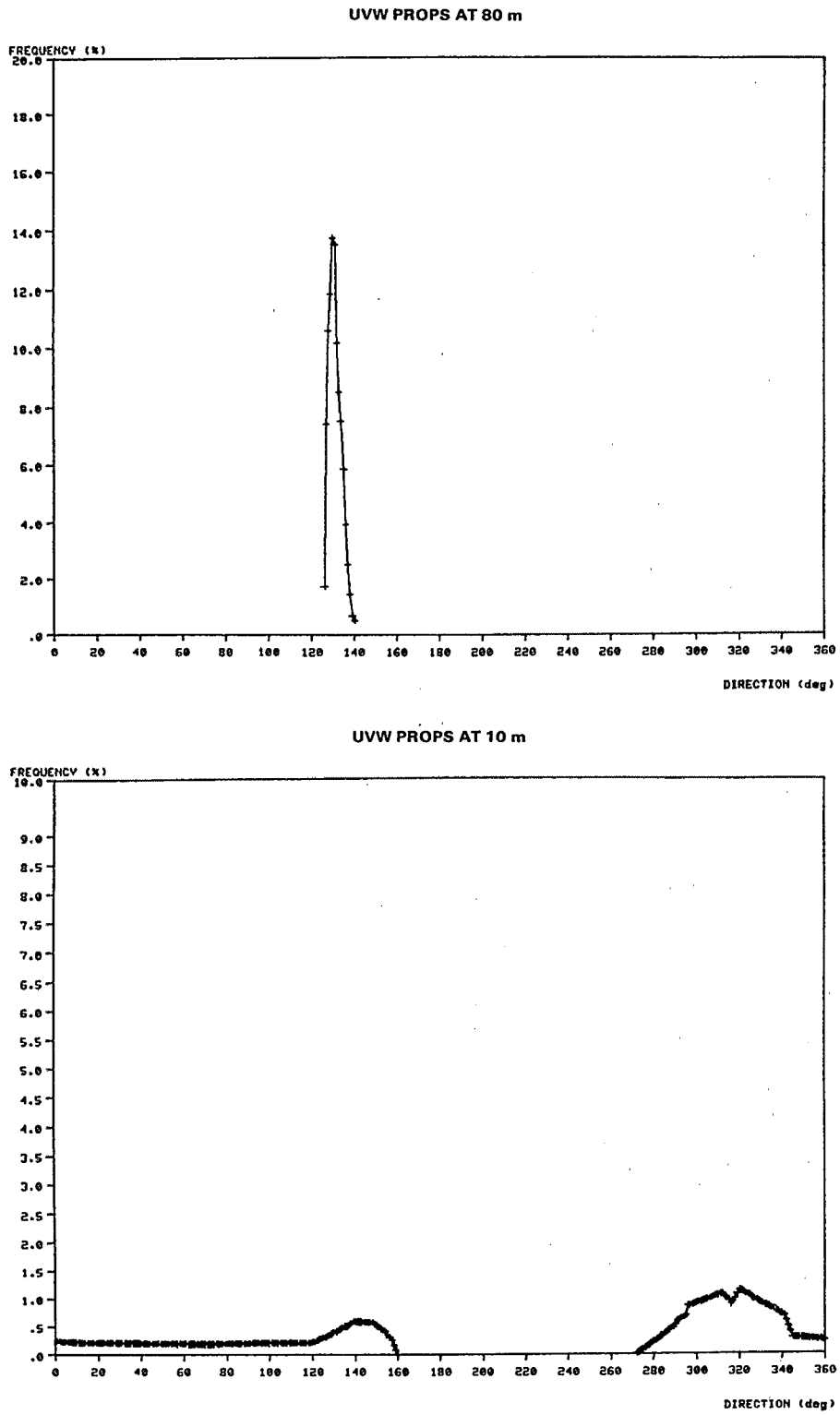

Figure 78. Calculated wind direction distribution functions for Experiment 206, Hour 8 (0700-0800 MST).

directions at the 80 m level are limited to about a 10° range. The 10° range remains indicative of the transport at plume elevation.

In summary, the hour is quite similar to hour 6. The plume was released at virtually the dividing streamline height, and the transport direction was very steady.

SF_6 Concentrations

The distribution of hourly averaged SF_6 concentrations over the surface of the hill is shown in Figure 79. Highest concentrations are found along the south side of the southeast draw and along the eastern face of the north peak. These concentrations lie between the 25 m and 50 m height contours. Other high concentrations are spread over the north peak and the saddle area.

This pattern is consistent with the observations and the photographs discussed above. The north peak area was frequently hit, but the plume was at times mixed down to the ground near the base of the draw, thereby producing the highest concentration measured during the hour. The broad distribution of higher concentrations on both the windward and leeward sides of the north peak indicates that plume material was mixed to the surface as it met the hill and was then advected directly over and around the hill top.

The distribution of 10-minute average SF_6 concentrations is presented in Figure 80. No information is available for the area near the impingement zone, but the data indicate that much of the material that came toward the north peak passed around toward the north side.

4.8.2 Model Performance

This hour is very similar to the previous hour discussed in Section 4.7.2. The plume was released very close to the calculated dividing streamline height, and so the Wrap model ought to work quite well.

All meteorological data were prepared for release height as in Section 4.1.2. The resulting values are summarized in Table 11.

The 1-hour average wind directions measured 25 m below and 45 m above the release height are 356° and 131°. However, the photographs suggest that the plume trajectory followed winds in the range of 127° to 170°. Therefore, 127° is used in the modeling along with the 80 m PDF.

Both Impingement and Wrap were run with the revised meteorological data, and the results are listed in Table 11, and plotted on a map of CCB in Figure 81.

The models do well in matching the observed concentration pattern. The highest observed concentrations occurred around the height of release; the maximum, 1,512 ppt, is measured at 25 m. The Wrap estimate at this height is 1,994 ppt, but Wrap estimates a maximum concentration of 2,345 ppt at a

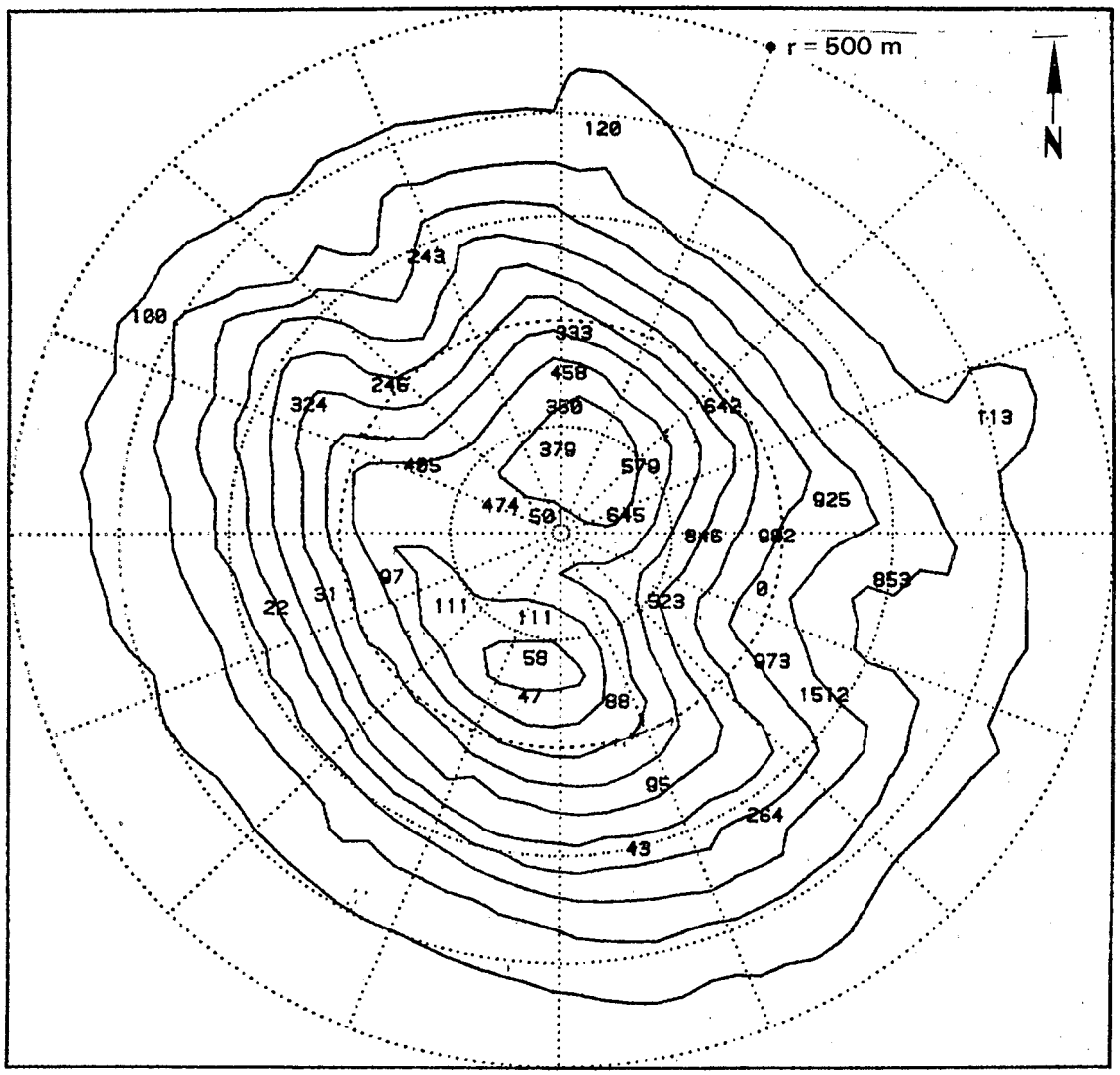

Figure 79. Observed SF_6 concentrations (ppt) for Experiment 206, Hour 8 (0700-0800 MST). Source: r = 595.9 m, θ = 123.6°, net height = 29.5 m, Q = .062 g/s.

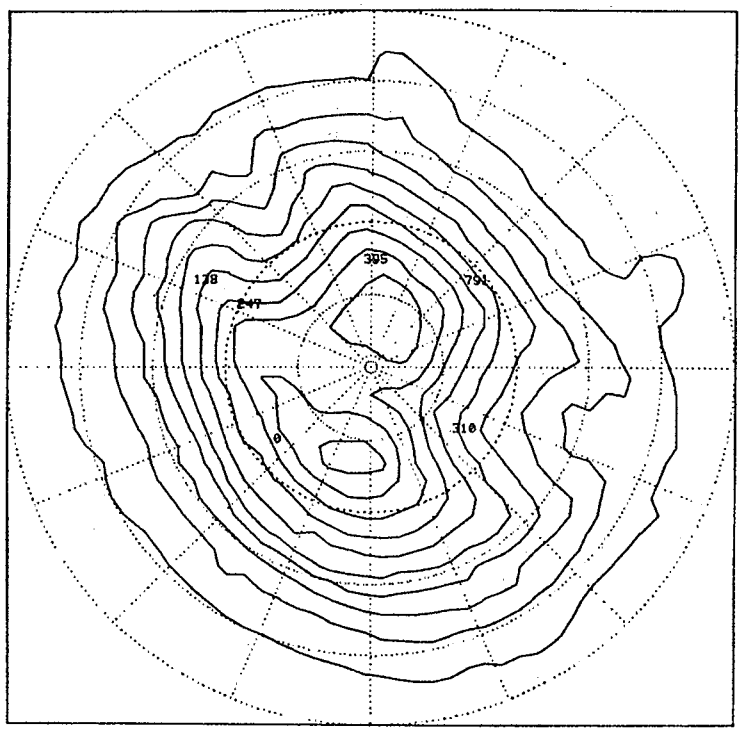

TIME PERIOD 0700-0710

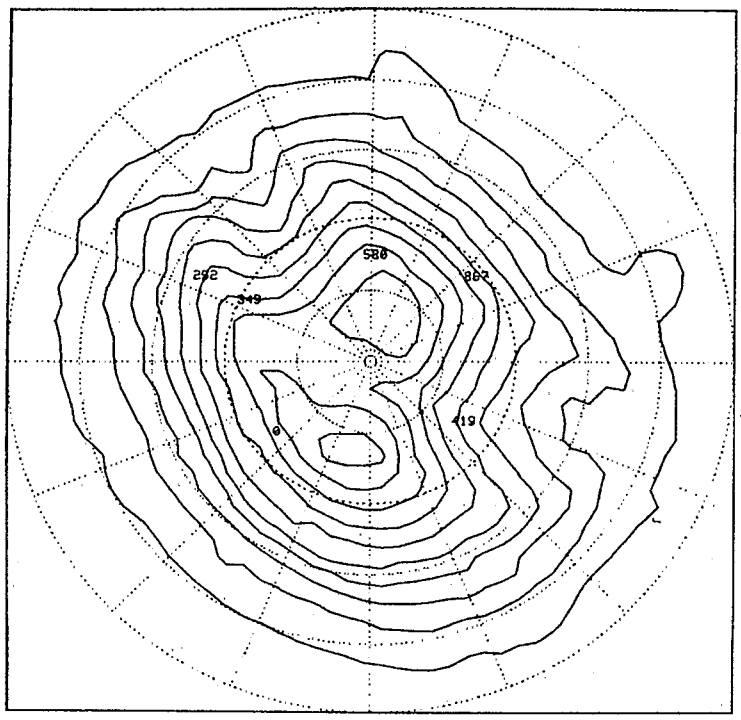

TIME PERIOD 0710-0720

Figure 80. Observed 10-minute average SF_6 concentrations for Experiment 206, Hour 8 (0700-0800 MST).

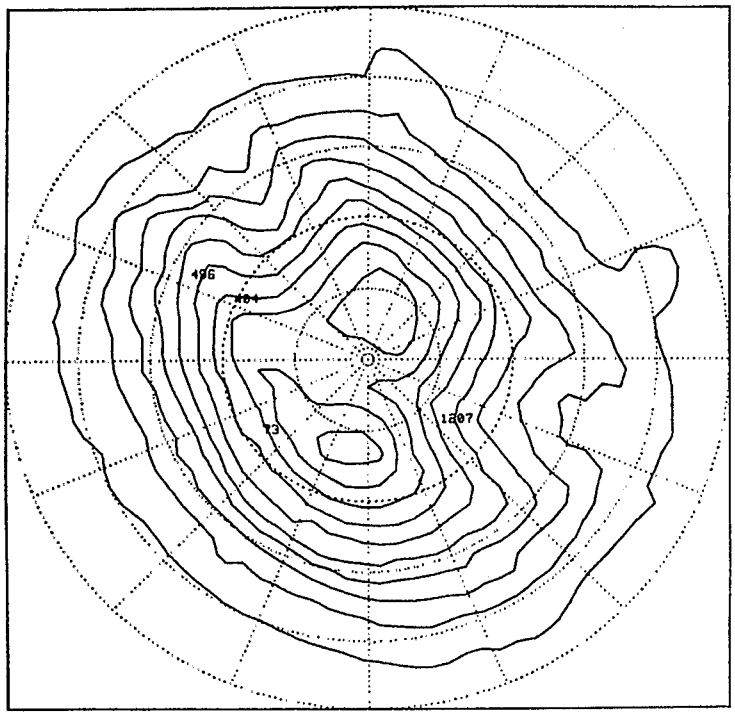

TIME PERIOD 0730-0740

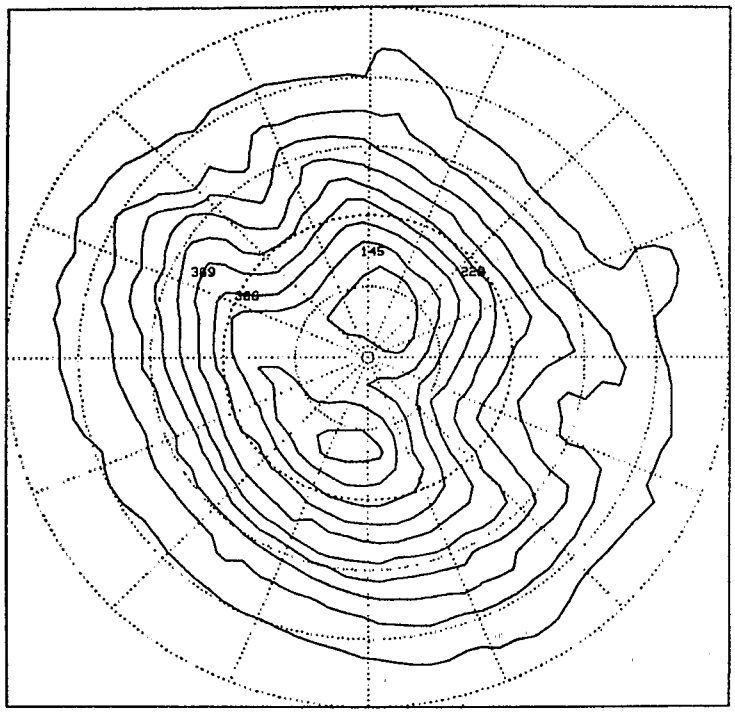

TIME PERIOD 0720-0730

Figure 80. Continued.

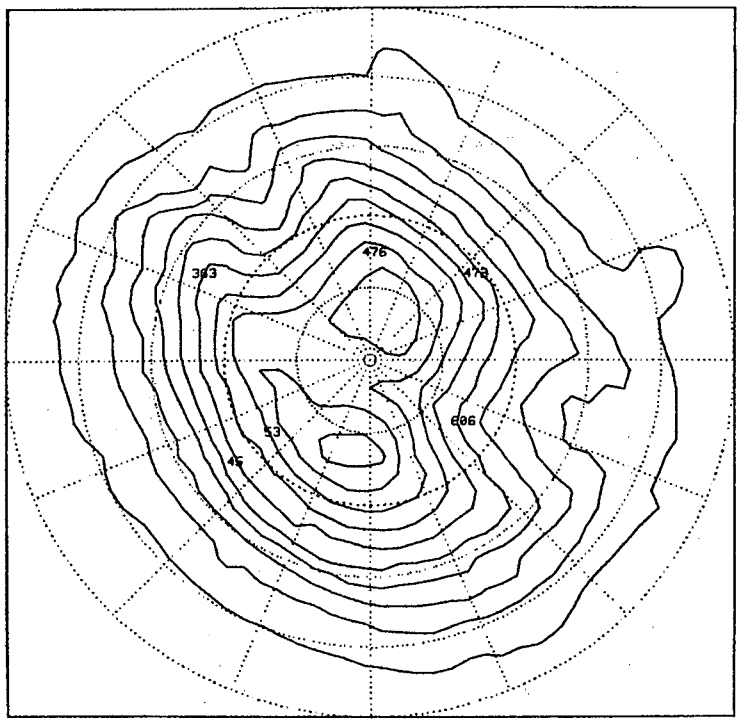

TIME PERIOD 0740-0750

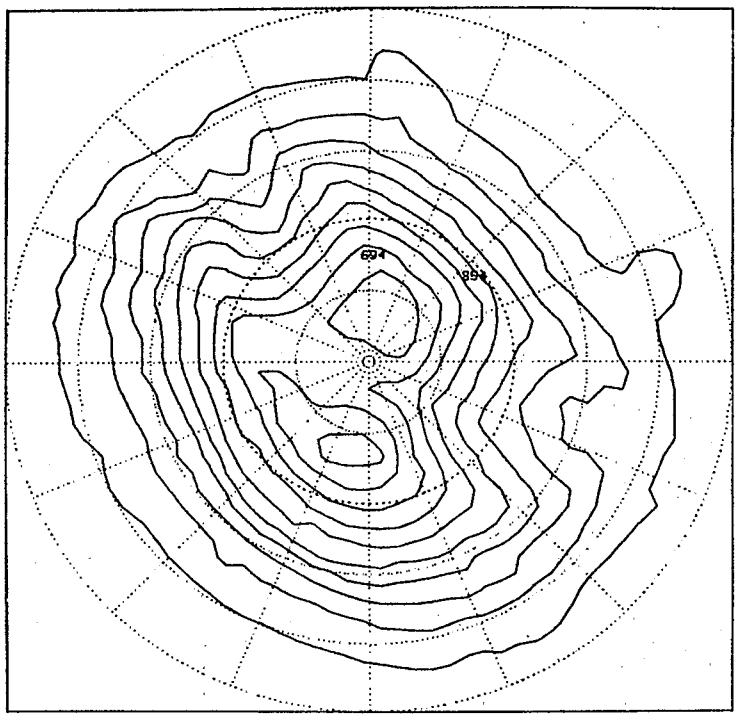

TIME PERIOD 0750-0800

Figure 80. Continued.

TABLE 11. IMPINGEMENT AND WRAP MODEL CALCULATIONS - EXPERIMENT 206, CASE HOUR 8

Meteorological Data

wind direction(deg)	=	127.
wind speed(m/s)	=	2.0
critical dividing streamline height(m)	=	37.0
Iz	=	.097
Iy	=	.180
N(1/s)	=	.040

Source Data

direction(deg)	=	124.
distance(m)	=	595.9
release height(m)	=	35.0
SF6 emission rate(g/s)	=	.062

Receptor Coordinates X(m)	Y(m)	Z(m)	Observed SF6 (ppt)	Impingement Predicted SF6 (ppt)	Wrap Predicted SF6 (ppt)
208.35	.00	31.25	981.70	408.91	1493.34
142.00	.00	50.00	846.10	325.42	1051.49
257.78	33.94	30.00	924.70	367.35	1329.21
72.15	19.88	80.00	645.40	49.79	67.83
404.91	111.59	10.00	112.70	188.81	508.63
159.04	122.04	46.91	642.40	240.12	822.14
85.15	64.88	80.00	578.60	52.07	84.82
51.04	387.66	11.78	119.50	129.77	399.02
20.07	152.45	81.06	457.90	48.34	95.30
15.97	121.29	90.94	349.70	25.77	38.27
10.61	80.56	91.97	379.20	23.97	34.46
25.15	190.88	65.00	333.20	103.60	287.82
2.15	18.88	80.00	500.70	51.28	104.22
-15.01	-113.99	98.96	58.30	8.87	5.77
-19.85	-149.12	90.00	47.00	22.02	22.43
-9.85	-76.12	90.00	110.90	21.98	22.35
-84.85	-65.12	90.00	110.60	27.07	39.78
-248.96	-66.71	32.90	21.80	161.76	576.34
-204.16	-54.70	52.26	30.60	136.49	451.16
-144.85	-38.12	80.00	96.80	50.23	106.88
77.87	-290.63	35.10	43.40	375.38	1376.19
95.80	-231.27	52.96	95.20	291.88	891.60
59.13	-154.04	80.00	88.40	46.85	54.56
199.06	-259.43	30.00	263.90	496.81	1815.01
256.81	-148.27	25.29	1512.10	575.91	1993.94
204.15	-117.12	30.00	973.30	636.25	2344.69
108.15	-61.12	50.00	523.10	471.23	1452.12
183.53	-49.18	30.00	.00	499.06	1823.52
312.38	-41.13	14.00	852.70	276.06	770.40
-359.96	207.82	8.94	100.40	87.68	270.97
-111.85	65.88	80.00	405.30	46.13	108.83
-40.85	28.88	80.00	474.40	45.99	108.78
-141.42	141.42	50.00	245.70	113.68	384.69
-109.07	263.31	30.00	242.70	144.55	511.33

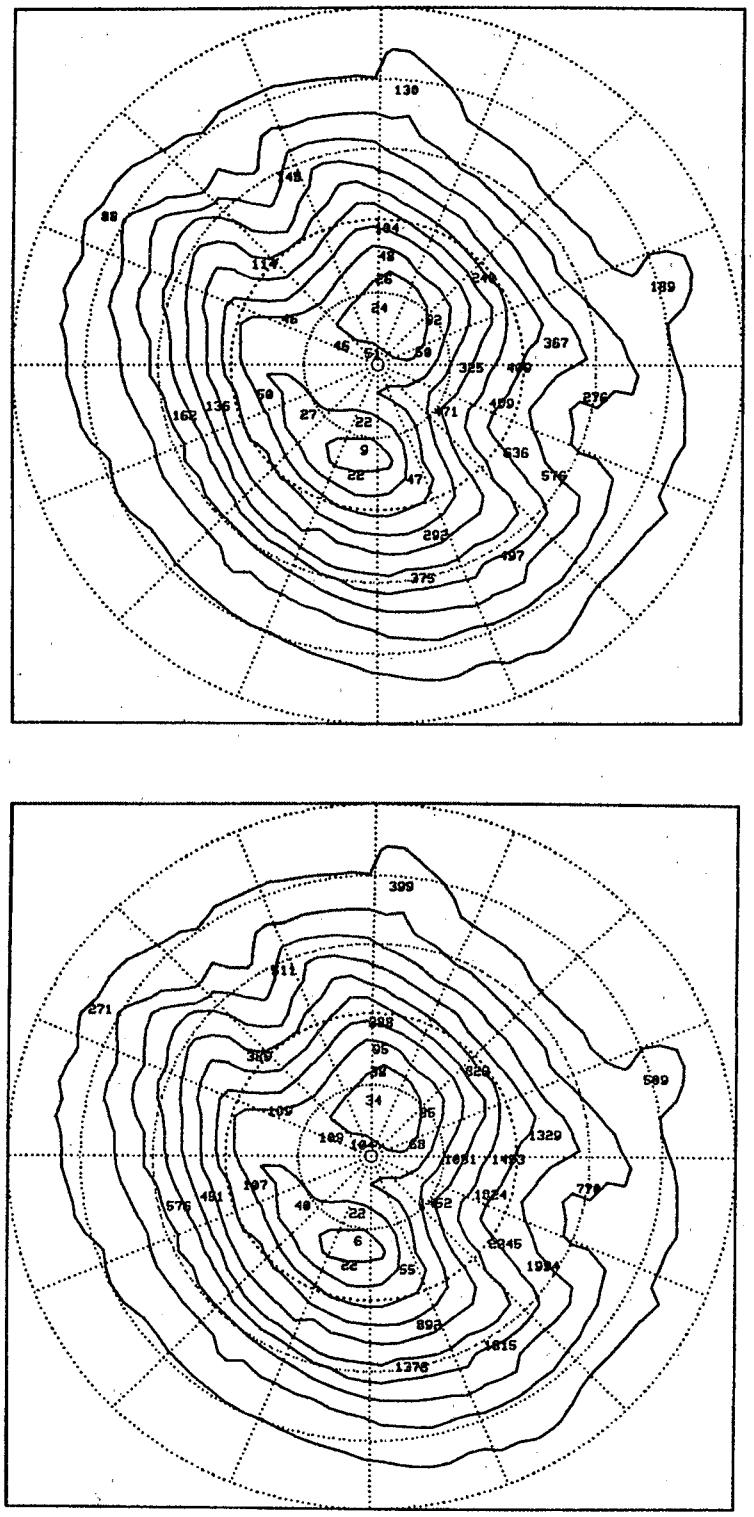

Figure 81. SF_6 concentrations (ppt) estimated for Experiment 206, Hour 8 by the Impingement (top) and Wrap (bottom) models.

height of 30 m (where the observed concentration was 973 ppt). In general, the predictions from Wrap are no more than 100% greater than the observed concentrations. On the other hand, the Impingement model underestimates the observations. The largest estimate is about 636 ppt, or roughly one-half the maximum observed. The difference between model estimates is directly related to the treatment of the wind direction probability distribution. In this case, the Gaussian distribution characterized by i_y underestimated the probability, and the assumed PDF overestimated it.

4.9 Experiment 209, Hour 1 (1700-1800 MST)

4.9.1 Summary Description

Thermofogger oil-fog and SF_6 tracer gas were released from the northwest side of the hill at 986.1 m, 315.9° for the entire hour. The release height was 40 m. Because the SF_6 was started at 1654 and terminated at 1759, the tracer plume was probably well established throughout the sampling hour.

Local terrain elevations near the release point are estimated to be -7.0 m relative to the zero of the hill coordinate system, so the net release height corresponded to the 33.0 m height level on the hill. The SF_6 release rate is computed to be 0.156 g/s with an estimated uncertainty of $\pm$5.9%. No Freon was released.

Plume Observations

During the course of this experiment, several people recorded their observations about the appearance and the trajectory of the oil- fog plume. Those comments applicable to the first hour are presented below.

Time: 1650 The jet fogger is up at 40 meters at site A2B. The plume looks quite unstable. There is a great deal of vertical development at the moment, and it appears to be headed right toward the hill. Looking from the back side of the hill, the plume looks like it goes to 2 hill heights at the moment.

Time: 1700 (?) Plume is starting out on a line toward the FAA tower and then curves to the north side. I see some plume material mixing down to the hillside at about the 20m elevation.

Time: 1715 Plume is fluctuating across the peaks. From the top, a little odor is noted, but most of the plume is going overhead.

Time: 1721 The plume is still continuing to go up the shoulder in the vicinity of tower F, and from the side view it looks like it is not touching the hill until it gets very near the top in the vicinity of tower B. In the lee, the plume descends quite a bit and looks like it almost reaches the ground again about a hill width away to the southeast.

Time: 1724 The plume is traveling right over B2 as it travels to the southeast.

Time: 1725 I am sitting at 48I, and the plume is passing right over this point.

Time: 1733 From southwest: plume goes towards draw, lifts up and over, and then comes back down on the lee side at a lower level than the approach height. The majority of the plume is going up the draw.

Time: 1740 Plume heading directly towards the blockhouse on the south end and then it bends around to the south (then back towards the east in the lee of the hill).

Time: 1745 Plume is midway between the blockhouse and tower E. It may be following this road along the south side.

Time: 1754 Plume has stabilized considerably over the last 5 minutes. It has a much smaller diameter as it approaches the hill and the loops are not nearly as great--they are almost gone near the release point.

Time: 1756 View from ERT Base: plume has a puffy appearance and is broken up somewhat.

These comments indicate that the plume went up and over the hill for much of the hour, apparently favoring the saddle area over the first half hour, and the south peak at times during the second half hour. The trajectory brought the plume up and over the hill, rather than directly into the hill, and little smoke odor was reported. A strong depression was reported in the lee of the hill, however. These features of the plume trajectory are consistent with weakly stratified flow (i.e., a hill Froude number of order 1).

Photographs of the plume document the described plume features on the upwind side of the hill. Four photos reproduced in Figure 82 show the plume trajectory at two times during the hour. One view is from behind the release crane at camera position B-1 (see Figure 46), and the other view is from a point off to the side of the plume trajectory, at camera position 0-3. Each individual photo is an automatic exposure, so it provides nearly instantaneous views of the plume rather than 5- or 10-minute averages.

The photos show that the plume trajectory was fairly steady over the hour and that the vertical dispersion was very large. During the first 5-minute period, the plume traveled toward the north peak. Over the next 15 minutes, however, it appears to have ridden steadily over the saddle between the two peaks. The lift in the plume as shown in the view from the side is quite significant, although the plume spread in the vertical appears great enough to have brought the visible plume material quite near the surface.

The plume tended to wander from the saddle toward the south peak over the next 15 minutes (periods 5-7) with little change in either plume spread

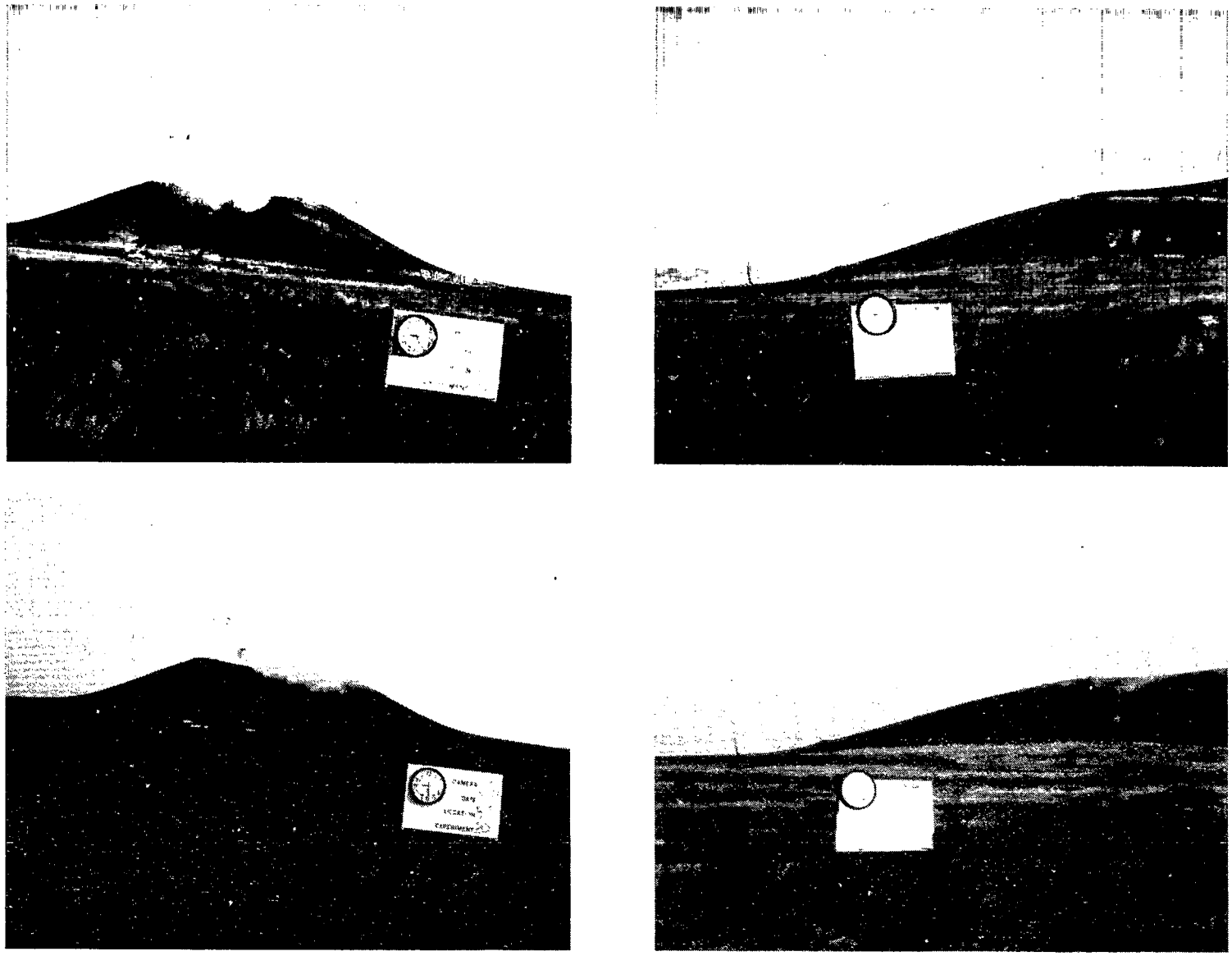

Figure 82. Two views of the plume trajectory at 1715 and 1746 MST taken from behind the release (position B-1) and taken off to the side of the release (position 3) during Experiment 209, Hour 1.

or plume lift. But during the remaining 20 minutes in the hour, the plume traveled preferentially over or around the south side of the hill. Some plume depression in the lee of the hill can be seen in period 10 (see Figure 82) as the plume hooked over the south peak. The scale of the vertical plume spread can be seen to decrease from period 9 to period 12.

Lidar data for this hour are quite extensive and permit quantification of the plume behavior noted above. The plume was sampled by the lidar along eight planes. Three of the planes were upwind of the hill, three were substantially over the hill, and two were in the lee. Plume centroid positions along these planes are plotted in Figure 83.

Centroid positions indicate that the plume trajectory was initially oriented toward the north side of the hill in period 2, but quickly shifted to the center of the hill through period 6. Later in the hour, the trajectory is seen to shift more toward the south peak. Estimates of the wind direction at source height, derived from the lidar data upwind of the hill, vary from 317° early in the hour to 323° in period 6, and then to as much as 330° later in the hour. Because the source is located at 316°, all but the earliest trajectories favor the south peak.

Meteorological Information

Wind and temperature data measured at tower A during this hour were used to characterize the flow in terms of H_c. The average of the 5-minute values over the hour is 5 m, and the average Fr_H above 5 m is 3.1. Because H_c was so low compared to the 40 m height of release, H_c should have had little impact on the SF_6 concentrations. Fr_L for the layer above H_c is 0.78, indicating that the stratification may have produced some streamline depression in the lee.

Figure 84 contains a time series plot of the calculated 5-minute H_c and Fr_H values for this experiment. H_c rises from a low of zero to about 9 m halfway through the hour and remains there for the rest of the hour. Fr_H is very large at the start of the hour but falls to 2.5 halfway through the hour. As the hour ends, Fr_H is as low as 2.3. Because H_c and Fr_H changed during the hour, the plume trajectory may not conform to that expected from average values of the Froude number. For example, Fr_L late in the hour is about 0.58, and more significant streamline depression in the lee would be expected in conjunction with this value. The observer log contains a reference to a pronounced depression in the lee at 1721, but it is unclear if such a depression might have occurred earlier or intensified later.

Hourly averaged wind speeds at 10 m and 40 m on tower A are 3.3 and 4.3 m/s, respectively. The 10 m winds were from 304°, and those at 40 m were from 311°. Wind shear (both speed and direction) was therefore small between the plume elevation and 10 m. Figure 85 shows the trend in wind speeds over the hour. Winds at all three levels from 10 m to 80 m were within 2 m/s of one another and were virtually constant over the hour. Therefore, the hourly average wind values are representative of the entire hour.

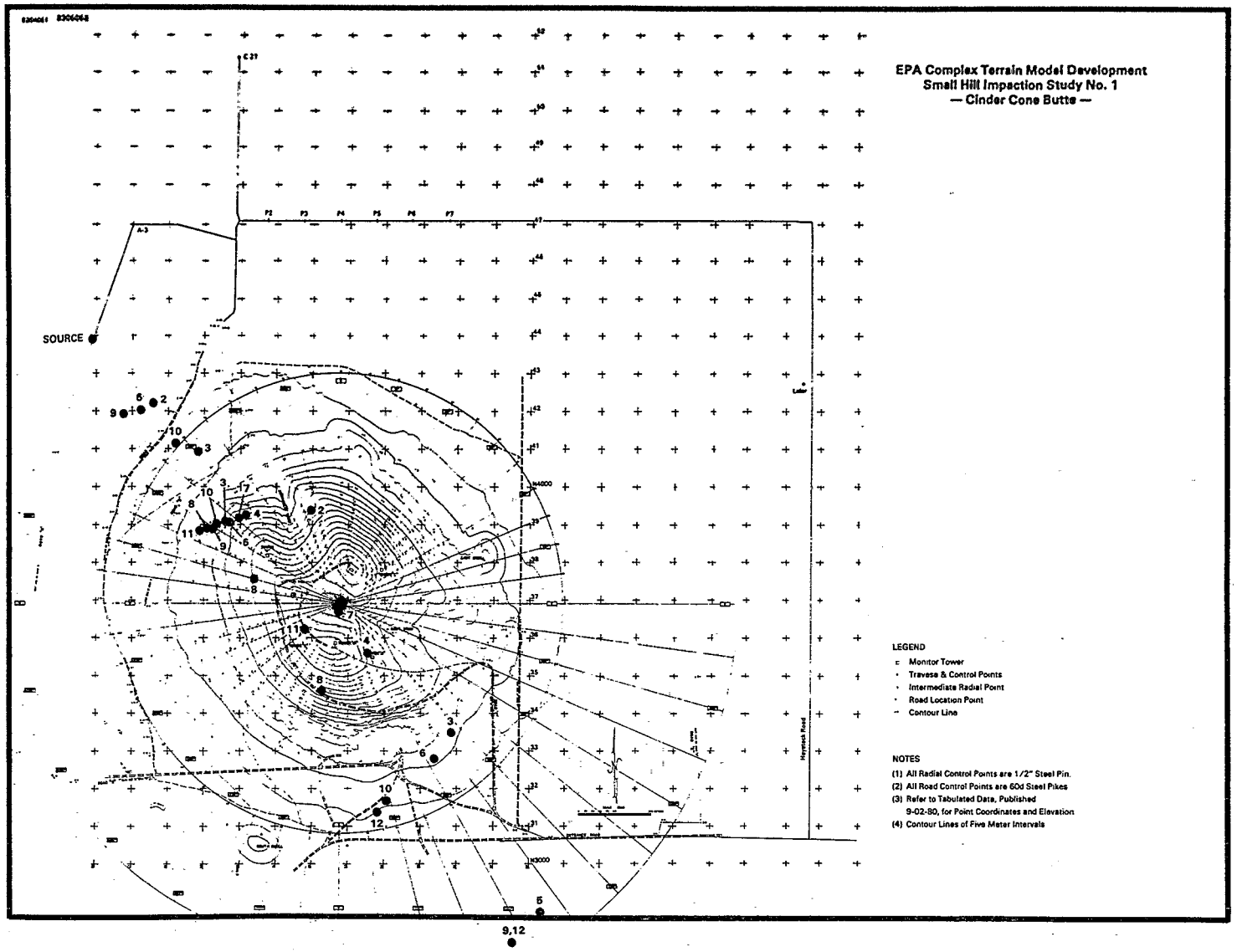

Figure 83. Plume centroid positions calculated from lidar data. Experiment 209, Hour 1 (1700-1800 MST).

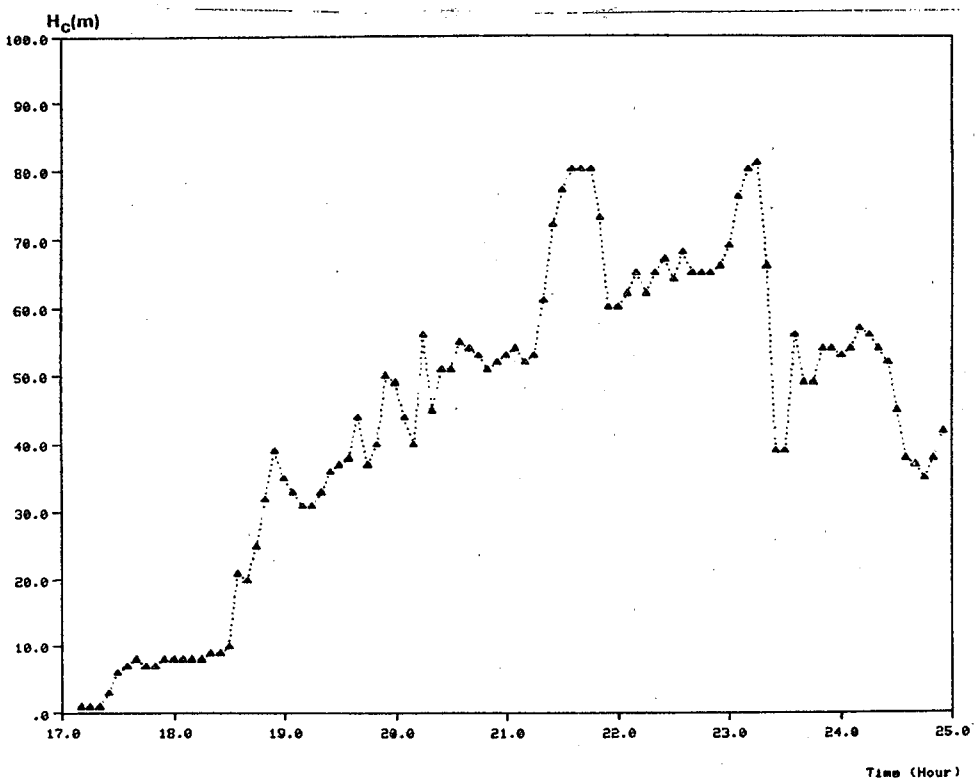

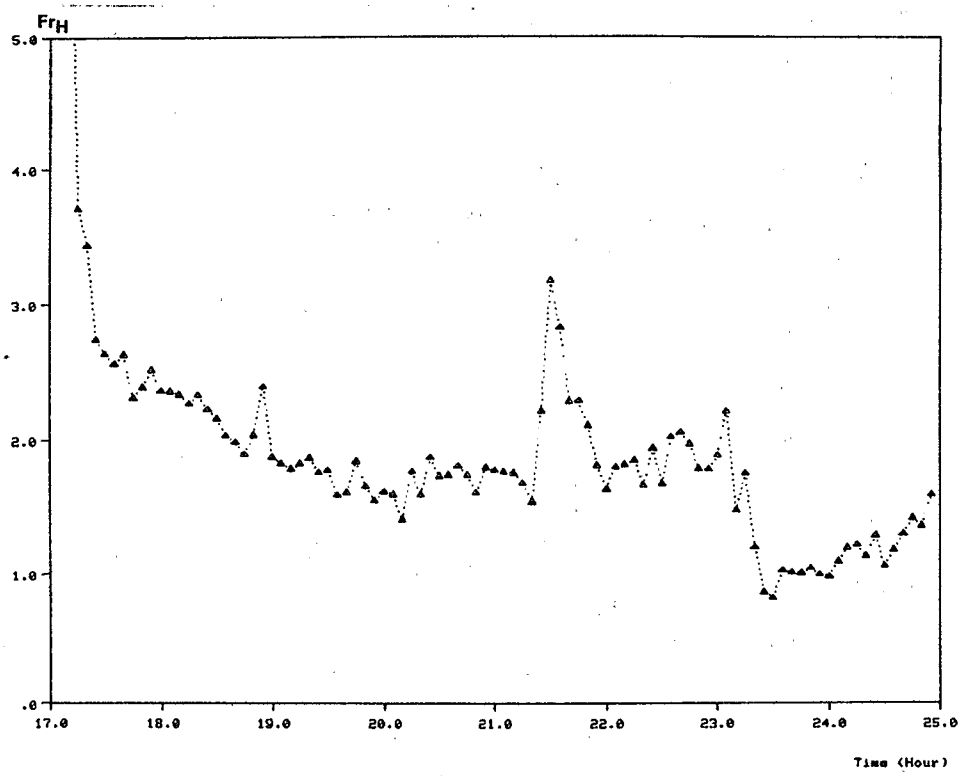

Figure 84. Calculated dividing streamline heights (H_C) and bulk hill Froude numbers above H_C (Fr_H) for Experiment 209.

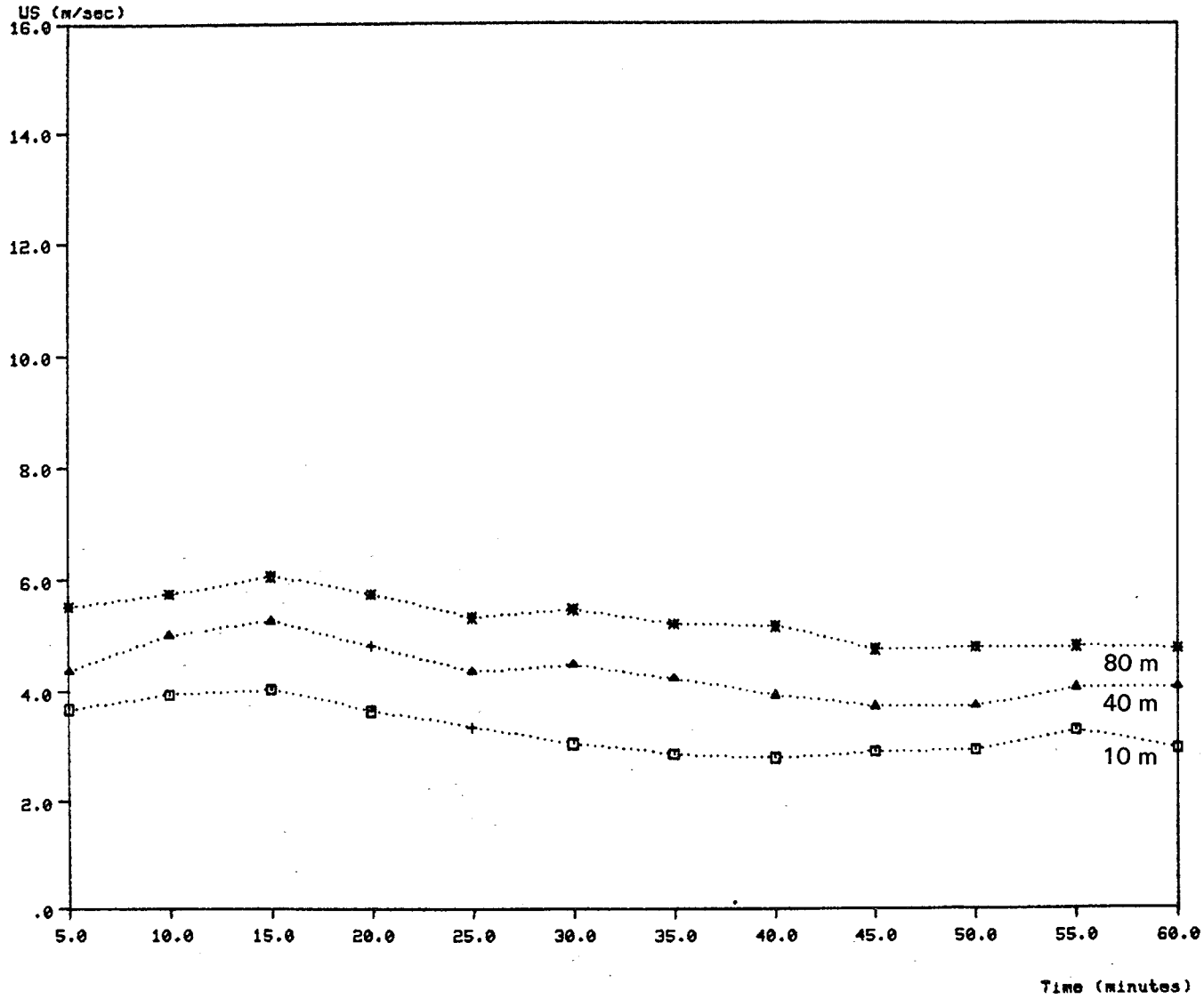

Figure 85. Tower A wind speeds during Experiment 209, Hour 1 (1700-1800 MST).

Variations in wind directions measured at 10 m and 40 m are shown in Figure 86 as frequency distributions. The 10 m wind directions were a little more variable than those at plume elevation primarily because of a shift toward 300° not seen at 40 m. However, the flow structure during this hour was not as complex as many other hours under study.

In summary, this hour may be characterized as nearly neutral with steady winds and little wind directional shear. The major complicating factor is the strengthening of the near-surface temperature gradient with time. On balance, the meteorology indicates that the plume should have traveled freely over the hill, much like plumes in a weakly stratified tow-tank experiment ($Fr_H \sim 1$).

SF_6 Concentrations

The distribution of hourly averaged SF_6 concentrations over the surface of the hill is shown in Figure 87. All concentrations are remarkably low, especially in view of the increased SF_6 emission rate begun in Experiment 209. Concentrations were measured on the windward side of the hill all the way up to the 60 m contour. Low concentrations were measured at lower elevations on either side of the hill and over the crest of the hill. The highest concentration is found near the base of the southeast draw in the lee of the hill.

This pattern is consistent with observations that the plume rose quite high over the hill and then descended in the lee. It is surprising, however, that the vertical mixing evident in the photos produced such small SF_6 concentrations at the surface.

The 10-minute average SF_6 concentration distributions are presented in Figure 88. They also show the lack of even moderate SF_6 concentrations on the windward site of the hill. Unfortunately, no 10-minute samplers were placed in the lee toward the base of the hill to document the time evolution of the higher concentrations during this hour.

4.9.2 Model Performance

This hour was modeled with the Lift model because all evidence indicates that the flow was nearly neutral (unstratified) and very steady. Meteorology for the release was prepared as in Section 4.1.2, except that no height interpolations were needed because the plume was released at 40 m, an instrumented level on Tower A. The data are summarized in Table 12.

The 1-hour average wind direction at the release height is 311°. However, the lidar and photographic data strongly suggest that the mean wind direction should be about 319°. Both the 10 m and 30 m levels on tower B recorded mean winds of 324°. Therefore, a mean direction of 319° is used in the modeling along with the PDF computed with the 40 m wind direction.

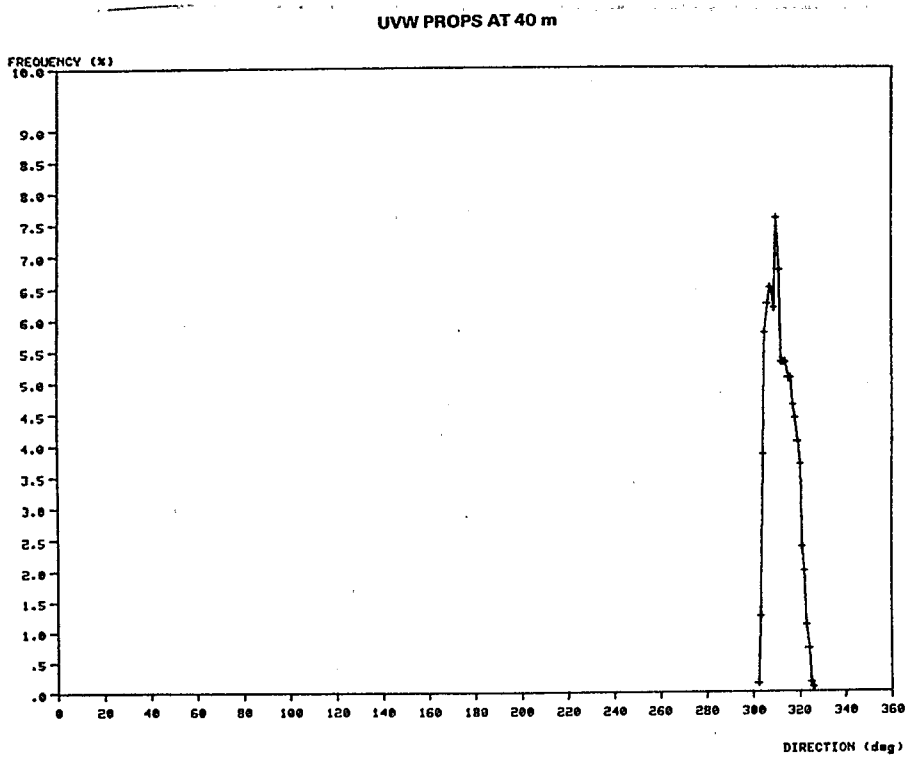

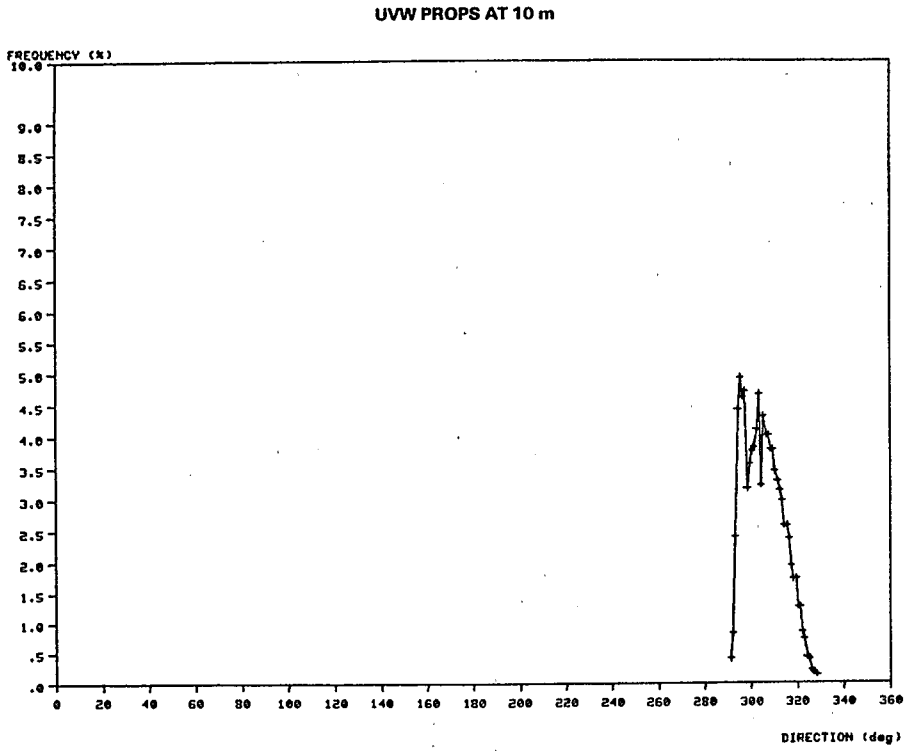

Figure 86. Calculated wind direction distribution functions for Experiment 209, Hour 1 (1700-1800 MST).

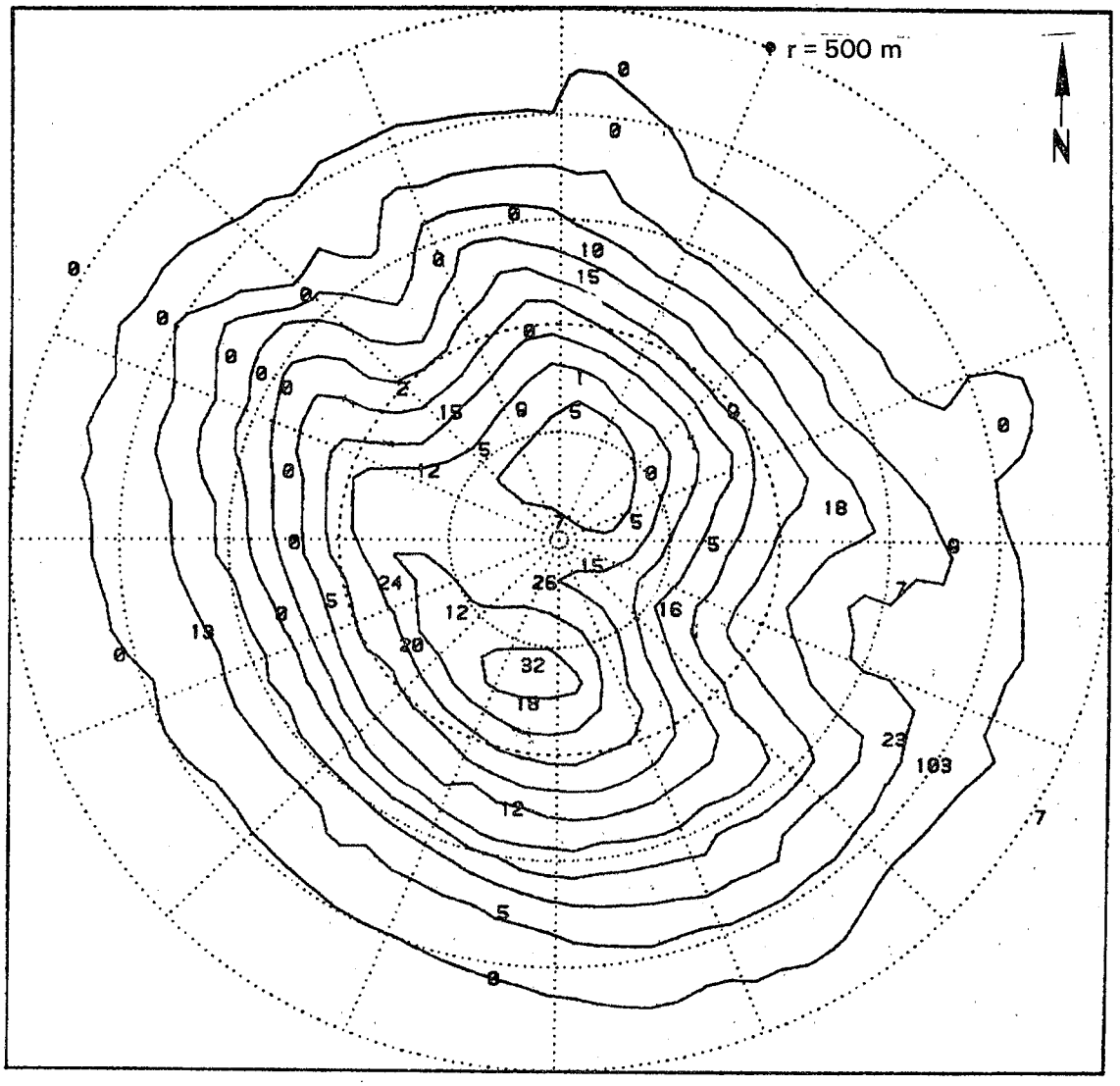

Figure 87. Observed SF_6 concentrations (ppt) for Experiment 209, Hour 1 (1700-1800 MST). Source: r = 986.1 m, θ = 315.9°, net height = 33 m, Q = .156 g/s.

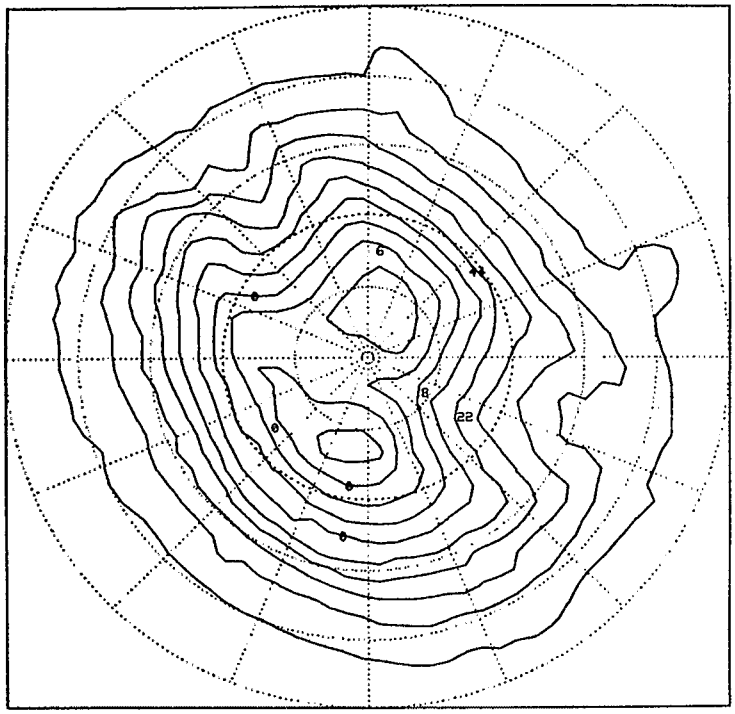

TIME PERIOD 1700-1710

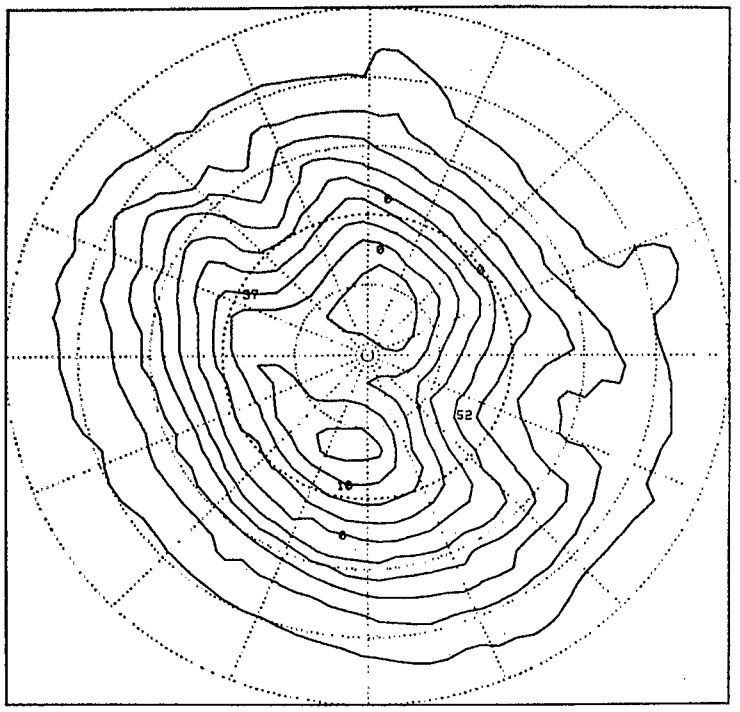

TIME PERIOD 1710-1720

Figure 88. Observed 10-minute average SF_6 concentrations (ppt) for Experiment 209, Hour 1 (1700-1800 MST).

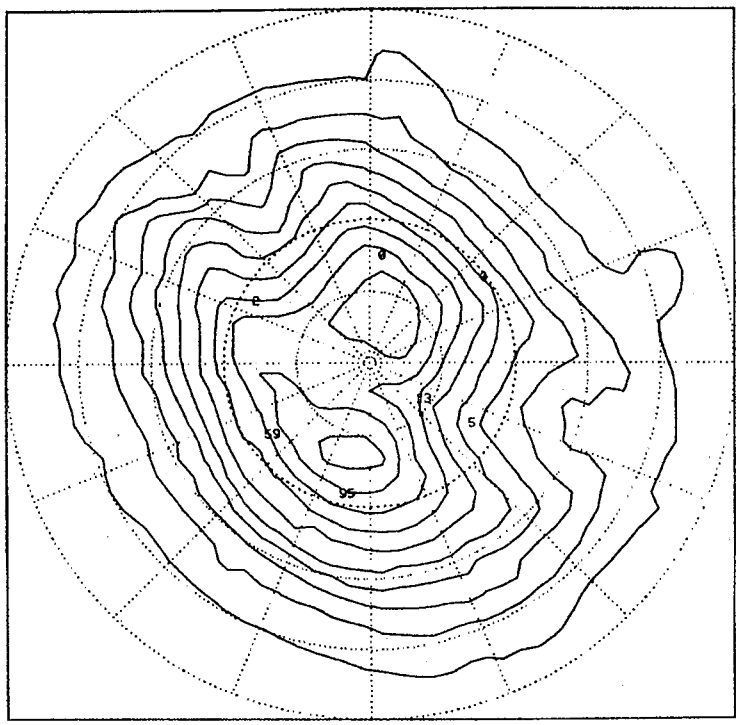

TIME PERIOD 1720-1730

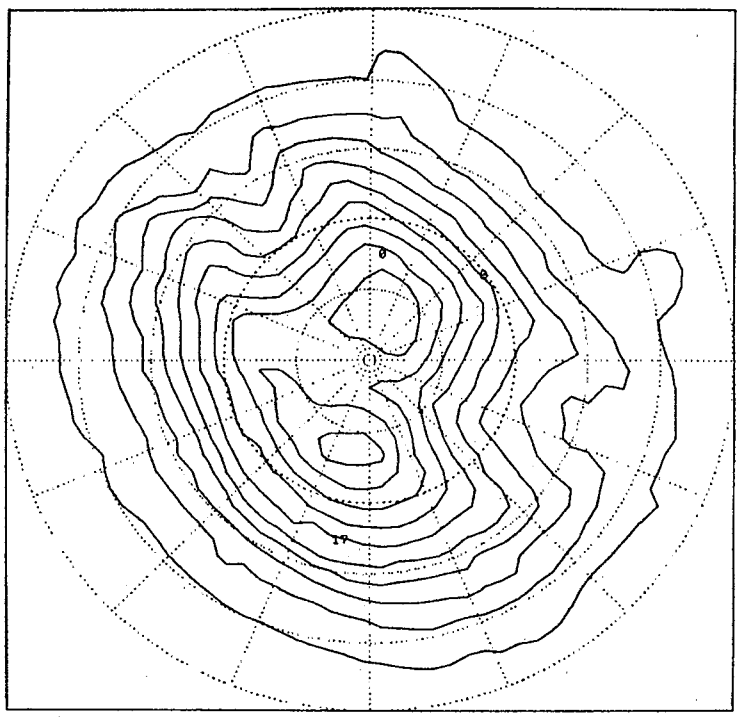

TIME PERIOD 1730-1740

Figure 88. Continued.

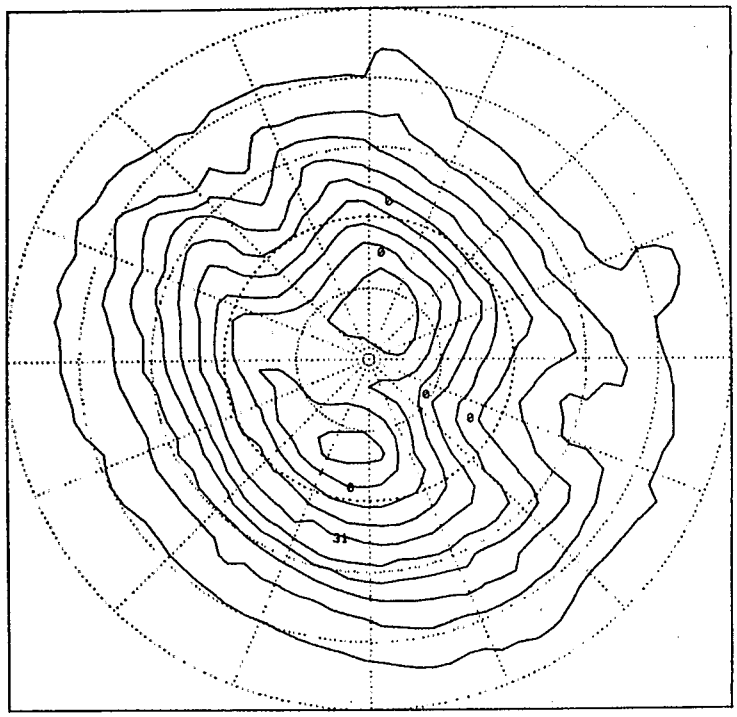

TIME PERIOD 1740-1750

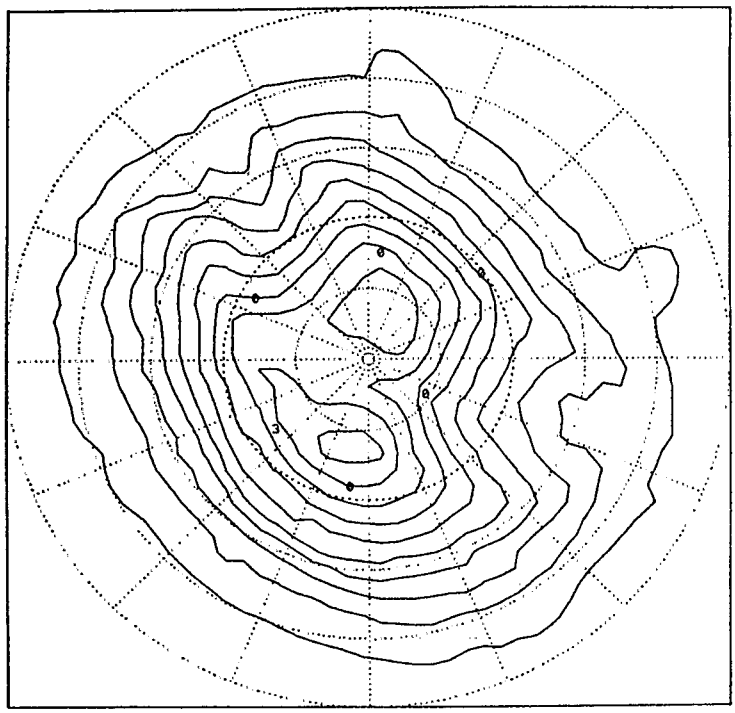

TIME PERIOD 1750-1800

Figure 88. Continued.

TABLE 12. NEUTRAL AND LIFT MODEL CALCULATIONS - EXPERIMENT 209, CASE HOUR 1

Meteorological Data

wind direction(deg)	=	319.
wind speed(m/s)	=	4.3
critical dividing streamline height(m)	=	5.0
Iz	=	.053
Iy	=	.093
N(1/s)	=	.018

Source Data

direction(deg)	=	316.
distance(m)	=	986.1
release height(m)	=	40.0
SF6 emission rate(g/s)	=	.156

Receptor Coordinates X(m)	Y(m)	Z(m)	Observed SF6 (ppt)	Neutral Predicted SF6 (ppt)	Lift Predicted SF6 (ppt)
360.22	.00	13.26	8.70	4.95	.00
142.00	.00	50.00	4.90	169.28	173.68
257.78	33.94	30.00	17.80	14.03	.00
72.15	19.88	80.00	4.90	313.81	272.88
404.91	111.59	10.00	.10	.11	.00
159.04	122.04	46.91	8.82	26.63	.00
85.15	64.88	80.00	.00	253.86	60.16
58.64	445.44	3.38	.00	.00	.00
51.04	387.66	11.78	.00	.00	.00
35.92	272.83	31.92	10.30	1.43	.00
32.61	247.73	41.74	14.50	6.02	.00
20.07	152.45	81.06	.98	235.54	8.12
15.97	121.29	90.94	5.00	302.00	63.69
2.15	18.88	80.00	6.50	407.88	313.65
-53.69	-407.79	3.82	.00	24.33	43.36
-45.46	-345.28	13.70	4.90	56.02	81.07
-15.01	-113.99	98.96	32.00	444.90	244.56
-23.49	-178.46	80.00	20.98	424.95	225.61
-19.85	-149.12	90.00	17.50	439.41	228.99
-4.85	-37.12	80.00	26.00	443.58	361.41
-84.85	-65.12	90.00	11.70	504.21	246.26
-396.68	-106.29	3.44	.00	.05	.00
-315.76	-84.61	13.24	12.50	3.97	.00
-248.96	-66.71	32.90	.00	49.00	37.45
-204.16	-54.70	52.26	4.90	308.73	121.05
-144.85	-38.12	80.00	23.60	542.60	233.87
-238.00	.00	50.00	.00	316.79	125.33
355.15	-205.04	5.69	102.70	82.95	140.43
313.62	-181.07	15.29	22.70	105.67	217.98
108.15	-61.12	50.00	16.30	301.06	289.44
37.15	-21.12	70.00	14.50	385.44	302.71
312.38	-41.13	14.00	6.90	20.97	.00
-243.41	65.22	50.00	.00	489.42	239.47
-441.92	255.14	-.90	.00	25.80	7.80
-359.96	207.82	8.94	.00	183.48	199.26
-297.11	171.54	28.07	.00	459.36	255.58
-269.62	155.66	38.07	.10	590.72	279.47
-246.20	142.14	47.96	.00	714.79	278.81
-111.85	65.88	80.00	11.70	550.56	353.48
-141.42	141.42	50.00	2.20	572.33	333.54
-229.81	229.81	30.00	.20	655.20	340.19
-91.99	119.88	64.94	14.60	467.78	339.87
-65.85	85.88	80.00	5.20	459.41	332.41
-109.07	263.31	30.00	.00	65.22	.00
-32.85	122.88	80.00	8.50	356.81	299.27
-40.46	307.35	30.00	.10	2.66	.00
-25.71	195.51	65.00	.10	184.04	.00

Neutral was rerun with the revised meteorological data. Instead of estimating a peak value that is 883% of the observed peak concentration, it produced a value 695% of the observed peak. Obviously, the model is bringing too much plume material to the surface, especially when the high modeled concentrations occur on the windward face of the hill where observed concentrations are nearly zero. Figure 89 shows the distribution of calculated concentrations plotted on a map of CCB, and the results are also summarized in Table 12.

Results from Lift computations are also displayed in Figure 89 and in Table 12. These concentrations are not quite as large as those from Neutral, but the peak modeled concentration is still 350% of the peak observed concentration. Both models produce σ_z values of 20 m to 30 m, and these are large enough to account for the substantial SF_6 impact on the hill according to the models.

The observations, however, tell a very different story. When terrain factors are computed from the observed concentration field and the output of the Lift model, T_o values are consistently near 2.0, which implies that the σ_z values are too large by approximately a factor of 2. Possible causes for the discrepancy between modeled and observed concentrations are being investigated.

4.10 Experiment 209, Hour 7 (2300-0000 MST)

4.10.1 Summary Description

SF_6 tracer gas was released from the east-southeast side of the hill at 999.2 m, 100.9° for the entire hour. The release height was 40 m. Because the SF_6 was not interrupted from the previous hour and continued through the end of the hour, the sampling data should represent the full hour. Oil-fog at 40 m was provided by the jet fogger from 2300 until 2329, so the visual plume was only operational for half the hour. A secondary oil-fog plume from the thermofogger was released at 30 m from a point on the northwest side of the hill (∿1155 m, 331°) between 2300 and 2340.

Local terrain elevations near the tracer release point are estimated to be -4.7 m relative to the zero of the hill coordinate system; the net release height corresponded to the 35.3 m height level on the hill. The SF_6 release rate is computed to be 0.160 g/s with an estimated uncertainty of ±1.5%. No Freon was released.

Plume Observations

During the experiment several people recorded their observations about the appearance and trajectory of the oil-fog plume. Comments applicable to this hour are presented below. Note that the comments actually begin during the preceding hour. These are included because the plume material released during the previous hour had an important impact during this hour.

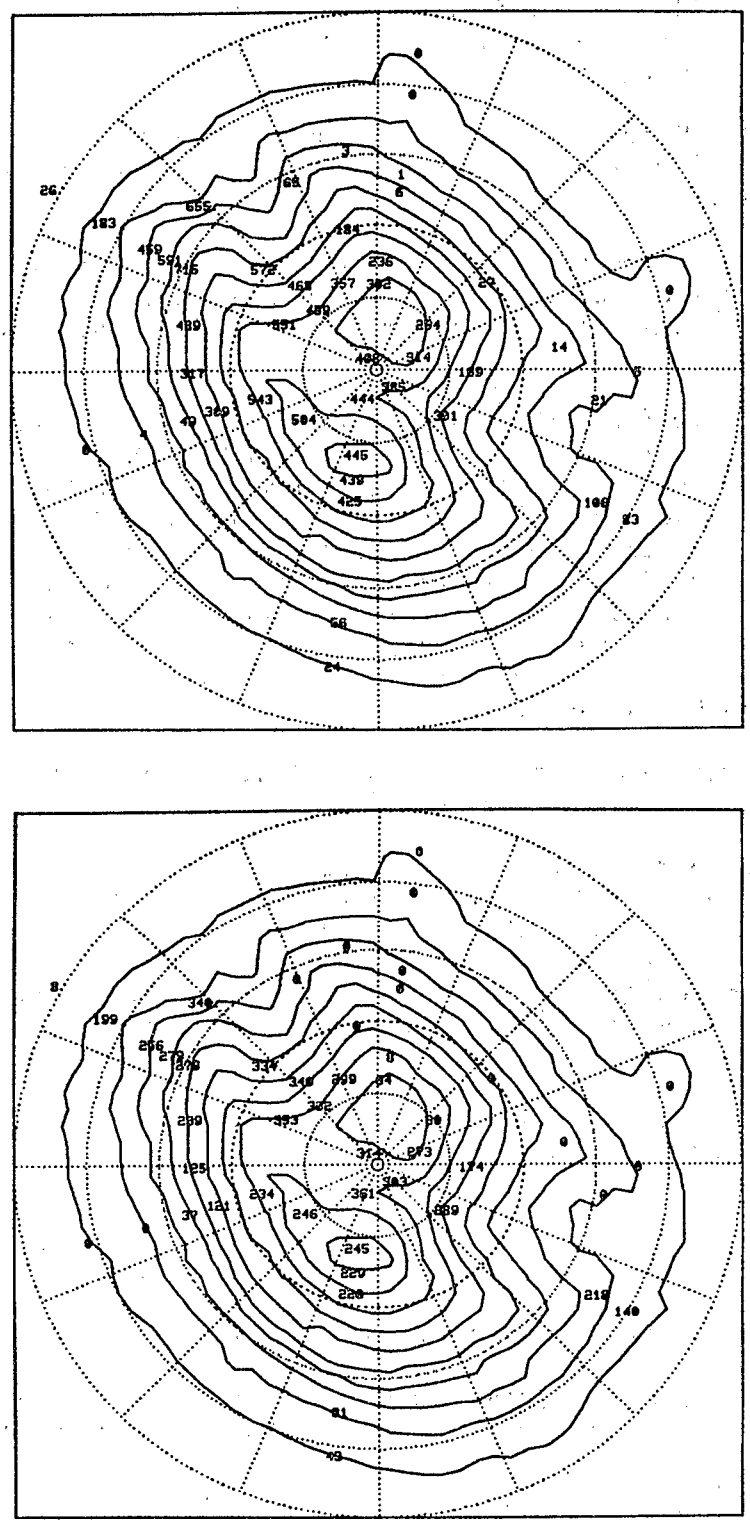

Figure 89. SF_6 concentrations (ppt) estimated for Experiment 209, Hour 1 by the Neutral (top) and Lift (bottom) models.

Time: 2235(?) Plume is heading a little more toward the hill, but it is hard to tell because the winds are so light that the fog is just pooling near the source.

Time: 2252 NAWC2 is at a point one-quarter mile south of the 150 m tower, and he is releasing a second thermofogger from 30 meters, and it is going to the west.

Time: 2255 The plume is still pooling a lot around the release area. A lot of fingers are extending in different directions. I still haven't seen a finger coming past road F. In fact, none of them have made it halfway to road F.

Time: 2304 There are several interesting things going on. One is that the release from E1 is just smearing back and forth, very very wide--a principal blob looks like it is headed toward the northeast knoll, and at this time is just beginning to get close to road F. It may even be over me now. In fact, yes, it is. The auxiliary release which is a quarter mile south of tower A (the release from the auxiliary crane) is traveling to the west under easterly flow and is relatively coherent, not showing the extreme meandering that we are seeing here. Winds at second release holding steady to the west. Tethersonde reports winds of about 2 m/s to the west.

Time: 2306 From road F, plume is about 1 hill width wide, and appears to be drifting toward north butte.

Time: 2309 From ERT base, the fog pool looks like it extends everywhere between the trailer and the hill. Second plume still heading out to the west with some meander.

Time: 2315 Smoke odor is reported at the sampler trailer. The fog is slowly traveling up the draw. Plume cloud looks like it is covering everything.

Time: 2320(?) Winds are shifting more to the north now at the second release. Fog from jet-fogger is cut down. No shift is seen at the tracer crane.

Time: 2327 I have had the rotating beacon going for about three minutes at about road F where radial 27 crosses road F.

Time: 2328 Butte is surrounded by smoke in all directions.

Time: 2329 Smoke has stopped. The jet fogger is out of oil. SF_6 is continuing. NAWC2 reports seeing plume smeared all over on all sides of the hill.

Time: 2330 I can smell the oil fog faintly on top of the hill. There is oil fog everywhere, particularly smeared now to the north, but it has also been visible on both sides of the hill according to other reports. It looks to me like it is at least two hill widths to the north, flying in very flat sheets although there is some definite vertical depth to it of maybe 10 to 15 meters. I feel like it would be terribly complicated in the analysis to cope with any kind of height change or break in the plume because it is smearing so widely so we are leaving the tracer up at 40 meters, and we are going to try to bring the thermofogger over and put it up near it at 30 meters.

These comments indicate that the concentrations measured on the hill from 2300 to 0000 may have been produced in part by plume material that had been spread out very widely in the horizontal to the south of the hill and then slowly advected toward the hill; for this hour, words like "blob" and "cloud" better describe the tracer material than does the word "plume."

A secondary plume released to the north of the hill was observed to travel toward the west during the same time period. It did not stagnate near the release, nor did it take on the appearance of a blob or cloud. Because the behavior of these two plumes is so different, it is unlikely that the meteorological data measured at tower A (also to the north of the hill) is representative of the meteorology at the primary release crane.

Photographs of the primary plume show its extraordinary behavior during the first half hour. Figure 90 contains two representative photos of the plume; the first was taken from the top of the north peak at camera position 0-15 (see Figure 46), and the second was taken from a position slightly behind the release at camera position 0-19. Each individual photo is a 5-minute time exposure.

The wide sheet of oil fog can be seen approaching the hill from the southeast during periods 2-5. This sheet apparently drifted past the hill by the sixth period, and the primary plume bent around to the north of the hill. The secondary plume cannot be seen in these photographs. No lidar data for this hour have yet been reduced.

Meteorological Information

Wind and temperature data measured at tower A during this hour were used to characterize the flow in terms of H_c. The average of the 5-minute values over the hour is 58 m, and the average Fr_H above H_c is 1.2. The Fr_L value corresponding to this bulk hill Froude number is 0.20. These values indicate that the flow during this hour was dominated by buoyancy effects. Streamlines above H_c should have exhibited lee wave behavior. Because the release height was 40 m, the plume was well below H_c and might be expected to have flowed around rather than over the hill.

Figure 84 contains a time series plot of the calculated 5-minute H_c and Fr_H values for this experiment. H_c rose from 75 m to 80 m during the first 15 minutes of the hour but then dropped rapidly during the next 10

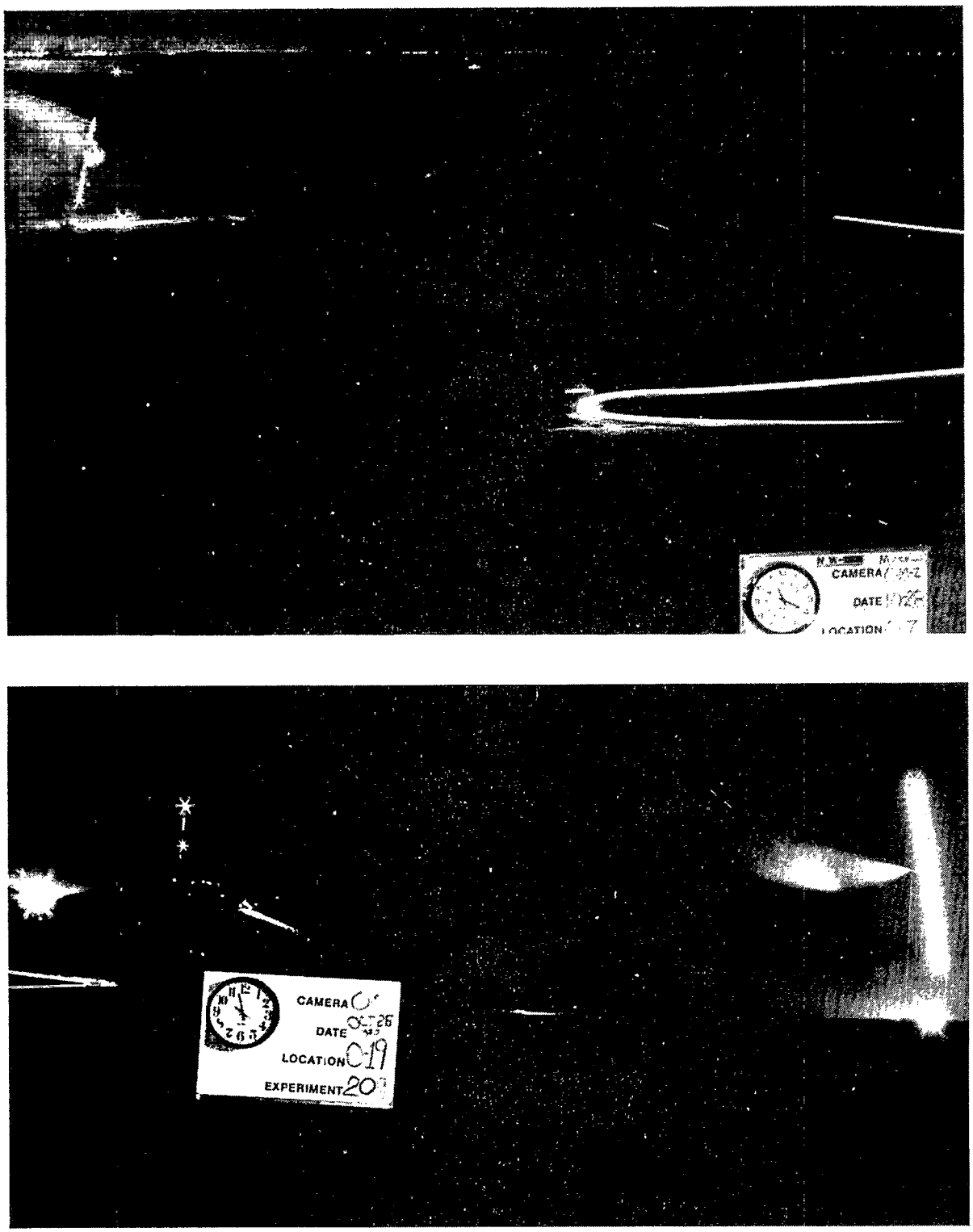

Figure 90. Two views of the plume trajectory between 2320 and 2325 MST taken from the top of the north peak (position 15) and taken from behind the release (position 19) during Experiment 209, Hour 7.

minutes to about 40 m. It held at 40 m for the next 5 minutes and then jumped to more than 55 m in the next 5 minutes. H_c remained between 50 m and 55 m for the remaining 25 minutes of the hour. Fr_H began the hour near 2.0 but dropped rapidly to less than 1.0 by half-past the hour and held near 1.0 for the remainder of the hour.

These large changes in H_c during the hour are interesting but may not be directly relevant to the tracer plume behavior. The observation logs indicate that a second oil-fog plume just north of the hill (approximately halfway to tower A) experienced a flow field that was totally different from that at the primary release site. At best, therefore, all we can learn from tower A is that the dramatic changes in the wind field were accompanied by similarly dramatic changes in the density structure.

The hourly averaged wind speed at 40 m on tower A was 2.5 m/s. During the previous hour, however, the average speed was only 0.6 m/s. Because the wind shift probably occurred at tower A before it occurred at the release site, the winds at the release early in the hour may have been close to 0.6 m/s. The mean wind direction at 40 m on tower A was 105°; once again, though, the wind direction during the previous hour was 045°, and this may be more indicative of average wind directions over the first part of the hour at the release point.

Figure 91 shows the trend in tower A wind speeds between 10 m and 80 m during the hour. Speeds at all levels are less than 3 m/s, and those at 40 m are slightly greater than those at either 10 m or 80 m. Variations in wind directions measured at 10 m and 40 m are displayed in Figure 92 as frequency distributions. It is not surprising that neither distribution satisfactorily summarizes the wind direction behavior seen at the primary release site. The 40 m distribution might be applicable to the release site once the wind shift had taken place.

In summary, winds appeared to be extremely light and variable at the release location during the hour, but the data from tower A indicate a steadier flow. H_c and Fr_H values during the hour indicate very stable flow conditions. Because tower A data is undoubtedly not representative of the flow at the release site early in the hour and because so much plume material from the previous hour could have been advected back over the hill, the measured concentration pattern may not be very useful for model development.

SF_6 Concentrations

The distribution of hourly averaged SF_6 concentrations over the surface of the hill is shown in Figure 93. The highest concentration measured is on the north face of the north peak near the 30 m height contour, the second highest is near the 75 m contour on the same hill face, and the third highest is located on the saddle point above the northwest draw. Most of the other nonzero concentrations were measured on the northwest side of the hill at contour elevations greater than 20 m. This is

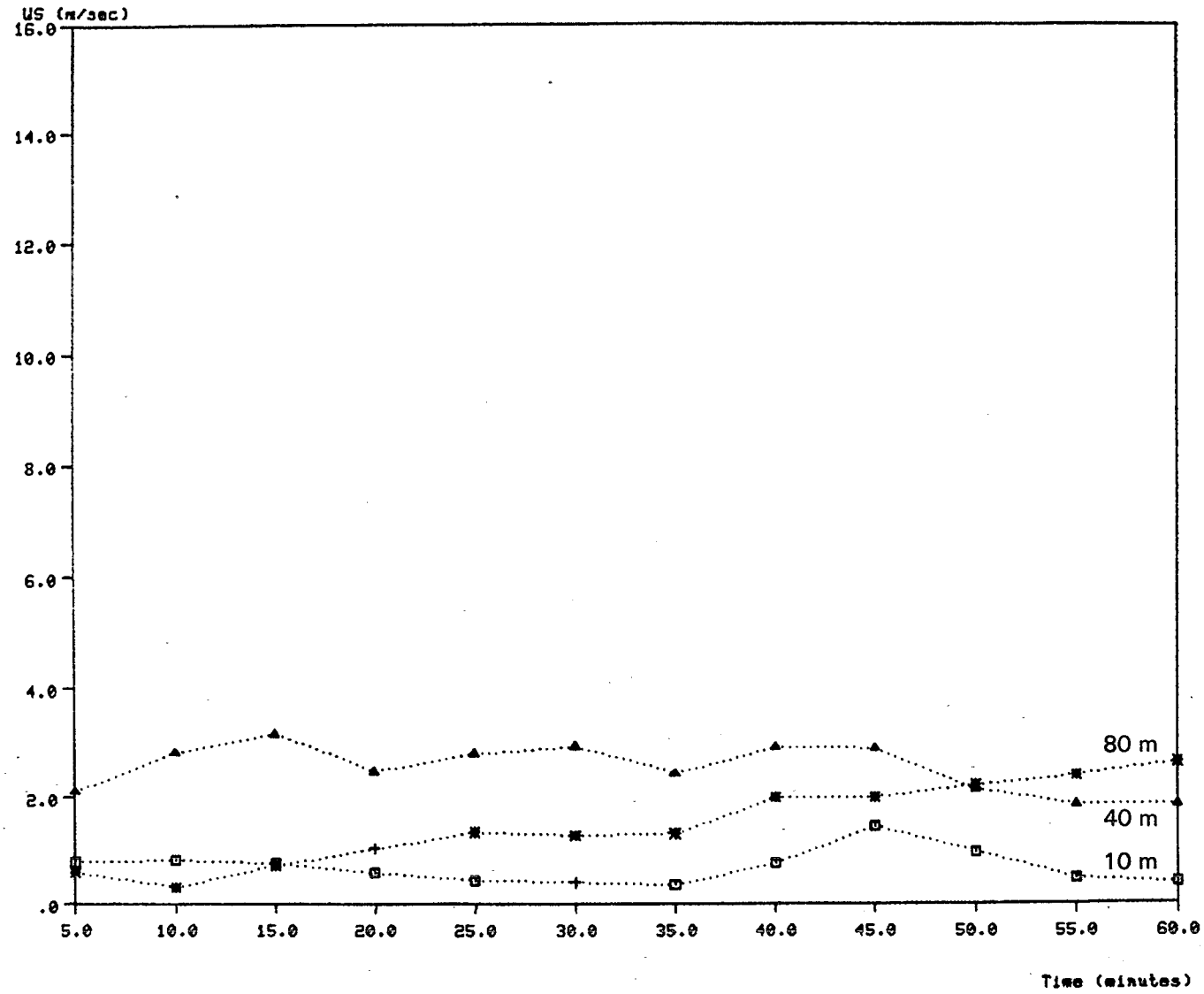

Figure 91. Tower A wind speeds during Experiment 209, Hour 7 (2300-0000 MST).

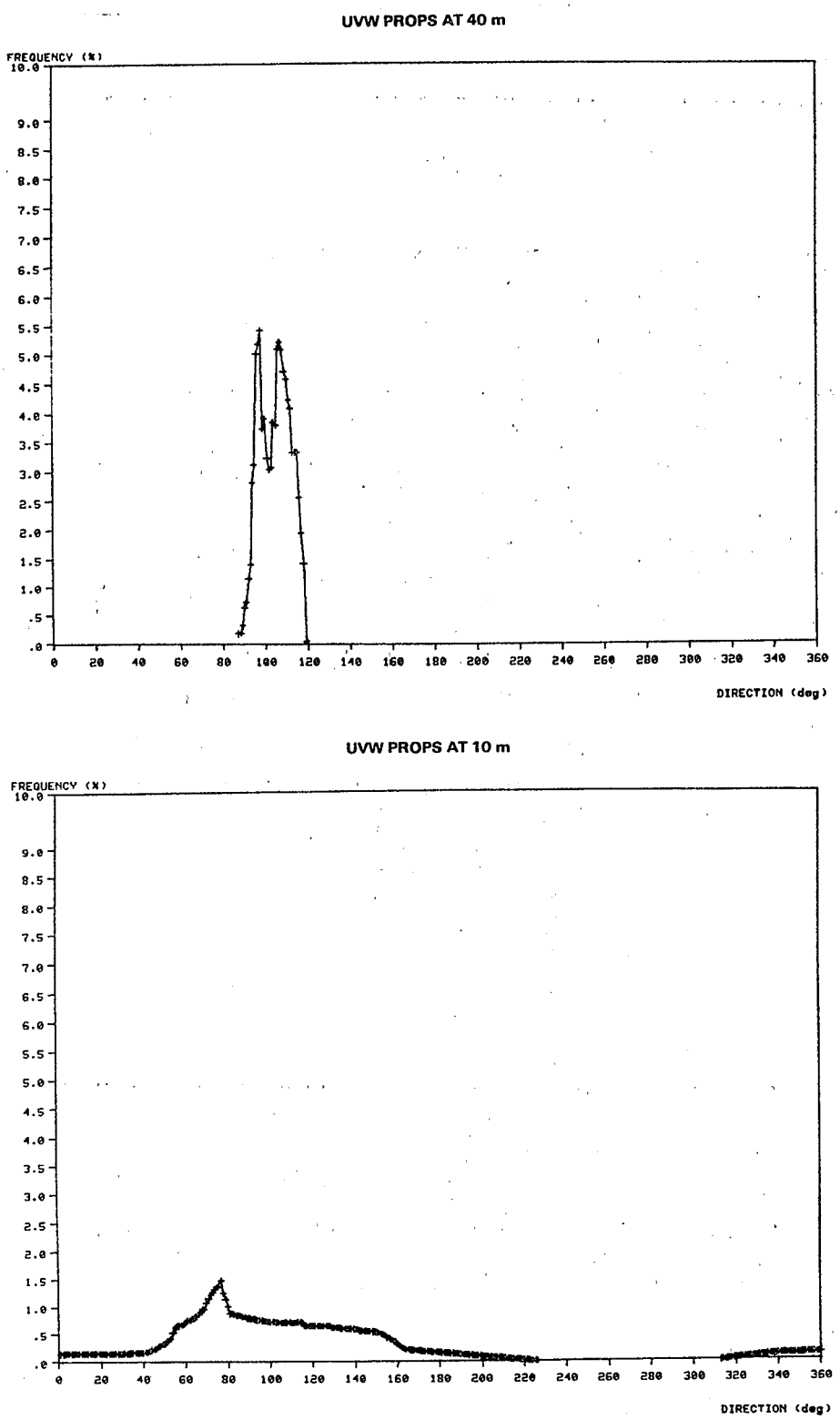

Figure 92. Calculated wind direction distribution functions for Experiment 209, Hour 7 (2300-0000 MST).

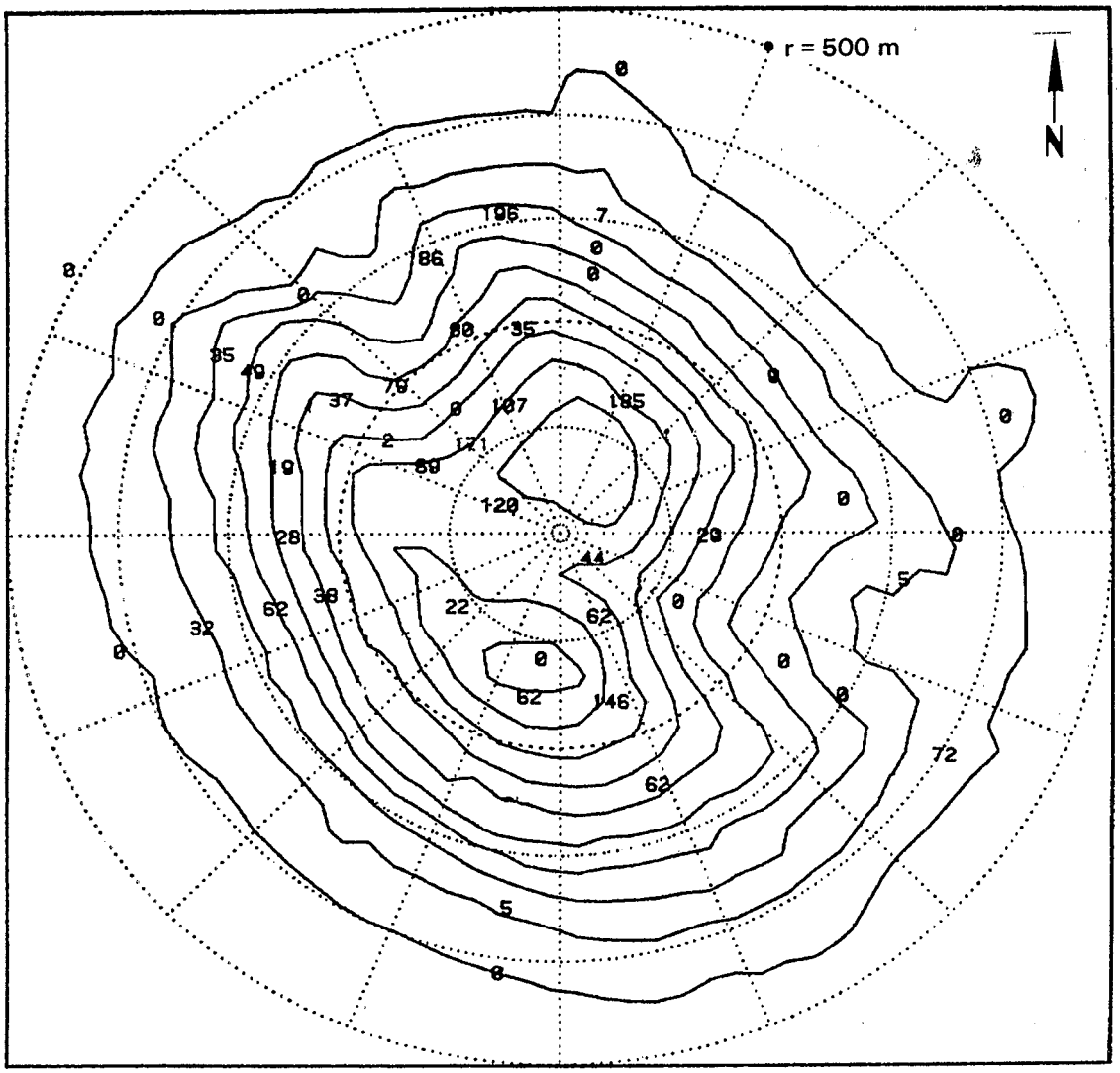

Figure 93. Observed SF_6 concentrations (ppt) for Experiment 209, Hour 7 (2300-0000 MST). Source: r = 999.2 m, θ = 100.9°, net height = 35.3 m, Q = .160 g/s.

surprising because the source was located to the southeast of the hill and most concentrations above 20 m on this side of the hill are zero. Perhaps the SF_6 measured in the lee of the hill circled round to the south of the hill and then shifted back across the southwest and west side of the hill amidst the changing wind directions.

This possibility is certainly suggested by the 10-minute average SF_6 concentration distributions presented in Figure 94. All concentrations on the hill were recorded during the half hour between 2310 and 2340, and a large concentration is seen on the south side of the hill in two out of the three 10-minute periods.

4.10.2 Model Performance

This hour is very difficult to model properly. Observed concentrations may have resulted from plume material released during the previous hour. Also, the meteorological data from tower A is not representative of conditions at the release point. Nonetheless, model calculations have been done to see what kind of correspondence between modeled and observed concentrations might be obtained. The Wrap and Impingement models were run because the release was substantially below H_c.

All meteorological data were prepared as in Section 4.1.2, except that no interpolation to source height was needed because the plume was released from 40 m, an instrumented height on Tower A. The resulting values are summarized in Table 13. Because of the large uncertainty in the winds at release height, the average 40 m wind direction (105°) was used in the modeling directly. Note, however, that tower B winds were from 160° and 188° at 10 m and 30 m, respectively.

Both Impingement and Wrap were run with the revised meteorological data; the results are listed in Table 13, and plotted on a map of CCB in Figure 95.

Although the release height of 40 m was well below H_c (58 m), some of the highest observed concentrations (ranging from 120 ppt to 185 ppt) occurred near the top of the hill at 80 m. This pattern cannot be reproduced by the models. The highest observed concentration of 196 ppt does, however, occur close to the release height. This value should be compared with the highest Wrap estimate of 174 ppt at 42 m. The estimates from Impingement are generally much higher than the observations, probably a result of the overestimation of the probability of the wind direction along the stagnation streamline. In any case, the apparent agreement in peak modeled (Wrap) and observed concentrations is probably accidental.

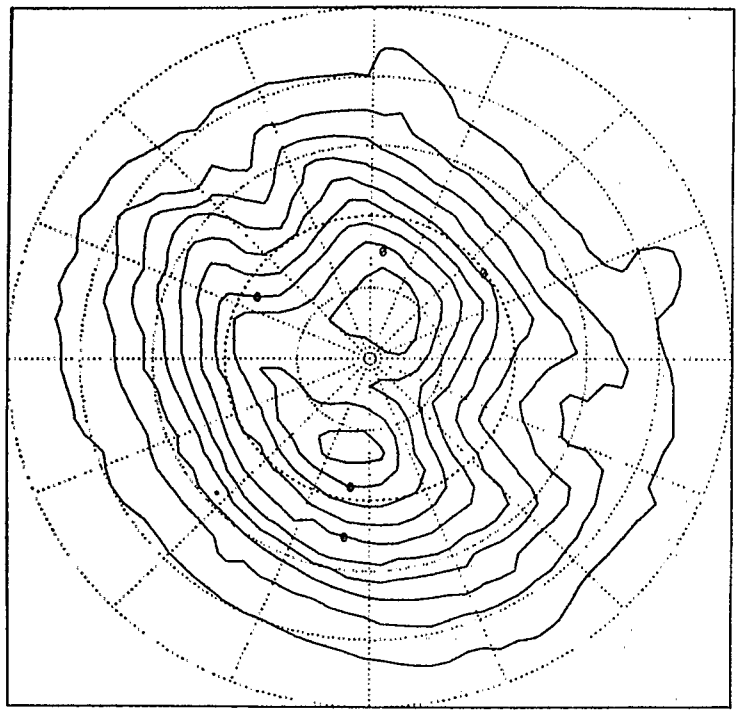

TIME PERIOD 2300-2310

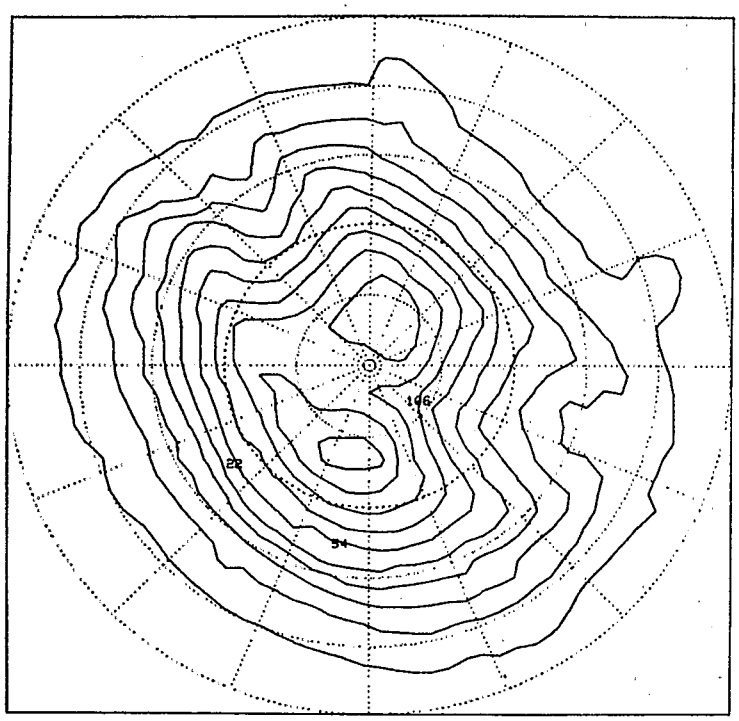

TIME PERIOD 2310-2320

Figure 94. Observed 10-minute average SF_6 concentrations (ppt) for Experiment 209, Hour 7 (2300-0000 MST).

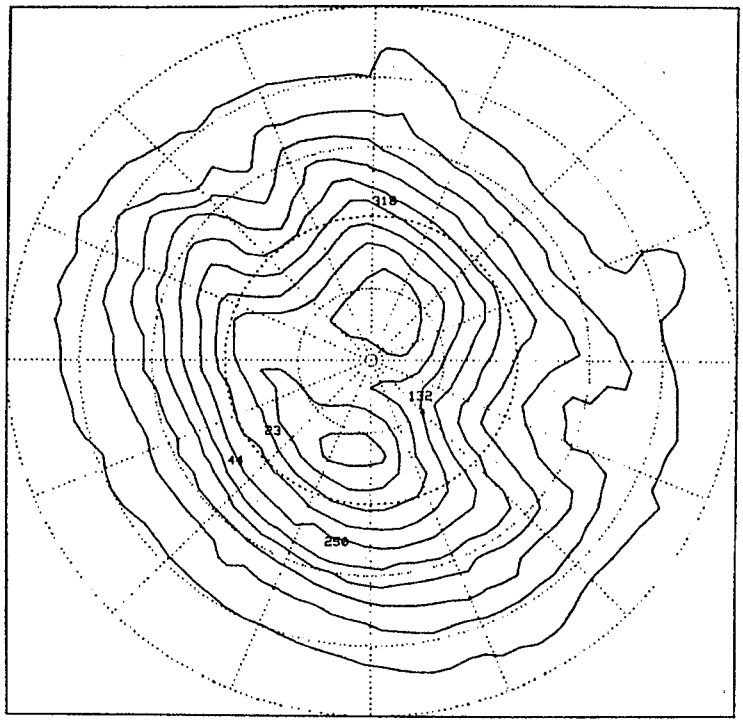

TIME PERIOD 2320-2330

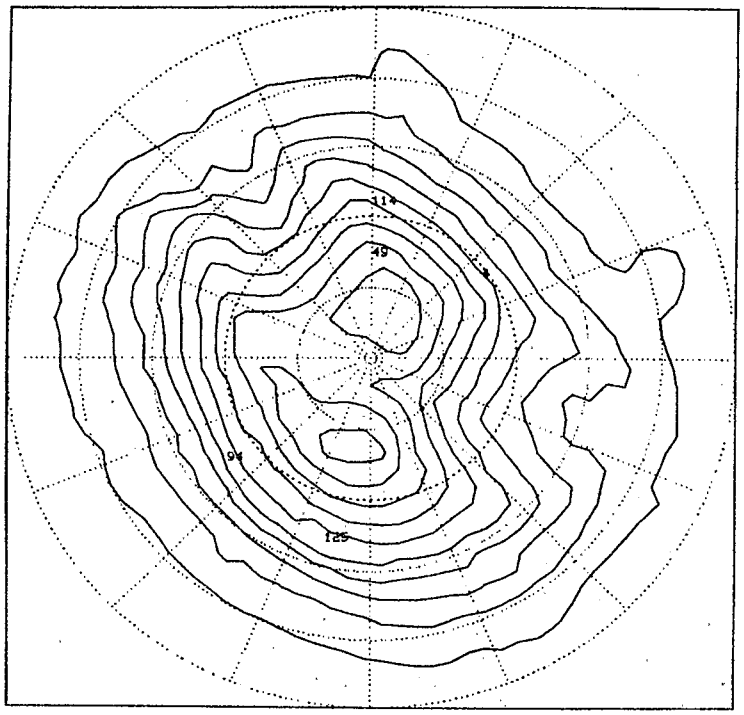

TIME PERIOD 2330-2340

Figure 94. Continued.

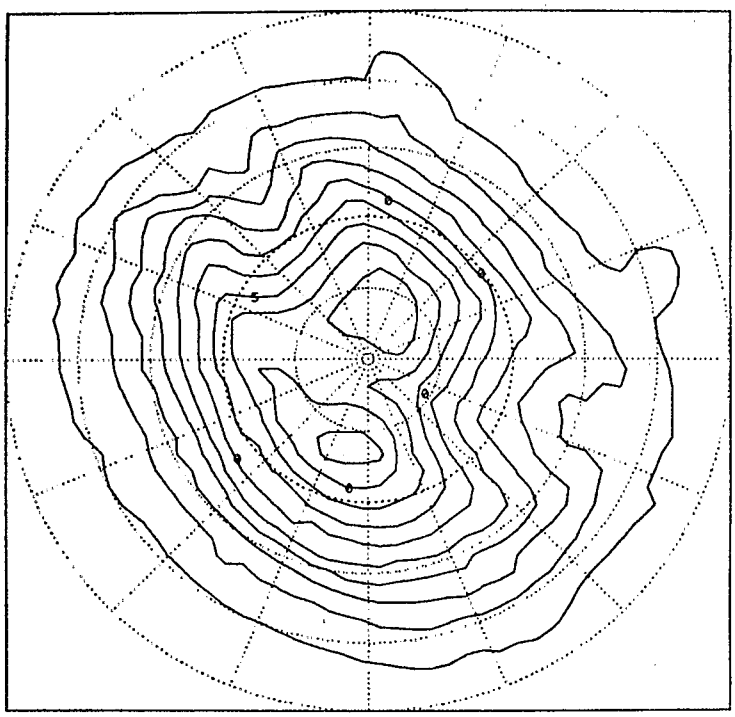

TIME PERIOD 2340-2350

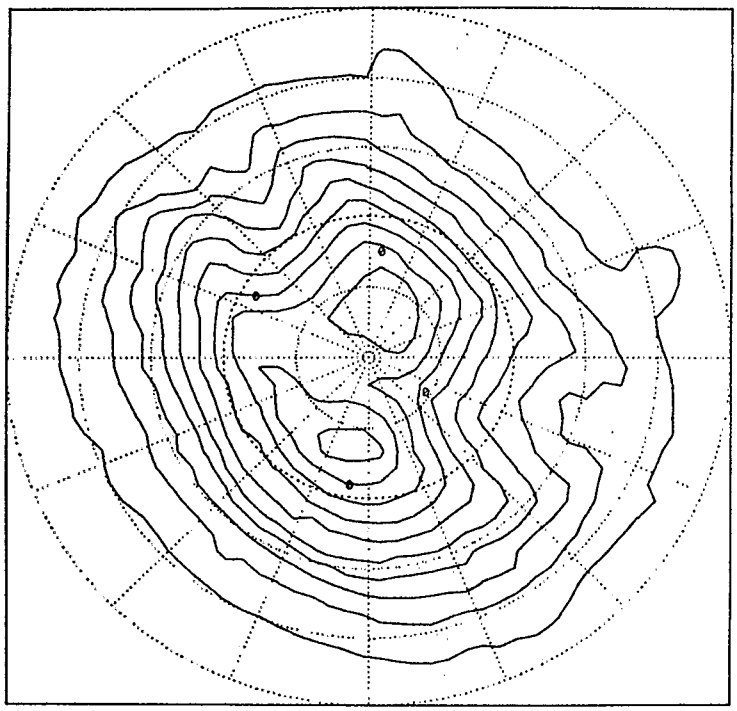

TIME PERIOD 2350-0000

Figure 94. Continued.

TABLE 13. IMPINGEMENT AND WRAP MODEL CALCULATIONS - EXPERIMENT 209, CASE HOUR 7

Meteorological Data

wind direction(deg)	=	105.
wind speed(m/s)	=	2.5
critical dividing streamline height(m)	=	58.0
Iz	=	.046
Iy	=	.121
N(1/s)	=	.094

Source Data

direction(deg)	=	101.
distance(m)	=	999.2
release height(m)	=	40.0
SF6 emission rate(g/s)	=	.160

Receptor Coordinates X(m)	Y(m)	Z(m)	Observed SF6 (ppt)	Impingement Predicted SF6 (ppt)	Wrap Predicted SF6 (ppt)
360.22	.00	13.26	.00	29.86	1.21
142.00	.00	50.00	28.80	891.52	139.86
257.78	33.94	30.00	.00	859.60	136.03
404.91	111.59	10.00	.00	13.81	.44
195.15	149.74	27.41	8.50	570.31	83.57
72.99	126.43	77.02	185.40	3.20	.07
66.30	505.92	-6.52	.00	.21	.00
58.14	445.44	3.38	.00	5.05	.14
40.17	305.14	22.10	6.80	263.02	31.90
35.92	272.83	31.92	.00	706.01	124.57
32.61	247.73	41.74	.00	898.49	173.73
-53.69	-407.79	3.82	.00	5.22	.14
-45.46	-345.28	13.70	4.90	60.54	4.14
-15.01	-113.99	98.96	.00	.00	.00
-19.85	-149.12	90.00	62.20	.05	.00
-84.85	-65.12	90.00	21.50	.15	.00
-396.67	-106.29	3.44	.00	9.69	.39
-315.76	-84.61	13.24	31.50	69.49	5.79
-248.96	-66.71	32.90	62.30	574.87	104.90
-204.16	-54.70	52.26	38.20	418.57	67.89
-238.00	.00	50.00	28.00	466.29	80.65
95.80	-231.27	52.96	61.60	531.87	77.47
59.13	-154.04	80.00	146.40	.92	.01
43.00	-74.48	80.00	62.20	.74	.01
355.15	-205.04	5.69	71.60	2.84	.05
256.81	-148.27	25.29	.00	462.20	57.31
204.15	-117.12	30.00	.00	857.36	135.76
108.15	-61.12	50.00	.00	858.89	135.94
37.15	-21.12	70.00	44.20	12.27	.36
312.38	-41.13	14.00	4.90	33.73	1.39
-243.41	65.22	50.00	18.70	455.70	78.98
-441.92	255.14	-.90	.00	3.59	.10
-359.96	207.82	8.94	.00	32.52	2.07
-297.11	171.54	28.07	34.70	420.55	69.10
-269.62	155.66	38.07	48.80	647.11	124.73
-111.85	65.88	80.00	69.30	4.49	.14
-40.85	28.88	80.00	120.30	4.27	.13
-141.42	141.42	50.00	79.00	505.60	86.76
-229.81	229.81	30.00	.00	505.60	86.76
-91.99	119.88	64.94	.00	91.31	8.17
-65.85	85.88	80.00	170.70	3.52	.09
-109.07	263.31	30.00	85.90	549.10	93.40
-80.75	194.94	50.00	79.70	549.10	93.40
-32.85	122.88	80.00	107.10	2.63	.06
-40.46	307.35	30.00	196.10	581.55	98.25
-25.71	195.51	65.00	35.10	84.57	6.90

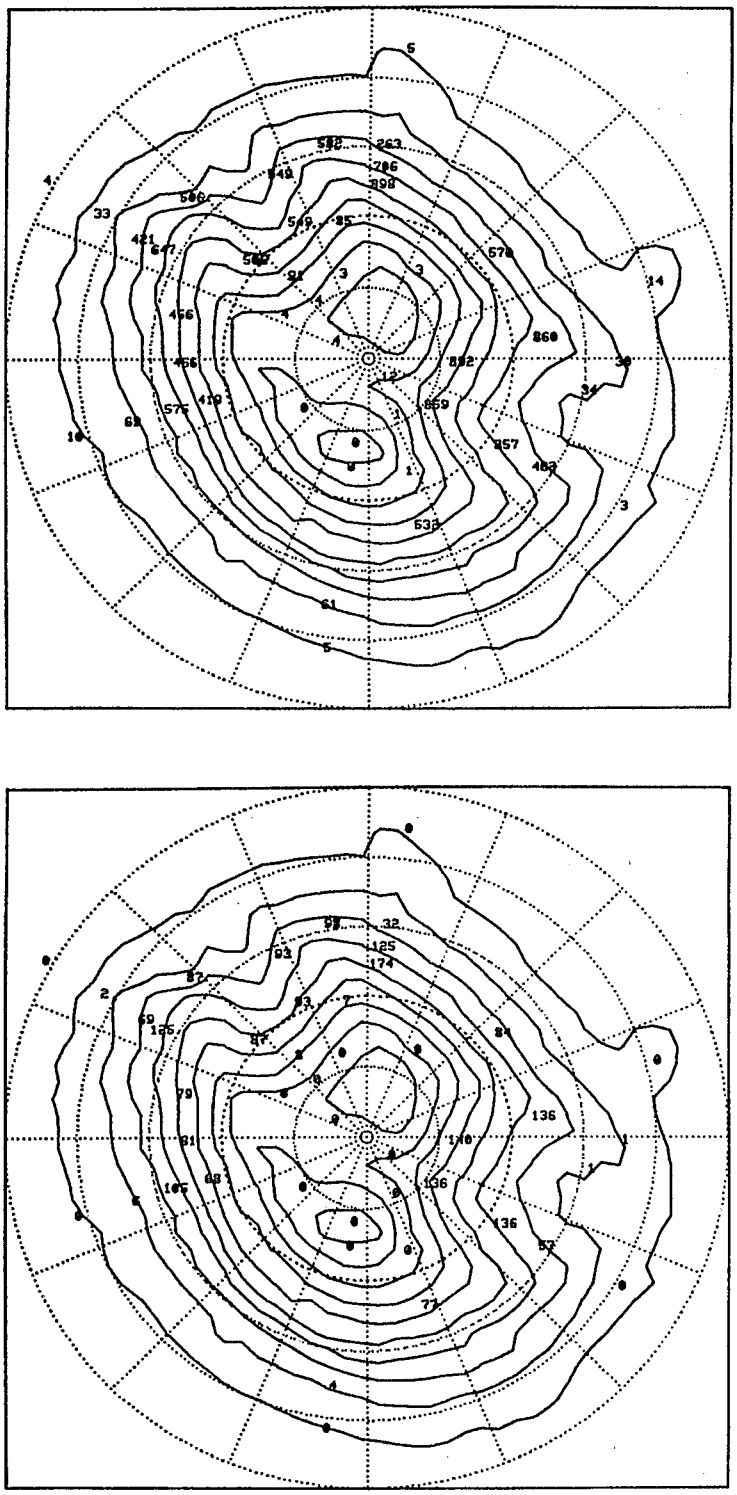

Figure 95. SF_6 concentrations (ppt) estimated for Experiment 209, Hour 7 by the Impingement (top) and Wrap (bottom) models.

4.11 Experiment 210, Hour 3 (0200-0300 MST)

4.11.1 Summary Description

Thermofogger oil-fog, SF_6, and Freon were released from the southeast side of the hill at 1084.3 m, 113.7° for the entire hour. The oil-fog and SF_6 were released at a height of 57 m, and the Freon was released at 30 m. Because all releases were continuous from the preceding hour, all tracer sampling data should be representative of the full hour.

Local terrain elevations near the release point are estimated to be -7.2 m relative to the zero of the hill coordinate system, so the net release height of the SF_6 and oil-fog correspond to the 49.8 m height level on the hill, and that for the Freon release corresponds to the 22.8 m height level. The SF_6 release rate is computed to be 0.169 g/s with an estimated uncertainty of $\pm 6.3\%$. The Freon release rate is 0.926 g/s $\pm 2.0\%$. No Freon concentration patterns have been modeled for this hour.

Plume Observations

Many observations about the plume appearance and trajectory were recorded during this experiment. Comments relevant to this hour are presented below.

Time: 0155 The plume looks like it is going around the south side at about the level of tower D.

Time: 0200 From south peak: Seeing some material come right up...

Time: 0202 Smoke odor is reported at tower D; I can see the plume coming into the vicinity of tower D, I believe it is on the south side of D and then rising quite a bit. The plume centerline is going directly towards the tower on the south peak. Presently the nephelometer crane seems to be right in the center of the plume.

Time: 0204 The plume now looks like it is going up the draw, not really touching the bottom of the draw, but going around the north side of the south peak.

Time: 0206 Plume is heading toward FAA tower, then it takes a sharp turn ($\sim$20°) and goes up the draw.

Time: 0208 The plume was going up the draw and then it swept right past me. I'm on the north butte, and it is barely going around the north side and up and over. I'm looking straight down the axis, and it comes right over the north edge of the flat area by the FAA tower. It is climbing quite a bit and going over at about 3 meters above the ground.

Time: 0210 I'm standing on the northeast point of the north flat area. The plume is going up and over me and I do not smell it, yet it is close enough that I feel like I can touch it. ERT 1, on the south butte, estimates that the centerline is maybe 9-10 m above the butte, with vertical dimensions of about 6 m. It is very coherent.

Time: 0213 Centerline has dropped maybe 5 m as the plume swings a little off to the north side--it is about even with the top of the hill. Plume is coherent and very visible; it is still almost touching the north side. After looking at another sweep, it's gone off the north side and has sunk down to the hill height.

Time: 0214 The plume is coming a little bit back over the top of the butte, about right over the very north extreme of the FAA flat area and now it is going up and over again. I cannot smell it, yet I feel like I can reach up and touch it. It is passing through the first white section of the FAA tower, which I would estimate, puts it at about 8 meters.

Time: 0216 The plume is passing right through the FAA tower, coming down as low as the top of the building at times.

Time: 0219 The plume now has moved just north of the FAA tower, and it is passing I would guess, about 5 to 8, maybe 10 meters above the ground. Now it is just streaming by here, yet, we cannot smell it.

Time: 0222 We're smelling the smoke now on top of the north butte.

Time: 0225 The plume is much more dispersed now horizontally and vertically. It's now approaching the north butte and going around the north side of the north butte. The top of the plume seems to be about even with the top of the hill right now, so the plume centerline is about 80 meters. There is quite a bit of plume meander evident between the hill and the source. The plume is very close to the top of the north peak, just barely off the north side, at time 0226.

Time: 0228 Ten meter winds at the ERT base are 130°, and are beginning to trend more toward the southeast.

Time: 0231 We have just had about a 10° change in wind direction at the source. Wind direction is now more to the southeast. It looks like about 130°, so we are missing the hill on the north side, and the plume is no longer rising as it approaches the hill. The plume is also more constricted now. There is a lot less horizontal and vertical mixing noticeable.

Time: 0233 The plume, as it is traveling over the northeast knoll, is not hitting the hill and is considerably more compact. As usual, we are seeing that as it gets off that stagnation streamline its character goes back to a more normal coherent compact plume.

Time: 0234 The plume centerline is slightly north of the north hill. You can see dramatic change in the centerline in about the point where it approaches the hill and the centerline turns to the right. It appears about 5° to 10° at that point.

Time: 0239 The plume is sweeping to the south now. Plume centerline is almost directly towards the draw. The plume still has a significant kink in it as it approaches the hill. It looks like the angle difference between the plume from the release point and the plume as it bends around the hill is at least 30°. The plume appears to be turning as it approaches the FAA tower.

Time: 0240 The plume is coming directly over on the north peak, but we cannot smell it. ERT 3 feels like if he were standing on top of my car that he could smell it. Looking at the source, it looks like the plume was swept back and is now aimed at the south shoulder.

Time: 0241 The plume is coming right at the draw and then dramatically rising and going through the draw at about the level of the two peaks. As I am looking across, the plume is obscuring the lower half of the 100-foot tower from me. It is going over the saddle and really diving on the back side. Occasionally a puff comes maybe 2, 3, maybe 4 meters below the level of the peaks (eye level looking across the two buttes).

Time: 0243 It is still going through the draw at about the height of the two peaks and just diving in the back. It looks like it may be going just barely south of tower F and really at the level of tower F. It really dives down, and we don't smell it on top of the hill. It looks to me like the height of the nephelometer intake on the northeast corner of the FAA fence is about 3 meters.

Time: 0250 The wind has picked up, and you can smell the plume now on the north butte. It looks quite a bit wider.

Time: 0254 I can faintly smell the plume on the north butte. It appears to be coming right at the FAA tower and going up and over.

These observations are quite extensive, providing a description of the plume during each 5-minute period. In summary, the plume initially streamed toward tower D or the southeast side of the hill during the first 5-minute period. It then shifted across the hill to the north side and remained either along the north shoulder of the hill, or over the north peak during periods 2-6. The plume shifted more to the north away from the hill in the seventh period, and remained there into period 8. Late in the eighth period, the plume again swept back toward the center of the hill and rose over the saddle between the peaks during period 9. In the last 15 minutes, the plume again flowed over the north peak.

Smoke odor was noted at several times during the hour, yet was noticeably absent at other times. Smoke odor was noted early when the plume was streaming near tower D, and it was also noted on top of the hill late in the hour after the wind speed increased. No smoke odor was noted at times in between because the plume was deflected directly over the north peak.

Two representative photographs of the oil-fog plume are presented in Figure 96. The first was taken from the top of the north peak at camera position 0-15 (see Figure 46), and the second was taken to the side of the plume at position 0-10. Each photo is a 5-minute time exposure.

The photos show the plume was near the southeast side of the hill during period 1, and over the north peak during periods 2-5. It then streamed around the north side of the hill during period 6, and shifted away from the hill to the north during period 7. The plume swept back toward the hill during period 8, and remained over the saddle or the south side of the north peak for the remainder of the hour. This is in substantial agreement with the recorded observer notes. The marked increase in plume dispersion in periods 10-12 noted by observers can also be seen in the photo record.

This photographic series clearly shows that the plume is able to rise over the hill at times, conforming to the hill shape but not mixing down to the surface. This behavior is a typical case in which the plume is compact enough, and the Froude number high enough, that the plume surmounts the hill with little impact.

Lidar data taken during this hour are extensive. The lidar sampled the plume along seven planes: three upwind of the hill, three over the hill, and one in the lee of the hill. Plume centroid positions derived from the lidar data are plotted in Figure 97. This figure shows that the plume preferentially traveled toward the north peak, either passing to the south, north, or directly over the top. The only periods in which the plume took a substantially different course are periods 1, 6, and 7. The plume passed to the north of the hill during periods 6 and 7, and it was directed more towards the southeast shoulder of the hill during the first period, as noted in the previous discussions.

Of additional interest is the plume centroid height in the lee of the hill. The lidar shows the centroid between 7 m and 33 m above the zero of the coordinate system in the lee, although it began at roughly 50 m in the sampling plane closest to the release point. Therefore, a marked streamline depression existed in the lee of the hill.

Initial wind directions at source height were calculated from centroid positions in the sampling planes closest to the release point. These vary from 106° in period 1, to 117° in period 6. Directions between these extremes vary from 108° to 114°. Because the source was located along the 113.7° ray, these wind directions should have taken the plume just left of the hill center. However, many of the centroid positions over the hill lie nearer the north peak. This shift may be due to uneven sampling in time at locations near the source, so wind directions were probably more southerly (say 118°-119°), taking the plume more toward the north peak.

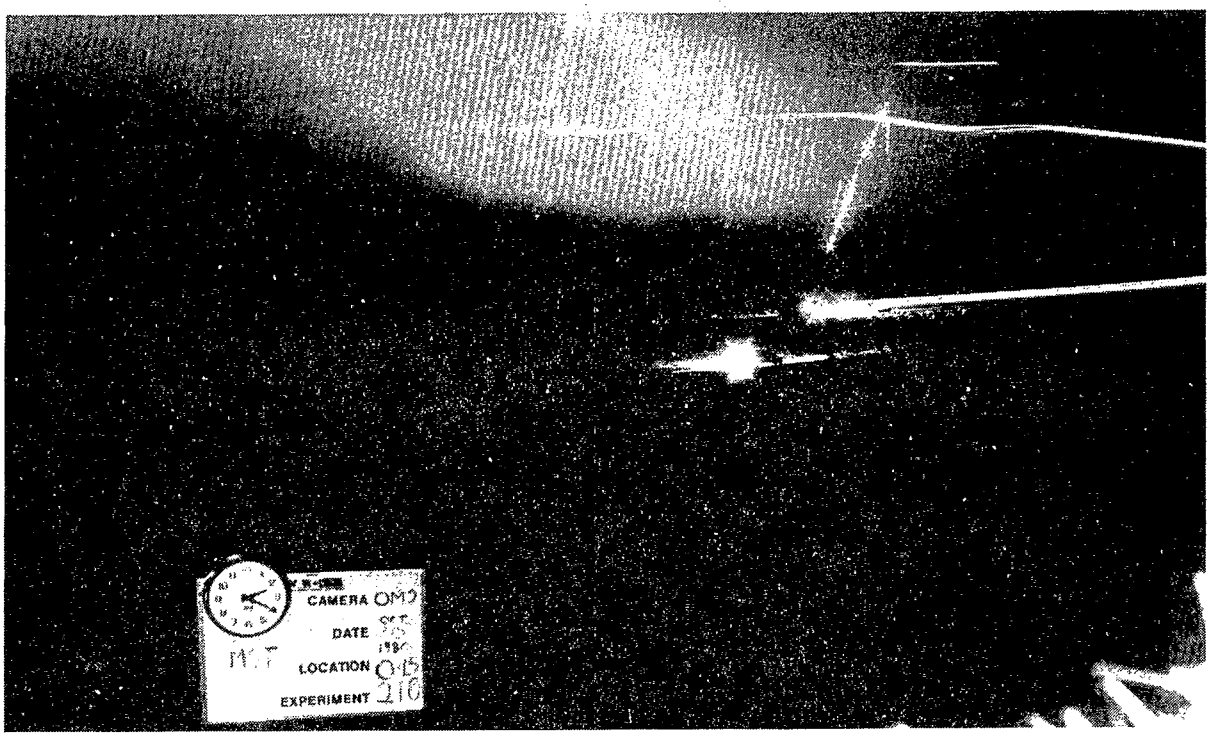

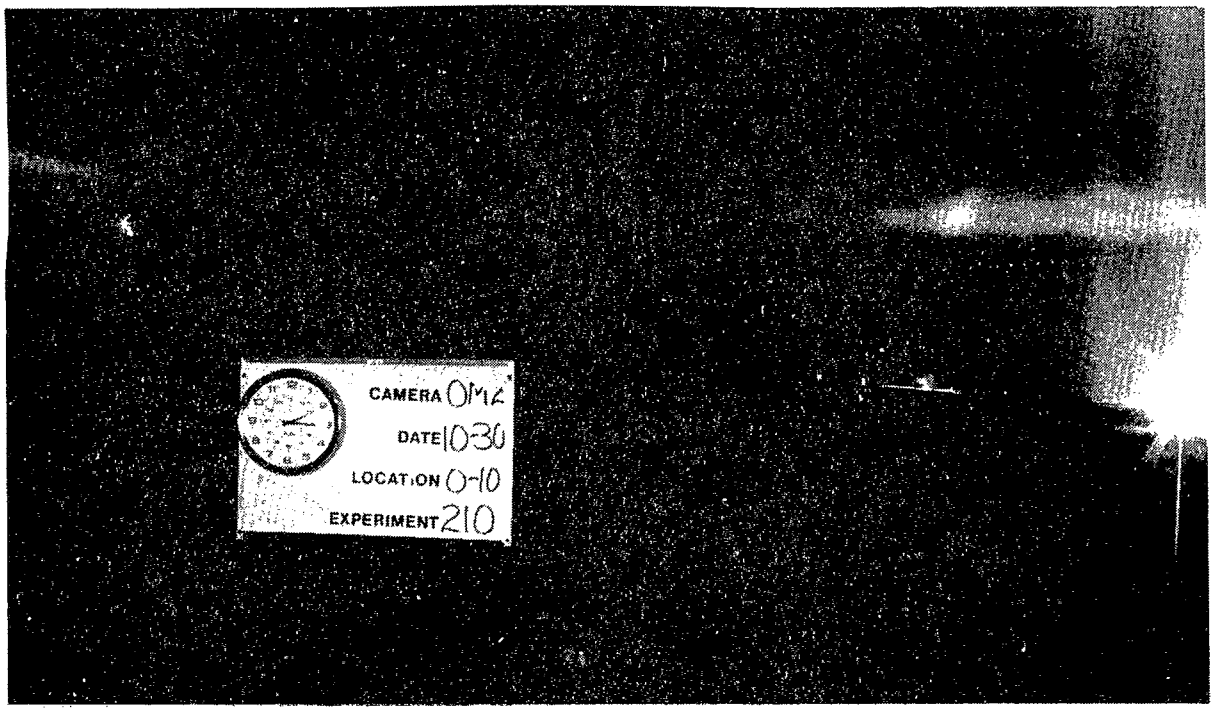

Figure 96. Two views of the plume trajectory between 0215 and 0220 MST taken from the top of the north peak (position 15) and taken off to the side of the release (position 10) during Experiment 210, Hour 3.

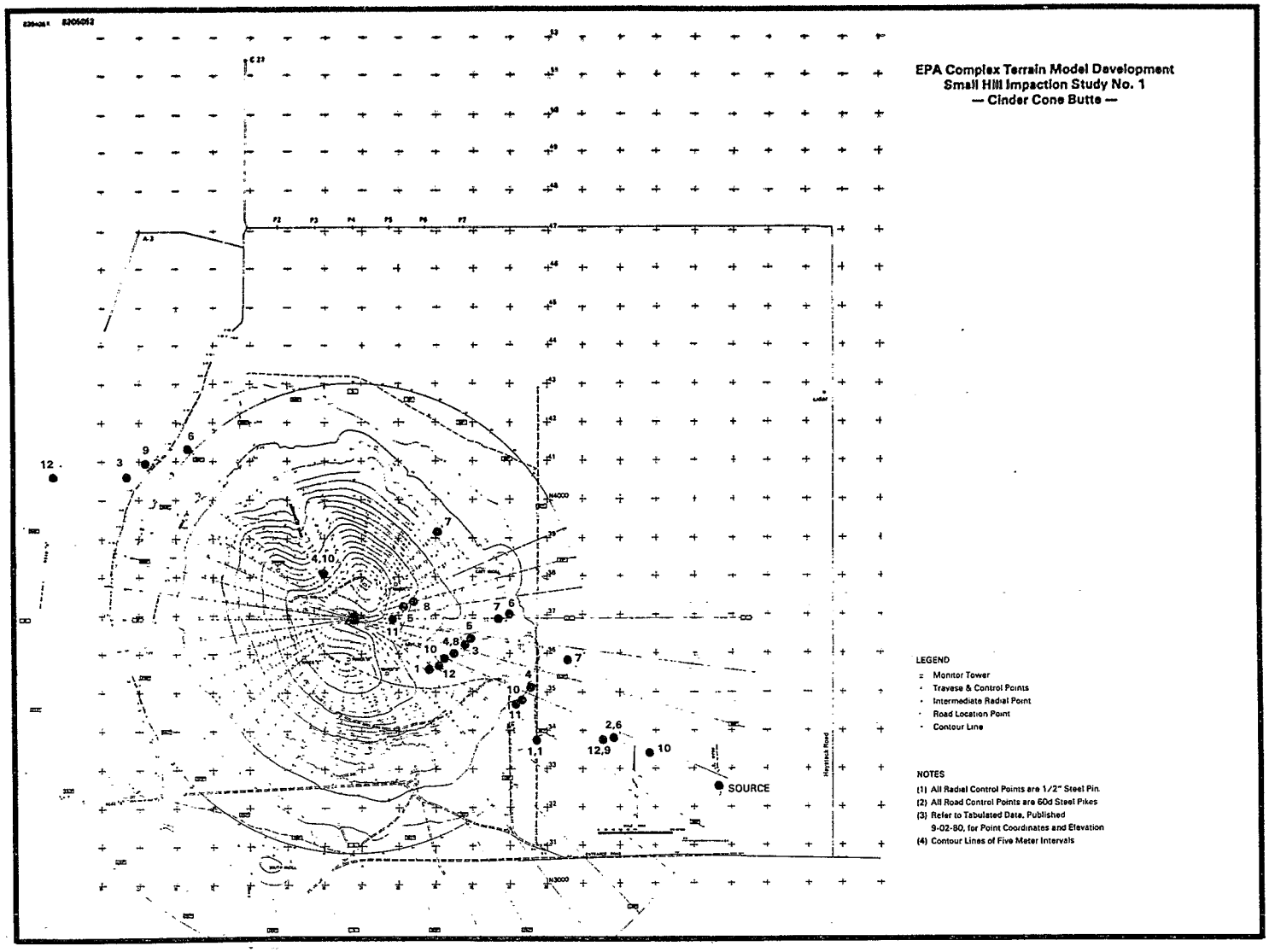

Figure 97. Plume centroid positions calculated from lidar data. Experiment 210, Hour 3 (0200-0300 MST).

Meteorological Information

Wind and temperature data measured at tower A during this hour were used to characterize the flow in terms of H_c. However, because of a partial failure of the 40 m wind set, 40 m wind speeds were inferred for each 5-minute period before calculating H_c. The method followed in calculating speeds at 40 m was outlined in Section 4.4.1.

The average H_c over this hour is 26 m, and Fr_H above this height is 2.1. Because the SF_6 plume was released at 57 m, its trajectory should have been similar to that for weakly stratified flows. Fr_L above 26 m is 0.55, so a significant streamline depression in the lee of the hill is expected. Lidar data in the lee of the hill indicate a substantial depression.

Figure 98 contains a time series plot of the calculated 5-minute H_c and Fr_H values for this experiment. H_c dropped from 25 m to 20 m during the first half hour, only to rise rapidly to 30 m until late in the hour, when it again dropped to 20 m. Fr_H rose from just under 2.0 to over 3.5. These changes in H_c probably had only a minor effect on surface SF_6 concentrations; however, the changes in Fr_H imply that the greatest streamline depression in the lee would have occurred early in the hour.

Hourly averaged wind speeds measured at 80 m and estimated at 40 m on tower A are 7.6 and 6.3 m/s, respectively. The 80 m wind direction, which is assumed to be applicable at source height, is 122°. Figure 99 shows the trend in wind speeds between 10 m and 80 m over the hour. The 10 m and 80 m winds are nearly constant, but the winds inferred at 40 m drop significantly in the eighth through eleventh 5-minute periods. This event coincides with a plume shift toward the center of the hill from a trajectory around the north side. If the wind at release height also dropped, then the hourly averaged concentrations over the saddle and the north peak may have been slightly greater than those calculated with the hourly average wind speed.

Variations in wind directions measured at 10 m and 80 m are shown in Figure 100 as frequency distributions. The 80 m distribution is much narrower than the 10 m distribution and is therefore indicative of the 57 m plume trajectories seen in the photographs. Because the plume was high above H_c (and high above the 10 m level, for that matter), the broad wind distribution at 10 m probably had little effect on measured SF_6 concentrations.

In summary, the plume was released well above H_c. Froude numbers were low enough to suggest the presence of lee waves, which were noted by the lidar.

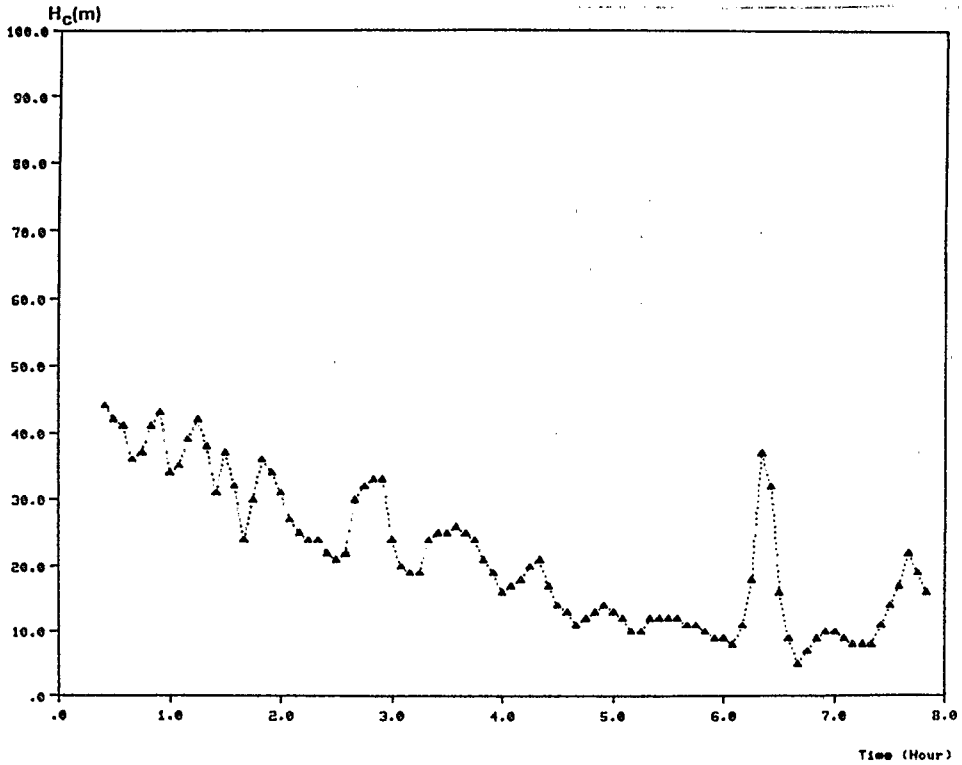

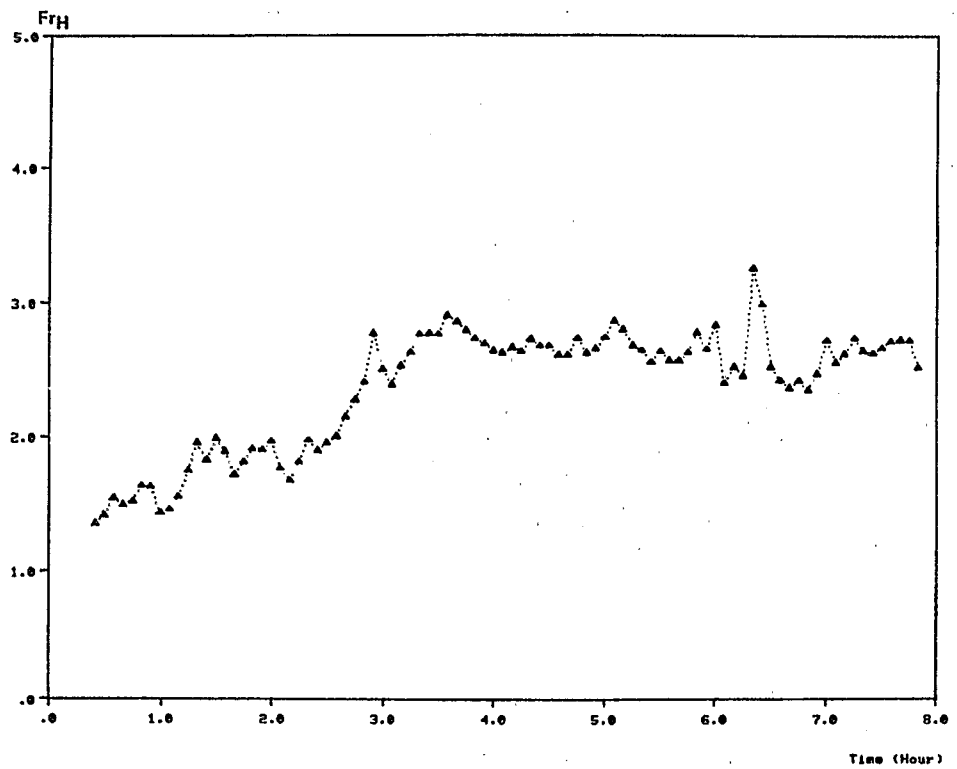

Figure 98. Calculated dividing streamline heights (H_c) and bulk hill Froude numbers above H_c (Fr_H) for Experiment 210.

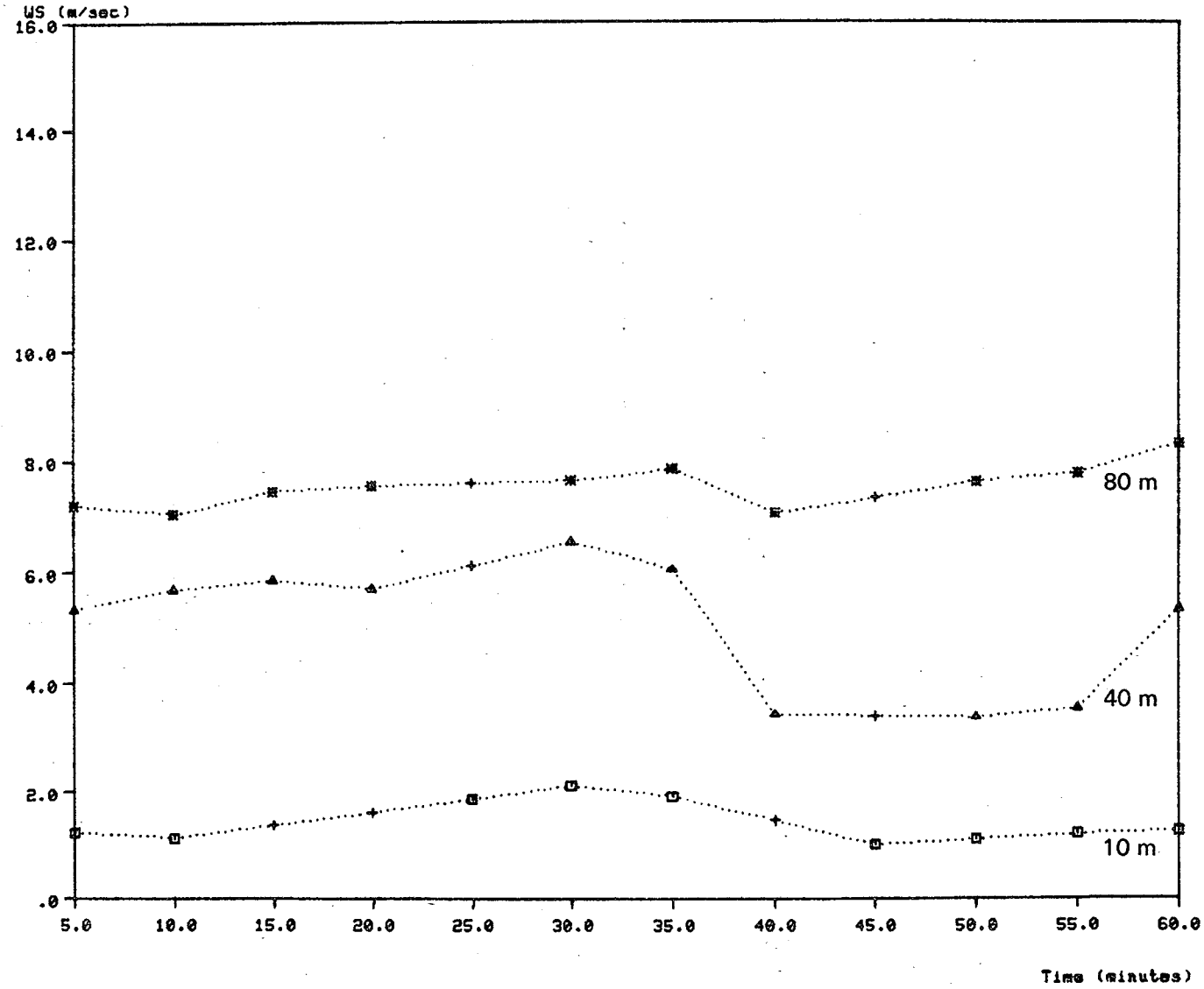

Figure 99. Tower A wind speeds during Experiment 210, Hour 3 (0200-0300 MST).

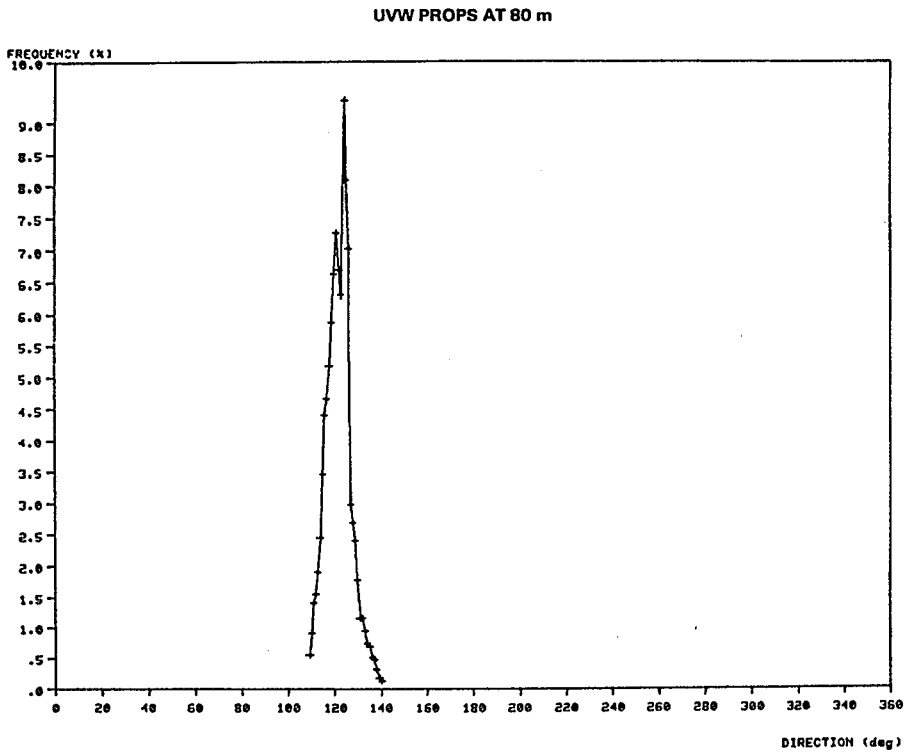

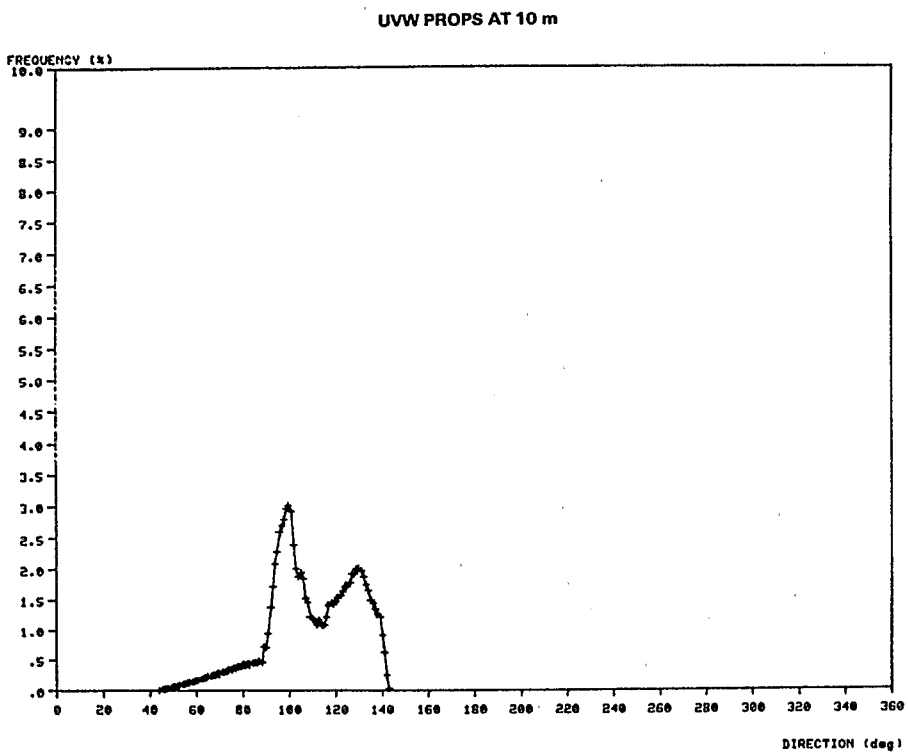

Figure 100. Calculated wind direction distribution functions for Experiment 210, Hour 3 (0200-0300 MST).

SF_6 Concentrations

The distribution of hourly averaged SF_6 concentrations over the surface of the hill is shown in Figure 101. All of the large concentrations measured lie at the base of the northwest draw in the lee of the hill. The largest is located at the downwind edge of the sampling network. Other sizeable concentrations are seen near the 80 m - 85 m height contour around both peaks and across the saddle. Concentrations below 30 m on the upwind side of the hill are very small.

This pattern is consistent with the observations and the photographs discussed above. The concentrations in the lee may be very large because the plume was depressed in the lee, and the moderate concentrations over the top of the hill may have arisen during those periods late in the hour when the plume appeared to undergo increased dispersion.

The distribution of 10-minute average SF_6 concentration presented in Figure 102 provides more information on the evolution of the pattern. The concentrations near the top of the north and south peaks arose in the first half hour, when the plume first traveled near the southeast side of the hill and then rested over the north peak. The sizable concentrations in the saddle area built up primarily during the last 10 minutes of the hour. This was the period of time when observers noted an increase in the dispersion of the plume.

4.11.2 Model Performance

This hour was modeled with the Lift model because all evidence indicates that streamlines at plume height traveled over the hill. Meteorology used in the modeling was prepared as in Section 4.1.2 and is summarized in Table 14.

The 1-hour wind directions measured 47 m below and 23 m above the release height are 113° and 122°, respectively. Directions at 10 m and 30 m on tower B are 119° and 124°, respectively. But the direction inferred from the lidar and photographic data indicate a wind direction of 118°-119°. Therefore, the model wind direction is set to 118°. The 80 m PDF is also used in the modeling.

Neutral was rerun with the new meteorological data. Instead of estimating a peak value 31% of the peak observed concentration, it produced a peak 8% of the peak observed. Figure 103 shows the distribution of calculated concentrations plotted on a map of CCB, and the results are also summarized in Table 14.

Results of the Lift computations are also displayed in Figure 103 and in Table 14. Once again, the computations produce extremely low concentrations: the peak modeled is only 4% of the peak observed.

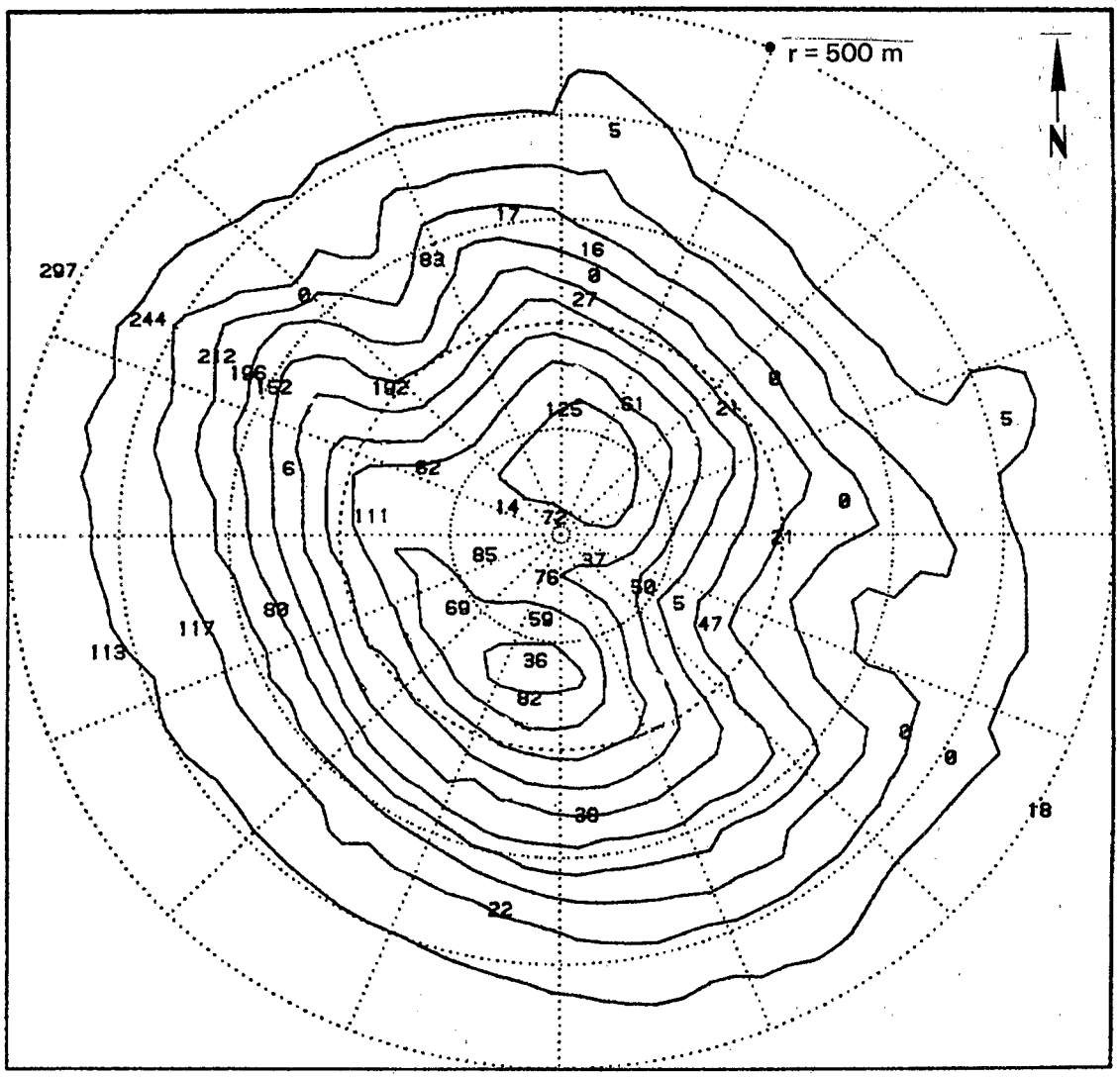

Figure 101. Observed SF_6 concentrations (ppt) for Experiment 210, Hour 3 (0200-0300 MST). Source: r = 1084.3 m, θ = 113.7°, net height = 49.8 m, Q = .169 g/s.

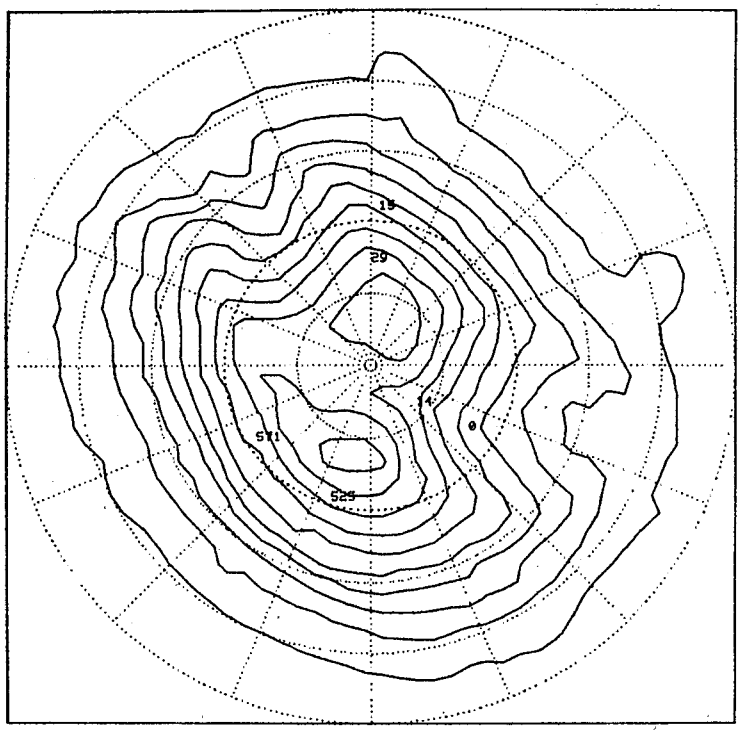

TIME PERIOD 0200-0210

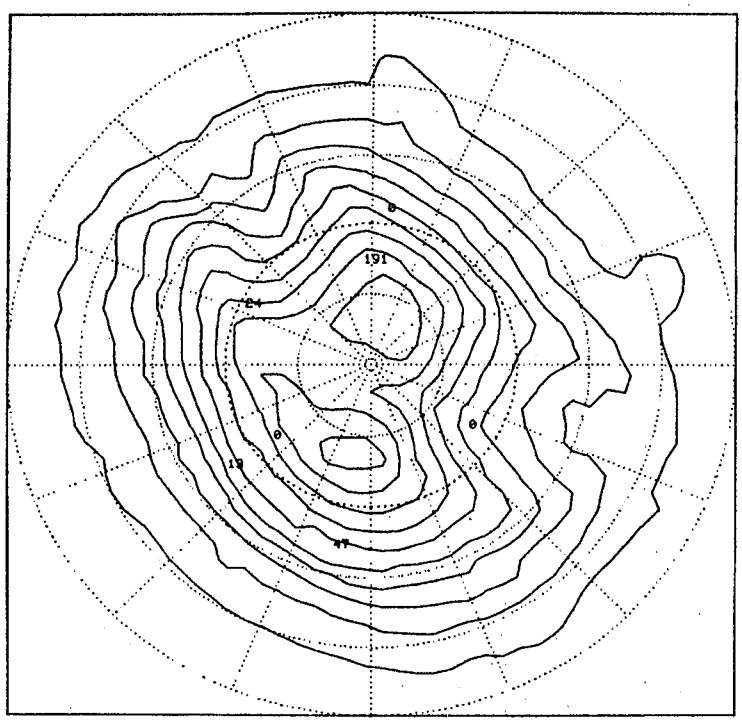

TIME PERIOD 0210-0220

Figure 102. Observed 10-minute average SF_6 concentrations (ppt) for Experiment 210, Hour 3 (0200-0300 MST).

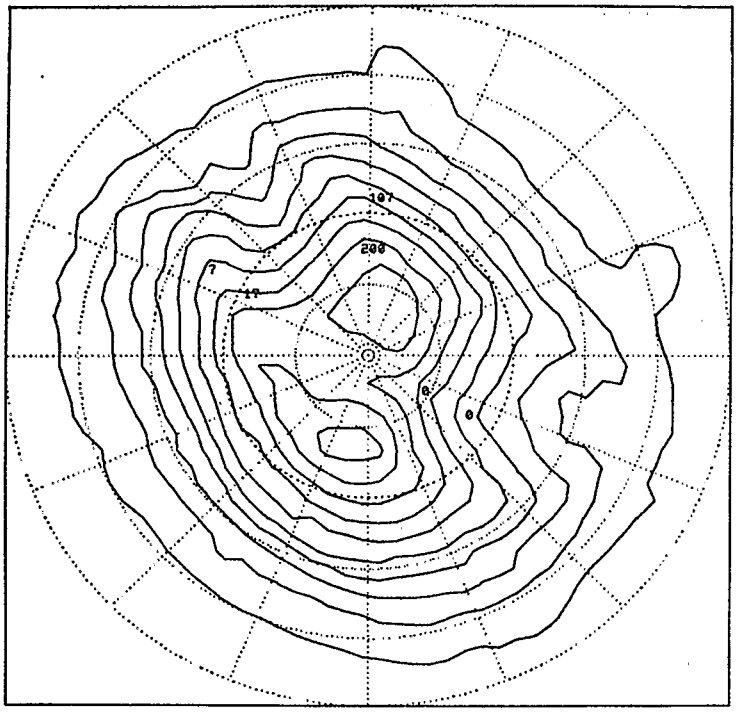

TIME PERIOD 0220-0230

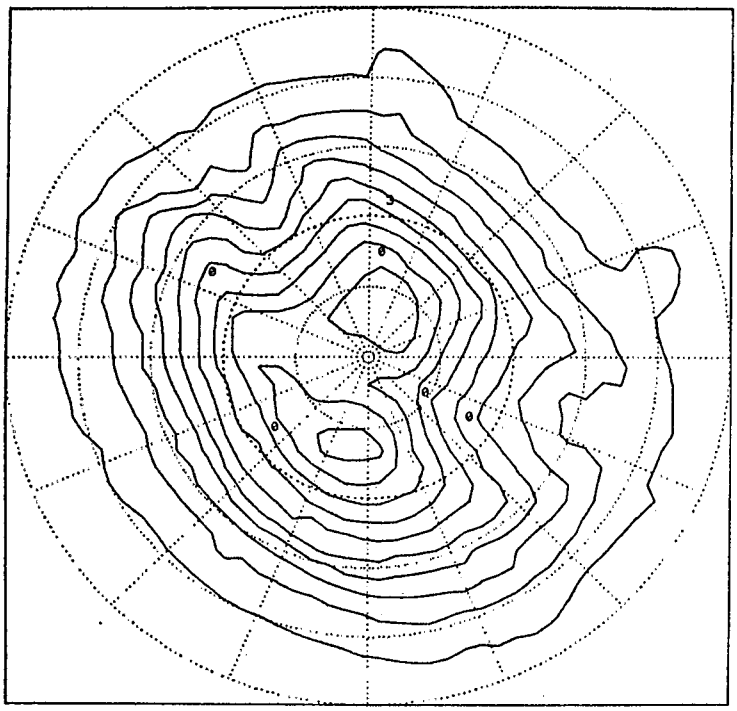

TIME PERIOD 0230-0240

Figure 102. Continued.

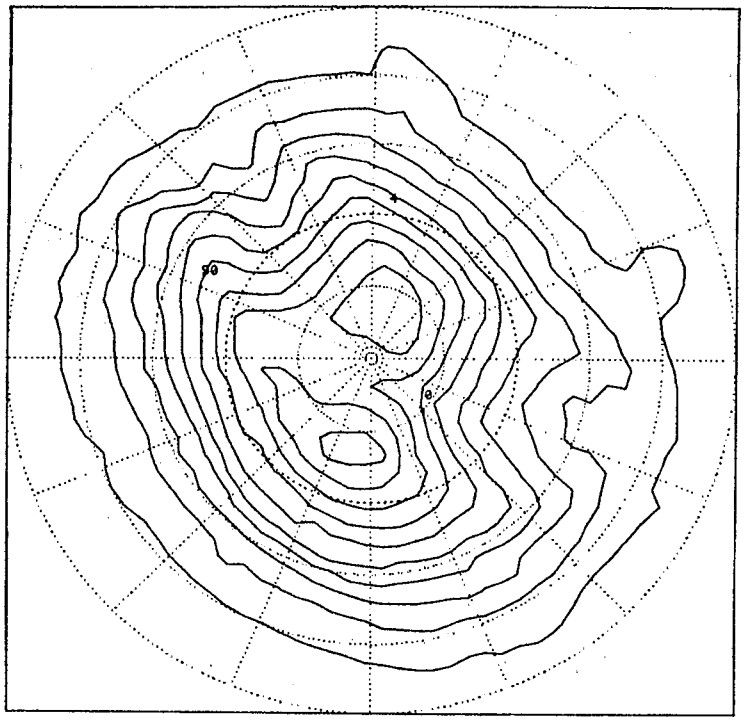

TIME PERIOD 0240-0250

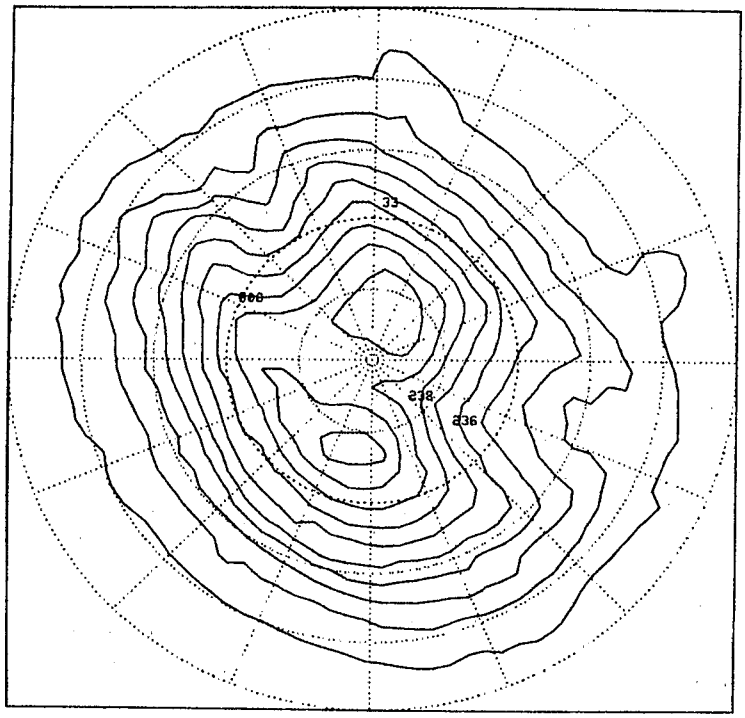

TIME PERIOD 0250-0300

Figure 102. Continued.

TABLE 14. NEUTRAL AND LIFT MODEL CALCULATIONS - EXPERIMENT 210, CASE HOUR 3

Meteorological Data

wind direction(deg)	=	118.
wind speed(m/s)	=	6.3
critical dividing streamline height(m)	=	26.0
Iz	=	.018
Iy	=	.105
N(1/s)	=	.044

Source Data

direction(deg)	=	114.
distance(m)	=	1084.3
release height(m)	=	57.0
SF6 emission rate(g/s)	=	.169

Receptor Coordinates X(m)	Y(m)	Z(m)	Observed SF6 (ppt)	Neutral Predicted SF6 (ppt)	Lift Predicted SF6 (ppt)
208.35	.00	31.25	20.80	.06	.44
257.78	33.94	30.00	.00	.02	.16
404.91	111.59	10.00	5.20	.00	.01
195.15	149.74	27.41	.20	.02	.26
159.04	122.04	46.91	20.86	2.06	.44
72.99	126.43	77.02	61.20	21.16	2.12
66.60	505.92	-6.52	.00	.00	.14
51.04	387.66	11.78	5.20	.00	.43
35.92	272.83	31.92	15.50	.18	.55
32.61	247.73	41.74	.00	1.26	1.07
29.59	224.79	51.51	26.98	6.84	1.14
15.97	121.29	90.94	125.00	24.15	2.19
2.15	18.88	80.00	71.70	18.68	1.65
-66.52	-505.24	-3.54	.00	.00	.00
-45.46	-345.28	13.70	21.90	.00	.00
-15.01	-113.99	98.96	36.20	8.44	.38
-19.85	-149.12	90.00	82.30	5.55	.19
-9.85	-76.12	90.00	58.60	10.70	.56
-4.85	-37.12	80.00	76.10	13.62	1.12
-84.85	-65.12	90.00	68.80	11.70	.65
-396.68	-106.29	3.44	112.70	.00	.00
-315.76	-84.61	13.24	117.40	.00	.49
-248.96	-66.71	32.90	80.40	.14	.98
-60.85	-16.12	80.00	84.90	15.62	1.56
31.69	-258.06	50.00	37.90	.05	.00
441.46	-254.87	-2.45	18.30	.00	.00
355.15	-205.04	5.69	.00	.00	.01
313.62	-181.07	15.29	.00	.00	.02
142.15	-81.12	40.00	47.30	.35	.39
108.15	-61.12	50.00	5.20	3.35	.54
82.15	-46.12	60.00	50.44	12.43	.68
37.15	-21.12	70.00	36.80	14.90	.96
-157.38	20.72	83.35	111.00	19.30	2.51
-243.41	65.22	50.00	5.70	8.88	3.60
-441.92	255.14	-.90	297.00	.01	11.28
-359.96	207.82	8.94	243.90	.04	7.79
-297.11	171.54	28.07	212.30	.70	6.43
-269.62	155.66	38.07	195.80	2.92	5.87
-246.20	142.14	47.96	152.30	10.62	5.40
-111.85	65.88	80.00	61.50	23.80	2.68
-40.85	28.88	80.00	13.80	19.94	1.83
-141.42	141.42	50.00	191.60	12.75	4.89
-229.81	229.81	30.00	.10	.94	6.43
-109.07	263.31	30.00	83.00	.50	5.26
-40.46	307.35	30.00	17.10	.23	1.19

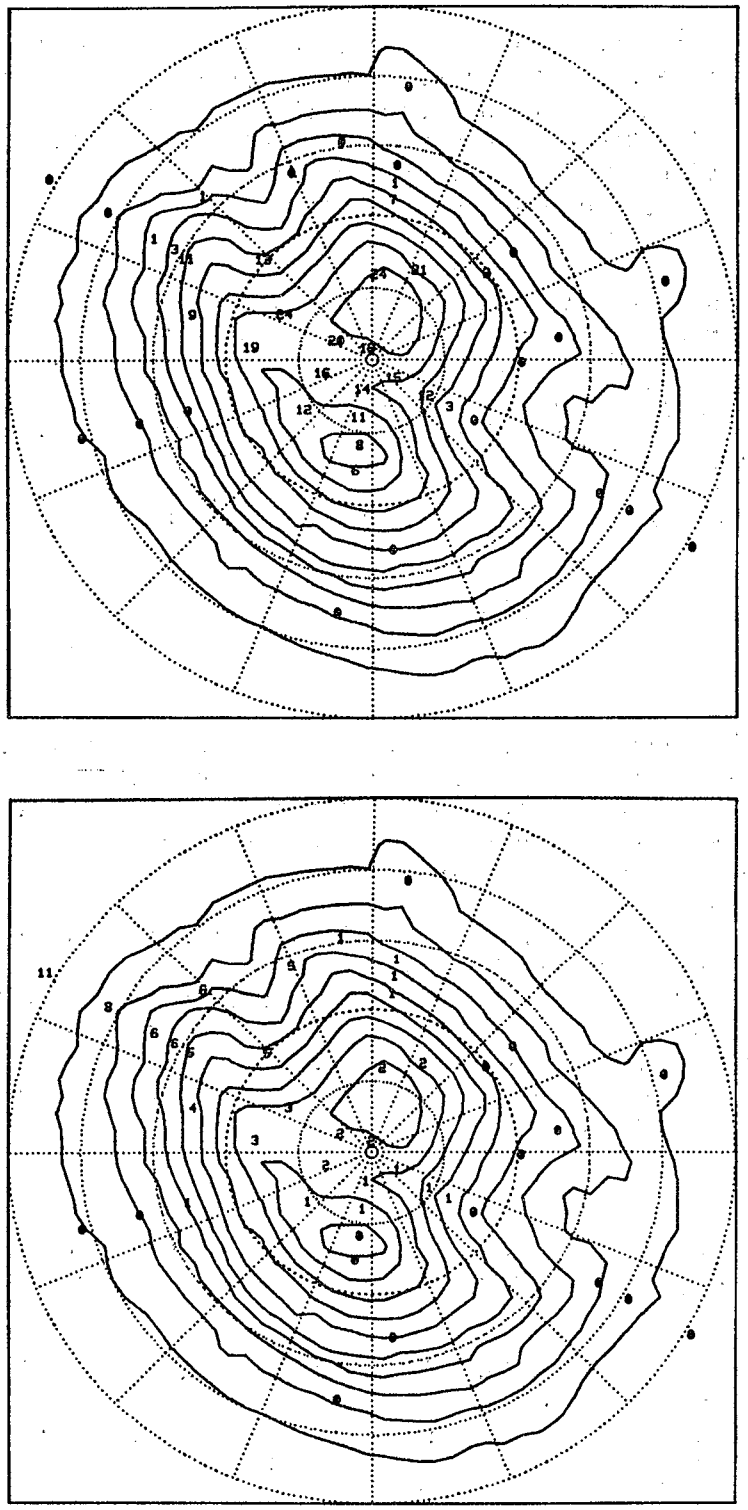

Figure 103. SF_6 concentrations (ppt) estimated for Experiment 210, Hour 3 by the Neutral (top) and Lift (bottom) models.

In both cases, the modeled concentrations are low everywhere across the hill. The observed concentrations are greater over much of the hill but become particularly greater at the base of the hill on the leeward side. Computed T_o values for these observed concentrations are about 0.6 in the southeast draw, 0.58 to 0.63 in the saddle area, 0.58 on the north peak, 0.50 on the south peak, and 0.48 to 0.50 near the base of the hill on the lee side.

These values suggest that the σ_z should be larger in order to reproduce the observed concentrations. As noted in the discussions above, the dispersion was seen to increase substantially late in the hour. This is already shown in the lidar data. The measured σ_z in a plane near the upwind base of the hill varied between 3.5 and 6.0 m for most of the hour. But during the last 10 minutes, σ_z increased to 11.0 m at 0252 and to nearly 15 m at 0256. Therefore, the key to modeling this hour successfully may be a careful treatment of the last 10 to 20 minutes.

4.12 Experiment 210, Hour 7 (0600-0700 MST)

4.12.1 Summary Description

Thermofogger oil-fog, SF_6, and Freon were released from the southeast side of the hill at 1086.2 m, 122.2° for the entire hour. The oil-fog and SF_6 were released at a height of 58 m, and the Freon was released at 30 m. All releases were continuous from the preceding hour, so all tracer sampling data should be representative of the full hour.

Local terrain elevations near the release point are estimated to be -8.2 m relative to the zero of the hill coordinate system, so the net release height of the SF_6 and the oil-fog corresponds to the 49.8 height level on the hill, and that for the Freon release corresponds to the 21.8 m height level. The SF_6 release rate is computed to be 0.178 g/s with an estimated uncertainty of $\pm$7.4%. The Freon release rate is 0.986 g/s $\pm$3.3%. No Freon concentration patterns have been modeled for this hour.

Plume Observations

Few observer comments and observations about the plume appearance and trajectory were recorded during this hour. The relevant ones are presented below.

Time: 0557 I am a third of a mile west of road A doing a north-south transect with my nose, and I can faintly smell the plume. I would estimate that it is about half of a hill width wide--that's very approximate.

Time: 0559 Looking back at the release, it is coming over the butte just south of tower B and then turning slightly north and then getting considerably wider as it comes out into the flats again.

Time: 0619 It's difficult to see, but it looks to me like the flow in the lee is no longer as attached as it was earlier, and it is not coming down as low. The dawn is just breaking so we will be able to see it better in about 15 minutes. The array I am asking them to analyze for Freon is again very extensive because we expect the lower level release to be meandering really all over the place. This analysis should be very interesting because the upper plume was very, very steady.

Time: 0702 The thermofogger is down being refueled and will go back up shortly. I have asked them to co-locate the Freon and SF_6 at the same level as the thermofogger, and we will be able to test how the system is working. The ERT crew is releasing flares all over the south shoulder of the hill, and most of them are going up the hill--the ones on the south face are going up the hill, the ones on the draw side of the shoulder are going across the hill, and the ones down low are going around the hill.

Although the notes are sketchy, they indicate that the plume was fairly steady during the first half hour, and that a strong depression in the lee of the hill at the start of the hour weakened over the same time period. More information on plume behavior upwind of the hill is contained in the photographs. Each photo is a 5-minute time exposure, except for one which covers a 10-minute period.

The available photos only cover 5-minute periods 1-7, but show that the oil-fog plume was fairly steady at least during the first half hour. It remained near the south peak, starting off the hour along the south shoulder of the peak, and ending over the saddle in period 7. As the plume sails over the south peak in periods 1-5, clear air can be seen beneath the bottom edge of the visible plume. SF_6 concentrations should therefore be small in this area. It is much harder to see if the oil-fog cleared the saddle by a similar amount, but it appears that the plume did rise high enough over the saddle to produce only small concentrations there too.

Two representative photos of the plume are reproduced in Figure 104. The first was taken from the top of the south peak at camera location 0-8 (see Figure 46), and the second was taken from behind the plume at location 0-19.

No photos are available to show what happened to the plume later in the hour, and no lidar data are yet available to provide this information.

Meteorological Information

Wind and temperature data from tower A were used to characterize the flow during the hour in terms of H_c. However, because of a partial failure of the 40 m wind set, 40 m wind speeds were estimated for each 5-minute period before calculating H_c. The method followed in calculating the 40 m speeds was outlined in Section 4.4.1.

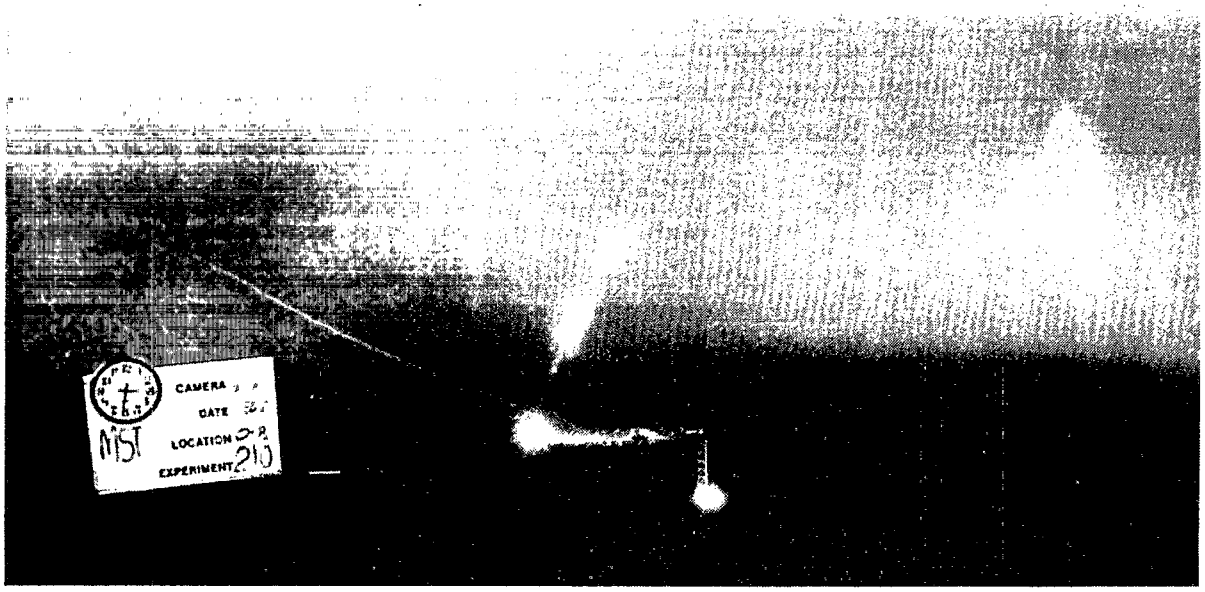

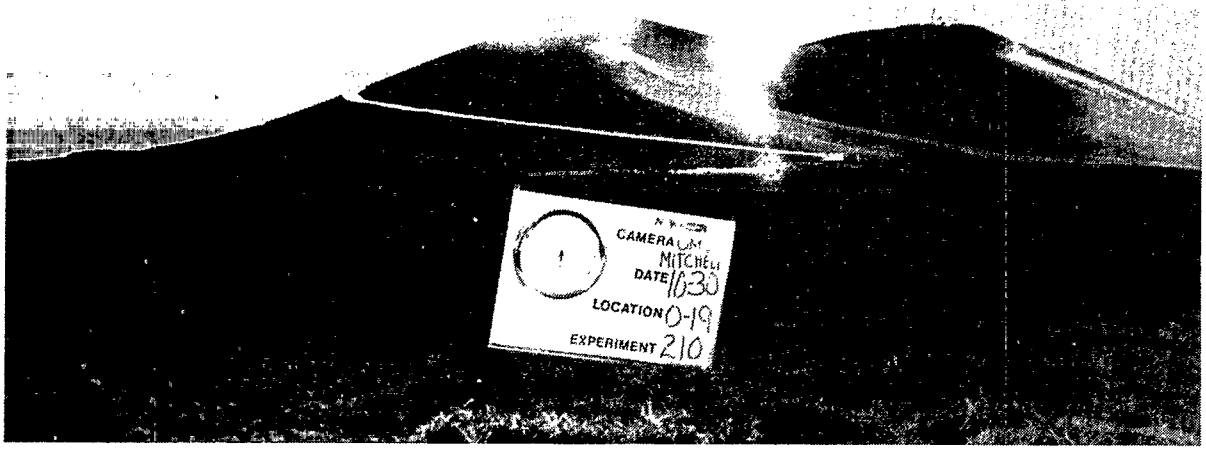

Figure 104. Two views of the plume trajectory between 0615 and 0620 (top), and between 0610 and 0620 MST (bottom) taken from the top of the south peak (position 8) and taken from behind the release (position 19) during Experiment 210, Hour 7.

The average H_c during this hour is 14 m, and the average Fr_H is 2.6. Because the SF_6 plume was released at 58 m, its trajectory should have been similar to that for weakly stratified flows. Fr_L above the H_c is 0.63, so some streamline depression in the lee of the hill may be expected.

Figure 98 contains a time series plot of the calculated 5-minute H_c and Fr_H values for this experiment. The H_c pattern exhibits a spike over the first half hour with a peak value of over 35 m. During the rest of the hour H_c is about 10 m. A much smaller spike is seen in the Fr_H trace. Its peak is centered on the fourth 5-minute period; this coincides with the observation that the depression of the plume in the lee of the hill was not as strong as it had been earlier. The peak Fr_H value corresponds to a Fr_L of 0.80. A weakening of the depression in the lee is consistent with a change toward greater Fr_L values.

Hourly averaged wind speeds measured at 80 m and estimated for 40 m on tower A are 9.0 and 7.3 m/s, respectively. The 80 m wind direction, which is assumed to be applicable to the source height, was 130°. Figure 105 shows the trend in wind speeds between 10 m and 80 m over the hour. A dramatic decrease in the 40 m speeds occurred during the fourth 5-minute period, and may be responsible for the changes in the flow parameters (H_c, Fr_H, Fr_L) discussed above.

Variations in wind directions measured at 10 and 80 m are shown in Figure 106 as frequency distributions. Each distribution has a mean of 130°, but the 10 m distribution is considerably broader. The 80 m distribution, undoubtedly more appropriate for the SF_6 release height, illustrates the steadiness observed in the plume trajectory over the hour.

In summary, the SF_6 plume was released well above H_c. Although wind directions were very steady at release height, wind speed changes produced a short period of flow alteration. The hourly SF_6 concentrations should be representative of a high release into a weakly stratified flow ($Fr_H > 1$).

SF_6 Concentrations

The distribution of hourly averaged SF_6 concentrations over the surface of the hill is shown in Figure 107. The highest concentration is found near the 80 m contour on the lee side of the south peak. Other high concentrations are found toward the base of the hill in the lee. Only zero concentrations are measured on the windward slope of the hill below 65 m. In fact, all but one sampler measured zero concentration in the southeast draw up toward the saddle. This pattern is consistent with weakly stratified flow over the hill.

The distribution of 10-minute SF_6 concentrations is presented in Figure 108. These plots also show the lack of any significant impact on the windward side of the hill. They illustrate the steadiness of the plume late in the hour when both photographic and lidar data are missing.

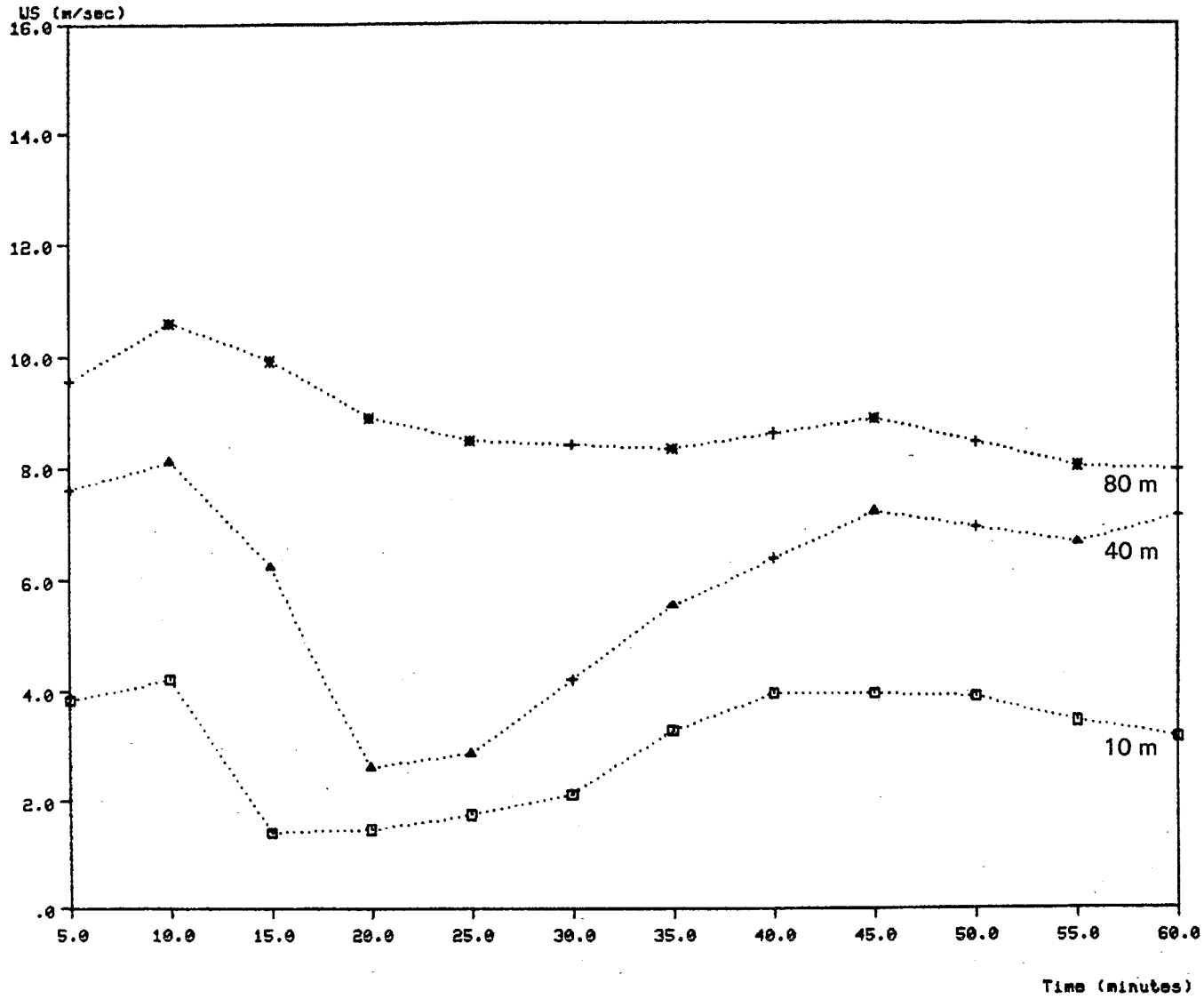

Figure 105. Tower A wind speeds during Experiment 210, Hour 7 (0600-0700 MST).

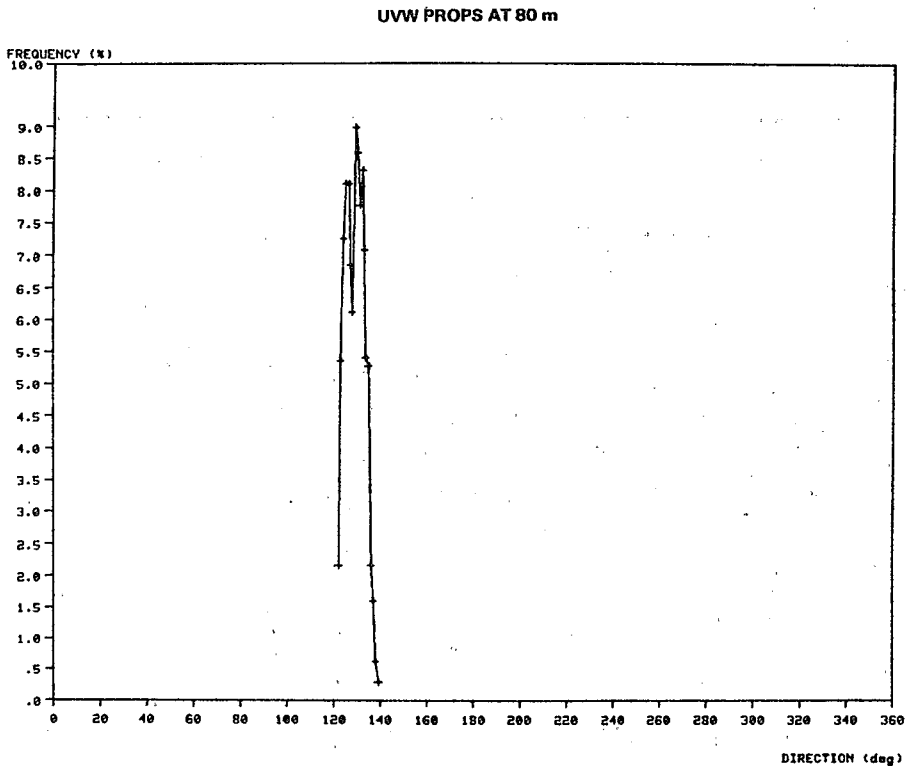

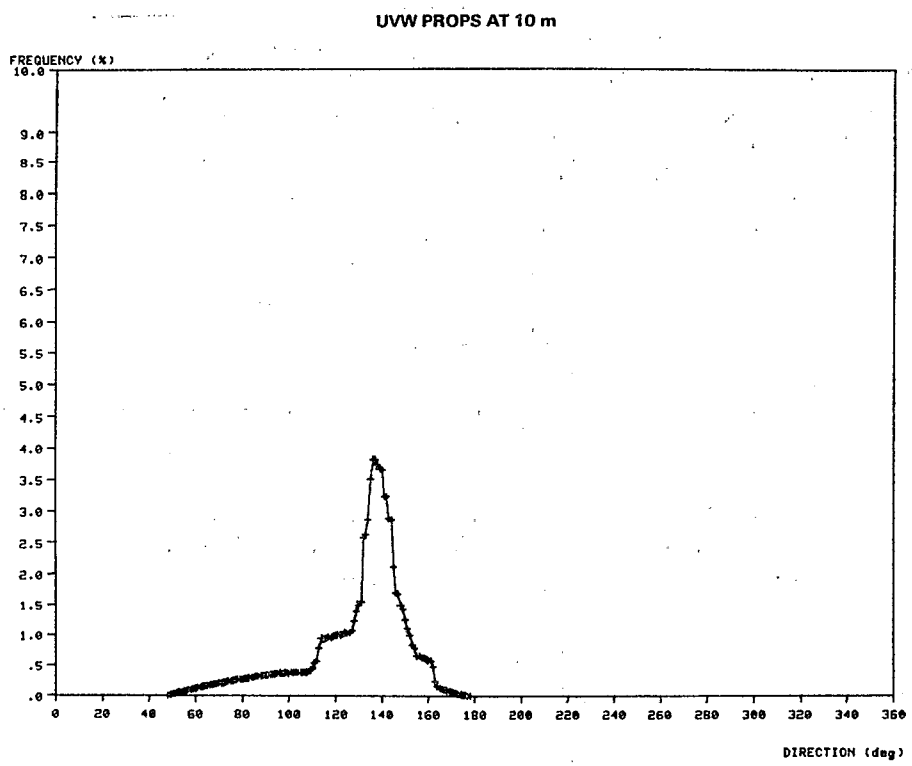

Figure 106. Calculated wind direction distribution functions for Experiment 210, Hour 7 (0600-0700 MST).

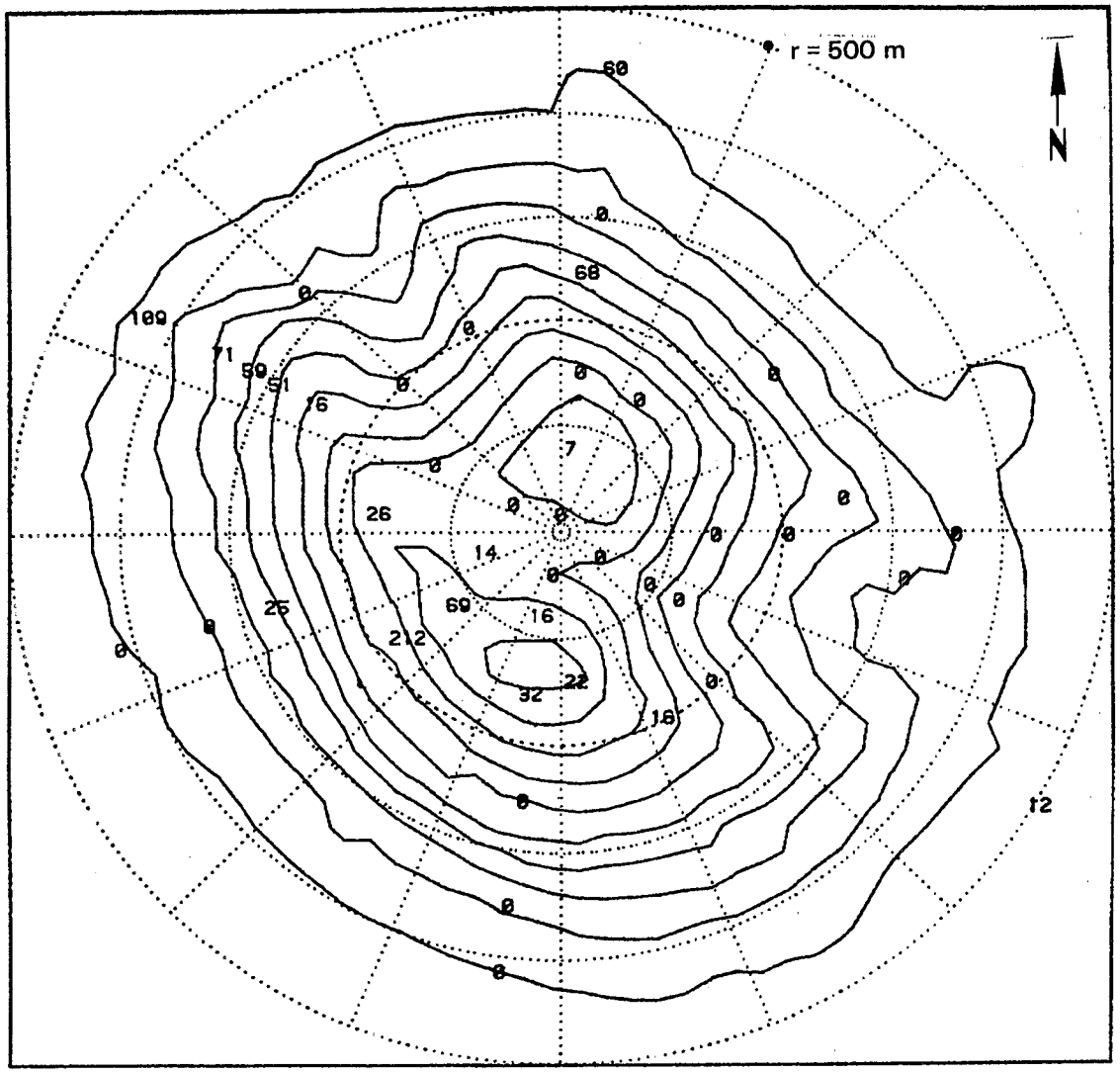

Figure 107. Observed SF_6 concentrations (ppt) for Experiment 210, Hour 7 (0600-0700 MST). Source: r = 1086.2 m, θ = 122.2°, net height = 49.8 m, Q = .178 g/s.

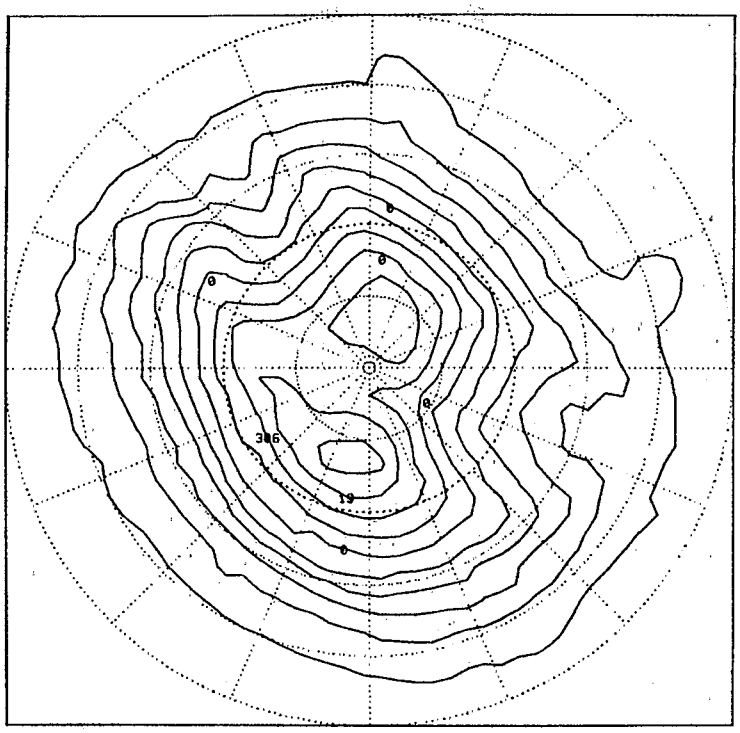

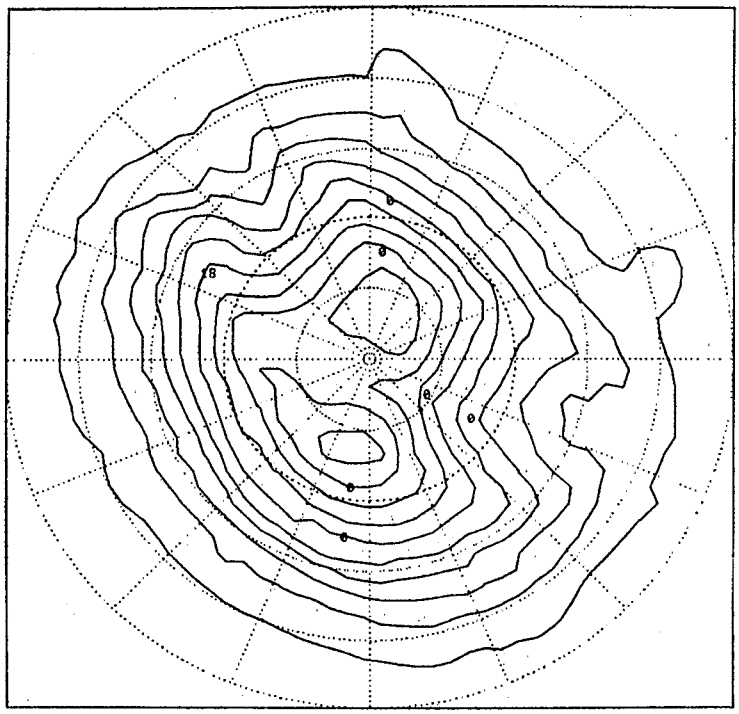

Figure 108. Observed 10-minute average SF_6 concentrations (ppt) for Experiment 210, Hour 7 (0600-0700 MST).

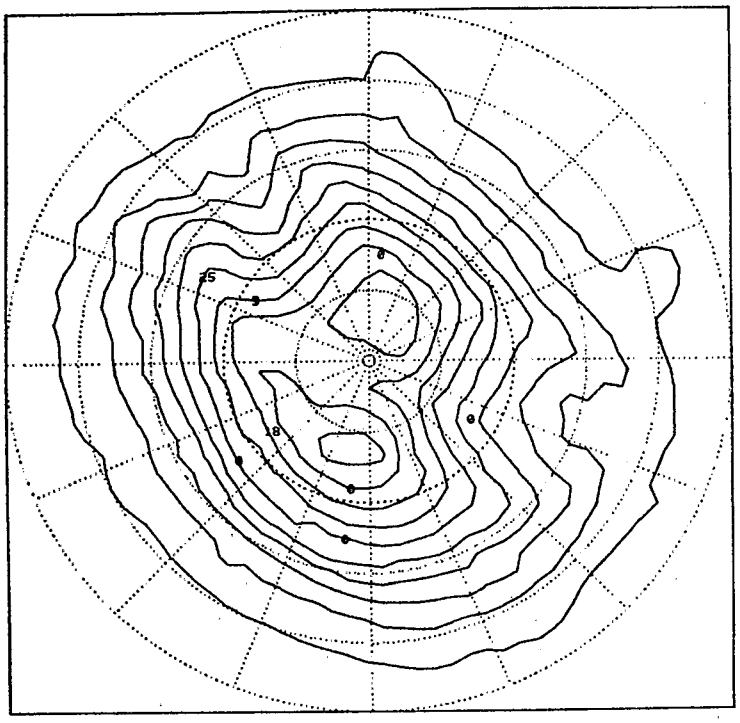

TIME PERIOD 0620-0630

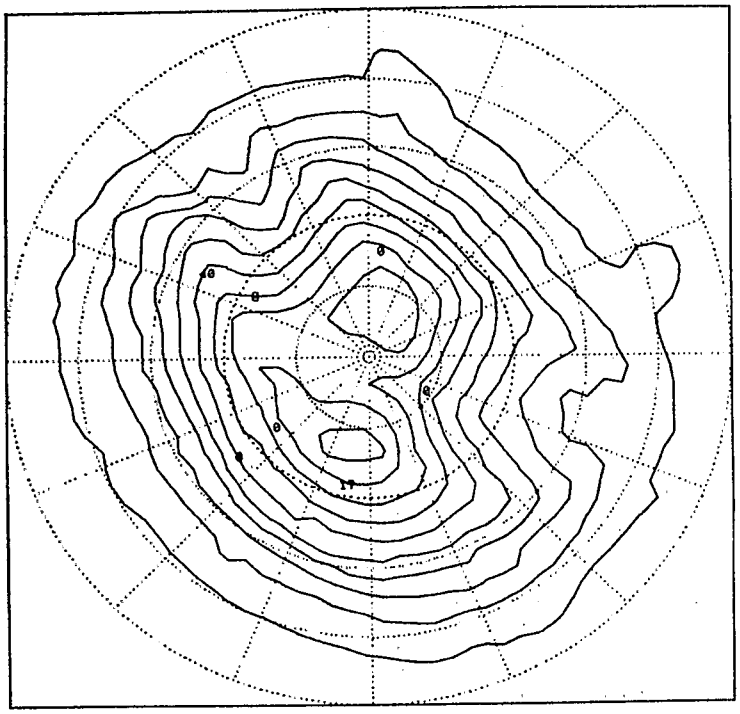

TIME PERIOD 0630-0640

Figure 108. Continued.

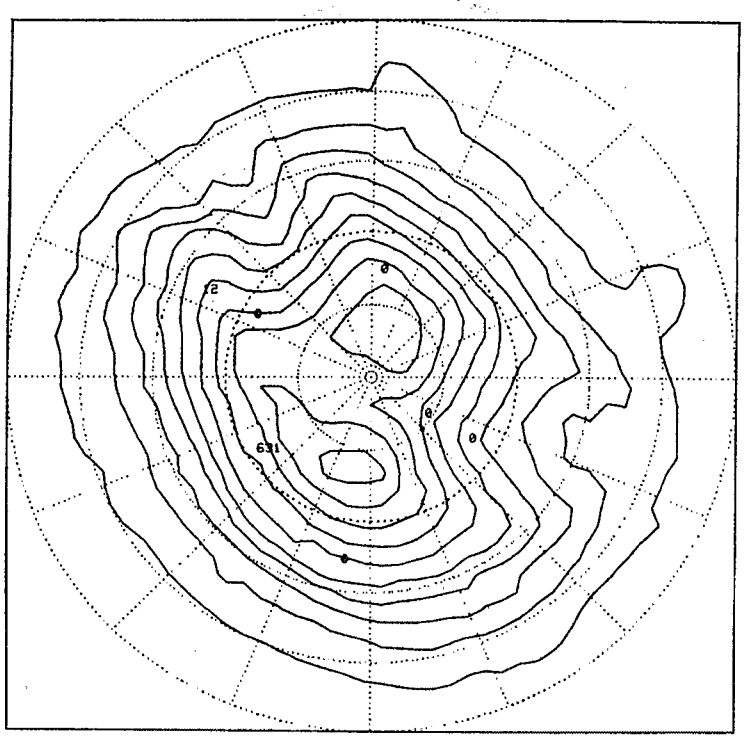

TIME PERIOD 0640-0650

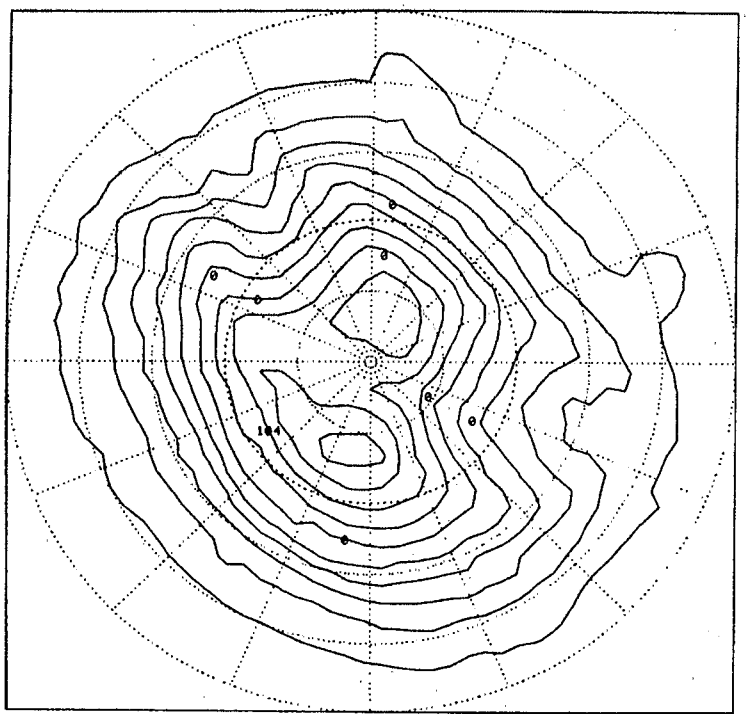

TIME PERIOD 0650-0700

Figure 108. Continued.

4.12.2 Model Performance

This hour has been modeled with the Lift model because all evidence indicates that streamlines at plume height traveled freely over the hill. Meteorology used in the modeling was prepared as in Section 4.1.2, and the data is summarized in Table 15. The 1-hour average wind directions measured 48 m below and 22 m above the release height are both 130°, although the peak of the PDF for each of these heights is considerably different. Wind directions measured at 10 m and 30 m on tower B are 118° and 123°, respectively, and directions inferred from the photographs during the first half hour lie between 117° and 120°. Therefore, considerable weight is given the data from 10 m on tower B, and the model wind direction is set to 118°. The 80 m PDF is deemed more appropriate than that from 10 m.

Neutral was rerun with the new meteorological data, and instead of estimating a peak value that is 92% of the observed peak value, it produced a value 112% of the peak observed. The peak observed value occurs in the lee of the south peak, and the modeled maximum occurs near the top of the windward face of the south peak. Figure 109 shows the distribution of calculated concentrations plotted on a map of CCB, and the results are also summarized in Table 15.

Results from Lift computations are also displayed in Figure 109 and in Table 15. The maximum occurs near the top of the hill and is 89% of the highest observed value. The model overestimates most of the observed concentrations, particularly on the windward side of the hill, over the south peak, and on the saddle. Concentrations in the lee are overestimated to a lesser degree. The degree of overestimation on the south peak produces a terrain factor (T_o) of 1.5 to 1.7, and that near the base of the hill in the lee produces T_o values between 1.0 and 1.4.

4.13 Experiment 211, Hour 1 (0000-0100 MST)

4.13.1 Summary Description

Thermofogger oil-fog, SF_6, and Freon were released from the east-southeast side of the hill at 1001.2 m, 101.4°. The SF_6 release began at 2350 and continued throughout the hour from a height of 30 m. The oil fogger started a half hour earlier at the same height, but stopped at 0055. The Freon release did not begin until 0045, released from a height of 20 m. The Freon samples are certainly not representative of a 1-hour average.

Local terrain elevations near the release point are estimated to be -4.7 m relative to the zero of the hill coordinate system, so the net release height of the SF_6 and the oil-fog corresponds to the 25.3 m height level on the hill, and that for Freon corresponds to the 15.3 m height level. The SF_6 release rate is computed to be 0.179 g/s with an estimated uncertainty of $\pm 5.1\%$. The Freon rate cannot be computed from the field log, but is estimated to be about 1.0 g/s. No Freon concentration patterns have been modeled for this hour.

TABLE 15. NEUTRAL AND LIFT MODEL CALCULATIONS - EXPERIMENT 210, CASE HOUR 7

Meteorological Data

wind direction(deg)	=	118.
wind speed(m/s)	=	7.3
critical dividing streamline height(m)	=	14.0
Iz	=	.057
Iy	=	.108
N(1/s)	=	.035

Source Data

direction(deg)	=	122.
distance(m)	=	1086.2
release height(m)	=	58.0
SF6 emission rate(g/s)	=	.178

Receptor Coordinates X(m)	Y(m)	Z(m)	Observed SF6 (ppt)	Neutral Predicted SF6 (ppt)	Lift Predicted SF6 (ppt)
360.22	.00	13.26	.00	1.47	.00
208.35	.00	31.25	.00	34.42	.00
142.00	.00	50.00	.00	84.07	13.64
257.78	33.94	30.00	.00	9.10	.00
195.15	149.74	27.41	.00	2.66	.00
72.99	126.43	77.02	.00	58.11	.00
66.60	505.92	-6.52	.00	.02	.00
58.64	445.44	3.38	60.40	.09	.00
40.17	305.14	22.10	.00	2.12	.00
32.61	247.73	41.74	68.40	7.68	.00
20.07	152.45	81.06	.07	67.70	.00
10.61	80.56	91.97	6.90	119.57	33.54
2.15	18.88	80.00	.20	158.26	113.75
-66.52	-505.24	-3.54	.00	.02	.00
-53.69	-407.79	3.82	.00	1.10	.00
-45.46	-345.28	13.70	.00	7.50	.00
-32.79	-249.09	48.82	.00	75.49	.00
-19.85	-149.12	90.00	31.80	229.15	173.60
-9.85	-76.12	90.00	16.40	214.38	182.86
-4.85	-37.12	80.00	.20	197.31	164.50
-125.24	-96.10	78.81	211.68	197.53	166.94
-84.85	-65.12	90.00	68.80	204.65	127.23
-396.68	-106.29	3.44	.00	34.85	.00
-315.76	-84.61	13.24	.00	61.80	102.17
-248.96	-66.71	32.90	24.80	107.56	158.22
-60.85	-16.12	80.00	14.20	190.52	161.20
21.74	-137.29	90.00	21.70	238.27	147.93
137.89	-137.89	50.00	.00	238.30	187.70
441.46	-254.87	-2.45	11.50	51.90	87.20
108.15	-61.12	50.00	.00	173.71	117.62
82.15	-46.12	60.00	.04	186.00	153.09
37.15	-21.12	70.00	.00	178.39	151.20
312.38	-41.13	14.00	.20	11.38	.00
-157.38	20.72	83.35	26.30	176.69	171.08
-359.96	207.82	8.94	109.00	73.89	123.64
-297.11	171.54	28.07	70.90	97.12	128.28
-269.62	155.66	38.07	59.30	110.48	130.34
-246.20	142.14	47.96	50.50	124.06	132.10
-111.85	65.88	80.00	.20	154.01	141.95
-40.85	28.88	80.00	.20	162.18	146.63
-141.42	141.42	50.00	.20	99.90	102.86
-229.81	229.81	30.00	.10	61.87	39.75
-80.75	194.94	50.00	.20	48.04	5.72

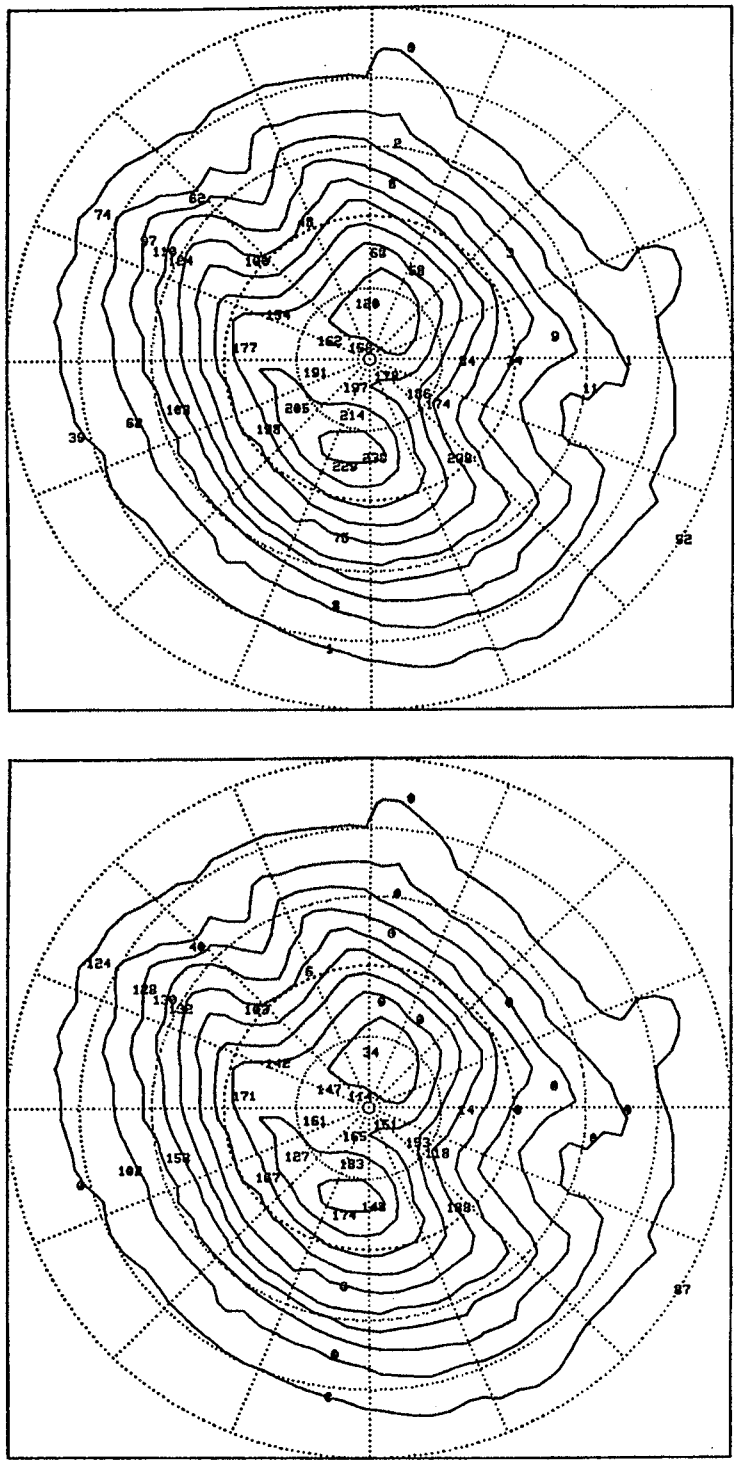

Figure 109. SF_6 concentrations (ppt) estimated for Experiment 210, Hour 7 by the Neutral (top) and Lift (bottom) models.

Plume Observations

The record of observer comments about the plume appearance and trajectory during this hour is presented below.

Time: 2350 SF_6 release started from E-1 at 30 m. Plume now appears to be heading over the east knoll.

Time: 2355 The fogger is up and I believe the tracer has started. The plume seems to be running south of the hill at this time. There is a great deal of mixing and vertical loops in the plume.

Time: 0000 I see a good deal of vertical mixing in plume.

Time: 0004 At the present time the plume is heading to the north of the butte, and it looks very stable. Approximately 5 minutes ago, the winds were light and variable. The plume did a complete 360 in its trajectory.

Time: 0005 Plume looks more stable now.

Time: 0006 The plume, after smearing and even doing 360 is headed around the north side of the hill and the first 1/3 of travel, on the plume, looks much more stable than the 2/3 that has gone out.

Time: 0011 The plume seems to be settled in and going around the north side right over the northeast knoll, and it is looking very stable at this time. The spotlight is going on the extension of the mobile crane road.

Time: 0015 Plume is back over the east knoll. The plume seems to have bend in it, and to my perspective it looks like it goes out horizontally and then begins to turn around the hill fairly early, considerably before it reaches road F. ERT 1 is describing the plume as a "pencil beam" at the moment. It is very compact. ERT 1 is also describing it as having a very dense central core.

Time: 0020 The plume is getting closer to the north side. ERT 1 is referring to it as a piece of yarn.

Time: 0022 The plume centerline is continuing to move towards the south and the plume centerline now appears to be directly towards the FAA tower. The horizontal dispersion has increased significantly as it is moving in that direction.

Time: 0025 The plume centerline now would take the plume significantly south of the hill and the horizontal dispersion still seems to be quite significant. The plume is south of the butte now.

Time: 0028 (?) The plume has definitely shifted toward the hill and is now looking considerably wider, and wispy, and with a lot of horizontal spreading. Looking north-northeast, it looks like the plume has been coming very close to the hill at that point.

Time: 0030 The plume has swung so it is headed more toward tower D. I can see some plume going in the vicinity of the draw and possibly up the draw. The plume is looking quite a bit wider and more difuse, a very radical change from what it was 10 or 12 minutes ago.

Time: 0035 Plume is headed toward the draw.

Time: 0038 The plume has moved back to the north side and is going around the north and the plume near the source is going back to that very stable coherent pencil beam look.

Time: 0040 The plume is going entirely north of the hill. It is very collimated and narrow and stable looking.

Time: 0051 The plume is going to the south, and the thermofogger is being brought down this time to check on some problems. The gas keeps on going now, since we've got those ropes holding up the tubes.

Time: 0107 The thermofogger is back up. The low level was going to the south, and the higher level flow looks like its going to the SW, and it should miss the butte. The wind is kind of rocking the car, I'm sitting here near tower B.

These comments indicate that the oil-fog plume trajectory varied over the hour from one side of the hill to the other. After initial wandering, the plume took on a stable appearance as it traveled around the hill on the north side, and it remained on the north side for most of the first half hour. By the fifth 5-minute period, however, it moved in close to the north peak and then shifted to the south side of the hill. As it crossed the hill, the horizontal spread increased significantly.

During period 7 the plume moved back between the two peaks, but within the next 5-minute period, it had swung over to the north side once again. It stayed to the north side until the last 10-15 minutes in the hour, when it again switched to the south. This sequence is documented in the photographs.

Only one view of the plume was suitable for analysis during this hour. It was taken from the top of the north peak at camera location 0-15 (see Figure 46). The camera was aimed toward magnetic bearings 105°, 90°, and 100° over the course of the hour. Each photo is a 5-minute exposure.

Some lidar data are also available for this hour. The lidar sampled the plume along five planes: two upwind of the hill and three over the hill. Plume centroid positions in these planes are presented in Figure 110. Most of the plume segment sampled followed trajectories toward

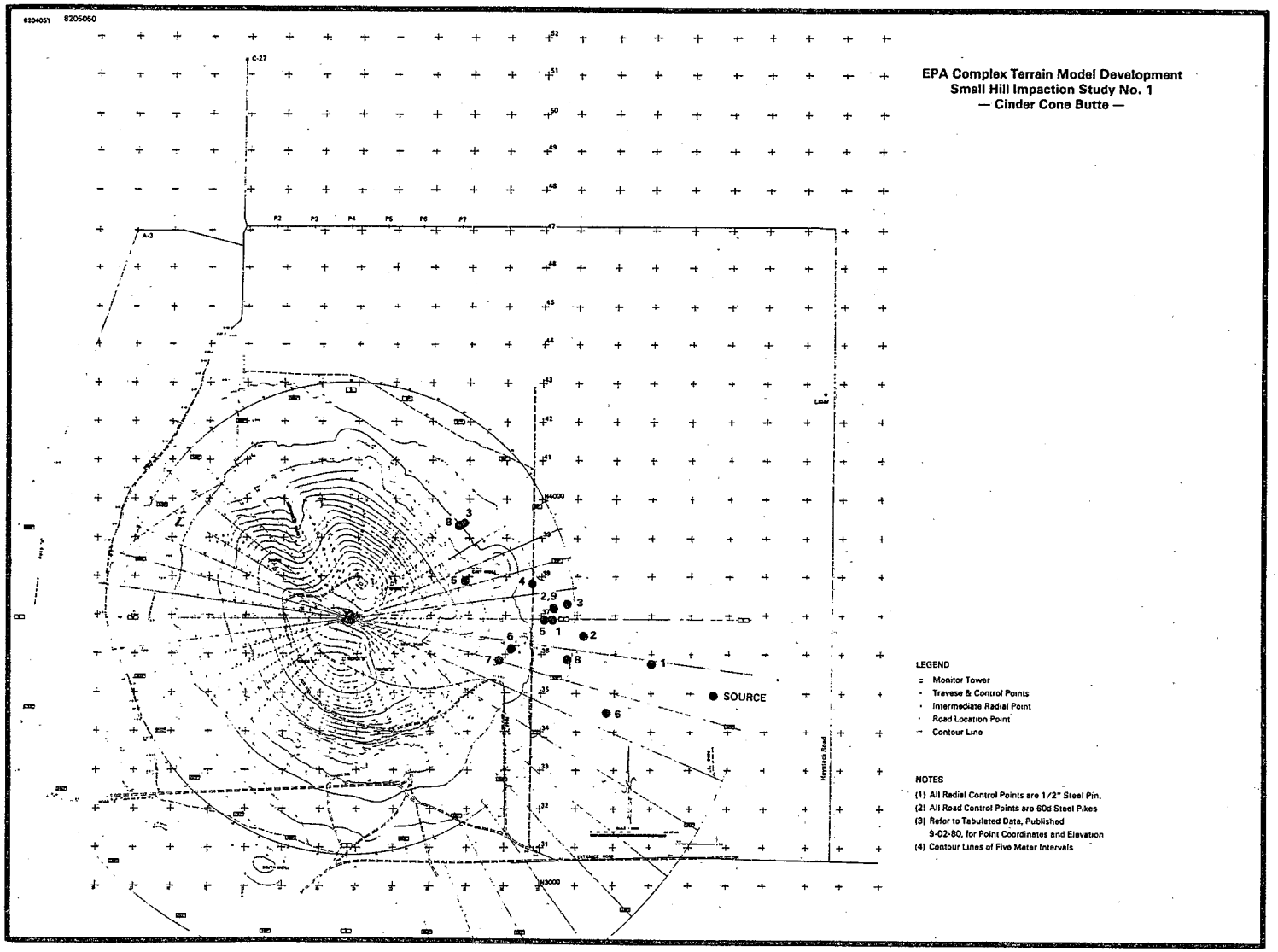

Figure 110. Plume centroid positions calculated from lidar data. Experiment 211, Hour 1 (0000-0100 MST).

the north side of the hill. These occurred during periods 1-5, 8, and 9. Periods 6 and 7 show the most tendency for plume travel toward the southern part of the hill, and this is consistent with the photographs.

Inferred wind direction estimates for the release height have been calculated based on the centroid positions closest to the source. They range from 73° to 118°. Because the source was located along the 101° ray, this range indicates that the wind trajectory carried the plume material well to the north and south of the hill at times.

Meteorological Information

Wind and temperature data measured at tower A during the hour have been used to characterize the flow in terms of H_c. However, because of a partial failure of the 40 m wind set, 40 m winds were estimated for each 5-minute period before H_c was calculated. The method followed in calculating speeds at 40 m was outlined in Section 4.4.1.

The average H_c over the hour is 45 m, and Fr_H above this height is 2.9. Because the SF_6 plume was released at 30 m, it was well below the computed dividing streamline of the flow. Figure 111 contains a time series plot of the calculated 5-minute values of H_c and Fr_H. H_c shows a weak tendency to increase during the hour, but the trend is small compared to the scatter about it. H_c tends to vary by 5 m about its mean value. Fr_H for the flow above H_c follows a stronger trend toward increasing values, but this is of little consequence because the tracer was released below H_c. Small variations in H_c illustrated in the plot are likely to have had only a small effect on surface concentrations, so the mean value should adequately characterize the hour.

Hourly averaged wind speeds measured at 10 m and estimated at 40 m on tower A are 2.2 and 1.8 m/s, respectively. The decrease from 10 m to 40 m may not be significant, however, because of the uncertainty inherent in estimating the 40 m wind speeds. The direction at 10 m was 353° and that at 80 m (which was used to estimate the 40 m winds) was 128°. With this kind of wind shear and light 2 m/s wind speeds, an estimation of the wind directions characteristic of the release height is subject to considerable error.

Figure 112 shows the trend in wind speeds between 10 and 80 m. The estimated 40 m wind speeds tend to follow the 80 m speeds, while the trend in the 10 m speeds remains distinctly different throughout the hour. It therefore seems likely that the low-level flow exerts only a small influence on the flow at 40 m, but it is not clear if the same can be said for its influence on the flow at 30 m.

Variations in wind directions measured at 10 m and 80 m are shown in Figure 113 as frequency distributions. Because the 80 m distribution spans 20° rather than 100°, it is considered more representative of the flow at release height. Two peaks can be seen in the distribution; this corroborates the photographic record, which shows the plume lying primarily on one side of the hill or the other.

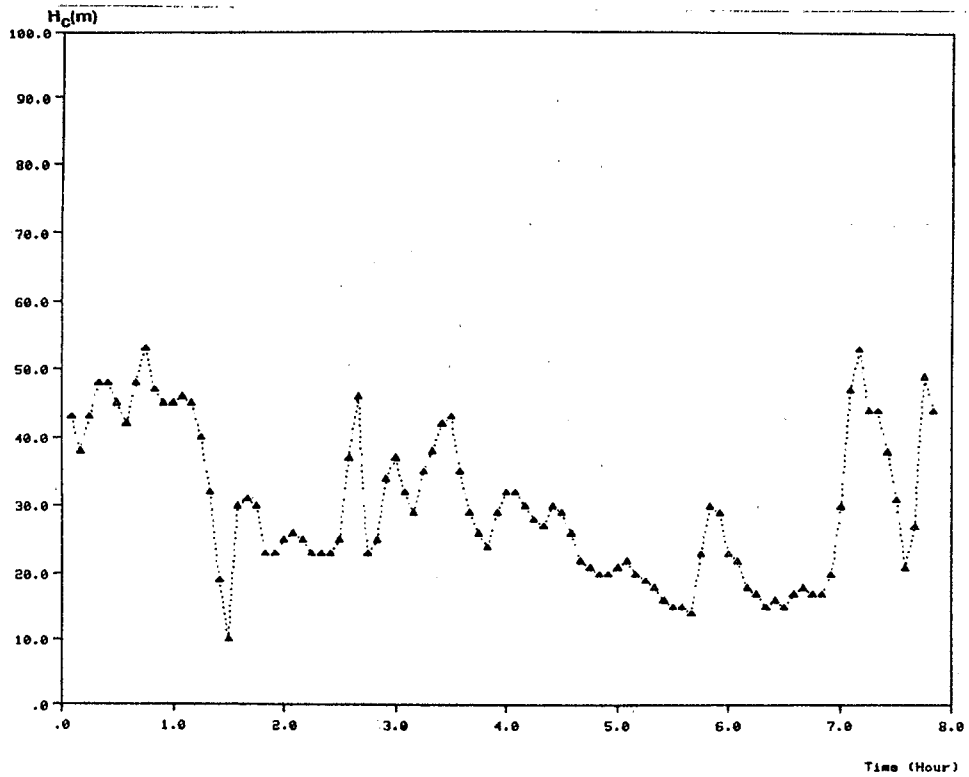

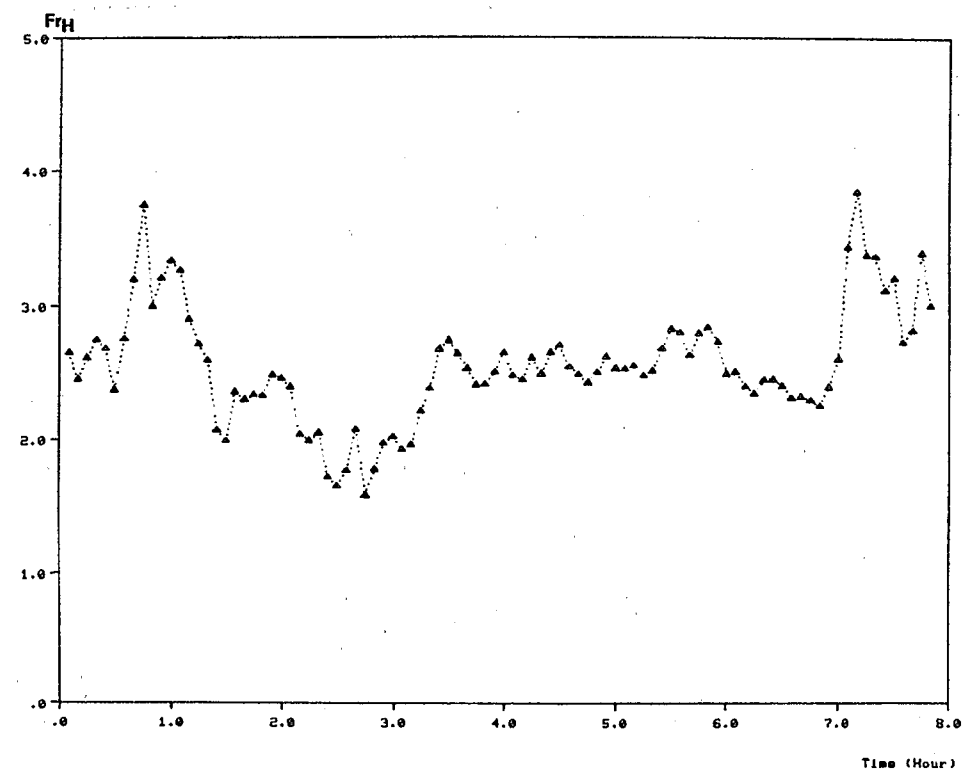

Figure 111. Calculated dividing streamline heights (H_c) and bulk hill Froude numbers above H_c (Fr_H) for Experiment 211.

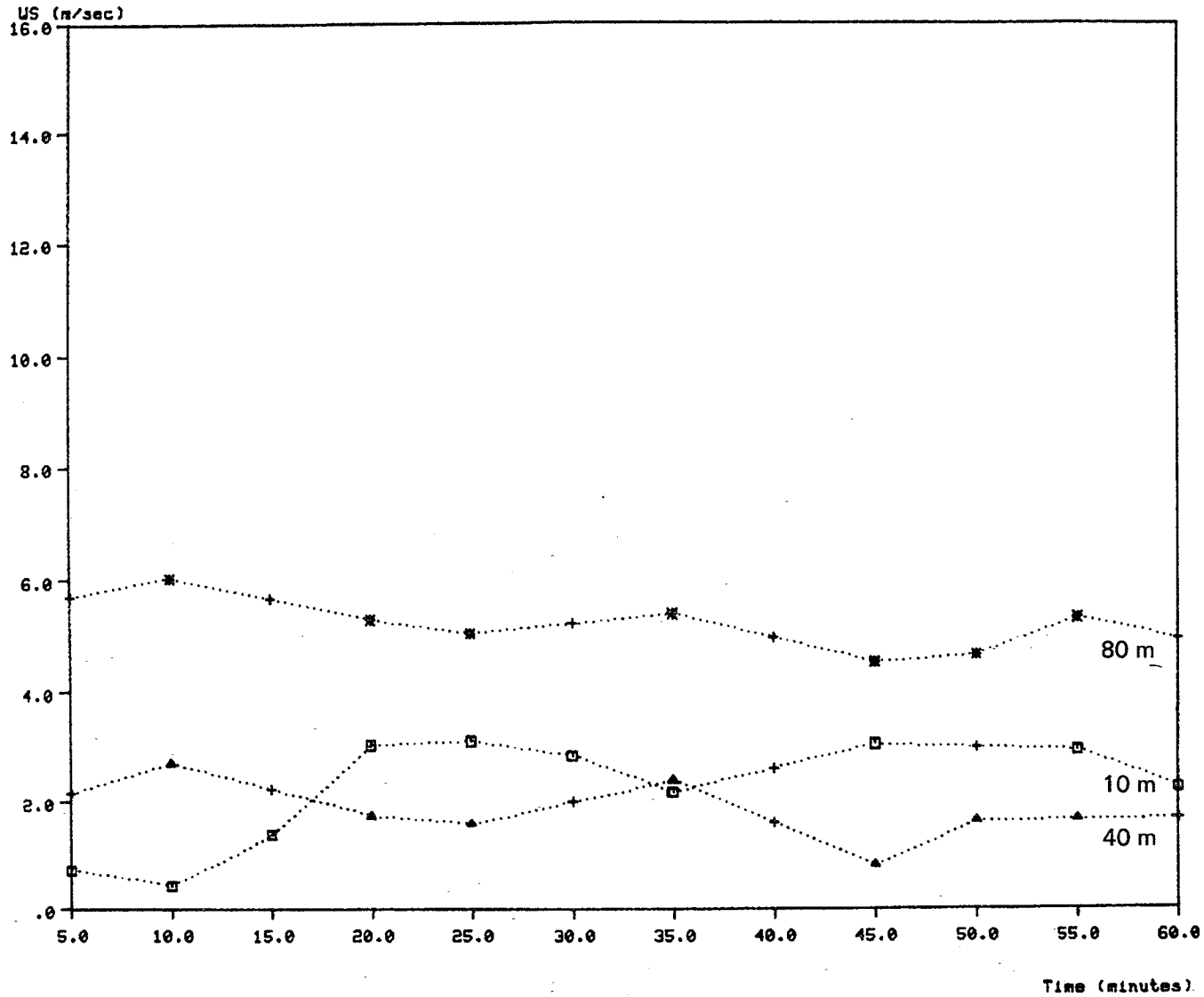

Figure 112. Tower A wind speeds during Experiment 211, Hour 1 (0000-0100 MST).

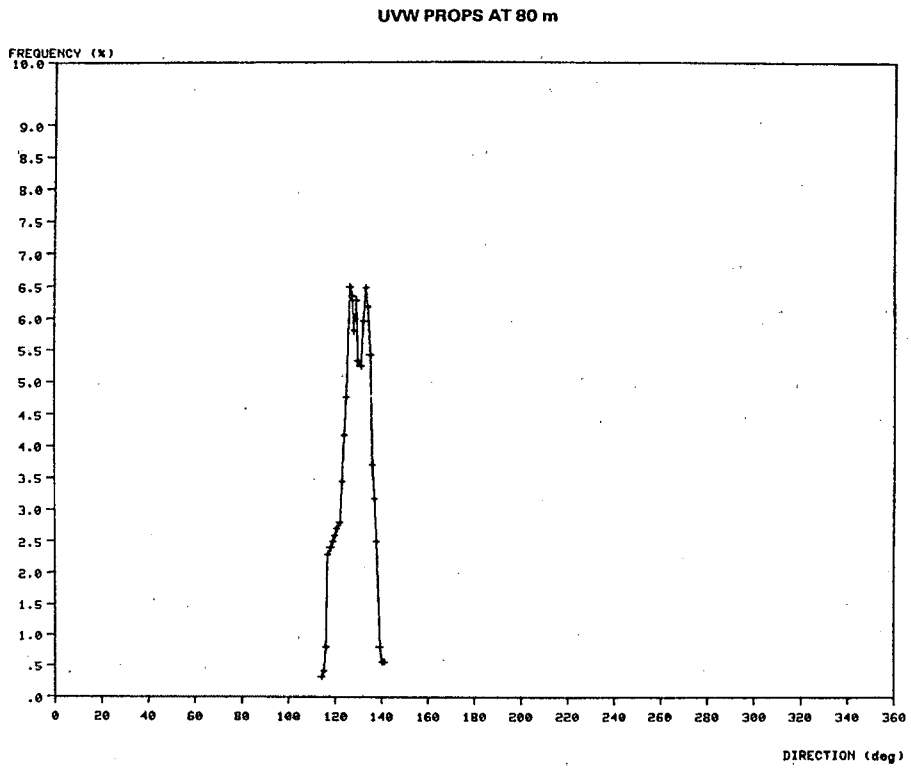

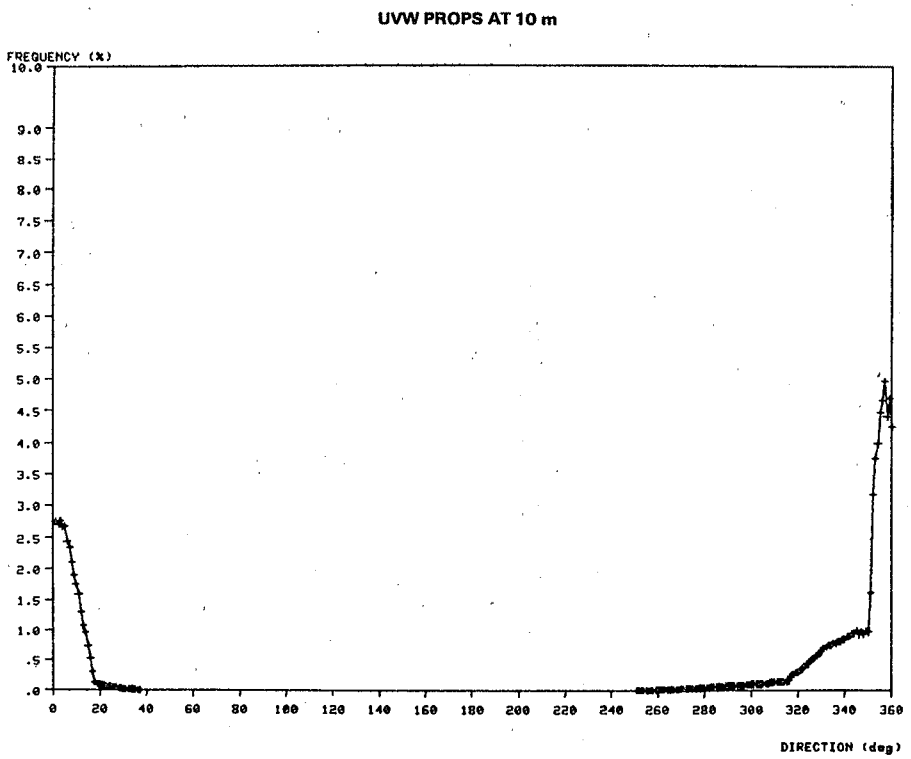

Figure 113. Calculated wind direction distribution functions for Experiment 211, Hour 1 (0000-0100 MST).

In summary, during this hour the plume was released into the flow substantially below H_c. Wind speeds were less than or nearly equal to 2 m/s, and variable; and are therefore difficult to characterize at the release height. The 80 m wind direction distribution, however, appears to be similar to what can be observed in the photographs.

SF_6 Concentrations

The distribution of hourly averaged SF_6 concentrations over the surface of the hill is shown in Figure 114. Highest concentrations are measured across the lower portion of the southeast draw from the 0 m contour to the 30-35 m contour. Moderately high concentrations cover the rest of the hill.

This pattern suggests that, with a relative release height of 25 m, the plume impinged on the hill surface near the draw consistently during the hour, and mixed enough in the vertical to produce a concentration maximum below the height of the plume centerline. However, the record of observations and the photographs indicate otherwise. The SF_6 pattern does not match what would be expected from the appearance and trajectory of the oil-fog plume over the hour.

The distribution of 10-minute average SF_6 concentrations presented in Figure 115, however, indicates that tracer material reached the hill several times during the hour even though this was not apparent from the photographs. Substantial concentrations are measured near the 60 m height contour in the southeast draw in four of the six 10-minute periods.

4.13.2 Model Performance

This hour has been modeled with the Wrap model because the plume was released significantly below the calculated dividing streamline height. Meteorological data were prepared for the release height as in Section 4.1.2, and the resulting values are listed in Table 16. Wind directions measured at tower A and tower B are not very helpful in selecting an appropriate wind direction for use in the modeling. The 10 m directions average to 353° and the 80 m directions average to 128° on tower A, whereas the directions at 10 m and 30 m on tower B average to 117° and 124°, respectively. The lidar data indicate that the mean direction should lie between 73° and 118°, and the photographs show the plume frequently on both sides of the hill. Therefore, the mean wind direction has been set equal to the direction from the source to the north peak (or 107°) because the plume appears to spend more time on the north side of the hill than on the south side. The 80 m PDF is also used because the 10 m PDF seems to be inappropriate.

Concentration estimates from both Impingement and Wrap are listed in Table 16 and plotted on a map of CCB in Figure 116. Although the observed SF_6 concentration distribution pattern was thought odd when compared with the photographs of the plume, the Wrap estimates are, in general,

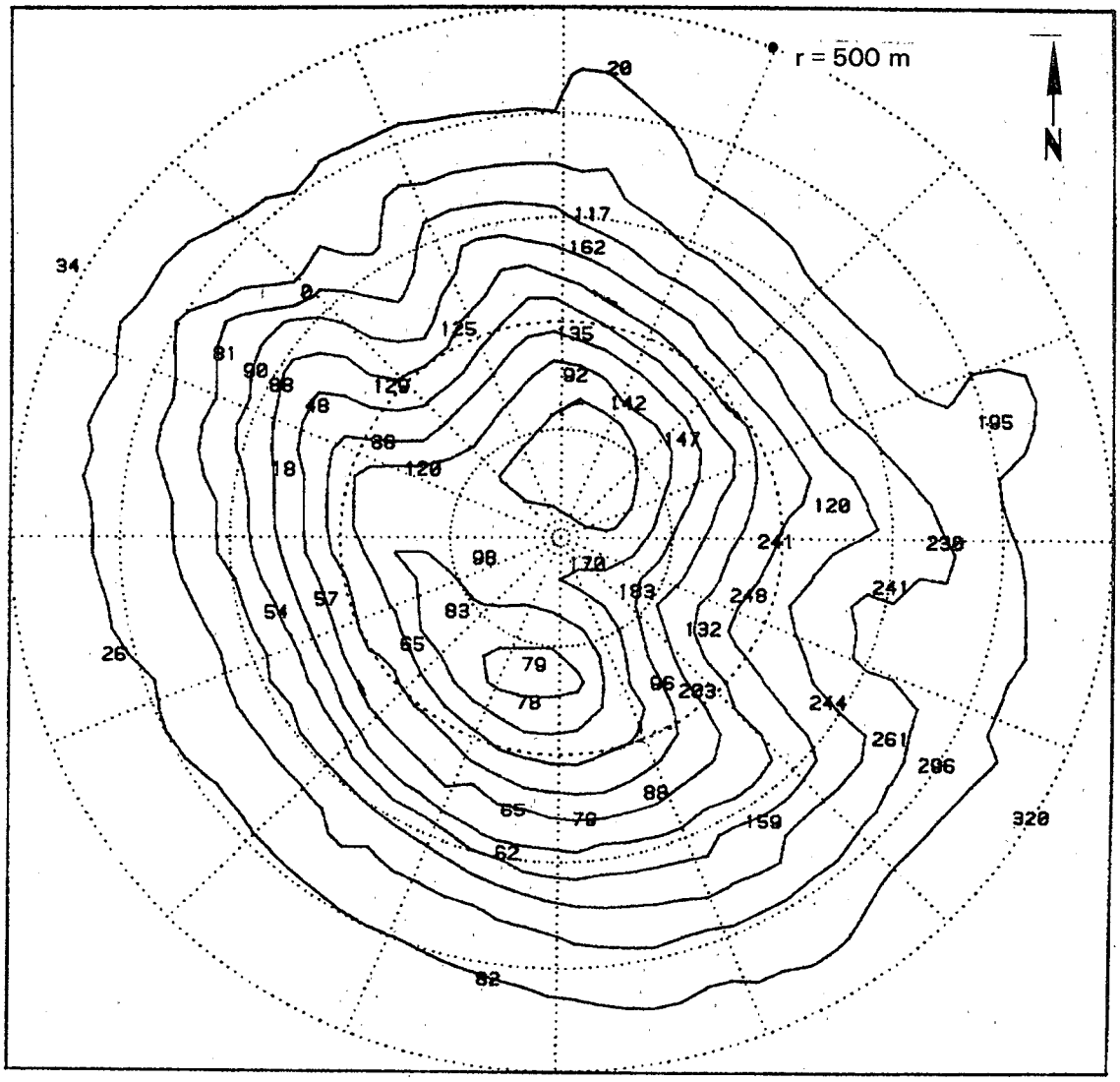

Figure 114. Observed SF_6 concentrations (ppt) for Experiment 211, Hour 1 (0000-0100 MST). Source: r = 1001.2 m, θ = 101.4°, net height = 25.3 m, Q = .179 g/s.

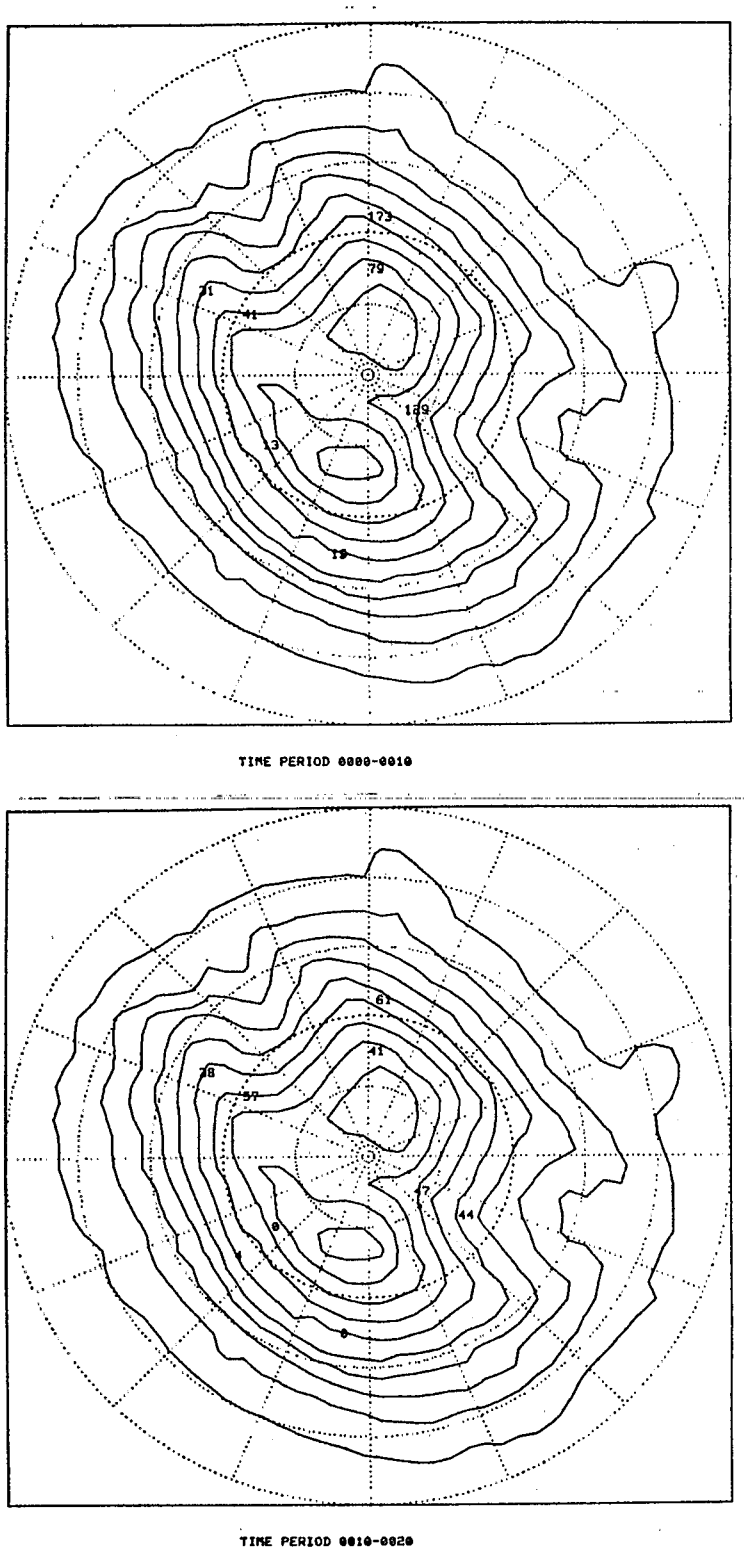

Figure 115. Observed 10-minute average SF_6 concentrations (ppt) for Experiment 211, Hour 1 (0000-0100 MST).

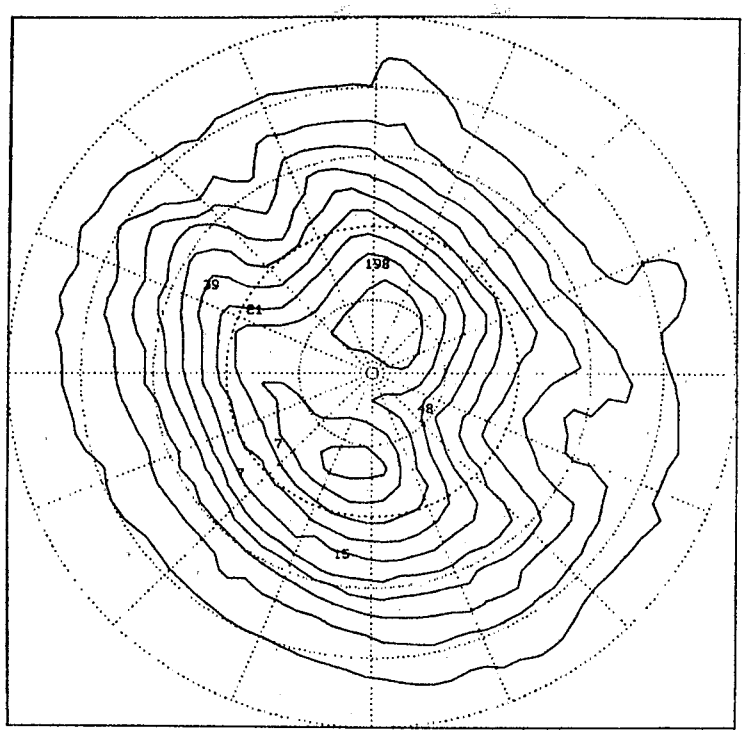

TIME PERIOD 0020-0030

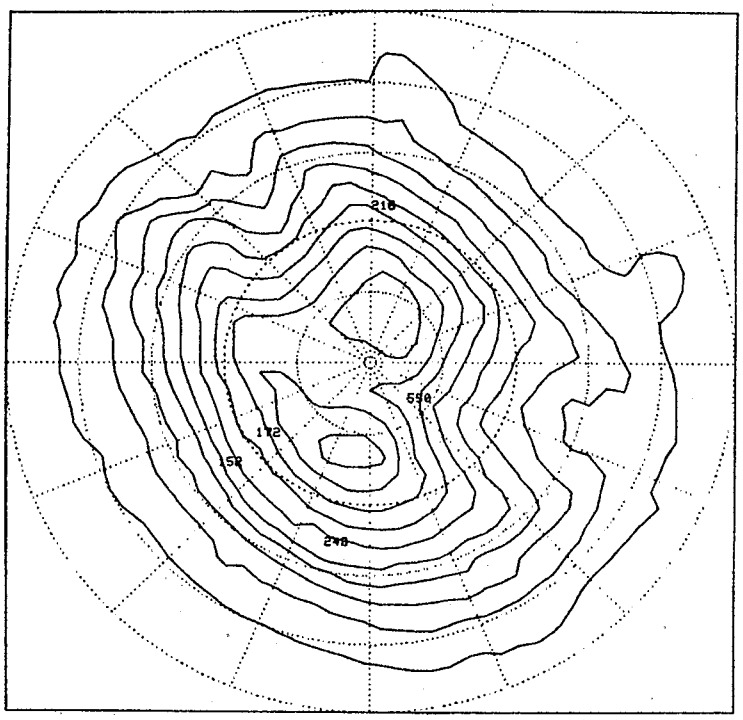

TIME PERIOD 0030-0040

Figure 115. Continued.

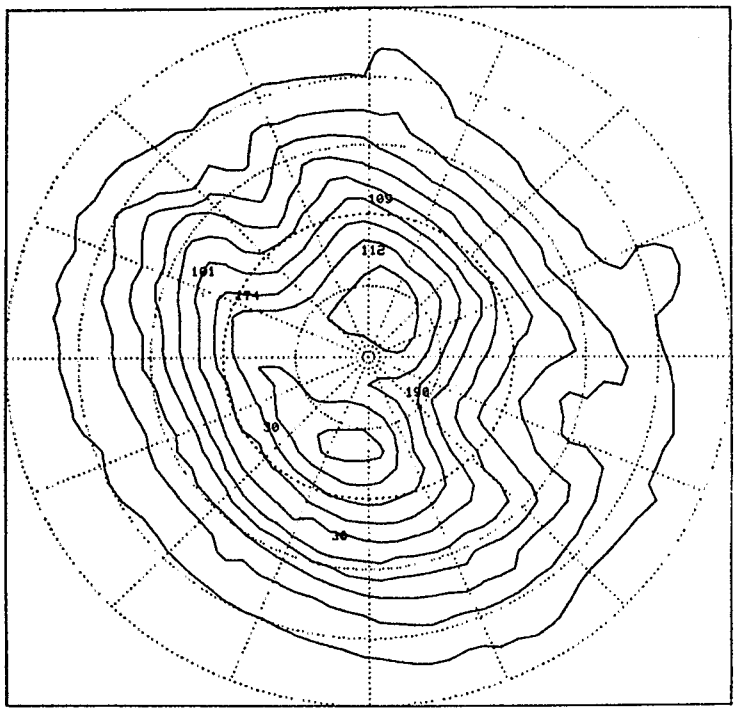

TIME PERIOD 0040-0050

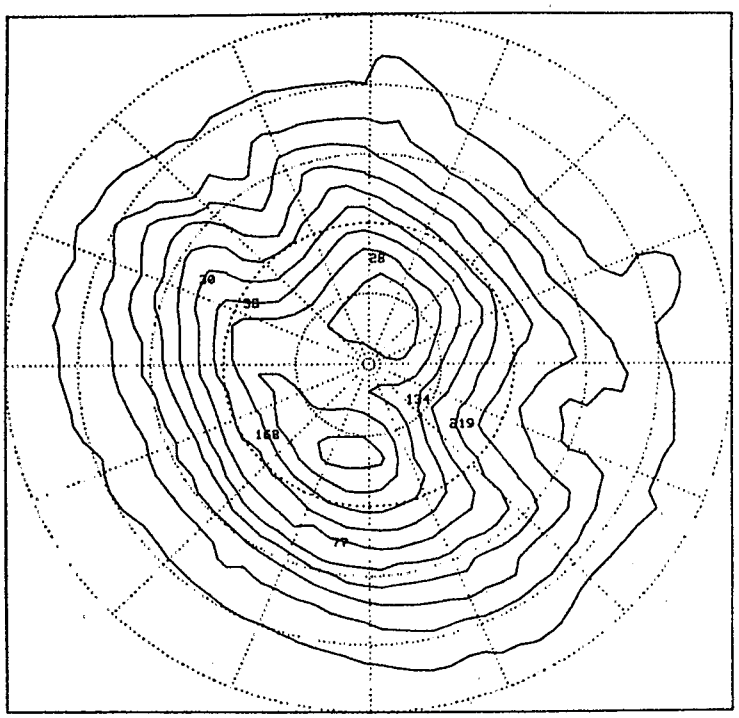

TIME PERIOD 0050-0100

Figure 115. Continued.

TABLE 16. IMPINGEMENT AND WRAP MODEL CLACULATIONS - EXPERIMENT 211, CASE HOUR 1

Meteorological Data

wind direction(deg)	=	107.
wind speed(m/s)	=	1.9
critical dividing streamline height(m)	=	45.0
Iz	=	.084
Iy	=	.326
N(1/s)	=	.058

Source Data

direction(deg)	=	101.
distance(m)	=	1001.2
release height(m)	=	30.0
SF6 emission rate(g/s)	=	.179

Receptor Coordinates X(m)	Y(m)	Z(m)	Observed SF6 (ppt)	Impingement Predicted SF6 (ppt)	Wrap Predicted SF6 (ppt)
360.22	.00	13.26	229.50	343.70	471.25
208.35	.00	31.25	241.20	502.79	807.87
257.78	33.94	30.00	119.90	472.17	758.40
404.91	111.59	10.00	194.70	268.00	350.15
72.99	126.43	77.02	141.60	34.39	22.74
58.64	445.44	3.38	20.10	144.95	179.14
40.17	305.14	22.10	116.90	262.45	408.76
35.92	272.83	31.92	162.40	276.98	440.54
20.07	152.45	81.06	91.66	25.35	15.88
25.15	190.88	65.00	134.60	90.21	92.68
-53.69	-407.79	3.82	82.10	152.15	188.04
-38.04	-288.98	32.94	61.50	288.98	459.05
-32.79	-249.09	48.82	64.85	208.29	291.09
-15.01	-113.99	98.96	78.80	3.21	.88
-19.85	-149.12	90.00	78.40	9.61	4.03
-125.24	-96.10	78.81	65.05	33.58	25.73
-84.85	-65.12	90.00	82.50	12.67	6.69
-396.68	-106.29	3.44	25.90	119.64	155.64
-248.96	-66.71	32.90	53.90	200.77	317.75
-204.16	-54.70	52.26	57.20	139.82	192.95
-60.85	-16.12	80.00	97.80	31.57	24.80
31.69	-258.06	50.00	78.60	213.42	290.42
95.80	-231.27	52.96	88.10	200.61	255.36
199.06	-259.43	30.00	158.80	395.47	633.19
137.89	-137.89	50.00	202.50	258.43	340.23
441.46	-254.87	-2.45	320.20	119.19	108.24
355.15	-205.04	5.69	296.30	218.21	254.46
313.62	-181.07	15.29	260.60	356.51	509.30
256.81	-148.27	25.29	243.60	459.80	729.74
82.15	-46.12	60.00	182.87	145.77	143.49
37.15	-21.12	70.00	170.20	58.12	39.15
183.53	-49.18	30.00	247.60	540.76	870.89
312.38	-41.13	14.00	240.50	373.98	516.29
-243.41	65.22	50.00	17.80	137.79	196.77
-441.92	255.14	-.90	33.60	97.46	119.00
-297.11	171.54	28.07	80.90	194.15	307.57
-269.62	155.66	38.07	90.00	185.69	289.26
-246.20	142.14	47.96	88.20	154.12	223.77
-153.85	89.88	70.00	66.12	61.10	62.51
-111.85	65.88	80.00	120.00	31.80	25.42
-141.42	141.42	50.00	129.10	154.37	218.27
-229.81	229.81	30.00	.00	209.23	332.06
-80.75	194.94	50.00	125.00	169.06	236.88

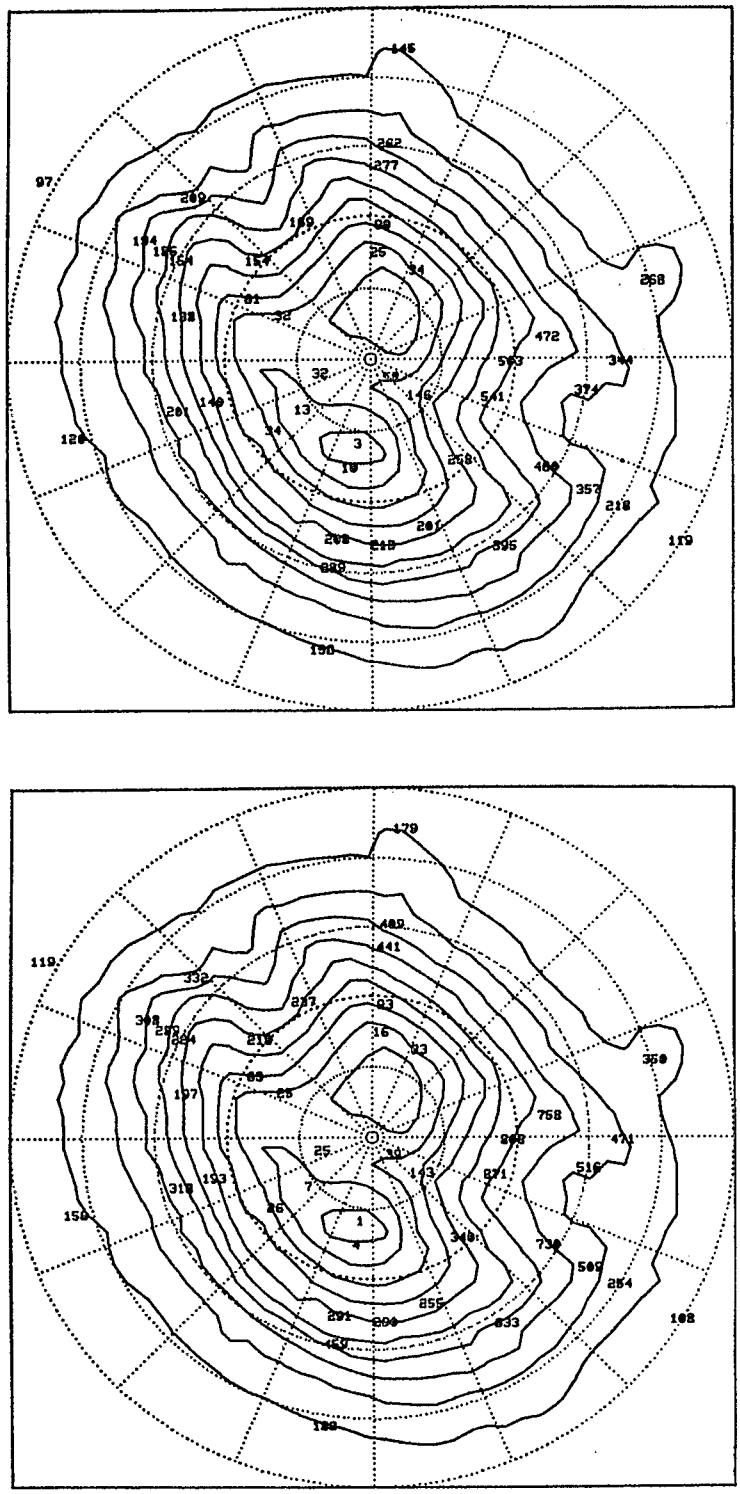

Figure 116. SF_6 concentrations (ppt) estimated for Experiment 211, Hour 1 by the Impingement (top) and Wrap (bottom) models.

supportive. The highest observed concentration, found at the base of the hill, is not simulated, but those across the face of the hill near release height are. At this height, the greatest observed SF_6 concentration is 248 ppt, and the greatest concentration estimate is 871 ppt. The largest modeled concentration from Impingement in the same area is 541 ppt. Both models overestimate the observed concentrations in this area; this might arise from overestimating the probability that the wind transported the plume along the stagnation streamline. In Impingement, the distribution is Gaussian and the 5.5° shift of the distribution still places the stagnation streamline near the peak of the distribution. In Wrap, the probability is taken from the PDF obtained from 80 m winds. This PDF could very well overestimate the steadiness of the wind direction at release height.

A second reason for the model overestimates may be related to the vertical dispersion near the hill. Neither model simulates the high concentration at the base of the hill. A σ_z large enough to do so would undoubtedly reduce the concentration estimates further up on the slope. Because a substantial wind shear existed between the release height and the surface, some enhanced dispersion near the hill might well be supposed.

4.14 Experiment 211, Hour 5 (0400-0500 MST)

4.14.1 Summary Description

Thermofogger oil-fog, SF_6, and Freon were released from the southeast side of the hill at 1155.1 m, 120.1°. The SF_6 release at 20 m and the Freon release at 58 m were continuous from the previous hour, so all tracer gas sampler data should be representative of the full sampling hour. The oil-fog was released at three heights over the course of the hour: 58 m (0400-0436), 45 m (0436-0444), and 20 m (0444-0500).

Local terrain elevations near the release point are estimated to be -9.9 m relative to the zero of the hill coordinate system, so the net release height of the SF_6 corresponds to the 11.1 m height level on the hill, and that for Freon corresponds to the 48.1 m height level. The SF_6 release rate is computed to be 0.175 g/s with an estimated error of $\pm$3.9%. The Freon release rate is 0.941 g/s $\pm$3.6%. No Freon concentration patterns have been modeled.

Plume Observations

An extensive record of observer comments about the appearance and the trajectory of the oil-fog plume during this hour is presented below.

Time: 0358 The plume centerline is at a point slightly to the north of the FAA tower.

Time: 0400 The plume is continuing to progress slightly northward. It's at a point now about half way down the hill. (It's approaching the nephelometer crane.) The plume is passing 20 m north of FAA tower, above tower C, but below the FAA tower (pretty close to release height).

Time: 0404 Plume is shifting more to the south--aimed more towards the FAA tower. Plume is going around the north shoulder of the hill with only a slight rise.

Time: 0406 Plume does rise quite a bit. It is even with the flat top of the north butte. The plume is passing just north (like I can reach out and touch it) of the north butte. This plume is passing overhead now, but I can't smell it. It's about as wide as the parking area here.

Time: 0407 The plume is passing up and over the north butte, just over the north edge. The plume is passing overhead, clearing by one tower section. It looks like about 1 tower section thick.

Time: 0408 The plume is passing directly overhead, and I am located right by the northeast corner of the parking lot on top of the north butte. I do not smell it, and it is going through the lowest white section on the FAA tower. It is clearing the top of the hill by about 8 m.

Time: 0411 The plume is now moving towards the south, approaching the draw. The plume centerline is now between the draw and the FAA tower.

Time: 0414 The plume trajectory is continuing to move south, now directed towards the tower on the south peak. It is rising quite high over the draw ($\sim$ 20 feet)

Time: 0416 The plume is shifting back toward the FAA tower. Plume top is just below lower red light (?).

Time: 0417 The plume trajectory was towards the south peak for a short period and then started drifting back to the north and is now at a point slightly north of the FAA tower. The nephelometer crane just passed through the plume.

Time: 0418 The plume meandered almost to the middle of the draw, then came back across the north butte and now it is entirely north of the butte and has gone below the level of the top of the butte. When the plume was going directly over the north butte, I couldn't smell it. It was very close to the ground, about 8 meters. As soon as it swings back off to the north it subsides to nearly its release altitude, and it does that subsiding back to that altitude very, very close to the hill.

Time: 0423 The plume centerline now is half way between the FAA tower and the northeast knoll.

Time: 0424 The plume is going around the north side, and it is significantly below the elevation of the north butte.

Time: 0432 Plume is north of the north butte. For a time, 15 or 20 minutes ago, the plume was passing up through the draw with a trajectory which took it probably 10 meters above the level of the two peaks here or 30 meters above the height of the draw. It's quite spectacular going up and over.

Time: 0438 At 45 m with the oil fog.

Time: 0439 The lower plume is absolutely creaming the hill, it's approaching it, it's quite wide and going up and through the draw. It's nearly extending from the FAA tower to the other side of the draw and I can smell it quite a bit.

Time: 0442 The plume is leaving the crane and spreading in a uniform "V" and when it hits the hill it's 1/3 of a hill width wide and it's going up and through the draw and I can smell it from time to time on the north butte. It's very dramatic, just filling up the whole draw.

Time: 0443 Release of smoke has been lowered to 20 m. The plume at 45 meters was creaming the hill right up through the draw. Now that the plume is at 20 meters, its aimed right at tower D. The whole mast set-up has probably been getting very much creamed all night.

Time: 0448 (?) Plume is approaching the hill, spreading out quite a bit. Most of it appears to be going around to the south.

Time: 0450 The lower plume spreads quite a bit, looks very stable and is almost dying in the draw and now that I walk in the draw it is definitely going up and through the draw.

Time: 0452 It looks to me like the nephelometers in the draw are really getting creamed right now, the smell of smoke is very thick on the south side of the parking area on the north butte. As I look down the northeast side it looks like part of the plume is also going around.

Time: 0453 Plume is approaching hill in a wide "V"; part of it is going around to the N. A lot of it is going up the draw, and I can smell it strongly at the FAA parking lot.

Time: 0455 The plume centerline continues to drift south and is now at a point about half way down the south slope or down about at the base of the hill.

Time: 0456 Plume is all over the place. It is approaching the hill in a wide "V".

Time: 0457 Now the plume appears to be heading towards the south shoulder and it's no longer got that very wide wedge.

Time: 0459 Plume is going south of south butte. It is a "pencil" plume as it goes over the cinder pit--no longer a "V". As the plume traversed the south flank, it tilted, and followed the contours, so that the horizontal axis paralleled the hill slope.

These observations indicate that the plume spent the first 20 minutes of the hour near the north peak, ranging from the saddle between the peaks to a point along the north side of the hill. Observers consistently reported no smoke odor as the plume passed overhead. The plume spent the next 10 minutes well north of the hill.

After the plume was lowered from 58 m (adjacent to the Freon release) to 45 m at the end of the eighth 5-minute period, the oil-fog traveled directly toward the hill and filled the draw and saddle between the two peaks as it went over the hill. Observers definitely reported smoke odor on the hill at this time.

The plume was lowered once again in the ninth period, and remained adjacent to the SF_6 release at 20 m for the rest of the hour. At this height, the oil-fog plume was directed toward the center of the south peak below the level of tower D. It was quite steady, and there was considerable spreading in the horizontal as plume material spread up the draw and over the saddle and the southern section of the north peak. A very strong smoke odor was reported on the hill during this episode. This lasted for a period of about 10 minutes before the plume swung to the south side of the hill for the last 5 minutes of the hour.

This sequence of events shows up very well in the photographs. Four photos showing the plume trajectory during two of the 5-minute periods is presented in Figure 117. One view is from behind the release crane at position 0-19 (see Figure 46); another is from the top of the south peak at location 0-8, and another view is from a point off to the side of the plume from location 0-11.

Besides illustrating the plume trajectories discussed above, these photos show the remarkable changes in plume spread as the plume travels toward the hill. For the high release, the spread is not especially striking, but the complete lift overhead is spectacular. As the plume is lowered to 20 m though, the spread is very remarkable, as is the lack of vertical lift. No lidar data for this hour are yet available.

Meteorological Information

Wind and temperature data measured at tower A during this hour were used to characterize the flow in terms of H_c. However, because of a partial failure of the 40 m wind set, 40 m winds were estimated for each 5-minute time period before H_c was calculated. The method followed in calculating speeds at 40 m is outlined in Section 4.4.1.

The average H_c over the hour is 26 m, and Fr_H above H_c is 2.5. The SF_6 was released at 20 m, marginally below the mean critical dividing streamline. Figure 111 contains a time series plot of the calculated

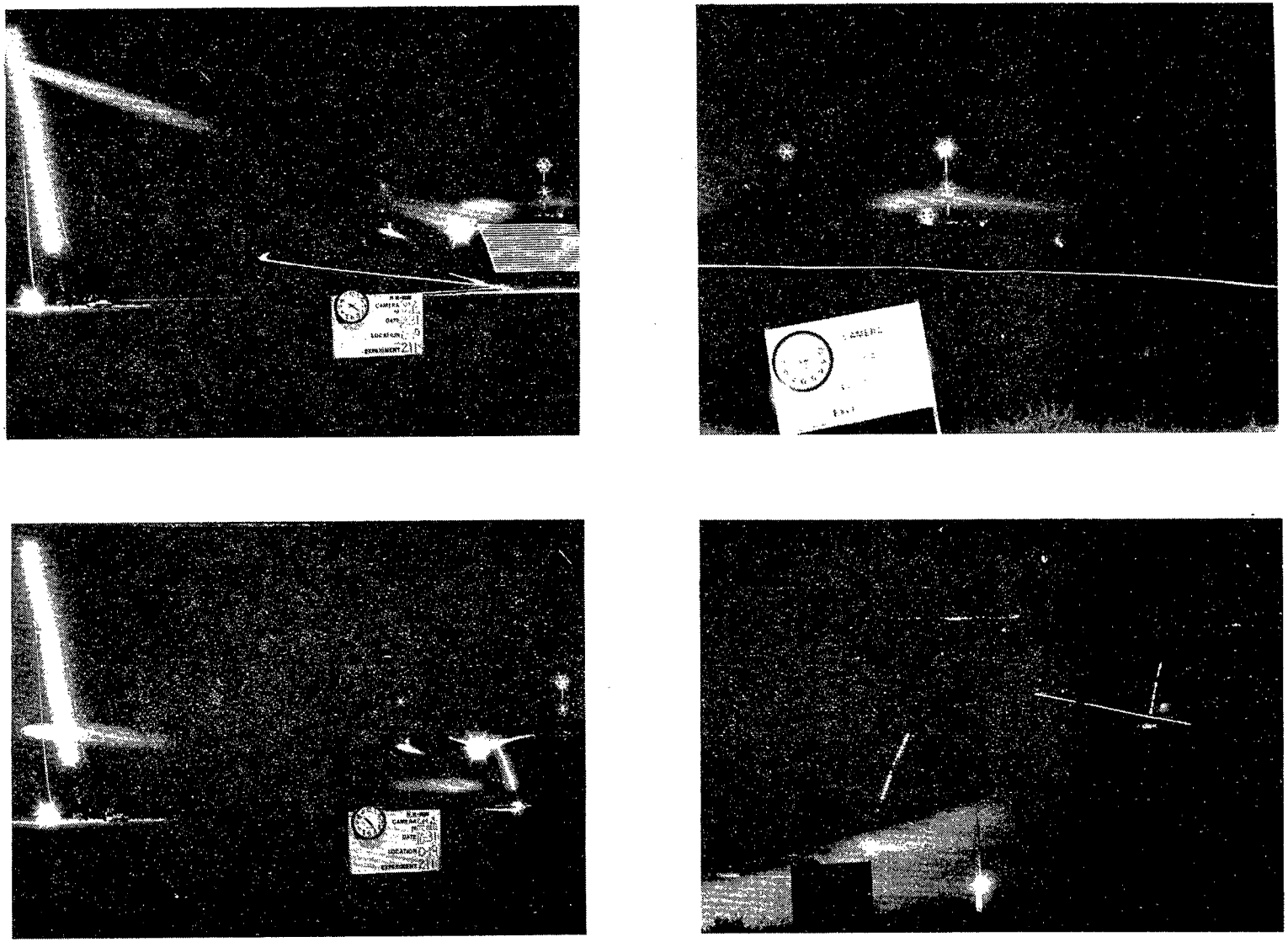

Figure 117. Three views of the plume trajectory between 0410 and 0415, and between 0450 and 0455 MST taken from behind the release (position 19), taken from the top of the south peak (position 8), and taken off to the side of the release (position 11) during Experiment 211, Hour 5.

5-minute H_c and Fr_H values for the experiment. Fr_H is very steady, exhibiting a variation of no more than 0.2. H_c, however, drops from 30 to 20 m over the first 40 minutes and then holds steady at 20 m for the rest of the hour. Therefore, the assumption that the SF_6 plume remained below H_c in the mean over the hour is not necessarily true, given the uncertainty in estimating H_c. The period of the time during which the smoke plume was placed alongside the SF_6 release corresponded to the period during which H_c was equal to the release height.

Hourly average wind speeds measured at 10 m and estimated at 40 m are 1.3 and 2.4 m/s, respectively. The 10 m mean wind direction was 094° and that at 80 m was 122°. Therefore, both wind direction and wind speed shears above 10 m were moderate. Figure 118 shows the trend in wind speeds between 10 and 80 m during the hour. The 10 m speeds become very low at times and rise as high as 2 m/s. Speeds at 40 m are quite steady, varying between 4 and 5 m/s. Winds at all levels tend to pick up toward the end of the hour, thereby producing the drop in H_c.

Variations in wind directions measured at 10 m and 80 m are shown in Figure 119 as frequency distributions. The 80 m distribution may be more representative of that at release height because it is directed more toward the hill; however, we cannot verify this from smoke plume observations. The pattern of SF_6 concentrations over the hill surface may confirm the choice of the 80 m distribution.

In summary, the plume was released close to the dividing streamline of the flow and might have spent much of the hour below it. Winds were 2 m/s or less and variable at the 10 m level but were presumably less variable and somewhat greater near the release height.

SF_6 Concentrations

The distribution of hourly averaged SF_6 concentrations over the surface of the hill is shown in Figure 120. Highest concentrations are measured between 15 m and 30 m in the southeast draw. Other concentrations across the hill surface are seen to be quite large and generally tend to favor the northern side of the hill. Those along the north side tend to fall into a band between the 25 m and 50 m contours. A fairly large value is also measured on the saddle toward the top of the northwest draw. Because the relative release height is 11 m, this pattern tends to confirm oil-fog plume observations made during the 15 minutes that the fog was released adjacent to the SF_6 source. The SF_6 was apparently transported straight toward the hill center or possibly the north peak for much of the hour, and little plume lift occurred.

The distribution of 10-minute average SF_6 concentrations is presented in Figure 121. Fortunately, the location of the largest 10-minute concentrations lies close to the location of the largest 1-hour average concentration. Therefore, the evolution of the largest 1-hour concentration may be seen in the 10-minute data. Large 10-minute concentrations occur in this area in only three of the six 10-minute periods. The first is between 0410 and 0420, and the other two are between 0440 and 0500--the period

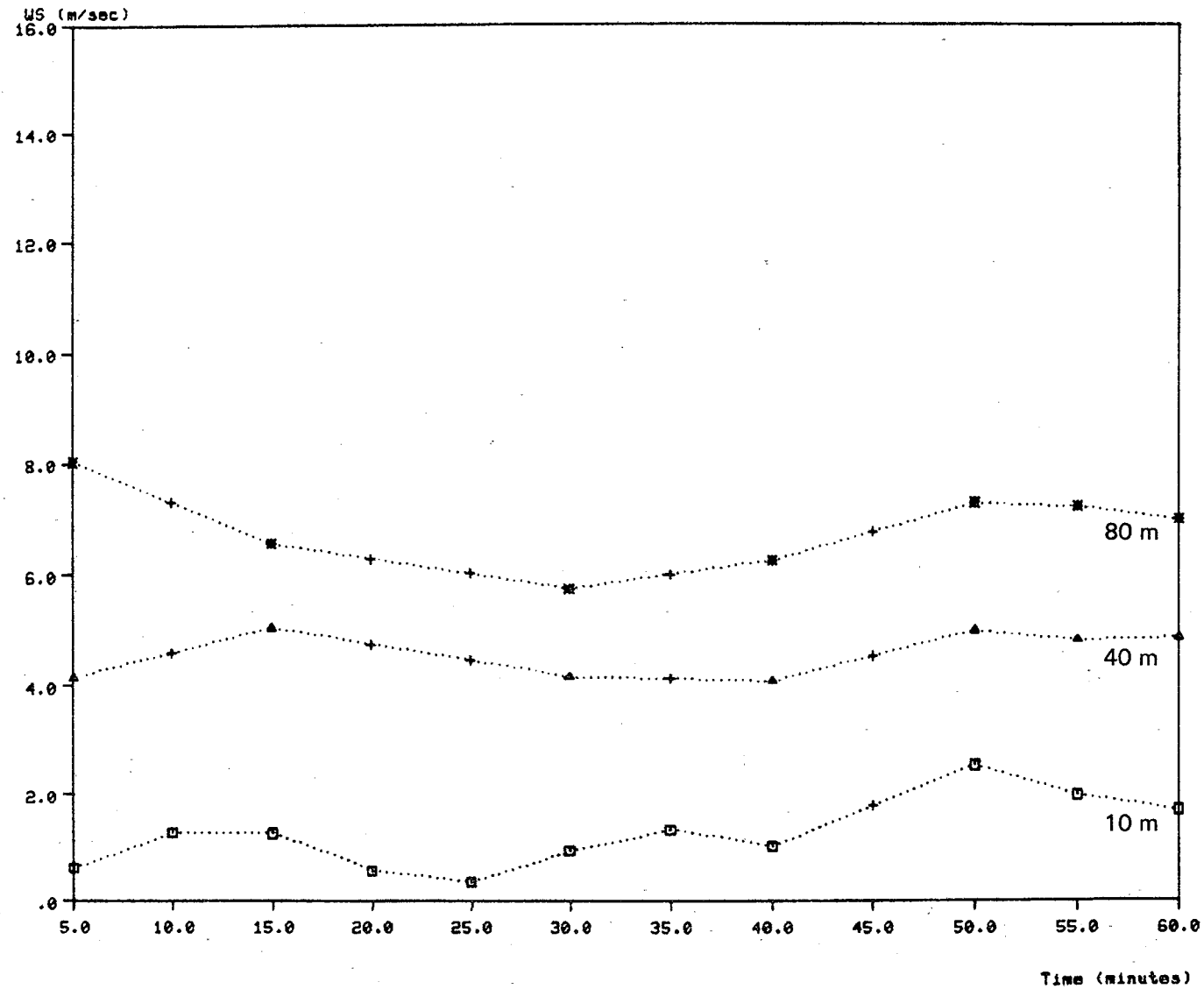

Figure 118. Tower A wind speeds during Experiment 211, Hour 5 (0400-0500 MST).

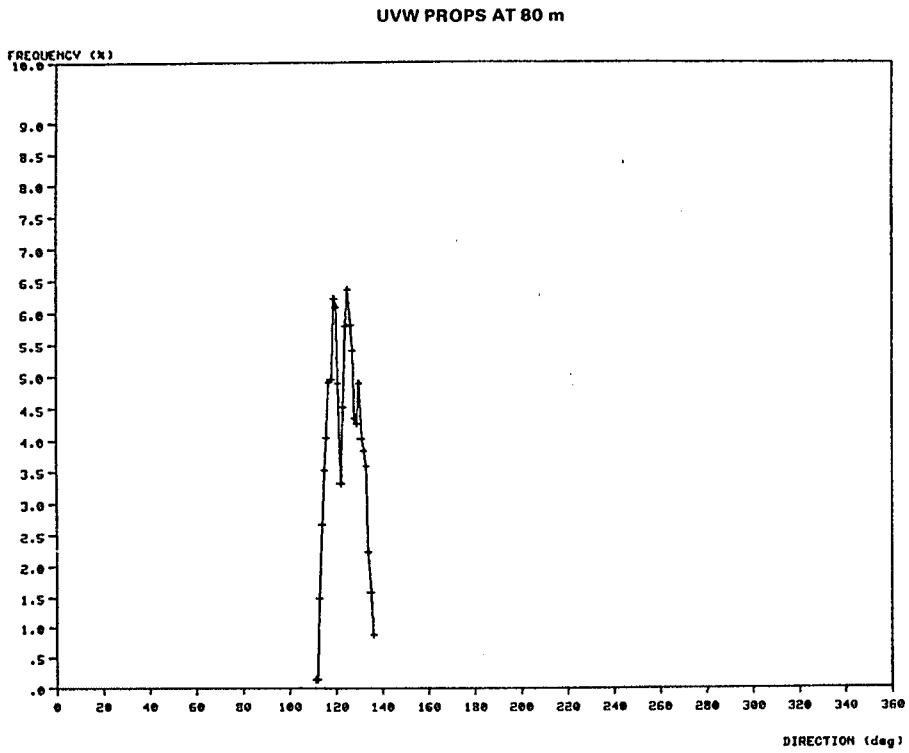

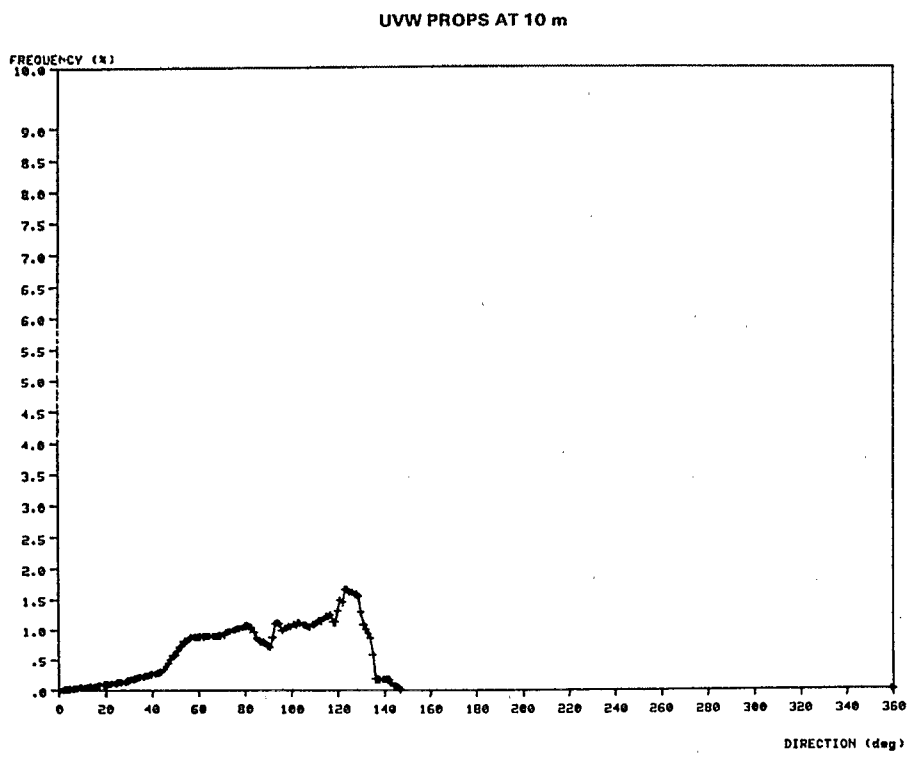

Figure 119. Calculated wind direction distribution functions for Experiment 211, Hour 5 (0400-0500 MST).

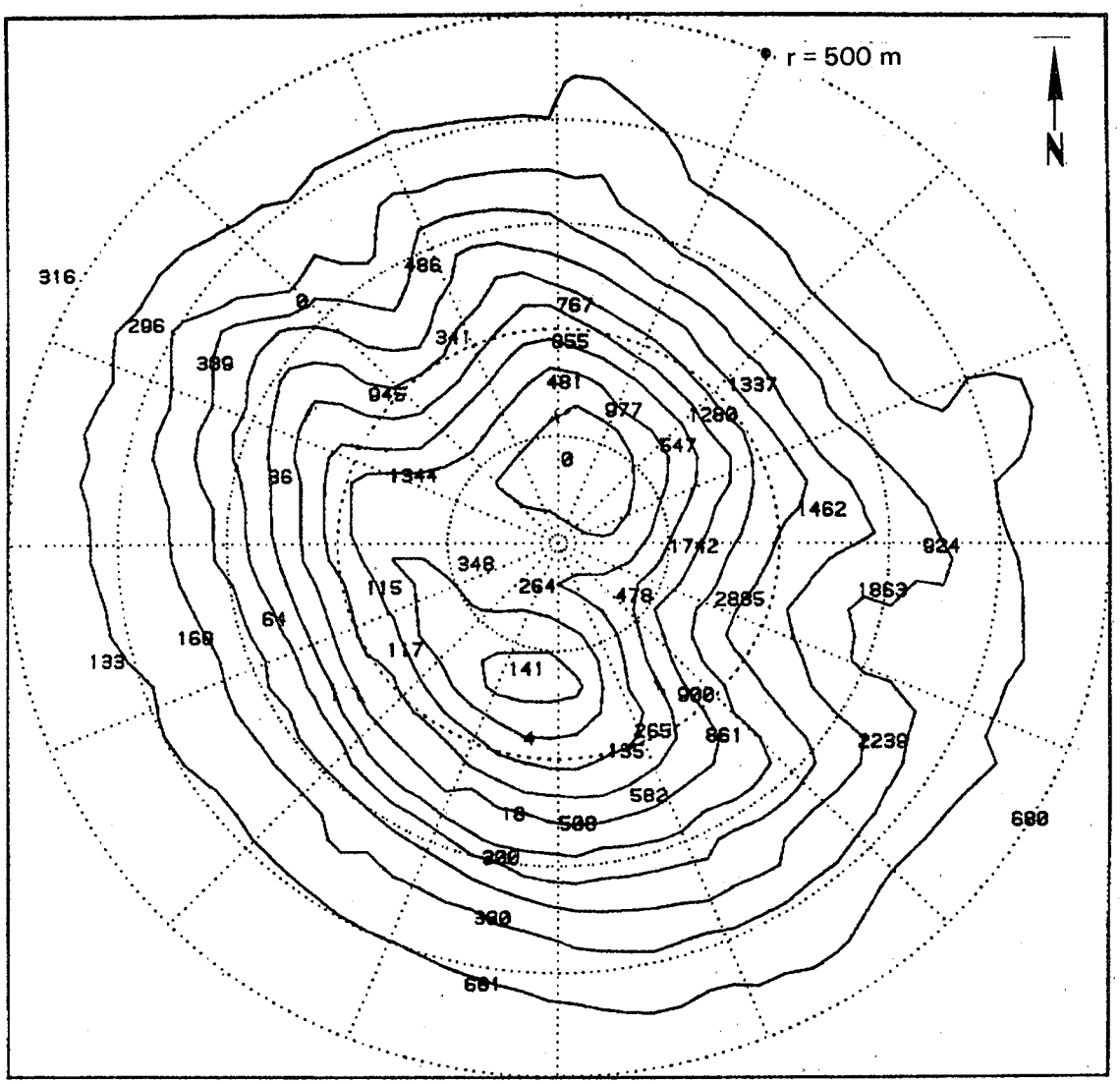

Figure 120. Observed SF_6 concentrations (ppt) for Experiment 211, Hour 5 (0400-0500 MST). Source: r = 1155.1 m, θ = 120.1°, net height = 11.1 m, Q = .175 g/s.

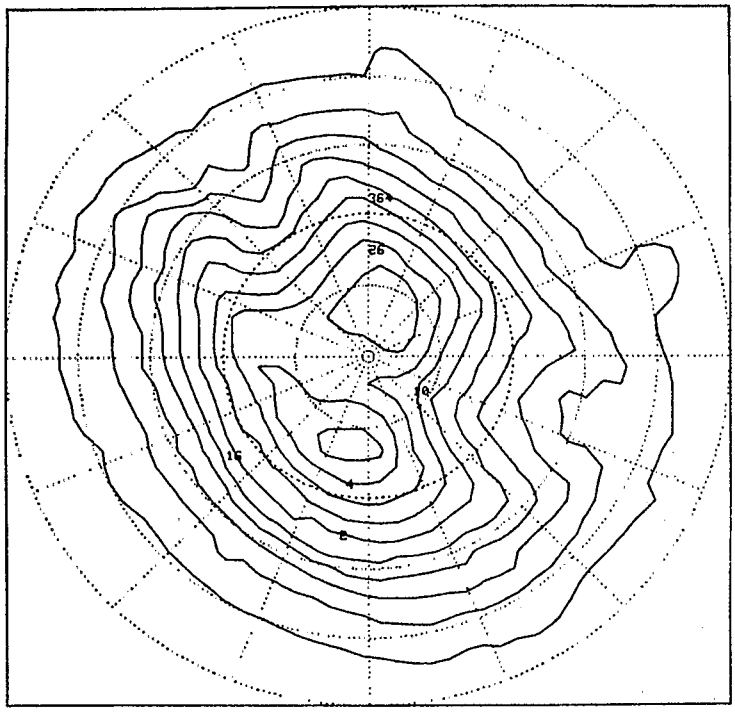

TIME PERIOD 0400-0410

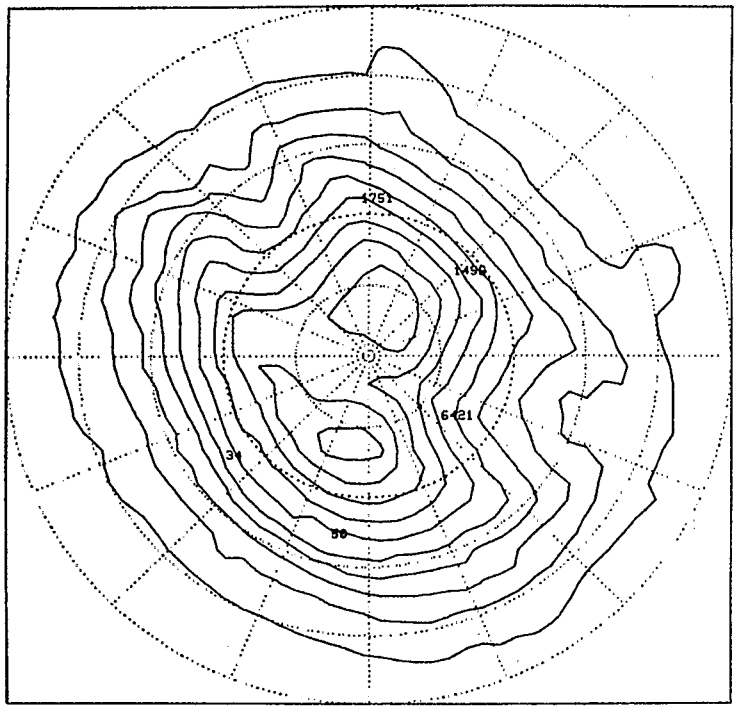

TIME PERIOD 0410-0420

Figure 121. Observed 10-minute average SF_6 concentrations (ppt) for Experiment 211, Hour 5 (0400-0500 MST).

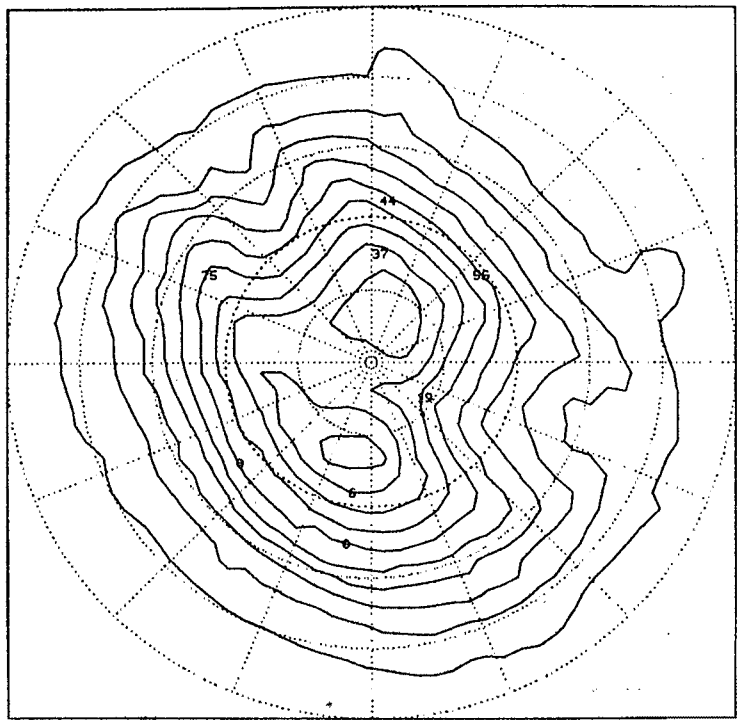

TIME PERIOD 0420-0430

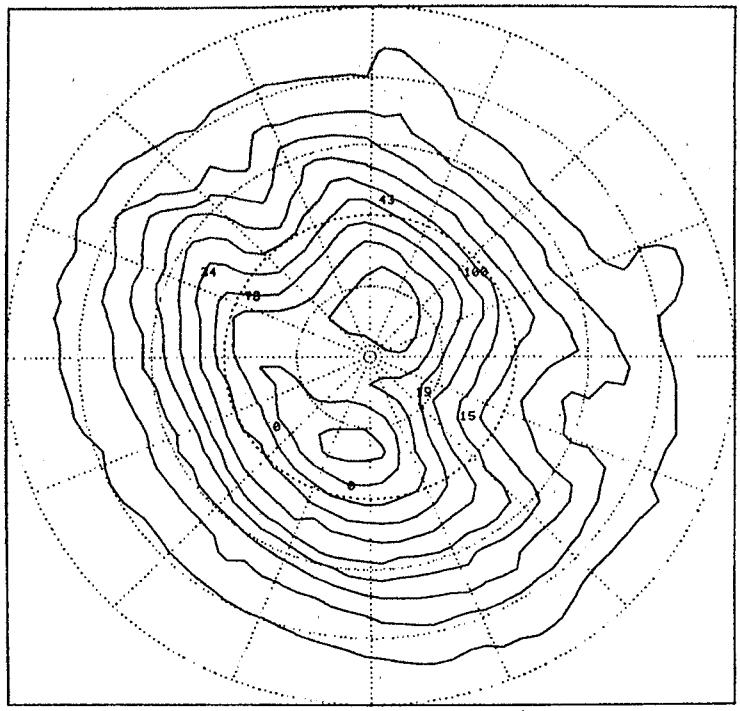

TIME PERIOD 0430-0440

Figure 121. Continued.

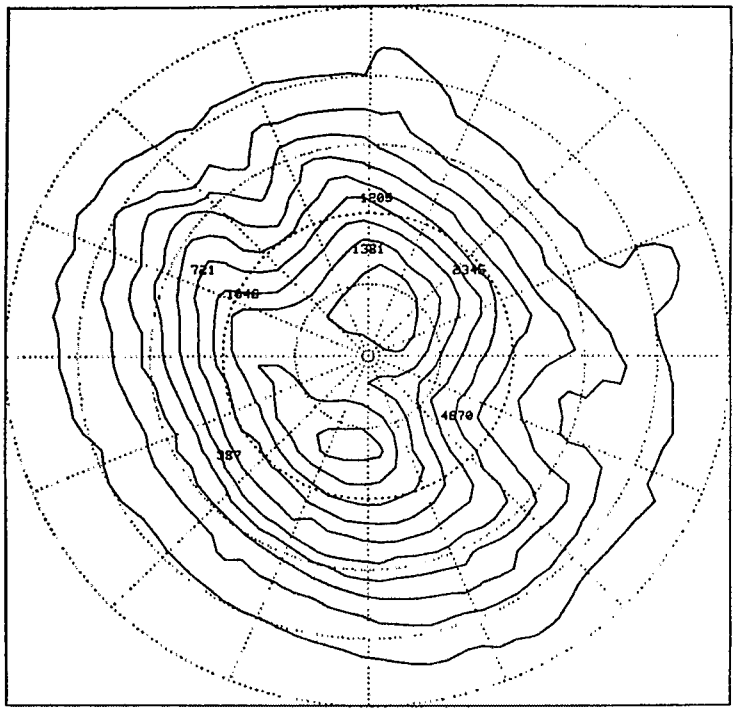

TIME PERIOD 0440-0450

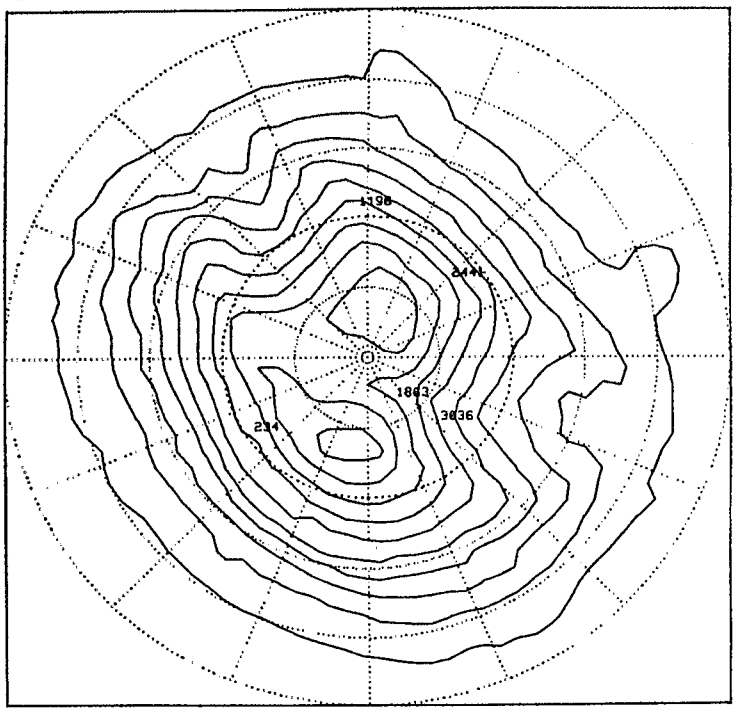

TIME PERIOD 0450-0500

Figure 121. Continued.

documented by the oil-fog plume in the photographs. This information implies that a peak in the PDF at release height should virtually line up with the flow toward the center of the hill.

4.14.2 Model Peformance

This hour has been modeled with the Wrap model because the plume was released slightly below the calculated dividing streamline height. However, because the plume was so near H_c, significant vertical smearing of plume concentrations on the hill was observed. This feature is not accounted for in the model.

In running the models, meteorological data were prepared as in Section 4.1.2, and the resulting values are listed in Table 17.

The 1-hour average wind directions 10 m below and 60 m above the release height are 094° and 122°, respectively. Directions at 10 m and 30 m on tower B are 120° and 126°, respectively. Unfortunately, all we know about the plume transport from photographs is obtained during the last 15 minutes of the hour, when the plume spent most of the time heading directly toward the hill center with a brief period of flow along the south edge of the hill. Because the photo documentation for the release height is incomplete, the model wind direction is chosen to be 120°, the direction from source to hill center. The 80 m PDF is also used in the modeling.

Concentration estimates from both Impingement and Wrap are listed in Table 17 and plotted on a map of CCB in Figure 122. Both models tend to underestimate peak observed SF_6 concentrations, but Wrap does better in estimating concentrations along the sides of the hill, and in the lee (if some compensation is made for differences between the heights of observed concentrations, and the heights of modeled concentrations).

Peak observed concentrations occur at higher elevations on the hill than do the peak modeled concentrations. The peak observed value is 3,885 ppt, and the peak modeled values are 565 ppt and 1,146 ppt for Impingement and Wrap, respectively.

Larger concentrations can be produced with Wrap if the mean wind direction is shifted slightly. The discussions above focused on the shape of the 80 m PDF. The 10-minute SF_6 data indicated that a peak of the PDF should be directed toward the hill center. The choice of 120° for the mean wind direction does not direct a peak of the PDF along the stagnation streamline. If the mean wind direction were changed from 120° to 118°, the probability that the wind blew along the stagnation streamline would increase from .0452 to .0635. This change would produce a peak concentration of 1,610 ppt or 56% of the peak observed.

TABLE 17. IMPINGEMENT AND WRAP MODEL CALCULATIONS - EXPERIMENT 211, CASE HOUR 5

Meteorological Data

wind direction(deg)	=	120.
wind speed(m/s)	=	2.4
critical dividing streamline height(m)	=	26.0
Iz	=	.068
Iy	=	.277
N(1/s)	=	.092

Source Data

direction(deg)	=	120.
distance(m)	=	1155.1
release height(m)	=	20.0
SF6 emission rate(g/s)	=	.175

Receptor Coordinates X(m)	Y(m)	Z(m)	Observed SF6 (ppt)	Impingement Predicted SF6 (ppt)	Wrap Predicted SF6 (ppt)
360.22	.00	13.26	923.50	417.45	831.39
142.00	.00	50.00	1742.00	71.70	72.47
257.78	33.94	30.00	1461.80	354.32	677.58
195.15	149.74	27.41	1337.30	316.63	628.96
159.04	122.04	46.91	1280.22	100.46	129.56
72.99	126.43	77.02	977.30	1.90	.59
66.60	505.92	-6.52	.00	96.81	137.19
29.59	224.79	51.51	767.08	64.04	77.91
10.61	80.56	91.97	.00	.16	.02
25.15	190.88	65.00	855.30	14.67	10.36
-53.69	-407.79	3.82	680.80	222.27	386.29
-45.46	-345.28	13.70	380.40	325.41	652.78
-38.04	-288.98	32.94	300.20	261.38	482.84
-15.01	-113.99	98.96	141.40	.01	.00
-4.85	-37.12	80.00	264.10	.72	.14
-396.68	-106.29	3.44	132.60	163.25	293.25
-315.76	-84.61	13.24	169.00	220.64	442.59
-248.96	-66.71	32.90	64.00	188.18	356.09
-144.85	-38.12	80.00	115.20	2.04	.74
-60.85	-16.12	80.00	348.20	2.04	.74
31.69	-258.06	50.00	508.30	73.82	81.26
95.80	-231.27	52.96	581.80	50.15	45.32
163.68	-175.52	50.00	860.80	69.49	66.07
137.89	-137.89	50.00	900.10	69.08	65.02
441.46	-254.87	-2.45	679.60	173.00	219.79
313.62	-181.07	15.29	2238.50	565.26	1146.27
183.53	-49.18	30.00	2884.70	415.60	787.57
312.38	-41.13	14.00	1863.40	451.27	904.90
-243.41	65.22	50.00	36.30	69.01	95.65
-441.92	255.14	-.90	315.80	114.68	196.01
-359.96	207.82	8.94	295.90	164.20	319.60
-297.11	171.54	28.07	389.30	175.28	349.33
-111.85	65.88	80.00	1344.10	3.10	1.43
-141.42	141.42	50.00	945.00	68.99	95.65
-229.81	229.81	30.00	.00	179.30	351.69
-109.07	263.31	30.00	486.30	198.17	387.64
-80.75	194.94	50.00	341.30	70.95	95.35

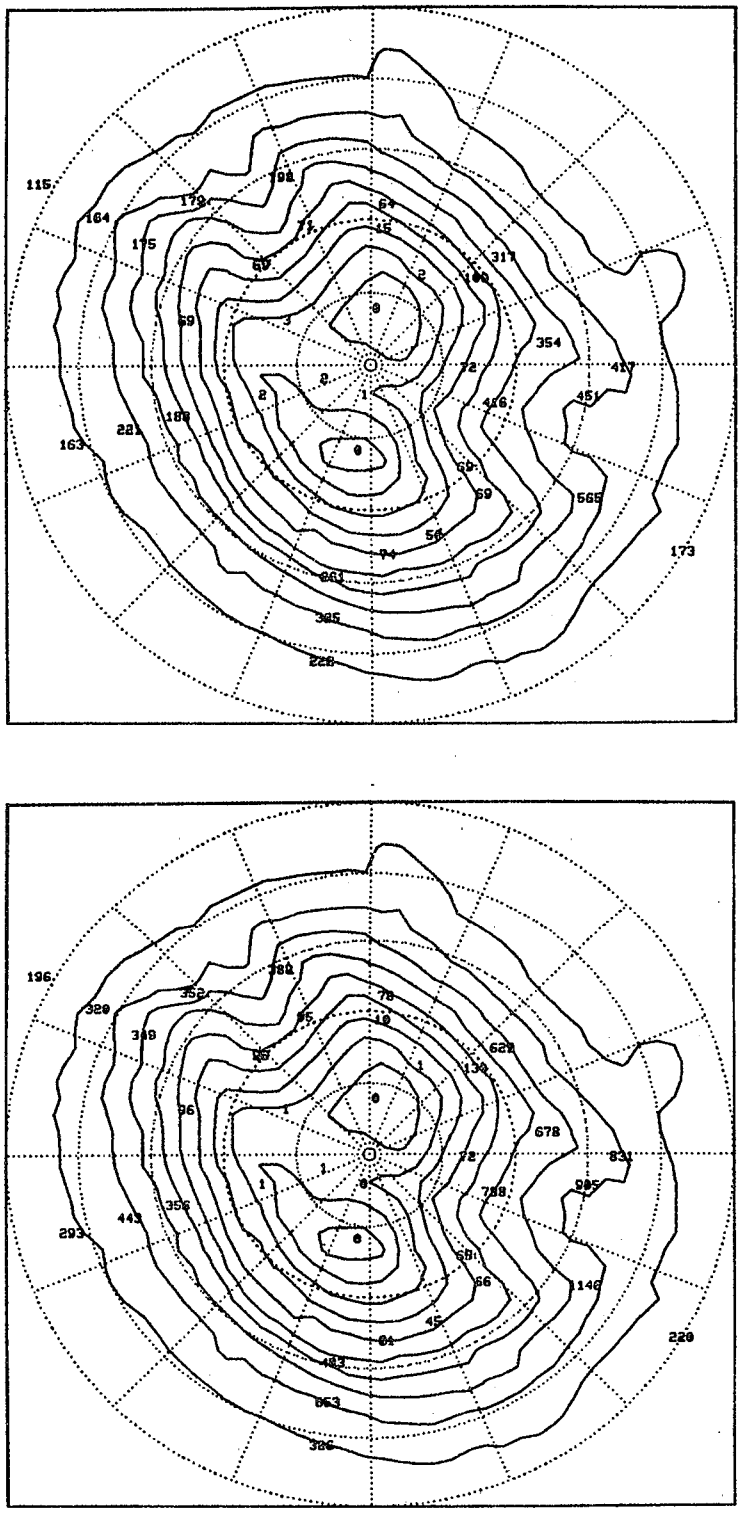

Figure 122. SF_6 concentrations (ppt) estimated for Experiment 211, Hour 5 by the Impingement (top) and Wrap (bottom) models.

4.15 Summary

Case study analyses of 14 hours of data collected at CCB have produced a wealth of information to guide the development of improved regulatory dispersion models for applicaton in rough terrain. From the assembled meteorological data, tracer concentrations, photographs, and lidar imagery, we have been able to construct detailed descriptions of plume paths over and around the hill under various meteorological conditions. Many of these descriptions are found to be consistent with expectations about plume behavior built upon theory and laboratory investigations. For example, the critical dividing streamline height (as calculated by the integral method) appears to be a good indicator of the basic modeling approach to be adopted--that is, whether the plume should be modeled with a Wrap or a Lift type of model.

Most of the experimental evidence supports these key findings about plume trajectory regimes:

- When the plume was released above H_c, it tended to travel over the hill. The plume path appeared to be consistent with streamlines in weakly stratified flow, as described both in theory and laboratory experiments.
- When it was released well below H_c, it tended to swing widely across the hill, preferring to travel around the hill, not over the hill.
- When it was released very near H_c, it tended to travel directly towards the hill, with only slight-to-moderate vertical displacement.

Table 18 helps to summarize the observationally-established relationships that appear to connect plume path behavior to the meteorological parameters. It lists for each hour the release height (z_r), the dividing streamline height (H_c), the difference between the two expressed as a function of the release height ($(z_r - H_c)/z_r$), as well as the location of the maximum observed concentrations. In addition, for those hours in which the release was above H_c, the table includes hourly average Froude numbers (Fr_H, Fr_L), inferred terrain factors (T_o), and observer notes on whether the streamlines appeared to be depressed in the lee of the hill. Terrain factors, as inferred from observed concentrations and the modeled plume dispersion and trajectory, can be useful in explaining changes in the relative magnitudes of the plume centerline height, plume distortion, and plume dilution--but only if interpreted properly. For example, because we assume that only the ratio of centerline height to σ_z should be adjusted in the terrain factor computations to make the model reproduce observed concentrations, the model must be using the "right" values of mean wind direction and horizontal spread. In addition, because we have assumed that the modeled centerline concentrations are "correct" in deriving the terrain factor, T_o can no longer properly account for changes in plume dilution; this places the burden on the model to use "correct" values of σ_z. When these conditions are violated, inferred T_o values can be misleading.

TABLE 18

SUMMARY OF METEOROLOGICAL DATA AND THE ASSOCIATED TRACER PLUME BEHAVIORS

Experiment	z_r	H_c	Fr_H	Fr_L	Streamline Depression			Inferred T_o			Location of C_{max} (m)	$\frac{z_r-H_c}{z_r}$	$U_o(z_r)$
					Obs.	Lidar	SF_6	Front	Top	Back			
202(4)	20	0	2.5	0.63	-	-	-	-	-	-	10 (side)	1.00	7.3
(5)	30	7	2.5	0.60	-	(plume to side)		0.77	-	-	10 (side)	0.77	7.8
204(1)	30	58	1.9	-	-	-	-	-	-	-	10 (side)	-0.93	2.1
205(4)	40	15	3.0	0.74	No	-	No	1.0	.7-.8	.8-1.0	80 (saddle)	0.63	5.9
(5)	50	24	3.3	0.86	No	?	No		(Bad SF_6)			0.52	6.5
206(4)	35	20	2.1	0.53	-	-	Yes	1.-1.5	.8-1.4	.7-1.4	90 (peak)	0.43	4.5
(5)	35	35	3.1	-	-	-	-	-	-	-	25 (front)	0.00	2.1
(8)	35	37	3.3	-	-	-	-	-	-	-	25 (front)	-0.06	2.0
209(1)	40	5	3.1	0.78*	Yes	-	?	2	2	2	10 (back)	0.88	4.3
(7)	40	58	1.2	-	-	-	-	-	-	-	30-75 (front)	-0.45	2.5
210(3)	57	26	2.1	0.55	-	Yes	?	0.6	0.6	0.5	0 (back)	0.54	6.3
(7)	58	14	2.6	0.63**	Yes	-	?	1	1.6	1.0	80 (back)	0.76	7.3
211(1)	30	45	2.9	-	-	-	-	-	-	-	0 (front)	-0.50	1.9
(5)	20	26	2.5	-	-	-	-	-	-	-	30 (front)	-0.30	2.4

*Varied during the hour - the low was 0.58
**Varied during the hour - the high was 0.80

For hours of release heights less than or equal to H_c, maximum concentrations were measured both above and below the level of the release height. One of these hours (209-7) is very difficult to interpret because the winds smeared SF_6 in all directions before the start of the hour; therefore, little definitive information can be extracted about plume behavior. However, data from the other hours for which $z_r \leq H_c$ indicates that the plume definitely "rode" up the hill slope at times, especially when z_r was nearly equal to the H_c. The data also indicate that when large directional shear was present, a complex flow interaction below the plume elevation could occur near the base of the hill. This interaction (for which we have qualitative evidence but as yet no good quantitative model) appears to have mixed the plume to the ground, producing maximum concentrations below the release height.

For release heights greater than H_c, maximum concentrations were measured either near the top of the hill or on the back side, provided that the mean wind was directed towards the hill center. The deciding factor that appears to govern whether the peak concentration lies near the top or in the lee is the ratio $(z_r - H_c)/\sigma_z$, not Fr_L. The observational evidence suggests that whenever Fr_L was between 0.5 and 0.7, a streamline depression effect appeared in the lee; but the inferred T_o values over the top of the hill and in the lee suggest that leeside concentrations were increased only moderately over what they might have been in the absence of a leeside streamline depression. This increase may cause a shift in peak concentrations from the top to the back of the hill. In cases where σ_z was small relative to the plume height, the concentrations across the top of the hill are likely to have been smaller than those near the base of the hill in the lee, regardless of the size of Fr_L.

Terrain factors inferred on the windward side of the hill suggest that subtracting the full value of H_c from the plume height may be too severe a correction in cases where H_c was a substantial fraction of the release height. Instead, the model should somehow account for the vertical deflection of H_c itself in order to better explain the observed concentrations on the windward face.

The geometry of CCB may also play a major role in determining the size of concentrations measured high on the windward side and in the saddle, because the shape of the hill tends to funnel the flow. At times, concentrations on the saddle were substantially lower than those measured on one peak or the other or those estimated by the models for plumes well above H_c. We conjecture that this may indicate a flow channeling effect: flow up the draw may have been funneled underneath the plume, tending to lift the plume somewhat, reducing tracer concentrations on the surface of the saddle. For cases in which the plume was below H_c, the same kind of channeling effect may have forced plume material over the saddle rather than to one side of the hill or the other. This would tend to promote large tracer concentrations high on the hill. (This supposed channeling effect is not taken into account by the Wrap model, which therefore always estimates small concentrations at elevations well above z_r.)

Many primary components of the Lift and Wrap models appear to be appropriate at CCB and need little modification. A comparison of model estimates with observed concentrations shows that major differences between modeled and observed concentrations can usually be explained by uncertainties in the meteorology prevailing at the release point, especially because of the observed spatial gradients and temporal changes in key meteorological variables. Therefore, improving the models to take fuller advantage of observational meteorological information turned out to be a mixed blessing; because the models rely more heavily on the details of the meteorology, they are not always better at estimating the observed concentration field.

The relative performance of the Lift, Wrap, Neutral, and Impingement models is summarized below for each of the case hours analyzed:

Experiment Case Hour	
202(4)	Neutral appears to be better than Lift because the PDF used in Lift seems to be too narrow. Neither version places the peak concentration correctly below the release height.
202(5)	Neutral does well, but the peak observed concentration again lies closer to the bottom of the windward slope. Lift would perform better if the PDF were a little broader and if a terrain factor between 0.7 and 0.8 were used.
204(1)	The peak concentration well to the side of the hill (nearly level terrain) cannot be reproduced by either model. Wrap is much better than Impingement in estimating other large concentrations because the PDF is highly non-Gaussian.
205(4)	Lift does better than Neutral. The PDF appears appropriate. (Model estimates would improve if the terrain factor over the hill top were about 0.8.)
205(5)	Questionable SF_6 pattern precludes model evaluation.
206(4)	Neutral does better than Lift. The PDF is too narrow, and subtracting H_c brings the plume too near the surface on the windward face of the hill.
206(6)	Wrap overestimates by a factor of 2; Impingement underestimates by the same factor. (Wrap with a larger σ_z and slightly broader PDF would work well.)
206(8)	Same as 206(6). (Both hours have very similar meteorological conditions).

209(1) Neutral and Lift both overestimate observed concentrations. Either the model σ_z is too large or the emission rate is grossly in error (not likely). PDF and Gaussian distribution appear equally suited.

209(7) Hour is impossible to model with tower A data.

210(3) Neutral and Lift estimates are uniformly low. An increase in σ_z late in the hour should be included in the estimates. PDF is probably adequate.

210(7) Lift estimates of the concentration distribution is better than that from Neutral, so the PDF is appropriate. Concentration estimates are too large on the windward face.

211(1) Wrap overestimates concentrations more than Impingement. Either the PDF is too narrow or σ_z is not large enough.

211(5) Wrap does better than Impingement because the PDF is a better representation of the wind distribution. Peak estimate is half the peak observed concentration. (A smaller σ_z with some plume lift would improve the model estimates.)

These observations indicate that the correct estimate of σ_z is absolutely crucial to model performance. In most cases when the release is above H_c, estimating σ_z only to within a factor of 1.5 to 2 introduces enough error in modeled concentrations to cause extreme over- or underestimates. In fact, because most reasonable estimates of T_o lie between 0.5 and 1.0, inferred values of T_o that fall repeatedly between 1.4 and 2.0 could indicate that the "appropriate" σ_z may be as much as twice as large in these cases.

In all but the lightest wind speed cases, it is not as important to be able to specify the horizontal distribution correctly. The use of a Gaussian distribution with interpolated values of i_y seems to provide an adequate description of the variability in the plume trajectory. Indeed, in some cases the Gaussian distribution offers a better description than does the PDF measured from the nearest "representative" level above or below the release height. But when wind speeds are light and variable, the distribution of wind directions can be highly non-Gaussian, and it is of the utmost importance, in such cases, to have available a truly representative PDF.

A quantitative measure of the performance of the Lift and Neutral models is presented in Table 19. The statistics describe the ability of the models to reproduce observed concentrations on a point-by-point basis for modeled and observed concentrations paired in space and time.

TABLE 19. SUMMARY PERFORMANCE STATISTICS FOR THE LIFT AND NEUTRAL MODELS

Lift Model

Case-Hr	Zr(m)	Theta(deg)	WD (deg)	Hc (m)	u (m/s)	N (1/s)	Iz	R**2	A	B	AGE(ppt)	RMSE(ppt)
202-4	20.0	319.0	327.0	.0	7.3	.0370	.0410	.3101	.6767	33.0827	-.0695	1.7385
202-5	30.0	319.0	326.0	7.0	7.8	.0470	.0370	.6887	2.1077	21.2766	-2.1417	5.0000
205-4	40.0	120.1	121.0	10.0	5.9	.0420	.0310	.5815	1.0404	38.1008	-.7733	1.1879
205-5	50.0	120.1	120.0	24.0	6.5	.0480	.0490	.5117	.3690	69.0225	.0152	.6303
206-4	35.0	123.6	128.0	20.0	4.5	.0440	.0310	.0773	.2336	68.3858	.1233	1.3763
209-1	40.0	315.9	319.0	5.0	4.3	.0180	.0530	.0127	.0142	7.9845	.9368	1.2349
210-3	57.0	113.7	118.0	26.0	6.3	.0440	.0180	.3843	18.1433	26.9123	-30.9949	42.4188
210-7	58.0	122.2	118.0	14.0	7.3	.0350	.0570	.0788	.1637	5.4271	.7794	1.0793

Neutral Model

Case-Hr	Zr(m)	Theta(deg)	WD (deg)	Hc (m)	u (m/s)	N (1/s)	Iz	R**2	A	B	AGE(ppt)	RMSE(ppt)
202-4	20.0	319.0	327.0	.0	7.3	.0370	.0410	.7142	1.0811	18.7519	-.3653	1.4165
202-5	30.0	319.0	326.0	7.0	7.8	.0470	.0370	.4199	.9009	23.3305	-.4096	2.2277
205-4	40.0	120.1	121.0	10.0	5.9	.0420	.0310	.5575	.5050	9.6890	.4357	.6180
205-5	50.0	120.1	120.0	24.0	6.5	.0480	.0490	.3728	.6285	54.7495	-.2469	.5513
206-4	35.0	123.6	128.0	20.0	4.5	.0440	.0310	.4538	.8773	-4.0268	.1590	.7565
209-1	40.0	315.9	319.0	5.0	4.3	.0180	.0530	.0048	-.0054	11.7708	.9629	1.2393
210-3	57.0	113.7	118.0	26.0	6.3	.0440	.0180	.0551	1.7054	48.1140	-6.5459	9.4489
210-7	58.0	122.2	118.0	14.0	7.3	.0350	.0570	.0382	.1107	7.1691	.8321	1.0315

A linear correlation method is used in which the observed concentration C_o is expressed as a linear function of the model concentration C_p plus a random variable ε

$$C_o = A\ C_p + B + \varepsilon \tag{57}$$

Ideally, A = 1 and B = 0. If A < 1, the model tends to overestimate concentrations; if A > 1, the model tends to underestimate concentrations. However, if A < 1 and B is large, the correlation between modeled and observed concentrations is likely to be small.

Table 19 contains the values of A and B as well as the correlation coefficient (R^2), the absolute gross error (AGE), and the root mean square error (RMSE).

$$AGE = \overline{C_o - C_p}/\overline{C_p} \tag{58}$$

$$RMSE = \overline{(C_o - C_p)^2}^{\,1/2}/\overline{C_p}$$

Only concentration samples taken at receptors above H_c are included in the statistics.

The correlation coefficient for Lift is better than for Neutral in case-hours 202(5), 205(4), 209(1), 210(3) and 210(7), but worse for case-hours 202(4) and 206(4). (No judgment is made in the case of 205(5) because the SF_6 pattern is questionable.) When the linear regression coefficients A and B are compared in the table for both models, Lift exhibits less of an improvement. All measures of model performance would be expected to improve, however, if input data uncertainty could be reduced.

Similar statistics for the Wrap and Impingement models are not presented because the model is not designed to give the complete concentration field--only concentrations near the stagnation streamline. The comparisons we presented between the two models only address the ability of each model to estimate the highest observed concentration on the hill. Table 20 summarizes peak modeled and observed concentrations for each of the fourteen case study hours. Note that these peak concentrations are not paired in space, so the table in no way reflects the ability of a model to estimate the spatial distribution of concentrations correctly. In all of the hours modeled by the Wrap and Impingement models except one, the Wrap estimate of the peak concentration lies closer to the peak observed concentrations than does the Impingement estimate. Furthermore, the Wrap model overestimates the peak concentration on the hill in all but one of the hours (excluding 209, hour 7). Therefore Wrap (with the PDF formulation) offers a clear improvement over Impingement.

TABLE 20

SUMMARY OF PEAK MODELED AND OBSERVED

1-HOUR AVERAGE SF_6 CONCENTRATIONS

Experiment	Hour	Observed	Peak Concentrations (ppt)[1]			
			Lift	Neutral	Wrap	Impingement
202	4	820	647	584	-	-
202	5	530	235	498	-	-
204	1	249[2]	-	-	195	262
205	4	288	207	372	-	-
205	5	(444)	(345)	(184)	-	-
206	4	956	1146	636	-	-
206	6	1921	-	-	3771	871
206	8	2439	-	-	3782	1026
209	1	66	232	420	-	-
209	7	(123)	-	-	(199)	(562)
210	3	176	7	14	-	-
210	7	119	105	135	-	-
211	1	179	-	-	487	302
211	5	1648	-	-	655	323

[1] Concentrations are scaled by 0.1 (g/s)/Q(g/s) to account for differences in SF_6 emission rates.

[2] The largest concentration measured on the hill was 129 ppt.

SECTION 5

QUALITY ASSURANCE AND REFINEMENT OF CCB DATA

Since the first milestone report, the quality of the data taken from the experiments has been substantially improved. ERT recently received the original records (strip charts and integrator outputs) of the tracer gas analysis performed at the North American Weather Consultants (NAWC) field office in Boise. NAWC also provided a quality assurance report on the CCB tracer data that indicated that some problems remained with the precision of the curves used to fit the gas chromatograph (GC) calibration data and with the interpolation in time between successive calibrations. These problems have been addressed by new approaches to the calibration of the GC outputs.

ERT has also received the meteorological instrument calibrations performed during installation and take-down of the tower data. These provide further documentation of the consistency of instrument response during the course of the experiments when compared with the data from the two field audits.

An important experiment with the UVW propellors was performed in the Colorado State University wind tunnel by staff of ERT's Western Measurements Division (WMD) in April 1982. This experiment checked the response of a completely assembled Climatronics triaxial wind component system. The departures from cosine response were substantially greater than those suggested by the curves in the manufacturer's literature. The data from this experiment were combined with the field experiment data from sites where cup and vane systems were co-located with propellor systems. This produced correction factors for the propellor data and, in turn, corrections for the effects of tower wakes. In addition, the locations of the tracer sources and the rates of tracer emissions were refined.

Because of these refinements to the experimental data, the precision and accuracy of the data base have been substantially improved. With these improvements, model development and evaluation can be based on a sounder foundation.

5.1 Refinement of Tracer Gas Data

NAWC's quality assurance report on the tracer gas samples taken at CCB pointed out two principal problems with the way the gas GCs were calibrated. First, the function used to represent the calibration data often did not fit the responses well at the lower concentrations; second, the interpolation of calibrations in time to determine an approximate calibration specific to each sample analysis was technically unjustified and

conceptually somewhat contrary to the quality assurance plan for the experiment. There is no reason to believe that a GC's calibration should drift linearly in time, and the calibration span checks run every four hours on each chromatograph were designed to keep the precision within 5% tolerance.

To correct these problems, all tracer gas concentrations had to be recalculated; this is described below.

5.1.1 Calibration Equations

GC responses to tracer gas samples were converted to concentrations of the tracer by applying calibration equations. These equations were determined by least-square fits of calibration functions to GC responses obtained during calibrations with standard gases.

All of the GCs exhibited responses that can be closely approximated by a power law for concentrations below about 1,500 ppt of SF_6. The AID GC followed the power-law response for both SF_6 and CF_3Br (Freon) over the entire range of concentrations used for calibrations, but the other GCs deviated from the power law above about 1,500 ppt. The following calibration function was used previously in an attempt to treat both the power-law and nonpower-law concentration ranges

$$R = A\,C\,[1 - \exp(-B/C)] \tag{59}$$

where R is GC response, C is the tracer gas concentration, and A and B are constants independent of concentration. Least-square fits were used to estimate A and B for each calibration.

An example of the fit of Equation 59 to a calibration is shown in Figure 123. The fitted function agrees well with the calibration results for concentrations higher than about 2,000 ppt of SF_6, but for lower concentrations the function deviates significantly from the measured responses and gives inaccurate concentration measurements. The manner in which the function deviates from the lower concentrations (higher or lower than the data) varies among GCs and calibrations.

New calibration curves were used to reduce these inaccuracies. They combine two functions: a power function for lower concentrations (below about 1,500 ppt) and an exponential function for higher levels

$$\begin{aligned} C &= A\,R^B, & R < R_o \\ &= A R_o^B \exp[B(R-R_o)/R_o], & R > R_o \end{aligned} \tag{60}$$

(The two functions are equal in value and slope at response R_o.) For each calibration, A and B were found first by linear least-square fit to the logarithm of concentration versus the logarithm of GC response for calibration values for concentrations below 1,500 ppt. R_o was then

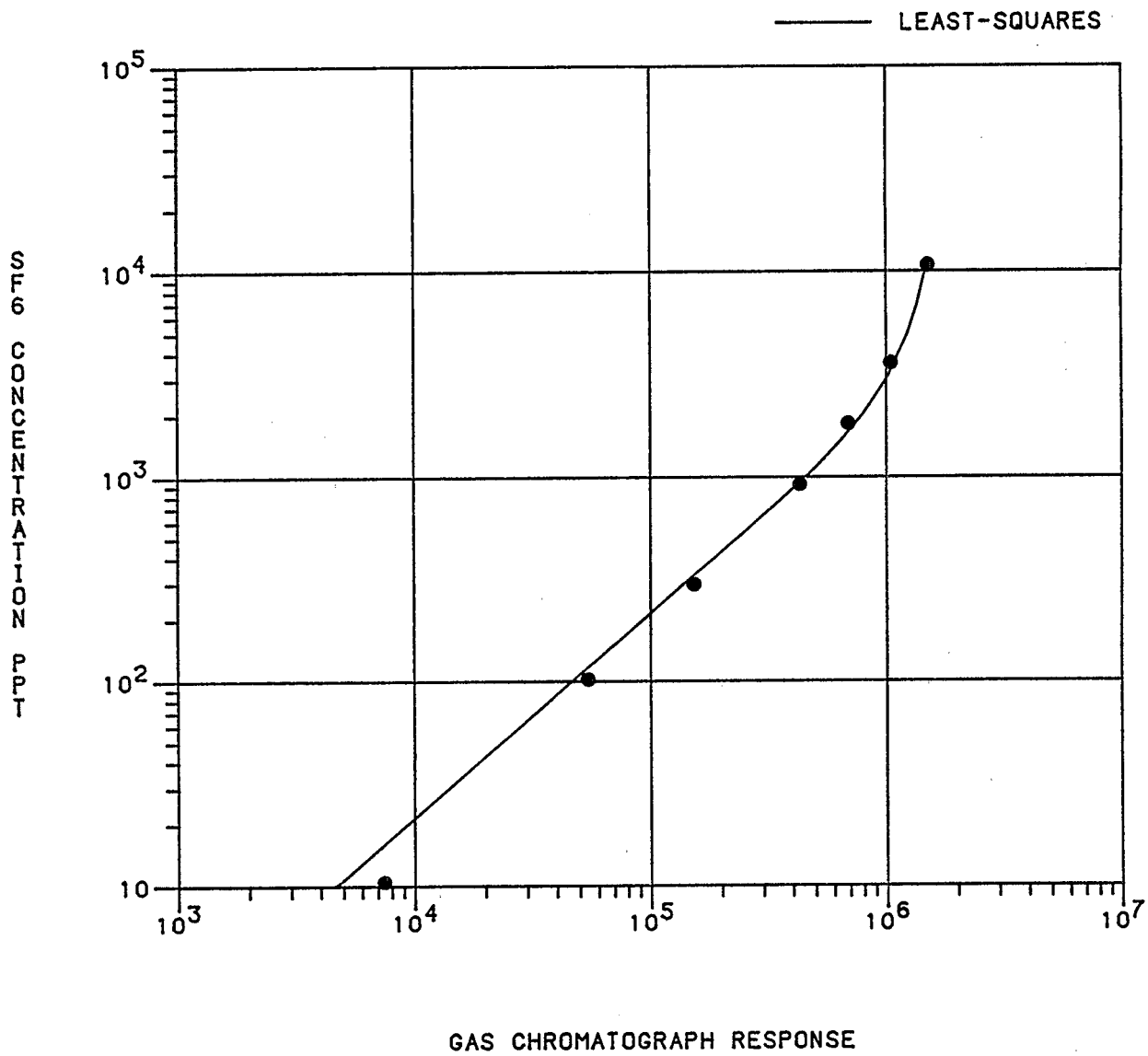

Figure 123. Least-squares fit of old calibration function to calibration of gas chromatograph No. 7, S^3, with SF_6 at 0615 MST on November 11, 1980. Note the consistent over-prediction of concentrations by the least-squares fit below 1,000 ppt.

8205076

determined by a nonlinear least-square fit to the rest of the data, that is, by finding the value of R_o that minimizes

$$\sum_{i=1}^{N} \{C_i - AR_o^B \exp[B(R_i - R_o)/R_o]\}^2 \tag{61}$$

where the subscript i denotes the ith calibration point above 1,500 ppt. R_o was constrained to fall between the last calibration point below 1,500 ppt and the last point in the calibration.

The calibration data showed that the GC response to the lowest SF_6 calibration concentration (which was either 10 or 12 ppt) was extremely variable. In many cases, for concentrations above the lowest value, a GC's responses agreed within 5% in consecutive calibrations, whereas the response to the lowest concentration might differ by as much as 50%. As discussed in Section 5.1.3, the lower quantifiable limit for SF_6 analysis was about 10 ppt. For these reasons, the lowest calibration concentration was excluded from the least-square fits of the calibration functions. (Note that the power-law concentration curve must go through the point (0,0).)

An example of the fit of the new function to calibrtion dta is shown in Figure 124. The agreement is good below about 2,000 ppt. Although percentage differences between the fitted functions and the data were usually larger above 2,000 ppt than below it, all data agreed with the function within about 15%.

As mentioned above, the AID GC response followed a power law throughout the entire calibration range, and only a power-law function was used to fit it. This GC was operated in several ranges selected through an electronic attenuator. Separate functins were not fit to the calibrtion data for each range; instead, the data were combined by multiplying the instrument response by the attenuation factor. In all cases, the responses at different attenuation factors agreed within a few percent when scaled to a common attenuation. The AID GC also exhibited vriable responses to the lowest SF_6 calibration concentration, which was therefore excluded from the least-square fits of the power law to the calibrations.

An example power-law fit to SF_6 calibrtion data for the AID instrument is shown in Figure 125. The figure shows that agreement with the data is good. The GC responses at two attentuations are plotted for all calibration gases but those with the highest and lowest concentrations. The near coincidence of the points demonstrates the validity of scaling the different ranges to a common attenuation. The plot also shows the deviation of the lowest concentration from the power law.

The AID GC was the only instrument used to measure Freon 13B1. A power law was used to fit the Freon 13B1 calibrations, and data from different ranges were scaled to a common attenuation. As with SF_6, the instrument responded variably to the lowest calibration concentration, 200 ppt; this concentration was excluded from the fits. Figure 126 shows an example of a fit to the Freon 13B1 calibration data.

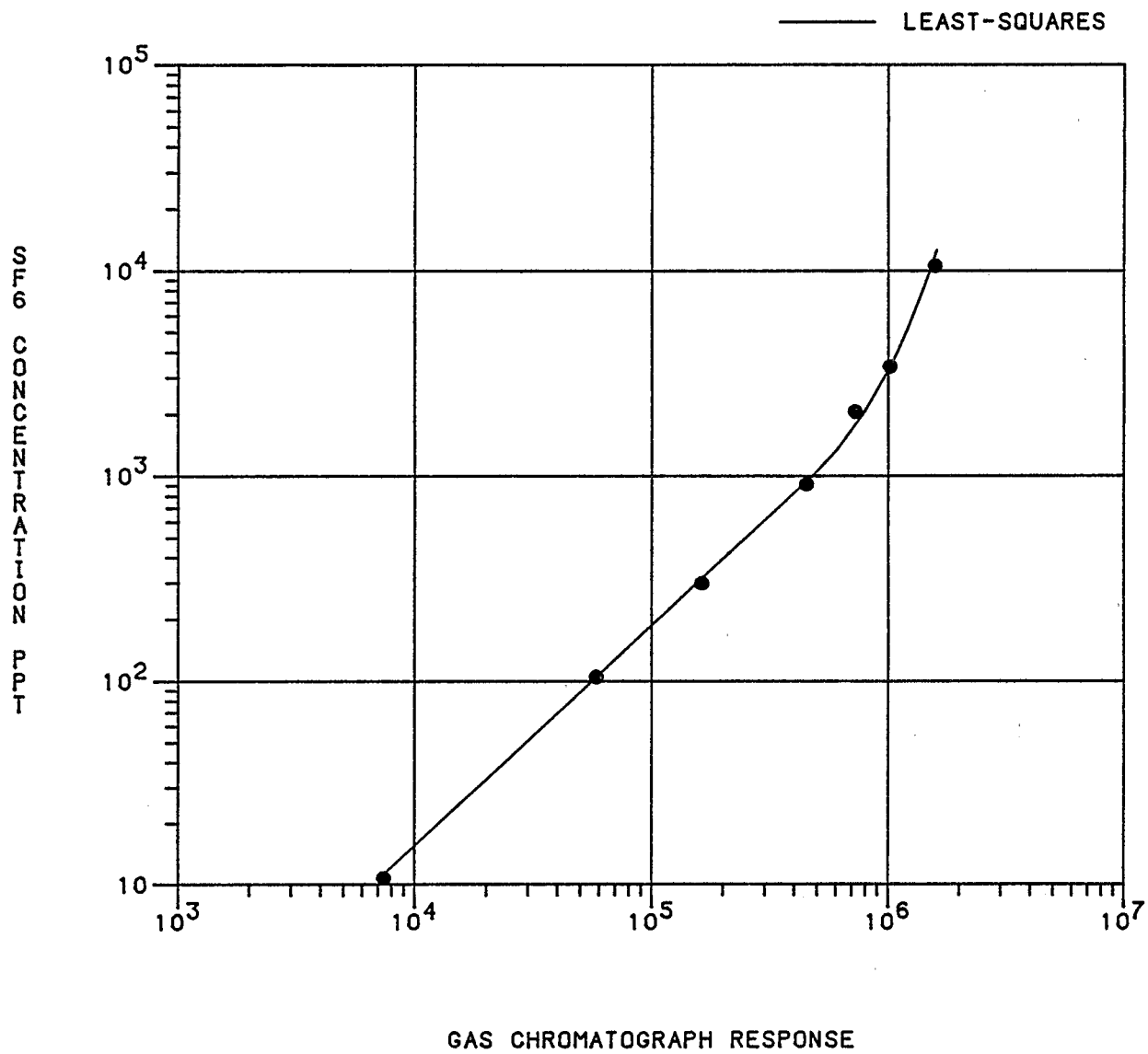

Figure 124. Least-squares fit of new calibration function to calibration of gas chromatograph No. 7, S^3, with SF_6 at 0615 MST on November 11, 1980. The new function fits concentrations below 1,000 ppt better than the old function shown in Figure 123.

8205075

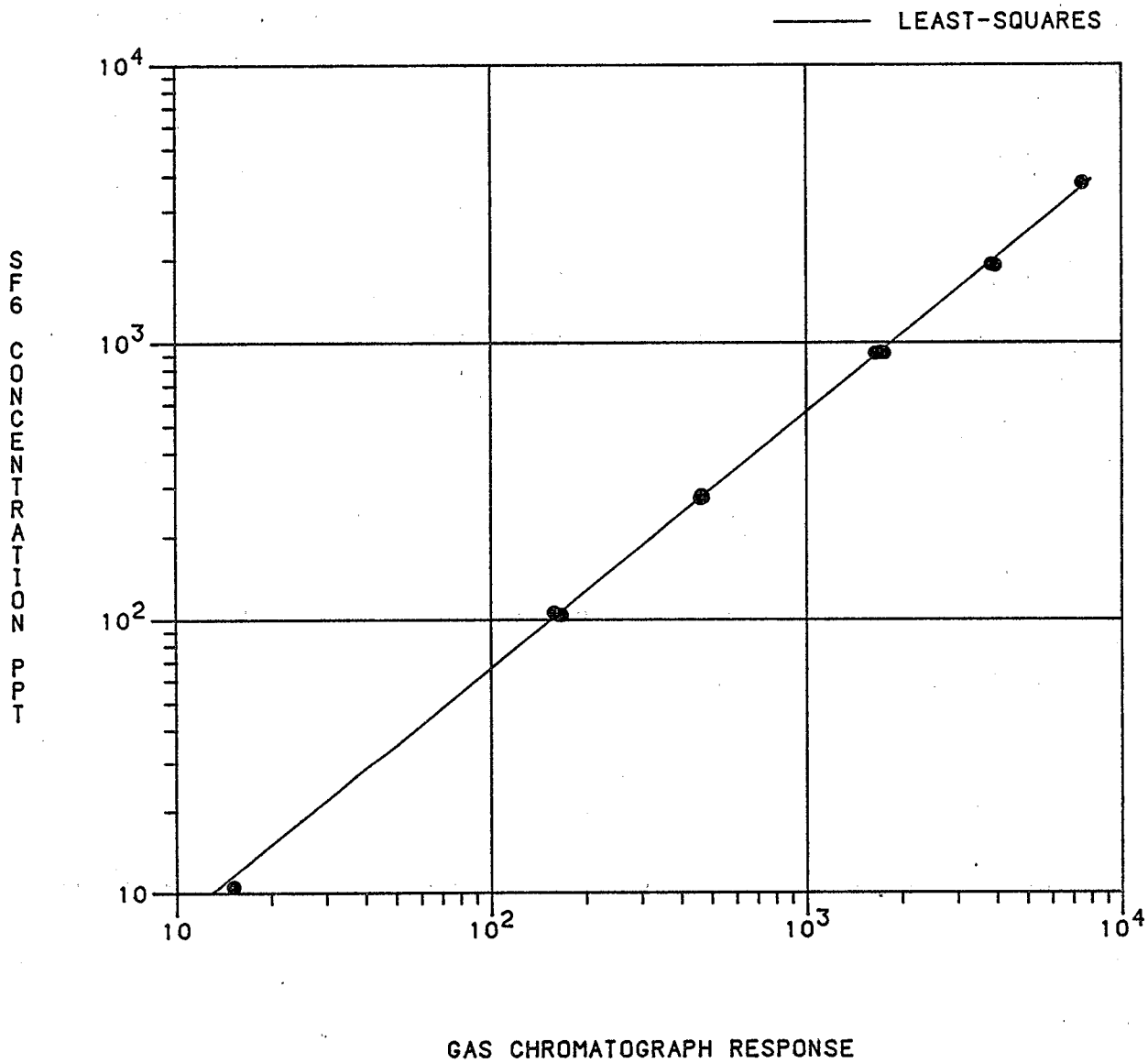

Figure 125. Least-squares fit of power-law function to calibration of the AID gas chromatograph with SF_6 at 0600 MST on November 11, 1980.

8205074

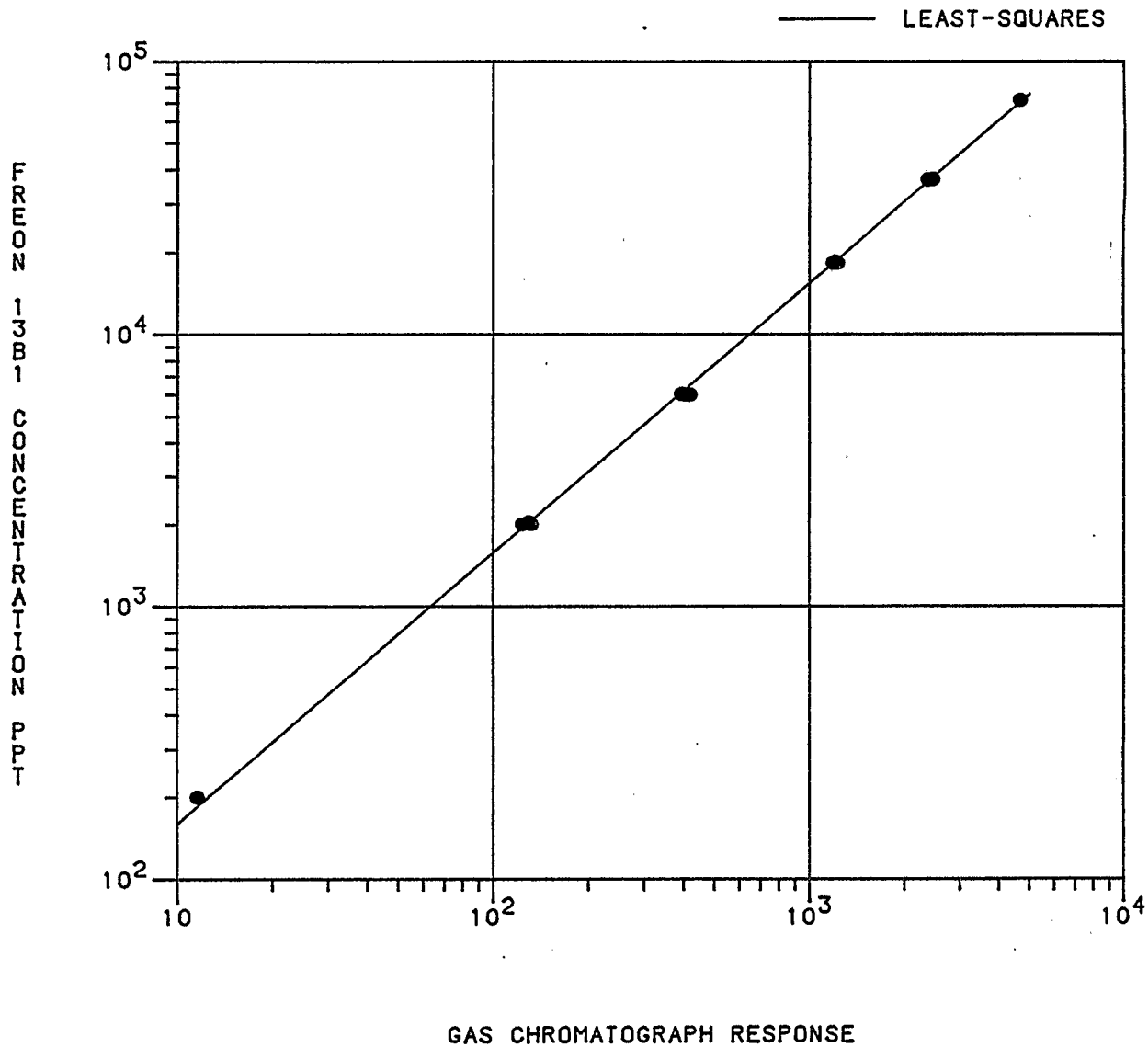

Figure 126. Least-squares fit of power-law function to calibration of the AID gas chromatograph with Freon 13B1 at 0615 MST on November 11, 1980.

8205073

5.1.2 Tracer Data Refinement

Tracer gas concentrations were recalculated from instrument responses by means of the new calibration functions. Previously, linear time interpolation of the calibration parameters (A and B in Equation 59) had been used to attempt to account for drifts in GC response between calibrations. However, data were not available to verify that changes in response were linear with time, and time interpolation was not used in reconstructing the data base. Instead, the most recent calibration was used to calculate concentrations. The response of each GC to a single calibration concentration was checked every four hours, and the instrument was recalibrated if the response differed by more than 5% from that obtained during the most recent calibration. Therefore, according to experimental design, drift between calibrations should not have introduced an error of more than 5% in the data. Because the Baseline GCs could not be kept within this limit, their use was abandoned after a few experiments.

Before concentrations could be recalculated for experiments 201 through 203, it was necessary to enter GC response and analysis time-of-day information into the data base. These data were not entered originally, because concentrations had been calculated manually for these experiments and entered directly into the computer. Some problems in the original data base were discovered and corrected during this data entry process:

- Erroneous recount results in experiment 201: Results of the first analysis of re-analyzed samples were entered instead of the results of the second analysis. These errors were identified by reviewing the recount log sheets, on which the results of recount analyses were recorded.

- Incorrect identification of GCs for some analyses in experiment 203: Corrections for these errors were discovered by comparing GC analysis log sheets, from which the data were entered originally, with GC strip charts and integrator printouts.

- Erroneous elimination of samples with collection times after midnight: These errors were identified by reviewing the field sampler log sheets, and the samples were restored to the data base.

The improvements in the SF_6 data can best be evaluated by examining recount data, which were obtained by repeating the analyses of some of the tracer gas samples. In almost all cases, the repeated analysis was not performed on the same GC as the first analysis, with the exception of samples that were analyzed for Freon, which could only be reanalyzed on the AID instrument. Therefore, deviations of the fitted calibration equations from the true GC response contributed to deviations between the two analyses. Table 21 shows average absolute percent deviations between the first and second analyses within various concentration ranges for the original and refined data bases. The numbers in the table were calculated only from recount data for samples that were not voided because of sample collection problems. The absolute percent deviations were calculated by

TABLE 21
AVERAGE ABSOLUTE PERCENT DIFFERENCES
OF RECOUNT DATA BY CONCENTRATION RANGES

Concentration (ppt)	Old Data Base	Number of Samples	Refined Data Base	Number of Samples
SF_6				
10-50	19.5	119	16.0	132
50-200	8.2	112	5.5	121
200-500	5.9	76	5.7	92
500-1000	5.9	35	3.8	33
1000	4.7	19	7.8	17
Overall	11.0	361	9.0	394
Freon 13B1				
200-500	10.0	10	14.6	6
500-1000	8.1	9	8.2	9
1000-6000	3.1	16	3.6	14
6000-12000	1.0	3	1.3	14
12000	2.0	1	1.4	1
Overall	5.8	39	5.3	44

$$d = \left| \frac{c_1 - c_2}{c_1} \right| \times 100 \tag{62}$$

where c_1 and c_2 are the first and second analyses of the sample. As seen in the table, the deviations were reduced substantially for SF_6 concentrations below 1,000 ppt. The average deviation tended to increase above that concentration, probably because the old calibration function (Equation 59) tended to fit the data better at high concentrations. However, the cumulative frequency distribution of measured SF_6 concentrations in Table 22 shows that more than 98% of the SF_6 measurements were below 1,000 ppt, and that 96% of the measurements above 10 ppt were below 1,000 ppt. Hence, the new calibration functions have resulted in significant improvement in the quality of a large majority of the SF_6 data.

5.1.3 Precision and Lower Quantifiable Limit

The recount data provide information to estimate the precision of the tracer analyses as a function of concentration and to estimate the lower quantifiable limit of the measurements. Precision is a measure of the agreement among individual measurements of the same quantity. Because of the inherent variability in any measurement process, replicate measurements of the same quantity by the same method yield different results. The precision can be defined as the standard deviation of an infinite number of replicate measurements. It cannot be determined exactly, but it can be estimated.

Several pairs of analyses of the same sample can be used to estimate the standard deviation of the measurement (EPA 1976)

$$\sigma \approx \frac{0.886}{N} \sum_{i=1}^{N} R_i \tag{63}$$

where N is the number of pairs of analyses and R_i is the absolute difference between the two values in the ith pair. The recount analyses were not replicate pairs of measurements of a single sample, but Equation 63 can be applied to estimate the precision within concentration ranges. This application assumes the precision is constant within the ranges used.

Table 23 lists the precision of the SF_6 analyses for various concentration ranges and gives the average absolute differences of the recount data and the estimated standard deviation as a percentage of the midpoint concentration in the concentration ranges. Between 10 and 30 ppt, the precision improves rapidly and σ decreases from 35% to 11% of the concentration. Between 50 and 1,000 ppt, σ is about 4% of the concentration; above 1,000 ppt, it averages about 6.5% of the concentration.

TABLE 22

CUMULATIVE FREQUENCY DISTRIBUTION

OF SF_6 CONCENTRATIONS

Concentration (ppt)	Number of Samples Below Concentration	Percent of Samples Below Concentration
5	6,228	51.3
10	6,952	57.3
20	7,677	63.3
50	8,691	71.6
70	9,092	74.9
100	9,526	78.5
200	10,389	85.6
300	10,923	90.0
500	11,469	94.5
750	11,777	97.1
1,000	11,936	98.4
2,000	12,082	99.6
5,000	12,130	99.98
9,821	12,133	100.0

TABLE 23

PRECISION OF SF_6 ANALYSIS

Concentration Range (ppt)	Number of Samples	Average Absolute Difference of Recount Data (ppt)	Standard Deviation of Analysis (Percent of Midpoint Concentration)
5-10	23	3.0	35
10-20	49	3.1	18
20-30	42	3.1	11
30-40	24	3.8	10
40-50	17	5.6	10
50-75	33	3.0	4
75-100	29	5.6	6
100-150	37	6.8	5
150-250	47	7.3	3
250-400	45	21.4	6
400-600	30	21.4	4
600-1000	25	30.8	4
1000	17	189.7	5*

*Highest concentration of first recount analysis was 6,420 ppt. Midpoint concentration of 3,710 ppt was used.

The lower quantifiable limit (LQL) is the lowest concentration that can be measured with a specified precision. Usually, it is defined as the concentration at which the precision is one-third of the value. For SF_6, this concentration is about 10 ppt; for Freon 13B1, it is about 220 ppt.

5.2 Refinement of Meteorological Data

5.2.1 Reasons for Refinement

As stated in the first milestone report, there were consistent differences in the wind speeds and directions derived from the cup-and-vane (Climatronics F460) and UVW propellor systems mounted at the same height on the same tower. This is because the propellor systems do not respond fully to the wind component along their axes. This deviation from cosine response has been documented in the past (Horst 1973, Wyngaard 1981, Pond et al. 1979, Gill 1975), but a preliminary examination of CCB data showed that the discrepancies in the wind speeds derived from the two systems were far greater than were expected on the basis of deviations from cosine response shown in the published reports. Accordingly, it was important to test the responses of a complete three-axis propellor set in a wind tunnel.

Tests on propellor sets could not be run at Colorado State University's tunnel in Fort Collins until early April 1982. In the two test days available, one complete set of UVW transmitters was tested for response at angles of attack incremented every 10° from 0° to 350° and additionally at 45°, 135°, 225°, and 315°. A second set was run to check consistency at a few angles.

Another characteristic of the wind data measured at CCB was an apparent effect caused by tower wakes. This appeared to disrupt the propellor data from the 150 m profile tower when the winds blew from directions between 90° and 125°. Because many experiments were run when the wind was blowing from these directions and because the wind profiles from these instruments must be used for estimating directions and speeds at source height, it was necessary to correct for these wakes.

Lastly, the information from the audits and calibration records of the sensors was evaluated to determine whether errors in orientation and calibration were sufficiently persistent or reproducible to justify correcting the instrument outputs. Errors in temperature sensors were evaluated as well as those in wind sensors.

5.2.2 Calibration Histories and Audits

Information on the accuracy of the calibrations of the meteorological instruments at CCB is contained in calibration records and the reports of two external performance audits. Each instrument was calibrated when it was installed in late September or early October 1980. The calibration was checked when the instruments were removed in the third week of November.

TRC Environmental Consultants, under subcontract to ERT, audited the performance of all the instruments during the first four days of November, and Mr. Thomas J. Lockhart of Meteorology Research, Inc. (MRI), under EPA contract, audited the performance of an easily accessible subset of the instruments a few days later.

TRC audited the systems using standard calibration techniques, including spinning wind-speed sensors at known rpm with synchronous motors, checking the orientation of wind vanes and triaxial propellor systems to true north, and immersing temperature probes in water baths whose temperatures were determined by precision thermometers certified by the National Bureau of Standards (NBS). The instruments' measurement values were determined by converting the voltage put out by the translator cards to engineering units. TRC's results are therefore directly comparable to the calibrations done by ERT's field personnel.

Mr. Lockhart's audit differed in two ways. First, he used the technique he has devised for auditing the performance of temperature probes by inserting them in "thermal masses." Second, instead of reporting the voltage outputs of the instruments' translator cards, he held the instruments in the audit condition for at least one full 5-minute averaging period of the data acquisition system and reported the output in engineering units produced by the data collection computer. Consequently, his audit checked not only instrument performance but the performance of other elements of the data system as well, principally the analogue-to-digital convertors in the microprocessors in the instrument shelters. (These converters had been separately checked by the TRC audit, however, and were found to be accurate within a few tenths of a percent.)

The results of the audits and calibrations of the instruments will be presented and discussed in greater detail in the forthcoming quality assurance report for the experiments, now in preparation.

5.2.3 Wind Tunnel Studies

Several wind tunnel studies have been performed on the CCB wind sets by ERT's Western Measurements Division (WMD) in Colorado State University's wind tunnel in Fort Collins. Both cup and propellor anemometers have been studied.

In October 1981 the linearity and calibration of six of the F460 cup anemometers used at CCB were checked. The frequency output of the cup sensors was converted to indicated wind speed by means of Climatronics' calibration curve for F460s with plastic cups

$$V_{mph} = Hz/9.5 + 0.5, \quad \text{or } V_{m/s} = Hz/21.25 + 0.224 \tag{64}$$

The range of wind speeds tested was 6 to 60 mph (2.7 to 27 m/s). The tunnel speeds were measured by ERT's cup anemometer with stainless steel cups that had been calibrated in the NBS wind tunnel in Gaithersburg, Maryland. A linear least-square regression was performed on the data from this NBS

calibration for tunnel speeds of 1.7, 5.3, 15.1, 25.2, and 35.2 mph and was used to convert the frequency output of this transmitter to actual tunnel speed for comparison with the cups under test. This regression line is

$$V_{mph} = Hz/10.10 + 0.529, \quad \text{or } V_{m/s} = Hz/22.59 + 0.236 \tag{65}$$

(The divisor of the frequency in this formula is larger than that shown above for the plastic cups because the stainless steel cups turn faster at a given speed.)

In the range 6 to 40 mph (2.7 to 18 m/s), which is relevant to the CCB data, all the speeds indicated by the CCB cup systems lay within 5% of the speeds measured by the NBS anemometer, over 85% lay within 3%, and over 50% within 2%.

The same sort of study was done with five individual Climatronics UVW wind component transmitters at 0° angle of attack. The manufacturer's calibration line of $V_{mph} = Hz/4.566$ was used to convert the propellor transmitters' frequency output to speed. These anemometers were even more accurate than the F460 cups. The largest difference between the speeds indicated by any propellor transmitter and by the NBS anemometer was only 2.2% for speeds less than 37 mph (16.5 m/s); the other points all lay within 2%.

The most significant experiment done at the CSU tunnel was the determination of the fraction of cosine response given by the U and V components of an assembled triaxial UVW propellor component system. WMD staff from the Fort Collins office did this study during the first week in April 1982. In the experiments with the cup and propellor anemometers described above, both the instrument being tested and the NBS cups were in the tunnel at the same time, situated side by side and at equal distances from the wall respectively closer to each. The speed measurements given by each were therefore taken simultaneously, so questions of variation of the flow are largely irrelevant. The triaxial propellor anemometer, however, is sufficiently large that both it and the NBS cups could not be placed simultaneously in the same tunnel section without one or the other getting too close to a tunnel wall.

As luck would have it, there were hurricane force winds in Fort Collins on the first day of the experiment, and there was some doubt about the stability of the tunnel controls in such conditions. However, before the test of the UVW set at each tunnel setting, the speed was measured by the NBS cups over a sequence of several periods, each at least 30 seconds long, to demonstrate that the speed was indeed reasonably steady. The first test was run at a very light wind speed. The mean value of the frequency output from the NBS cups during eight 30-second periods was 13.28 Hz with a standard deviation of only 0.331 Hz. The calibration line for the NBS cups at 13.28 Hz yields a speed of 0.82 m/s, but the error in the calibration at such low frequencies is large because of the zero intercept of 0.236 m/s. The original data from the calibration of this wind set when it was certified by NBS show that the instrument's output frequency was 14.1 Hz at approximately 1.7 mph or 0.76 m/s. Linear extrapolation of the NBS data

from the calibration points at 48.0 Hz and 14.1 Hz down to 13.28 Hz gives an approximate speed of 0.72 m/s.

With the tunnel controls held constant, the output frequencies of the U and V sensors were measured at angles of attack varying from 0° to 350° in 10° increments as well as at 45°, 135°, 225°, and 315°, where vector resultant speed is expected to be a minimum fraction of actual flow speed. The frequency outputs of the U and V arms were converted to meters per second by the Climatronics formula $V_{m/s} = 0.447\ (Hz/4.566) = Hz/10.214$. At the end of the light wind test, the tunnel speed was again measured for 30 seconds by the NBS cups, which now gave a reduced frequency of 9.17 Hz. Extrapolating down from the NBS calibration data gives 1.2 mph (0.53 m/s) as the tunnel speed at that time. This is probably a high estimate, however, because of the diminishing responsiveness of the cups at light speeds. The data from this first test are apparently not reliable because of the drop in tunnel speed.

The second tunnel setting gave a frequency output from the NBS cups of 105.9 Hz with no variation in four consecutive 30-second periods; a similar check for 43 seconds after this test yielded a frequency of 105.7 Hz. Data from this higher speed test are probably quite reliable therefore. The calibration line for the NBS sensor gives a speed of 4.92 m/s for a frequency of 105.9 Hz.

The third test of the UVW sensor response was run at a still higher wind speed. Six periods varying in length from 30 to 60 seconds gave a mean frequency output from the NBS cups of 222.16 Hz with a standard deviation of 0.75 Hz. A 30-second check at the end of this test yielded a frequency of 222.12 Hz; again the data seem reliable. The calibration line of the NBS cups gives 10.07 m/s for 222.16 Hz.

During this experiment, the W propellor never turned, nor did the U and V propellors when the flow was normal to them, just as one would expect.

The results of these experiments are shown in Figures 127 and 128 (set A), in which the plotted values are the observed fractions of cosine response from the U and V arms of the anemometer; i.e.

$$F_u = -\frac{u}{u_o \sin\theta}, \quad F_v = -\frac{v}{u_o \cos\theta} \tag{66}$$

where u_o is the tunnel speed indicated by the NBS-calibrated cups, and θ is the wind direction as it would be with the instruments mounted in the field; that is, $u>0$ for winds with westerly components and $v>0$ for winds with southerly components. In order to display the symmetry of the responses of the U and V components, the data are plotted together for the two components in Figure 129. Here the wind direction for the V response θ_v has been set to $\theta_v = 90° - \theta$. This makes a wind from 90° blow with an attack angle of 0° (directly onto the outward-facing side of the propellor), and a wind from 270° blow from the junction block of the three component arms down the shaft of the arm to the back side of the propellor.

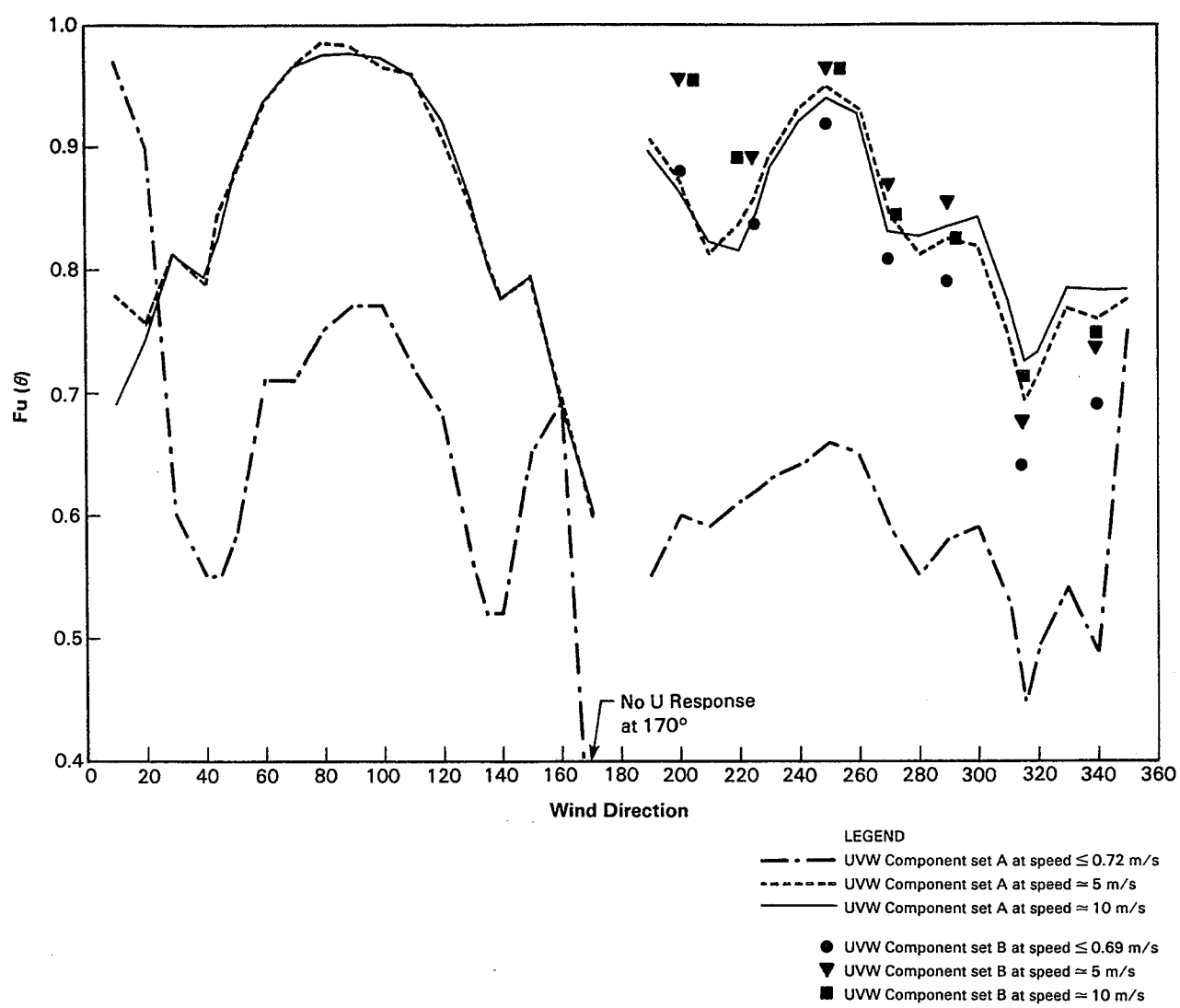

Figure 127. F_u, fraction of cosine response of U-propellor, from wind tunnel experiments as a function of wind direction as mounted in the field.

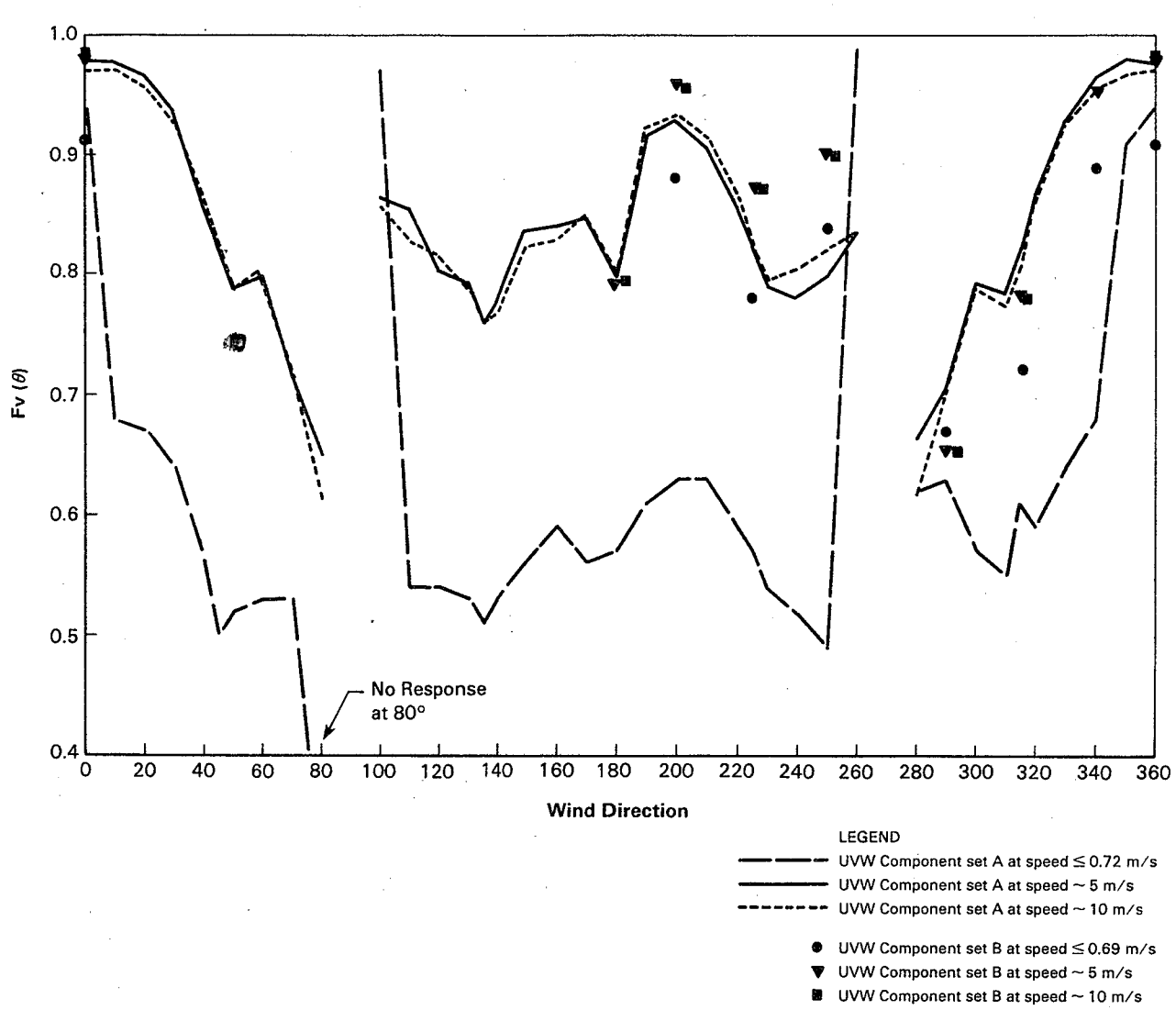

Figure 128. F_V, fraction of cosine response of V-propellor, from wind tunnel experiments as a function of wind direction as mounted in the field.

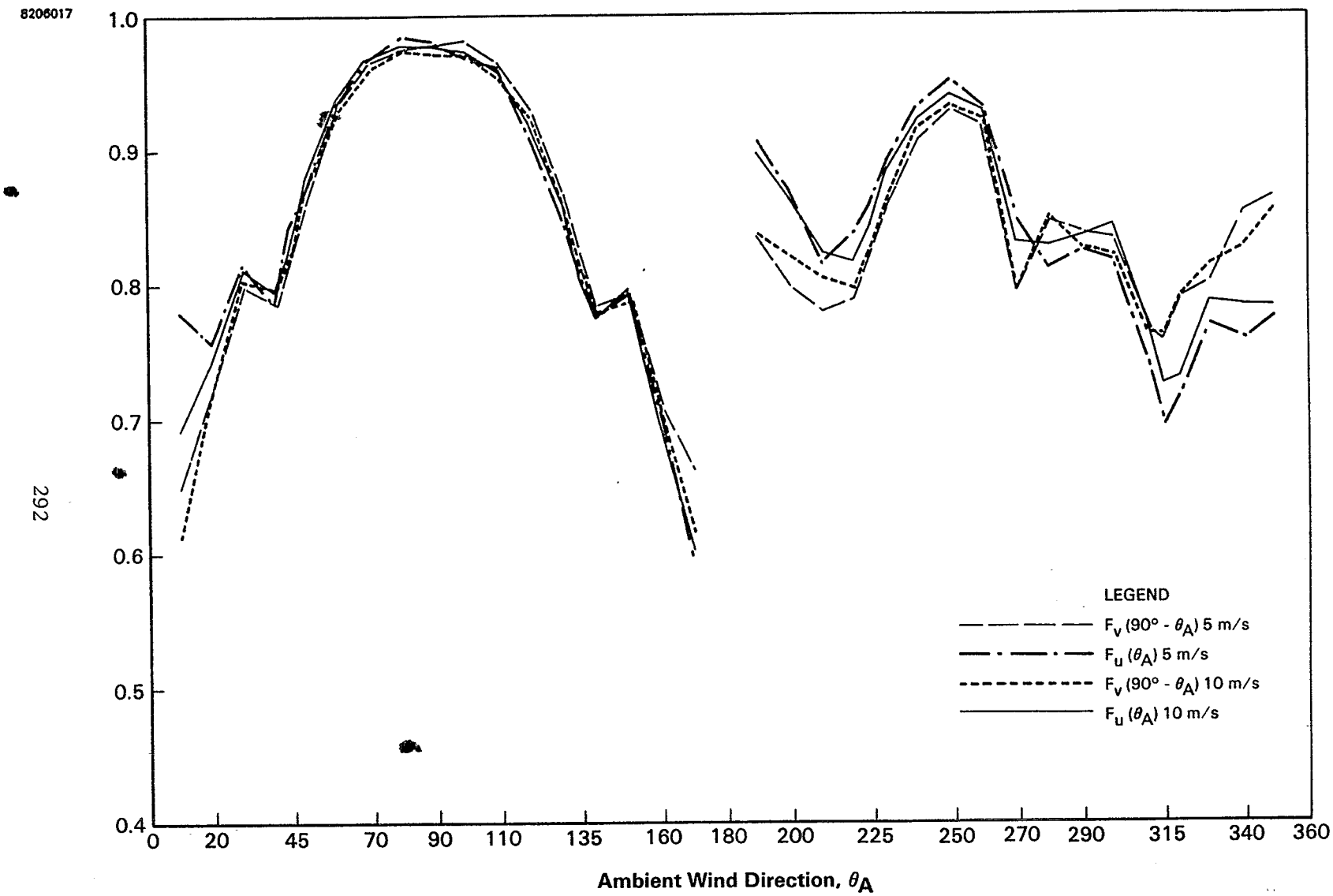

Figure 129. F_u and F_v from wind tunnel experiments plotted symmetrically (θ_V = 90° - θ_A). Responses at 5 and 10 m/s for UVW set A only. (θ_A is "ambient" direction as instruments are mounted in the field).

The data from the experiment with the tunnel speed less than 1.0 m/s have been omitted.

Several characteristics of this plot are noteworthy. First, the responses at 5 m/s and 10 m/s are nearly identical except where the angle of attack on the propellor approaches 90°. Second, the UVW system seems to behave quite symmetrically as a whole, but the responses of the individual arms are not symmetrical about attack angles along the axes of the transmitters. For example, the responses at 60° are different from those at 120°, and the responses at 250° are different from those at 290°. This asymmetry is attributable to the wake of one component sensor acting on the other at 290° and not at 250°, but it is unclear why this should be the case near 90°, where it would seem that no part of one arm could affect the other. However, the asymmetry is small in this region. A third obvious characteristic of the data is the large impact of the sensor components themselves when they are upwind. This was noted by Gill (1975) during tests of his early designs, and he modified his later instruments so that the U and V arms extended from the vertical shaft at different heights, and the bulky cube at the "origin" of the three arms was eliminated. The Climatronics system retains the cube and has no vertical offset of the arms.

Another remarkable feature of the experimental data is the increased response of the transmitters when the wind is ±60° from the axis of the propellor, that is, at winds from 30° and 150°. This feature is clearly defined in the data from both arms and at both tunnel speeds, but no explanation for it is obvious.

A second set of UVW components was assembled and tested at a few angles of attack to check the reproducibility of the results from the first set. The people performing the experiment noted that the hardware joining one arm to the central block caused the angle between the U and V arms to differ by a few degrees from a right angle. The data from this windset are therefore somewhat suspect, but they have been plotted as points on Figures 127 and 128 (Set B) nonetheless and appear only slightly displaced from the results of the more complete experiment with the first set of UVW transmitters.

Wind data from the CCB experiments were analyzed for comparison to the results of the wind tunnel experiments. Cup-and-vane and UVW anemometers were located at the same tower levels at nine sites in the network, but the winds at the 2 m level of tower A were not analyzed because the speeds there were so light that the instruments were operating at or near their response thresholds a large part of the time. Plots of the differences between cup-and-vane wind directions and propellor wind directions at the 2 m level show large scatter and no consistent pattern; the differences in wind speeds measured by the two systems show similar scatter. The data from the co-located instruments at 10 m on the four towers on the flanks of the butte (towers C through F) were not analyzed because the large vertical component of the wind at these sites would confound the analysis. Up to fairly large angles of attack, cup anemometers respond positively to vertical motions, either up or down, but at larger angles to the flow they respond negatively, until they actually turn backwards at very large angles. Only the data from

the 10 m and 150 m levels of tower A and the 10 m and 30 m levels of tower B were judged suitable for this analysis.

After correction for orientation of the vanes and UVW sets to true north, all the valid 5-minute wind data taken at each of these four sites during the tracer experiments were classified according to vane direction into 36 groups, each 10° wide (0°-10°, 10°-20, etc.). Within each direction class, the data were further classified according to whether the 5-minute vector-resultant wind speed from the propellors was less than 1.5 m/s, between 1.5 and 5.0 m/s, or greater than 5.0 m/s. The cup-and-vane data were assumed to be accurate measures of the mean speed and direction of the flow. Except for very light wind periods, this assumption seems reasonable because the generally low turbulence intensities during the experiments mean that overspeeding of the cups was minor.

The fraction of cosine response, F_u and F_v, from each horizontal arm of the propellor system were calculated in a manner identical to that used for the wind tunnel data. The number of points in each wind direction group and the sample mean and standard deviation of the fractional responses in each group were then calculated and listed. Data groups whose standard deviations exceeded 10% of their means were excluded from further consideration. This latter criterion excluded all the data with propellor-derived speeds less than 1.5 m/s. The remaining data in the two speed groups above 1.5 m/s were combined, and the sample means (and standard deviations) of the fractional responses were again calculated to give an overall average fractional response for each U and V arm for each 10° direction class and at each of the four sites.

The average F_u's and F_v's were in turn averaged across the four tower sites, with any site average excluded if the standard deviation of the responses at that site exceeded 10% of the mean, but only if there were data with less variation at some other site. In general, the data show a satisfactory lack of scatter for wind directions that had a high frequency of occurrence, were not taken from very high angles of attack, and did not cause tower wakes on the sensors. These directions are naturally those which occurred most frequently during the experiments, that is, northwest and southeast.

The F_u and F_v results from the wind tunnel experiments at 5 m/s and 10 m/s were averaged at each angle of attack. For application to the CCB data, a running two-angle averaging was then done. (Data from three angles of attack were averaged for the 40°-50°, 130°-140°, 220°-230°, and 310°-320° sectors because of the data also taken at the central angle of the sectors.) This averaging was done not only because the ambient data had been averaged in 10° sectors, but also because the sharp peaks and valleys of the propellor responses in the wind tunnel would have been smoothed out somewhat by turbulence and meander in the atmosphere.

Finally, the average wind tunnel and ambient F_u's and F_v's were themselves averaged to give the values to be used in the correction of the CCB data. Table 24 lists the average ambient values, the average wind tunnel values, and the values used in the data correction. For wind

TABLE 24

AVERAGE FRACTIONS OF COSINE RESPONSE SHOWN BY U AND V PROPELLOR ANEMOMETERS: CCB FIELD DATA, CSU WIND TUNNEL DATA, AND VALUE APPLIED AS CORRECTION FACTOR TO FIELD DATA

Direction Sector	Average Fu			Average Fv		
	CCB Data	Wind Tunnel	Applied	CCB Data	Wind Tunnel	Applied
0-10	(.927)	(.736)	.736	.949	.975	.962
10-20	(.751)	.743	.743	.927	.969	.948
20-30	--	.781	.781	.909	.947	.928
30-40	(.811)	.802	.807	.843	.897	.870
40-50	(.846)	.833	.840	(.814)	.825	.820
50-60	(.916)	.904	.910	.707	.794	.758
60-70	.979	.950	.965	.626	.758	.709
70-80	.959	.974	.966	(.694)	.672	.683
80-90	1.004	.980	.992	(1.410)	(.631)	.694
90-100	.980	.975	.978	(.686)	(.860)	.821
100-110	.972	.965	.968	.917	.850	.884
110-120	.932	.937	.935	.870	.824	.847
120-130	.862	.882	.872	.826	.799	.813
130-140	.781	.811	.796	.798	.773	.786
140-150	.746	.785	.766	.844	.799	.822
150-160	.680	.747	.714	.823	.831	.827
160-170	(.600)	.650	.625	.806	.841	.824
170-180	(-.109)	(.601)	.677	.796	.822	.809
180-190	(.398)	(.827)	.827	.839	.858	.849
190-200	(1.037)	.884	.935	.831	.926	.879
200-210	(.833)	.843	.843	(.700)	.921	.921
210-220	(.800)	.823	.823	(.908)	.885	.897
220-230	(1.010)	.855	.855	(.800)	.825	.813
230-240	(.712)	.907	.907	(.739)	.792	.766
240-250	.912	.936	.924	(.802)	.801	.801
250-260	.866	.939	.903	.875	.823	.849
260-270	.877	.885	.881	.866	(.836)	.792
270-280	.845	.880	.863	(.765)	(.640)	.703
280-290	.875	.828	.852	.760	.672	.716
290-300	.814	.831	.823	.820	.748	.784
300-310	.767	.796	.782	.815	.786	.801
310-320	.748	.731	.740	.866	.820	.843
320-330	.769	.754	.762	.937	.896	.917
330-340	.767	.776	.771	.941	.943	.942
340-350	.621	.776	.699	.960	.967	.964
350-360	(.484)	(.780)	.632	.970	(.975)	.972

Note: Numbers in parentheses are questionable because of small sample or high variability.

directions in which the CCB data showed substantial scatter, the ambient average is enclosed by parentheses, and heavier weight has been given the wind tunnel result unless it is very close to the ambient value. For those cases with very few and inconsistent data from CCB, the wind tunnel value has been used.

5.2.4 Procedures for Refining Meteorological Data

The first milestone report describes the results of the performance audits of the meteorological instruments by TRC and MRI and points out some inconsistencies in the differences between instrument responses and audit values. These audit data have been reexamined together with data from the calibrations done by WMD at the time of installation and at take-down to try to find consistent response errors. Where such are found, corrections have been made to the data. All the audit and calibration information will be presented in the forthcoming quality assurance report so that other users of the data base may make any appropriate modifications.

The refinements made to the meteorological data in response to the audit and calibration data and the wind tunnel studies are described below.

Cup and Vane Wind Data

The performance audit done by TRC checked the response of the F460 cup anemometers by spinning the sensor shafts at 360 rpm with a synchronous motor. This corresponds to a wind speed of 8.69 m/s according to Climatronics' specified calibration line u(mph) = Hz/9.5 + 0.5, or u(m/s) = Hz/21.25 + 0.224.

The responses of the F460s on towers A and B, the 150 m tower north of the butte, and the 30 m tower on top of the south peak of the butte, showed a very consistent error of 0.15 or 0.16 m/s (except at the 30 m level of tower B, where the error was 0.26 m/s)(see first milestone report). The F460s on towers C through F, the 10 m masts on the flanks of the butte, also showed a consistent error between -0.16 and -0.13 m/s at the audit speed of 8.69 m/s. The calibration records of the translator cards on these instruments show the reason for both the precision and sign of these errors: on towers A and B the translator cards were calibrated to 0.045 (0.45 m/s) vdc at 0 shaft rpm or 0.0 Hz, whereas on towers C through F, they were zeroed to 0.000 vdc. The span calibration of the translators of all F460s was done with an oscillator giving 524.8 Hz, which corresponds to 25 m/s or 2.5 vdc, half the scale of these 0-5 v, 0-50 m/s instruments. In fact, the instruments should have been zeroed at the voltage corresponding to 0.50 mph (0.224 m/s) or 0.022 vdc.

The output from the F460s (in meters per second) has been "recalibrated" to give the proper 25 m/s response at 524.8 Hz and the proper 0.224 m/s response at 0 Hz. This recalibration was done with the correction

corrected speed (m/s) = 1.008 x (uncorrected speed) - 0.214(m/s) for towers A and B

corrected speed (m/s) = 0.991 x (uncorrected speed) + 0.224 (m/s)
for towers C through F

TRC also audited the orientation of the F460 vanes to true north and the linearity of the potentiometers (and translators). The mean value of the total error for each vane, including mean nonlinearity, was used to correct its output.

Temperature Data

The audit and calibration data for the temperature and temperature difference systems were examined for consistency. The general variability of the errors, even between the two audits done only a few days apart, is so large that no corrections have been made to the temperature data. The differences between audit or calibration values and output measurements are, in any case, quite small for most of the temperature sensors. All but two indicated errors (both from MRI's audit) are less than 0.2°C in magnitude.

UVW Wind Component Data

The audit and calibration data from the UVW propellor sensors are fairly consistent for some sensors and not for others. The errors are generally less than 0.1 m/s, and because these sensors' deviations from cosine response result in errors far larger than 0.1 m/s, no changes to the sensor outputs have yet been made to correct any apparent calibration errors. Effort has been directed instead to the problem of noncosine response.

The wind tunnel experiments with these sensors and the derivation of the average fractions of cosine response by the U and V arms in the tunnel and at CCB have been described above. To correct the wind component data, each measured component value was simply multiplied by the inverse of the average fraction of cosine response appropriate to the wind direction (see Table 24).

The wind direction was initially estimated by correcting the wind direction WD resulting from the measured U and V components by means of the function

$$WD_1 = WD + 4 \sin (4WD) \qquad (67)$$

This sinusoidal correction is an approximation to the observed difference between actual wind direction in the wind tunnel and the wind direction resulting from the U and V sensor responses. According to the tunnel data, it corrects the direction to within 2.0° in all wind directions.

This corrected wind direction was then used to find the appropriate values of F_u and F_v from Table 24. The values for a specific wind direction were derived by linear interpolation in this table, with the tabulated values for wind sectors 0°-10°, 10°-20°, etc., ascribed to wind directions 5°, 15°, etc. The measured values of U and V were corrected by

dividing by F_u and F_v, respectively. Corrected wind direction and speed were in turn calculated by changing the corrected U and V values to polar coordinates.

Corrections for Tower Wakes

Plots of the differences between 5-minute vector-resultant wind speeds derived from cup-and-vane data (SP) and from propellor data (WS) versus 5-minute vector-resultant vane direction (DR) showed a pattern of deficit in WS in certain wind directions that corresponds to periods when the propellor sensors were in the lee of the tower. Figure 130 is the plot of this wind speed difference at the 150 m level of tower A, where the pattern is best defined because of the steady winds at that height. (The data plotted have not been corrected for propellor response.) There is a region between 90° and 125° and centered near 110° in which the propellor speed is low, apparently only about 40% of the cup speed in the core of the region. To the left (north) of this region is a less well-defined deficit in cup speed relative to propellor speed. Figure 131 is a sketch, approximately to scale, of the 150 m level of tower A; the 10 m level was the same. Because no cup-and-vane sets were mounted at the 40 m and 80 m levels, the UVW component sensors were not offset to the north on a crossarm, and the wake of the tower should be most pronounced at wind directions slightly south of 90°.

Studies of tower wakes in wind tunnels (Gill et al. 1967, Cermak and Horn 1968) and in the atmosphere (Izumi and Barad 1970, Moses and Daubek 1961) have indicated substantial speed deficits in the lee of towers. The amount of the deficit depends on the tower structure, the distance of the sensors from the tower, and the orientation of the sensors with respect to the "legs" or sides of the tower. The width of the tower wake stays approximately constant at 1.5 tower diameters for distances up to 6 diameters downwind. For distances from the tower at which the sensors were mounted at CCB (3 to 4 diameters, a diameter being the length of a tower leg), the speed deficit at the center of the wake is expected to be 20% to 30%. The factor of 2 speed deficit in the core of the wake is therefore somewhat surprising, but the boom carriages of the instrument elevator presented solid obstacles about 0.5 m square. This may account for the increased speed deficit shown in the data.

Speed deficits in the tower wakes were corrected by the function

$$C_T = 1 + C - \frac{2C}{W}\ \theta_o - \theta \quad \text{for } \theta \text{ in region } \theta_o - \theta \leq W/2 \qquad (68)$$

$$C_T = 1 \qquad \text{for } \theta \text{ elsewhere.}$$

Here C is the speed deficit assumed in the center of the wake (at wind direction θ_o), W is the "width" of the wake in degrees, and θ is the wind direction derived from propellor sensors after correction for noncosine response. Wake locations and widths were estimated from the geometry of the towers and sensors. For the 10 m and 150 m levels of tower A, C_T for the propellor speeds was calculated with C = 0.7,

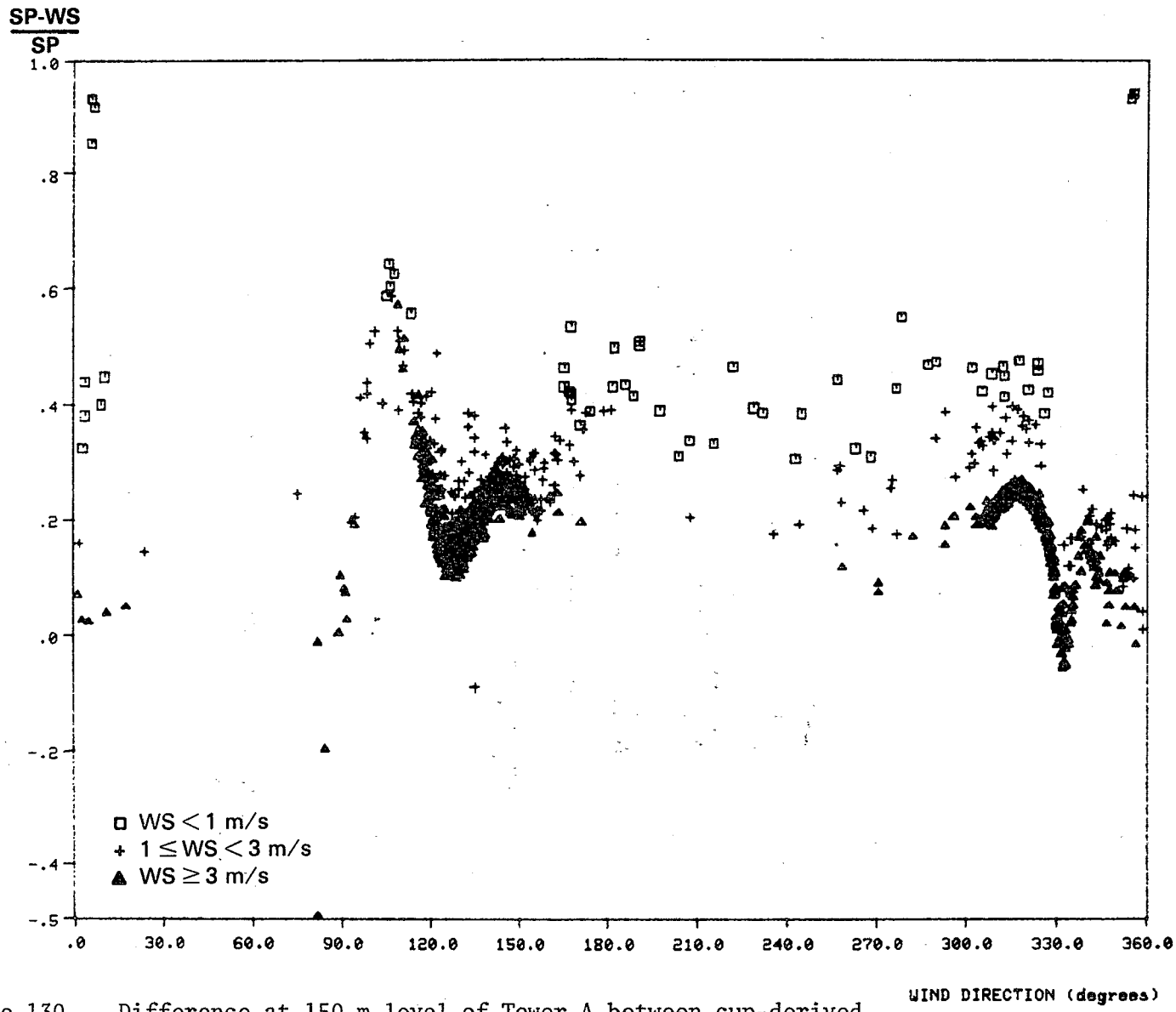

Figure 130. Difference at 150 m level of Tower A between cup-derived wind speed SP and propellor-derived wind speed WS plotted as ratio (SP-WS)/SP as a function of vane direction DR before correction of data.

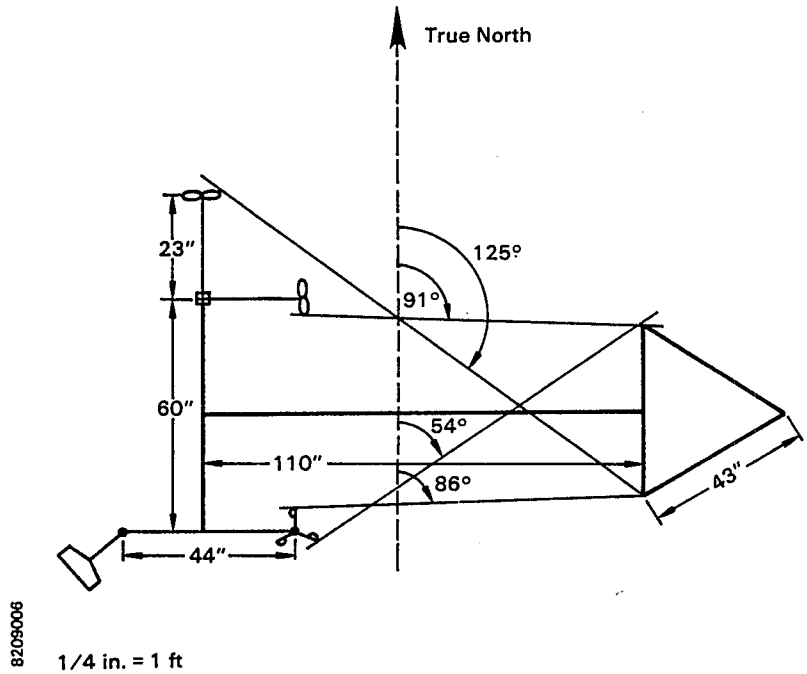

Figure 131. Sketch of geometry of tower, booms, and wind instruments at 150 m level, Tower A.

$W = 31°$, and $\theta_o = 107.5$. For the 40 m and 80 m levels of tower A, the wake on the propellors was assumed to be centered at 92° with a wake 35° wide. Wake correction for the cups on tower A was calculated with $C = 0.7$, $W = 30°$, and $\theta_o = 70°$, and for the cups at 10 m and 30 m on tower B with $C = 0.26$, $W = 20°$, and $\theta_o = 263°$. The wake on the propellors at 10 m and 30 m on tower B was corrected with $C = 0.3$, $W = 30°$, and $\theta_o = 227.5°$. There are few data from the appropriate wind directions on tower B with which to evaluate the corrections for wake effects, and the corrections used more closely follow the suggestions of Gill et al. (1967).

Wind tunnel studies indicate that there is a speed increment at the edge of a tower wake amounting to about 10%. No attempt has been made to correct the CCB data for this increment; it has been assumed that changes of wind direction caused by turbulence during each 5-minute averaging period would tend to put the wind sensors alternately in the increment and deficit regions, which would diminish this effect.

Figure 132 is a plot of the same data after correction that were plotted in uncorrected form in Figure 130. The general improvement in correspondence between cup-and-vane measurements and propellor measurements is obvious. The correction for tower wakes has not been completely successful in eliminating the peakiness in the plots near 90° and 120°. How much of these apparent errors is attributable to overspeeding of one sensor at the edge of a wake and how much to underspeeding at the other is hard to assess. The strange peak centered at 330° also remains. This feature appears, though less distinctly, in the data from 10 m and 30 m on tower B. It is tentatively attributed to the effect of the UVW propellor system on the cup anemometer. If this premise is true, the UVW wind speed is probably a more accurate measurement when the wind is near 330° on these towers since the propellors are upwind of the cups.

Corrections to Turbulence Intensities

The UVW anemometers were used at CCB primarily to determine the intensities of turbulence i_x, i_y, and i_z. Corrections have been derived by Horst (1973) for measurements of those variables made with R.M. Young instruments. Because of the now partially documented disparity in response between the Young and Climatronics versions of the propellor systems, and because Horst's corrections were developed from data taken in only two periods of approximately one-half hour each (neither of which was stable), the applicability of these corrections to the CCB data is doubtful.

The 5-minute values of intensity of turbulence have therefore not been altered. We have elected to leave them alone rather than correct them inappropriately. To some extent the departure from cosine response of the propellor sensors is self-correcting in the calculation of the intensities because both the numerator and denominator of the intensity are "scaled" by the fraction of cosine response achieved by the instruments. However, in the CCB measurements, the ratio of crosswind intensity i_y to alongwind intensity i_x becomes notably smaller as the wind direction approaches the axis of one propellor transmitter, which is expected given the response characteristics. This means that the horizontal turbulence intensities

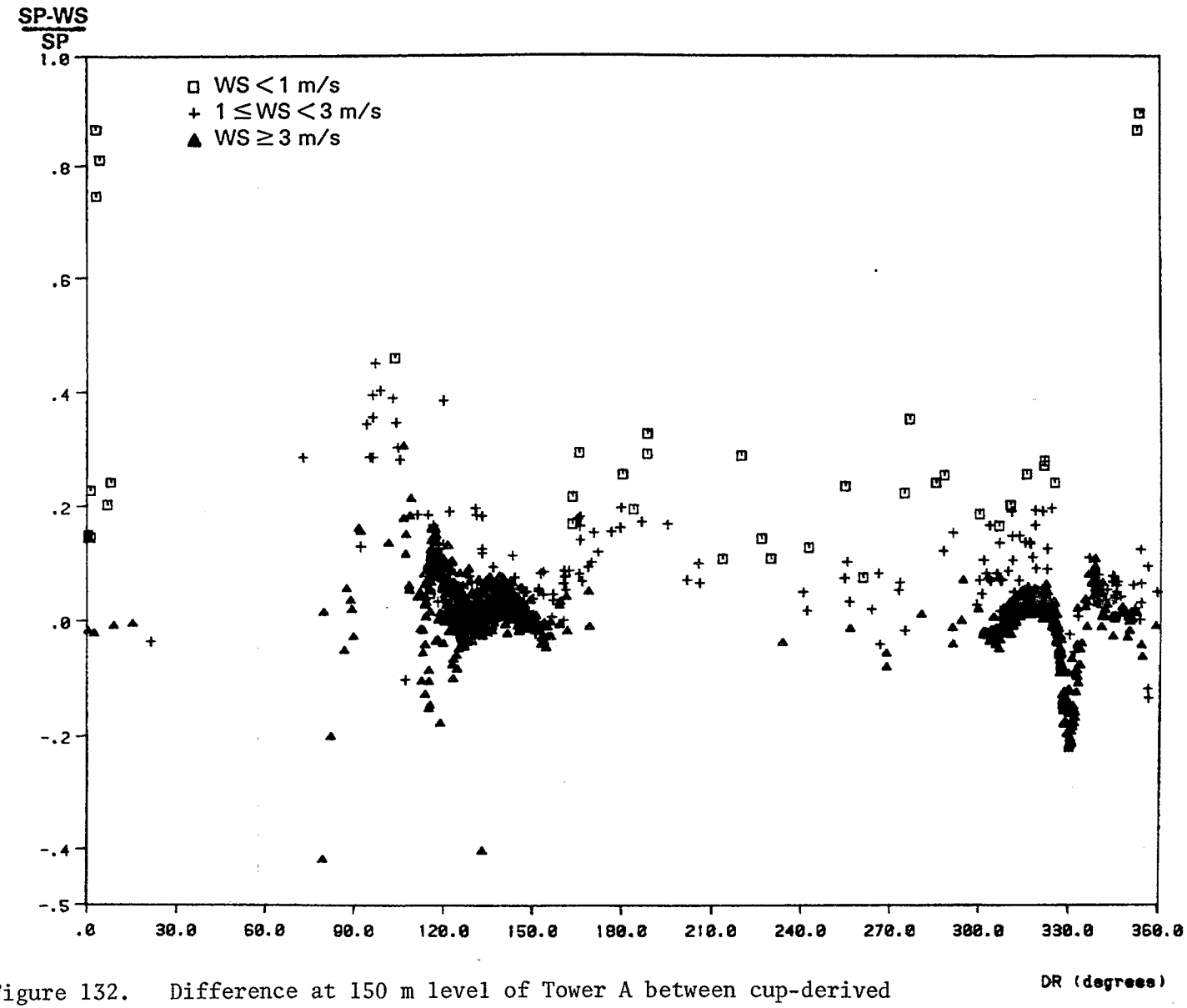

Figure 132. Difference at 150 m level of Tower A between cup-derived wind speed SP and propellor-derived wind speed WS plotted as ratio (SP-WS)/SP as a function of vane direction DR, after correction of data.

recorded in the data base are not simply wrong by some scaling factor, but that their errors are functions of wind direction. The vertical turbulence intensity measurements are almost assuredly underestimates, particularly near the ground and where the mean vertical components are low. This underestimate results not only from the poor cosine response of the propellors to mean flow at high angles of attack but also from the response distance of approximately 1 meter, which limits the response of the propellor to high-frequency oscillations in the vertical.

5.2.5 Results of Data Refinements and Conclusions

The improvement in correspondences between wind speeds derived from propellor systems and wind speeds from cup anemometers has been shown from one sample site, the 150 m level of tower A, in Figures 130 and 132. Figures 133 and 134 show the correspondence between wind directions derived from the two systems at the same site after application of the corrections described above. A large part of the improvement results from simply correcting the data for misorientation of the sensors to true north; the correction for the UVW data at 150 m was +7° and for the vane data, -2°. The changes resulting from the corrections for propellor response have removed most of the cyclic quality of the disparities in direction measurements also. Nevertheless, the sample plots show that there remain anomalies in the comparative data, one of which is probably an effect of wakes on wind direction. This effect is complicated by the fact that the U and V propellors are not normally in the same part of the wake at the same time. Users of the data should be advised to give precedence to data taken from outside wakes whenever possible.

In general, clear improvements have been made in the precision and accuracy of both the tracer and meteorological data from the CCB experiments. Recalibration of the tracer data has resulted in increased precision and reliability of the concentrations. Wind tunnel studies have explained a large portion of the discrepancies between propellor and cup-and-vane data, but some anomalies remain. Corrections for orientation of wind sets has improved the accuracy of wind direction data.

Other improvements in data quality may be possible, but no firm basis for making them is apparent. The calibration and audit data for a few of the meteorological instruments show some consistency, but whether this results from chance or a truly persistent error in response remains a question because so much of this data shows such large variations.

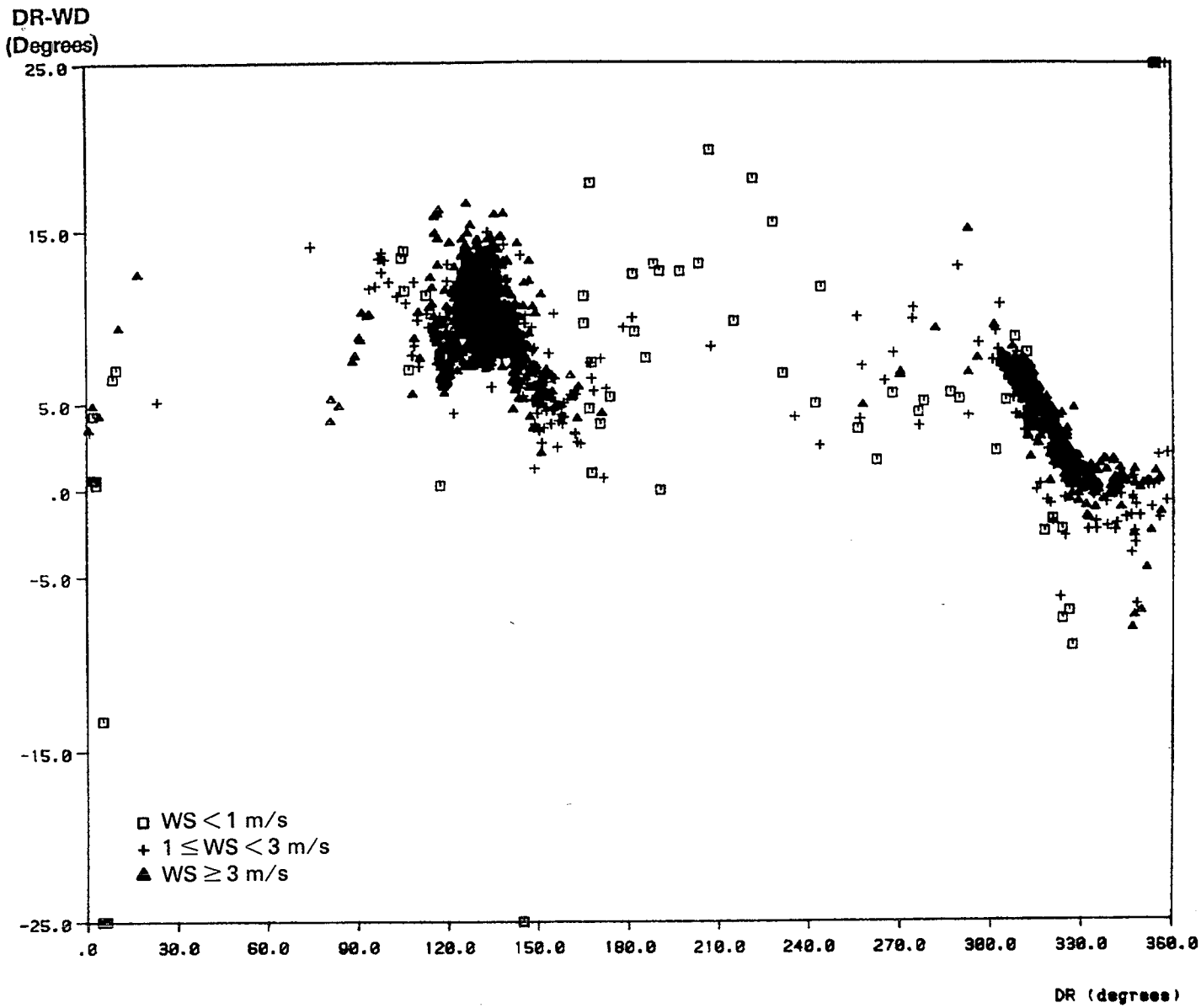

Figure 133. Difference (in degrees) at 150 m level of Tower A between wind direction DR derived from cup-and-vane set and direction WD derived from propellors as a function of DR before correction.

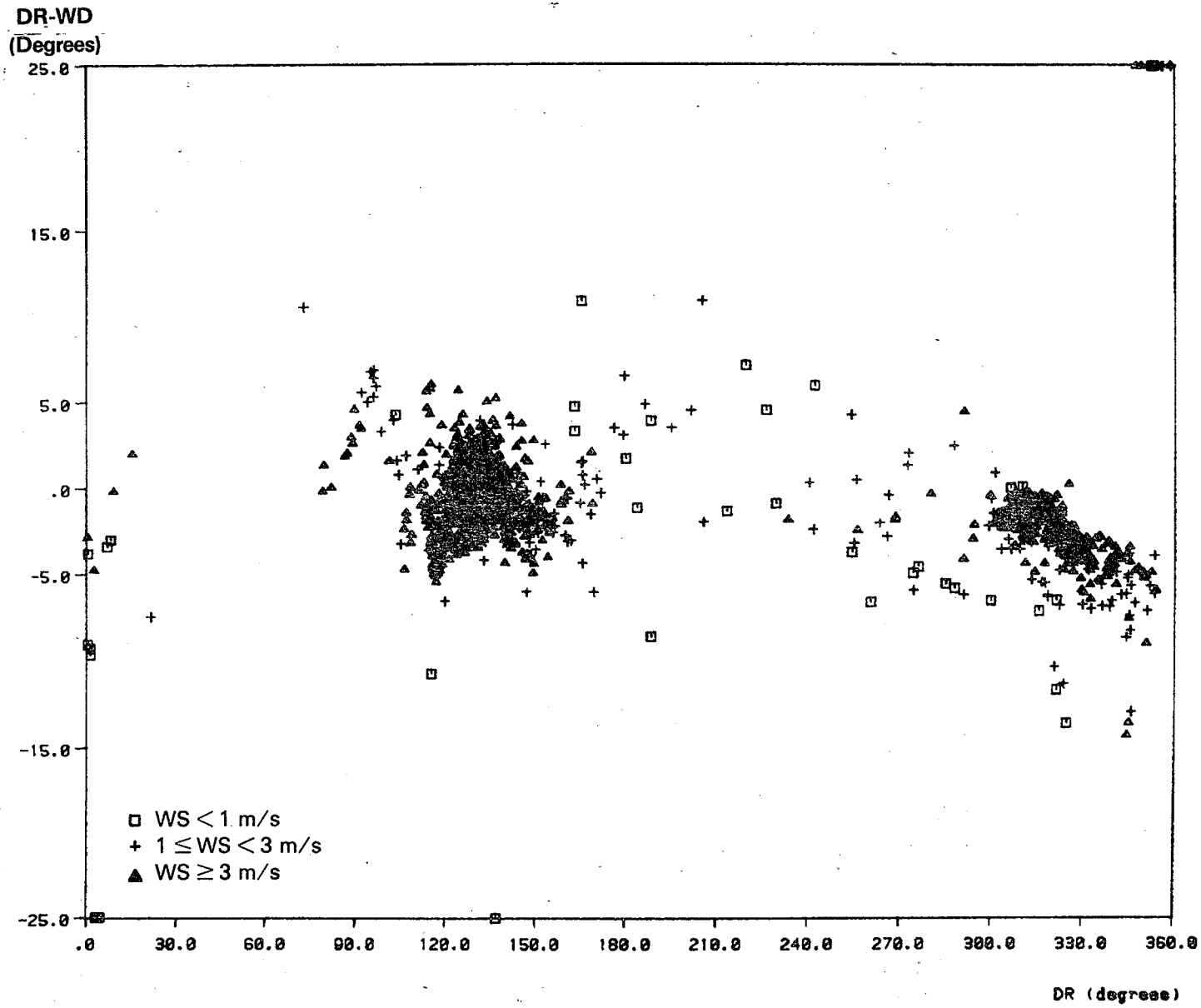

Figure 134. Difference (in degrees) at 150 m level at Tower A between wind direction DR derived from cup-and-vane set and wind direction WD derived from propellors after correction.

SECTION 6

SUMMARY, CONCLUSIONS, AND RECOMMENDATIONS FOR FURTHER STUDY

This document has described in detail the further progress to date in correcting and refining the CCB data bases, analyzing the case study experimental hours selected for intensive study, and in improving the preliminary Neutral and Impingement models and evaluating their performance. In this section we present an overview of conclusions reached so far. Much of the technical analysis that underlies these findings is of very recent completion, and further review, evaluation, and augmentation of these conclusions will undoubtedly be required.

6.1 Principal Accomplishments and Key Findings

6.1.1 Data Base Refinements

The first milestone report described some of the major uncertainties and likely sources of error in the data obtained at CCB. During the study phase just completed, considerable effort was expended to revise the tracer concentrations and meteorological data. This sub-section summarizes these activities.

Tracer Concentration Data

The mathematical functions used to fit gas chromatograph calibrations were revised in order to reduce errors in tracer gas concentrations. All concentrations were recalculated by means of the new calibration functions. The SF_6 and Freon 13B1 recount results were analyzed to estimate the precision and lower quantifiable limits of the tracer gas analysis.

The new calibration functions fit the calibration data within 15% for all concentrations. For concentrations below 1500 ppt the calibration fit is within 5%. The precision (expressed as the standard deviation) of the SF_6 analyses varies with concentration. In the range 10-20 ppt, the mean precision is about 18% of the concentration; in the range 20-50 ppt the mean precision is about 10%; above 50 ppt the mean precision is about 5%.

The lower quantifiable limit (defined as the concentration at which the standard deviation of the analysis is 33% of the concentration) is about 10 ppt for SF_6. The precision of the Freon 13B1 analysis is about 74 ppt, independent of concentration. Therefore, the lower quantifiable limit for Freon 13B1 analysis is about 220 ppt.

Meteorological Data

In addition to problems of data loss or simple instrument malfunctions, major difficulties which required corrective measures are associated with basic inadequacies of the propellor anemometer (UVW) wind systems. In retrospect it is clear that their response characteristics differed significantly from those of the cup and vane systems at CCB. In particular the UVW wind speed components were underestimated--sometimes slightly, sometimes to a large degree--depending upon wind direction. So far as we have been able to determine, the patterns of UVW system underestimation were caused by some combinations of:

- non-cosine response characteristics of the propellors used;
- wake effects of one propellor on another;
- wake effects of a propellor shaft or junction box on an adjacent propellor; and
- wake effects (shadowing) caused by the supporting tower.

The tower wake also affected winds measured by the cup and vane systems for some wind directions.

Corrections have been devised from comparisons of the UVW data with the cup and vane data and from a recent wind tunnel test of the entire UVW wind set. These corrections improve the correspondence between winds measured by the cups and props at the same heights. The agreement is also improved by correcting for errors made in orienting the wind sets to true north. The improvements are best, characteristically, for wind directions that do not leave a wind set in the tower's wake.

Although the 5-minute turbulence intensity data obtained by the UVW wind sets undoubtedly contain similar deficiencies as those noted above, we do not know of an appropriate method for "correcting" i_y and i_z for the errors in propellor response characteristics. In particular, the vertical turbulence measurements, so critical to describing σ_z in the model, are almost assuredly underestimates of the actual turbulence experienced. Rather than running the risk of "correcting" them inappropriately, we have elected to leave them as they are. However, in modeling and data analysis applications requiring 1-hour i_z data we have adjusted the data base i_z values in two ways. Firstly, a new 1-hour σ_w is computed from the 5-minute i_z and wind speed values, and this σ_w is then scaled by the 1-hour scalar average horizontal wind speed. Secondly, adjustments for prop response suggested by Horst (1973) were applied.

The temperature data have not been adjusted on the basis of the QA audit dta. The maximum error detected in the QA audits of the temperature systems was 0.4°C, but it was not duplicated in the two audits done only a few days apart. In fact, the general inconsistency between the errors in temperature systems found in the two audits suggestes that the magnitude of the errors approaches the resolution of the audit procedures.

Overall, the revised tracer and meteorological data bases provide a much better foundation for model development and evaluation, and we are confident that the many lessons learned at CCB will directly benefit the quality of data obtained in the next field program.

6.1.2 Investigations of Plume Growth

Some exploratory work has been done to compare the photographic evidence for vertical plume spread with contemporaneous tower data. The vertical growth of the visible plume as determined from the plume photographs agrees reasonably well with tower observations of vertical turbulence intensity for time averages of 30 minutes or more, but the agreement for time averages of five minutes is poor. In some light wind cases, the sinusoidal-like variations in vertical dispersion seen in the photos are out of phase by 20 to 30 minutes with the variations identified in the tower data.

In a parallel effort, the lidar measurements of short term average σ_y and σ_z have been plotted as functions of downwind distance x. These show very little variation with x, but when plume meander is accounted for in the hourly averages, σ_y is seen to be proportional to x and the proportionality factor is equal to the lateral turbulence intensity. Light wind, stable conditions appear to be necessary but not sufficient for large values of i_y. Under the same conditions vertical turbulence intensity can be high, due perhaps to transfer of gravity wave energy into the vertical component.

A number of time series analyses were made to examine the spectral characteristics of the wind components. These analyses show turbulent energy maximums at periods of one or two hours, suggesting that this energy may translate into gradual meandering of the plume across CCB during the course of an hour.

One-hour average σ_z values (computed from Equation 47 with 1-hour i_z values adjusted for prop response characteristics and interpolated to release height) have been compared with effective 1-hour average σ_z values obtained from lidar data. The comparisons indicate that, in general, Equation 47 estimates σ_z to within a factor of 2 when the parameter p is set equal to 1.5.

6.1.3 Investigations of Flow Patterns

The integral method of calculating H_c appears to be a successful estimator of dividing streamline heights (and therefore of plume flow regions) at CCB. Plumes released below H_c tended to wander from side to side without flowing directly over the hill; plumes released close to H_c travelled directly into the hill, rising along the surface as they flowed either around one side of the hill or over the saddle; plumes released well above H_c travelled freely over the top of the hill, usually with very small impact.

The isentrope analysis suggests that flow above H_c behaves much like a weakly stratified flow ($Fr_H \geq 1$). The streamline heights over the south peak of CCB were plotted against their inferred heights well upwind. Although the scatter is large, the points do show a tendency to cluster in a near-neutral zone, as predicted from physical modeling studies and theory. The analysis explicitly accounts for a dead layer below H_c, and the results suggest that a modeling method which subtracts out the dead layer of height H_c and then treats the flow above H_c as neutral flow may be consistent with flows over CCB.

Theory predicts that in weakly stratified flow over a hill, lee wave effects begin to influence the pattern of flow over the hill when Fr_L is less than about unity. Observer comments, photos, and lidar data at CCB all suggest that streamline depressions occurred in the lee of CCB for values of $Fr_L < 0.7$. SF_6 measurements show that tracer concentrations on the lee side were often larger than those on the windward side of the hill. However, the role of streamline depression and plume distortion in producing the larger concentrations has not been established.

As expected, the relative locations of peak tracer concentrations on CCB depended to a great extent on the ratio of release height to H_c. When plumes were released above H_c, the larger concentrations were generally found either over the top of the hill or on the lee side. The position of these larger concentrations appears to be dictated more by the size of σ_z rather than by Fr_L. When plumes were released below H_c, the larger concentrations were found primarily on the windward side of the hill, but not necessarily near the release height. Although some degree of streamline lift was visually evident, vertical mixing at times was sufficient to produce peak concentrations at receptors below the release height.

Effects of directional wind shear can be of central importance for low release heights at CCB. Some evidence of increased plume dispersion close to the base of the hill may be associated with such a shear zone. In these cases the highest concentrations were found below the release heights.

6.1.4 Model Modifications and Testing

Several modifications have been made to the Impingement and Neutral models since their evaluation in the first milestone report. The purposes of these changes is to increase their applicability to more general terrain shapes, and to increase their ability to respond to changes in important meteorological parameters. The new versions of these models have been named Wrap and Lift, respectively.

The formulation for σ_z has been altered in both models. Now σ_z (Equation 47) grows like $\sigma_w t$ for travel times small compared to $1/N$, where N is the Brunt-Vaisala frequency. This change has very little effect on the size of σ_z for most values of N encountered at CCB. However, when N becomes small (weak density stratification), the new expression for σ_z no longer tends to overestimate the size of the plume.

The Gaussian probability density function for the wind direction was replaced by the probability density function (PDF) constructed from the 5-minute averaged wind directions. With this change, both models are able to simulate concentration patterns better when the wind distribution is decidedly non-Gaussian.

The Wrap model allows estimates of concentrations in a band around the hill for elevations near the height of release. Formerly, the model only provided a concentration estimate for the stagnation point.

The Lift model allows for broad differences in hill shape. The shape of the hill in the crosswind direction is characterized by an overall radius of curvature which determines the amount of horizontal distortion produced in the plume as the plume travels over the hill. A large radius characterizes a very broad terrain feature, and produces relatively little horizontal plume distortion. The curvature is also used to interpolate between empirically suggested limits for the terrain correction factor (T_c): 0.5 for $R/H \sim 1$, 1.0 for $R/H >> 1$.

In addition,the Lift model accounts for stratification effects by treating the layer below H_c as a "dead" layer. This supposes that the dynamics of the flow above H_c are similar to weakly stratified (near neutral) flow. However, because none of the flow below H_c is allowed over the hill, the plume above H_c passes closer to the hill surface as H_c is increased.

An evaluation of both the new and old versions of the models has been completed for 14 of the 45 hours modeled in the first milestone report. The results are presented in Section 4, and summarized in detail in Section 4.15. These are the general qualitative results:

- Use of the actual wind direction PDF rather than a Gaussian distribution is critical when the winds are light and variable - especially for Wrap model calculations. This modification is the major reason for the improved results of the Wrap model. However, use of a PDF when winds are fairly steady could degrade model performance if wind data at the release height are unavailable. In this case a Gaussian distribution may be a fair approximation to a peaked PDF. Use of a Gaussian distribution with i_y values interpolated to release height is often better than use of the nearest "representative" PDF measured at some other height on the tower.

- Lift overestimates concentrations on the windward side of the hill at times. To alleviate this problem, further modifications may be needed to account for a "dynamic" H_c surface (one that may rise part way up the hill), or to account for (as yet conjectured) convergence effects caused by the topography at CCB.

- A good estimate of σ_z (x) in the absence of the hill is crucial to evaluating the structure of the models. Both Neutral

and Lift overestimate concentrations by a wide margin at times, apparently because σ_z is too large.

- The T_c expression used in Lift should be replaced by a function of the local terrain height (as it was previously in Neutral). Away from the hill T_c should be identically 1. Over the hill top T_c may be a function of meteorology as well as hill shape, but we cannot now quantify the relationship because of uncertainties in the magnitude of σ_z at CCB.

- Concentrations on the lee side of the hill may depend only weakly on Fr_L (the interpretation is based on T_c values inferred over the top and on the lee side of the hill). Therefore, streamline depression in the lee may cause some increase in surface concentrations.

- In plume impingement cases, the location of the maximum observed concentration is frequently above the release height. The Wrap model simulates the magnitude of these concentrations to within a factor of 2 (generally), but cannot identify the location of the maximum observed concentration accurately.

- The Wrap model appears to be appropriate for plume release heights close to as well as much less than H_c.

6.2 Conclusions

Results from the analyses undertaken to date on the refined CCB data base are leading us toward a complex terrain modeling system with two major flow components. The usefulness of H_c as a parameter to differentiate two distinct plume flow regimes has been amply demonstrated at CCB. Plume trajectories well below H_c are substantially consistent with low Froude number theory; plume trajectories well above H_c are consistent with high Froude number theory. The behavior of trajectories near H_c is difficult to describe analytically, but in practice the plume behavior on the windward face of the hill appears to be amenable to low Froude number modeling so long as some empirical adjustments are made to plume spread and concentrations. Plume transport and dispersion concepts contained in the Wrap model appear applicable to plumes released below or very near H_c, and concepts contained in the Lift model are applicable to plumes released above H_c.

Because H_c is a central parameter in modeling stable flow in complex terrain, the use of this two-model approach in a regulatory setting will require representative on-site wind and temperature information. We have attempted, without good success, to relate the character of profiles measured at CCB to 'surface' meteorological data (that is, winds and temperatures measured at 10 m.) Vertical profiles of wind and temperature, although burdensome to obtain, are absolutely necessary because there is no substitute for H_c to differentiate among impingement cases and near-neutral flow cases.

The modifications we have made to the models encourage their applicability to sites other than CCB, and make them more useful for estimating concentrations over several hours. The Lift model incorporates a measure of the crosswind aspect ratio of the terrain feature. The Wrap model estimates concentrations at more than one point across the hill surface. For both models, estimates can be averaged over a 24-hour period, for example.

The Wrap model estimates (and, in fact, the observed concentrations) are very sensitive to the actual shape of the horizontal wind direction distribution when the winds are very light and variable. When the plume is released above H_c, concentrations over the top of the hill are extremely sensitive to the size of σ_z. Therefore, the meteorological data should be measured on-site, at levels representative of plume height. This is strongly underscored by the CCB field results; often the meteorological data available within 20-30 m of the release height were inadequate to describe wind characteristics at release height at the same moment in time. This is especially true under conditions of light winds and very stable flow.

A number of uncertainties must be better bounded to make further progress in the development of these complex terrain models. Because of uncertain σ_z values for a number of the case hours studied, an adequate evaluation of the terrain factor formulation in Lift could not be completed. We need to decide, with better assurance than we now have, whether or not the simple way we interpolated T_c is appropriate (for CCB at least); and we also must learn whether the scheme is appropriate for other differently-shaped hills. We expect, for example, that the strength of the thermal stratification above and below H_c may influence T_c but any such effects in the case studies at CCB were probably masked by σ_z uncertainties.

Although H_c differentiated well between "neutral" and "stable" layers at CCB, we must see if the H_c parameter works as well in distinguishing flow regimes for two-dimensional ridges. Most of the modeling concepts we have adopted should be evaluated at a ridge site. These include: terrain correction factors, plume distortion, and dynamics of flow around (or along) the terrain. At CCB, plume material below H_c could pass over the saddle--but we cannot answer the question: How high might the plume have risen if there were no draw or saddle at CCB?

We have also made some untested conjectures about convergence or channeling effects in the draws at CCB. These should be evaluated, because they could have broad applicability to a wide range of terrain shapes.

Some recommended approaches for addressing these problems are presented in the next section.

6.3 Recommendations for Further Study

More information is needed to better evaluate the individual algorithms describing flow and dispersion around CCB, and also to extend the formulation to other sites. This information can be acquired through additional analyses of the CCB data base, new and old fluid modeling investigations, and new or recently acquired field measurements.

Flow, Turbulence, Waves, and Eddies

Although 1-hour i_z data measured away from the hill at Tower A compare favorably with 1-hour i_z values inferred from averages of photographic and lidar scanning of the oil-fog plume, the correspondence among 5-minute data was not as good. This was attributed in part to spatial and temporal variability in the turbulence field. Because there appeared to be some organization to this variability, the role of gravity waves and eddies was postulated. More analysis of the data is needed to better define the source of this variability, and to understand the mechanisms of turbulence production in the flow at CCB.

Because the flow structure over the hill changes over periods of one hour, and because the turbulence also changes, any relationship between the flow field and the turbulence field could be important in modeling the 1-hour average concentration field correctly. Analyses of profiles of winds, turbulence, and temperatures measured away from the hill at Tower A and over the hill at Tower B will be undertaken to identify the characteristics of the spatial and temporal variability in the turbulence field (particularly i_z), to relate these characteristics to the local dynamic stability of the flow reflected in the wind and temperature profiles, and to assess the importance of flow variability and turbulence intermittancy in modeling 1-hour average concentrations.

σ_z

The expression for σ_z currently in the models includes a trend with distance that is in general agreement with 1-hour averages of lidar measurements upwind of CCB. Because the interpretation of concentrations over the top and back sides of the hill depends critically on knowing what the "flat terrain" value of σ_z would have been at corresponding distances, the assumed distance dependence of σ_z should be validated at larger distances from the source. In addition, because the σ_z equation was adjusted to the lidar data through the parameter p, an independent check on the value of this parameter is needed.

Information required to perform these analyses may indeed be available in the CCB lidar data base, but at present we simply do not know whether or not sufficient lidar sampling data were obtained from plumes passing well to the side of the hill, because to date only a portion of the CCB lidar data has been reduced. Supplementary information may also be available from the experiments conducted at the BAO tower by WPL; again, we do not know at present. This is one of the key modeling purposes, we feel, to be addressed

in a comprehensive lidar plume sampling program. Plans should be made to sample plumes released during this fall's field experiment at the Hogback with this in mind.

Analysis of T_c

The terrain correction factor T_c is controlled by turbulence levels over the hill in concert with plume deformation. Therefore, we do not expect T_c to be a simple function of overall terrain shape only. Neither do we anticipate that all complex terrain modeling can be formulated wholly in terms of T_c and level terrain Gaussian plume models. However, we do feel that T_c, as inferred from observed concentrations and estimated (level terrain) concentrations, can be useful in assessing the importance of deformation and turbulence as a function of hill shape, meteorology, and location (i.e., crest, lee, or windward face).

With progress in reliably estimating plume growth (see σ_z discussion above) in stably stratified flows over flat terrain, especially over downwind distances of 1-2 km at CCB, inferred T_c patterns may be more instructive. However, a better method for calculating T_c patterns is needed to remove differences between the modeled plume trajectory and the average of observed plume trajectories (as reflected in the distribution of tracer gas concentrations). One method to be evaluated is a wind direction optimization scheme which would compute a plume trajectory that would be consistent with the observed concentration field. Once useful T_c patterns are developed, they will guide the investigation of plume deformation and turbulence mechanisms. This study will rely on analyses of wind and temperature data from the five meteorological towers on CCB to discern flow field characteristics, and it will also rely on an analysis of turbulence data measured at these towers as well as those measured in the flow away from the hill (tower A) to discern changes in turbulence over the hill.

Additional information can be extracted from fluid modeling studies already completed for a range of simplified terrain shapes and meteorology. Further analyses of these studies should help in interpreting the more complicated patterns of T_c values inferred from observed concentrations at CCB; and they should also provide an additional source of data for developing and testing models for estimating the effects of flow deformation and turbulence on plumes in complex terrain. The data to be obtained at the Hogback will similarly help to illuminate the structure of T_c for flows in ridge geometries

Generalization of H_c

H_c has been found to be a very useful measure to differentiate flow behavior at CCB. Because the simple energy balance argument implicit in H_c is at least as applicable to ideal two-dimensional flows as it is to a three-dimensional hill, H_c should be, we expect, equally useful in describing flows near long ridges. Because flows over ridges at low Froude numbers are very difficult to simulate correctly in tow tanks because of nonstationarity (see Appendix), the field program at the Hogback offers the

best present opportunity to acquire physical data to evaluate the usefulness of H_c in describing flows toward a ridge feature.

Dynamics of the H_c Surface

Flows above and below H_c have been modeled as though the two regions were completely independent. This is a convenient simplification, but it fails to reproduce important features of the observed flow field and tracer concentration pattern. Because the theory describing the dynamics of the flow near H_c is inherently non-linear, simple adjustments are better parameterized and validated through field experiment and fluid modeling. By putting more emphasis on describing the structure of the flow near the H_c surface, we hope to make progress in coupling the Lift and Wrap model concepts together in one model for complex terrain applications.

Much has already been learned from fluid modeling studies of stratified flow over simple hill shapes. This information should be included in the model formulations. Also, more information may be obtained from additional analyses of the CCB temperature data (e.g., performing the isentropic analysis with the data from the 10-m towers on CCB).

Flow Channeling Effects

Small scale variations in the inferred terrain correction factors may arise because of local terrain effects. The analysis of concentration patterns at CCB suggest the possibility of flow channeling, which is important because it would tend to encourage plume material to flow up and over the saddle between the two peaks in very stable conditions (when the plume might otherwise be expected to travel around the sides) and also because it would tend to lift a plume in neutral flow farther from the surface of the saddle.

Perhaps the best method for studying this type of topographical effect is fluid modeling: a simple experiment could be designed to compare streamline heights over the center of a model of CCB with streamline heights over a modified model of CCB with the peaks removed. (Other small irregularities would be smoothed out of both models). The intent of such an experiment is to search for a suitable parameterization of channeling effects, which could be applied in the model for terrain features with gaps.

REFERENCES

Briggs, G.A., 1973. Diffusion Estimation for Small Emissions, ATDL Cont. File No. 79, Atmospheric Turbulence and Diffusion Laboratory, Oak Ridge, TN.

Britter, R.E., J.C.R. Hunt and K.J. Richards 1981. Analysis and Wind-Tunnel Studies of Speed Up, Roughness Effects and Turbulence Over A Two-Dimensional Hill. Quart. J.R. Met. Soc., 88: 91.

Businger, J.A., 1973. Turbulent Transfer in the Atmospheric Surface Layer, Workshop on Micrometeorology, ed. D. Haugen. Am. Meteorol. Soc., Boston, MA.

Cermak, J.E. and J.D. Horn, 1967. Tower Shadow Effect. Journal of Geophysical Research, 73: 1869-1876.

Cooley, J.W. and J.W. Tukey, 1965. An Algorithm for the Machine Calculation of Complex Fourier Series. Maths. Comput., 19: 297-301.

Drazin, P.G. 1961. On the Steady Flow of a Fluid of Variable Density Past an Obstacle. Tellus, 13: 239-251.

Egan, B.A. 1975. Turbulent Diffusion in Complex Terrain. Lectures on Air Pollution and Environmental Impact Analyses. Am. Meteorol. Soc. Boston, MA.

Gifford, F.A., 1977. Tropospheric Relative Diffusion Observations. J. Appl. Meteorol., 16: 311-313.

Gill, G.C., L.E. Olsson, J. Sela, and M. Suda, 1967. Accuracy of Wind Measurements on Towers or Stacks. Bulletin of the AMS, 48, 9: 665-674.

Gill, G.C. 1975. Development and Use of the Gill UVW Anemometer. Boundary Layer Meteorology, 8: 475-495.

Hanna S.R., 1981. Lagrangian and Eulerian Time-Scale Relations in the Daytime Boundary Layer. J. Appl. Meteorol, 20: 243-249.

Holzworth, G.C. 1980. The EPA Program for Dispersion Model Development for Sources in Complex Terrain. Second Joint Conference on Applications of Air Pollution Meteorology, New Orleans, LA. Am. Meteorol. Soc., Boston, MA.

Horst, T.W., 1973. Corrections for Response Errors in a Three-Component Propeller Anemometer. J. Appl. Meteorol., 12: 716-725.

Hovind, E.L., M.W. Edelstein, and V.C. Sutherland 1979. Workshop on Atmospheric Dispersion Models in Complex Terrain. EPA-600/9-79-041. U.S. Environmental Protection Agency, Research Triangle Park, NC.

Hunt, J.C.R., 1982. Diffusion in the Stable Boundary Layer. In Atmospheric Turbulence and Air Pollution Modelling, D. Reidel Publishing Company, Dordrecht, Holland.

Hunt, J.C.R., and R.J. Mulhearn 1973. Turbulent Dispersion from Sources Near Two-Dimensional Obstacles. J. Fluid Mech., 61: 245-274.

Hunt, J.C.R. and J.S. Puttock, and W.H. Snyder 1979. Turbulent Diffusion from a Point Source in Stratified and Neutral Flows Around A Three-Dimensional Hill (Part I - Diffusion Equation Analysis). Atmos. Environ., 13: 1227-1239.

Hunt, J.C.R., and K.J. Richards, 1982. Stratified Shear Flow Over Low Hills. To be published.

Hunt, J.C.R. and W.H. Snyder 1978. Flow Structure and Turbulent Diffusion Around A Three-Dimensional Hill. (Part II - Surface Concentrations Due to Upstream Sources - unpublished manuscript).

Hunt, J.C.R. and W.H. Snyder 1980. Experiments on Stably and Neutrally Stratified Flow Over A Model Three-Dimensional Hill. J. Fluid Mech., 96: 671-704.

Irwin, J.S., 1979. Estimating Plume Dispersion-A Recommended Generalized Scheme. In preprints of Fourth Symposium on Turbulence, Diffusion, and Air Pollution, Reno, NV, Jan 15-18, 1979, pp62-79, Am. Meteorol. Soc., Boston, MA.

Izumi, Y., Barad, M.L. 1970. Wind Speeds as Measured by Cup and Sonic Anemometers and Influenced by Tower Structure. J. Appl. Meteorol., 9: 851-6.

Jackson, P.S. and J.C.R. Hunt, 1975. Turbulent Wind Flow Over A Low Hill. Quart. J.R. Met. Soc., 101: 929-955.

Lavery, T.F., A. Bass, D.G. Strimaitis, A. Venkatram, B.R. Greene, P.J. Drivas and B.A. Egan, 1982. EPA Complex Terrain Model Development Program: First Milestone Report - 1981. EPA-600/3-82-036, U.S. Environmental Protection Agency, Research Triangle Park, NC, 304p.

Moses, H. and H.G. Danbek, 1961. Errors in Wind Measurements Associated with Tower-Mounted Anemometers. Bulletin of AMS, 42: 190-194.

Panofsky, H.A., 1982. Personal Communication.

Pasquill, F., 1976. Atmospheric Dispersion Parameters in Gaussian Plume Modeling: Part II, Possible Requirements for Change in the Turner Workbook Values. Report EPA-600/4-760306, U.S. Environmental Protection Agency.

Pond, S., W.G. Large, M. Miyake, and R.W. Burling, 1979. A Gill Twin Propeller-Vane Anemometer for Flux Measurements During Moderate and Strong Winds. Boundary Layer Meteorology, 16: 351-364.

Rayment, R., 1970. Introduction to the Fast Fourier Transform (FFT) in the Production of Spectra, Met. Mag., 99: 261-269.

Rowe, R.D., S.F. Benjamin, K.P. Chung, J.J. Havlena, and C.Z. Lee, 1982. Field Studies of Stable Air Flow Over and Around A Ridge. Atmos. Env. 16: 643-653.

Scorer, R.S., 1949. Theory of Waves in the Lee of Mountains. Quart. J.R. Met. Soc., 75: 41-55.

Sheppard, P.A., 1956. Airflow Over Mountains, Quart. J. R. Meteor. Soc., 82: 528-529.

Smith, R.B. 1980. Linear Theory of Stratified Hydrostatic Flow Past an Isolated Mountain. Tellus, 32: 348-364.

Snyder, W.H., R.E. Britter and J.C.R. Hunt, 1980. A Fluid Modeling Study of the Flow Structure and Plume Impingement on a Three-Dimensional Hill in Stably Stratified Flow. Proc. Fifth Int. Conf. on Wind Engr. (J.E. Cermak, ed.), 1: 319-329, Pergamon Press, NY, NY.

U.S. E.P.A., 1976. Quality Assurance Handbook for Air Pollution Measurement Systems. Vol. I Principles. Research Triangle Park, N.C. EPA 600/9-76-005.

Van Ulden, A.P. 1978. Simple Estimates for Vertical Diffusion from Sources Near the Ground. Atmos. Environ., 12: 2125-2129.

Wyngaard, J.C. 1981. Cup, Propeller, Vane, and Sonic Anemometers in Turbulence Research. Annual Review of Fluid Mechanics, 13: 399-423.

APPENDIX A

THE STRUCTURE OF STRONGLY STRATIFIED FLOW OVER HILLS

DIVIDING STREAMLINE CONCEPT

THE STRUCTURE OF STRONGLY STRATIFIED FLOW OVER HILLS
Dividing-Streamline Concept

William H. Snyder[1]
Roger S. Thompson
Robert E. Eskridge[1]
Robert E. Lawson, Jr.[1]

Meteorology & Assessment Division
Environmental Sciences Research Laboratory
Environmental Protection Agency
Research Triangle Park, NC 27711

Ian P. Castro
Department of Mechanical Engineering
University of Surrey
Guildford, Surrey, England GU2 5XH

J.T. Lee
Los Alamos National Laboratory
Los Alamos, NM 87545

Julian C.R. Hunt[2]
Department of Applied Mathematics and Theoretical Physics
University of Cambridge
Cambridge, England CB3 9EW

Yasushi Ogawa
National Institute for Environmental Studies
P.O. Yatabe, Ibaraki 305, Japan

August 1982

1) On assignment from the National Oceanic and Atmospheric Administration, U.S. Department of Commerce.

2) Also, Department of Engineering.

PREFACE

This report pulls together the results of a whole series of experiments done by numerous investigators and for a variety of different purposes. The overall objective, of course, was to gain fundamental understanding of flow and diffusion under stably stratified conditions in complex terrain, but the individual projects were designed with very specific purposes in mind. Nevertheless, one aspect of each of the projects was to examine the concept of a dividing-streamline height, as it has very important consequences in the assessment of pollutant concentrations in complex terrain. This paper was written for submission to a journal for possible publication; its inclusion as an appendix to the CTMD second milestone report is felt to be justified on the basis of providing additional support and guidance to (1) mathematical modelers attempting to expand their models to include a wide variety of terrain shapes and approach flows and (2) planners of the second Small Hill Impaction Study which is to take place at The Hogback Ridge in northwestern New Mexico, a very long, 100 m high ridge of fairly steep slope that is cut periodically by narrow river valleys. Because of the urgency in getting information to the planners and modelers as soon as possible, the paper is included here in essentially draft stage.

ABSTRACT

Several laboratory experiments are described that test the applicability of an integral formula for the dividing-streamline height in strongly stable flow over hills. The dividing-streamline concept is based upon simple energy arguments; fluid parcels originating far upstream of a hill at elevations H_R above the dividing-streamline height H_S will have sufficient kinetic energy to rise over the top, whereas those below H_S must pass around the sides. The concept is found to be valid when interpreted as a necessary but not sufficient condition for wide ranges of hill shapes, density profile shapes, and wind angles, and in strong shear flows as well. Further, studies on strongly stratified flow over two-dimensional hills show that steady-state conditions are not established in a finite-length towing tank; these measurements also suggest that a very long tank would be required for steady-state conditions to be established upstream of long ridges with small gaps and cast doubt upon the validity of previous laboratory studies.

SECTION 1

INTRODUCTION

Hunt and Snyder (1980) conducted towing-tank experiments to test Drazin's (1961) theory for low-Froude-number flow over three-dimensional obstacles. They verified that for a bell-shaped hill, a linearly stratified environment and an effectively uniform approach-flow velocity profile, Drazin's theory was applicable in the range $F<0.4$, where F is the Froude number ($F=U/Nh$, U being the towing speed, N the Brunt-Vaisala frequency and h the hill height). They showed evidence for a dividing streamline (on the center plane determined by the flow and the axis of the axisymmetric hill) of height H_s such that streamlines below H_s would impinge on the hill surface and follow the surface around the sides, whereas streamlines above H_s would go over the top. Moreover, they suggested the simple formula

$$H_s = h(1-F) \tag{1}$$

as the criterion for determining whether a plume embedded in the flow approaching the hill would impact on the surface or surmount the top, for $0 \leq F \leq 1$.

Snyder et al. (1980) presented further laboratory evidence in support of the simple formula; they showed that it was applicable to other shapes of axisymmetric hills, including a cone and a hemisphere. Furthermore, they presented another simple formula (and experimental data to support it) for determining whether an elevated (step) inversion would surmount a hill. This second formula is

$$U_\infty/(gh_o\Delta\rho/\rho_1)^{1/2} = (2(h/h_o-1))^{1/2} \tag{2}$$

where g is the acceleration due to gravity, h_o is the height of the interface, $\Delta\rho$ is the density difference across the interface, and ρ_1 is the density of the fluid between the interface and the surface.

A more general formula for determining this dividing-streamline height was, in fact, suggested by Sheppard (1956), based upon simple energy arguments. He asked the question: in a strongly stratified flow approaching a hill, does a particular fluid parcel at some height upstream

possess sufficient kinetic energy to overcome the potential energy required to lift the parcel through the (potential) density gradient from its upstream elevation to the top of the hill? His formula may be written as

$$\frac{1}{2}\rho U_{\infty}^{2}(H_s) = g\int_{H_s}^{h}(h-z)\left(-\frac{\partial\rho}{\partial z}\right)dz \qquad (3)$$

where the left side may be interpreted as the kinetic energy of the fluid parcel far upstream at elevation H_s, and the right side as the potential energy gained by the parcel in being lifted from the dividing streamline H_s to the hill top h through the density gradient $d\rho/dz$. This integral formula is, of course, applicable to a fluid with any shape of stable density profile and, presumably, with any shape of approach-flow velocity profile. In practice, it must be solved in iterative fashion, since the unknown H_s is the lower limit of integration. It is not difficult to show that the formula reduces to the simpler formulas (1) and (2) using the boundary conditions applicable to those special cases.

The concept of a dividing-streamline height, of course, has very important consequences in the assessment of pollutant concentrations from sources located in or near complex terrain. For example, because of the essentially horizontal flow field below H_s, plume diffusion from a point source can be modeled by considering horizontal flow and horizontal diffusion alone, i.e., the three-dimensional problem is reduced to a two-dimensional one of diffusion from a line source about a circular cylinder (Hunt et al. 1979). This treatment suggests, and experiments by Snyder et al. (1980) support, that maximum surface concentrations under such conditions may approach or even exceed those that would have existed at the center of the plume in the absence of the hill. These concentrations are, of course, very much larger than would be obtained from a plume diffusing normally onto a surface.

Questions that naturally arise concern the applicability of the simple integral formula and these laboratory results to the atmosphere. For example, is the formula still applicable as the hill is elongated into a ridge? What if the ridge is not perpendicular to the approach wind? Is the hill slope important? What is the effect of shear in the approach flow, as most certainly occurs in the atmosphere? And, of course, the density structure of the approach flow is seldom linear; more typical is a strong surface-based inversion with a weaker gradient approaching neutral above.

A few other studies have shed light on some of these problems. Baines (1979), for example, conducted towing tank studies of low-Froude-number flows around a barrier with a gap. His results suggest

$$H_s/h = 1-2F \qquad (4)$$

for barriers with very small gaps, tending toward $H_s/h = 1-F$ for those with wider gaps. Weil et al. (1981) conducted similar towing-tank studies, extending the work of Baines, and found quite similar results. However, some doubts are expressed (see later discussion) concerning (1) the experimental techniques, (2) the establishment of "steady-state" conditions, and (3) the interpretation of results in view of the fairly substantial scatter in the data.

Data from a field study by Rowe et al. (1982) of stable air flow over a "long" ridge show much better agreement with the data for axisymmetric hills (Equation 1) than for ridges with gaps (Equation 4).

A major field study was designed (Holzworth 1980) and the first phase was conducted (Spangler and Taylor 1982; Lavery et al. 1982 a&b) based partly upon the results of the laboratory studies described above. This field study also tended to confirm Equation 3; indeed, H_s was computed in real-time from incoming meteorological data and used to determine operational strategy during the field experiment.

In conjunction with that field study, several more laboratory experiments were conducted to test the general validity of the integral formula (Equation 3) and to assess its limits of applicability. These laboratory experiments included:

1) Towing tank studies on a model of the field-study hill called Cinder Cone Butte in southwestern Idaho. It is an isolated, 100 m high, roughly axisymmetric hill in the flat, broad Snake River Basin. Density profiles were set up in the tank to simulate (in somewhat idealized fashion) those expected during the field-study period, i.e., strong surface-based inversions over a fraction of the hill height with weaker (but stable) gradients above to several hill heights, and towing speeds were established to simulate field conditions. Dividing-streamline heights were calculated according to Equation 3 and neutrally buoyant, different-colored dyes were released upstream slightly above, at and slightly below the calculated H_s. Visual and photographic observations were made to establish an observed dividing-streamline height, which was then compared with the predicted dividing-streamline height.
2) Towing tank studies on truncated, steep-sided ridges of various crosswind aspect ratios. These included examination of upstream "blockage" regions, surface flow patterns and lee-wave structure and will be reported separately (Castro and Snyder 1982); only those aspects dealing specifically with the dividing-streamline concept will be reported here.
3) Stratified wind tunnel studies on <u>shear</u> flow over vertical fences of various crosswind aspect ratios and over a model of Cinder Cone Butte.
4) Towing tank studies on a truncated sinusoidal ridge with a maximum slope of 40° positioned perpendicular and at other angles to the approach wind direction.

5) Towing tank studies on an "infinite" triangular ridge and a long sinusoidal ridge to test the validity of the "steady-state" assumption of flow upwind of an obstacle under strongly stratified conditions.

The results of these laboratory experiments are reported herein. Section 2 provides a rigorous derivation of Sheppard's integral formula and presents a discussion of blockage effects and upstream influence. Experimental apparatus, techniques and models are described in Section 3. Results are presented in Section 4 and conclusions in Section 5.

SECTION 2

REVIEW OF THEORY AND EXPERIMENTS

2.1 Overview

Several theoretical and experimental studies have been performed to analyze the influence of two-dimensional objects on stratified flow. Much of the work has been concerned with describing the formation and structure of lee waves. Some effort, however, has been directed towards determining conditions under which the upstream flow may be "blocked" by the obstacle. A description of the path of the dividing streamline for two-dimensional hills would prove useful in determining the fate of pollutants released upwind of such hills.

Laboratory studies have been performed by towing freely-mounted or surface-mounted, two-dimensional objects in layered or continuously stratified tanks. Many questions remain as to how the results of these experiments performed in a tank of finite depth and length apply to the atmosphere. The dimensions of the tank determine possible wave motions of the fluid.

One feature of stratified experiments conducted in finite towing tanks that has not been adequately addressed is how the upstream conditions change during a tow. A fixed end on the tank provides a uniform approach velocity profile at a distance upstream of the obstacle that varies as the experiment progresses. If fluid is blocked by the obstacle, the density gradient will be modified by the blocked fluid as the blockage influence is observed farther and farther upstream. The assumption usually made, that the approach flow density gradient remains, throughout the tow, equivalent to the density gradient at the onset of the tow, could lead to a misinterpretation of the observations.

In applying the theory of the dividing-streamline height to three-dimensional axisymmetric hills, the portion of the flow with insufficient energy to surmount the hill top was able to pass around the sides. However, the fluid blocked by a two-dimensional hill is trapped upstream. If the aspect ratio (width of hill perpendicular to flow divided by hill height) is taken as the experimental variable, the value at which the centerline flow deviates from the patterns established for axisymmetric cases can be determined. A complication that arises in towing tank experiments is that the amount of the test section cross-sectional area that is blocked must remain below some limiting value. As will be discussed later, the ratio of the area occupied by the model to the area that would be occupied if the model were extended to the width of the tank is important in stratified flow.

Long (1953, 1954, 1955) performed both theoretical and experimental analyses of two-layer and continuously stratified flow over "easy" shapes in a finite tank. Long made the hypothesis of an undisturbed approach flow at a sufficient distance upstream of the obstacle. He was interested in the upstream propagation of gravity waves rather than blockage effects, and thus, did not perform experiments at low Froude numbers. The reality of Long's hypothesis has been the subject of much controversy and has been discussed by Long (1972), McIntyre (1972) and more recently by Baines (1977). Application of Long's hypothesis to a tank experiment implies that for a portion of the experiment, presumably near the middle of the tow, a "steady-state" exists.

Wei et al. (1975) towed a 1-inch circular cylinder, a 2-inch circular cylinder, and a 1-inch flat plate through a linearly stratified fluid. Upstream columnar disturbance modes were observed for Froude numbers based on the half depth of the tank from 0.084 to 0.24. The disturbances appeared as unattenuated horizontal jets. Froude numbers based on the radius of the cylinders (or half-width of the plate) ranged from 0.78 to 4.72. The larger cylinder towed at a Froude number of 0.78 was the only case with a Froude number less than 1.0. In this case, the fluid to at least 27 radii upstream approached the cylinder at a speed of about 0.7 times the towing speed. A layer of blocked fluid was not apparent. A tow at a Froude number of 1.10 exhibited a fluid layer upstream of the cylinder with a speed toward the cylinder of 0.9 times the towing speed. This layer extended upstream a distance of at least 27 times the radius of the cylinder.

Baines (1979) studied stratified flow past a surface-mounted, two-dimensional barrier and barriers with gaps at the ends with gap widths $G = 1/16$, $1/8$ and $3/8$ (G is defined as the fraction of area removed from the model that spans the width of the tank). The cross-section of the hill was a "Witch of Agnesi" shape with a maximum slope of 39.4°. Neutrally buoyant beads were placed in the fluid to observe the flow over the two-dimensional model. The flow over models with gaps was observed by releasing dye at various heights upstream. The density of the dye was adjusted to be neutrally buoyant at approximately one-half of the barrier height. Thus, when the release was below this height, the dye was buoyant. The magnitude of the errors introduced by this buoyancy was not addressed.

Baines made his observation "after steady-state was reached (estimated by direct observation) and before the reflected upstream motions arrived". The criterion for the existence of blocked fluid upstream of a two-dimensional barrier was found to be $F < 0.5$ (± 0.05) based on the barrier height. The depth of blocked fluid was found to be approximately 0.5 and essentially independent of Froude number. For the barriers with gaps of $G = 1/16$ and $1/8$, he concluded that the blockage criterion for the two-dimensional case applied. Further, the height of the dividing streamline was found to be given by $h(1-2F)$. However, for the barrier with $G = 3/8$, the dividing-streamline height (as deduced from Baines' Figure 7) was more nearly $h(1-0.7F)$.

Overall, observations of Weil et al. (1981) tended to support those of Baines (1979), but regarding the depth of blocked fluid upwind of a two-dimensional ridge, Weil et al. found $z_b/h = 1-2F$, as opposed to the nearly constant depth of $z_b/h = 0.5$ for $0 \leq F \leq 0.5$ found by Baines.

One other point needs to be made here. Baines (1979) assumed that $H_s/h \rightarrow 1$ as $G \rightarrow 1$ (for all F), and his Figure 7 shows that result. Presumably, this idea derives from the thought that, if the hill were "needle-like", all streamlines would easily pass around it, independent of F. However, in neutral flow, even for a "needle-like" hill, all streamlines originating in the centerplane pass over the crest, even a branch of one that was on the surface far upwind. The contention here is that, in a stratified flow, $H_s/h = 1-F$ when $G = 1$, because the streamline at upstream elevation H_s will branch at the needle, with a portion following the surface over the top and other portions going round the sides.

Kitabayashi (1977) performed a stratified wind-tunnel study of the flow upstream of two different smooth two-dimensional hills (maximum slope of 10° and 15°). He found a critical Froude number of $F = 2.3$ below which a stagnant layer can form. However, the approach wind profile was not uniform and the density profile was not linear, so the Froude numbers he calculated are not directly comparable to those for more idealized laboratory studies.

Kitabayashi (1981) continued his studies of stratified flow over two-dimensional objects by analyzing the flow over thin vertical barriers. He used the wind-tunnel test section depth in defining his Froude number but concludes that a critical Froude number based on the barrier height should be adopted. His data (Figure 19; Kitabayashi 1981) can be used to support the argument for a critical Froude number for upstream blocking based on hill height of $F \simeq 1.0$.

2.2 Derivation of Integral Formula for Dividing-Streamline Height

An integral formula for calculating the height of the dividing streamline for flow in the atmosphere or in a laboratory water tank can be derived using the "parcel method". The idea is to calculate the height attainable by a parcel of fluid if its kinetic energy of horizontal motion were converted into potential energy of buoyancy. The derivation presented here closely follows that of Sheppard (1956).

The parcel method assumes that a parcel or small volume of fluid can be identified and followed as it moves through the environment. The pressure within the parcel remains equal to that of the local enviornment which is assumed to be in hydrostatic balance. Frictional forces are neglected. In the atmosphere, the parcel motion is therefore adiabatic and in the water tank the parcel maintains its original density.

Under these assumptions, the equation of conservation of energy can be expressed as

$$\frac{d}{dt}\left(\frac{1}{2}q^2 + gz\right) + \frac{1}{\rho}\frac{dP}{dt} = 0 \qquad (5)$$

The hydrostatic balance of the atmosphere can be expressed as

$$\frac{dP_e}{dz} = g\rho_e \tag{6}$$

where the subscript e is used to denote a local environmental value. Recall the assumption that $P = P_e$ and combine Equations 5 and 6 to get

$$d\left(\frac{q^2}{2} + gz\right) = \frac{\rho_e}{\rho} g\, dz \tag{7}$$

Application of the equation of state for dry air yields

$$d\left(\frac{q^2}{2}\right) = \left(\frac{T-T_e}{T_e}\right) g\, dz \tag{8}$$

where T is the absolute temperature. Assuming the existence of a streamline originating at a height H_s that approaches a stagnation point on the hilltop (z=h), Equation 8 can be integrated between these limits to obtain the integral formula

$$q^2(H_s) = 2g\int_{H_s}^{h} \left(\frac{T-T_e}{T_e}\right) dz \tag{9}$$

Since the parcel moves adiabatically, $T = T_e(H_s) + \gamma_d(z-H_s)$, where γ_d is the dry adiabatic lapse rate. Thus,

$$q^2(H_s) = -2g\int_{H_s}^{h} \frac{T_e(H_s) + \gamma_d(z-H_s) - T_e(z)}{T_e(z)} dz \tag{10}$$

This expression can be written in terms of potential temperature θ through the application of Poisson's equation

$$\frac{T}{\theta} = \left(\frac{P}{1000}\right)^{0.286} \tag{11}$$

Integrating by parts, and noting that $\theta_e(H_s)/\theta_e(z) \simeq 1$,

$$q^2(H_s) = 2g\int_{H_s}^{h} \frac{h-z}{\theta_\rho(z)} \left(\frac{d\theta e}{dz}\right) dz \tag{12}$$

Equation (10), however, is a simpler computational form.

To obtain a corresponding formula for flow in a water tank, Equation 7 can be written as

$$d\left(\frac{q^2}{2}\right) = g\left(\frac{\rho-\rho_e}{\rho}\right) dz^* \tag{13}$$

where z^* is directed downward (models are inverted and towed along the surface of the water tank). Again, assuming the existence of a dividing streamline, Equation 13 can be integrated to obtain

$$q^2(H_s^*) = \frac{2g}{\rho_e(H_s^*)} \int_{H_s^*}^{h} \rho_e(z^*)dz^* - g(h-H_s^*) \tag{14}$$

Adding and subtracting $h\rho_e(h)$ and integrating by parts gives

$$q^2(H_s^*) = \frac{2g}{\rho_e(H_s^*)} \int_{H_s^*}^{h} (h-z^*) \left(\frac{d\rho_e}{dz^*}\right) dz^* \tag{15}$$

In general, these formulas must be solved iteratively to obtain the height of the dividing streamline.

As was pointed out earlier, this formula may be reduced to $H_s/h = 1-F$ under conditions of uniform velocity and linear density gradient. This assumes that all kinetic energy is converted into potential energy. A more general formula allowing for only a portion of the kinetic energy to be converted is $H_s/h = 1 - \alpha F$, with $\alpha \leq 1$. In neutral flows, the pressure field set up by the body will allow kinetic energy along a streamline to increase (e.g., speed-up over a hill). Hence, α is not necessarily less than 1 for all F, but the pressure effects are expected to be small for $F \leq 1$. The data of Baines (1979) and Weil et al. (1981), however, suggest that α is greater than 1.0, indeed, as large as 2.0 for long ridges with narrow gaps. As discussed in the next section and as shown by the experiments described in Section 4, the validity of their experiments, or at least the applicability of their results to the atmosphere, is questioned.

2.3 The Squashing Phenomenon

Drazin's (1961) theory of flow over hills suggests that in the limit of extreme stability ($F \to 0$), vertical motions are inhibited, i.e., the flow is constrained to move in horizontal planes. Let us now imagine a stratified towing tank of finite length L in which we tow a two-dimensional obstacle of finite height h at very low speed (i.e., approaching $F = 0$). Let us further imagine that the fluid is incompressible and that the tow is begun at one end of the tank. The fluid initially in the layer between the

top and bottom of the obstacle must conserve its volume (Lh) because of the incompressibility assumption. Hence, as the distance between the obstacle and the opposite end wall of the tank decreases (even infinitesimally), the height of the layer increases (also infinitesimally). What happens in practice, of course, is that this fluid spills over the top and/or bottom of the obstacle, filling the void behind it. If the obstacle moves a distance x down the tank, a volume hx is displaced and fills the void in the lee. Because of the inhibition of vertical motions, the fluid filling the void must come from thin layers just below the top and just above the bottom of the obstacle. Because there are no dynamics involved ($U \to 0$), these layers must extend from the obstacle to the opposite end of the tank, and their thicknesses are $xh/2(L-x)$ each.

The fluid remaining in the space ahead of the obstacle has its density gradient modified by the multiplicative factor $1-x/L$. This phenomenon will be referred to as the "squashing" phenomenon in analogy with water spilling over the top of a bucket when the sides are "squashed". These finite changes in height of fluid parcels upstream of the obstacle are prohibited by Drazin's theory, which allows only infinitesimal changes of elevation as the velocity approaches zero.

Of course, in a real towing tank, the obstacle must be towed at some finite speed, so that dynamics must become important. However, Drazin's theory has been largely confirmed experimentally and extended (ultimately to $F = 1$) by Riley et al. (1976), Brighton (1978) and Hunt and Snyder (1980), and the experiments to be described in Section 4 certainly confirm the existence of essentially horizontal flow around three-dimensional obstacles (including very long ridges) below some height H_s (indeed, the formula $H_s/h = 1-F$ was derived by Hunt and Snyder (1980) on the basis of Drazin's theory, not as a special case from Sheppard's integral formula). Hence, we might expect Drazin's theory (and Sheppard's formula) to apply to <u>all</u> obstacle shapes, including two-dimensional ones.

The results of Baines (1979) and Weil et al. (1981) for two-dimensional ridges and ridges with small gaps were surprising because they suggested that fluid parcels could surmount the hills even though they had insufficient kinetic energy far upwind to do so. It is here suggested that their results are due largely to the squashing phenomenon, i.e., the gaps in their ridges were insufficiently large to allow a "relief value" to avoid the squashing.

This squashing phenomenon seems to have no counterpart in the atmosphere. If true blocking occurred upwind of an "infinite" ridge in the atmosphere, it seems that the flow would be blocked to infinity upwind (i.e., there is no "end-wall" forcing the flow toward the ridge). In more practical terms, "blocking" upstream of a very long ridge would imply "upstream influence" to very large distances, possibly through an upstream propagating front, which would imply non-steady-state behavior. From another viewpoint, there are no infinite ridges, so that fluid parcels can always be diverted around the obstacles without changing their elevation.

2.4 Upstream Influence and Blocking of Flow over Hills

The energy argument given in Section 2.2 assumes steady-state conditions upwind of the obstacle. The very low Froude number arguments of Section 2.3 show that the density profile is continuously modified as an obstacle is towed along the tank, due to the squashing phenomenon. At small but finite Froude number (say, $0.1 < F < 1$), it is well known that the steady-state assumption is incorrect upwind of two-dimensional obstacles. "Columnar disturbance modes", which are gravity waves of wave number zero, can propagate upstream. They are not generated near the obstacle, but in the tails or terminal zones of the lee waves (McIntyre, 1972).

The dispersion equation for waves in a tank of finite depth d is (see Turner 1979; Wei et al. 1975)

$$w^2 \left(k + \frac{4n^2\pi^2}{d^2}\right) - N^2 k^2 = 0 \tag{16}$$

where $k=2\pi/\lambda$ is the horizontal wave number, n is the mode in the vertical, and w is the circular frequency. Columnar disturbance modes, $k=0$, have frequency $w=0$, but group velocity

$$C_g(n) = \frac{\partial w}{\partial k} = \frac{Nd}{n\pi} \tag{17}$$

Since energy is transported at the group velocity, when $C_g(n) > U$, energy will be transmitted upstream of the obstacle. Upstream disturbances are thus generated whenever

$$F_i = \frac{U}{Nd} < \frac{1}{n\pi} \tag{18}$$

When $1/2\pi < F < 1/\pi$, only one mode can propagate upstream; when $1/3\pi < F < 1/2\pi$, modes 1 and 2 can propagate upstream, etc. However, as Baines (1979) has pointed out, if the obstacle height h is such that $h>d/2n$, the nth mode will be inhibited because the obstacle height will exceed 1/4 of its verical wavelength and extend into the region of "reversed" flow for that particular wavelength.

It is clear that the upstream, long waves arrive first, yielding a broad velocity profile. Short waves, which travel more slowly, arrive later and result in a region that moves with the velocity of the cylinder. These waves eventually reflect from the upstream end-wall of the tank, then propagate back downstream to influence the flow in the vicinity of the obstacle. Baines (1979) believed that valid observations could be made of

the flow over and around the obstacle in isolation (in the absence of end effects) by making the observations after steady state was reached (estimated by direct observation) and before the reflected upstream motions arrived. Evidently, he believed that a local steady state was achieved in that at some not-too-distant point upstream of the obstacle, steady-state velocity and density profiles were established before the reflected motions returned to modify them. His results, however, were not specified based upon the local steady-state conditions, but rather upon the towing speed and initial density gradient.

The goal of the experiments to be described in Section 4.5 was to test whether a local steady-state condition is in fact achieved at some not-too-distant point upstream. For example, does there exist a portion of the tow wherein the density profile is in steady state, i.e., where it does not change shape with distance? Another way of asking the question is: At some point upwind of the obstacle (say ten hill heights), is there a significant period of time during the tow (in which to make observations) wherein all upstream propagating modes have passed the point (and so that a steady-state has been reached) and, at the same time, no upstream modes have been reflected from the end-wall of the tank and returned to influence the flow at the point?

2.5 Effects of Shear and Hill Slope on Flow Structure

In the first order solution of Drazin (1961), the flow is assumed to be inviscid and two-dimensional in horizontal planes with no vertical coupling. Brighton (1978) has shown how to extend this solution to higher order, and has shown how to calculate small vertical deflections of streamlines arising from the vertical pressure gradients requried by the two-dimensionality of the flow. For an obstacle with circular contours of radius R_o (and in the absence of rotation), Brighton has shown that the streamline deflection

$$\delta = \frac{1}{N^2}\left[U_o \frac{dU_o}{dz}\frac{R_o^2}{r^2}\left(2\cos 2\theta - \frac{R_o^2}{r^2}\right) + \frac{2U_o^2}{r^2} R_o \frac{dR_o}{dz}\left(\cos 2\theta - \frac{R_o^2}{r^2}\right)\right] \tag{19}$$

where U_o is the approach flow velocity ($U_o = U_o(z)$), and (r,θ) are cylindrical coordinates. The first term represents the displacement due to shear in the approach flow and the second, that due to the slope of the hill. Assuming $dU_o/dz > 0$ and $dR_o/dz < 0$, it is easily seen that the shear leads to a drop in the streamline upstream of the hill and a rise as the fluid passes round the sides. The slope of the hill has just the opposite effect, a rise upstream and a drop as the fluid passes round the sides. Note that at the stagnation point, the deflection due to the slope is zero, whereas that due to the shear is negative $(-U_o/N^2)\,(dU_o/dz)$.

It should be pointed out that Equation 19 is valid only when

$$\delta \ll R_o/(dR_o/dz) \sim h \tag{20}$$

Let us calculate some typical values to obtain a feel for the contributions due to the two effects. Let U_o = 4 m/s at z=50m, N=0.1/s (very strong stratification), R_o =500 m, h=100 m, and dR_o/dz=2 (26.5° slope). The contribution of the shear term at the stagnation point is 32 m, a value that violates Equation 20, but is certainly indicative of the strong effect the shear can have. The maximum deflection due to the slope term occurs at θ=90°, and is -26 m, again violating Equation 20 and again indicating strong effects. Considering the variability of instantaneous wind and temperature profiles occurring in a typical nighttime stable atmosphere, it is not difficult to imagine an extreme variability in plume behavior as a plume encounters a hill!

For a general body where dR_o/dz=0 (as for flow about vertical fences or flat plates),

$$\delta = -\frac{1}{N^2}\left[U_o \frac{dU_o}{dz}\left(1 - \frac{U^2 + V^2}{U_o^2}\right)\right] \tag{21}$$

where U and V are the horizontal mean velocity components. It is useful to note that at the stagnation points, where vertical deflections of streamlines may be expected to be largest, this expression reduces to

$$\delta = -\frac{U_o}{N^2}\frac{dU_o}{dz} \tag{22}$$

which is independent of the plate width. Hence, the centerplane flow structure of strongly stratified flows about vertical plates (indeed, any vertical-walled object) may be expected to be independent of aspect ratio.

SECTION 3

APPARATUS

3.1 Towing Tank Experiments

Most of the experiments to be described were conducted in the large stratified towing tank of the EPA Fluid Modeling Facility. The tank is 1.2 m deep, 2.4 m wide and 24 m long. The sides and bottom are lined with acrylic plastic for viewing purposes. The model hills were mounted flush on a 2.4 m square baseplate which was inverted and suspended from a carriage such that the surface of the baseplate was submerged approximately 4 mm below the water surface. The carriage permitted towing speeds from 3 to 50 cm/s. For additional details, see Thompson and Snyder (1976) or Hunt et al. (1978).

Salt water was used to obtain stable density profiles and for the present work with linear profiles, the Brunt-Vaisala frequencies were nominally 1.33 rad/s. Towing of the models slowly eroded the linearity of the density profiles at the top; this non-linear layer was skimmed-off daily and the water height (108 cm) was restored by filling from the bottom with saturated salt water (for additional details, see Castro and Snyder 1982). The linearity and slope were well-maintained, but there was an increasingly deep region of saturated salt water at the bottom. In all cases, the depth of the linear layer exceeded 80 cm (>8 hill heights), so that this changing bottom boundary condition is not believed to have significantly affected the results.

Twelve tows were made with the Cinder Cone Butte (CCB) model under different density profiles, towing speeds, and dye-release heights as shown in Table A-1. The density profiles consisted of strong near-surface gradients ($N \sim 2.5$ rad/s) and weaker gradients above ($N \sim 0.86$ rad/s) (in actuality the weaker gradients were below the stronger gradients, as the models were towed upside down, but for purposes of clarity, the experiments will be described as if the model were right-side-up). The depth of the surface layer was initially set at 18 cm (1.25 h); this depth was successively reduced (by skimming) on subsequent tows to 13, 8, and 5 (0.9, 0.56, and 0.35 h) to simulate different depths of typical nighttime stable atmospheric flows. These density profiles are shown in Figure A-1, where it may be observed that the initially sharp break-point between the two layers was eroded slightly, but for practical purposes, the profiles are well-described as two linear-gradient layers. The changes in the Brunt-Vaisala frequencies were due primarily to changes in the reference densities as opposed to changes in the slopes of the curves.

TABLE A-1

SCHEDULE OF TOWS FOR CCB MODEL

Tow No.	Breakpoint Ht., cm	N_ℓ rad/s	N_u rad/s	Release Ht., cm	Speed cm/s
0	18	2.6	0.86	10	5.0
1				8	10.5
2				8	10.5
3				5	18.3
4				2	25.4
5	13	2.4	0.86	2	25.4
6	8	2.2	0.86	8	5.7
7				5	12.5
8				2	21.5
9	5	2.3	0.89	7	5.8
10				4	11.3
11				2	17.4

Notes

height of hill, h = 14.4 cm
height of saddle point = 11.9 cm

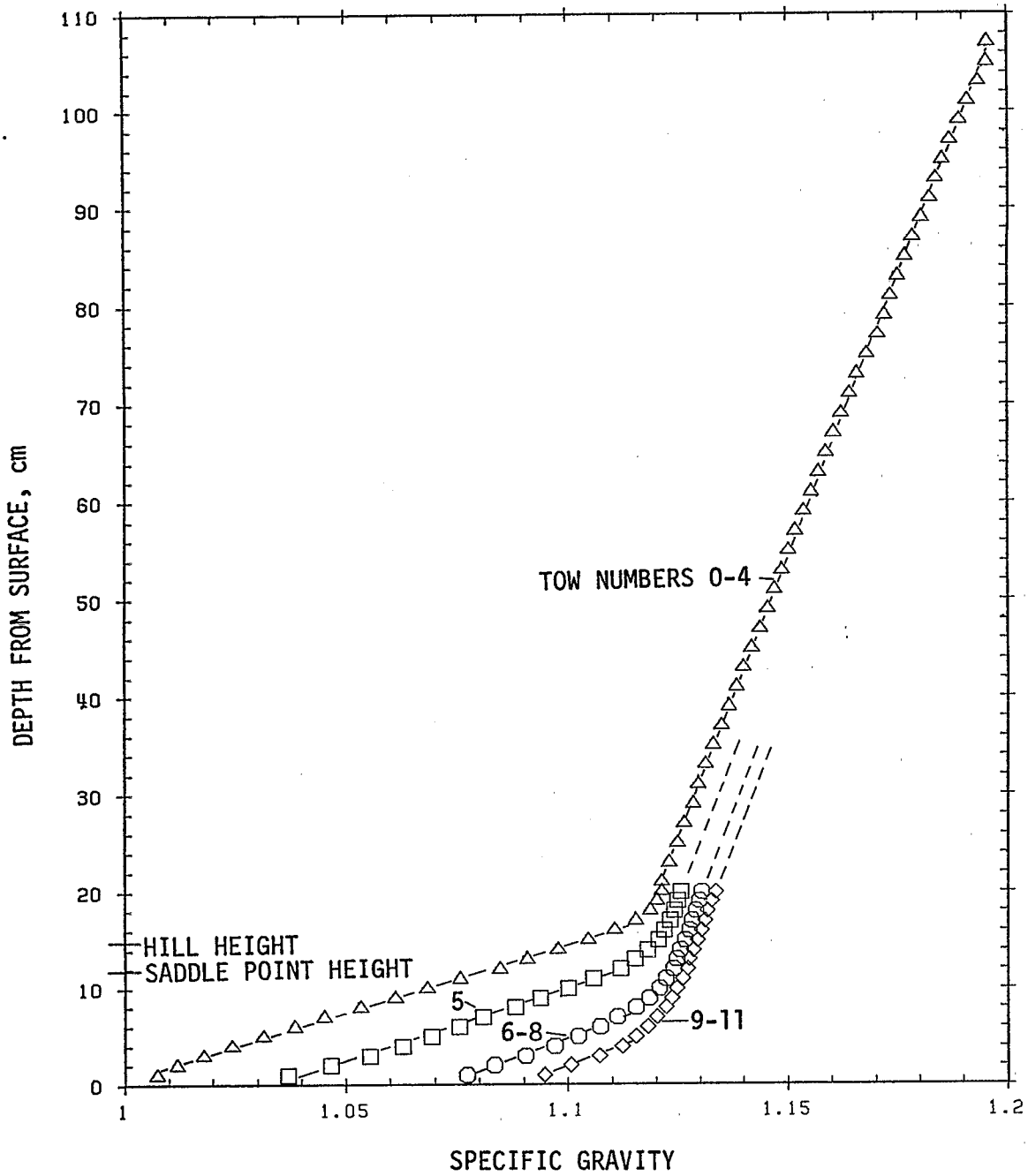

Figure A-1. Density Profiles for CCB model tows.

Water samples were drawn each day from up to 100 elevations using a rake and vacuum system. The density of each sample was determined by measuring the displaced weight of a plumb bob suspended in the sample from an electronic balance. The standard deviation in repetitive measurements of specific gravity of a typical sample has been determined to be 0.0002.

These density profiles were fed into a PDP 11/40 minicomputer system where the numerical integration of Equation 3 was performed to calculate the towing speed required to obtain a desired H_s value. Dye mixtures were emitted horizontally at each of three elevations at a distance of 160 cm upstream of the hill center. Each dye solution was neutrally buoyant at its release elevation. Red dye was emitted at H_s and blue dye 1 cm above and below H_s through 1.6 mm diameter tubing. According to the dividing streamline concept, the upper streamer should pass freely over the hill and the lower one should pass round the sides; the middle one, because of its finite thickness, should split, with the upper portion passing over and the lower portion passing round the sides. Visual and photographic observations were thus made during each tow to ascertain the validity of Equation 3. In practice, the accuracy of this determination was assessed to be approximately ± 0.5 cm or ± 0.03 h.

The CCB model was constructed of acrylic plastic by vacuum molding onto a wooden form. It was a 1:690 scale model made from enlarged U.S. Geological Survey maps. A contour map (Figure A-2) shows it to be double-peaked with a height of approximately 100 m (model height 14.4 cm), a saddlepoint height of 83 m (model height 11.9 cm), and base diameter of 1 km (model dia. 1.6 m). The maximum slope was approximately 26°. The wind direction simulated during this series of tows was 110°, nearly perpendicular to a line connecting the two peaks; hence, the flow tended to be channelled through the draw between the two peaks. The appropriate hill height was thus the saddle point height of 11.9 cm; this height was used in calculating the dividing-streamline height from Equation 3 and the experimental criterion was whether or not the dye streamers succeeded in passing through the draw.

The ridge models were triangular in cross-section with height (9 cm) equal to base length (63° slope). They were made of acrylic plastic. Four models were used such that the spanwise width between the vertical end faces was 1, 2, 4 or 8 h. They were mounted 10 h downstream from the leading edge of the baseplate such that the ridge axes were normal to the tow direction. A fairly substantial tripwire (5x5 mm) was mounted 5 cm from the leading edge of the baseplate. Further details on these models may be obtained from Castro and Snyder (1982). Dye releases were made on the ridge centerlines about 8 h upstream at $H_s \pm 1$ cm, as described for the CCB model above. Full-depth linear density profiles were maintained by skimming; density profiles were measured prior to each tow and the towing speed required to obtain the desired H_s was calculated from the density profiles as described above. Filming by motion picture camera was used in addition to the normal visual and photographic observations.

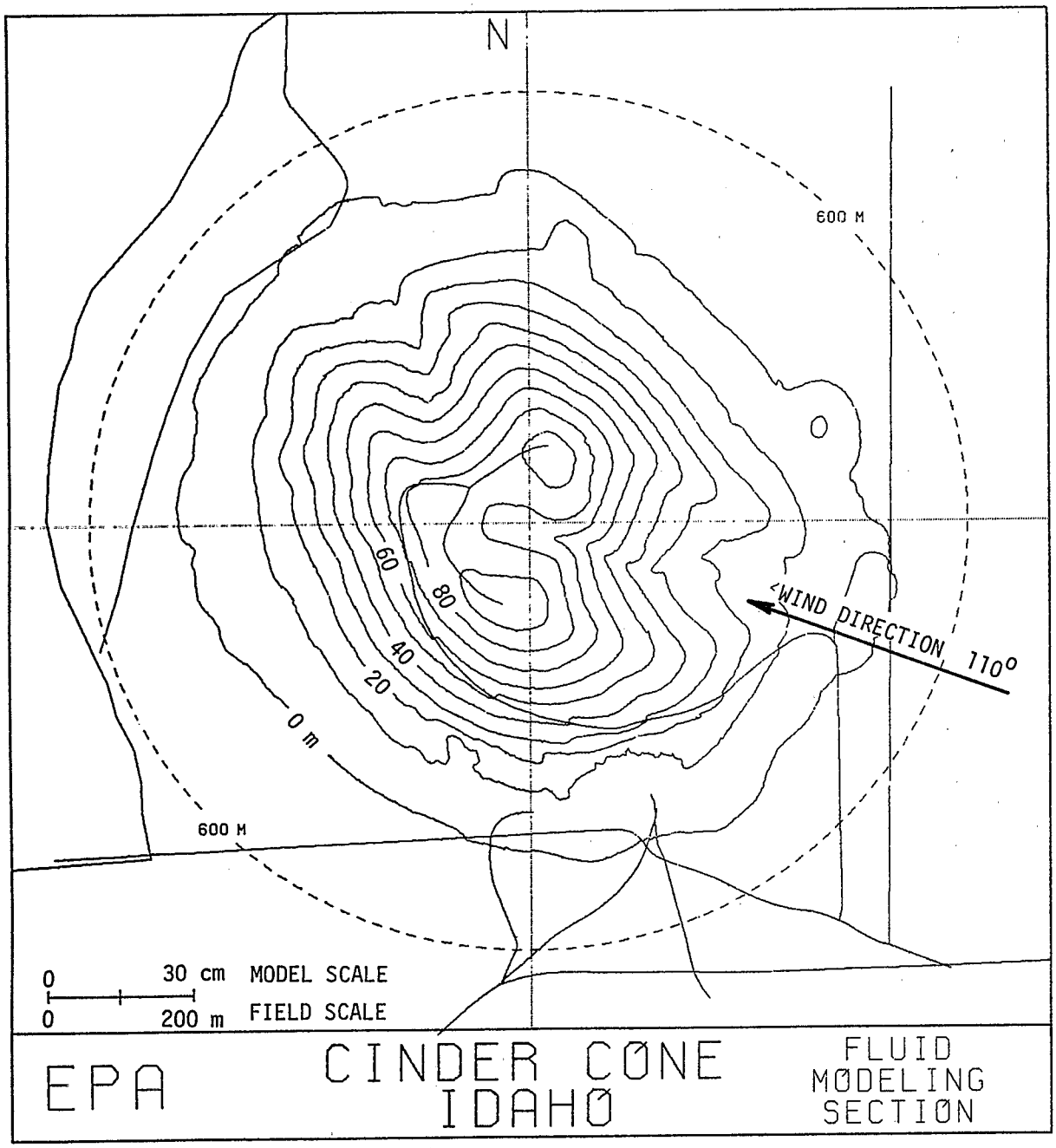

Figure A-2. Contour map of Cinder Cone Butte.

The sinusoidal hill is sketched in Figure A-3. The cross-sectional shape is described by

$$z = \frac{h}{2} (1 + \cos (2 \pi x/W)),$$

where h=10 cm and W=37 cm, giving a maximum slope of 40°. This was a truncated ridge with the length of the straight section being 163 cm. The end caps were of the same vertical cross-section and semi-circular in horizontal planes. The skirt of the hill was molded in integral fashion into a flat circular plate that fitted flush into the carriage baseplate. Thus, the wind direction θ could easily be changed. When oriented perpendicular to the tow direction, the cross-sectional area of this hill was 75% of the area of an "infinite" ridge of the same height stretching across the width of the channel, i.e., the gap width as defined by Baines (1979) was G = 0.25.

Tows of this model were made with linear density profiles, Froude numbers of 0.3, 0.5, and 0.7 and wind angles of 90°, 60°, 30°. In this series of tests, neutrally buoyant red dye was released at the upstream edge of the baseplate (x = -1.2 m) on the centerline at an elevation of H_s + 1 cm and blue dye at H_s-1 cm. Additionally, some dye releases were made during the θ = 30° case, all releases being at the same elevation but separated in the lateral direction. The purpose was to examine possible changes in H_s with source offset from the centerline, as will be discussed later.

In the "infinite" ridge studies designed to test the "steady-state" assumptions, the same triangular ridge was used as discussed above except that it's length was extended fully across the width of the tank and sponge rubber pads were inserted to seal the small gaps getween the ridge ends and the tank sidewalls. In this case, the ridge was towed at Froude numbers of 0.25 and 0.5 (based on the near-linear ambient density profiles), and samples of fluid were drawn during the tow through vertical sampling rakes positioned at 0.1 m (1 h) and 1.0 m (11 h) upwind of the ridge. The rakes sampled the fluid at 21 levels each with spacing between individual tubes of 1 cm. The two rakes were laterally offset by 12 cm on opposite sides of the centerline to avoid influences of the upstream rake on the downstream one. The total length of the tow was 20 m (222 h). The intention was to take rapid samples at four points of each tow, i.e., during the first and last meter and at the one-third and two-thirds points of each tow. Because of logistics problems in switching banks of tubes, the length of the sampling intervals varied from 1.0 to 2.5 m and the centerpoints of the sampling varied slightly from the precise one-third-points, but the basic objective was accomplished, i.e., to determine whether a local steady state was realized by comparing the density profiles measured at different periods during the tow.

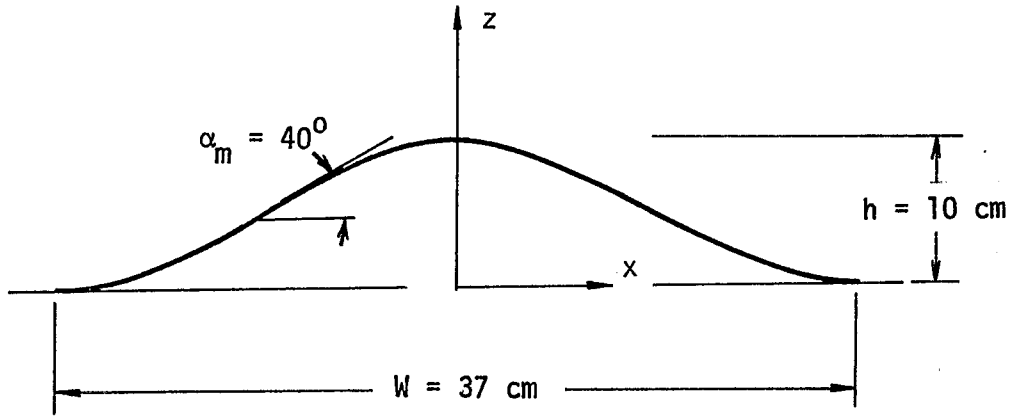

a) cross-sectional view

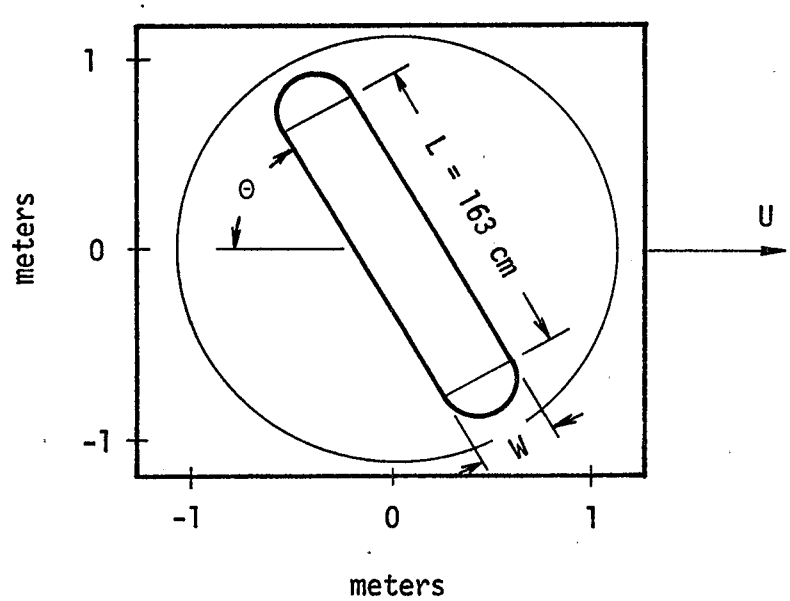

b) plan view of hill on baseplate

Figure A-3. Details of the sinusoidal hill model.

3.2 Wind Tunnel Experiments

One series of expermients was conducted in the stratified wind tunnel of the National Institute for Environmental Studies of the Japan Environment Agency (Ogawa et al. 1981). This vertical, closed-return wind tunnel has a test section 3 m wide, 2 m high and 24 m long. The speed in the test section may be controlled from 0.1 to 10 m/s and the ambient air temperature may be maintained at any value between 12 and 87°C. A temperature-profile cart (TPC) at the entrance to the test section allows the creation of vertical temperature gradients; the TPC is essentially a series of heaters dividing the 2 m height of the test section into 20 horizontal sections, each section (10 cm height) independently increasing the temperature of the incoming air by a controlled amount (maximum of 30°C). The temperature of each 3x3 m floor panel may be independently controlled between 7 and 112°C with a uniformity of ± 0.2°C. Previous experience had shown that at high ambient air temperatues, secondary flows (downward along the test-section walls) were created; interior sidewalls made of 1 m high aluminum plates were placed 30 cm from the tunnel walls to minimize these secondary flows (Ogawa et al. 1981).

The tunnel was designed for rather more weakly stable flows (i.e., wind speeds greater than $\sim$ 1 m/s) and difficulties were encountered in attempting to obtain the very low bulk Froude numbers ($0.2<F<1$) required for the present experiments. Reverse flows were observed which changed remarkably in depth and elevation with very small changes in fan speed. After considerable experimentation and the installation of thick felt pads at the entrance and exit of the test section, a range of operating modes was found that yielded reasonably strong shear layers with depths more than twice the depth of the fences (h=15 cm) in conjunction with strong stable temperature gradients.

The controlled temperatures were as follows. The floor panels were set at 6°C, and the ambient air temperature (that approaching the TPC) was set at 50°C. The TPC was set at: T_1=50°C (level 1, lowest, 0 to 10 cm); T_2=56°C, T_n=(60 + n)°C for n=3 to 20, so that T_{20}=80°C (level 20, highest, 190 to 200 cm). This condition was chosen and is referred to as "maximum stratification" because it yielded the strongest temperature gradient over the height of the model while maintaining a slight stability in the air layers above.

The fences were constructed of 6 mm acrylic plastic as sketched in Figure A-4. They were 15 cm high, with lengths of 7.5, 15, 30, 60 and 120 cm. They were centered in the tunnel perpendicular to the tunnel centerline and with the flange along the floor pointing downstream.

For the CCB studies, the model was identical to that used in the towing tank studies. Because of the special floor panels in the wind tunnel, the model could not be recessed, so it was simply set on the tunnel floor. The overall height of this model was thus 15.4 cm (14.4 cm hill height and 1 cm skirt thickness).

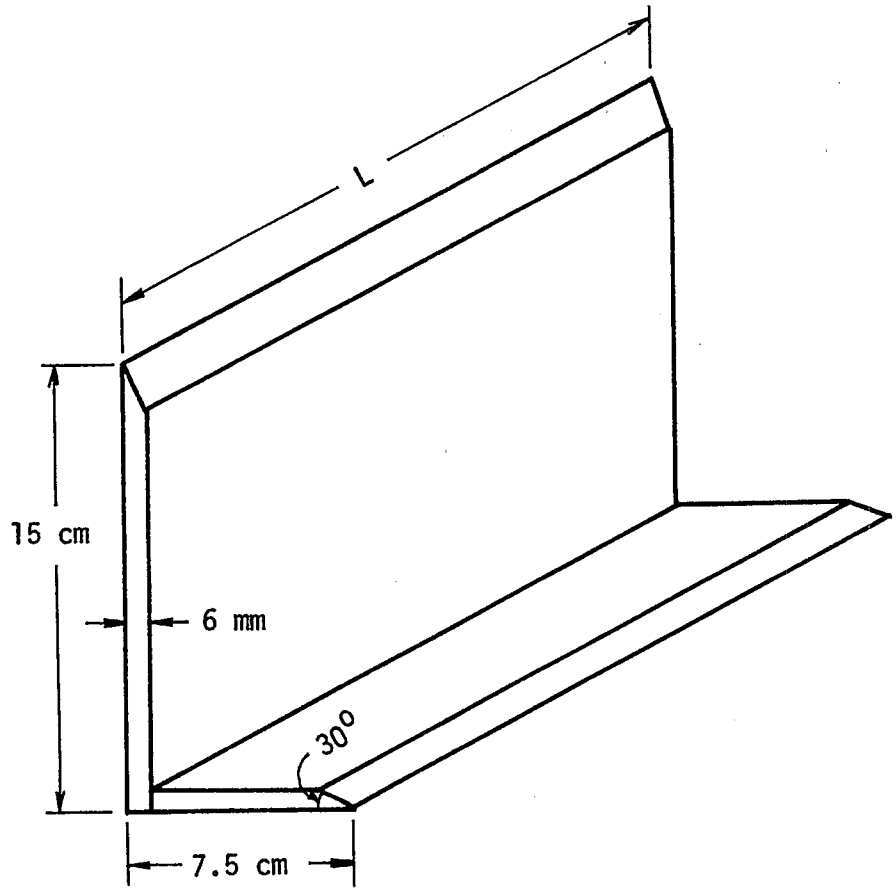

Figure A-4. Model fences.

For these flow visualization studies, a flattened, 10 mm diameter horizontal tube was fastened to a vertical standpipe of 6 mm diameter to emit smoke at the desired elevation. Mixtures of nitrogen and helium were fed into a smoke generator (electrical heating element wrapped around glass wool soaked in paraffin oil), then to the "stack". The fraction of helium to be used was determined by trial and error in the absence of the fence, i.e., the fence was removed from the tunnel, the gas mixture was adjusted to obtain a neutrally buoyant plume, then the fence was installed and photographic observations were made while maintaining the nitrogen and helium flow rates.

For temperature profile measurements, a Tokyo-Denpa quartz thermometer was used. For velocity profiles, a sonic anenometer (Kaijo Denki Co., Ltd., model DA-390) with an x-sensor head oriented to measure horizontal components of velocity (U and V) was used. This anemometer was specially constructed for wind tunnel measurements, with a separation distance between heads of 10 cm. Separate tests showed the velocity indications to be independent of air temperature over the range of 15 to 50°C. A minicomputer was used to sample the outputs from the anemometer and to calculate means and standard deviations of the signals. One-hundred-second averages were found to be adequate from the velocity measurements.

Photographic equipment included a TOPCON 4x5 graphics camera equipped with a polaroid back, an Olympus OM-1 camera equipped with a databack (for unique marking of each photograph), and a Sony Betamax video-tape recorder.

SECTION 4

PRESENTATION AND DISCUSSION OF RESULTS

4.1 Towing Tank Studies with CCB Model

The schedule of tows of the CCB Model was shown in Table A-1 and the density profiles were shown in Figure A-1. For each tow, a particular source height (center tube) was chosen and Equation 3 was integrated numerically using the measured density profile to predict the towing speed required such that the center streamer would rise just to the elevation of the saddle point, i.e., the minimum height of the draw between the two peaks. If the formula were correct, then, the lower streamer would be observed to go around the sides of the hill, the upper streamer over the top, and the center one, because of its finite thickness, would split, with the upper portions going over and the lower portions round the sides. Visual observations and periodic photographs were taken during the full length (20 m) of each tow.

Figure A-5 shows the results of the integrations of Equation 3 for each density profile as well as the experimentally observed results of the twelve tows. The agreement between the predictions and observations is regarded as excellent. The error bars indicate the best judgement of variability during the observation. For example, tow number 0 showed little or no deviation of the splitting of the center steramer, so that the error was judged as zero. Tow number 3, on the other hand, showed occasional wisps of the lower streamer rising over the top and of the upper streamer going around the hill. Figure A-6 shows top and side views of impinging streamers during a typical tow.

This set of experiments in conjunction with the results of Hunt and Snyder (1980) and Snyder et al. (1980) for full-depth, linear density profiles as well as elevated inversions has demonstrated the validity of the general integral formula for predicting the dividing-streamline height as a function of wind speed for a wide range of shapes of stable density profiles. The remainder of the towing tank studies to be described used only full-depth, linear density profiles.

4.2 Towing Tank Studies with Truncated Triangular Ridges

Figure A-7 shows the observations made during twelve tows of the triangular ridges with aspect ratios of 1 (L=h) and 8 (L=8 h). It is apparent that the dividing-streamline height followed the "1-F" rule for

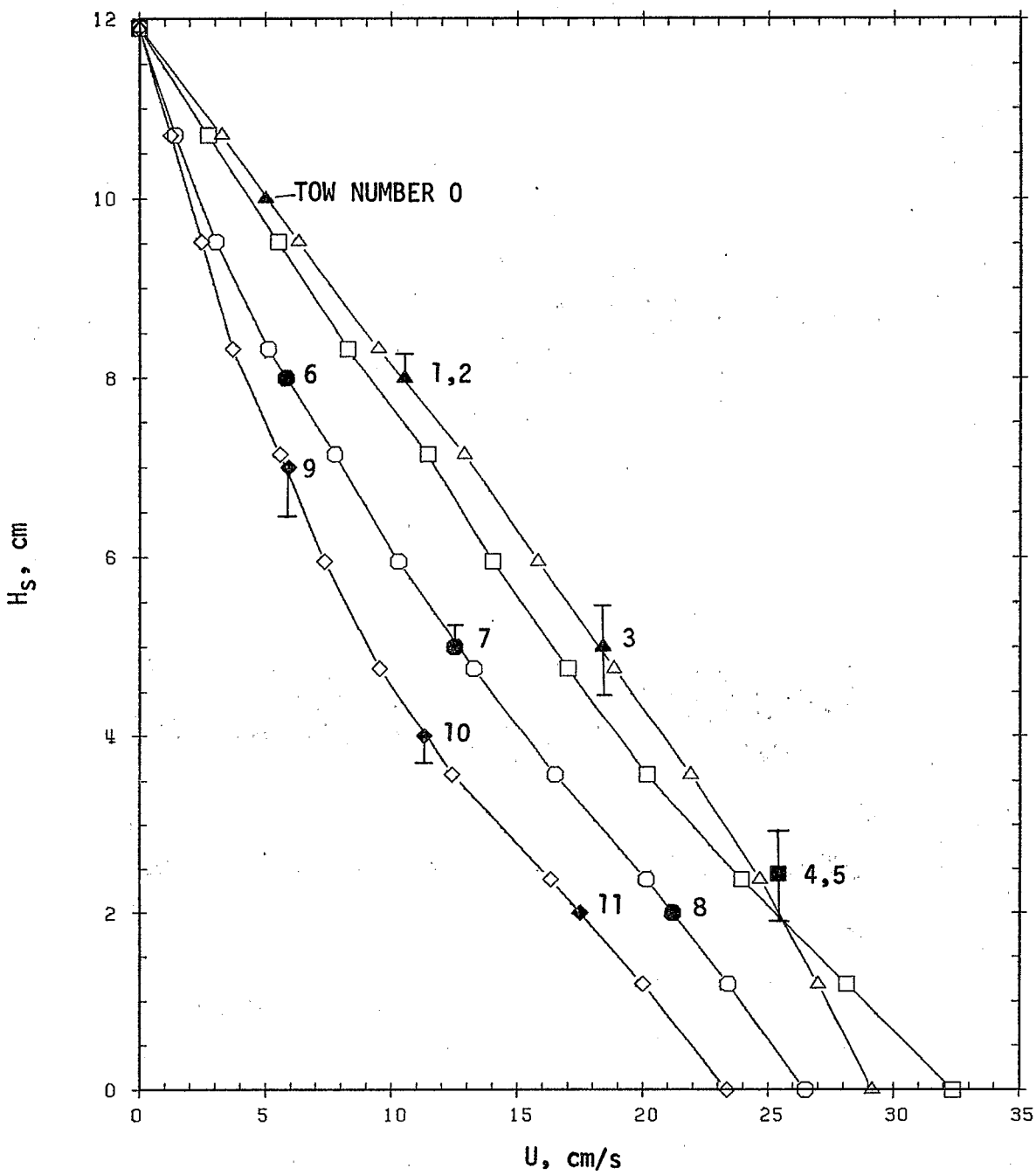

Figure A-5. Predictions and observations of dividing-streamline heights (open symbols: predictions; closed symbols: observations).

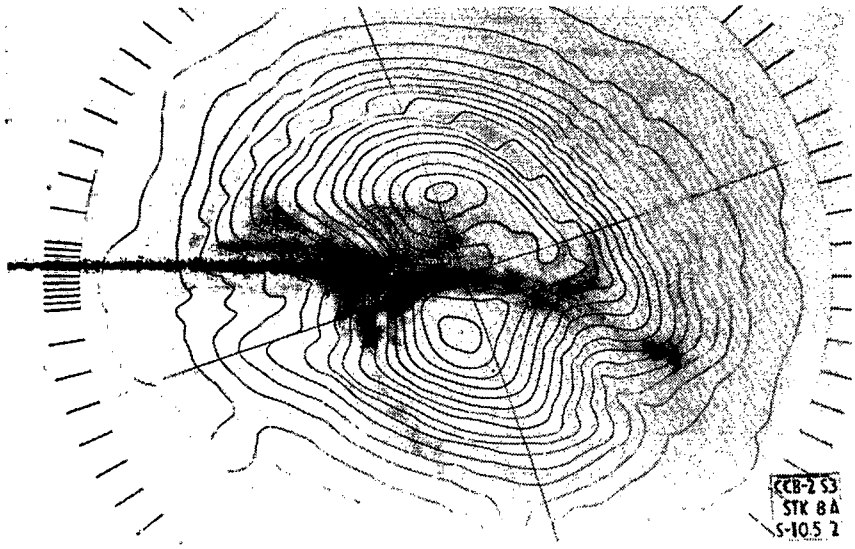

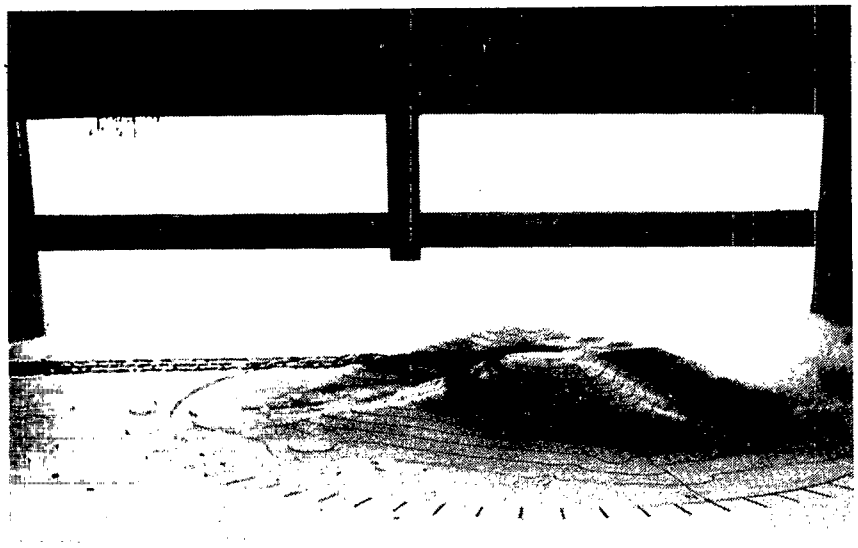

Figure A-6. Top and side views of streamers impinging on the Cinder Cone Butte model.

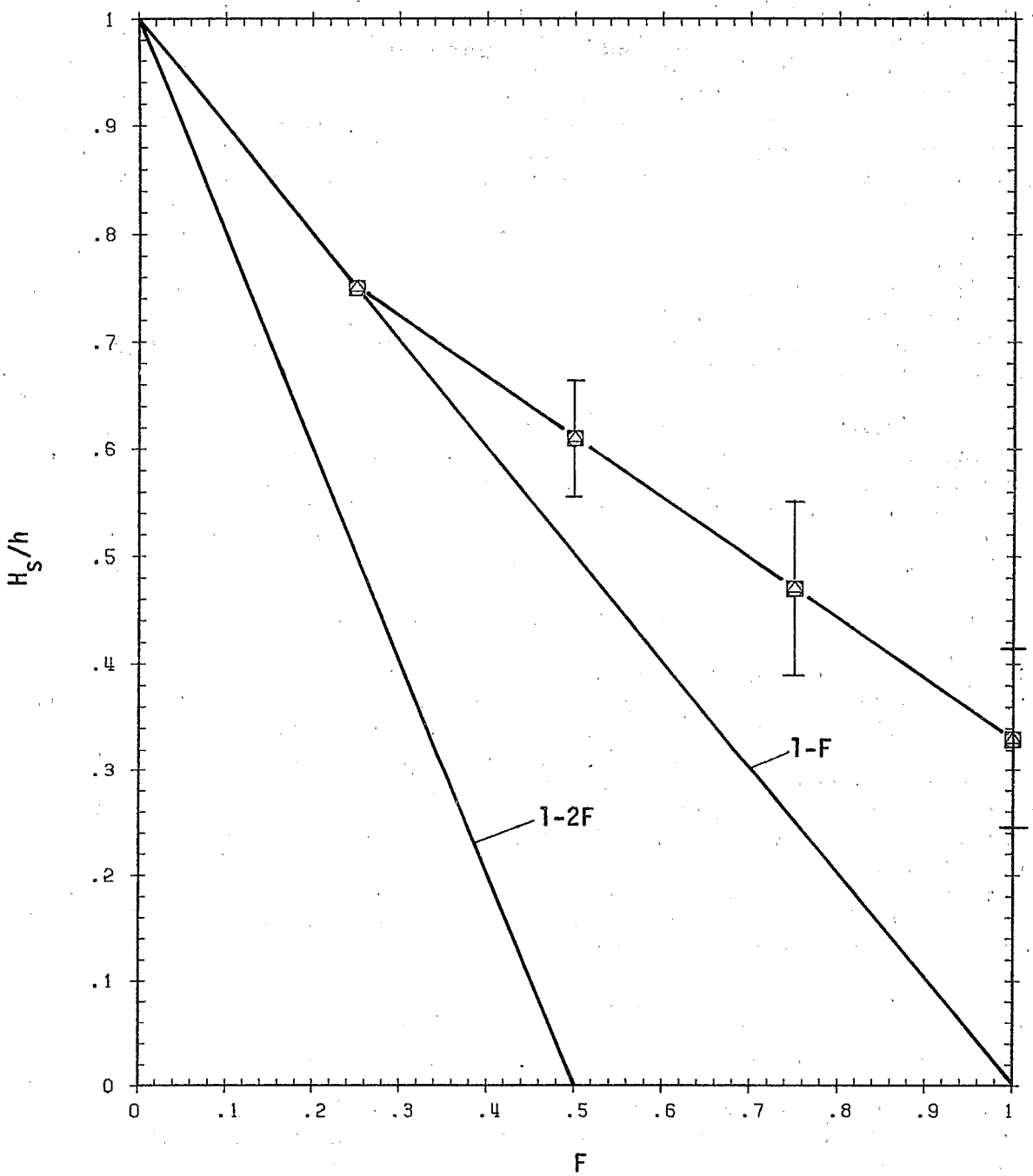

Figure A-7. Dividing-streamline height from the triangular ridge study.

$F \leq 0.25$, and deviated strongly for $F > 0.25$, but there were no observable differences due to the difference in aspect ratio. The deviation from the "1-F" rule is due to the formation of an upwind vortex that produces a downward flow on the front face of the ridge. It is apparently due to the combination of the steep upwind slope of the ridge and the shear in the approach flow - as was mentioned earlier, the boundary layer was tripped by a fairly substantial tripwire and, of course, grew in depth over nearly 1 m of baseplate upwind of the ridges. The structure of this vortex may be seen in Figure A-8; its diameter (and, hence, vertical extent) increased as the Froude number increased, reaching a maximum of about 0.6 h at F=1.0.

Notice that the data in Figure A-7 are on the opposite side of the "1-F" line from the "1-2F" line suggested by Baines (1979), even for the ridge with aspect ratio 8. But, of course, the "gap" ratio (as defined by Baines) was very large (0.7).

The conclusion from this set of experiments is that H_s is independent of the width of the hill and that it deviates from the "1-F" rule because of the combination of the steep upwind slope and the shear in the approach flow. Unfortunately, it was not possible to further investigate the nature of the boundary layer in this case, but work in the stratified wind tunnel, to be described in the next section, tends to support these conclusions.

4.3 Stratified Wind-Tunnel Study of Shear Flow over Fences

Figure A-9 shows the mean velocity profiles measured with the sonic anemometer. Nine profiles are plotted, eight under "maximum" stratification and one under neutral conditions. The temperature boundary conditions were maintained constant and the stratification was varied by changing the fan speed. Reverse curvature in the pofiles may be observed at fan speds below 220 revolutions per minute (rpm), and reverse flow in the lowest 4 cm was observed at 200 rpm. A slight overshoot of the velocity is observed near the top of the boundary layer under neutral conditions; this overshoot seems to be enhanced by the addition of stratification. The depth of the boundary layer was about 15 cm in the neutral case and gradually increased to 40 to 50 cm as the stratification increased.

Figure A-10 shows the corresponding temperature profiles. Temperatures near the floor systematically decreased and temperature gradients increased slightly as the fan speed was reduced.

Crosswind mean velocities are shown in Figure A-11. A positive V implies that a plume could veer to the right (looking downstream) as it was transported down the tunnel. In neutral flow, the largest crosswind velocity was 0.9 cm/s, which is to be compared with the streamwise velocity of 85 cm/s at the same elevation, implying an angle of 0.6°. This is indeed a very small angle and it is probably not within the capability of the sonic anemometer to measure such a small deviation. The largest crosswind velocity was -6.6 cm/s at 220 rpm; this is to be compared with the streamwise velocity of 40 cm/s, implying an angle of 10°, not-at-all insignificant. Indeed, smoke from a vertical rake was frequently observed

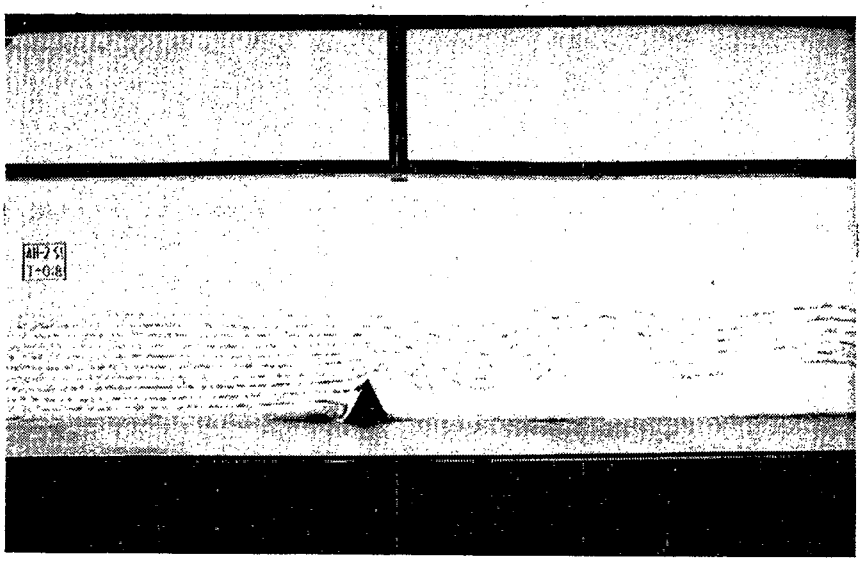

(a)

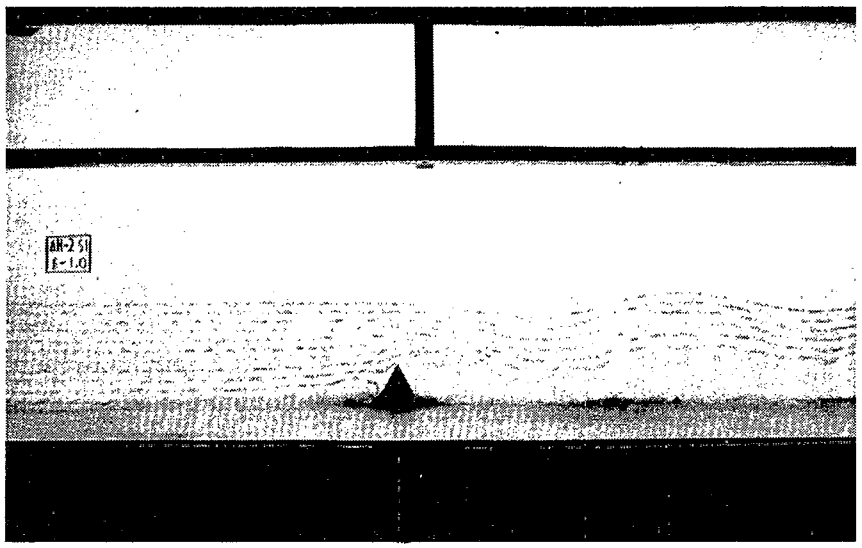

(b)

Figure A-8. Multilevel dye release upwind of a triangular ridge with an aspect ratio of 2: (a) F=0.8; (b) F=1.0.

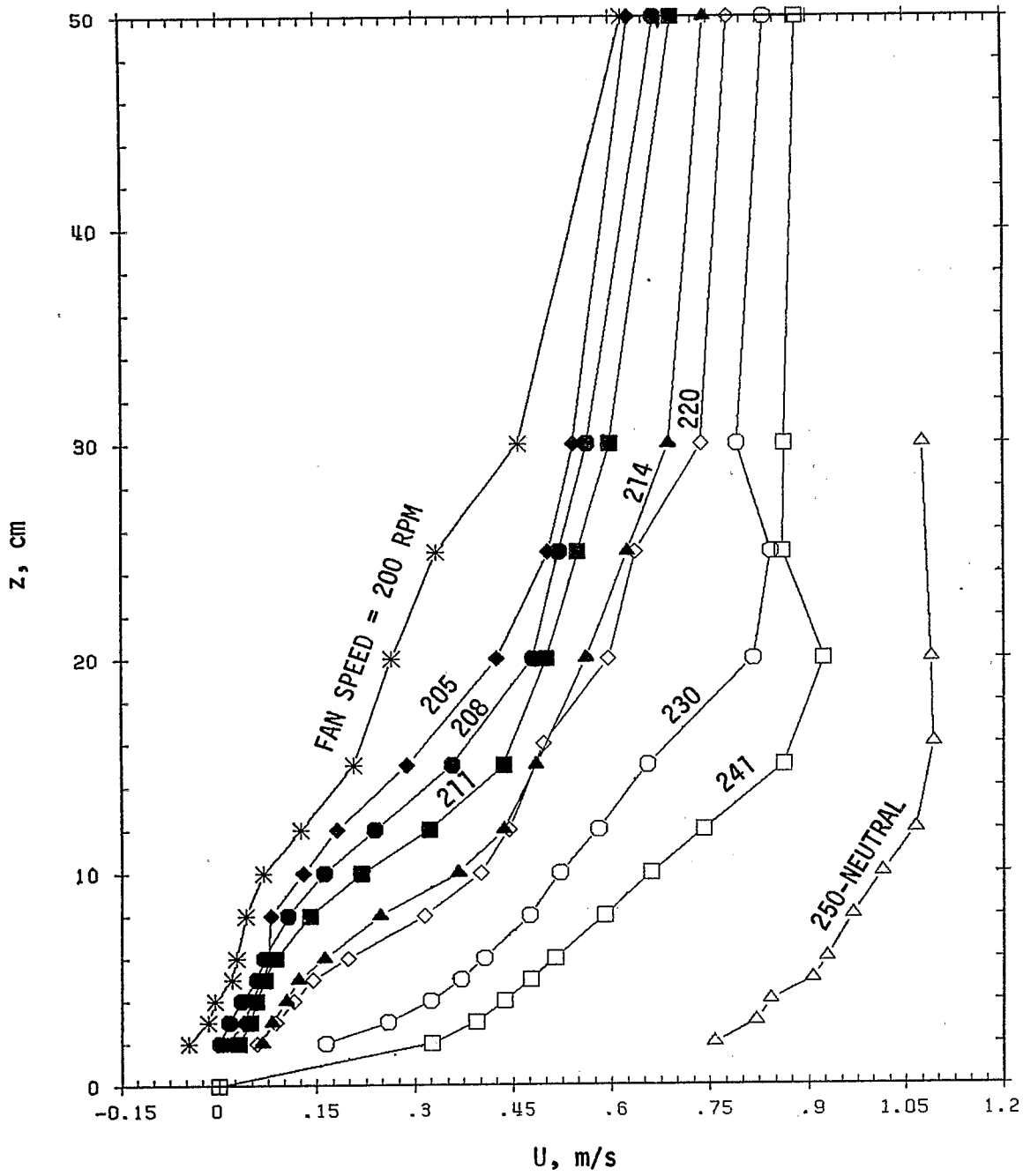

Figure A-9. Mean velocity profiles in the stratified wind tunnel.

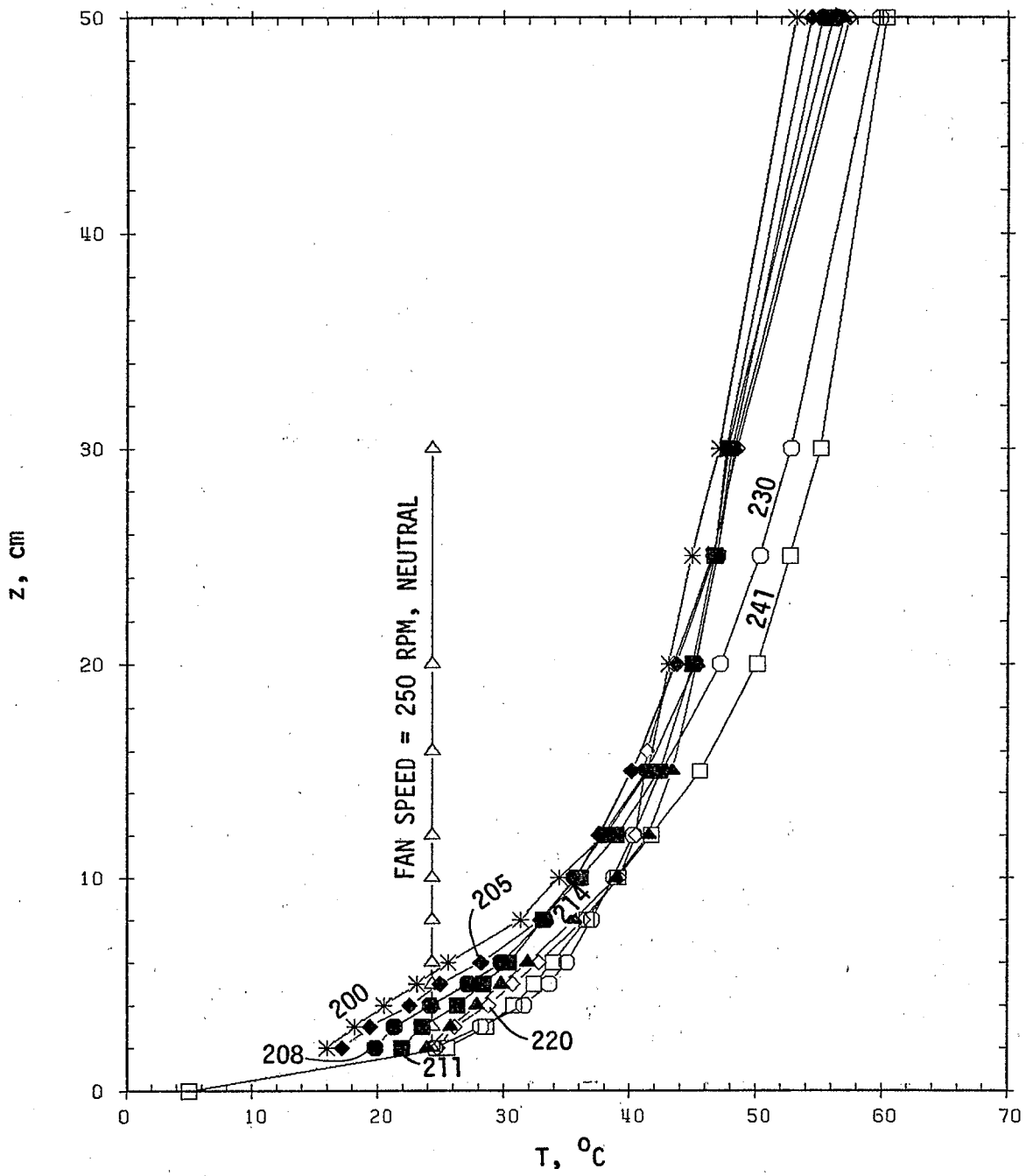

Figure A-10. Temperature profiles in the stratified wind tunnel.

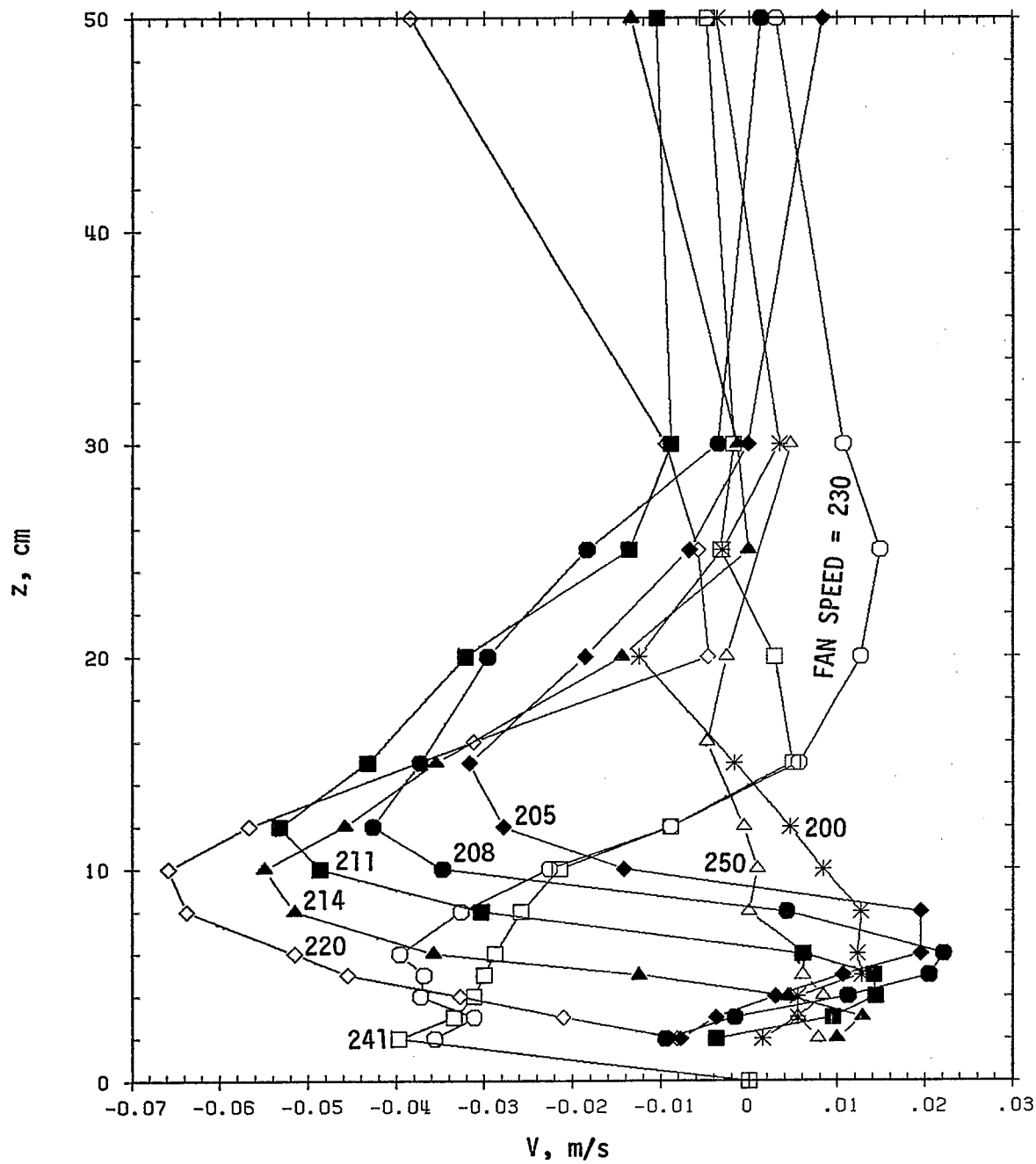

Figure A-11. Crosswind mean velocity profiles in the stratified wind tunnel.

to veer away from the tunnel centerline and to follow the directions indicated in the figure. This crosswind component is not believed to have had a significant influence on the structure of the flow over the fence.

Longitudinal and lateral turbulence intensity profiles are shown in Figures A-12 and A-13, respectively. The most notable characteristic of the stratified profiles is the elevated maxima, unlike the neutral case where the maximum was much nearer ground level. Most noticeable are the very large intensities at 241 rpm, where the peak value is located at an elevation of 12 cm and the value is 2.5 times the maximum neutral value. This corresponds with visual observations of smoke, where Kelvin-Helmholz rolls were observed. These measurements are indicative of relatively large scales of turbulence only, since, because of the large path-length, the sonic anemometer could not resolve scales smaller than about 10 cm. Visual observations, in fact, suggested there was little energy at scales smaller than that.

Repeat measurements of longitudinal and lateral mean velocity profiles are shown in Figures A-14 and A-15, respectively. The repeatability is regarded as excellent; the data seem to imply that the crosswind velocity component can be repeated to within ± 0.5 cm/s! The data also indicate the very good repeatability of the flow in the tunnel, as the profiles at 205 rpm were taken 5 days apart. Similar repeat measurements of temperature and turbulence intensities (not shown) also showed excellent correspondence.

From these velocity and temperature profiles, the dividing-streamline height was calculated using Equation 3. The results are graphed in Figure A-16; the data appear to fall on a straight line from 10.5 cm at 200 rpm to 0 at 241 rpm. These data were used to characterize the stratification and the results will be described in terms of release height relative to this dividing-streamline height.

A large number of photographs of smoke plumes flowing over and around the various fences were obtained. It is not possible to reproduce all of them here, but a representative set is presented in Figures A-17 through A-19. At 205 rpm, (Figure A-17), the dividing-streamline height calculated from Equation 3 (Figure A-16) was approximately 9 cm or 0.6 h. It is obvious from the photographs, however, that the plume from the 9 cm stack did not split over the fence top, as would be expected from the dividing-streamline concept. Instead, it went totally around the sides of the fence, for all aspect ratios. Indeed, only a tiny fraction of the 12 cm plume (0.8 h) surmounted the fence, and only about half the 15 cm plume (1 h) passed over the top. Moreover, this behavior was essentially independent of aspect ratio. Such behavior appears to be due to an upwind vortex, with downward flow along the front face of the fence; it is very similar to that observed on the front faces of buildings in <u>shear</u> flows (at least in wind-tunnel studies!). One difference, however, is quite evident: there is a bottom limit to this vortex; it does not extend to the tunnel floor as would be expected in a neutral shear flow. Instead, the streamline originating far upstream at fence-top elevation appears to be limited in how far <u>down</u> it can travel, presumably by the amount of kinetic energy it possessed initially, i.e., its kinetic energy is used-up in moving

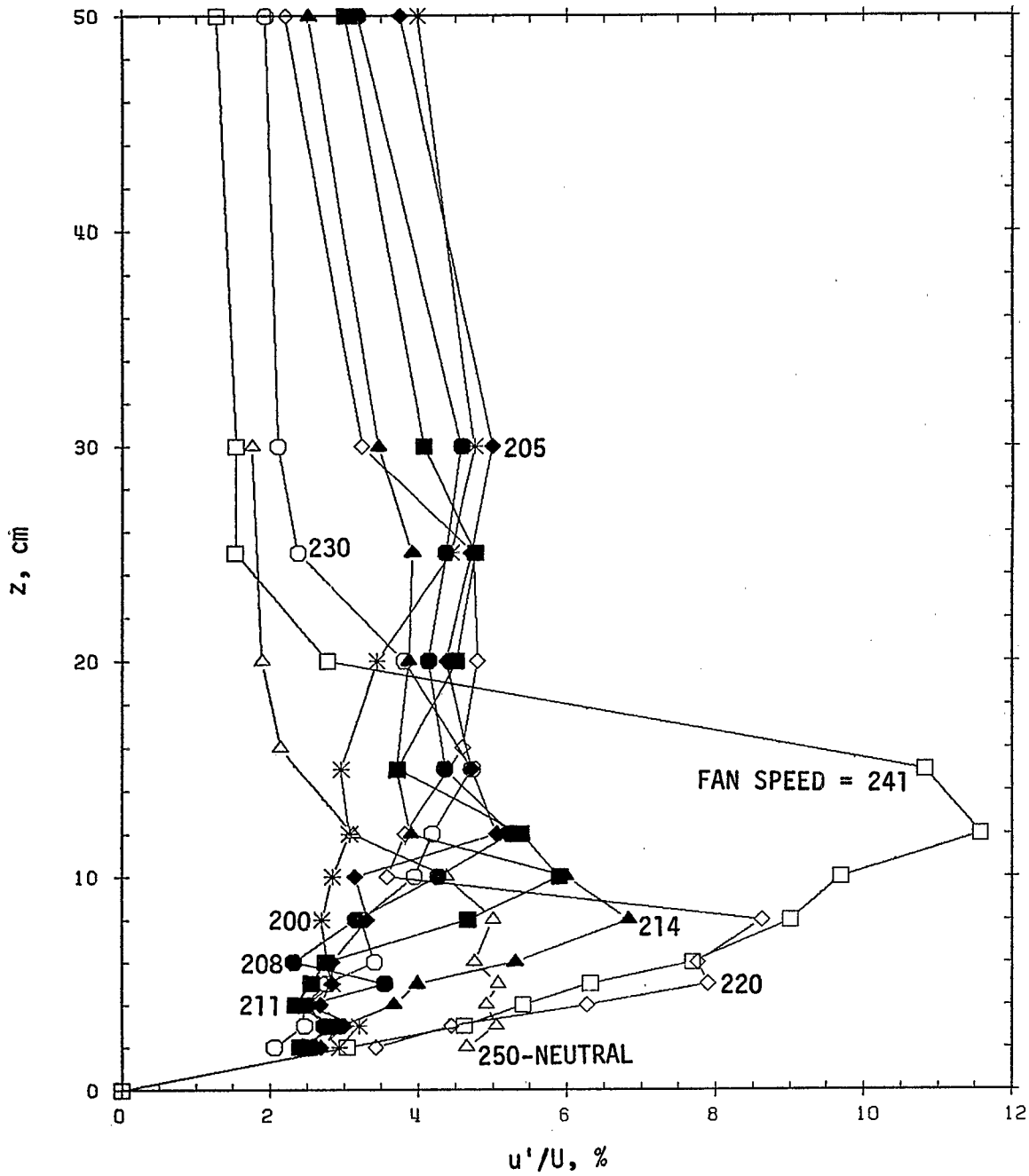

Figure A-12. Longitudinal turbulence intensity profiles.

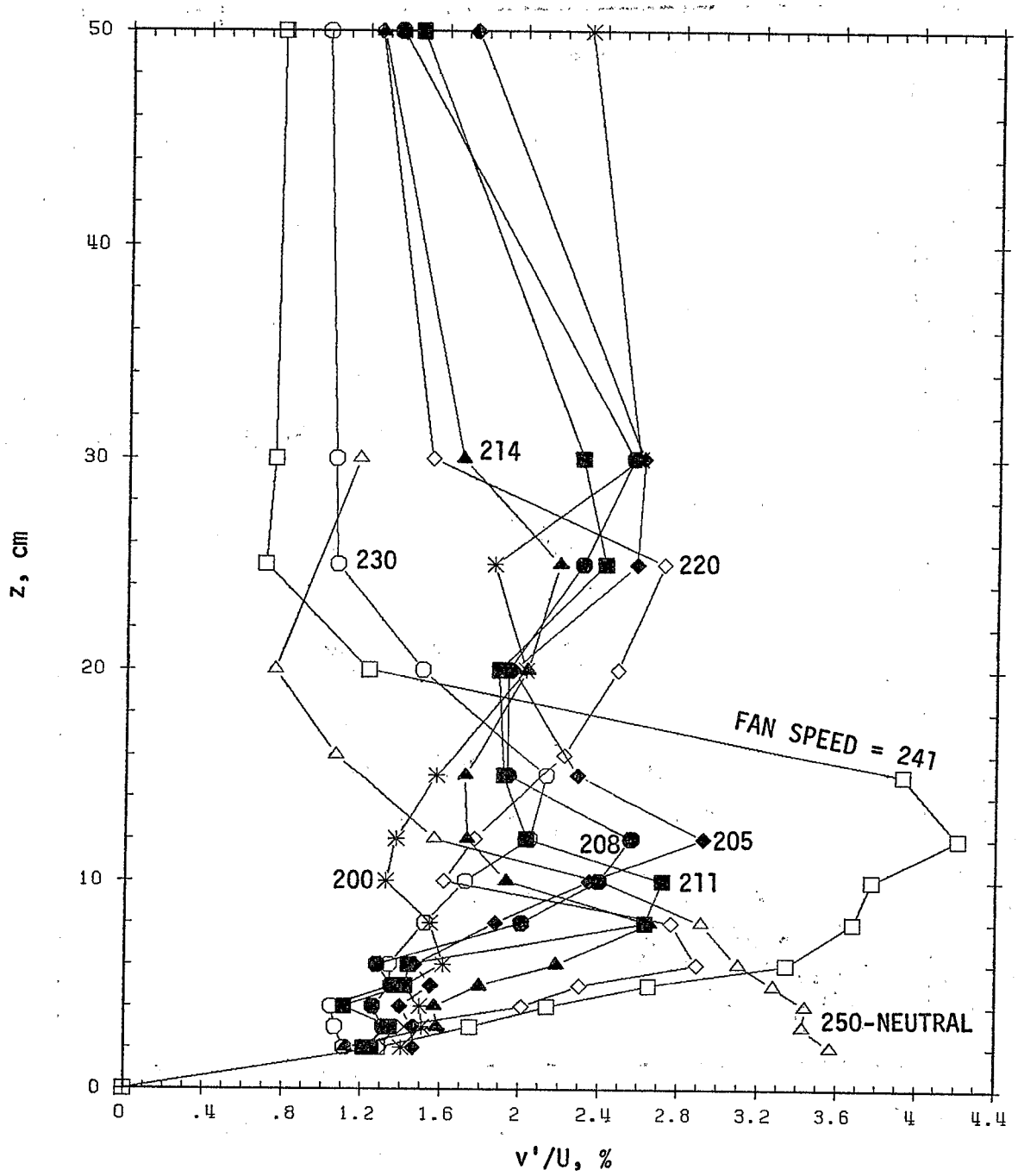

Figure A-13. Lateral turbulence intensity profiles.

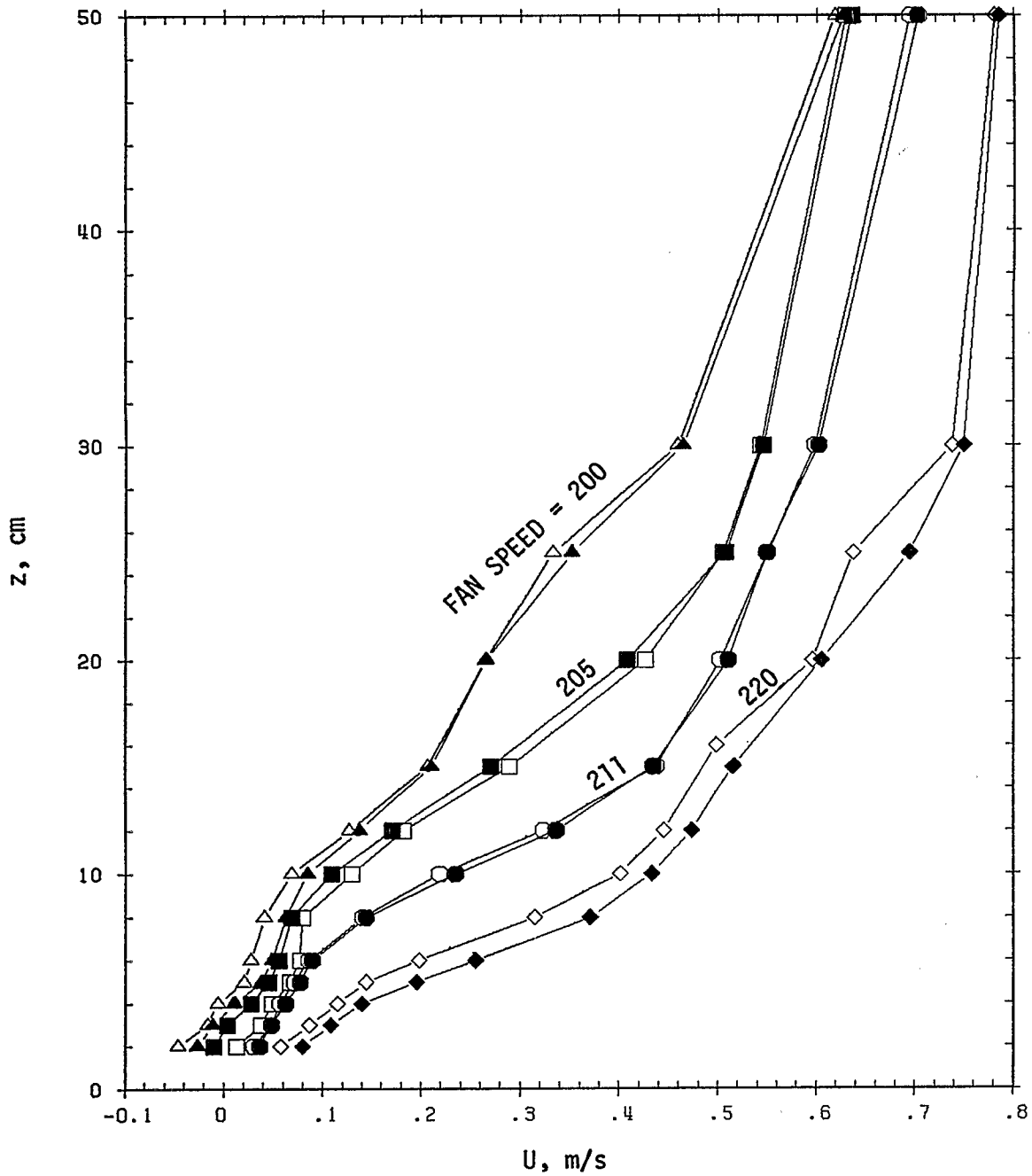

Figure A-14. Repeated measurements of longitudinal mean velocity profiles.

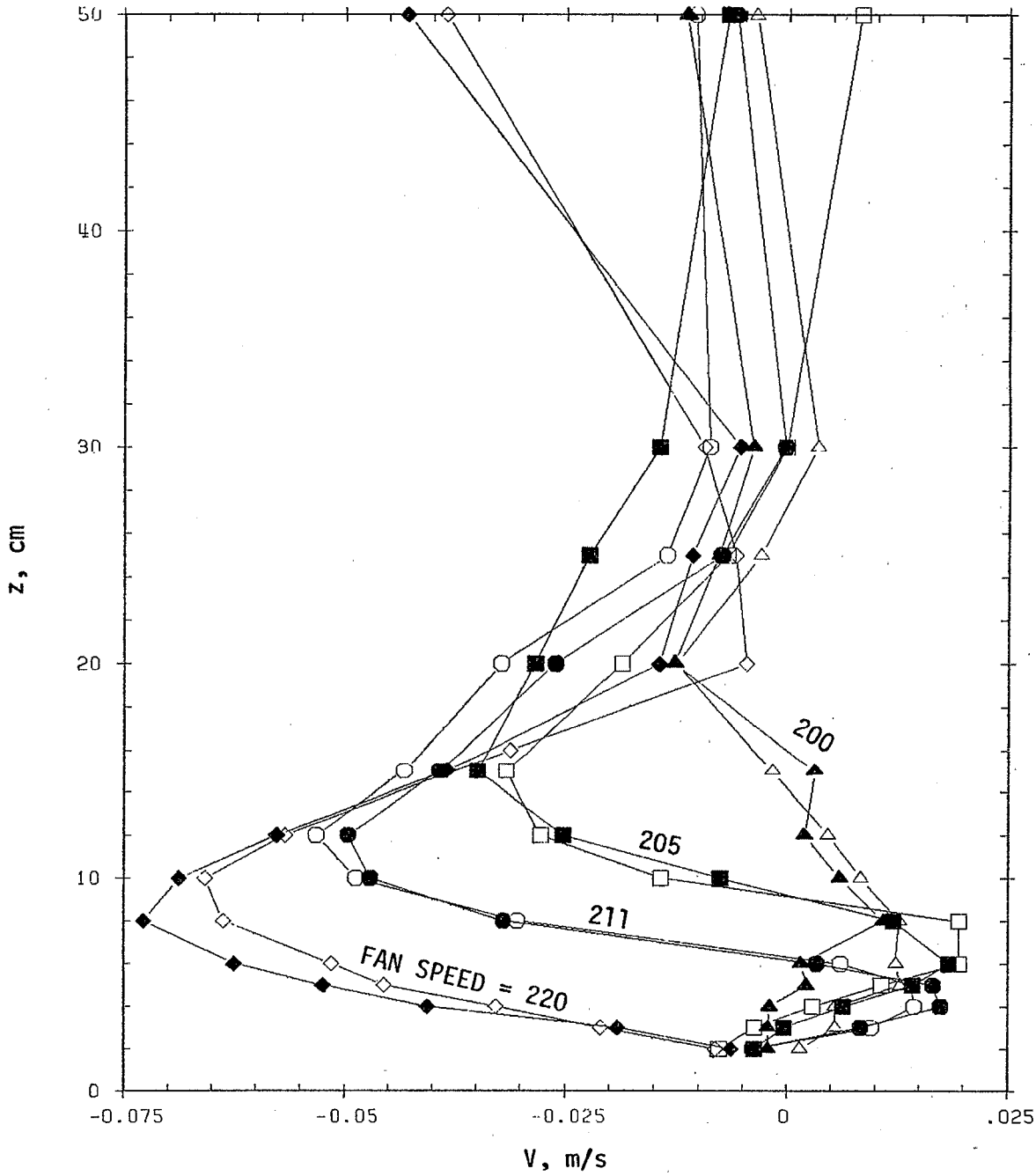

Figure A-15. Repeated measurements of lateral mean velocity profiles.

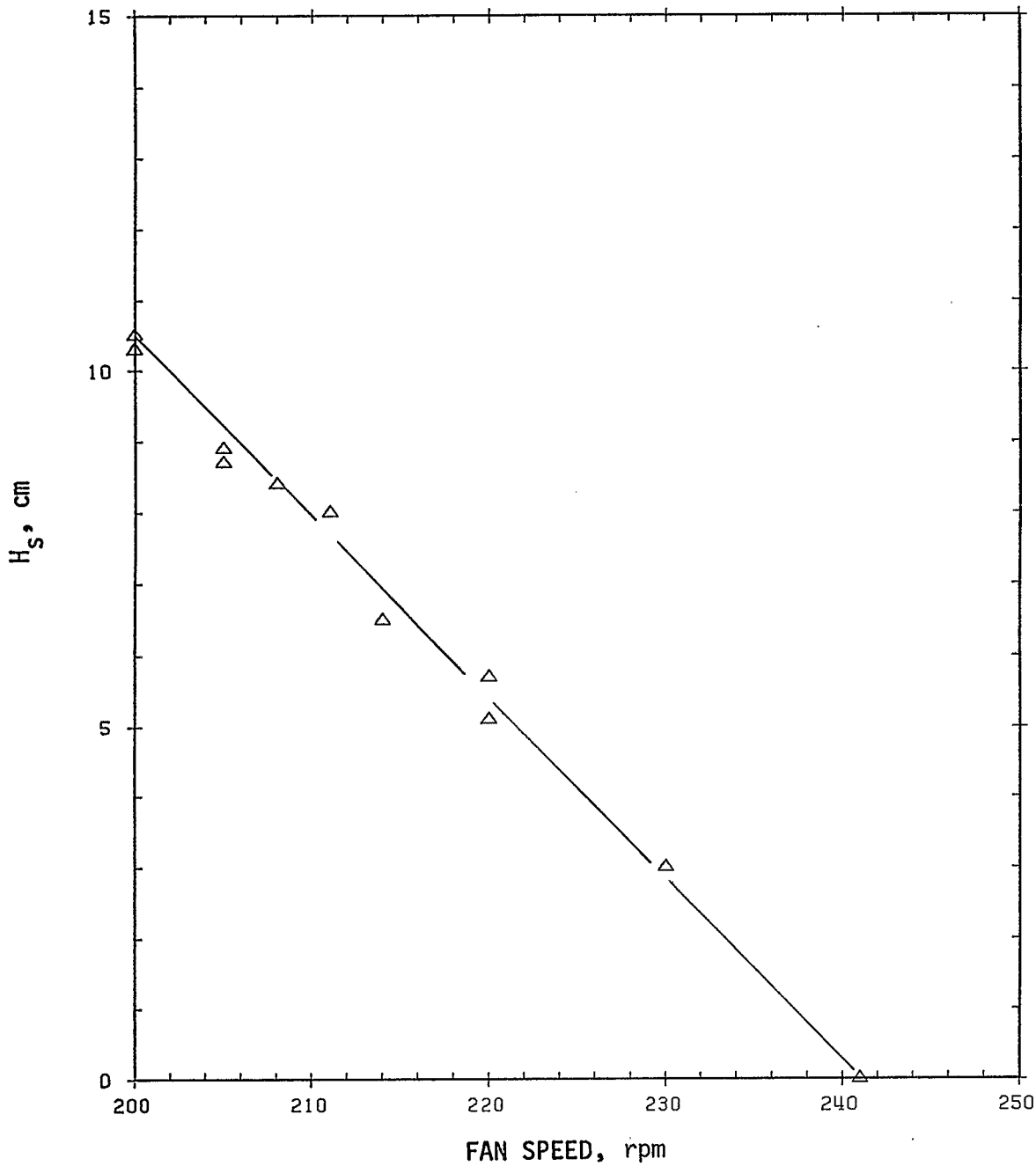

Figure A-16. Dividing-streamline height for the 15 cm hill as function of fan speed.

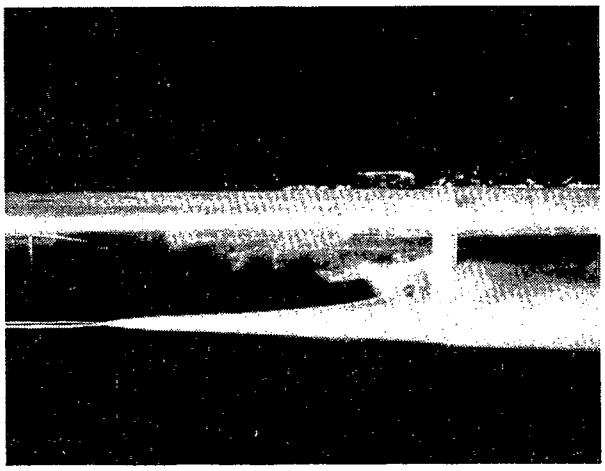

H_R=h L=4h

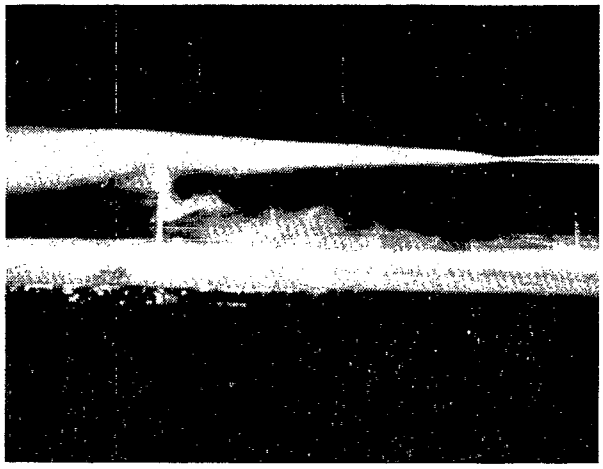

H_R=h L=h

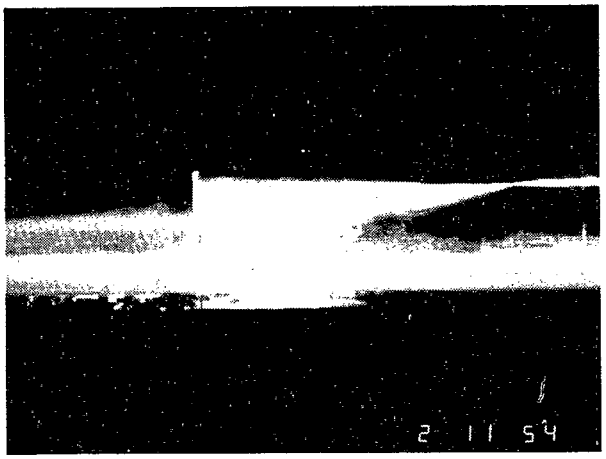

H_R=0.8h L=4h

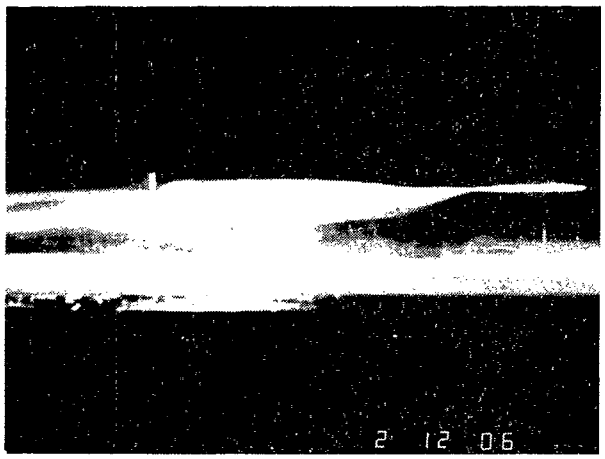

H_R=0.8h L=h

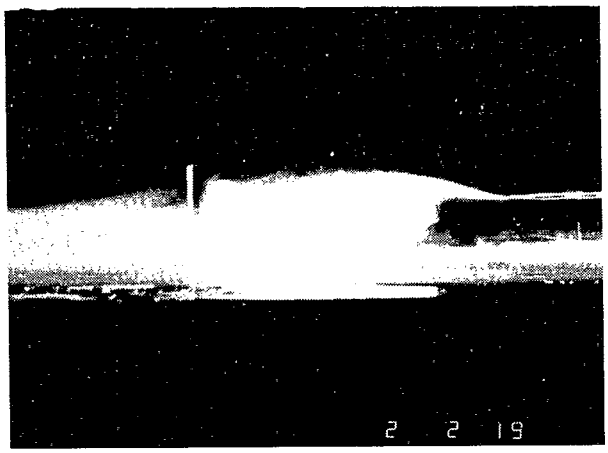

H_R=0.6h L=4h

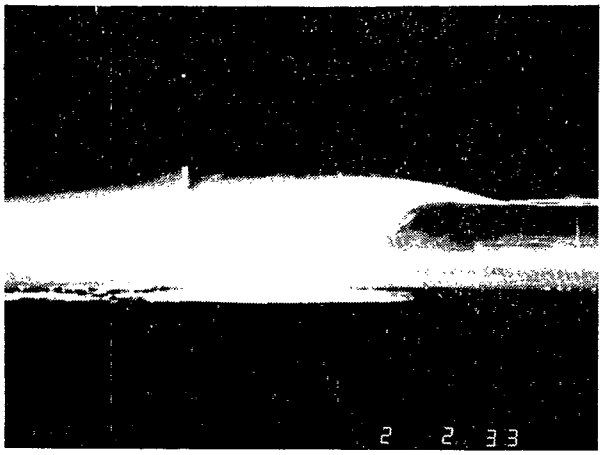

H_R=0.6h L=h

Figure A-17. Views of smoke streamers over a vertical fence; H_s=0.6h.

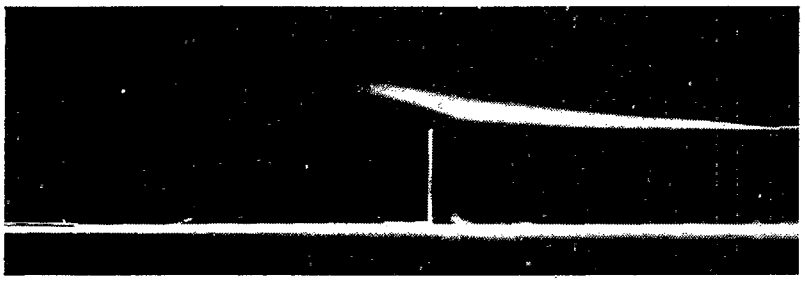

$H_R = h$

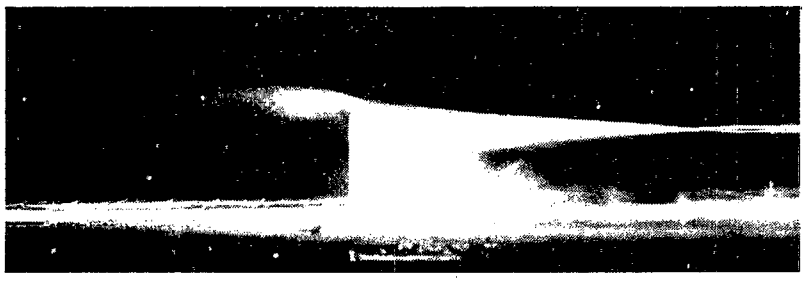

$H_R = 0.8h$

$H_R = 0.6h$

$H_R = 0.4h$

Figure A-18. Views of smoke streamers over a vertical fence; H_s=0.36h, L=2h.

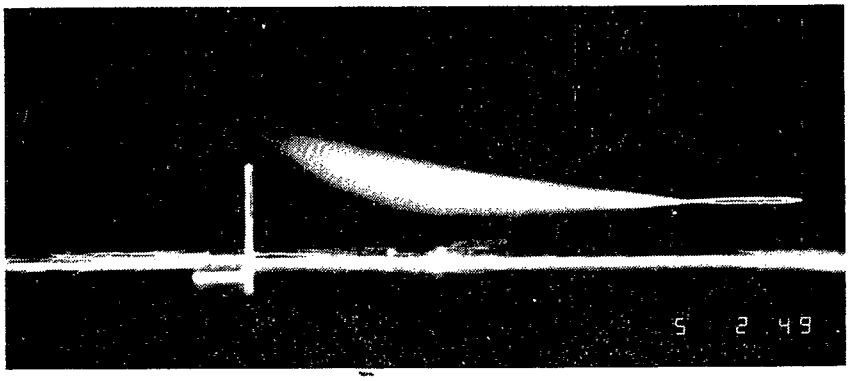

L = 8h

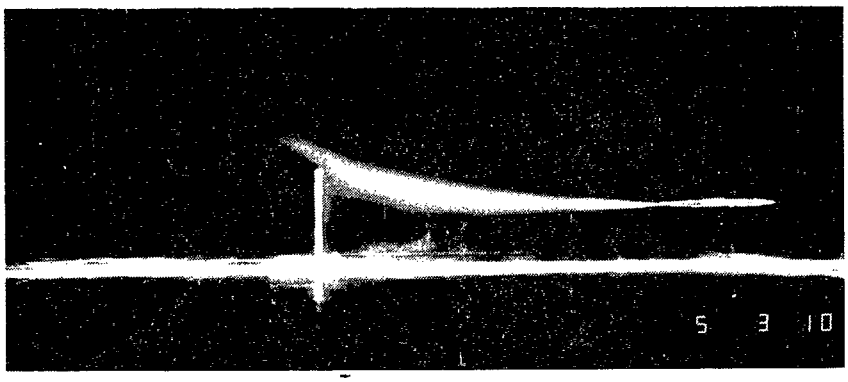

L = 2h

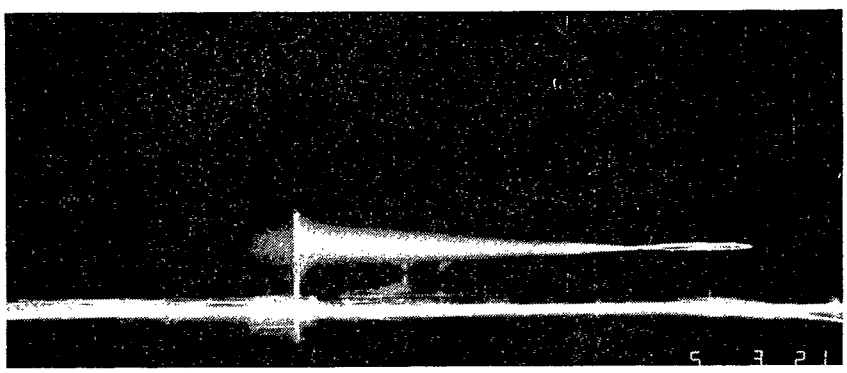

L = 0.5h

Figure A-19. Views of smoke streamers over a vertical fence; neutral flow, H_R=0.6h.

vertically through the density gradient (increasing its potential energy). Indeed, the bulk Froude number based on the (far upstream) fence-top velocity was 0.67. From another viewpoint, the velocity gradient is nearly constant over the full depth of the fence and the temperature gradient decreases with height, so that the Richardson number also decreases with height, i.e., an "outer" layer behaves more like neutral flow and an "inner" layer exhibits strongly stable, horizontally constrained flow characteristics.

At 220 rpm (Figure A-18), the calculated dividing-streamline height (from Figure A-16) was approximately 5.5 cm (0.36 h). The plume behavior was somewhat similar to the previous case, but here the 15 cm plume completely surmounted all fences and the upwind vortex appeared to reach the tunnel floor. Evidently, the streamlines impinging just below the top of the fence possessed sufficient kinetic energy to overcome the potential energy difference between the top and base of the fence. Indeed, the bulk Froude number based on the (far upstream) fence-top velocity was 1.1.

In neutral flow (Figure A-19), the plume behavior appeared to be much more dependent upon the fence aspect ratio. For long fences, the plume appeared to surmount the fence (even for the 3 cm plume), whereas for the short fences, most of the plume appeared to go around rather than over the fences (even the 12 cm plume).

To summarize, it is evident that even a relatively small amount of stratification drastically alters the flow structure over fences. And the shear seems to have an overwhelming influence! Tentative conclusions are (1) for strongly stratified flows, the basic flow structure is independent of aspect ratio, (2) the shear creates an upwind vortex so that upwind plumes are downwashed on the front face of fences and (3) under strong stratification, the downward penetration of elevated streamlines is limited; the extent of this downward penetration appears to be predicatable as a balance between kinetic and potential energies (hence, characterized by the Froude number), using arguments similar to those from the dividing-streamline theory.

Later flow visualization studies with the CCB model under these same stratified flow conditions showed no evidence of upwind vortex formation, but systematic studies to locate H_s were not conducted. However, concentration measurements (to be described in another paper) on the hill surface from an upwind source of 48 mm elevation first showed evidence of flow through the draw between the two peaks at a fan speed of 220 rpm, where the calculated dividing-streamline height (based on the saddle-point height) was 45 mm. These results suggest that, because of the relatively low upwind slope of the CCB model, the formation of an upwind vortex was not possible. They also suggest that Equation 3 may be a good indicator of dividing streamline heights, even in strong shear flows, for the vast majority of real hills (i.e., maximum slopes less than 26°).

The strong effect of the shear in the fence studies is not surprising in light of the discussion in Section 2.5. The slope term dR_o/dz, which normally tends to counteract the shear term, was zero. In the CCB model,

the minimum value of dR_o/dz was 2.0, so that the slope term evidently roughly balanced the shear term, thus inhibiting the upwind vortex formation. Also, as indicated in Section 2.5, it is not surprising that the centerline flow structure was independent of hill aspect ratio; however, because of the very large streamline deflections, it is not appropriate to make estimates using Equation 19.

4.4 Towing Tank Studies with the Sinusoidal Ridge

A total of 19 tows were made of the truncated sinusoidal ridge at Froude numbers of 0.3, 0.5, 0.7 and 1.0, and wind directions of 90°, 60°, and 30°. To conserve space, data from the 90° and 60° cases are not shown, but these data were completely consistent with all previous data for axisymmetric hills and supported the "1-F" rule (within the resolution of the method, ± 0.1 h). Data from the 30° case are shown in Figure A-20, where the release heights of the dye streamers are plotted versus Froude number; open symbols indicate that the streamers passed freely over the ridge, closed symbols show they were diverted around the ridge, and the half-filled symbol indicates the streamer split, with half going over the top and half going round the end. These data suggest something like $H_s/h = 1-0.7F$, as the streamers were diverted around the hill even though they had sufficient kinetic energy to pass over the top. It should be pointed out that this does not violate Sheppard's (1956) concept; just because a fluid parcel far upwind has sufficient kinetic energy to surmount the hill does not necessarily mean it will do so. In this 30° case, the flow, in some sense, followed the path of least resistance in travelling round the end of the ridge.

These streamers were released on the centerline of the towing tank and, hence, were not on (or even near) a stagnation streamline. A few tows were made with F=0.5 releasing dye from three tubes positioned at the same elevation but at different lateral positions. These releases showed the stagnation streamline to be located very near the most-upwind end of the ridge, as was also found experimentally and theoretically by Weil et al. (1981). Further tows showed that streamers released above (at $z/h=0.6$) the stagnation streamline travelled over the ridge ($H_s/h=0.5$) and that streamers released 1 h on either side of the center streamer travelled around opposite ends of the ridge, even though their elevation was above H_s. When the center streamer was released at $z/h=0.4$ (below H_s), it travelled round the sides, periodically switching from one side to the other. These data are consistent with Sheppard's (1956) criterion interpreted as a necessary but not sufficient condition on the kinetic energy of a fluid parcel far upstream.

These experiments also suggest that the lateral offset of the source from the stagnation streamline can be a very important parameter affecting the location and value of the maximum surface concentration, especially when the elevation of the source is below H_s. The data of Figure A-20, however, suggest that lateral offset can be extremely important even when the source is above H_s. Other tows with truncated ridges (both sinusoidal and triangular ones) oriented perpendicular to the tow direction suggested

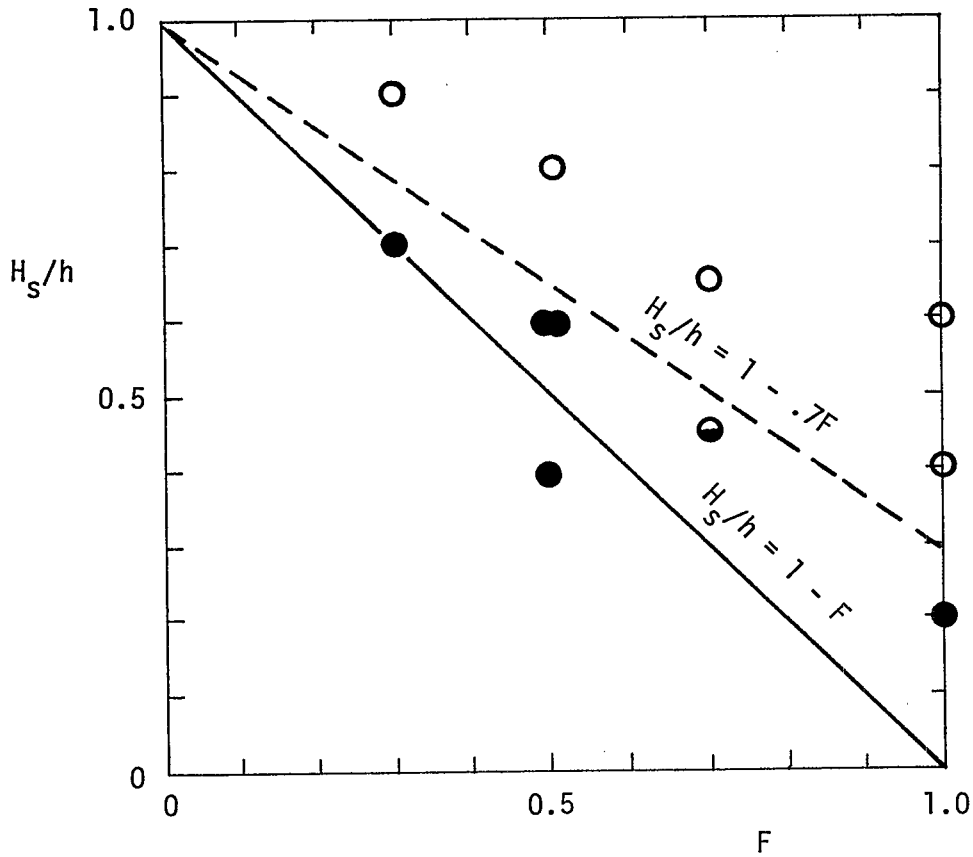

Figure A-20. Dividing-streamline height for a truncated sinusoidal ridge at 30° to tow direction.

that lateral offset was not a significant parameter when the source was located above H_s unless it was also located very near the ends of the ridges. Hence, the question of whether a plume will impact on a ridge is expected to be a function of both the source height relative to the dividing-streamline height and lateral offset; lateral offset, however, greatly increases in significance as the angle between the ridge axis and the wind direction is reduced.

4.5 Strongly stratified towing tank experiments with two-dimensional triangular ridges

Two tows were made of the two-dimensional triangular ridge at Froude numbers (based on the tow speed and the undisturbed density profiles) of 0.3 and 0.5. Figure A-21 shows the sampling positions and intervals. One sampling rake was positioned at the leading edge of the baseplate (11 hill heights upstream) and the other 10 cm (1.1 hill heights) upstream. A typical set of density profiles is compared with the initial density profile in Figure A-22. It is clear that the initial near-linear density profile was continuously modified during the tow at a position 11 hill heights upstream and that upstream conditions did not reach a steady state. The profiles tended toward neutral at elevations below half the hill height. These results tend to support the squashing model described in Section 2.3. The profiles taken at 1.1 h upstream and those at F=0.3 showed similar tendencies, but with the tendency-toward-neutral behavior occurring over larger depths, i.e., to approximately 0.8 h.

The density profiles measured at 11 h upstream were used to calculate H_s according to Sheppard's integral formula assuming a uniform approach wind profile. The results are shown in Figure A-23. Because the density gradients below hill top were reduced, the dividing-streamline heights were also reduced as the tow progressed. This behavior was also substantiated by observing dye streamers released simultaneously at various elevations during the tow.

It should be pointed out that in Baines (1979) experiments on ridges with gaps, the dye-release rake was hinged in such a way that dye was released at 8 different elevations. However, the rake was pivoted from one elevation to the next during the length of the tow, so that observations of dye behavior at each level took place for, at most, 1 m. It is not difficult to imagine that, because of the systematic change of release elevation with tow distance in conjunction with the decrease in H_s with tow distance, the results were interpreted incorrectly to arrive at $H_s/h = 1-2F$.

Some additional experiments with the truncated sinusoidal ridge ($G = 0.25$, $W/h = 16$) show that, even though the $H_s/h = 1-F$ formula is well-verified, a very long time period (or a long length of tow) is required for steady-state conditions to be established at 10 hill heights upwind.

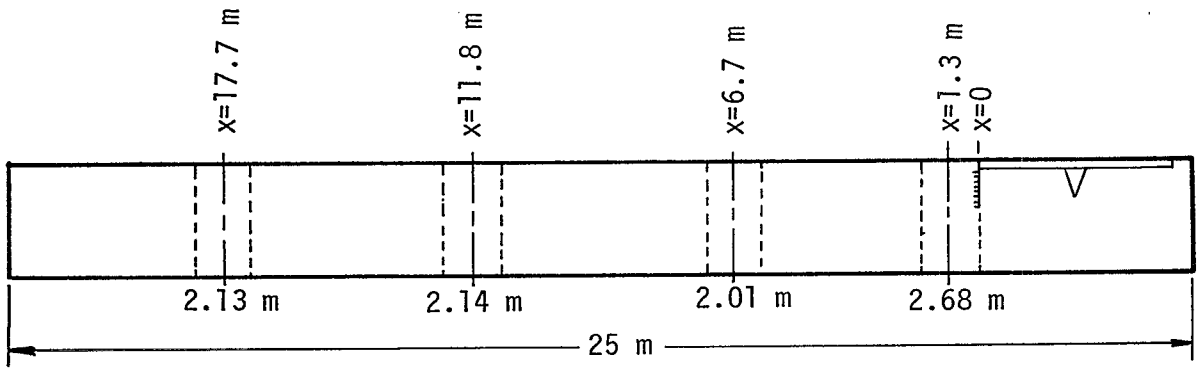

Figure A-21. Sketch showing sampling intervals and locations for the two-dimensional ridge tow at F=0.5.

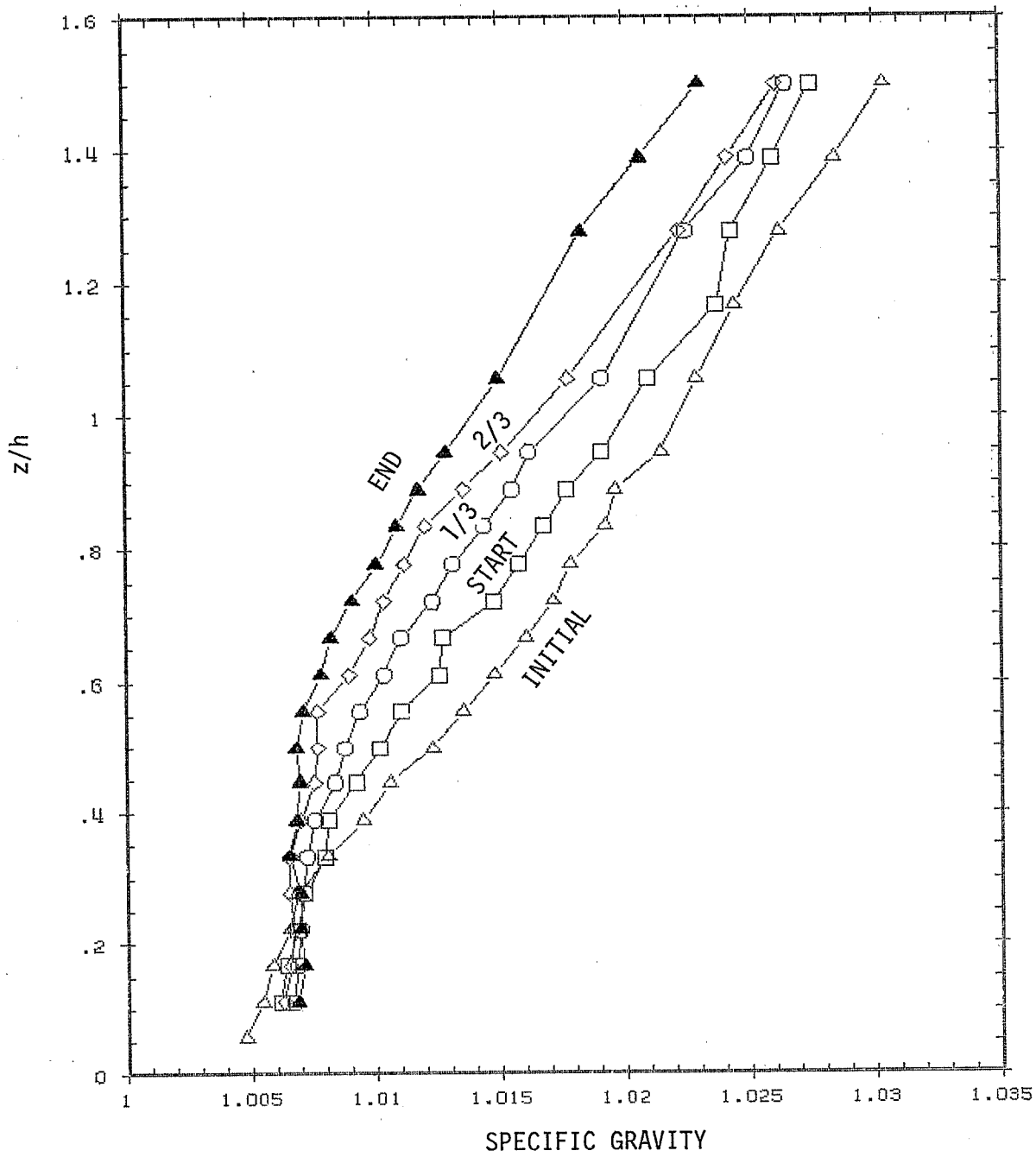

Figure A-22. Density profiles measured upstream of the two-dimensional triangular ridge.

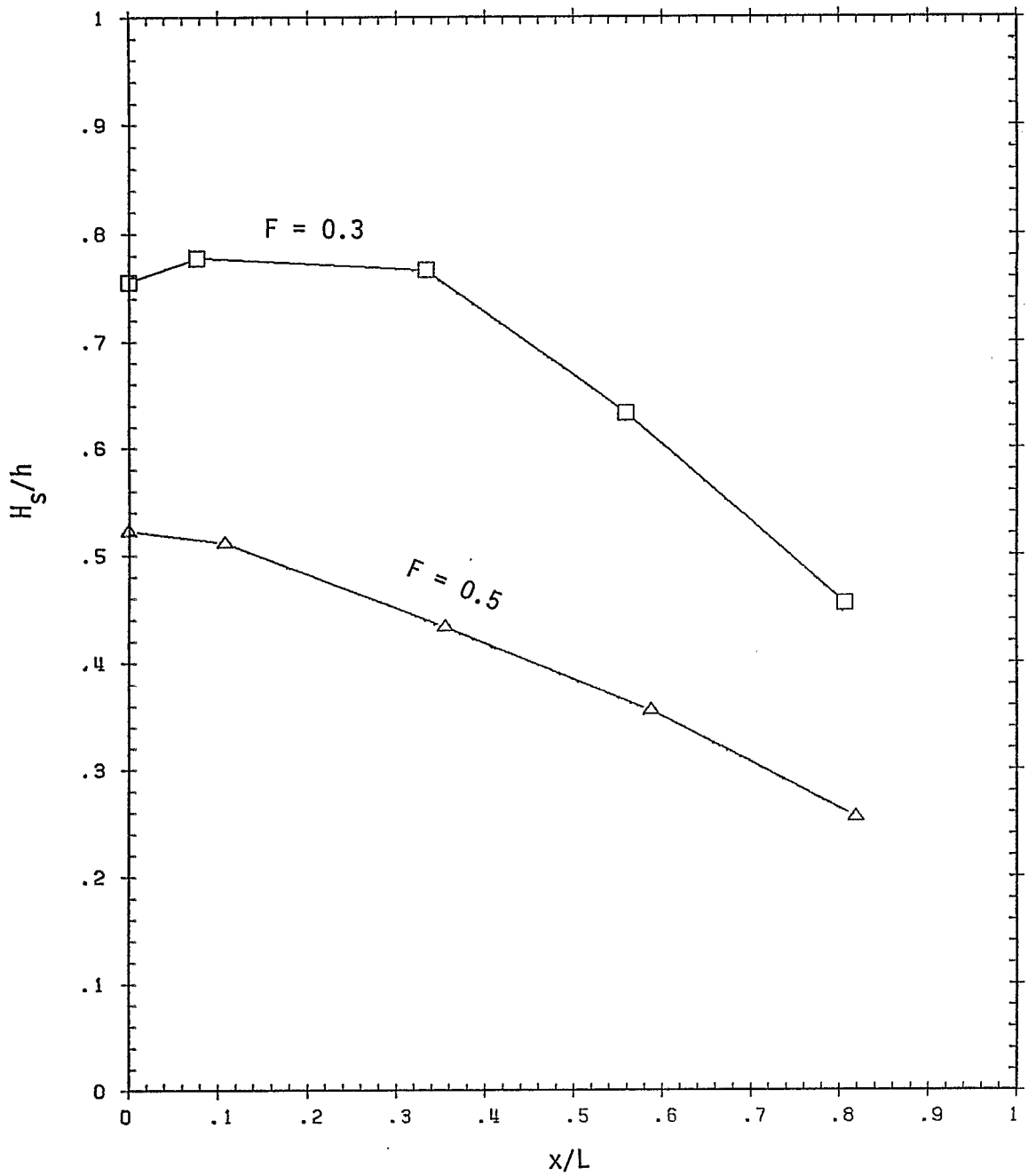

Figure A-23. Dividing streamline height as function of towing distance for the two-dimensional triangular ridge.

SECTION 5

CONCLUSIONS

(1) From previous work as well as current studies with the CCB model, it is concluded that the integral formula of Sheppard (1956) is valid for predicting the height of the dividing streamline for a wide range of shapes of stable density profiles and a wide range of roughly axisymmetric hill shapes.

(2) From the studies with the truncated triangular and sinusoidal ridges perpendicular to the wind, it is concluded that the aspect ratio, per se, does not have a significant influence on the dividing-streamline height H_s. Deviations from the $H_s/h = 1-F$ rule are attributed to the combination of shear in the approach flow and the steep slope of the triangular ridges, which resulted in the formation of an upwind vortex with downward flow on the front face of the ridges. The "1-F" rule was validated for the sinusoidal ridge with a length-to-height ratio greater than 16:1; in this case, the shear in the approach flow was much less pronounced and the upwind slope was substantially smaller. Note that the above deviations from the "1-F" rule do not invalidate Sheppard's concept; the rule should be interpreted as a necessary but not sufficient condition, i.e., a fluid parcel may possess sufficient kinetic energy to surmount a hill, but it does not necessarily do so.

(3) In the stratified wind tunnel studies, a range of operating modes was found that yielded reasonably strong shear layers with depths more than twice the hill heights in conjunction with strong stable temperature gradients. These provided dividing-streamline heights as large as 0.75 h. In the vertical fence studies with a stratified approach flow, the shear was found to have an overwhelming influence. Conclusions are: (a) as in the triangular ridge studies, the aspect ratio was relatively unimportant; the basic flow structure was independent of aspect ratio, (b) the shear (in conjunction with the steep slope) created an upwind vortex such that plumes were downwashed on the front faces and (c) under strong enough stratification, there was a limit to the downward penetration of elevated streamlines; the extent of this penetration is apparently predictable as a balance between kinetic and potential energies. With these same shear flows approaching the much lower sloped CCB model, however, there was <u>no</u> evidence of upwind vortex formation. Limited concentration measurements on the CCB model suggested that Sheppard's integral formula correctly predicted the height of the dividing streamline.

(4) From the sinusoidal ridge studies with wind angles at other-than-90°, it is concluded that the effect of deviations in wind direction (from 90°) are relatively insignificant until the wind direction is something like 45° to the ridge axis. At 30°, significant departures from the $H_s/h = 1-F$ rule were observed; the fluid had sufficient kinetic energy to surmount the ridge but, presumably, found a path of lower resistance in travelling round the end of the ridge. When the streamers were moved closer to the upstream stagnation streamlines (upwind of the upwind edge of the ridge), they behaved according to the $H_s/h = 1-F$ rule.

These experiments suggest that the lateral offset of the source from the (probably contorted) plane of stagnation streamlines is an important parameter to consider in determining the location and value of surface concentrations, especially when the wind is at a small angle to the ridge axis (say, <45°).

(5) The two-dimensional triangular ridge studies showed that steady-state conditions are not established in strongly stratified flows (say, $F<1$). The squashing phenomenon and upstream columnar disturbances continuously changed the shapes of the "approach flow" velocity and density profiles. Thus, these experiments have no analog in the real atmosphere. Further, since long ridges cut by periodic small gaps require very long tow distances in order for steady state to be established, it is concluded that previous laboratory studies are not valid; specifically the $H_s/h = 1-2F$ formula proposed for flow about ridges with small gaps is not expected to be valid in the real atmosphere. Finally, a suggestion is made that the gap ratio must exced 25% in order for steady-state conditions to be established in the usual size and shape of towing tank. More work is required to firmly establish the relationships between model size and shape, stability, and tank size and shape in order to determine limits of applicability of fluid modeling and ranges of tranferability to the atmosphere.

REFERENCES

Baines, P.G., 1977. Upstream Influence and Long's Model in Stratified Flows, J. Fluid Mech., v. 82, pt. 1, pp. 147-59

Baines, P.G., 1979. Observations of Stratified Flow Past Three-Dimensional Barriers, J. Geophys. Res., v. 84, no. C12, p. 7834-8, Dec.

Brighton, P.W.M., 1978. Stongly Stratified Flow Past Three-Dimensional Obstacles, Quart. J. Roy. Meteorol. Soc., v. 104, p. 289-307.

Castro, I.P. and Snyder, W.H., 1982. Stratified Flow over Three-Dimensional Ridges, (in preparation).

Drazin, P.G., 1961. On the Steady Flow of a Fluid of Variable Density Past an Obstacle, Tellus, v. XIII, no. 2, p. 239-251.

Holzworth, G.C., 1980. The EPA Program for Dispersion Model Development for Sources in Complex Terrain, Pres. at 2nd Jt. Conf. on Appl. of Air Poll. Meteorol., March 24-27, New Orleans, LA, 4p.

Hunt, J.C.R., Snyder, W.H., and Lawson, R.E. Jr., 1978. Flow Structure and Turbulent Diffusion around a Three-Dimensional Hill: Fluid Modeling Study on Effects of Stratification; Part I: Flow Structure, Envir. Prot. Agcy. Rpt. No. EPA 600/4-78-041, Res. Tri. Pk., NC.

Hunt, J.C.R., Puttock, J.S. and Snyder, W.H., 1979. Turbulent Diffusion from a Point Source in Stratified and Neutral Flows around a Three-Dimensional Hill: Part I: Diffusion Equation Analysis, Atmos. Envir., v. 13, p. 1227-39.

Hunt, J.C.R. and Snyder, W.H., 1980. Experiments on Stably and Neutrally Stratified Flow over a Model Three-Dimensional Hill, J. Fluid Mech., v. 96, pt. 4, p. 671-704.

Kitabayashi, K., 1977. Wind Tunnel and Field Studies of Stagnant Flow Upstream of a Ridge, J. Meteorol. Soc. of Japan, v. 55, no. 2, p. 193-204, April.

Kitabayashi, K., 1981. On the Stagnant Zone Upstream of an Obstacle within a Stably Stratified Flow in the Atmosphere, J. Meteorol. Soc. of Japan, v. 59, no. 3, p. 373-86.

Lavery, T.F., Bass, A., Greene, B.R., Hatcher, R.V., Venkatram, A. and Egan, B.A., 1982. The Cinder Cone Butte Dispersion Experiment, Paper no. 11.3, Proc. 3rd Jt. Conf. on Appl. of Air Poll. Meteorol., Jan 12-15, San Antonio, TX, Am. Meteorol. Soc., Boston, MA.

Lavery, T.F., Bass, A., Strimaitis, D.G., Venkatram, A., Greene, B.R., Drivas, P.J. and Egan, B.A., 1982: EPA Complex Terrain Modeling Program: First Milestone Report - 1981, Rpt. No. EPA-600/3-82-036, Envir. Prot. Agcy., Res. Tri. Pk., NC, 304p.

Long, R.R., 1953. Some Aspects of the Flow of Stratified Fluids: I. A Theoretical Investigation, Tellus, v. 5, no. 1, p. 42-57.

Long, R.R., 1954. Some Aspects of the Flow of Stratified Fluids: II. Experiments with a Two-Fluid System, Tellus, v. 6, no. 2, p. 97-115

Long, R.R., 1955. Some Aspects of the Flow of Stratified Fluids: III. Continuous Density Gradients, Tellus, v. 7, no. 3, p. 341-57.

Long, R.R., 1972. Finite Amplitude Disturbances in the Flow of Inviscid Rotating and Stratified Fluids over Obstacles, Ann. Rev. Fluid Mech., v. 4, p. 19-92.

McIntyre, M.E., 1972. On Long's Hypothesis of no Upstream Influence in Uniformly Stratified or Rotating Fluid, J. Fluid Mech., v. 52, pt. 2, p. 209-243.

Ogawa, Y., Diosey, P.G., Uehara, K., and Ueda, H., 1981. A Wind Tunnel for Studying the Effects of Thermal Stratification in the Atmosphere, Atmos. Envir., v. 15, no. 5, p. 807-821.

Riley, J.J., Liu, H.T. and Geller, E.W., 1976. A Numerical and Experimental Study of Stably Stratified Flow Around Complex Terrain, Envir. Prot. Agcy. Rpt. No. EPA-600/4-76-021, Res. Tri. Pk., NC, 41p.

Rowe, R.D., Benjamin, S.F., Chung, K.P., Havlena, J.J. and Lee, C.Z., 1982. Field Studies of Stable Air Flow Over and Around a Ridge, Atmos. Envir., v. 16, no. 4, p. 643-53.

Sheppard, P.A., 1956. Airflow over Mountains, Quart. J. Roy. Meteor. Soc., v. 82, p. 528-9.

Snyder, W.H., Britter, R.E. and Hunt, J.C.R., 1980. A Fluid Modeling Study of the Flow Structure and Plume Impingement on a Three-Dimensional Hill in Stably Stratified Flow, Proc. Fifth Int. Conf. on Wind Engr. (J.E. Cermak, ed.), v. 1, p. 319-29, Pergamon Press, NY, NY.

Spangler, T.C. and Taylor, G.H., 1982. Flow Simulation Techniques Used in the Small Hill Impaction Study, Paper no. 11.4, Proc. 3rd Jt. Conf. on Appl. of Air Poll. Meteorol., Jan. 12-15, San Antonio, TX, Am. Meteorol. Soc., Boston, MA.

Thompson, R.S. and Snyder, W.H., 1976. EPA Fluid Modeling Facility, Proc. Conf. on Envir. Modeling and Simulation, Envir. Prot. Agcy. Rpt. No. EPA 600/9-76-016, Wash. D.C., July.

Turner, J.S., 1979. Buoyancy Effects in Fluids, Cambridge Univ. Press, Cambridge, England, 368p.

Wei, S.N., Kao, T.W. and Pao, H.P., 1975. Experimental Study of Upstream Influence in the Two-dimensional Flow of a Stratified Fluid Over an Obstacle, Geophys. Fluid Dyn., v. 6, p. 315-36.

Weil, J.C., Traugott, S.C. and Wong, D.K., 1981. Stack Plume Interaction and Flow Characteristics for a Notched Ridge, Rpt. No. PPRP-61, Maryland Power Plant Siting Program, Martin Marietta Corp., Baltimore, MD, 92p.